Terms and Conditions of Use of Digitised Theses from Trinity College Library Dublin

Copyright statement

All material supplied by Trinity College Library is protected by copyright (under the Copyright and Related Rights Act, 2000 as amended) and other relevant Intellectual Property Rights. By accessing and using a Digitised Thesis from Trinity College Library you acknowledge that all Intellectual Property Rights in any Works supplied are the sole and exclusive property of the copyright and/or other IPR holder. Specific copyright holders may not be explicitly identified. Use of materials from other sources within a thesis should not be construed as a claim over them.

A non-exclusive, non-transferable licence is hereby granted to those using or reproducing, in whole or in part, the material for valid purposes, providing the copyright owners are acknowledged using the normal conventions. Where specific permission to use material is required, this is identified and such permission must be sought from the copyright holder or agency cited.

Liability statement

By using a Digitised Thesis, I accept that Trinity College Dublin bears no legal responsibility for the accuracy, legality or comprehensiveness of materials contained within the thesis, and that Trinity College Dublin accepts no liability for indirect, consequential, or incidental, damages or losses arising from use of the thesis for whatever reason. Information located in a thesis may be subject to specific use constraints, details of which may not be explicitly described. It is the responsibility of potential and actual users to be aware of such constraints and to abide by them. By making use of material from a digitised thesis, you accept these copyright and disclaimer provisions. Where it is brought to the attention of Trinity College Library that there may be a breach of copyright or other restraint, it is the policy to withdraw or take down access to a thesis while the issue is being resolved.

Access Agreement

By using a Digitised Thesis from Trinity College Library you are bound by the following Terms & Conditions. Please read them carefully.

I have read and I understand the following statement: All material supplied via a Digitised Thesis from Trinity College Library is protected by copyright and other intellectual property rights, and duplication or sale of all or part of any of a thesis is not permitted, except that material may be duplicated by you for your research use or for educational purposes in electronic or print form providing the copyright owners are acknowledged using the normal conventions. You must obtain permission for any other use. Electronic or print copies may not be offered, whether for sale or otherwise to anyone. This copy has been supplied on the understanding that it is copyright material and that no quotation from the thesis may be published without proper acknowledgement.

Mechanistic and functional studies on biliverdin IXα reductase from the cyanobacterium *Synechocystis* sp. PCC6803

A thesis submitted to the University of Dublin, Trinity College for the degree of Doctor of Philosophy

Jerrard Michael Hayes

School of Biochemistry & Immunology,

Trinity College,

Dublin.

2008

DECLARATION

This thesis is submitted by the undersigned to the University of Dublin for the examination of Doctorate in Philosophy. The work described in this thesis is entirely my own and has not been submitted for any degree in this or any other university. The library at Trinity college, Dublin has my full permission to lend or copy this thesis on request

TABLE OF CONTENTS

CHAPTER 3 Recombinant production of the proteins of heme metabolism and phycobilin biosynthesis from *Synechocystis*

ACKNOWLEDGEMENTS

First and foremost I would like to sincerely thank my supervisor Dr. Tim Mantle for his support, advice, guidance and enthusiasm.

I would also like to express my sincere gratitude to Dr. Vincent Kelly for his help and expertise with many aspects of this thesis and for his advice and guidance,

Immense gratitude is due to the members of Tim's lab, both past and present. Mainly past however as apart from Tim I am now the only present member. A special thanks to Ed who up until recently was my only labmate for his friendship and help. A special thanks to Coilin also who is the first person I run to when I have a question about most things, particularly computers. Thanks to Seamus, Gavin, Bertie (el mexicano muy molestando), Conor (HPV lab) and Liam.

I would like to thank the Irish Research Council for Science, Engineering and Technology (IRCSET) for funding this work.

Last but certainly not least a very special thanks to my family, to my mother Una and my father Jim, to my brothers James and John and to my sister Jemma for your financial and moral support, without which this would not have been achievable. I am sure that this means as much to you as it does to me.

ABSTRACT

The enzymes of heme metabolism and phycobilin biosynthesis in the cyanobacterium *Synechocystis* sp. PCC6803, along with their reducing partners, ferredoxin and ferredoxin reductase were produced through recombinant DNA techniques and displayed the appropriate molecular weights on SDS-PAGE. Antibodies were raised against the recombinant heme oxygenase 1 (HO1), biliverdin IXα reductase (sBVR-A) and phycocyanobilin ferredoxin oxidoreductase (PcyA).

The initial rate kinetics were performed on the recombinant sBVR-A with biliverdin IXα, NADPH and NADH as the variable substrates. Kinetic parameters were determined for the enzyme and have shown that like mammalian BVR-As NADPH is the preferred nucleotide over NADH for reduction of biliverdin with a K_m value of approximately 10μM for NADPH and 200μM for NADH. The k_{cat} for the enzyme was determined to be approximately 0.4 s^{-1} for NADPH and 0.2 s^{-1} for NADH showing that sBVR-A is quite a "slow" enzyme. The K_m for biliverdin IXα was approximately 2μM. A complete product inhibition study was performed by varying the concentrations of the products bilirubin IXα, NADPH or NADH against varying concentrations of the substrates at saturating and non-saturating levels and the modes of inhibition and inhibition parameters were determined. sBVR-A was not substrate inhibited by biliverdin IXα up to 50μM unlike the mammalian BVR-As and the kinetic mechanism under optimum conditions was shown to be compulsory ordered with NAD(P)H the first substrate to bind and bilirubin IXα the first product to leave. This is the first description of the kinetic mechanism of any BVR-A under optimum conditions.

A complete pH study and the effect of pH on the kinetic parameters of sBVR-A was undertaken. The pH optimum was approximately 5 with all substrates. When the k_{cat} data were plotted as a function of pH with NADPH and NADH as co-factors a pK of approximately 5.4 was determined from the "less-acidic" limb of the pH curve. It is possible that a co-operative pK of approximately 4 is also in effect in the "more-acidic" limb of the curve which "turns-off" the enzyme by approximately 50%. However, the enzyme was shown to be extremely unstable at low pH with a half-life of only 30 sec at pH 4. Based on the pH studies and the pK of 5.4 determined from the k_{cat} *versus* pH data a histidine residue was predicted to be involved in the enzymatic mechanism of sBVR-A, in substrate binding or catalysis or both and must be protonated at pH 5 in order to carry out these functions.

It was also possible that an acidic residue (Asp or Glu) with a pK of 4 was also required and must be deprotonated at pH 5. A series of residues were mutated and the effect of the mutation on the activity of the enzyme and its ability to bind substrates was analysed. His 84 was shown to be involved in the binding of biliverdin to the enzyme and proton transfer to the reaction, Glu 101 was also shown to be involved in the binding of biliverdin to the enzyme and Tyr 102 was shown to be involved in the binding of biliverdin to the enzyme in the correct orientation for efficient catalysis to occur.

Initial rate *versus* enzyme concentration curves for sBVR-A were shown to deviate from linearity at protein concentrations above 20-30μg/ml with NADPH and NADH as co-factor. Analytical unltracentrifugation (sedimentation velocity and sedimentation equilibrium), laser light scattering and size-exclusion chromatography suggested that sBVR-A exists with a molecular weight of approximately 70kDa. The theoretical molecular weight, based on amino acid sequence of sBVR-A is 36kDa which suggests that sBVR-A exists as a stable dimer in solution, the first BVR-A to be described as such. It is proposed that sBVR-A dimerises through the interface of a C-terminal β-sheet, present in the crystal structures of the rat and human BVR-As and the sBVR-A model, similar to a number of protein dimers present in the literature.

The sBVR-A gene in *Synechocystis* sp. PCC6803 was disrupted by interposon mutagenesis and the absence of sBVR-A was verified by western blotting. Preliminary evidence suggests that growth is retarded in the absence of sBVR-A, particularly under conditions of oxidative stress induced by high light conditions. The presence of bilirubin in the growth medium of these cells suggests that bilirubin can enhance growth of the wild-type cells under stress conditions and possibly return the sBVR-A mutant cells to the wild-type growth phenotype under the same conditions. Through HPLC analysis, levels of chlorophyll are shown to be decreased in the mutant cells in comparison to the wild-type cells under light stress conditions, possibly coupled with an increase in protective carotenoids. Western blotting has shown that under oxidative stress conditions levels of HO1 decrease, levels of PcyA remain constant and levels of sBVR-A increase. This may suggest that under oxidative stress conditions light-harvesting is down-regulated by decreasing the levels of HO1 and increasing the levels of sBVR-A. sBVR-A and its metabolite bilirubin IXα may be playing an ancient anti-oxidative role in these organisms.

ABBREVIATIONS

ALA	5-aminolaevulinic acid
bp	Base pairs
BAP	Bacterial alkaline phosphatase
BSA	Bovine serum albumin
BVR-A	Biliverdin IXα reductase
cfu	Colony forming unit
Da	Dalton
DMSO	Dimethyl sulfoxide
dNTP	Deoxyribonucleotide triphosphate
DTT	Dithiothreitol
EDTA	Ethylenediaminetetraacetic acid
GSH	Glutathione
GST	Glutathione-*S*-transferase
HO	Haem oxygenase
IPTG	Isopropylthio-β-D-galactose
kDa	kiloDalton
mA	miliAmpere
MBP	Maltose binding
M_r	Relative molecular mass
NADPH	Nicotinamide adenine dinucleotide phosphate (reduced)
$NADP^+$	Nicotinamide adenine dinucleotide phosphate (oxidised)
NADH	Nicotinamide adenine dinucleotide (reduced)
NAD^+	Nicotinamide adenine dinucleotide (oxidised)
NFW	Nuclease free water
NP-40	Nonidet P-40
OD	Optical density
PBS	Phosphate buffered saline
PCR	Polymerase chain reaction
PcyA	Phycocyanobilin ferredoxin oxidoreductase

PebA	Phycoerythrobilin ferredoxin oxidoreductase
PEG	Polyethyleneglycol
PSI	Photosystem I
PSII	Photosystem II
rpm	Revolutions per minute
sBVR-A	*Synechocystis* biliverdin IXα reductase
SDS	Sodium dodecyl sulfate
SDS-PAGE	SDS-polyacrylamide gel electrophoresis
TAE	Tris-acetate/EDTA electrophoresis buffer
TBE	Tris-borate/EDTA electrophoresis buffer
TE	Tris/EDTA buffer
TEMED	*N*,*N*,*N*',*N*'-tetramethylenediamide
Tm	Melting temperature
Tris	2-amino-2-(hydroxymethyl)-propane-1,3-diol
TTBS	Tris/Tween 20 buffered saline
Tween 20	polyoxyethylene (20) sorbitan monolaurate

CHAPTER 1

INTRODUCTION

1.1 Cyanobacteria - a general introduction

Cyanobacteria are a large family of aquatic, free-living autotrophic bacteria that can manufacture their own "food" through the process of photosynthesis. Although they are often referred to as "blue-green" algae, they are a phylum of bacteria that are not directly related to any eukaryotic algal group. This can be demonstrated by their clear lack of a nucleus and internal organelles. In fact, their simple structure contains no internal compartments, except for the thylakoid membrane and the name "blue-green algae" is simply due to their superficial resemblance to eukaryotic green algae. The name cyanobacterium comes from the Greek "cyano" meaning blue, due to the pigment phycocyanin. With regard to their internal structure however, it should be noted that some cyanobacteria contain gas vesicles, heterocysts for nitrogen fixation, polyphosphate granules and carboxysomes.

Cyanobacteria are the oldest known organisms on the planet and the first to utilise photosynthesis and produce oxygen as a by-product. Their fossil record dates back 2.8 billion years, the oldest of any known organism. They were the first to produce oxygen and gave rise to oxygenic life on this planet during the Archean and Proterozoic eras. Even today cyanobacteria are ecologically important, releasing vast amounts of oxygen to the atmosphere, particularly from the oceans. Oxygen production is not the only reason why they are essential to the environment and life as we know it. They are important for the health and growth of many plants, mainly through their ability to fix nitrogen. They are one of only a small number of groups, which can convert inert atmospheric nitrogen into an organic form, such as nitrate or ammonia. It is this form that plants need to grow and they must obtain it from the soil. This nitrogen fixation can only occur in the absence of oxygen and occurs in specialised cells called heterocysts. Not all cyanobacteria have the ability to fix nitrogen however, but those that can contribute significantly to the total amount of nitogen fixed on the planet eg. *Trichodesmium* is the major nitrogen fixer in the open ocean.

The structure of a typical cyanobacterium is very simple (see Fig. 1.1). They are Gram negative bacteria, approximately 2μm in diameter with a tough outer cell wall composed of small amounts of peptidoglycan compared to Gram positive bacteria and lipopolysaccharide. They can be organised into a variety of structures, including filaments, unicells or packets of cells in mucilage. Most have infoldings of the cell membrane to form the photosynthetic thylakoid membrane, with the phycobilisomes attached to photosystem II.

Cyanobacteria are not very diverse in form but are rich in chemical diversity. Although they get their name from the blue pigment phycocyanin, not all cyanobacteria are blue, some species are red due to another photosynthetic accessory pigment, phycoerythrin. The red sea for example gets its name from large blooms of red cyanobacteria called *Oscillatoria* and African flamingos get their pink colour from eating the same cyanobacteria. They can be found in a tremendous variety of environments, practically anywhere near the surface of the earth. Typical environments include freshwater and marine habitats, hotsprings, soil and in a fairly broad range of pH but not in extremely acidic environments.

Some species can form mass populations of cyanobacteria known as algal blooms, such as *Anabaena, Aphanizomenon* and *Microcystis.* During the summer months, when there is increased eutrophication, rivers and lakes are often affected by these algal blooms. Phosphate is typically the limiting nutrient in freshwater so the most effective way of reducing cyanobacterial blooms is to reduce phosphate input. Among these bloom-forming cyanobacteria are some species, which produce toxic compounds such as the heptapeptide microcystin, and these are therefore potentially toxic and harmful to both humans and animals.

1.2 Cyanobacteria – The evolutionary ancestor to chloroplasts

The site of photosynthesis in plants and algae, the chloroplast is a membraneous organelle known as a plastid (see Fig 1.2). It is now known that this highly specialised organelle evolved through an endosymbiotic relationship with primitive cyanobacteria. Although genomic (Martin *et al.,* 2002) and molecular phylogenetic (Douglas & Raven, 2003) evidence makes cyanobacteria the closest bacterial homologue to plastids, this was not always widely accepted. When Mereschkowsky first proposed this in 1905 he was greeted with scepticism (see Martin & Kowallik, 1993 for a translation of the original paper). However, advances in biochemical, genetic, phylogenetic and microscopical techniques lend strong support to this theory.

It is generally accepted that a requirement for endosymbiosis between a cyanobacterium and a plant is that there is large-scale gene transfer from the chloroplast/cyanobacterium to the nucleus. This was thought to be impossible but it is now known that many of the proteins needed for photosynthesis and other chloroplast functions are indeed encoded in the nuclear genome of plants resulting from wholescale uptake of cyanobacteria by plants followed by gene transfer from the cyanobacterium to the nucleus of the plant (Boucher *et al.,* 2003). It is also now known that gene transfer occurs naturally from chloroplast to nucleus in tobacco plants (Huang *et al.,* 2003). There is also other evidence that lends support to this theory. Cyanobacteria and plants are the only photosynthetic organisms that contain two photosystems (PSI and PSII), which they use to split

water (PSII). It is also known that chloroplasts contain their own DNA and RNA that is distinct from the nucleus, providing evidence for an early "independent" existence.

1.3 Photosynthesis – an overview

1.3.1 Photosynthesis in higher plants

In eukaryotes, such as plants and algae, the chloroplast is the site of photosynthesis. This is a member of a family of membraneous organelles exclusive to plants known as plastids. The basic structure of a chloroplast is similar to that of mitochondria, consisting of a highly permeable outer membrane and a nearly impermeable inner membrane separated by an intermembrane space (see Fig. 1.2). The stroma contains the DNA/RNA and ribosomes involved in the synthesis of many chloroplast proteins and enzymes and this is enclosed by the innermembrane. The thylakoid is the structural unit of photosynthesis in both prokaryotes and eukaryotes and this is surrounded by the stroma. It is a flattened vesicle consisting of stacks called grana and it contains the chemicals involved in photosynthesis. Invaginations in the innermembrane lead to the formation of the thylakoid membrane, the photosynthetic membrane of cyanobacteria and higher plants.

Photosynthesis is a two-stage process. The first stage requires direct energy from light to make NADPH and ATP. These energy carrier molecules are then used in the second process. The first stage reactions are therefore known as the light reactions. The second stage is light independent. It occurs in the dark if the energy carrier molecules from the first stage are present and uses NADPH and ATP to drive the synthesis of carbohydrate from CO_2 and H_2O. These are known as the dark reactions. The light reactions occur in the grana, in the thylakoid membrane while the dark reactions occur in the stroma. In the first stage (light reactions) light is absorbed by chlorophyll *a*. Light that is absorbed by antenna chlorophylls and accessory pigments is transferred to photosynthetic reaction centres, where the primary reaction of photosynthesis takes place. In this process electrons from excited chlorophyll molecules are passed through a series of acceptors, which convert electronic energy to chemical energy (see Fig 1.3). The photosynthetic reaction centre is a transmembrane protein containing a variety of chromophores. It was the first transmembrane protein to be described in atomic detail and consists of eleven α-helices (Deisenhofer *et al.*, 1984).

Photosystems are arrangements of chlorophyll molecules and other accessory pigments packed into thylakoids. Plants and cyanobacteria contain two photosystems, PSI and PSII. Electrons are transferred from PSII to PSI (see Fig. 1.3). $NADP^+$ is reduced by a strong reductant produced by PSI while PSII produces a strong oxidant which is capable of oxidising H_2O. During photosynthesis in plants and cyanobacteria, both photosystems function to transfer electrons from

H_2O to $NADP^+$ to form O_2 and NADPH. PSI uses a chlorophyll *a* known as p700 while PSII uses a chlorophyll *a* known as p680. This photosynthetic electron transport drives the formation of a proton gradient, similar to that found in mitochondria. ATP is synthesised by the process of photophosphorylation, driven by the dissipation of the pH gradient, which closely resembles that of oxidative phosphorylation in mitochondria. In the light reactions light energy is harnessed to generate ATP and NADPH but it is in the dark reactions that these products are used to synthesise carbohydrates from carbon dioxide. The series of biochemical, enzyme-mediated reactions by which plants take atmospheric CO_2 and reduce and incorporate it into carbohydrates is known as the Calvin cycle, and was elucidated by (Bassham *et al.*, 1950) using radioactive CO_2 to trace its metabolic fate

1.3.2 Photosynthesis in cyanobacteria

The process of photosynthesis and photosynthetic electron transport in cyanobacteria is essentially the same as that described above for eukaryotes. However, there are a number of subtle differences. The most notable difference is that cyanobacteria do not possess chloroplasts and can actually be seen as self-contained free-living chloroplasts. They do however possess the photosynthetic thylakoid membrane. Cyanobacteria also possess phycobilisomes, attached to PSII in their thylakoid membranes. These are multiprotein complexes consisting of phycobiliproteins, proteins with covalently attached linear tetrapyrroles which are unique to cyanobacteria and red algae. These tetrapyrroles are used together with chlorophyll as light harvesting antennae in cyanobacteria. The main function of these complexes is to harvest light that is outside the wavelengths 450-550nm because this is almost completely absorbed by passage through metres of water. Phycobilisomes and phycobiliproteins are discussed in more detail below.

Some species of cyanobacteria also have the ability to fix nitrogen and are the only nitrogen-fixing organisms (diaxotroph) that also produce oxygen. The enzyme found in those cyanobacteria which fix nitrogen into a form that can be incorporated into biological molecules is known as nitrogenase (Zehr *et al.*, 1998) but it is not encoded in any eukaryotic genome. However, this enzyme is inhibited by molecular oxygen which is produced during photosynthesis so these cyanobacteria must overcome its presence through oxygen protection mechanisms including anti-oxidative molecules such as carotenoids and anti-oxidative enzymes such as catalase.

1.4 The phycobilisome

The phycobilisome is the photosynthetic apparatus which cyanobacteria and red algae use to harvest light energy from the sun and pass on their excitations to PSI and PSII in the thylakoid membrane. The phycobilins are linear tetrapyrroles covalently attached to the phycobiliproteins of

the phycobilisome through thioether linkages. These tetrapyrroles are highly coloured, highly fluorescent compounds that function as the light absorbing molecules of cyanobacteria and red algae. Phycobiliproteins are classified on the basis of their colour into two large groups, the phycoerythrins (red) and the phycocyanins (blue). Absorption maxima for phycoerythrins lie between 490 and 570 nm while absorption maxima for phycocyanins are found between 610 and 665 nm. As a group, the phycobiliproteins absorb visible light in the range 450-660nm. The typical phycobilisome consists of a core of allophycocyanin attached to the terminal pigment. Phycocyanin and phycoerythrin extend out from the core of the phycobilisome to form rod like structures (see Fig. 1.4). This structure is then stabilised by linker peptides. All of the phycobiliproteins absorb incident light directly, but in addition they participate in the following energy transfer chain within the phycobilisome:

phycoerythrin ⟶ phycocyanin ⟶ allophycocyanin ⟶ chlorophyll a

1.5 The biological importance of tetrapyrroles

Life as we know it would not exist without tetrapyrroles such as heme, chlorophyll, cytochromes and phycobilins, which function in a broad range of important biological processes ranging from heme mediated oxygen transport, light harvesting by chlorophyll and the phycobilins, electron transport by the cytochromes and decomposition of hydrogen peroxide by catalase. In these processes heme functions as a covalently bound protein prosthetic group. Tetrapyrroles of biological importance can be cyclic, such as heme and chlorophyll (see Fig 1.5 and 1.6) or linear such as the plant signalling chromophore, phytochrome and the light harvesting phycobilins of cyanobacteria and red algae. In mammals, heme derived linear tetrapyrroles such as biliverdin and bilirubin have also been shown to have numerous other important biological functions including antioxidative effects (Baranano *et al.*, 2002, Sedlak & Snyder, 2004), immunosuppressive effects after organ transplantation (Yamashita *et al.*, 2004) and a role in embryogenesis in frogs (Montorzi *et al.*, 2002).

1.6 Heme and chlorophyll

One of the most important ways in which metal ions are involved in biochemistry is in complex with a macrocyclic ligand known as a porphyrin and the two most important metal complexes of porphyrins are heme in mammals and chlorophyll in plants. Heme consists of an iron ion chelated to the porphyrin ring to form a structure known as protoporphyrin IX. Iron is the most widespread of the transition metals found in living systems, where its compounds participate in a variety of biological activities, most importantly, transport of oxygen as oxy-hemoglobin and mediation in electron transfer chains as cytochromes. In all cases, the heme group functions in association with

a protein molecule, through which it is tightly bound through extensive hydrophobic and hydrogen bonding interactions. The most important of these heme proteins in mammals are hemoglobin, myoglobin, cytochromes (including P_{450}) and enzymes such as catalase and peroxidase. In these proteins the porphyrin derived heterocyclic ring system of heme consists of four pyrrole rings, linked by methene bridges, with a particular arrangement of two vinyl sidechains, two propionate sidechains and four methyl sidechains with a centrally bound iron atom (see Fig 1.5).

Plants synthesise four major tetrapyrrole molecules: heme, chlorophyll, phytochromobilin and sirohaem, while cyanobacteria also make phyocyanobilin and phycoerythrobilin. Although plants and cyanobacteria have an essential requirement for heme for respiratory cytochromes and hemoproteins such as peroxidase, chlorophyll is needed in far greater amounts for photosynthesis. Like heme, chlorophyll is biosynthetically derived from protoporphyrin IX and serves as the major light harvesting pigment for photosynthesis. Chlorophyll differs from heme by having a centrally bound magnesium ion instead of iron, the propionyl side chain of ring IV is esterified to a tetraisoprenoid alcohol, ring V is fused to pyrrole ring III to form a cyclopentanone ring and in chlorophyll *a* and *b* pyrrole ring IV is partially reduced (see Fig. 1.6).

1.7 Heme and chlorophyll biosynthesis

The pathways of heme biosynthesis in mammals, plants and cyanobacteria and of chlorophyll biosynthesis in plants and cyanobacteria are similar. 5-aminolaevulinic (ALA) is the starting point for both heme and chlorophyll synthesis. Plants and cyanobacteria use the carbon skeleton of glutamate to form ALA through a series of enzyme reactions. This is then further converted into uroporphyrinogen III, the precursor of all tetrapyrroles and in the case of heme an iron atom is inserted into the porphyrin structure to form protoporphyrin IX, catalysed by ferrochelatase. In the case of chlorophyll, a magnesium ion is inserted instead of iron, catalysed this time by magnesium chelatase. This is then converted into chlorophyll *a* and chlorophyll *b* (see Fig. 1.7). In mammals ALA is formed from the condensation of glycine and succinyl-CoA. This is also converted to uroporphyrinogen III through a series of enzyme reactions and eventually into protoporphyrin IX, followed by insertion of an iron atom, similar to the reaction seen in plants and cyanobacteria.

1.8 Heme metabolism and phycobilin biosynthesis

1.8.1 Heme metabolism in mammals-an overview

Heme metabolism in mammals occurs mostly in the spleen from the breakdown of hemoglobin in red blood cells. The ability to degrade heme however is not restricted to the spleen and can occur in the resident macrophages of the liver (Kupffer cells) which are responsible for the degradation

of erythroid and non-erythroid heme, particularly hepatic hemoproteins such as cythochrome P450 and catalase (Granick & Beale, 1978). The first step of heme degradation involves the oxidative cleavage of the porphyrin ring to form biliverdin, catalysed by the enzyme heme oxygenase (Tenhunen *et al.,* 1968). This enzyme was shown to be NADPH and cytochrome P450 reductase dependent. The next step of heme metabolism in mammals involves the enzyme biliverdin IXα reductase (BVR-A). This enzyme uses electrons from NADPH/NADH to reduce the C10 methene bridge of biliverdin IXα to form the lipophilic tetrapyrrole bilirubin IXα. The insoluble bilirubin is released into the bloodstream where it is complexed to serum albumin and transported to the liver. In the hepatic sinusoids of the liver, the albumin-bound bilirubin dissociates and migrates across the sinusoidal endothelium into the "space of Disse" and the free bilirubin is taken up by the hepatocytes via active transporters on the basolateral membrane of the hepatocyte. Once in the hepatocyte it is bound by the Alpha class of glutathione S-transferases (Hayes *et al.,* 2005) and Z-protein. This complex then migrates to the endoplasmic reticulum where the bilirubin is conjugated with glucuronic acid by the enzyme bilirubin UDP-glucuronosyl transferase (UGT1A1) (Jansen *et al.,* 1977). Bilirubin diglucuronide is more water soluble than bilirubin and is transported out of the cytosol and into the bile ducts by the ATP-dependent anion transporter, Mrp2 (Gerk & Vore, 2002). Bilirubin diglucuronide then passes through the bile ducts and into the gall bladder before being emptied into the duodenum. Here it is modified to form water-soluble colourless metabolites such as mesobilinogen, urobilinogen and stercobilinogen by the actions of the enzyme β-glucuronidase and anaerobic intestinal bacteria. On exposure to air these colourless compounds are oxidised to the corresponding bile pigments, urobilin, stercobilin and mesobilin and these water-soluble metabolites are then excreted from the body (see Fig. 1.8 for the pathway of heme metabolism in mammals).

1.8.2 Heme metabolism and phycobilin biosynthesis in cyanobacteria

Cyanobacteria, red algae and plants "open" the macrocyclic ring system of heme to form biliverdin IXα and in a series of ferredoxin dependent reactions produce the phycobilins for use in light harvesting. Surprisingly they also express biliverdin IXα reductase (Schluchter & Glazer, 1997), the function of which is unclear although Schluchter & Glazer, (1997) suggest that the product bilirubin IXα may be involved in regulating phycobiliprotein biosynthesis. In cyanobacteria, red algae and plants biliverdin IXα is derived from heme by the action of ferredoxin dependent heme oxygenase (Cornejo *et al.,* 1998). Following heme oxygenase catalysed conversion of heme to biliverdin IXα the biliverdin IXα procedes down one of two metabolic pathways (see Fig 1.9). The first is similar to mammals and is NAD(P)H dependent, where biliverdin IXα is converted to bilirubin IXα through the action of a cyanobacterial

NAD(P)H dependent biliverdin IXα reductase (Schluchter & Glazer, 1997). The other branch of the pathway is ferredoxin dependent and leads to the formation of the phycobilins, phycocyanobilin and phycoerythrobilin through the action of ferredoxin dependent bilin reductases (Beale & Cornejo, 1991). These ferredoxin dependent bilin reductases, named phycocyanobilin ferredoxin oxidoreductase (PcyA) and phycoerythrobilin ferredoxin oxidoreductase (pebB) catalyse two and four electron reductions of biliverdin IXα and 15,16 dihydrobiliverdin respectively (Frankenberg *et al.,* 2001). However, not all cyanobacteria make both phycobilins. *Synechocystis* sp. PCC6803 for example only makes phycocyanobilin (see Fig. 1.10). The Arabidopsis HY2 gene encodes a related ferredoxin dependent biliverdin reductase in plants, phytochromobilin synthase, which converts biliverdin into the plant chromophore phytochromobilin (Kohchi *et al.,* 2001).

1.9 Heme metabolites: biliverdin, bilirubin, phycocyanobilin and phycoerythrobilin

Biliverdin and bilirubin are the bile pigments found in mammals, plants and cyanobacteria, which result from the breakdown of heme. Depending on which of the meso bridges of heme are cleaved four different isomers of biliverdin IX can be produced (α, β, γ or δ), see Fig. 1.11. If this reaction is carried out *in vitro*, using ascorbate as reductant, all four isomers are formed in approximately equal amounts (McDonagh, 1979). *In vivo* heme oxygenase is specific in generating biliverdin IXα. The term bile pigment was once reserved for the pyrrolic pigments found in bile but now it is used to describe all linear tetrapyrroles with the skeletal structure shown in Fig. 1.12A and with oxygen at the terminal positions (Mcdonagh, 1979). Biliverdin is a green biliatriene (three unsaturated bridges) resulting from heme oxygenase catalysed cleavage of the porphyrin ring of heme. It consists of four linearly attached pyrrole rings linked by single bridging carbon atoms, with differing sidechains in the substituent positions. Biliverdin IXα is the predominant form found in adult mammals, plants and cyanobacteria and consists of four methyl sidechains in the 2, 7, 13 and 17 positions, 2 vinyl sidechains in the 3 and 18 positions and 2 propionate sidechains in the 8 and 12 positions (see Fig. 1.12B)

Bilirubin, yellow bilidiene (two unsaturated bridges) is formed from the enzymatic reduction of biliverdin by the enzyme biliverdin reductase. The IXα isomer of bilirubin is the most abundant form found in mammals. It is highly lipophilic and like other lipophilic metabolites, such as free fatty acids is transported in the blood in complex with serum albumin. Reduction of the C10 position of biliverdin by BVR-A allows rotation which facilitates the formation of the so-called "ridge-tile" structure where the propionate sidechains hydrogen bond to the terminal lactams (Lightner & McDonagh, 2001). This "ties up" the functional groups that can interact with water internally so that bilirubin IXα is highly insoluble in aqueous solvents. It is similar to biliverdin

IXα with regard to the arrangement of side-chains (see Fig. 1.12C) and can also exist as four different isomers. The approximate ratio of bilirubin isomers in adult mammals is 95-97% IXα and 3-5% IXβ. However, this ratio is different in the neonate, which has only 6% IXα and 87% IXβ. The origins of the IXβ isomer are currently unclear. When the blood contains excessive amounts of bilirubin it is deposited, causing yellowing of the skin and eyes. This so-called physiological jaundice of the newborn occurs because the livers of new born babies do not yet make sufficient amounts of the enzyme bilirubin glucuronyl transferase (UGT1A1) to deal with the high levels of bilirubin (Berk *et al.,* 1969). Conjugated bilirubin is more soluble than unconjugated bilirubin and is more easily excreted. Unconjugated bilirubin leads to elevated serum bilirubin levels resulting in so-called neonatal jaundice. Although excess bilirubin is toxic it is easily treated, usually through photo-therapy (Maisels & McDonagh, 2008).

Phycocyanobilin is the linear tetrapyrrole chromophore of cyanobacteria and red algae that is responsible for the absorption of light in the red and far-red region of the electromagnetic spectrum. It is therefore intensely blue in colour. Phycocyanobilin is a bilatriene similar to biliverdin IXα, with the same arrangement of substituent sidechains, except that the vinyl side chain in the C18 position of the D ring has been oxidised to an ethyl group and the C2 carbon on the A ring has been reduced (see Fig. 1.12D).

Phycoerythrobilin is also a linear tetrapyrrole used to harvest light energy in cyanobacteria and red algae but in this case it absorbs light in the blue region of the spectrum. This accounts for the red colour of this chromophore. Together with phycocyanobilin and chlorophyll, these photosynthetic pigments absorb most of the visible light in the solar spectrum. Phycoerythrobilin is also a bilatriene, like phycocyanobilin but in this case the carbon in the 15 position is reduced (see Fig. 1.12E).

1.10 The enzymes of heme metabolism and phycobilin biosynthesis

1.10.1 Heme oxygenase (HO)

Heme oxygenase activity was first described by Tenhunen *et al.,* (1968) who reported that rat liver microsomal fractions exhibited heme oxygenase activity, catalysing the formation of equimolar amounts of biliverdin IXα, Fe^{2+} and carbon monoxide from heme. This activity was later shown to be dependent on NADPH, NADPH-cytochrome P450 reductase and molecular oxygen (Tenhunen *et al.,* 1968). Heme oxygenase catalyses the oxidative cleavage of the porphyrin ring of heme to yield one of four biliverdin isomers (α, β, γ or δ). However, all of the mammalian heme oxygenases reported to date cleave the α-methene bridge of heme to form biliverdin IXα. As a result biliverdin IXα is the predominant form found in adult mammals. A heme oxygenase that

produces 70% biliverdin IXα and 30% biliverdin IXβ has been described in *Pseudomonas aeruginosa* (Caignan *et al.,* 2002), biliverdin IXγ has been reported in the insect *Pieris brassica* (Rudiger *et al.,* 1969) and biliverdin IXδ has been reported in the marine snail *Turbo cornutu* (Benedikt *et al.,* 1988). These findings suggest the existence of non α-methene bridge specific heme oxygenases. It is now known that there are two forms of heme oxygenase in mammals. HO1 is highly inducible by a wide variety of agents including heavy metals, phenylhydrazine and bromobenzene and is the form mainly found in the spleen (Braggins *et al.,* 1986). HO2, the constitutive form is found in immune privileged sites such as the brain and testis. A third form, HO3 from rat brain was described by McCoubrey *et al.,* (1997). However, recent work suggests that this may be a pseudogene, derived from the HO2 gene (Hayashi *et al.,* 2004).

Cyanobacteria are now known to encode two heme oxygenases which are highly similar to the mammalian enzymes. Cornejo *et al.,* (1998) first described the cloning and overexpression of a soluble ferredoxin dependent heme oxygenase (HO1) from the cyanobacterium *Synechocystis sp.* PCC6803. The enzyme was reported to catalyse the formation of biliverdin from heme but in contrast to the mammalian enzyme, it was shown to obtain its reducing equivalents from ferredoxin. The same group cloned the gene for HO2 but reported that the enzyme was inactive and that they could not detect any mRNA for the protein (Cornejo *et al.,* 1998). However, using a synthetic HO2 gene Zhang *et al.,* (2005) described the overexpression of a soluble and active HO2 protein, which bound hemin stoichiometrically to form an enzyme-heme complex which degraded to form biliverdin IXα, CO and iron. The HO2 protein was again shown to use the ferredoxin/ferredoxin reductase/NADPH reducing system.

The crystal structure for HO1 from the cyanobacterium *Synechocystis sp.* PCC6803 was determined by Sugishima *et al.*, (2004) and was shown to be composed of 8 α-helices with an overall fold similar to other heme oxygenases (see Fig. 1.13A). Ferredoxin provides the reducing equivalents to the heme oxygenase reaction and is a small acidic iron-sulphur protein which docks to the HO1 protein through electrostatic interactions involving basic residues on the surface of HO1 (see Fig. 1.13B). The heme binding site is positively charged and is composed of highly conserved amino acids, including His17 which is co-ordinated to the heme iron, Gly130 which hydrogen bonds to the distal ligand and basic amino acid residues, Arg10, Lys168 and Arg172 which stabilise the orientation of the heme molecule through electrostatic interactions. Tyr125 also hydrogen bonds to the propionate groups of the heme molecule which further stabilises the complex (Sugishima *et al.,* 2004).

1.10.2 Biliverdin reductase

In mammals, biliverdin IXα is produced from heme by the microsomal enzyme heme oxygenase. Biliverdin is further metabolised by biliverdin IXα reductase (BVR-A) to form bilirubin IXα. This is a highly specific reaction but was for a long time believed to be non-specific. The first report of an enzyme that could specifically reduce biliverdin to form bilirubin came when Singleton *et al.,* (1965) partially purified an enzyme which displayed this activity from the liver of guinea pigs. However it was not until Noguchi *et al.,* (1979) that the first biliverdin reductase enzyme was successfully purified from pig spleen. The enzyme has been reported in a variety of tissues and species since, including human liver (Yamaguchi *et al.,* 1994), ox kidney (Rigney *et al.,* 1988), rat liver (Kutty & Maines, 1981), mouse (Franklin *et al.,* 2007), salmon (Elliot, 1996), cyanobacteria (Schluchter & Glazer, 1997) and *Xenopus tropicalis* (Franklin *et al.,* 2007). Biliverdin IXα reductase has been described as a monomer of molecular weight 34kDa in most mammalian species including pig spleen and rat liver (Noguchi *et al.,* 1979), rat liver (Kutty & Maines, 1981), human liver (Maines & Trakshel, 1993) and ox kidney (Rigney & Mantle, 1988). However, human biliverdin IXα reductase migrates with an apparent molecular weight of 42 kDa on SDS-Page (Maines & Trakshel, 1993). A molecular weight of 34 kDa is determined from the amino acid composition suggesting the anomalous migration on SDS-PAGE of human BVR-A, possibly due to modification of the enzyme. The mammalian enzyme is cytoplasmic and its activity has been shown to be pyridine nucleotide dependent. BVR-A is able to use either NADPH or NADH to reduce biliverdin however the low Km for NADPH suggests that this is the physiological substrate (Colleran & O'Carra, 1970). It is an oxidoreductase, displaying a high degree of specificity for the meso C10 bridge of biliverdin IXα. The reaction mechanism for the ox kidney enzyme at pH 9 is ordered sequential (Rigney *et al.,* 1988) and the transfer of hydride is stereospecific from the B-face of the pyridine nucleotide (Ennis *et al.,* 1997).

The crystal structure of the rat BVR-A enzyme was elucidated using X-ray crystallography by Kikuchi *et al.,* (2001) and shows that the enzyme consists of two well defined domains that are tightly packed together (see Fig 1.14A). The N-terminal domain consists of a core of one anti-parallel and six parallel β-strands, flanked on both sides by five α-helices (Kikuchi *et al.,* 2001). This αβ structure is nearly symmetrical and resembles the classic lactate dehydrogenase fold (Abad-Zapatero *et al.,* 1987). The N-terminal domain of BVR-A is therefore characteristic of a Rossman dinucleotide binding fold and is the likely binding site for NAD(P)H, where enzyme–NADPH interactions would be mediated through the hydrogen bonds of phosphate moieties and sugar hydroxyl groups of the co-factor with the amide groups of the enzyme (Bellamacina, 1996). Although no tertiary structure with $NAD(P)^+$ and biliverdin is currently available for any BVR-A

the crystal structure of the rat enzyme shows NAD^+ in the co-factor binding site (Whitby *et al.*, 2002). However, the position of the nucleotide, shape of the binding pocket and residues involved would suggest that this is not the correct orientation for nucleotide binding. The adenine ring is stacked over the nicotinamide in this structure, which would prevent productive binding of biliverdin. Whitby *et al.*, (2002) have suggested that in the crystal Lys72, from a neighbouring monomer packs into the space that in solution would be occupied by the adenine moiety. Recently a crystal structure has been solved for human BVR-A enzyme and shows that the overall structure is highly similar to the rat enzyme with two well defined domains and the $NADP^+$ in this structure is in the predicted open conformation (Fig. 1.14B) to allow biliverdin to enter the active site and catalysis to occur with the adenine ring in this case folding back out of the active site and allowing entry of the second substrate biliverdin (Kavanagh *et al.*, unpublished).

Biliverdin IXα reductase was for a long time believed to be an essentially mammalian enzyme, although reports of activity in fish and some birds suggests a broader phylogenetic distribution. Schluchter & Glazer, (1997) first reported the existence of a biliverdin IXα reductase in an ancient cyanobacterium, *Synechocystis sp.* PCC 6803. The enzyme was cloned and overexpressed and was found to convert biliverdin IXα to bilirubin IXα in the presence of NADPH. Although this activity could in theory divert the biosynthesis of phycobilin precursors to a metabolic "dead-end" to date there are no reports of bilirubin IXα in cyanobacteria. Bioinformatic analysis of further cyanobacterial genomes has revealed DNA sequences which are also likely to encode ancient biliverdin IXα reductases (see Section 5.5.1).

A second form of biliverdin reductase exists in mammals which is capable of using biliverdin IXβ as a substrate to make bilirubin IXβ but which cannot reduce biliverdin IXα. This enzyme, known as biliverdin IXβ reductase (BVR-B) was first described by Yamaguchi *et al.*, (1994) from human liver and was later shown by Shalloe *et al.*, (1996) to be capable of reducing riboflavin and to be identical to flavin reductase. In the human foetus biliverdin IXβ has been shown to be the major bile pigment up to 20 weeks (Yamaguchi & Nakajima, 1995). The switch in heme degradation from the IXβ pathway to the IXα pathway may be coupled to the switch from foetal to adult haemoglobin.

1.10.3 Phycocyanobilin ferredoxin oxidoreductase (PcyA) and phycoerythrobilin ferredoxin oxidoreductase (PebB)

Cyanobacteria and red algae possess ferredoxin-dependent bilin reductases which are unique to these organisms for the synthesis of the linear tetrapyrrole precursors of their phycobiliprotein light harvesting complexes. Beale & Cornejo, (1991) were the first to describe the existence of

these enzymes, which could synthesise the light harvesting tetrapyrroles phycocyanobilin and phycoerythrobilin from biliverdin IXα using electrons from reduced ferredoxin. Plants contain a ferredoxin-dependent homologue to these bilin reductases, which can reduce biliverdin to form phytochromobilin, the light sensing tetrapyrrole of plant phytochrome. Kohchi *et al.,* (2001) cloned the enzyme, phytochromobilin synthase (HY2), which is responsible for this ferredoxin-dependent reduction and showed that it reduced biliverdin to form the plant chromophore phytochromobilin.

Frankenberg *et al.,* (2001) identified and biochemically analysed the HY2 family of ferredoxin-dependent bilin reductases from three cyanobacteria, *Synechocystis sp.* PCC 6803, *Anabaena sp.* PCC7120 and *Nostoc punctiforme.* They showed that the enzyme PcyA catalyses the four electron reduction of biliverdin IXα to form phycocyanobilin. This phycocyanobilin is then incorporated and covalently attached to the protein phycocyanin for use in light harvesting. This direct conversion of biliverdin to phycocyanobilin in cyanobacteria is different from phycocyanobilin biosynthesis in the red algae *Cyanidium caldarium*, which synthesizes phycocyanobilin from the intermediate phycoerythrobilin (Beale, 1994).

It was later shown by Tu *et al.,* (2004) that biliverdin reduction by cyanobacterial PcyA proceeds via linear tetrapyrrole radical intermediates. Many other enzymes have been shown to produce organic radical intermediates during their reactions, including the photosynthetic oxygen evolving complex (Gilchrist *et al.,* 1995), cytochrome C peroxidase (Sivaraja *et al.,* 1989) and class I ribonucleotide reductases (Sjoberg & Gräslund, 1977). Using an anaerobic coupled electron transfer system it was shown that PcyA mediates reduction of biliverdin to phycocyanobilin via four one electron transfers from individual reduced ferredoxin molecules to tightly associated PcyA:bilin complexes and that the bilin radical intermediates are stable, with a half life of 10-20 minutes (Tu *et al.,* 2004).

Two phycoerythrobilin ferredoxin oxidoreductases (PebA and PebB) have also been identified by Frankenberg and colleagues from *Synechococcus sp.* WH8020 and *Nostoc punctiforme* but not *Synechocystis.* However, only one (PebA) is capable of reducing biliverdin IXα to a compound identified as 15,16-dihydrobiliverdin. This was then shown to be a substrate for PebB to form phycoerythrobilin (Frankenberg *et al.,* 2001). The same group hypothesize that the PebA and PebB enzymes function as a dual enzyme complex. As *Synechocystis* lacks both phycoerythrin apoprotein and the two ferredoxin dependent phycoerythrobilin synthesizing enzymes it suggests that phycocyanobilin is synthesised via an independent pathway

Recently, the crystal structure of the first ferredoxin-dependent bilin reductase (PcyA from *Synechocystis sp.* PCC6803) was determined and was shown to be folded in a three layer α/β/α sandwich structure consisting of four N-terminal α-helices, an anti-parellel β-sheet consisting of seven strands and five C-terminal α-helices in which biliverdin IXα is positioned between the β-sheet and C-terminal α-helices (see Fig. 1.15A) (Hagiwara *et al.* 2006). Ferredoxin is a small, 10kDa acidic protein and docks to a basic patch of amino acids on the PcyA surface allowing for direct transfer of electrons to biliverdin (see Fig. 1.15B). Hagiwara *et al.*, (2006) propose that the orientation of biliverdin is fixed in the PcyA structure by the shape of the biliverdin binding pocket and held in place by hydrogen bonds or salt bridges between the hydrophilic functional groups of biliverdin to PcyA. In particular, Lys221 of PcyA is salt bridged to the propionate group of the B ring of biliverdin and is hydrogen bonded to Arg149, Trp154 and Asn219 through water molecules. In addition, Arg149 is hydrogen bonded to Ser114 and salt bridged to the propionate group of the C ring of biliverdin, which together with the other residues mentioned fix the propionate groups of biliverdin and thereby fix biliverdin tightly in the substrate binding pocket of PcyA (Hagiwara *et al.*, 2006).

1.11 Carotenoids

Carotenoids are a large group of naturally occurring lipid soluble pigments found primarily in plants, algae and photosynthetic bacteria. They are also found in yeasts, moulds, some non-photosynthetic bacteria and animals. However, animals appear to be incapable of synthesizing carotenoid pigments and must obtain them from their diets. These pigments are responsible for the array of colours found in nature such as the reds, yellows and oranges found in leaves, fruit, flowers and much of the colour found in birds, insects and fish. More than 600 carotenoids are known to occur naturally which are characterized and defined by their chemical structure and it is this structure which determines the physiological function of a particular carotenoid. The majority are formed from a backbone consisting of a 40-carbon polyene chain which may or may not be terminated with cyclic end groups and oxygen containing functional groups (see Fig. 1.16).

When cyanobacteria first began to utilize photosynthesis they had to deal with the problem of photooxidation and photoinhibition of the photosynthetic reaction centres caused by the generation of reactive oxygen species and it was crucial to develop mechanisms to cope with this stress and protect the photosynthetic apparatus. Oxidative stress is generated by hydrogen peroxide, by singlet oxygen ($^1O_2$) directly, by energy transfer from triplet chlorophyll to oxygen or by electron transfer to oxygen yielding superoxide (O_2-).This leads to damage to the photosynthetic apparatus, cell membranes, DNA, proteins and other cell constituents. Cyanobacteria evolved mechanisms to prevent the formation and accumulation of these reactive oxygen species, mainly through the

enzymes catalase and peroxidase and anti-oxidant molecules such as carotenoids. In plants and cyanobacteria carotenoids can dissipate the energy from photosensitised molecules like chlorophyll and singlet oxygen and can also inactivate peroxy radicals, making these lipid soluble molecules essential for the survival of these organisms. The distinctive pattern of alternating single and double bonds in the polyene backbone of carotenoids is what allows them to absorb the excess energy from other molecules.

Carotenoids are synthesised from isoprenoid precursors, beginning with the conversion of acetyl-CoA to mevalonic acid and eventually leading to the synthesis of phytoene. Four desaturation reactions convert phytoene to lycopene. Each desaturation reaction increases the number of conjugated double bonds by two so that the number increases from three in phytoene to eleven in lycopene. Two cyclization reactions convert lycopene to β-carotene which is then converted to other carotenoids by the addition of various oxygen containing side groups (see Fig. 1.16 for carotenoid biosynthesis in *Synechocystis* sp. PCC6803).

1.12 Proposed study

At present there are two crystal structures available for biliverdin IXα reductase from different species and while this provides valuable information on the folding and overall structure of the enzyme the rat crystal structure of Kikuchi *et al.,* (2001) does not have any substrates present and therefore no information on the binding of NAD(P)H or biliverdin. Similarly, the rat crystal structure of Whitby *et al.,* (2002) has $NADP^+$ bound but not in a conformation which supports the binding of biliverdin. Recently the human BVR-A structure was solved by Kavanagh *et al.*, (unpublished) and while this does have $NADP^+$ bound in the predicted conformation to support biliverdin binding it also does not have biliverdin present. For these reasons there is no ternary structure available for any BVR-A and it is an aim of this project to crystallize the *Synechocystis* BVR-A with biliverdin and $NADP^+$ bound. This will prove extremely informative in the study of biliverdin binding to BVR-A and in the study of any potential inhibitors to the enzyme. Because the *Synechocystis* enzyme was the first biliverdin IXα reductase to appear in evolution, it's structure will provide valuable information on the evolution of this enzyme and any structural and functional changes which have taken place in its development from primitive cyanobacteria to mammals. Studies examining the secondary, tertiary and quaternary structure and binding of biliverdin will also be conducted on the *Synechocystis* BVR-A in the absence of a crystal structure.

Mammalian BVR-As have proved refractory to mechanistic analysis mainly due to the potent substrate inhibition by biliverdin. As a result the initial rate kinetics with biliverdin as the variable substrate cannot be performed satisfactorily. To date, only the mechanism of the ox kidney BVR-

A (Rigney & Mantle, 1988) has been determined but not under optimum conditions. It is an aim of this study to determine if the *Synechocystis* BVR-A is subject to the same potent substrate inhibition and if not to determine the kinetic mechanism of the enzyme under optimum conditions. By performing kinetic analysis on the purified *Synechocystis* enzyme and comparing its activity to that of mammals, such as the human enzyme any evolutionary changes in its activity, activation and use of substrates and co-factors can be studied.

Biliverdin IXα reductase is a two substrate enzyme with NAD(P)H and biliverdin IXα the substrates. The enzymatic mechanism of the enzyme has not been definitively determined for any BVR-A, although certain residues have been implicated. The chemical mechanism of the *Synechocystis* BVR-A will be examined under optimum conditions if the enzyme is not substrate inhibited by biliverdin. A complete pH study will be performed and the effect of pH on the kinetic parameters of the enzyme will be analysed. In addition to the pH studies, examination of the multiple sequence alignment of all known and putative BVR-As and the active sites of the rat and human crystal structures will allow the identification of putative catalytic residues. Following identification of possible residues involved in catalysis and substrate binding these residues will be mutated by site-directed mutagenesis. The effects of these mutations will be evaluated and the enzymatic mechanism of the *Synechocystis* BVR-A under optimum conditions will be determined in this way.

The function of biliverdin IXα reductase and its product bilirubin in cyanobacteria is unclear. Schluchter & Glazer (1997) have suggested that the enzyme may have a regulatory role and may be required for normal phycobilin biosynthesis. However, through personal communication it was revealed that the authors inadvertently inactivated a protein required for phycocyanobilin incorporation into the phycobiliprotein phycocyanin. There is also no evidence that cyanobacteria make bilirubin. For these reasons it is a major aim of this study to determine the function of BVR-A in *Synechocystis*. This will be done by inactivating the BVR-A gene through prokaryotic transgenic techniques. This will allow the role of BVR-A and its metabolite bilirubin to be investigated *in vivo*. It has been proposed in mammals that the BVR-A mediated redox cycling of biliverdin and bilirubin serves as a major anti-oxidant mechanism but this is still controversial. This BVR-A "knock-out" mutant will allow these primitive cyanobacteria to be used as a "model" organism and may provide evidence as to the role of bilirubin in higher organisms and whether it is indeed acting as an anti-oxidant. Antibodies will also be raised against the purified heme oxygenase, phycocyanocyanobilin ferredoxin oxidoreductase and biliverdin IXα reductase. These antibodies will be used to examine the expression levels of the enzymes under various conditions and together with the BVR-A mutant work will help to determine the function of sBVR-A.

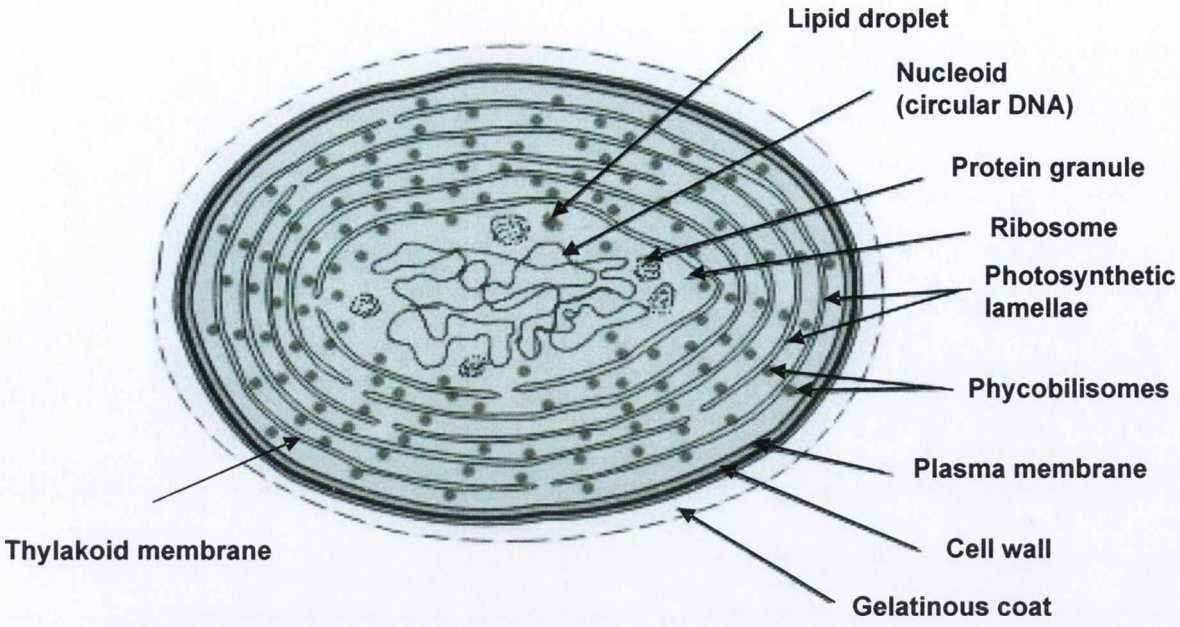

Figure 1.1 Structure of a typical cyanobacterium

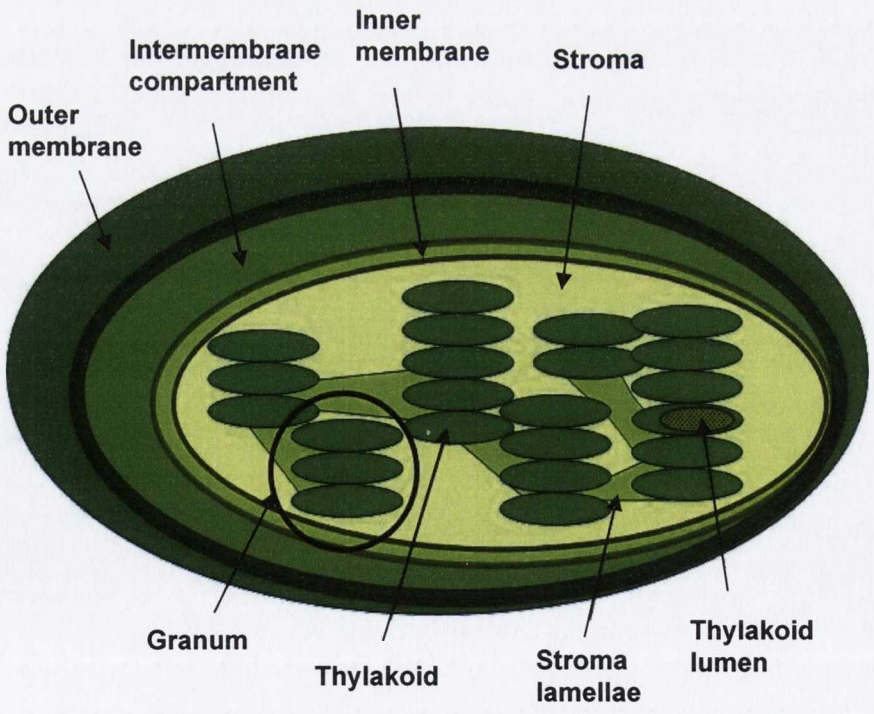

Figure 1.2 Structure of a chloroplast

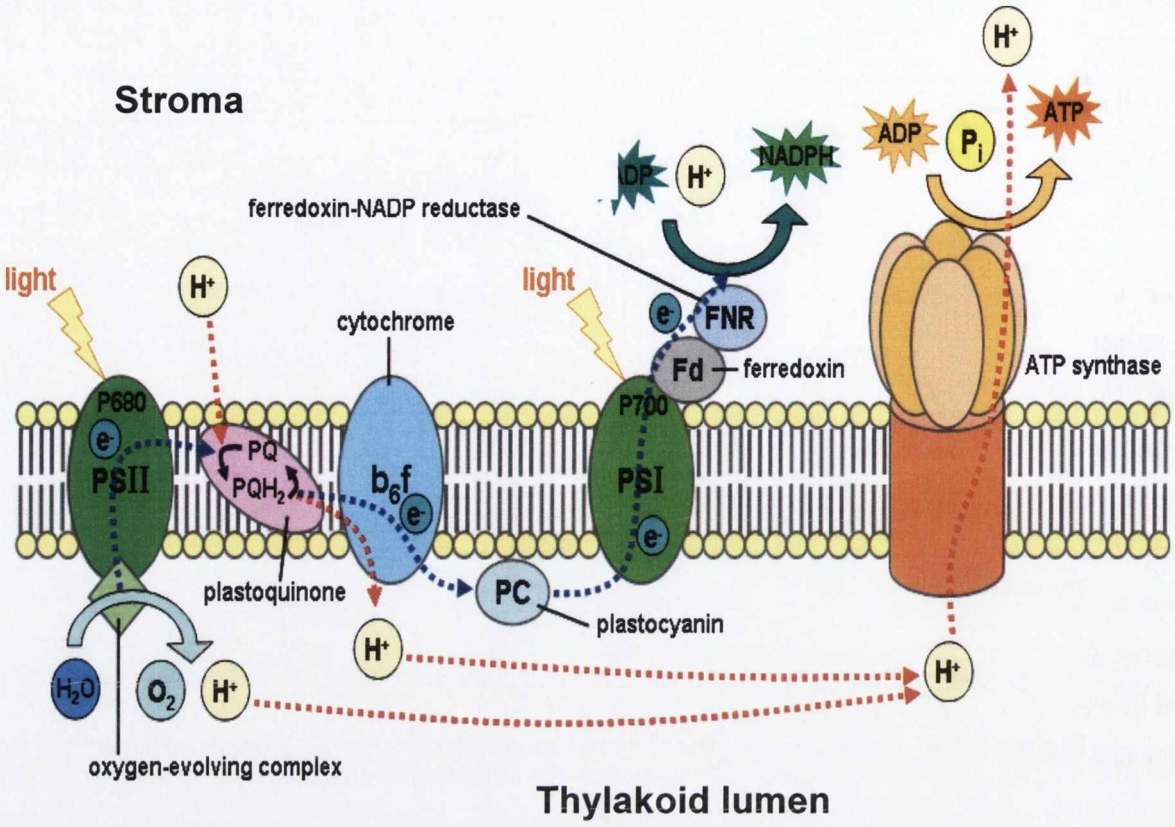

Figure 1.3 A diagramatic representation of the photosynthetic thylakoid membrane showing the components of the electron transport chain

The system consists of three protein complexes: PSI, PSII and the cytochrome b6f complex which are electrically connected by the diffusion of the electron carriers plastoquinol (PQ) and plastocyanin (PC). Light drives the transport of electrons from water to NADP+ to form NADPH (blue arrows). This drives the transport of protons into the thylakoid space (red arrows). The resulting proton gradient powers the synthesis of ATP by the CF1CF0 proton translocating ATP synthase. The thylakoid membrane also contains chlorophyll molecules and phycobilisomes (cyanobacteria) for light harvesting and electron transfer to PSI and PSII. The ATP and NADPH produced in the light reactions is then used to make carbohydrates from CO_2 and H_2O. This electron transport during photosynthesis is the same in both cyanobacteria and eukaryotes.

Adapted from Biochemistry (Voet & Voet) 1995. John Wiley & Sons Inc.

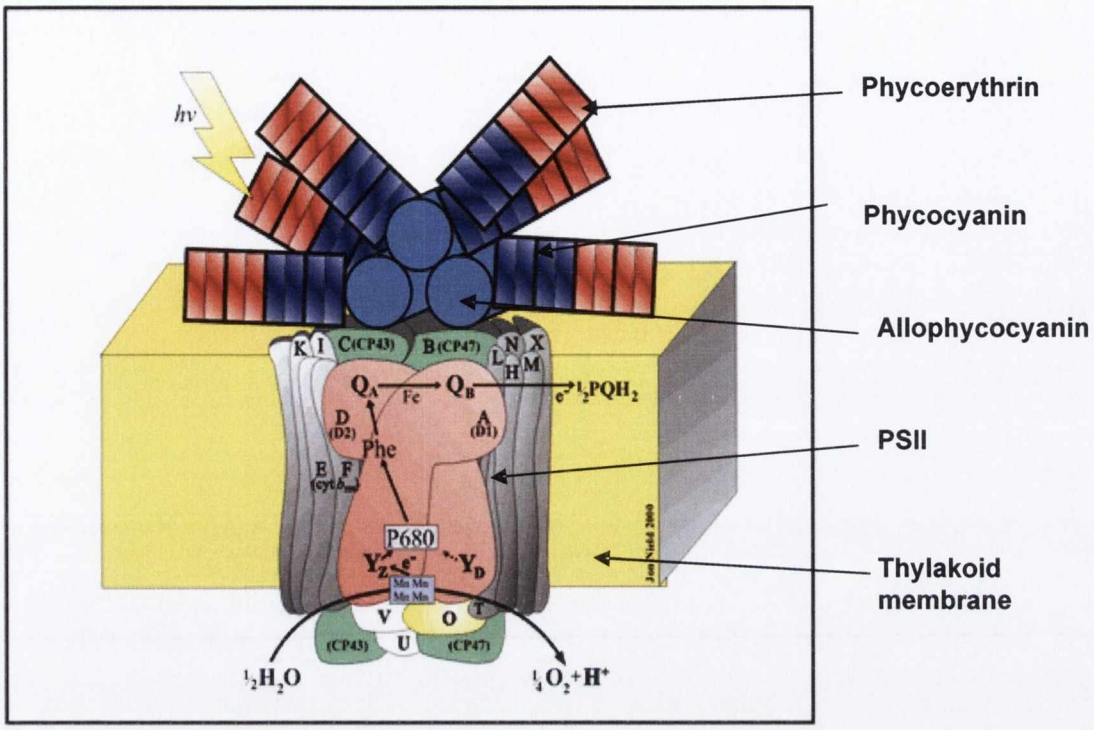

Figure 1.4. Structure of a typical multiprotein cyanobacterial phycobilisome complex.

The typical cyanobacterial phycobilisome consists of a core of allophycocyanin attached to photosystem II (PSII) in the thylakoid membrane. Phycocyanin and phycoerythrin extend out from the core of the phycobilisome to form rod like structures

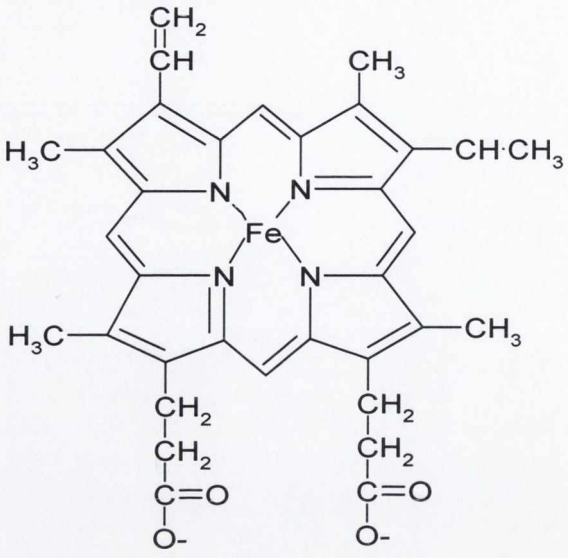

Figure 1.5. Molecular structure of ferrous protoporphyrin IX (Heme).

The heme molecule consists of 4 pyrrole rings, linked by methene bridges with a particular arrangement of 4 methyl, 2 vinyl and 2 propionate side chains.

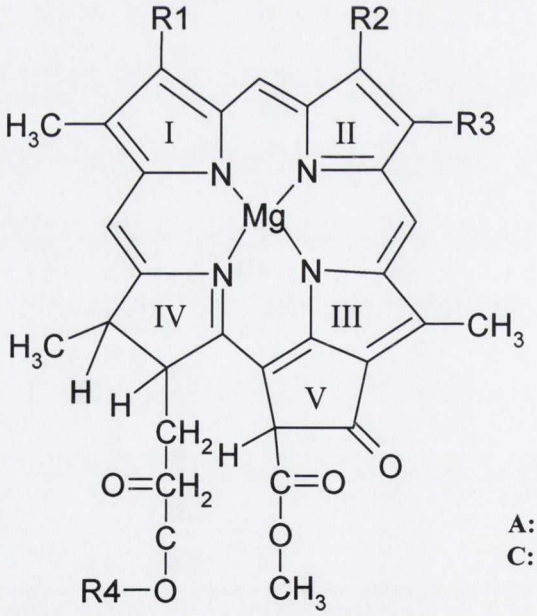

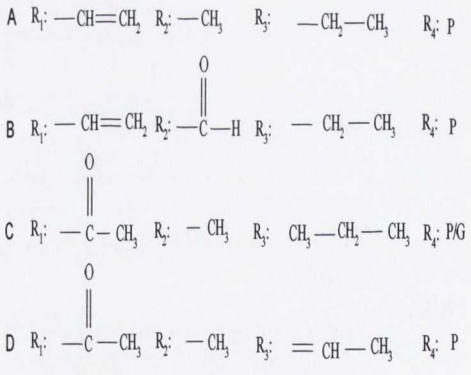

A: chlorophyll a **B: chlorophyll b**
C: bacteriochlorophyll a **D: bacteriochlorophyll b**

Figure 1.6. Molecular structure of chlorophyll

Chlorophyll has a centrally bound magnesium ion, the propionyl side chain of ring IV is esterified to a tetraisoprenoid alcohol (R_4), ring V is fused to pyrrole ring III to form a cyclopentanone ring and in chlorophyll a and b pyrrole ring IV is partially reduced. Side chains indicating the type of chlorophyll molecule are indicated

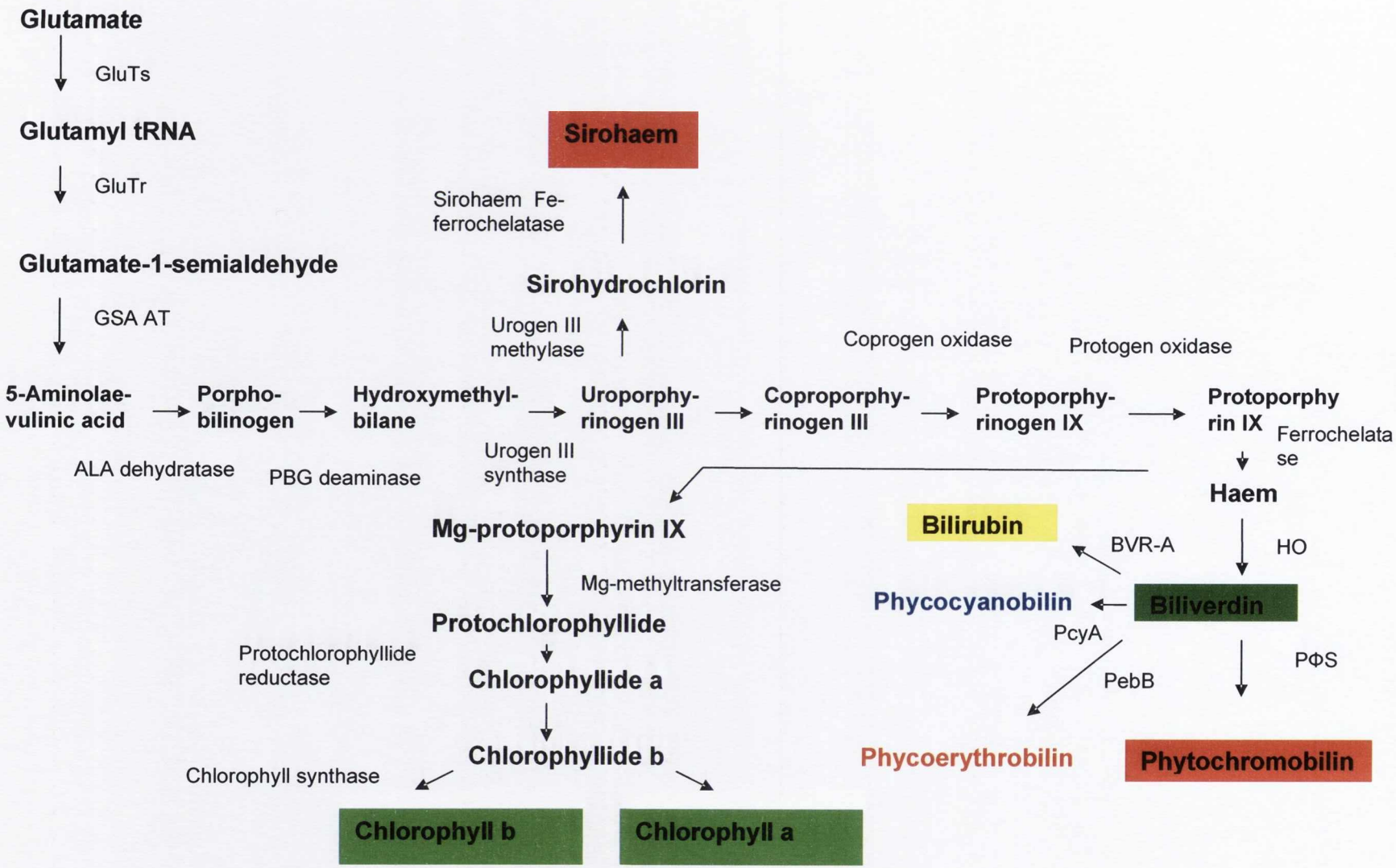

Figure 1.7 Pathways of heme and chlorophyll biosynthesis in plants and cyanobacteria and phycobilin biosynthesis in cyanobacteria

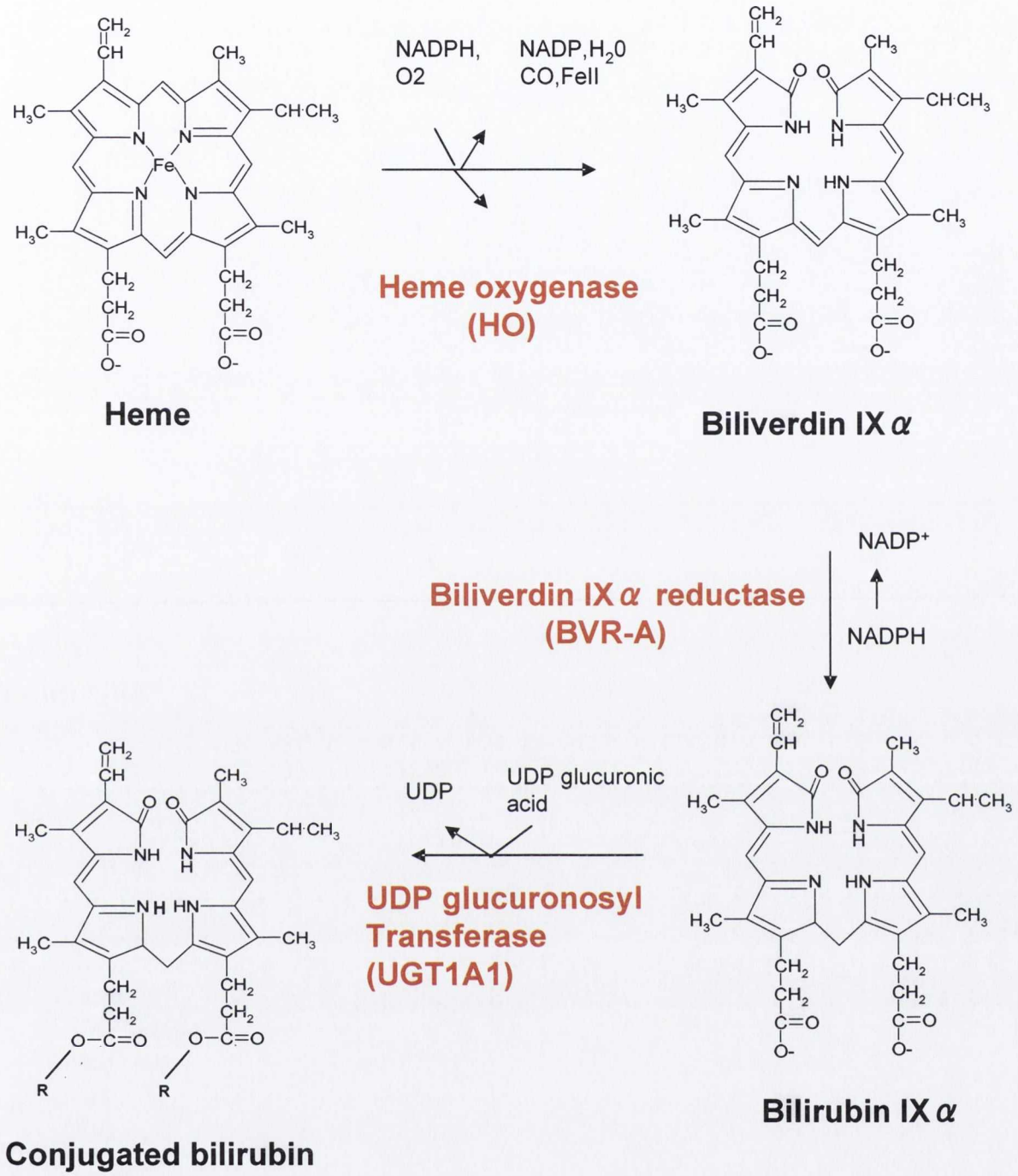

Figure 1.8 Pathway of heme metabolism in mammals and the enzymes involved

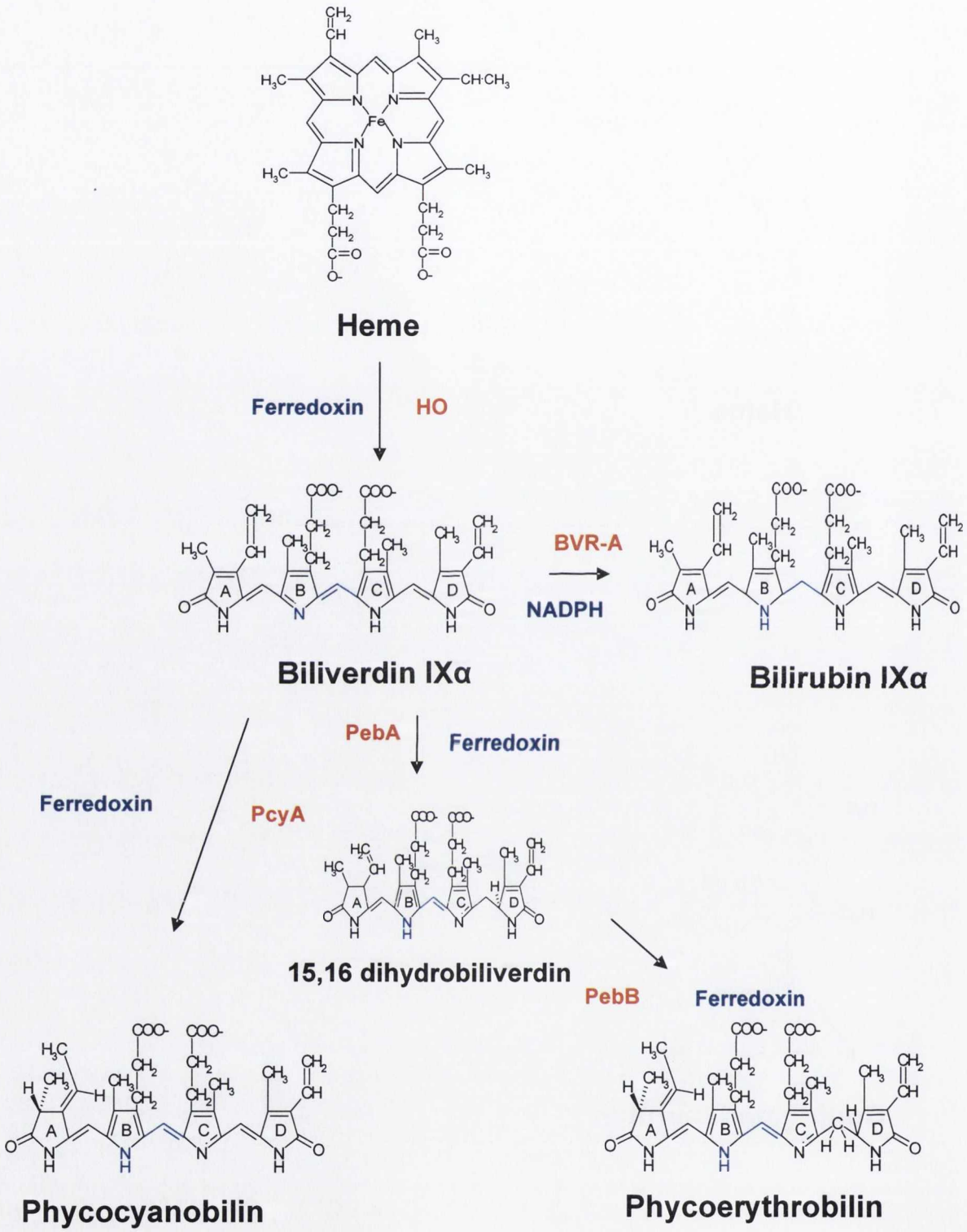

Figure 1.9 Pathway of heme metabolism and phycobilin biosynthesis in cyanobacteria

Shown in the red are the enzymes involved and in blue the source of reducing equivalents

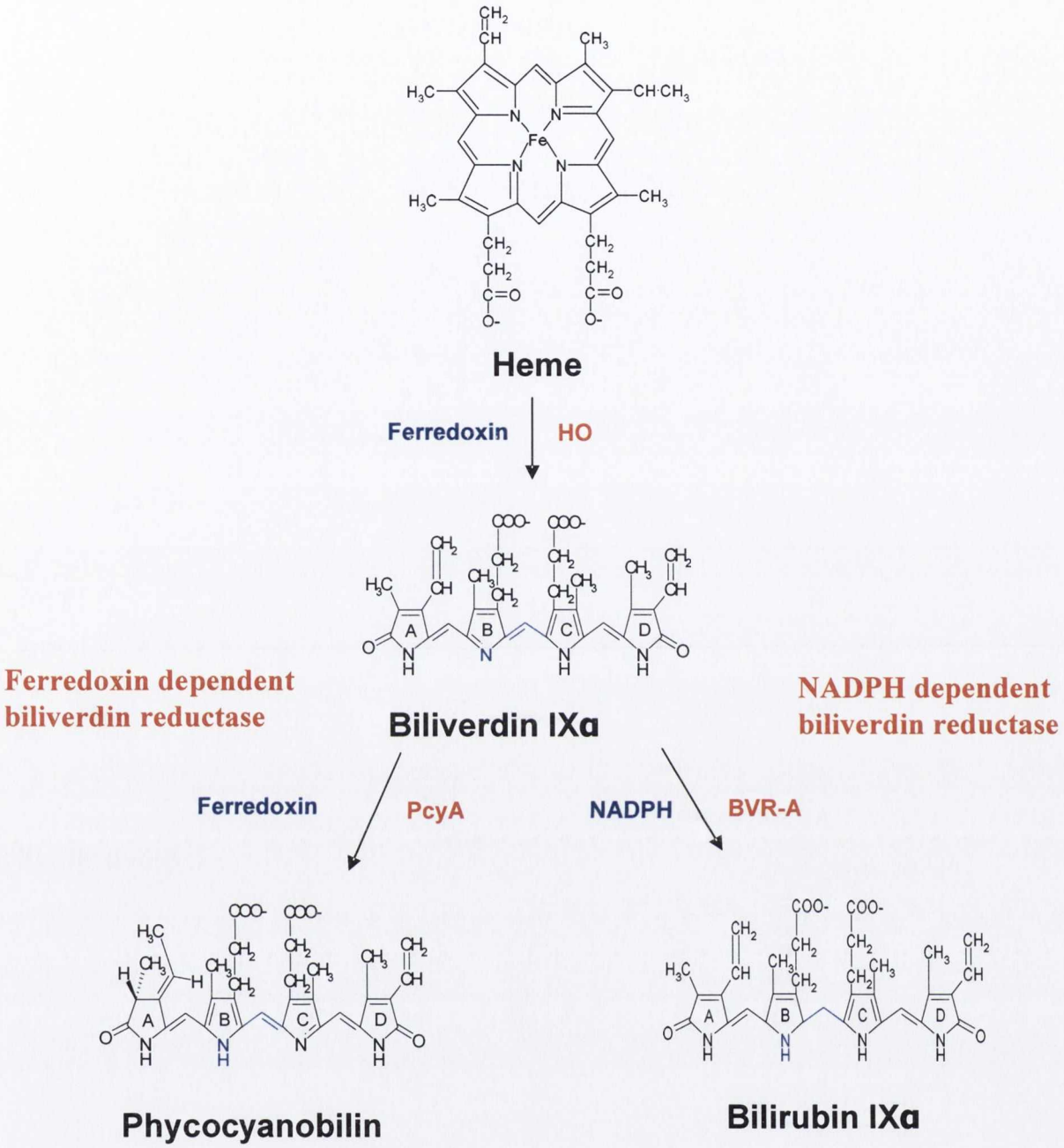

Figure 1.10 Pathway of heme metabolism and phycobilin biosynthesis in the cyanobacterium Synechocystis sp. PCC6803

Shown in the red are the enzymes involved and in blue the source of reducing equivalents

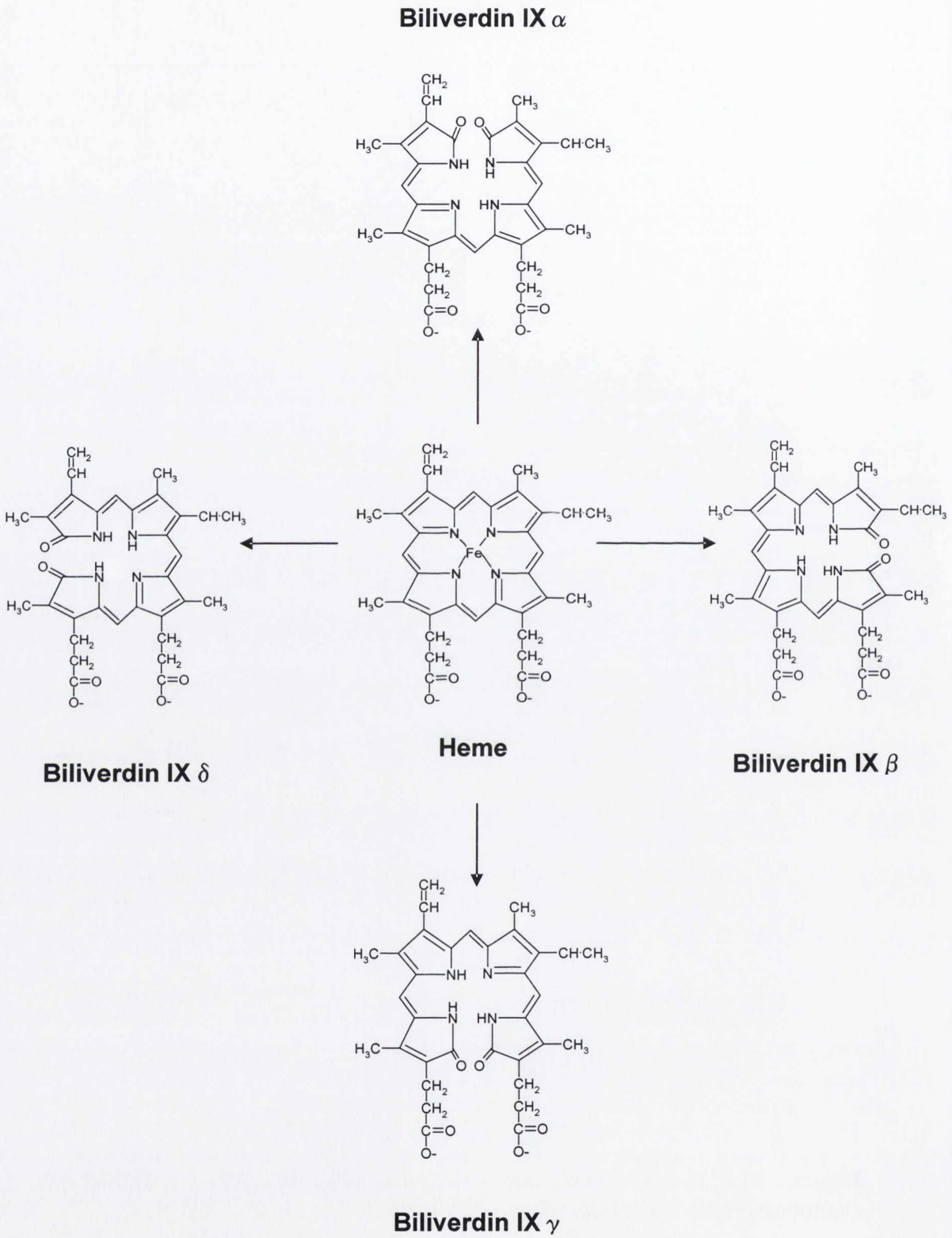

Figure 1.11 Heme and the biliverdin isomers

Depending on which of the methene bridges of heme is cleaved can yield one of four biliverdin IX isomers, α, β, γ or δ

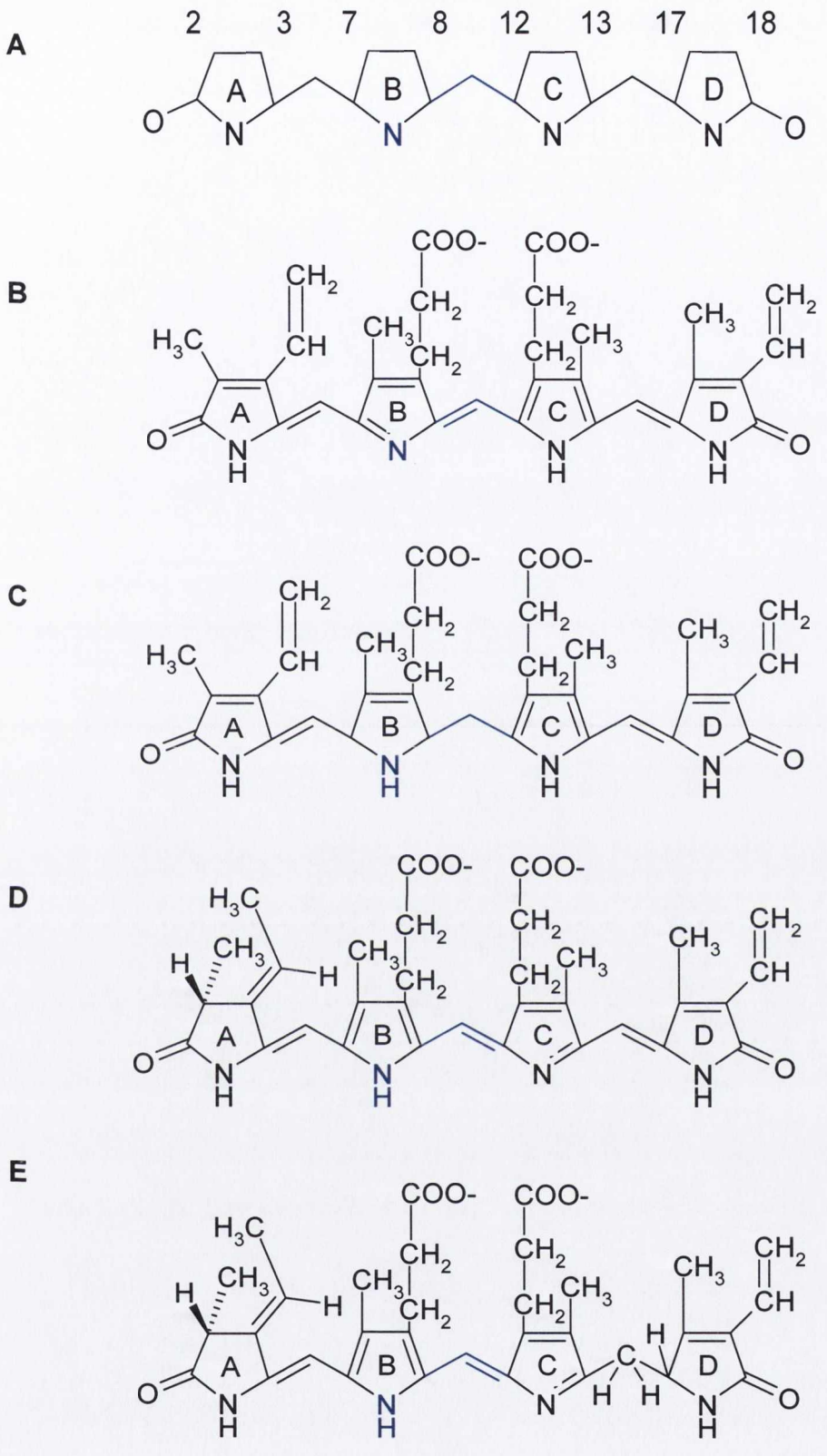

Figure 1.12. Molecular structures of linear tetrapyrroles

A. Structure of the open chain linear tetrapyrrole bilin skeleton with oxygen at the terminal positions. Each of the pyrrole rings is labeled A-D. Carbon atoms are numbered. **B**. Biliverdin IX α **C**. Bilirubin IX α **D**. Phycocyanobilin **E**. Phycoerythrobilin. The C10 bridge is shown in blue

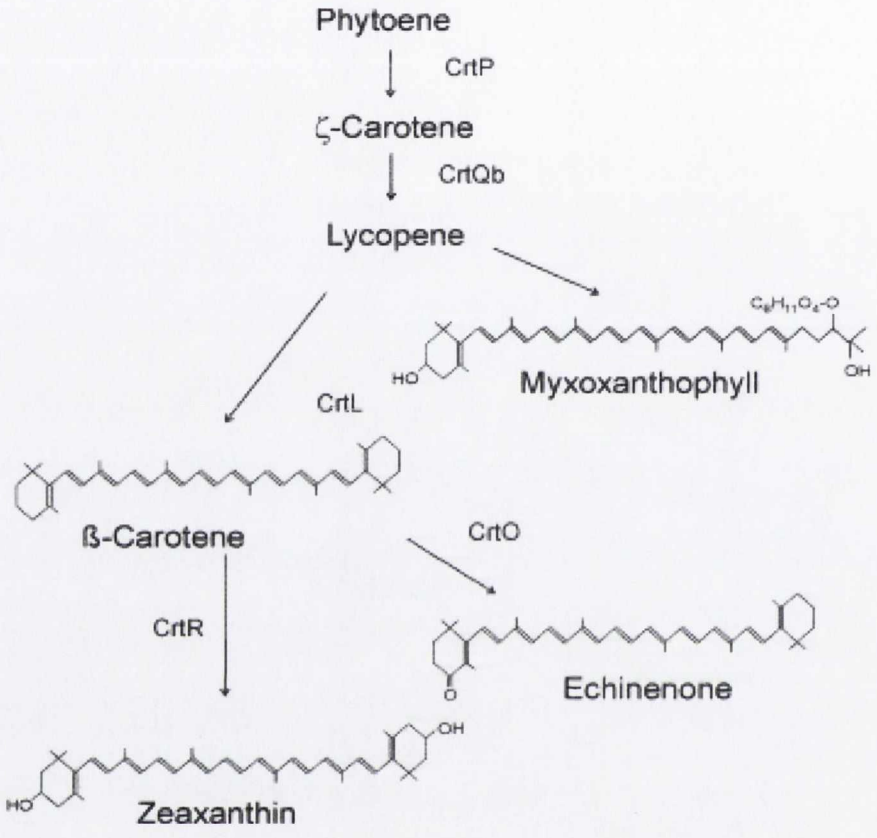

Figure 1.16 Pathway of carotenoid biosynthesis in *Synechocystis* sp. PCC6803

A

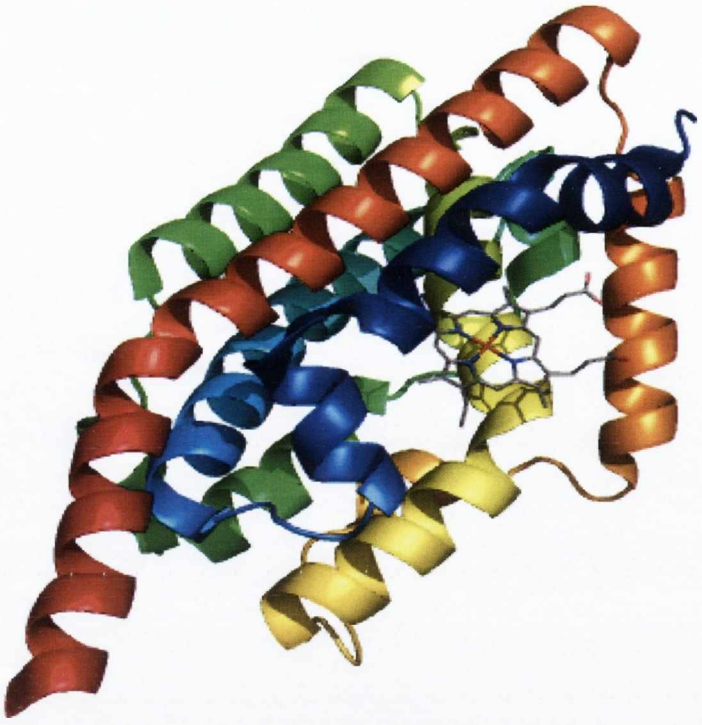

B

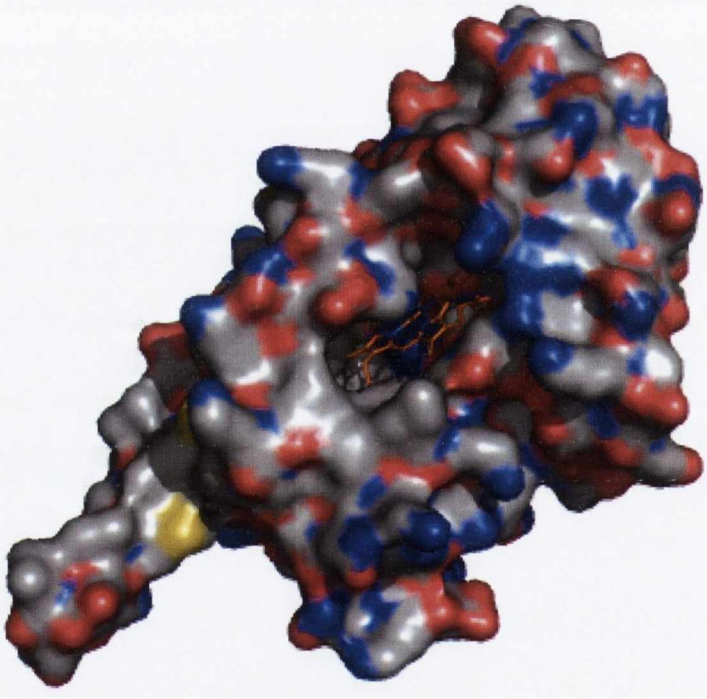

Figure 1.13 Crystal structure of *Synechocystis* heme oxygenase 1

A. Cartoon representation of HO1 showing heme bound in the active site

B. Surface representation of HO1 showing heme bound in the active site. Also shown in blue are the positive patch of amino acids around the active site where acidic ferredoxin binds

Structures were modeled using Pymol (Delano Scientific, 2002) using PDB accession number 1we1

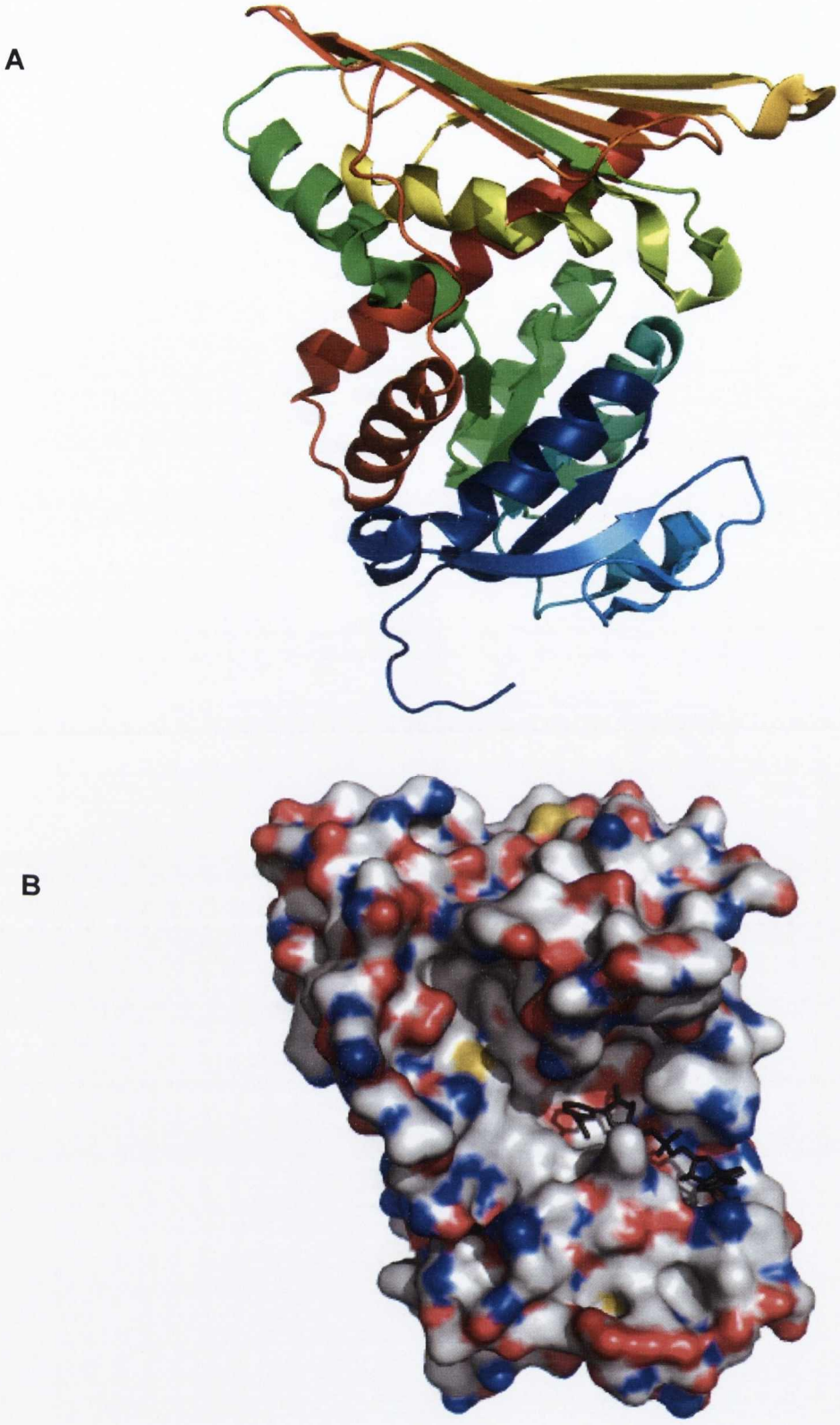

Figure 1.14 Crystal structure of biliverdin IXα reductase

A. Cartoon representation of rat BVR-A (PDB accession number: 1gcu)

B. Surface representation of human BVR-A showing $NADP^+$ bound in the active site (PDB accession number (2h63)

Structures were modeled using Pymol (Delano Scientific, 2002)

A

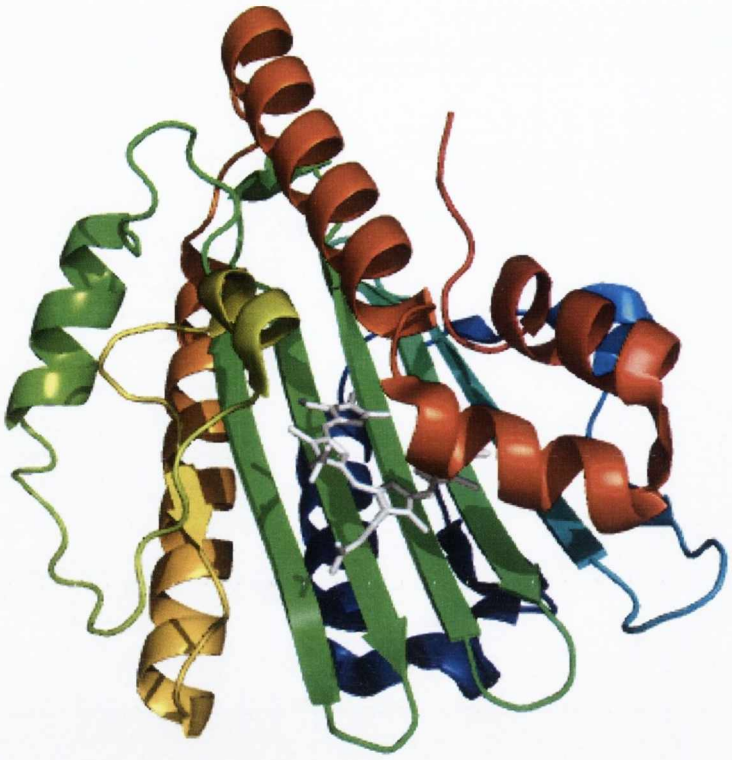

B

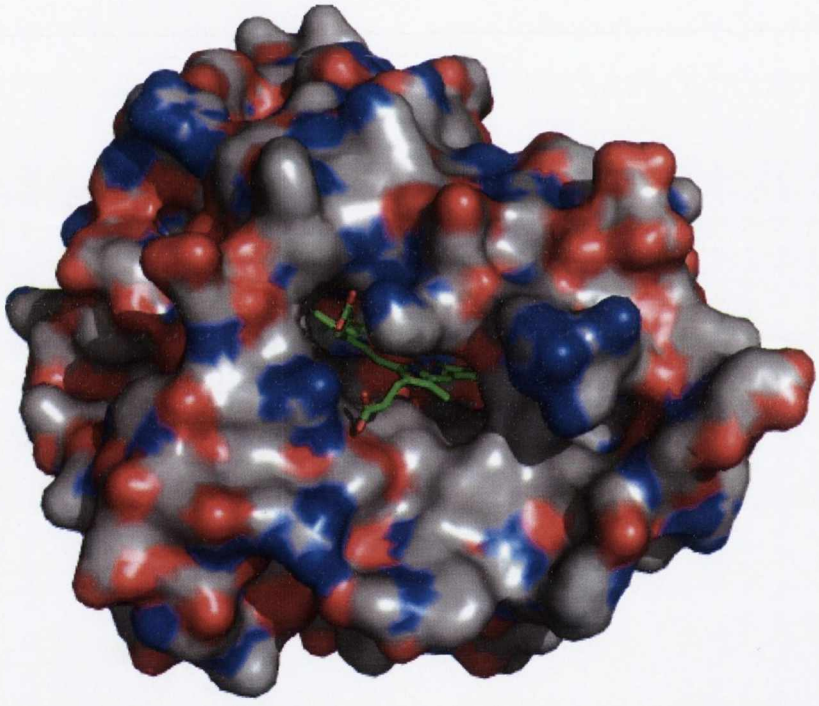

Figure 1.15 Crystal structure of *Synechocystis* phycocyanobilin ferredoxin oxidoreductase

A. Cartoon representation of PcyA showing biliverdin IXα bound in the active site

B. Surface representation of PcyA showing biliverdin IXα bound in the active site Also shown in blue are the positive patch of amino acids around the active site where acidic ferredoxin binds

Structures were modeled using Pymol (Delano Scientific, 2002) using PDB accession number 2d1e

CHAPTER 2

MATERIALS & METHODS

2.1 Materials

The biochemical reagents and chemicals used were of analytical grade, where possible, and obtained from BDH, Reidel-de Haen and Sigma.

Materials	Source
Acrylamide/Bis Solution	National Diagnostics
Adenosine diphosphate	Sigma
Adenosine triphosphate	Sigma
2'5' ADP Sepharose	Sigma
Agarose (molecular biology grade)	Promega
Agarose Gel DNA Extraction Kit	Qiagen
Anti-rabbit secondary antibody (Donkey)	Amersham Biosciences
Ampicillin, sodium salt	Sigma
Bacto-Tryptone	Difco
Bacto-Yeast	Difco
Bacto-Agar	Difco
Biliverdin IXα	Chromatrin
Bilirubin IXα	Frontier Scientific
Dialysis tubing (10kDa cut-off)	Medicell International
Dimethylsulfoxide	Sigma
DNA molecular weight marker VII	Boehringer Mannheim
dNTPs (100 μM stock)	Takara
ECL reagents	Millipore
Folin and Ciocalteau's reagent	Sigma
Freund's adjuvant, complete	Sigma

Freund's adjuvant, incomplete	Sigma
Glutathione, reduced	Sigma
GoTaq polymerase	Promega
Immobilin P membrane	Millipore
Kanamycin sulphate	Sigma
LATaq polymerase	Takara
Ligation kit 2.1.1	Takara
Lysozyme	Sigma
Nicotinamide adenine dinucleotide (reduced)	Calbiochem
Nicotinamide adenine dinucleotide (oxidised)	Calbiochem
Nicotinamide adenine dinucleotide phosphate (reduced)	Calbiochem
Nicotinamide adenine dinucleotide phosphate (oxidised)	Calbiochem
Nitrocellulose paper	Sigma
N-lauryl sarcosine	Sigma
Oligonucleotide primers	MWG Biotech
Plasmid DNA purification kit	Qiagen
Prestained Molecular Markers SDS-7B	Sigma
Restriction enzymes	Roche/Promega
S-hexyl glutathione	Sigma
Sephadex G-25	Sigma
Sepharose 6B	Sigma
Supelco discovery C18 reverse phase HPLC column	Sigma
T_4 DNA Ligase	Promega
Taq DNA polymerase	Promega

2.2 Methods

2.2.1 Bacterial strains, culture media and plasmid vectors

The strains of *E.coli* used for the genetic manipulation, propagation and expression of clones during the course of this work included XL1-Blue, TOP10 and BL21 (DE3) and BL21(DE3) RIL. XL1-Blue cells were obtained from Stratagene, Top10 from Invitrogen, BL21 (DE3) and BL21 (DE3) RIL from Novagen. Genotypes of E.coli strains used during the course of this work can be found in *Appendix* 1.

The media used for the preparation, culturing, and transformation of *E.coli* were all prepared following methods described in Sambrook *et al.,* (2000) and included LB broth, LB agar, SOC medium and PSI broth (see Table 2.1)

Synechocystis sp. PCC6803 cells were purchased from the Pasteur Institute, Paris and were cultured in Bg11 medium plus supplements according to the supplier's recommendations (see Table 2.2). Glucose tolerant *Synechocystis sp.* PCC6803 cells were a generous gift from Dr. Julian Eaton-Rye (University of New Zealand)

All molecular biology reagents, antibiotics, IPTG and lysozyme were prepared as described in Sambrook *et al.,* (2000), and were sterilised either by autoclaving at 121°C for 20 min or by 0.22 μm filtration. All water used in molecular biology experiments was Milli Q treated Nuclease Free Water (NFW).

The plasmid vector pMAL-c2 was obtained from New England Biolabs, pBluescript SK+ from Stratagene, pET41a from Novagen and pUC4K from Amersham Biosciences.

2.2.2 Culturing of *Synechocystis sp.* PCC6803 cells

Under normal conditions *Synechocystis sp.* PCC6803 cells were grown under cool white light with shaking (50rpm) using a New Brunswick scientific Inova 4340 illuminated incubator shaker with a light output of 447 μEinsteins m^{-2} s^{-1} and 30°C with a light/dark cycle of 8 hours light/16 hours dark and an atmosphere of 3% CO_2. Liquid cultures were grown in Bg11 medium plus supplements (see Table 2.2). For growth on plates, Bg11 medium was supplemented with 15g/l agar, 3g/l sodium thiosulphate and 10mM TES-NaOH (pH 8.2). Glucose tolerant cells were grown in Bg11 medium supplemented with 5mM glucose. sBVR-A "knock-out" cells were also grown in the presence of 50-100μg/ml kanamycin.

2.2.3 Purification of cyanobacterial genomic DNA

2.2.3.1 Large scale genomic DNA purification

A fresh *Synechocystis* culture (50ml) was grown in Bg11 medium for 4-5 days until the optical density at 730nm (OD_{730}) was approximately 0.5. The cells were transferred to a sterile 50ml Falcon tube and harvested by centrifugation at 2760 x g for 5min at 4°C in an Eppendorf 5810R refrigerated centrifuge. The cells were resuspended in saturated sodium iodide [2ml (2g NaI/ml H_2O] per gram cell paste) and incubated at 37°C for 30mins. 20ml ddH_2O was added to dilute the NaI and the cells were centrifuged at 2760 x g for 10min at 4°C. The resulting pellet was resuspended in 8ml Tris buffer (50mM Tris-HCl, 50mM NaCl, 5mM EDTA, pH8) per gram of wet cells. An 18 gauge needle was used to ensure that the cells were completely resuspended. Lysozyme was added to a final concentration of 50µg/ml; the solution was mixed gently and incubated at 37°C for 20mins. 1ml 10% N-lauryl sarcosine was added per gram of cells followed by 1ml 10% SDS, the solution was mixed gently and incubated at 37°C for 20mins. Proteinase K (Qiagen) was added to 50µg/ml final concentration and incubated at 50°C for 1 hour with shaking. The lysate was then transferred to a 50ml phenol-resistant screw-cap plastic tube and an equal volume of Tris-HCl (pH>7.8) equilibrated phenol was added. The solution was mixed gently for 1hour and centrifuged at 2760 x g for 10mins at 4°C. The upper aqueous phase was transferred to a clean phenol resistant tube. An equal volume of chloroform, containing 1/25 volume of isoamylalcohol was added to the aqueous phase and mixed gently for a further 45mins. This was then centrifuged again at 2760 x g for 10mins at 4°C and the aqueous phase was transferred to another clean phenol-resistant tube. The DNA was precipitated by adding $1/10^{th}$ volume of 3M sodium acetate (pH5), followed by 2½ volumes of 100% ethanol. This was shaken gently to mix and then stored at -20°C for 1hour to aid the precipitation of the DNA. The solution was centrifuged at 23,000 x g for 15mins at 4°C in a Sorvall RC 5C plus refrigerated centrifuge and the ethanol was removed using a pipette. The resulting genomic DNA pellet was washed with chilled 70% ethanol (-20°C) and again centrifuged at 2760 x g for 5mins at 4°C. The ethanol was again carefully removed. This was further centrifuged at 2760 x g for 30secs at 4°C and the last of the ethanol was completely removed. Air drying the pellet was avoided as this greatly reduced the solubility of the DNA. The DNA pellet was then solubilised in 1ml nuclease free water (NFW), analysed by agarose gel electrophoresis, quantified as described in Section 2.2.6 and stored at -20°C.

2.2.3.2 Small scale rapid genomic DNA purification

A fresh *Synechocystis* (1ml) culture was grown for 2-3 days in Bg11 medium until OD_{730} was approximately 0.5. 400µl of this culture was transferred to a sterile phenol resistant 1ml minifuge

tube and centrifuged at 7000 x g for 2min at 4°C in an Eppendorf 5415R refrigerated centrifuge. The cell pellet was washed with sterile ddH_2O and resuspended in 200µl saturated sodium iodide (2g NaI/ml H_2O) and incubated at 37°C for 10mins. NFW (1ml) was added to dilute the NaI and the cells were centrifuged at 13,600 x g at 4°C for 1min. The resulting pellet was resuspended in 400µl Tris buffer (50mM Tris-HCl, 50mM NaCl, 5mM EDTA, pH8). 20µl lysozyme (1mg/ml) was added and the solution was mixed gently and incubated at 37°C for 10mins. 100µl of 10% N-lauryl sarcosine was added followed by 50µl of 10% SDS (final concentration 0.1%) and the solution was mixed gently and incubated at 37°C for 10mins. Proteinase K was added to 50µg/ml final concentration and incubated at 50°C for 1 hour with shaking. 600µl phenol/chloroform containing isoamylalcohol (1/25 volume) was added and the solution was mixed gently for 5-10mins. This was then centrifuged at 13,600 x g for 10mins and the upper aqueous phase was transferred to a clean phenol resistant 1ml minifuge tube. 3M sodium acetate (100µl), pH5 was added to precipitate the DNA, followed by 800µl isopropanol. This was mixed well and incubated on ice for 5-10mins. The solution was centrifuged at 13,600 x g for 10mins at 4°C and the isopropanol was removed using a pipette. The resulting genomic DNA pellet was washed with chilled 70% ethanol (-20°C) and again centrifuged at 13,600 x g for 2mins at 4°C. The ethanol was again removed. This was further centrifuged at 13,600 x g for 10sec at room temperature and the last of the ethanol was completely removed using a pipette. The DNA was then resuspended in 50µl NFW, analysed by agarose gel electrophoresis, quantified as described in Section 2.2.6 and stored at -20°C.

2.2.4 Purification of plasmid DNA

Plasmid DNA was extracted and purified using either Qiagen's Midi prep (100µg plasmid DNA) or Mini prep (20µg of plasmid DNA) kits. The DNA was extracted according to the manufacturer's instructions. Qiagen's plasmid–purification procedures are based on a modified alkaline lysis procedure, followed by binding of plasmid DNA to an anion-exchange resin under appropriate low-salt and pH conditions. RNA, proteins, dyes and low-molecular-mass impurities are removed by a medium-salt wash. Plasmid DNA is then eluted in a high-salt buffer, concentrated and de-salted by isopropanol precipitation, resuspended in NFW, quantified as decribed in Section 2.2.6, analysed and either used immediately or stored at -20°C.

2.2.5 Electrophoresis of DNA

DNA was routinely electrophoresed through 1% agarose gels at 100V for 1 hour in Tris-Acetate buffer (TAE) [0.04 M Tris, 1.1% (v/v) acetic acid, 0.001 M EDTA, pH 8.5]. A 10µl volume of the sample to be analysed was mixed with 5µl 5 X DNA loading dye (Promega). Following

electrophoresis, gels were stained in ethidium bromide solution (final concentration, 0.5μg/ml) and bands were visualised with minimum exposure to UV irradiation.

2.2.6 Quantification of DNA concentration

The concentration of DNA was routinely determined by measuring the A_{260} using a Philips PU8625 spectrophotometer and the following formula:

$$A_{260} \times 50 \times \text{dilution factor} = \text{DNA } (\mu g/ml)$$

This method is not suitable if unincorporated nucleotides are present as these also absorb light at 260nm. Under such conditions, estimates of DNA concentration were obtained by comparing the intensity of the band of the unknown sample to that of known standards following electrophoresis.

2.2.7 Genetic manipulation techniques

2.2.7.1 Polymerase chain reaction (PCR)

PCR reactions were carried out using a PTC-200 Peltier thermal cycler (MJ Research). The exact components of each PCR reaction and the PCR cycling conditions can be seen in Tables 2.3 and 2.4. Primer design is tabulated in the relevant sections. The normal reaction volume was 25 or 50μl. When cloning, only proof-reading polymerases, such as Stratagene *pfu* or Takara LATaq, were used to amplify the desired DNA fragment, ensuring the lowest possible occurrence of random point mutations. However, when screening *E.coli* colonies a less stringent polymerase such as GoTaq (Promega) was sufficient. PCR primers were designed based on each individual DNA fragment's sequence, taking into account the required restriction sites for cloning into the selected vector. PCR products were analysed by agarose gel electrophoresis and purified.

2.2.7.2 Purification of linear DNA fragments

Linear DNA fragments were purified using Qiagen's "Quick PCR purification" kit according to the manufacturer's instructions. DNA fragments containing salts, restriction enzymes other impurities were applied to Qiagen's silica spin columns and centrifuged at 13,600 x g for 1min at room temperature. The supernatant was discarded and the DNA was washed with chilled 70% ethanol. Following removal of the ethanol, the DNA was solubilised and eluted with NFW. The sample was centrifuged at 13,600 x g for 2min at RT and used immediately or stored at -20°C.

2.2.7.3 Extraction and purification of DNA fragments from agarose gels

DNA fragments obtained after digestion with restriction enzyme were electrophoresed through 1% agarose gels made with NFW and TAE buffer (also made with NFW). The DNA was visualised very briefly under UV light following "in gel" staining with ethidium bromide (10μg/ml).

Digested DNA fragments were then purified using Qiagen's agarose gel DNA extraction kit according to the manufacturer's instructions. The DNA bands of interest were carefully excised using a sterile razor blade and transferred to pre-weighed 1ml minifuge tubes. Solubilisation buffer (300µl) was added for every 100mg of agarose. This was incubated at 50°C with intermittent vortexing until all the agarose had completely melted. The resulting solution was then transferred to the silica spin columns provided with the kit. The DNA-agarose mixture was centrifuged at 13,600 x g for 1min at room temperature and the supernatant discarded. 1ml column wash buffer (containing ethanol, 10% v/v) was added and the spin column was again centrifuged at 13,600 x g for 1min at room temperature. The supernatant was again discarded and the spin column centrifuged at 13,600 x g for 2min at room temperature. This step was to remove any residual ethanol. The bound and washed DNA was then eluted with 32µl NFW by centrifugation at 13,600 x g for 1min at room temperature. The purified DNA was then analysed by agarose gel electrophoresis and used immediately or stored at -20°C.

2.2.7.4 Restriction enzyme digestion of DNA

All restriction enzymes used in the digestion of genomic DNA, plasmid DNA and PCR products were obtained from either Roche or New England Biolabs. A typical digestion reaction contained 1µg DNA, 1 unit of the appropriate restriction enzyme and 5µl of a suitable 10X reaction buffer. The reaction volume was brought to 50µl using NFW, incubated at 37°C for 1.5-2 hours and then analysed by agarose gel electrophoresis.

2.2.8 Ligation reactions

2.2.8.1 Preparation of DNA for ligation reactions

Ligation of successfully amplified PCR products and other DNA fragments into plasmids was achieved by digesting both the plasmid and the PCR product with the appropriate restriction enzymes, as described in the previous section. Following inactivation of the restriction enzymes by heating at 65°C for 15 min a 1µl volume of Takara's bacterial alkaline phosphatase (BAP) was added to the reaction and incubated at 55°C for 1h. The phosphatase-treated linearised plasmid DNA and digested DNA fragments were then purified using Qiagen's "PCR Quick clean up kit", as described below.

2.2.8.2 Purification of DNA following restriction digestion

Purification of PCR products and other DNA fragments before and after digestion with restriction enzymes was performed using Qiagen's "PCR Quick clean up kit". Plasmid DNA, DNA following restriction digestion or BAP treatment, was purified by the same method according to the

manufacturer's instructions. Using this method salts, restriction enzymes and other contaminants which might interfere with the ligation reaction were removed.

2.2.8.3 Ligation of linear DNA fragments into plasmids

Ligation reactions were performed using Takara's Version 2.1.1 Rapid ligation kit. This kit uses an optimised buffer system and T_4 DNA ligase to achieve high ligation efficiency. Ligation reaction volumes were always 10µl and were set up as detailed in Table 2.5 and incubated overnight at 16°C. The entire contents (10µl) of these reactions were used in the subsequent transformation reactions. A number of controls were also set up to aid the identification of true positive clones following transformation. In the first ligation control water replaced the ligase solution. This would identify the percentage of clones which had plasmid without any insert present. In the second ligation control water replaced the DNA insert. This would identify the percentage of clones which had plasmids that were not BAP treated or that were only cut once and could re-circularise following ligase treatment without any insert.

2.2.9 Transformation of *E. coli* competent cells

2.2.9.1 Preparation of ultra–competent *E. coli* cells for heat shock transformation

This protocol is a modification of the method of Inoue *et al.*, (1990) for the preparation of "ultra-competent" *E. coli*. For details of the buffers used in this process see Table 2.6. Overnight cultures (3.5 ml) were grown at 37°C (in the appropriate antibiotic) and 1ml was used to inoculate 100ml of PSI or LB culture broth containing the appropriate antibiotic and incubated at 37°C for approximately 1.5-2 hours until the OD_{600} was between 0.2-0.4. At this point the culture was placed immediately on ice for 15 min and the cells were then harvested by centrifugation (2,500 x g for 10 min at 4°C). The supernatant was discarded and the cell pellets were each resuspended in 5 ml sterile $CaCl_2$ (75mM) on ice for 20min. The cells were harvested as before and the supernatant was discarded. The pellets were suspended in a total volume of 4ml of TfBII buffer (see Table 2.6) and incubated on ice for 20min. The cells were then either used immediately or snap frozen in liquid nitrogen and stored at -80°C. A 100µl volume of cells was used for most ligation reactions. The expected transformation efficiency of cells prepared using this protocol was $1x10^8$ cfu/µg DNA.

2.2.9.2 Transformation of *E. coli* competent cells by heat shock

The entire 10µl volume of the ligation reaction (see Table 2.5) was added to the suspension of competent cells, mixed gently and incubated on ice for 30min. The cells were heat shocked at 42°C for 90 seconds and immediately cooled on ice for a further 2min. SOC medium or LB broth

(1ml) was added to each transformation followed by a further incubation at 37°C for 1h with moderate shaking (200rpm). The cells were spread onto LB agar plates containing the appropriate antibiotic and incubated at 37°C overnight. The resulting colonies were then screened for the presence of the correct DNA fragment. Purified, intact plasmids (1µl) were transformed into *E.coli* cells using the same method.

2.2.10 Screening for positive clones

2.2.10.1 Screening by restriction analysis

Antibiotic resistant clones (usually 10) were picked from the original transformation plate and re-plated onto fresh antibiotic resistant plates to create single plates of each clone. Single colonies were then picked from this permanent plate and their plasmids purified as described in Section 2.2.4. The purified plasmid DNA was then digested using the same restriction enzymes that were originally used to clone the DNA fragment. If the selected clone was positive and the required DNA insert was present the appropriate fragment was visible on agarose gel electrophoresis following restriction digestion.

2.2.10.2 Screening by PCR

With PCR screening, up to 20-50 original colonies were picked and re-plated to create permanent plates for each clone. Each individual clone was cultured in 500µl LB medium in 1ml minifuge tubes and grown at 37°C with shaking for a number of hours, until the solution appeared turbid. 1µl of each culture was then removed and placed into a PCR reaction, containing all the components shown in Table 2.7. The PCR conditions were also changed according to the conditions required for the screening polymerase (see Table 2.8). If the required DNA fragment was present it was visualised by agarose gel electrophoresis after amplification by PCR.

2.2.11 Site–directed mutagenesis

The construction of the desired mutations was based on the method of Stratagene's commercially available "QuikChange site-directed mutagenesis kit". The individual mutagenesis reactions were performed using *PfuTurbo* DNA polymerase and a PTC-200 Peltier thermal cycler (MJ Research). The basic procedure utilizes a supercoiled double-stranded DNA (dsDNA) vector with the insert of interest and two synthetic oligonucleotide primers containing the desired mutation. The oligonucleotide primers, each complementary to opposite strands of the vector, are extended during temperature cycling by *PfuTurbo* DNA polymerase. This enzyme ensures that both plasmid strands are replicated with high fidelity without displacing the mutant oligonucleotide primers. Incorporation of the oligonucleotide primers generates a mutated plasmid containing staggered

nicks. Following the amplification reaction, the product was treated with *Dpn* I. The *Dpn* I endonuclease (target sequence: 5′-Gm6ATC-3′) is specific for methylated and hemimethylated DNA and is used to digest the parental DNA template and to select for newly synthesized DNA containing the desired mutation. DNA isolated from almost all *E.coli* strains is dam methylated and therefore susceptible to *Dpn* I digestion. The nicked vector DNA containing the desired mutations was then transformed into XL1-Blue supercompetent cells as described in Section 2.2.9.2. Exact details regarding primer design and details about the individual PCR reaction are in the relevant section. Plasmids were purified from the resulting antibiotic resistant colonies and sequenced as described below to ensure the correct mutations had been introduced but no other unintended mutations were present. Only plasmids with the correct mutations present were then transformed into competent BL21(DE3) cells as described in Section 2.2.9.2.

2.2.12 DNA sequencing

Purified plasmids were sequenced by MWG Biotech (Eurofins MWG operon, Fraunoferstr. 22, 82152 Martinsreid, Germany). The DNA to be sequenced was prepared and purified from either plasmid minipreps or midipreps as described in Section 2.2.4. Each plasmid (1-5μg) was dehydrated by spinning under a vacuum for 30-45mins in a speedi-vac. Usually, two aliquots of each plasmid to be sequenced were prepared, one for the forward read and one for the reverse read. This ensured all of the DNA sequence was read. Primers used to sequence the DNA inserts in plasmids were usually standard primers and can be seen in Table 2.9.

2.2.13 Preparation of permanent frozen stocks

LB broth (5ml) was inoculated with a single *E.coli* colony and incubated at 37°C overnight with shaking (270rpm). The cell suspension was centrifuged at 5000rpm and 4°C in an Eppendorf 5415R centrifuge. The supernatant was removed and the cells were resuspended in fresh LB medium (1ml). Sterile glycerol was added to a final concentration of 15% (w/v) and the samples were vortexed and stored immediately at -80°C in sterile culture cap tubes.

2.2.14 Growth, harvesting and lysis of *E.coli* transformants containing expression plasmids

A single *E.coli* colony containing the selected expression plasmid was used to inoculate a 10ml overnight LB culture containing the appropriate antibiotic. The overnight cultures were grown at 37°C and 270rpm for approximately 14hours. The following morning the overnight cultures were centrifuged as previously described, resuspended in 1ml fresh LB medium and used to inoculate large 500ml LB cultures which contained the appropriate antibiotic. These cultures were grown at 30°C and 270 rpm until the OD_{600} reached 0.6-1, at which point they were induced to express

protein by the addition of IPTG to a final concentration of 250μM. The temperature was reduced to 27°C and the cultures were grown for a further 16h. The cells were then harvested by centrifugation for 8min at 8000 x g and 4°C as previously described. The resulting pellet was stored at -20°C overnight. The next day, the cell pellets were resuspended in 100ml phosphate-buffered saline (PBS: 0.9% NaCl, 10mM potassium phosphate, pH7.2) or Tris buffered saline (TBS: 0.9% NaCl, 20mM Tris, pH7.5) depending on the protein. Lysozyme was added to a final concentration of 100μg/ml and the solution was incubated on ice for 1h followed by sonication using a Dawe soniprobe type 7532A with a power output of 5 and a duty cycle of 50% for a total of 4 min. Sonication was also performed on ice as the sonication process leads to heating of the sample. The resulting sonicate was centrifuged at 16,000 x g for 45 min and 4°C as described previously.

2.2.15 Protein purification techniques

2.2.15.1 Affinity chromatography

2.2.15.1a Glutathione–Sepharose affinity chromatography

Glutathione-Sepharose was used to purify GST fusion proteins from supernatants by affinity chromatography. This affinity resin is composed of glutathione covalently attached to the porous and insoluble Sepharose by cyanogen bromide. The resin was packed into a glass column (15 x 2cm) and equilibrated with 10 column volumes of TBS or PBS. The cell lysate supernatant (prepared as described in Section 2.2.14) was loaded onto the affinity column at a flow rate of 0.1ml/min and washed at a flow rate of 1ml/min until the A_{280} of the eluent was below 0.005. The fusion protein was then eluted using 5mM reduced glutathione (GSH) in 25 mM Tris, pH 7.5, 100mM NaCl. Fractions with an A_{280} value greater than 0.5 were pooled, cleaved and purified further.

2.2.15.1b Affinity chromatography of proteins tagged with the maltose binding protein (MBP)

Affinity chromatography of cell-lysate supernatant containing maltose binding fusion proteins (prepared as described in Section 2.2.14) was carried out using amylose resin. This resin, an agarose-amylose composite, was packed in a glass column (15 x 2cm) and equilibrated with 10 column volumes of PBS, pH 7.2. The supernatant was loaded onto the column washed with 10 column volumes of PBS containing 1mM EDTA. The fusion protein was eluted with 5mM maltose in equilibration buffer in 1ml fractions. Fractions with an A_{280} greater than 0.5 were pooled, cleaved with precission protease and further purified.

2.2.15.1c Affinity chromatography of His-tagged proteins

His-tagged proteins were purifed from cell lysate supernatants (prepared as described in Section 2.2.14) using Ni^{2+}-agarose. Before use, the Ni^{2+}-agarose was equilibrated with 10 column volumes of equilibration buffer (20 mM potassium phosphate, 100 mM NaCl, 20 mM imidazole, pH 7.5). The supernatant was mixed with 2ml Ni^{2+}-agarose for 1h at 4°C and poured into a glass column (15 x 2 cm) and washed with equilibration buffer until the A_{280} was below 0.005. The resin was then washed with two column volumes of 20 mM KH_2PO_4, 1 M NaCl, pH 7.5 followed by elution of the fusion protein by 20 mM KH_2PO_4, 250 mM imidazole, 100 mM NaCl, pH 7.5. Samples containing fusion protein were detected using the Bradford assay.

2.2.15.1d Affinity chromatography using 2'5' ADP-Sepharose

2'5' ADP-Sepharose binds NADPH/$NADP^+$binding proteins. The resin was carefully packed into a glass column (15 x 2cm) and equilibrated with 10 column volumes of Tris buffer (25 mM Tris pH 7.5, 150mM NaCl). Partially purified BVR-A in 25 mM Tris buffer, pH 7.5 containing 150mM NaCl was slowly loaded onto the column and washed with 10 column volumes of equilibration buffer, followed by 10 column volumes of 25 mM Tris, 250mM NaCl, pH 7.5. BVR-A was eluted using 25 mM Tris, 1M NaCl pH 7.5). The protein was then dialysed or gel filtered to remove the NaCl.

2.2.15.2 Dialysis of protein samples

Dialysis membrane (cut-off 10,000 kDa) was prepared by boiling for 5min in 1mM EDTA followed by extensive washing with ddH_2O. The protein solution was carefully pipetted into the knotted membrane and dialysed against 3 x 5 litres of the required buffer for 3 hours each time.

2.2.15.3 Sephadex G-25 Gel filtration chromatography

2.2.15.3a Large scale G-25 gel filtration

The Sephadex G-25 was carefully packed into a glass column (50 x 1.0 cm) and equilibrated with Tris buffer (25mM Tris pH 7.5, 150mM NaCl). It was calibrated using 2ml Blue Dextran (5mg/ml) and 2ml para-nitrophenol (2mg/ml) in order to determine the void and included volumes. Following calibration, the protein solution (samples above 2-3ml) was applied to the column at a flow rate of 1ml/min and when the void volume had eluted fractions (3ml) were collected. The protein content of the various fractions was monitored by the A_{280}.

2.2.15.3b Small scale G-25 gel-filtration using PD-10 columns

Protein samples from 0-2ml were desalted or buffer-exchanged using PD-10 columns (Amersham). Proteins in a total volume of 2ml were applied to pre-equilibrated PD-10 columns, washed with 2ml of the required buffer and eluted in 3ml of the same buffer. Samples containing protein were monitored by the A_{280}.

2.2.15.4 Sephadex-200 Gel filtration chromatography

Size exclusion chromatography using Sephadex S-200 was used to purify proteins based on their molecular mass and was also used to determine the molecular weight of sBVR-A. The Sephadex S-200 was carefully packed into a glass column (100 x 1cm) and equilibrated with Tris buffer (25mM Tris, pH 7.5, 100mM NaCl) or citrate buffer (25mM sodium citrate, pH5, 100mM NaCl) and then calibrated with Blue Dextran (5mg/ml) and para-nitrophenol (2mg/ml) in order to determine the void and included volumes. Calibrating proteins [β-amylase (200kDa), alcohol dehydrogenase (150kDa), bovine serum albumin (66kDa), carbonic anhydrase (29kDa) and cytochrome C (12.4kDa)] were then individually applied to the column and their elution volumes also recorded and used to construct a standard curve of log molecular weight *versus* elution volume. The standard curve was used to estimate the molecular weight of sBVR-A. Fractions (2ml) were collected and the presence of protein detected by the absorbance at 280nm or by a positive reaction with Bradford reagent.

2.2.15.5 Diethylaminoethyl (DEAE) ion-exchange chromatography

DEAE-cellulose was swollen and equilibrated in a buffer depending on the isoelectric point of the protein of interest. Usually this buffer was 25mM Tris-HCl, pH8.2, 25mM NaCl. The swollen resin was packed into a column (20 x 2cm) and equilibrated with 10 column volumes of the same buffer. The protein solution was applied to the column and samples which did not bind were collected and their absorbances measured at 280nm. The DEAE was then washed with 10 column volumes of equilibration buffer. Bound protein was eluted using a salt gradient (100-500mM NaCl in the same buffer), absorbances at 280nm were again monitored and protein was desalted as described in Section 2.2.15.3.

2.2.16 Cleavage of fusion proteins

2.2.16.1 Cleavage of eluted proteins

Proteins eluted as described in Section 2.2.15 were cleaved to remove their fusion tags using either thrombin (target sequence: LeuValProArgGlySer). Cleavage is between the Arg and Gly residues) or Precision protease (target sequence: LeuGluValLeuPheGlnGlyPro. Cleavage is between the Gln

and Gly residues). The fusion protein was incubated overnight at 4°C with mixing in the presence of 1unit of protease/μg fusion protein.

2.2.16.2 On-column cleavage of fusion proteins using Glutathione-Sepharose

GST fusion proteins were loaded onto a glass column packed with glutathione-Sepharose as described in Section 2.2.15.1a. Following the wash step, the fusion protein was not eluted as before but 40units thrombin protease in thrombin cleavage buffer (50mM Tris-HCL, 150mM NaCl, 2.5mM $CaCl_2$, pH 7.5) was added to the top of the column and allowed to soak into the resin. The column flow was then stopped and left overnight. The following morning the cleaved protein was released from the column by washing with buffer while the GST moiety remained bound to the resin.

2.2.17 Concentration of proteins

2.2.17.1 Concentration of proteins by ultra-filtration

Ultra-filtration concentration was carried out using Centriplus concentrator columns according to the manufacturer's instructions. The sample reservoir was connected to the filtrate vial and the sample (10ml) was applied. The assembled concentrator was centrifuged at 3000 x g at 4°C until the desired concentration was achieved. The sample reservoir was then inverted into the retentate vial and centrifuged at 2000 x g at 4°C for 3-4min to recover the sample.

2.2.17.2 Concentration of proteins by osmosis

Using this method, PEG 80,000 was dissolved in the desired buffer until a very viscous solution was formed. The protein solution was put into dialysis membrane as previously described, placed into a 500ml beaker of the concentrated PEG solution and stirred slowly. The concentrated PEG solution removes the water by osmosis resulting in concentration of the protein sample. Alternatively solid PEG 80,000 was placed around the dialysis membrane and used to remove the water by osmosis.

2.2.18 Determination of protein concentration

2.2.18.1 Absorbance at 280nm

For routine column monitoring, the absorbance at 280nm was measured and a value of 1 was assumed to be equivalent to a protein concentration of approximately 1 mg/ml. For more accurate protein determination, the Bradford assay or method of Markwell *et al.* (1978) was used.

2.2.18.2 Markwell assay

The Markwell assay was performed according to the procedure of Markwell *et al.*, (1978). Bovine serum albumin (BSA) was used as a protein standard to construct the standard curve. Three reagents were required, reagent A [2% (w/v) sodium carbonate, 0.4% (w/v) sodium hydroxide, 0.16% (w/v) potassium tartrate, 1% (w/v) SDS], reagent B [4% (w/v) copper sulfate] and reagent C, made by mixing 99ml reagent A and 1ml reagent B. The BSA (0–100µg) or unknown protein, in a volume of 1ml, was mixed with 1.5 ml reagent C and incubated for 10min at RT. 200µl, 50% Folins-Ciocalteau solution was added, the solutions were vortexed and left to develop for 45min at RT. The absorbances were then measured at 660nm using a Molecular Devices Spectra max 340PC plate reader. The absorbance values of the standards were fitted to a straight line using a least-squares procedure and this standard curve was used to estimate the protein concentration of the unknown samples.

2.2.18.3 Bradford assay

The Bradford assay was performed according to the procedure of Bradford, (1976). BSA was used as the protein standard. 10µl unknown protein or standard (0-500µg) was mixed with 200µl Bradford reagent (Bio-rad) and 10µl of each sample (including standards) was added to the well of a 96 well plate and the absorbance at 595nm was measured. The concentration of unknown protein samples was determined from the standard curve of absorbance *versus* the concentration of BSA standard.

2.2.19 Protein electrophoresis and immunoblotting

2.2.19.1 Sodium dodecyl-sulphate polyacrylamide gel electrophoresis (SDS-PAGE)

2.2.19.1a Gel preparation and electrophoresis

SDS–PAGE was carried out using the discontinuous system of Laemmli, (1970).

The composition of the polymerising gel mixtures for the mini-gels (5cm) and large gels (16cm) are outlined in Table 2.10. The components of the resolving gel were mixed, poured into an ATTO gel mould (mini-gel) or Amersham SE 600 Ruby gel mould to approximately 1-2cm (mini-gel) or 3-4cm (large gel) below the top and covered with a layer of water-saturated butanol. Once polymerised, the water-saturated butanol was removed and the gel carefully rinsed with ddH_2O. The stacking gel was then added and a teflon comb consisting of 12 wells (minigel) or 15 wells (large gel) was inserted into the stacking gel. The comb was removed when the stacking gel had polymerised the wells were washed with ddH_2O before use. All mini-gels were run in an ATTO AE-6400 mini-gel system and large gels in an Amersham SE 600 Ruby system with electrode

chambers filled with running buffer (0.38M glycine, 0.05M Tris and 0.1% (w/v) SDS, pH8.3). Electrophoresis for mini-gels was carried out at 30mA/gel and larger gels at 9-10mA/gel until the tracking dye reached the bottom of the gel. Temperature was controlled at 13°C for large gels by a refrigerated, circulating water bath.

2.2.19.1b Sample preparation

Samples were prepared for electrophoresis by boiling (usually 5-10 µg for mini-gels or 100-200µg for large gels) in sample buffer for 2mins. The sample buffer consisted of 2% (w/v) SDS, 0.5% (v/v) 2-mercaptoethanol, 25 mM Tris-HCl, pH6.8, 0.0012% (w/v) bromophenol blue and 10% (v/v) glycerol.

2.2.19.1c Preparation of *Synechocystis* cytosol for SDS-PAGE and Western blotting

Synechocystis cultures (usually 50ml) were grown as described in Section 2.2.2 in the presence of glucose until the OD_{730} was 0.5-0.8. Prior to treatment glucose and antibiotics were removed as described in Section 2.2.33.1. At this point the cells were either treated or harvested by centrifugation and stored at -20°C overnight. Cell number in each sample was normalised by recording the OD_{730} and diluting the sample with fresh Bg11 medium until the OD_{730} was exactly 0.5. A 50ml sample of Synechocystis cells with an OD_{730} of 0.5 is approximately equal to 7.5 x 10^9 cells. The cells were resuspended and washed with ice-cold PBS and finally resuspended in 0.5ml Tris buffer (50mM Tris-HCl, 150mM NaCl, 5mM EDTA, 10µl complete protease inhibitor cocktail (Sigma), pH 7.5) Acid-washed glass beads (2µm diameter) were added to 1cm below the surface of the cell suspension and the cells were lysed by 3 cycles of vortexing for 1min followed by 2min on ice. Unlysed cells and insoluble cell debris was then removed by centrifugation at 16,000 x g for 2min at 4°C. Samples were prepared for electrophoresis as described above.

2.2.19.2 Staining and destaining procedures

When the gel had run to completion it was stained with 1.25% (w/v) Coomassie Brilliant Blue R in 50% (v/v) methanol, 10% (v/v) acetic acid for 30 min, washed in ddH_2O and destained overnight in 10% (v/v) methanol, 10% (v/v) acetic acid.

2.2.19.3 Western blotting

Western blotting was carried out using a semi-dry blotting apparatus (Semi-Phor, Hoeffer Scientific Instruments, Model TE70). SDS-PAGE was performed as described above. When electrophoresis was complete, the gel was equilibrated for 15 min in cathode buffer (25 mM Tris-HCl, 192 mM glycine, pH 8.3). Proteins were electrophoretically transferred to Immobilon P

membrane (Milli-Pore) for probing with antibodies. The membrane was first treated by immersion in methanol for 15sec, followed by rinsing for 2min in MilliQ water and equilibration in anode buffer 2 (25mM Tris, 10% methanol, pH10.4) for 5min. Filter paper (2 pieces) was also soaked in anode buffer 2 for at least 30sec, 1 piece in anode buffer 1 (300mM Tris, 10% methanol, pH10.4) and 3 pieces in cathode buffer (25mM Tris, 40mM glycine, 10% methanol, ph9.4). The blot "sandwich" was prepared by placing the 2 pieces of filter paper soaked in anode buffer 1 in the centre of the anode electrode plate, followed by the filter paper soaked in anode buffer 2. The membrane was placed on top of the filter paper and the gel was placed on top of the membrane. The 3 pieces of filter paper soaked in cathode buffer were placed on top of the gel and finally the cathode electrode plate was placed on top of the stack. Care was taken to ensure that no air bubbles were trapped between the gel and the membrane. The semi-dry blotting apparatus was attached to an ATTO Crosspower 500 power pack and transfer of proteins was achieved using a constant current of 110 mA for 1-1.5 hours.

2.2.19.4 Development of Western blots

Following electrophoretic transfer, the Immobilon P membrane was removed from the cassette and incubated in blocking buffer [TTBS [20 mM Tris-HCl, 500 mM NaCl, pH 7.5 containing 0.05% (v/v) Tween–20] containing 10% (w/v) commercial dried milk product (Marvel) for 1h at room temperature. This solution blocked non-specific binding sites on the Immobilon P membrane.

The membrane was then rinsed in TTBS and incubated for 1 hour at room temperature with primary antibody (diluted 1:1000 with TTBS containing 1% (w/v) Marvel) on a shaking platform. The membrane was washed three times with TTBS for 10min followed by a 1 hour incubation at RT with donkey anti-rabbit horse radish peroxidase-conjugated secondary antibody (Amersham) at a dilution of 1:20,000 in blocking buffer as described above. Following incubation, the membrane was washed as described previously.

Western blots were developed by enzyme-linked chemiluminescence (ECL), according to the manufacturer's instructions. In dark conditions equal volumes of MilliPore ECL reagent 1 and 2 (usually 1ml of each) were mixed and pipetted over the membrane a number of times. Following removal of excess ECL reagents the membrane was sandwiched between two sheets of acetate paper (normally used for overhead projectors) and placed into a light proof developing cassette. X-ray film (Fuji) was placed over the membrane and left for a period of time, usually 30sec-5min, depending on the strength of the signal. The film was then fixed and developed using a Fuji Colenta Mediphot 937 X-ray developer.

2.2.20 Production of anti-sera against *Synechocystis* heme oxygenase I, biliverdin IXα reductase and phycocyanobilin ferredoxin oxidoreductase.

2.2.20.1 Preparation of proteins for immunisation

All three proteins were cloned, overexpressed and purified as fusion proteins as described in Section 2.2.15. The proteins (8 aliquots of 250µg of each protein) were then shipped on dry ice to Harlan Sera-lab Ltd. (Hillcrest, Dodgeford Lane, Belton, Loughborough, UK.) who raised the respective anti-bodies in New-Zealand white rabbits.

2.2.20.2 The immunisation schedule

On the day before the schedule commenced a 10ml blood sample was taken from each rabbit and was used to prepare a sample of pre-immune serum. On day 1 of the schedule 350µg of each purified protein was mixed with 500µl of Freund's complete and incomplete adjuvant in a total volume of 1ml. The resulting emulsion of each protein was injected into multiple sites of the back of individual rabbits (one rabbit per protein).

On day 14 of the schedule, a booster injection was prepared in the same way and injected into the leg of each rabbit. 2 weeks later a second booster was injected into each rabbit. The first test bleed (10ml) was taken one week after the second booster. A third booster was injected 1 week later, followed by another 10ml test bleed 1 week after that. A fourth booster was injected 1 week later followed by a third test bleed 1 week after that. The fifth and final booster was injected after 1 more week, 2 months and 10 days after the schedule began and the terminal bleed was taken 1 week later.The individual anti-sera containing antibodies raised against *Synechocystis* HO1, BVR-A and PcyA was then shipped from Harlan-Seralab and stored at -20°C.

2.2.21 Purification of antibodies

2.2.21.1 Preparation of cyanogen-bromide activated protein-Sepharose matrix

Recombinant protein (20mg) was purified as described in Section 2.2.15 in buffer A (100mM sodium phosphate, 150mM NaCl, pH8). Cyanogen-bromide activated Sepharose (3g) was swollen in cold 1mM HCl and washed extensively with buffer A (al least 200ml/g resin) followed by washing with 10 column volumes of ddH_2O and equilibration with 15ml (5ml/g resin) buffer A. The protein solution was then immediately transferred to the activated Sepharose for coupling as the reactive groups hydrolyse in basic solution. The protein-Sepharose mixture was mixed gently end-over-end overnight at 4°C and unreacted protein was washed away using the same buffer as above. Unreacted groups on the Sepharose were also blocked with 200mM glycine, pH8 for 2 hours at RT. The resin was washed extensively with the coupling buffer to remove the blocking

solution followed by an acidic wash with 100mM sodium acetate, 500mM NaCl, pH 4. This wash cycle of high to low pH was repeated at least 5 times followed by equilibration with PBS.

2.2.21.2 Purification of antibodies by affinity binding to protein-Sepharose matrix

Following equilibration of the matrix the Sepharose was packed into a glass column (1cm x 5cm) and washed with a further 10 column volumes of PBS. Anti-sera (5ml) was then slowly applied to the resin and the flow-through collected. The resin was washed with a further 10 column volumes of PBS, followed by a high salt wash (250mM NaCl in PBS). Antibodies were eluted by lowering the pH with 200mM glycine, pH2.5. 1ml fractions were collected and their A_{280} monitored. Following elution the pH was immediately brought back to pH 7.2 by addition of 1M PBS and the purified antibodies were stored in 10% glycerol at -80°C.

2.2.22 Purification of phycocyanobilin

A fresh *Synechocystis* culture (250ml) was grown in Bg11 medium supplemented with 5mM glucose under medium light until the OD_{730} was approximately 1.5. Cells were harvested by centrifugation at 10,000 x g for 10min at 4°C and stored at -20°C. Harvested cells were washed twice in ice cold sodium phosphate (10mM), pH7 by resuspension and centrifugation and disrupted by sonication. Sonication was carried out on ice with 5sec pulses using a Dawe soniprobe type 7532A with a power output of 5 and a duty cycle of 50% for a total of 5 min. Cell debris and unbroken cells were removed by centrifugation at 15,000 x g at 4°C for 30min. Phycocyanin was precipitated by adding ammonium sulphate to a final concentration of 50% w/v with gentle mixing at 4°C for approximately 12 hours. Precipitated protein was removed by centrifugation at 25,000 x g at 4°C for 20min. Precipitated protein was resuspended in 20mM Tris/HCl, 25mM NaCl pH 8 and ammonium sulphate and other impurities were removed by extensive dialysis in the same buffer (3 x 5 litres for at least 3 hours each). Phycocyanin was further purified by ion-exchange chromatography as described in Section 2.2.15.5 and eluted with a gradient of 25-500mM NaCl. Eluted phycocyanin was dialysed as before using 20mM sodium phosphate, pH7. Purified phycocyanin was precipitated using 1% w/v trichloroacetic acid for 1hour at 4°C in the dark and collected by centrifugation at 30,000 x g for 20min at 4°C. The pellet was washed twice with 20ml of 100% HPLC grade methanol by resuspension and centrifugation at 30,000 x g for 20min at 4°C. The blue pellet was resuspended in 100% HPLC grade methanol containing 2mg/ml mercury chloride ($HgCl_2$) and incubated at 42°C in the dark for 24hours. Protein was removed by centrifugation at 10,000 x g for 10min at 4°C. 2-mercapthoethanol (1µl/ml) was added to the supernatant to precipitate the dissolved mercuric ion which was also

removed by centrifugation at 30,000 g for 30min at 4°C. The crude phycocyanobilin was stored at 4°C in the dark prior to purification by HPLC.

Crude phycocyanobilin was purified by reverse phase HPLC using a Shimadzu LC10AT HPLC system with online photo-diode array detector set from 200-700nm. The crude PCB solution was centrifuged at 13,000 rpm at 4°C for 10min and immediately loaded onto a "Supelco Discovery" C18 reversed phase HPLC column (25mm x 4mm) equilibrated in 56% 100mM ammonium phosphate, 44% HPLC grade methanol, pH3.4. PCB was eluted using a gradient of 30-100% (v/v) HPLC grade methanol over 15min followed by 100% methanol for a further 15min. PCB was identified by its absorption spectrum and fractions (500µl) were collected. Solvent was evaporated off under a vacuum in the dark and PCB was resuspended in DMSO (100%).

2.2.23 Kinetic studies

2.2.23.1 Kinetic studies on *Synechocystis* biliverdin IXα reductase

The biliverdin reductase activity of *Synechocystis* BVR-A was measured using a colourimetric assay and monitored spectrophotometrically using a Thermospectronic Heλios spectrophotometer with online Kipp & Zonen chart recorder. Temperature was maintained at 30°C by a circulating water bath.The activity of the enzyme was monitored by the increase in absorbance at 460nm due to the appearance of bilirubin IXα. The typical reaction mixture contained 1-5µg purified sBVR-A, 100mM sodium citrate buffer, pH5 and various concentrations of the substrate biliverdin and co-factor NAD(P)H. The reaction was performed at 30°C and initiated by the addition of enzyme or NAD(P)H and followed continuously by the appearance of bilirubin IXα at 460nm with the chart recorder set at 10 mm/min and 50mV (this corresponds to a full scale deflection of 0.1 absorbance units). Stock solutions of biliverdin IXα (1mM or 100µM), NAD(P)H (10mM and 100mM) and $NAD(P)^+$ (10mM and 100mM) were made fresh daily in 10mM sodium phosphate, pH7. Stock solutions of bilirubin IXα (1mM or 100µM) and phycocyanobilin (1mM or 100µM) were made fresh daily in DMSO (100%). The Beer-Lambert law ($A=\varepsilon.c.l$) was used to obtain exact concentrations of substrates. Extinction co-efficients (ε) for the substrates used are:

Biliverdin IXα at 660nm and pH7	=	12.5×10^3 $mol^{-1}.l^{-1}.cm^{-1}$
Bilirubin IXα at 460nm and pH7	=	45.85×10^3 $mol^{-1}.l^{-1}.cm^{-1}$
Phycocyanobilin at 374nm and pH7	=	47.9×10^3 $mol^{-1}.l^{-1}.cm^{-1}$
NAD(P)H at 340nm and pH7	=	6.22×10^3 $mol^{-1}.l^{-1}.cm^{-1}$
$NAD(P)^+$ at 260 nm and pH7	=	1.74×10^4 $mol^{-1}.l^{-1}.cm^{-1}$

For initial rate kinetics data points (in triplicate) were fitted to the Michaelis-Menten equation (equation 1) using the least squares fitting routine and the computer program Prism (Graphpad) or Wincurve Fit, version 1.3 (Kevin Raner Software, Mt. Waverly, Australia.

Equation 1:

$$v = \frac{V_{max}[S]}{K_m + [S]}$$

Where v is the initial rate, V_{max} is the maximum velocity, [S] is the substrate concentration and K_m is the Michaelis constant. The rectangular hyperbolas generated from these curves were used to obtain values for V_{max} and K_m.

For inhibition studies initial rates were converted to double reciprocal plots and the data were then fitted to a straight line using y = *m*x+c. However, this was for illustration purposes only and was not used to determine inhibition constants. To determine inhibition constants involving slope ($appK_m/appV_{max}$) effects the slope of the relevant double reciprocal plot was re-plotted against the concentration of inhibitory product. The straight line intercepted the x axis at $-K_{is}$ to give the inhibition constant for the slope effect. For inhibition constants involving intercept effects the $1/appV_{max}$ values from the initial rate data was plotted against the concentration of inhibitory product and the inhibition constant for the intercept effect (K_{ii}) was determined from where the line intercepted the x axis at $-K_{ii}$.

For pH studies and the determination of pK the data were fitted to the Richards generalised logistic function for pK:

Equation 2:

$$f(x) = \frac{a1 - c1}{1 + 10^{p1(-pH + pK1)}} + c1$$

In this expression a1 represents the upper limit of the sigmoid, c1 represents the lower limit of the sigmoid, p1 represents the Hill co-efficient and pH and pK represent the pH and pK of interest respectively.

2.2.24 Analytical ultracentrifugation

2.2.24.1 Sedimentation velocity analysis

Protein samples (0.42ml) were centrifuged in 1.2cm pathlength 2-sector epon meniscus-matching centrepiece cells (sample in RH sector, reference buffer in LH sector) with sapphire windows in an 8-place An-50 Ti analytical rotor running in an Optima XL-I analytical ultracentrifuge (Beckman Instruments, Inc., Palo Alto, California 94304) at 50,000rpm and at a temperature of 11°C or 20°C. Changes in solute concentration were detected by Rayleigh interference and radial absorbance scans at 287nm. 122 scans of each cell were collected during a 9 hour period.

Results were analysed by whole-boundary profile analysis using the program Sedfit v 9.4 (Schuck, P., 2000). The distribution co-efficient, c(s) for sBVR-A was determined by modelling to the Lamm equation (equation 3) using Sedfit.

Equation 3:

$$\frac{\partial c}{\partial t} = \frac{1}{r}\frac{\partial c}{\partial r}\left[rD\frac{\partial c}{\partial r} - cs\omega^2 r^2 \right]$$

This equation describes the evolution of the concentration distribution c(r,t) of a species with sedimentation coefficient s and diffusion coefficient D in a sector-shaped volume and in the centrifugal field $\omega^2 r$, t and r are the time and radius, D is the diffusion constant, s is the sedimentation co-efficient, ω is the rotor angular velocity. Both D and s are strongly dependent on molar mass and are related by the Svedberg equation (equation 4).

Equation 4: $\mathbf{M = RTs / D (1 - \bar{\nu}_b \rho)}$

Where M is the relative molecular mass (Mr), R is the gas constant, T is the temperature in degrees Kelvin, s is the sedimentation co-efficient (Svedbergs), D is the diffusion co-efficient, $\bar{\nu}_b$ is the partial specific volume of the solute (calculated from the amino acid compositon) and ρ is the solvent density.

Buffer densities and viscosities were calculated using the program Sednterp (Laue, *et al.*, 1992).

2.2.24.2 Sedimentation equilibrium analysis

Protein samples (0.1ml) were centrifuged in 1.2cm pathlength 6-sector epon centrepiece cells (samples in RH sectors, reference buffer in LH sectors) with sapphire windows in a 4-place An-60 Ti analytical rotor running in an Optima XL-I analytical ultracentrifuge (Beckman Instruments, Inc., Palo Alto, California 94304) at a temperature of 4°C at 12,000rpm, 15,000rpm and 18,000rpm. sBVR-A concentrations used were 0.1, 0.3 and 1mg/ml. Radial absorbance scans at 275nm (10 replicates, radial step size 0.001 cm) were performed at intervals of 5h. Interference scans were also collected. Scans were judged to be at equilibrium by plotting radial offset versus time using the program WinMatch (David A. Yphantis). The results were analysed and the data were fitted to a one species model (equation 5) using a least squares fitting routine or a monomer-dimer self-associating model (equation 6) using the program Sedanal V 4.34 (Stafford, W.F., Sherwood, P.J. 2004). For a single ideal species at sedimentation equilibrium the data obtained can be described by equation 5 and the self-association model described by equation 6 incorporates a single self-association reaction where a monomer is in equilibrium with another monomer to form a dimer. Fits with small, randomly distributed residuals indicated a good fit to the model. A goodness of fit parameter, RMSD (root mean squared deviations) was used to determine the best fit to a particular model.

Buffer densities and viscosities were also calculated using the program Sednterp (Laue, *et al.*, 1992).

Equation 5: $$S(r, \lambda) = \delta_\lambda + \varepsilon_\lambda C_0 \exp [M^* \theta (r^2 - r^2_0)]$$

where S(r, λ) is the radially-dependent signal at wavelength λ. This signal can correspond to absorbance, refractive index increment, or fluorescence intensity. $\delta\gamma$ is the baseline offset at wavelength λ, $\varepsilon\lambda$ is the molar extinction coefficient at wavelength λ. C_0 is the molar concentration of the monomer at the arbitrary reference distance r_0, M^* is the monomer buoyant molecular weight and θ is given by:

$$\theta = \omega^2 / 2RT$$

where ω is the angular velocity of the rotor in radians/sec, R is the molar gas constant (83,144,000 erg/mol/K) and T is the absolute temperature. The buoyant molecular weight, M^*, is defined by:

$$M^* = M\,(1-\square\rho)$$

where M is the monomer molar mass, □ is the partial specific volume, and ρ is the solvent density.

Equation 6: $$S(r,\lambda) = \delta_\lambda + \varepsilon_\lambda C_0 \exp\left[M^*\theta\,(r^2-r^2_0)\right] + N\varepsilon_\lambda C_0^{\,N}\exp\left[\ln K + NM^*\theta\,(r^2-r^2_0)\right]$$

Where N is the stoichiometry of the association reaction and lnK is the natural logarithm of the association constant, K. The extinction coefficient should be expressed in typical units of signal/Molar, so that the association constant K is defined is in units of molar. For example, in a monomer-dimer system K is obtained in units of M^{-1} and is defined by:

$$K = [D] / [M]^2$$

2.2.25 Light scattering

Light scattering was performed on sBVR-A at pH5 and pH7.5 and room temperature (18-20°C). Recombinant sBVR-A was purified as described in Section 3.4.3. Protein samples (0.25mg/ml) were clarified using a 0.22μm filter and applied to an S-200 Superdex HR gel-filtration column (Amersham Biosciences) in a total volume of 1ml. The gel-filtration column was connected to an AKTA FPLC system (Amersham Biosciences) and the column was run at room temperature (18°C) and a flow rate of 0.5ml/min in the desired equilibration buffer (25mM sodium citrate, pH5, 100mM NaCl or 25mM Tris, pH7.5, 100mM NaCl). The gel-filtration column was connected online to the following flow detectors: a multiwavelength UV/Vis detector (Amersham biosciences), a miniDawn Tristar light scattering detector (Wyatt Technology) and an Optilab rEX Rayleigh interference detector (Wyatt Technology). The sBVR-A was fractionated according to its molecular weight (Mr) on the S-200 HR gel-filtration column and the molecular mass then analysed from the absolute measurement of the laser scattered light intensity measured by the light scattering (LS) detector. The computer software Astra solved the equation based on Zimm's formalism (equation 7 below) that relates the excess scattered light to the concentration and weight-average molar mass of sBVR-A.

Equation 7: $$K^*c\,/R(\theta) = 1/W_w P(\theta) + 2A_2 c$$

Where $R(\theta)$ is the excess intensity of scattered light at DAWN angle θ , c is the sample concentration, M_w is the weight-average molecular weight (molar mass), A_2 is a second virial coefficient, K* is an optical parameter equal to $4p^2n^2 (dn/dc)^2 / (l_o^4 N_A)$, n is the solvent refractive index and dn/dc is the refractive index increment , N_A is Avogadro's number, l_o is the wavelength of the scattered light in a vacuum. The function $P(\theta)$ describes the angular dependence of scattered light.

2.2.26 UV/Vis spectrophotometric analysis of recombinant proteins

Recombinant proteins were purified as described in Chapter 3 and analysed by UV/Vis spectrometry in the 250-800nm range using a Cary 300 Bio scanning UV-Visible spectrophotometer. Purified recombinant protein (usually 2ml of 0.5mg/ml) in Tris buffer pH7.5, containing 100mM NaCl was placed in a quartz cuvette and the absorbance spectrum measured from 250-800nm.

2.2.27 High performance liquid chromatography (HPLC) separation of ATP, $NADP^+$, NADPH, NAD^+ and NADH standards

Each nucleotide standard (stock 1mM) was freshly prepared in 10mM potassium phosphate buffer, pH7. HPLC analysis was performed using a Shimadzu LC10AT HPLC system with online fluorescence detector (excitation wavelength set at 340nm and emission wavelength set at 460nm) and online photo-diode array detector set from 200-400nm. All buffers were filtered though 0.22μm filters prior to use. The "Supelco Discovery" C18 reversed phase HPLC column (25mm x 4mm) was equilibrated in 100mM potassium phosphate, pH6. Each nucleotide standard (50μl of 100μM) was individually auto-injected onto the HPLC column and run at a flow rate of 0.5ml/min in 100mM potassium phosphate, pH6. A mixture (50μl) containing each standard (100μM) was seperately injected. Elution was achieved using a linear gradient of 40% methanol, 60% potassium phosphate (100mM), pH6 over a 50 minute period. The fluorescence of the eluted compounds was measured by an online fluorescence detector with an excitation wavelength of 340nm and emission set at 460nm and absorption spectra were recorded continuously by an online photodiode array detector in the 220-400nm range.

2.2.28 HPLC analysis of recombinant sBVR-A

sBVR-A purified as described in Section 3.4.3 was analysed using a Shimadzu LC10AT HPLC system with online fluorescence detector (excitation wavelength set at 340nm and emission wavelength set at 460nm) and online photo-diode array detector set from 200-400nm. All buffers were filtered though 0.22μm filters prior to use. The "Supelco Discovery" C18 reversed phase

HPLC column (25mm x 4mm) was equilibrated in 100mM potassium phosphate, pH6. sBVR-A (50µl of 1mg/ml) was mixed with 50µl 12M urea and heated at 85°C for 2min and immediately placed on ice. Precipitated protein was removed by centrifugation at 13,600 x g for 2min at 4°C. 50µl of the supernatant was immediately subjected to HPLC analysis at flow rate of 0.5ml/min in 100mM potassium phosphate, pH6. Elution was achieved using a linear gradient of 0-40% methanol in the same buffer over a 50min period. Detection was by fluorescence and absorbance as described above.

2.2.29 Crystallisation trials of sBVR-A

2.2.29.1 Preparation of protein for crystallisation trials

sBVR-A was cloned, overexpressed and purified as described in Section 3.4. The protein was further purified using 2'5' ADP-Sepharose affinity chromatography as described in Section 2.2.15.1d and gel filtered using Sephadex-200 as described in Section 2.2.15.4 to remove protein aggregates. Following purification the protein was concentrated to approximately 2-5mg/ml as described in Section 2.2.17 in preparation for initial crystallisation screening trials.

2.2.29.2 Initial crystallisation screening trials

Initial screening for crystallisation conditions for sBVR-A was done using the crystallography screening kits Wizard I and Wizard II (Hampton research). These kits contain a large range of buffer and salt conditions which may suit crystallisation of sBVR-A. Initial crystallisation trials were performed using the hanging drop vapour diffusion method in 96 well plates. A 10µl sample of purified sBVR-A was added to 10µl of each buffer on a coverslip. The coverslip was then inverted over a well containing 1ml of the same buffer and sealed using a lubricant. The plates were covered and then left at 4°C or RT and viewed daily using a stereo microscope.

2.2.30 Circular dichroism (CD) analysis of sBVR-A

sBVR-A and sBVR-A mutants were analysed by circular dichroism using a Jasco-J815 CD spectrometer. Proteins were purified as described in Section 3.4.3 and gel-filtered into a buffer suitable for CD analysis in the far UV region as described in Section 2.2.15.3b. This buffer was free from NaCl as chloride ions absorb in the far UV region of the spectrum and phosphate buffer replaced Tris, which also absorbs in this region. For far UV analysis the buffer system used was 50mM NaFl, 100mM NaH_2PO_4, pH7. sBVR-A and sBVR-A mutants at a concentration of 0.5mg/ml were analysed in a 0.1mm path length cuvette. Parameters were as follows: wavelength range of 185-260nm, standard sensitivity (100mdeg), 0.1 nm data pitch, continuous scanning mode, 50nm/min scanning speed, 1 sec response, 1nm bandwidth and an accumulation of 4 scans.

For secondary structure analysis protein was analysed in the 285-260nm range as described above and results were analysed using the online CD analysis program DICHROWEB (Whitmore & Wallace, Lobley *et al.*, 2002). The CD spectra of recombinant sBVR-A was analyzed using the five algorithms available in DICHROWEB and the algorithm which gave the best fit with the lowest normalized root mean squared deviation (nrmsd) was employed. The algorithm CDSSTR and the variable selection method using protein reference set 6 was therefore used for the analysis of sBVR-A.

For analysis of biliverdin binding to sBVR-A and sBVR-A mutants in the visible region (300-700nm) protein (1mg/ml) in 25mM Tris pH7.5, 100mM NaCl was incubated with 10-30μM biliverdin IXα and 100μM $NADP^+$ and CD spectra recorded. Parameters were as follows: 0.1mm path length, wavelength range 300-700nm, 0.1 nm data pitch, continuous scanning mode, 100nm/min scanning speed, 1 sec response, 1nm bandwidth and an accumulation of 4 scans.

2.2.31 Homology modelling of sBVR-A

This is a technique which uses computer software to build a model of an unknown structure by "threading" its amino acid sequence to templates of known and related proteins whose 3D structures has been solved. Three online homology modelling programs were used: Swissmodel (http://www.swissmodel.expasy.org), Phyre (http://www.sbg.bio.ic.ac.uk/phyre/), and ESypred 3D (http://www.esypred-help@urbm.fundp.ac.be) to build the models of sBVR-A. The following proteins were used as templates: rat BVR-A, human BVR-A, glucose-fructose oxidoreductase from *Zymomonas mobilis*, human glyceraldehyde-3-phosphate dehydrogenase, an oxidoreductase from *Thermotoga maritima,* a putative virulence factor oxidoereductase, monkey dihydrodiol dehydrogenase, a flavoprotein from *Photobacterium leiognathi,* LuxP from *Vibrio harveyi*, flavoprotein 390 and yeast enolase. The predicted structures were then modelled and structural alignments performed using Pymol (Delano Scientific).

2.2.32 Construction of the sBVR-A knock-out mutant in *Synechocystis sp.* PCC6803

2.2.32.1 Design of the sBVR-A knock-out construct

The general strategy to inactivate the sBVR-A gene, involved isolating a genomic DNA fragment, which included the sBVR-A gene, plus 250 base pairs upstream and 267 base pairs downstream of the gene. These extra base pairs on either side of the sBVR-A gene would be used as "homology arms" and through homologous recombination would be used to insert an antibiotic resistance "cassette" into the middle of the sBVR-A gene. This strategy was designed to disrupt the sBVR-A gene by separating essential conserved domains required for activity. The antibiotic resistance

gene would also be used to screen for positive transformants by conferring resistance to the antibiotic kanamycin, which is lethal to wild-type *Synechocystis* cells.

2.2.32.2 Construction of the sBVR-A knock-out construct

The DNA sequence of the sBVR-A gene, plus the homology regions was retrieved from the cyanobacterial genome database (www.kazusa.or.jp/cyano/). This genomic DNA fragment was 1500 base pairs in length. PCR primers were designed to amplify this fragment from *Synechocystis sp.* PCC6803 genomic DNA. Following successful amplification, this fragment was cloned into the cloning vector pBluescript SK+ (Stratagene). A unique Hpa-1 restriction site within the sBVR-A gene was selected to create maximum disruption of the gene by insertion of the kanamycin resistance cassette. The transposon Tn903 was selected to insert into the sBVR-A gene. This transposon contains a kanamycin resistance gene, which codes for kanamycin aminoglycoside which degrades kanamycin. The Tn903 transposon also contains the promoters, terminators and regulatory elements required for successful expression of the kanamycin aminoglycosidase gene in *Synechocystis.* The Tn903 transposon was acquired by digestion of the plasmid pUC4K (Amersham Biosciences) with the restriction enzyme Pvu-II. The sBVR-A gene, cloned into pBluescript was digested at the unique Hpa-1 site within the gene. Following purification of the linearised plasmid containing the sBVR-A gene and homology regions the Tn903 transposon was blunt end cloned into the Hpa-1 site within the sBVR-A gene to create the sBVR-A knock-out construct pBBVR-Akan.

2.2.32.3 Screening and sequencing of the pBBVR-Akan knock-out construct

The Tn903 transposon was "blunt end" cloned into the sBVR-A gene meaning it could be inserted in either the forward or reverse orientation. Any positive transformants should now grow on both ampicillin and kanamycin resistant agar because the pBluescript vector confers ampicillin resistance while the Tn903 transposon confers kanamycin resistance. Positive clones were isolated, re-streaked to make individual plates and the plasmid DNA purified as described in Section 2.24. Purified plasmids were then screened by restriction analysis to determine the orientation of the cassette. Plasmids with the sBVR-A gene and the Tn903 transposon in both orientations were verified by sequencing.

2.2.32.4 Transformation of *Synechocystis sp.* PCC6803 cells with the pBBVR-Akan knock-out construct

Synechocystis sp. PCC6803 cells are naturally transformable, meaning they can take up exogenous DNA naturally from their environment and do not need any prior treatment or electroporation in order to introduce exogenous DNA.

A fresh *Synechocystis* culture (50ml) was grown in sterile Bg11 medium, supplemented with 5mM glucose as described in Section 2.2.2 under medium light conditions (447 μEinsteins m^{-2} s^{-1}). This was grown for 2-3 days until the OD_{730} was 0.5. It was important not to let the density exceed this as transformation efficiency declines in late log phase. Under sterile conditions, the cells were then transferred to a sterile 50ml falcon tube and centrifuged at 2760 x g for 5 minutes at room temperature as described previously. The supernatant was discarded and the pellet was resuspended in fresh Bg11 medium (2ml). The cells were diluted to give an OD_{730} of 2.5 put into 0.5ml volumes in sterile culture-cap tubes. 2-10μg of purified pBBVR-Akan DNA was then added to each tube and shaken gently. One tube was left without any DNA as a control. The tubes were placed in the illuminated incubator under medium light for 6 hours, with shaking once after 3 hours. Nucleopore 0.2μm PVDF filters were placed on fresh Bg11 plates supplemented with 5mM glucose. The purpose of these filters was to allow the bacteria to grow on the plates but also to allow for easy transfer to fresh plates. 200μl of the transformation cells were then plated onto these filters on the Bg11 plates. The filters were allowed to dry and then transferred to the illuminated incubator and allowed to grow for 12 hours under medium light. After 12 hours the filters were removed from the Bg11 plates and transferred to fresh Bg11 plates which also contained 12.5μg/ml kanamycin. After a further 3 days the filters were transferred to fresh Bg11 plates which contained 25μg/ml kanamycin and were allowed to grow under medium light for 2 weeks. After approximately 3-4 days the wild-type cells died and after a further 1-2 weeks kanamycin resistant colonies appeared. Antibiotic resistant colonies (100) were picked and re-plated on fresh Bg11 plates containing 5mM glucose and 25μg/ml kanamycin.

2.2.32.5 Genomic screening of antibiotic resistant clones

2.2.32.5a Screening by PCR

A number of PCR protocols were designed to determine if the "knock-out" construct had inserted into the correct place in the *Synechocystis* genome and to examine the degree of segregation of wild-type from knock-out alleles. The first PCR protocol was used to verify correct placement of the construct in the genome. Primers for this PCR were designed to bind to a region of genomic DNA that was upstream of the sBVR-A gene and outside the homologous region used for

recombination (forward primer) and within the kanamycin resistant cassette (reverse primer), which was not present in wild type *Synechocystis* genomic DNA. Using this method, the only possible way a PCR product of the correct size could be obtained was if the cassette was located in the correct place in the *Synechocystis* genome. Individual primer sequences are shown in Table 7.1. Primers were also designed to estimate the level of segregation of knock-out alleles from wild-type alleles. In this case the primers were designed to flank the sBVR-A gene. The forward primer was designed to bind to a region of genomic DNA that was upstream of the sBVR-A gene and outside the homologous region used for recombination and the reverse primer was designed to bind to a region of genomic DNA downstream of the sBVR-A gene and outside the homologous region used for recombination. Using this method, 2 PCR products would be obtained, depending on the level of segregation. If the knock-out construct was not present or was present only in a small number of copies, then the PCR product obtained would be mostly the wild-type sBVR-A gene plus homology regions and extra DNA. This would show up as the major band on an agarose gel. A second PCR product consisting of the wild type fragment plus the 1550 bp kanamycin resistant cassette would not be present in many copies and would be the minor band on the agarose gel. As segregation increases and the knock-out allele becomes more dominant, eventually replacing all wild-type copies of the gene this can be visualised on an agarose gel. If segregation does not occur then the bands will not change in intensity and the major band will always be the wild-type allele. Using this protocol the degree of segregation of the wild-type allele from the knock-out allele can be monitored.

A knock-out allele specific PCR was also designed to differentiate between wild-type and targeted alleles. Purified wild-type or targeted genomic DNA (2μg) was digested with 0.5units Xho-1. There is a Xho-1 restriction site within the kanamycin resistant cassette but not in the sBVR-A gene or homology regions. 20ng of the digested DNA was purified using Qiagen's "PCR quick" purification kit and used in the PCR reaction shown in Table 2.3, using the segregation screening primers as described above.

2.2.32.5b Screening by Western blotting

A number of selected clones were cultured in Bgll medium supplemented with 5mM glucose and 50μg/ml kanamycin until the OD_{730} was approximately 0.7. *Synechocystis* cytosols were prepared for western blotting as described in Section 2.2.19.1c and probed with anti-sBVR-A antibodies at a dilution of 1:1000 in TBST containing 10% (w/v) Marvel. Blots were washed and probed with HRP conjugated anti- rabbit secondary antibody at a dilution of 1:20,000 and developed as described in Section 2.2.19.4.

2.2.33 Analysis of the sBVR-A mutant phenotype

2.2.33.1 Analysis of the growth characteristics of wild-type and sBVR-A knock-out cells

Wild-type *Synechocystis* (50ml) and sBVR-A mutant cells (50ml) were cultured as described in Section 2.2.2 in Bg11 medium supplemented with 5mM glucose until the OD_{730} was 0.5-0.8. At this point the cells were transferred to sterile 50ml tubes and harvested by centrifugation at 4000 x g at 4°C for 5 min. Cells were washed 3 times by repeated resuspension in fresh Bg11 medium and centrifugation to remove all traces of glucose and antibiotic. After the final wash step the cells were resuspended in 5ml fresh Bg11 medium and their OD_{730} was recorded. Fresh 50ml Bg11 cultures were prepared and inoculated with the cultures from the previous step until the OD_{730} was exactly 0.05. Cultures were grown under medium light (447 μEinsteins m^{-2} s^{-1}) with 12hours light/12 hours dark at 30°C and the cell number in each culture was determined every 24hours by their OD_{730} or by counting using a haemocytometer and a stereo microscope and used to build growth curves. Growth conditions were varied by increasing the amount of light or making additions to the growth medium. Growth characteristics of wild-type and sBVR-A mutant cells were also evaluated under conditions of light stress (895 μEinsteins m^{-2} s^{-1} and 24hours light). Growth characteristics in the presence of bilirubin IXα were investigated by growing cultures until the OD_{730} was 0.5-0.8 and diluted into fresh Bg11 medium until the OD_{730} was 0.05 as described above. At this point 100nM bilirubin IXα was added to the culture and the culture was placed in the growth chamber in the dark for 12 hours. Cell number was evaluated as described above. Cells were treated with 100nM bilirubin IXα and left in the dark for 1hour per day following bilirubin treatment until the OD_{730} was approximately 0.3. Bilirubin concentration was increased to 1μM per 24 hours for the remainder of the growth period.

2.2.33.2 Analysis of the photosynthetic and carotenoid pigments of wild-type *Synechocystis* and sBVR-A mutant cells

2.2.33.2a Preparation of pigments

Cells were cultured (50ml) in BG11 medium under low (224 μEinsteins m^{-2} s^{-1}), medium (447 μEinsteins m^{-2} s^{-1}) or high light (895 μEinsteins m^{-2} s^{-1}) until the OD_{730} was 0.7. Cells were harvested by centrifugation washed with ice cold PBS and immediately snap-frozen in liquid nitrogen and freeze-dried overnight at -50°C under a vacuum using a Labconco Freezone Plus Freeze-dry system and stored at -80°C. Pigments were extracted from freeze-dried cells by three successive extractions by resuspension and centrifugation with 100% methanol containing 0.1% NH_4OH in the dark and on ice. The extracts were then combined and either concentrated under a stream of nitrogen or diluted in 100% methanol containing 0.1% NH_4OH prior to analysis.

2.2.33.2b HPLC analysis of the pigment extracts

Pigments extracted using this method were usually too concentrated for HPLC analysis and were therefore diluted 1:10 (v/v) with 100% methanol containing 0.1% NH_4OH and immediately subjected to HPLC analysis using a Shimadzu LC10AT HPLC and a "Supelco Discovery" C18 reversed phase HPLC column (25mm x 4mm). The column was equilibrated with acetonitrile-water-triethylamine (9:1:0.01, vol/vol/vol). Pigments were eluted with a linear 18min gradient of ethyl acetate (0-95%) at a flow rate of 1ml/min. The absorption spectra of the eluted pigments were recorded continuously by an online photodiode array detector in the 280-660nm range.

2.2.33.2c Mass-spectrometry analysis of pigments

Selected pigments were subjected to further analysis by mass-spectrometry. Pigments separated by HPLC as described above were collected in individual fractions (100-500µl). This was repeated several times to obtain sufficient amounts for analysis and the fractions of individual pigments were pooled, concentrated under a stream of nitrogen in the dark and stored overnight at -80°C. The individual pigments were either diluted 1 in 10 (v/v) or 1 in 2 (v/v) in 100% HPLC grade methanol (depending on the signal) as the solvent and subjected to mass analysis and mass spectra were obtained by matrix-assisted laser desorption ionisation time of flight (MALDI-TOF) mass spectrometry using a Waters Q-TOF premier mass spectrometer in electrospray + mode.

2.2.34 Electron microscopy using immuno-gold labelled antibodies

Synechocystis cells were cultured as described in Section 2.2.2 under medium levels of light (447 Einsteins m^{-2} s^{-1}) and in the presence of 5mM glucose until the OD_{730} was approximately 0.5. At this point the cells were harvested by centrifugation and washed with ice cold PBS (10mM potassium phosphate, 150mM NaCl, pH 7.4). Cell pellets were fixed at room temperature for 2 hours in a solution containing 4% (v/v) paraformaldehyde and 2% glutaraldehyde in PBS as the fixative. Samples were then transferred to fresh fixative and stored overnight at 4°C. For ultrastructure examination samples were embedded in Spurr resin according to the manufacturer's instructions were then cut into 80nm sections using a microtome and mounted on copper grids. For immunolabelling, samples were embedded in LR White medium grade resin, cut into 90-100nm thick sections using a microtome and mounted on Formvar-coated nickel grids. Sections were incubated for 1.5 hours with anti-BVR-A antiserum (purified as described in Section 2.2.21 at a final dilution of 1:500 (v/v) in PBS. The samples were then washed (4 x 3 min) with 1% (w/v) BSA in PBS. Immunogold (6nm) - conjugated goat anti-rabbit IgG was added at a dilution of 1:100 (v/v) in PBS and the samples were incubated at room temperature for 2 hours or overnight at 4°C. Samples were washed (4 x 3 min) with PBS and rinsed with a gentle stream of de-ionised

water. Sections were stained with uranyl acetate and lead citrate and viewed with a transmission electron microscope at an operating voltage of 75kV.

Luria-Bertani (LB) Broth

10 g/l NaCl
10 g/l Tryptone
5 g/l yeast extract
Made up to 1litre with ddH_20

Autoclaved at 121°C for 20 min and stored at 4°C

LB agar

10 g/l NaCl
10 g/l Tryptone
5 g/l yeast extract
15 g/l agar
Made up to 1litre with ddH_20

Autoclaved at 121°C for 20 min and stored at 4°C

PSI Broth

5 g/l yeast extract
20 g/l Tryptone
5 g/l magnesium sulphate
Made up to 1litre with ddH_20

Autoclaved at 121°C for 20 min and stored at 4°C

SOC medium

20 g/l Tryptone
5 g/l yeast extract
0.5 g/l NaCl
2.5 ml KCl (1M)
Made up to 1litre with ddH_20

Autoclaved at 121°C for 20 min and stored at 4oC

Table 2.1 Media used for the preparation, culturing, and transformation of *E.coli*

Bg11 medium	
$NaNO_3$	1.5 g/l
$MgSO_4.7H_20$	75 mg/l
$CaCl_2.2H_20$	36 mg/l
Citric acid	0.6 mg/l
NaEDTA (250mM), pH 8	11.2 µl
Ammonium iron (III) citrate	0.006 mg/l
Na_2CO_3	0.02 mg/l
K_2HPO_4	0.0305mg/l
5mM HEPES, pH8	
Trace minerals (see below)	1ml / l
ddH20	to 1 litre
Usually a 100 x stock is made and autoclaved and diluted 1 in 100 in ddH20 and autoclaved prior to use Autoclaved at 121°C for 20 min and stored at 4°C	

Trace minerals	
H_3BO_3	2.86 g/l
$MnCl_2.4H_20$	1.8 g/l
$ZnSO_4.7H_20$	0.222 g/l
$Na_2MoO_4.2H_20$	0.39 g/l
$CuSO_4.5H_20$	0.079 g/l
$Co(NO_3)_2.6H_20$	0.0494 g/l

Table 2.2 Composition of Bg11 medium for the culturing of *Synechocystis* sp. PCC6803

Components of PCR reaction	Volume
DNA Template (10ng/µl)	1.0µl
pfu turbo reaction buffer (5x)	2.5µl
dNTPs (2mM each)	2.0µl
Gene specific Forward primer(10pmoles/µl)	1.0µl
Gene specific Reverse primer (10pmoles/µl)	1.0µl
Nuclease Free Water (NFW)	17.0µl
pfu turbo polymerase (1unit/µl)	0.5µl

Table 2.3 Components of the PCR reaction.

The DNA template is usually genomic DNA purified from *Synechocystis* sp. PCC6803cells. Primer sequences can be seen in the sections relevant to a particular PCR. The total reaction volume is 25µl

Step	Cycle name	Temperature (^{o}C)	Time (min)
1	Hot start	95	2
2	Denaturation	95	0.5
3	Annealing	*	0.5
4	Elongation	72	1
5	No. Cycles	32 x step 2	
6	Polishing	72	7
7	Hold & Cool	4	∞

Table 2.4 PCR cycle conditions.

The conditions are identical for amplification of all DNA fragments using *pfu* described in the relevant sections. The annealing temperature is changed to suit the melting temperature of the specific primers. For sBVR-A the annealing temperature was 55^{o}C, HO1/HO2: 60^{o}C, PcyA: 62^{o}C, Fer/FNR: 55^{o}C and for the sBVR-A knock-out fragment: 60^{o}C

Component	Ligation reaction (µl)	Control reaction (µl)
DNA Insert	4	0
Plasmid	1	1
Takara Ligation Mix	5	5
NFW	0	4
Total Volume	10	10

Table 2.5 Components of the ligation reaction.

The reaction was set up as described and incubated at 16°C overnight. The entire reaction mix was used to transform competent cells the next day.

Compound	Final Conc.
MOPS (pH7)	10 mM
Calcium chloride	75 mM
Rubidium chloride	10 mM
Glycerol	15% (v/v)
Filtered through a 0.22µm filter	

Table 2.6 Components of buffer TfBII used for the preparation of competent cells.

Component	Final volume (µl)	Final concentration
5 x green or colorless GoTaq Flexi buffer	5	1 x
MgCl2 solution (25mM)	2	2mM
Takara dNTP mix (2.5mM each)	4	0.2mM each dNTP
Forward primer (10pmol/µl)	1	0.4µM
Reverse primer (10pmol/µl)	1	0.4µM
E.coli culture	2	
MiliQ H20	9.75	
GoTaq polymerase (5units/µl)	0.25	1.25 units

Table 2.7 Components of the PCR reaction used for screening for positive clones

Step	Cycle name	Temperature (^{o}C)	Time (min)
1	Hot start	95	5
2	Denaturation	98	0.16
3	Annealing	60	0.5
4	Elongation	72	2
5	No. Cycles	35 x step 2	
6	Polishing	72	8
7	Hold & Cool	4	∞

Table 2.8 PCR cycling conditions for screening for positive clones

Primer	Sequence	Size	Tm (°C)	GC (%
M13 rev (-29)	CAGGAAACAGCTATGACC	18	53.7	50
M13 rev (-49)	GAGCGGATAACAATTTCACACAGG	24	61	46
M13 uni (-21)	TGTAAAACGACGGCCAGT	18	53.7	50
M13 uni (-43)	AGGGTTTTCCCAGTCACGACGTT	23	62.4	52
M13 (-96)	TGAGTTTCGTCACCAGTA	18	51.4	44
SP6	CATTTAGGTGACACTATAG	19	50.2	37
T3	AATTAACCCTCACTAAAGGG	20	53.2	40
T7	TAATACGACTCACTATAGGG	20	53.3	40
T7 term	CTAGTTATTGCTCAGCGGT	19	54.5	47
pGex for	ATAGCATGGCCTTTGCAGG	19	56.7	53
pGex rev	GAGCTGCATGTGTCAGAGG	19	58.8	58

Table 2.9 List of standard sequencing primers used to sequence cloned DNA fragments in plasmids

Component	12% Resolving gel (ml) 5cm/16cm gel	5% stacking gel (ml) 5cm/16cm gel
Acrylamide (30%)	3.33 / 15	0.54 / 1.08
Bis-acrylamide (0.8%)	0.67 / 2.6	0.13 / .26
Tris (1.5 M, pH 8.8)	2.5 / 10	0
Tris (1 M, pH 6.8)	0	0.5 / 1
Distilled water	3.3 / 13.2	2.7 / 5.5
SDS (10%, w/v)	0.1 / 0.4	0.04 / 0.08
TEMED	0.004 / 0.016	0.004 / 0.008
Ammonium persulfate (10% w/v)	0.1 / 0.4	0.04 / 0.08

Table 2.10 Components of the 12% SDS polyacrylamide gel

CHAPTER 3

RECOMBINANT PRODUCTION OF THE PROTEINS OF HEME METABOLISM AND PHYCOBILIN BIOSYNTHESIS FROM *SYNECHOCYSTIS*

3.1 Introduction

Phycobiliproteins are the major light-harvesting proteins in cyanobacteria. Phycobilins (phycocyanobilin and phycoerythrobilin), the linear tetrapyrrole chromophores of the phycobiliproteins which serve as the light-harvesting pigments of cyanobacteria are synthesised from heme by the action of a ferredoxin-dependent heme oxygenase (HO). Phycocyanobilin ferredoxin oxidoreductase (PcyA) and biliverdin IXα reductase (sBVR-A) in turn convert the product of the heme oxygenase reaction, biliverdin IXα, to phycocyanobilin and bilirubin IXα respectively. This system is crucial for the growth and survival of cyanobacteria and it is possible that the system or some of its components participate in other unknown functions. By studying this system and its components *in vitro* it is hoped to gain information about how it functions *in vivo*.

3.2 Production and purification of recombinant *Synechocystis sp.* PCC6803 heme oxygenase 1 (HO1)

3.2.1 Amplification of HO1 DNA

The DNA coding for HO1 was amplified from *Synechocystis sp.* PCC6803 genomic DNA using synthetic oligonucleotide primers. PCR primers were designed based on sequences retrieved from Cyanobase (www.bacteria.kazusa.or.jp/cyanobase/.) The forward primer (Oligo. 1 in Table 3.1) contained a BamH1 site in the 5' sequence and the reverse primer (Oligo. 2 in Table 3.1) contained a HindIII site. Both primers contained 3 base pair overhangs, which facilitated binding of the particular restriction endonuclease. The exact components of the HO1 PCR reaction and the cycle conditions used for amplification are described in Tables 2.3 and 2.4. The products of the PCR reaction (10μl) were analysed by agarose gel electrophoresis. The predicted PCR product for HO1 was 723 bps which was consistent with the mobility on agarose gel electrophoresis (see Fig. 3.1A).

3.2.2 Cloning of HO1 into the expression plasmid pET41a (mod)

3.2.2.1 Restriction enzyme digestion of HO1 and pET41a (mod)

The HO1 PCR product was analysed by agarose gel electrophoresis, extracted from the gel and purified as described in Section 2.2.7.3. The pET41a (mod) vector was purified, as described in Section 2.2.4. The HO1 PCR product had compatible "sticky" ends for "in-frame" cloning into the BamH1 and HindIII sites of pET41a (mod). The restriction enzyme reactions for HO1 and pET41a

(mod) were carried out as described in Section 2.2.7.4. and the products analysed by agarose gel electrophoresis and purified as described in Sections 2.2.5 and 2.2.7.2.

3.2.2.2 Ligation of HO1 DNA into the expression vector pET41a (mod)

The linearised expression vector was treated with bacterial alkaline phosphatase (BAP) to prevent self-religation and purified as described in Section 2.2.7.2. Ligation was carried out using Takara's ligation kit, version 2.1.1. The ligation reactions were incubated overnight at 16°C and the next day the complete contents of the reaction were used to transform competent *E.coli* XL-1 Blue cells as described in Section 2.2.9.

3.2.3 Screening for positive pET.HO1 transformants by restriction analysis

When ligation controls were clear, single colonies were picked from the ligation plates and re-plated onto kanamycin resistant master plates. Single colonies were cultured and the purified plasmid DNA was subjected to restriction analysis as described previously. The agarose gel electrophoresis analysis in Fig. 3.1B shows two clearly visible bands. A large molecular weight band (approximately 6000bp) corresponds to the linearised pET41a (mod) vector and a smaller band (approximately 700-800bp) that corresponds to the HO1 DNA insert. Following identification of positive clones pET41a (mod).HO1 was renamed pET.HO1 and the purified plasmid DNA containing the HO1 insert was sequenced as described in Section 2.2.12. The purified pET.HO1 was then transformed into *E.coli* BL21 (DE3) cells for expression of recombinant protein. In addition, permanent glycerol stocks of the expression plasmids were made as described in Section 2.2.13.

3.2.4 Purification of recombinant *Synechocystis* HO1

E.coli BL21 (DE3) cells transformed with the pET.HO1 plasmid were verified by their ability to grow on kanamycin agar. The cells were cultured and harvested as described in Section 2.2.14. The harvested cells were pale green in colour, indicating the overexpression of heme oxygenase and the formation of biliverdin or verdohaem. The pelleted cells were then stored at -20 °C overnight.

3.2.4.1 Glutathione-Sepharose affinity chromatography of GST-HO1

The harvested *E.coli* cells were resuspended, incubated with lysozyme, sonicated and centrifuged as described in Section 2.2.14. The glutathione-Sepharose affinity column was equilibrated as described in Section 2.2.15.1a. The cell lysate supernatant was loaded onto the glutathione-Sepharose affinity column, washed with 10 column volumes of Tris buffer (25mM Tris, 150mM

NaCl, pH7.5) and eluted with 5mM reduced glutathione in equilibration buffer. Fractions (2ml) were collected, the absorbance at 280nm was monitored and the peak fractions were pooled. After this initial purification step, the GST-HO1 fusion protein was approximately 50% pure, as judged by SDS-PAGE (see lane 6 of Fig. 3.2).

3.2.4.2 Ni^{2+}-Sepharose affinity chromatography of GST-HO1

The modified pET41a expression vector has an internal hexahistidine tag, in addition to the GST tag. This property was exploited to purify the fusion protein by Ni^{2+}-Sepharose affinity chromatography. This was prepared and equilibrated as described in Section 2.2.15.1c. The fusion protein was loaded, washed and eluted with 250mM imidazole. Fractions (2ml) were collected, the absorbance at 280nm was monitored and the peak fractions were pooled. Imidazole also absorbs at 280nm and the spectrophotometer was blanked against the elution buffer which contained 250mM imidazole in equilibration buffer. After this purification step the protein was approximately 70% pure (see lane 7 in Fig. 3.2).

3.2.4.3 G25 gel filtration chromatography

The pooled fractions were gel filtered as described in Section 2.2.15.3 to remove the imidazole. The void volume was determined using Blue dextran to be 175ml. Fractions (2ml) were collected and the absorbance at 280nm was monitored. The GST-HO1 fusion protein eluted in the void volume. The peak fractions were again pooled.

3.2.4.4 On-column cleavage and removal of the GST fusion protein

Following gel filtration the fusion protein was cleaved using thrombin and the GST moiety removed on S-hexyl glutathione-Sepharose. The GST-HO1 fusion protein was loaded onto the S-hexyl glutathione-Sepharose column and washed with 10 column volumes of Tris buffer (see Section 3.6.1). Thrombin (40units) in thrombin cleavage buffer (50mM Tris/HCL, 2.5mM $CaCl_2$, 150mM NaCl, pH7.8) was slowly loaded onto the column and the column then clamped and left at 4°C overnight. The next day the column was unclamped and HO1 eluted. After this purification step the protein was judged by SDS-PAGE to be more than 95% pure (see lane 8, Fig. 3.2). Purified protein was stored at -80°C in 10% (v/v) glycerol.

3.3 UV/Vis spectrometry analysis of recombinant HO1

The recombinant HO1 purified in the previous sections was pale green in colour indicating the presence of a bound chromophore. The chromophore was analysed by UV/Vis spectrophotometry.

Fig. 3.3 shows that the spectrum obtained tentatively identifies the chromophore as biliverdin with absorbance maxima at 678nm and 378nm.

3.4 Production and purification of recombinant *Synechocystis* biliverdin IXα reductase (sBVR-A)

3.4.1 Amplification and cloning of sBVR-A DNA

Synthetic oligonucleotide primers used to amplify the protein coding DNA sequence of sBVR-A were designed based on sequences retrieved from Cyanobase and are shown in Table 3.1. *Synechocystis sp.* PCC6803 genomic DNA served as the target for amplification. The forward primer (Oligo. 3 in Table 3.1) incorporated a BamH1 site which facilitated "in-frame" cloning and the reverse primer (Oligo. 4 in Table 3.1) contained an Xho-1 site for cloning into the expression vector pET41a (mod). The PCR reaction components and cycle conditions can be seen in Tables 2.3 and 2.4. When the PCR reaction was complete samples (10μl) were analysed by agarose gel electrophoresis. The PCR product for sBVR-A was predicted to be 953bp. In the agarose gel electrophoresis analysis in Fig. 3.4A a band corresponding to this mobility is shown. The PCR product was extracted and purified from the agarose gel as described in Section 2.2.7.3 and digested with BamH1 and Xho-1 for cloning into the pET41a (mod) expression vector. The purified pET41a (mod) vector was also digested with BamH1 and Xho-1 and treated with bacterial alkaline phosphatase and purified as described in Section 2.2.4. The protocols for the ligation and transformation reactions are described in Sections 2.2.8 and 2.2.9, respectively.

3.4.2 Screening of pET.BVR-A transformants by restriction analysis

Antibiotic resistant clones were picked, re-plated on master plates and their plasmid DNA isolated and analysed by restriction analysis (see Section 2.2.7.4). The restriction analysis shows a large molecular weight band (approximately 6000bp) that corresponds to the linearised vector and a smaller band (approximately 1000bp) that corresponds to the sBVR-A DNA insert (see Fig 3.4B). Following identification of positive clones, the expression plasmid was renamed pET.BVR-A, sequenced and transformed into BL21 (DE3) cells.

3.4.3 Purification of recombinant *Synechocystis* BVR-A

BL21 (DE3) cells transformed with the pET.BVR-A expression plasmid were cultured, induced, harvested and lysed as described in Section 2.2.14.

3.4.3.1 Glutathione -Sepharose affinity chromatography of GST-BVR-A

The GST-BVR-A fusion protein was purified from the cell lysate supernatant using glutathione-Sepharose affinity chromatography as described in Section 2.2.15.1a. Following this initial purification step the GST-BVR-A fusion protein was approximately 90% pure, as estimated by SDS-PAGE (see lane 6 of Fig. 3.5).

3.4.3.2 Cleavage of the GST-BVR-A fusion protein

The fusion protein eluted from the glutathione-Sepharose affinity column was cleaved overnight in thrombin buffer containing 0.01% (v/v) NP-40 and thrombin (40units) with gentle mixing. The following day the protein was gel filtered to remove unwanted solutes as described in Section 2.2.15.3.

3.4.3.3 Removal of the GST moiety by S-hexylglutathione-Sepharose affinity chromatography

The GST moiety, following cleavage from the BVR-A was removed by S-hexyl glutathione-Sepharose affinity chromatography. The S-hexylglutathione Sepharose was prepared and equilibrated as described in Section 2.2.15.1a. The affinity resin (10ml) was added to the cleaved GST/BVR-A protein mixture and mixed gently for 45min at 4°C. The S-hexylglutathione-Sepharose protein mix was then loaded into a 5ml column (10 x 1cm) and clamped. The column was unclamped and the BVR-A released in the eluate while the GST remained bound to the S-hexylglutathione Sepharose. After this final purification step the sBVR-A was judged to be more than 95% pure, as estimated by SDS-PAGE (see lane 9 of Fig. 3.5). The sBVR-A protein was either further purified or stored at -80°C in 10% (v/v) glycerol.

3.5 UV/Vis spectrometric analysis of recombinant sBVR-A

The recombinant sBVR-A purified in the previous sections was colourless, however, the normal protein absorbance peak at 280nm was masked by an additional absorbance at 260nm. The absorbance spectrum in Fig. 3.6 shows that the major peak is shifted from the expected maximum at 280nm to a maximum at 260nm indicating the presence of an additional component that absorbs at 260nm. The nature of this component was investigated further (see below).

3.6 A_{280}/A_{260} ratio of recombinant sBVR-A

Spectral analysis of sBVR-A indicates an absorption peak with a maximum at 260nm. The A_{280}/A_{260} ratio of sBVR-A is low, between 0.5 and 1, indicating the presence of bound nucleotide in protein as an absorbance at 260nm is consistent with a nucleotide.

3.7 HPLC analysis of the nucleotide bound to sBVR-A

3.7.1 HPLC separation of ATP, $NADP^+$, NADPH, NAD^+ and NADH

The reversed phase HPLC method of Markham *et al.,* (2004) was used to separate a mixture of ATP, $NADP^+$, NADPH, NAD^+, and NADH standards for identification of the nucleotide bound to sBVR-A. A mixture of each standard (50µl of 100µM) was loaded onto a "Supelco Discovery" C18 reversed phase HPLC column at a flow rate of 0.5ml/min in 100mM potassium phosphate, pH6. The HPLC column was pre-equilibrated in the same buffer. Elution was achieved using a gradient of 40% methanol, 60% potassium phosphate (100mM), pH6 over a 50 minute period. Fig. 3.7 shows the successful separation of the following nucleotides with the retention times indicated in brackets ATP (12min), $NADP^+$ (29min), NADPH (38min), NAD^+ (39min) and NADH (42min). The elution of the compounds was detected at 254nm using a photo-diode array detector and also a fluorescence detector with the excitation wavelength set at 340nm and emission wavelength at 460nm (see Fig. 3.8). The absorbance spectra of the eluted compounds are shown in Fig. 3.9.

3.7.2 HPLC analysis of sBVR-A and bound nucleotide

The HPLC analysis of sBVR-A was performed as described in Section 2.11. The urea and heat treated protein sample (50µl) was centrifuged at 13,000 x g for 5min and immediately loaded onto the C18 reverse phase HPLC column and eluted using the same buffer and elution system described in Section 2.2.27. The absorbance and fluorescence were also detected as described in Section 3.6.1. The elution profile shown in Fig. 3.10 shows a number of peaks which absorb at 254nm. Only one of these peaks was easily identifiable as a pyridine nucleotide. The retention time (Fig. 3.10), fluorescence (Fig. 3.11) and absorbance spectrum (Fig. 3.12) made the tentative identification of peak C at 38min as NADPH. However, with the exception of peak A in Fig. 3.10 at 5min which was identified as protein through a positive reaction with Bradford reagent there were a number of peaks which absorbed at 254nm which were not easily identifiable.

3.8 2'5' ADP-Sepharose affinity chromatography analysis of nucleotide bound to sBVR-A

Affinity chromatography was conducted using 2'5' ADP-Sepharose as described in Section 2.2.15.1d. The idea behind these experiments was to test the hypothesis that a common nucleotide binding site on sBVR-A is able to bind to a matrix bound 2'5' ADP and therefore promote desorption of reversibly bound nucleotide which can then be analysed by reverse phase HPLC. Binding to the affinity matrix must promote exchange of the bound nucleotide with the immobilised ADP. Whatever is released from the protein or remains bound can then be analysed by reverse phase HPLC. Figs 3.13, 3.14, 3.15 clearly show that adsorption of sBVR-A to the affinity matrix promotes release of all other components which are then released in the flow

through. When compared with Fig. 3.10 it is clear that the only peak which is missing in Fig. 3.13 is that of the protein (peak A). Fig. 3.16 clearly shows that when the bound protein was eluted and analysed by reverse phase HPLC it was now free from nucleotide as only the protein peak was now present. These experiments account for the protein and all the compounds bound, although the identity of peaks B and D has not been defined. The tight binding of peaks B and D to the enzyme would not be inconsistent with 2'5' ADP or some related structure.

3.9 Cloning and purification of *Synechocystis* phycocyanobilin ferredoxin oxidoreductase (PcyA)

3.9.1 Amplification and cloning of PcyA DNA

Synthetic oligonucleotide primers were used to amplify the protein coding sequence of PcyA from *Synechocystis sp.* PCC6803 genomic DNA and are shown in Table 3.1. The forward primer (Oligo. 5 in Table 3.1) incorporated a BamH1 site and the reverse primer (Oligo. 6 in Table 3.1) contained a Pst1 restriction site, for cloning into the vectors pBluescript SK+ and pET41a (mod). The PCR conditions and components are shown in Tables 2.3 and 2.4. When the PCR reaction was complete samples (10µl) were analysed by agarose gel electrophoresis. Figure 3.17A shows that a PCR product of the predicted size (793bp) was obtained. The PcyA PCR product was extracted from the gel, purified and digested sequentially with BamH1 and Pst1. The cloning vector pBluescript SK+ was also digested with BamH1 and Pst1 and purified as described in Sections 2.2.7.4 and 2.2.7.2. Following treatment of the vector with bacterial alkaline phosphatase the purified PcyA PCR product was ligated into pBluescript SK+ and transformed into *E.coli* XL-1 Blue cells as described in Sections 2.2.8.3 and 2.2.9.2.

3.9.2 Screening for positive pBlue.PcyA transformants by restriction analysis

Ampicillin resistant clones were picked, replated and analysed by restriction analysis (see Section 2.2.10.1). The plasmid was cut sequentially, first with BamH1 and then with Pst1. The analysis in Fig. 3.17B (lanes 2-4) shows two bands; a large molecular weight band (approximately 3000bp) that corresponds to the linearised vector and a smaller band (approximately 700-800bp) that corresponds to the PcyA DNA insert. Positive clones were renamed pBlue.PcyA.

3.9.3 Subcloning of PcyA into the expression vector pET41 (mod)

The PcyA DNA was excised from the pBluescript SK+ cloning vector using BamH1 and Pst1, fractionated on an agarose gel, extracted and purified. pET41a (mod) was also digested with BamH1 and HindIII and purified. The PcyA DNA was then ligated into the bacterial alkaline phosphatase treated pET41a (mod) expression vector as described in Section 2.2.8.3. Positive

clones were identified by restriction analysis (see Section 3.14.2) and renamed pET.PcyA. The results of this analysis are shown in Fig. 3.17B (lanes 5-10). Plasmid DNA was isolated from pET.PcyA clones, sequenced and transformed into BL21 (DE3) cells and permanent glycerol stocks were made as described in Section 2.2.13.

3.9.4 Purification of recombinant *Synechocystis* PcyA

Recombinant PcyA was purified as described in Section 3.6. *E.coli* BL21 (DE3) cells transformed with the pET.PcyA expression plasmid were cultured, induced with IPTG, harvested and lysed as described in Section 2.2.14. The cell lysate supernatant was loaded onto a glutathione-Sepharose affinity column equilibrated with Tris buffer (25mM Tris, 150mM NaCL, pH7.5), washed with the same buffer until the absorbance at 280nm was below 0.04 and the GST-PcyA fusion protein eluted in the same buffer containing 5mM reduced glutathione. The fusion protein was approximately 70% pure after this initial purification step (see lane 6 in Fig. 3.18). The fusion protein was then loaded onto the Ni^{2+} affinity column, washed and eluted as described in Section 2.2.15.1c. After this second affinity chromatography step the fusion protein was approximately 80% pure as estimated by SDS-PAGE (see lane 7 in Fig. 3.18). The fusion protein was gel-filtered and cleaved with thrombin on an S-hexylglutathione Sepharose affinity column as described in Section 2.2.16.2. This step released PcyA which was eluted with running buffer, leaving the GST moiety bound to the affinity resin. The recombinant PcyA was judged to be 90% pure after this final purification step, as estimated by SDS-PAGE (see lane 8 in Fig. 3.18).

3.10 UV/Vis spectrometric analysis of recombinant PcyA

The recombinant PcyA purified in the previous sections was further analysed by UV/Vis spectrometry. The protein was colourless and Fig. 3.19 shows that the spectrum obtained contains the protein peak at 280nm, although there is absorbance from 300-500nm which is consistent with bound ferredoxin (see Fig. 3.18).

3.11 Production and purification of recombinant *Synechocystis* Ferredoxin and Ferredoxin $NADP^+$ reductase (FNR)

3.11.1 Amplification and cloning of *Synechocystis* Ferredoxin and Ferredoxin $NADP^+$ reductase (FNR)

Synthetic oligonucleotide primers used for the amplification of the protein coding sequences of ferredoxin and ferredoxin $NADP^+$ reductase were designed based on DNA sequences retrieved from Cyanobase and are shown in Table 3.1. The forward primers (Oligos. 7 and 9 in Table 3.1)

incorporated a BamH1 site and the reverse primers (Oligos. 8 and 10 in Table 3.1) contained a HindIII restriction site, for cloning into the expression vector pET41a (mod). Genomic DNA from *Synechocystis* sp. PCC6803 served as the target for amplification. The PCR reaction components and cycling conditions are shown in Tables 2.3 and 2.4. When the PCR reactions were complete samples (10µl) of each were analysed by agarose gel electrophoresis. Fig. 3.20A shows the PCR product of the predicted size (297bp) for ferredoxin and Fig. 3.20B shows the PCR product of the predicted size (1242bp) for FNR. The ferredoxin and FNR PCR products were extracted from the agarose gels, purified and digested sequentially with BamH1 and HindIII. The expression vector pET41a (mod) was also digested with BamH1 and HindIII and purified as described previously in Sections 2.2.7.4 and 2.2.7.2. Following treatment of the vector with bacterial alkaline phosphatase the purified ferredoxin and FNR PCR products were ligated into pET41a (mod) and transformed into *E.coli* XL1-Blue cells as described in Sections 2.2.8.3 and 2.2.9.2.

3.11.2 Screening for pET.Fer and pET.FNR clones by PCR

Following transformation into *E.coli* XL-1 Blue cells, colonies of each ferredoxin and ferredoxin reductase transformation were picked, re-plated on master plates and cultured in 500µl of LB medium at 37°C as described in Section 2.2.10.2. When the culture appeared turbid samples (2µl) were added to the PCR reaction shown in Table 2.7 and the PCR reaction was carried out under the conditions shown in Table 2.8. If the required insert was present it was re-amplified from the plasmid vector and was visualised by agarose gel electrophoresis. Fig. 3.21 shows positive clones could easily be identified by the presence of a re-amplified fragment of the correct size. Fig. 3.21A shows the PCR analysis of the ferredoxin clones and Fig. 3.21B shows the analysis of the FNR clones. Positive ferredoxin clones were renamed pET.Fer and sequenced and positive FNR clones were renamed pET.FNR and sequenced and both were transformed into *E.coli* BL21 (DE3) cells and permanent glycerol stocks were made as described in Sections 2.2.9.2 and 2.2.13.

3.11.3 Purification of recombinant *Synechocystis* ferredoxin

Recombinant ferredoxin was cloned as a GST fusion protein and purified by glutathione Sepharose affinity chromatography as described in Section 2.2.15.1a. The transformed *E.coli* BL21 (DE3) cells were cultured in LB medium supplemented with 5mM ferrous ammonium sulphate. Ferredoxin is an iron-sulphur protein so the addition of ferrous ammonium sulphate to the medium supported the incorporation of the iron-sulphur cluster into the protein. *E.coli* BL21 (DE3) cells transformed with the pET.Fer expression plasmid were cultured in medium supplemented with ferrous ammonium sulphate, induced with IPTG, harvested and lysed as described in Section 2.2.14. The harvested cells were dark brown in colour indicating the

overexpression of ferredoxin. The cell lysate supernatant was loaded onto a glutathione-Sepharose affinity column equilibrated with Tris buffer (25mM Tris, 150mM NaCL, pH7.5) washed with the same buffer until the absorbance at 280nm was below 0.04 and the GST-Fer fusion protein eluted in the same buffer containing 5mM reduced glutathione. Following elution the fusion protein was not cleaved because the recombinant GST-ferredoxin was active as a fusion protein. The fusion protein was approximately 70-80% pure at this stage (see Fig. 3.22).

3.11.4 Purification of recombinant *Synechocystis sp.* PCC6803 ferredoxin $NADP^+$ reductase

Ferredoxin $NADP^+$ reductase was also cloned and purified as a GST fusion protein. The *E.coli* BL21 (DE3) cells were cultured, harvested and lysed as described in Section 2.2.14. The harvested cells were yellow at this stage, indicating the overexpression of ferredoxin $NADP^+$ reductase, which is yellow due to the presence of the flavin prosthetic group. The GST-ferredoxin $NADP^+$ reductase was purified by glutathione-Sepharose affinity chromatography. Following elution from the glutathione-Sepharose the fusion protein was cleaved using thrombin as described in Section 2.2.16.1. At the end of the purification the ferredoxin $NADP^+$ reductase was approximately 95% pure as estimated by SDS-PAGE (see Fig. 3.23).

3.12 UV/Vis spectrometric analysis of recombinant ferredoxin

The recombinant ferredoxin was reddish-brown in colour indicating the presence of the bound 2Fe-2S iron-sulphur cluster. This protein was further analysed by UV/Vis spectrometry. Fig. 3.24 shows the spectrum obtained with absorption peaks at approximately 550nm, 450nm and 350nm. This spectrum was characteristic of holo ferredoxin and indicated that recombinant GST-ferredoxin folds correctly and is able to incorporate the iron sulphur centre while being over-produced.

3.13 UV/Vis spectrometric analysis of recombinant ferredoxin $NADP^+$ reductase

The recombinant FNR was yellow in colour indicating the presence of a bound flavin group. The protein was further analysed by UV/Vis spectrometry. Fig. 3.25 shows the characteristic spectrum obtained for FNR with absorption peaks at 450nm and 350nm. This indicated that recombinant FNR had the required fold and prosthetic group required for activity.

Cyanobacteria require phycobilins for the process of light harvesting. This light energy is ultimately converted to chemical energy through photosynthesis. Heme oxygenase (HO) synthesises biliverdin IXα from heme. At this point biliverdin can be converted to the phycocyanobilin by the action of phycocyanobilin ferredoxin oxidoreductase (PcyA) or to bilirubin IXα by biliverdin IXα reductase (sBVR-A). Both HO and PcyA are ferredoxin dependent, which is kept in its reduced state by ferredoxin $NADP^+$ oxidoreductase (FNR). This system is crucial for the growth and survival of cyanobacteria. In order to study the system *in vitro* and gain insight into the reactions involved, the enzymes HO1, PcyA and sBVR-A and related proteins ferredoxin and FNR were heterologously produced through recombinant DNA techniques. The cyanobacteria *Synechocystis sp.* PCC6803 contains up to twelve copies of their genome per cell, arranged as circular chromosomes. They do not contain any introns. The lack of non-coding introns made the cloning of protein coding regions directly from genomic DNA possible, thus facilitating the construction of vectors for heterologous expression. The *Synechocystis sp.* PCC6803 genome has also been sequenced (Kazusa DNA Research Institute) and this information is available from the online cyanobacteria database (www.bacteria.kazusa.or.jp/cyanobase/.) Because all of the sequences required were freely available it made the design of primers and subsequent cloning of the required DNA fragments possible.

The genome of *Synechocystis sp.* PCC6803 contains two open reading frames (sll1184 and sll1185) which are highly similar to known heme oxygenases and could possibly encode two heme oxygenases in *Synechocystis.* HO1 (sll1184) was first cloned and overexpressed by Cornejo *et al.,* (1998). They reported that the enzyme was soluble and ferredoxin dependent. The enzyme is 20-22% identical to the mammalian heme oxygenases with highly conserved domains required for catalytic activity. The *Synechocystis* HO1 expression construct described in the present study was overexpressed efficiently in *E.coli* as a soluble GST fusion protein and although the bulk of the protein was insoluble and found in inclusion bodies; a large proportion was retained in the supernatant and could be purified by glutathione-Sepharose affinity chromatography. The protein was green in colour and when a full UV/Vis spectrum was analysed, the green colour was tentatively identified as biliverdin bound to the protein (λmax 678nm and 378nm, consistent with results reported by Saito *et al.,* 1982). This suggests that in *E.coli* cells overexpressing HO1, low levels of heme can be subverted and converted to biliverdin without deleterious effects on the cells. Cornejo *et al.*, (1998) also described the presence of biliverdin in HO1 purified from *E.coli.* Difficulties were encountered in the present study when attempts were made to obtain a

homogenous preparation of enzyme. These problems were overcome in a 4-step purification procedure. After the initial glutathione-Sepharose affinity chromatography step the fusion protein was found to be only 60-70% pure (see Fig. 3.2). This was unusual as other proteins were generally obtained at a much higher level of purity after this initial purification step. A likely explanation for this is that other proteins were attracted to the HO1 via electrostatic interactions. HO1 has a patch of positive amino acid residues on its surface where the acidic ferredoxin binds. This is likely to be the region where proteins with negative charges would be attracted to HO1. The next purification step involved a second round of affinity chromatography with Ni^{2+} Sepharose. Because the pET41a (mod) expression vector has an internal hexahistidine tag, the fusion protein could be further purified in this way. After this step the fusion protein was estimated to be 70-80% pure by SDS-PAGE (see Fig 3.2). The fourth and final purification step removed the GST and released the pure HO1. Cleavage *in situ* on the S-hexyl glutathione-Sepharose column was the method of choice because the HO1 protein was not stable during dialysis overnight and precipitated easily. Any contaminating proteins that remained were washed off prior to on-column cleavage. This purification procedure alleviated the need for dialysis. The protein was not left in unfavourable conditions and was purified, frozen and stored in a short space of time. Using this method 10mg of purified HO1 per litre of culture was obtained.

HO2 (sll1185) was also cloned but all efforts to overexpress the protein in *E.coli* failed. The cloned putative HO2 gene was sequenced and verified as sll1185 from *Synechocystis* sp. PCC6803. This ruled out the possibility that a mutation was preventing its expression. The HO2 gene was cloned as a fusion protein with GST and MBP but failed to express in either vector. Many different conditions, such as IPTG concentration and temperature were investigated to induce expression without any success. It is a possibility that codon bias prevented expression. This can occur if the recombinant gene has a codon usage that differs greatly from that utilised by *E.coli*. To test this the pET.HO2 and pMal.HO2 plasmids were transformed into competent BL21 RIL cells. These cells are specialised to express "difficult proteins" and can rescue expression of genes derived from AT and GC-rich genomes. However, no expression was detected in these cells. Cornejo *et al.*, (2001) reported the cloning of an insoluble and inactive HO2 protein from *Synechocystis* sp. PCC6803 and they could not detect any mRNA for the protein in *Synechocystis* cells. For this reason it was decided to concentrate on HO1 as the HO2 gene appears not to be expressed or may not code for a true heme oxygenase.

Biliverdin IXα reductase in *Synechocystis sp.* PCC6803 was first discovered by Schluchter & Glazer (1997) who described the cloning and overexpression of a soluble protein which was capable of reducing biliverdin IXα to bilirubin IXα at pH5.8. The protein is approximately 20%

identical to mammalian BVR-As. The *Synechocystis* BVR-A was cloned, overexpressed and purified as a GST fusion protein. Only one round of affinity chromatography, followed by thrombin cleavage, gel-filtration and removal of the GST on S-hexylglutathione Sepharose was required for the purification of sBVR-A to approximately 95% purity (see Fig. 3.5). For applications where the protein must be as close to 100% pure as possible, such as crystallisation and raising antisera the sBVR-A was further purified using 2'5' ADP-Sepharose affinity chromatography. This technique utilises the ability of sBVR-A to bind to $NADP^+$ analogues such as the 2'5' ADP immobilised to this matrix and resulted in a highly pure enzyme preparation. Dialysis was avoided due to stability problems and protein precipitation. The final yield of purified sBVR-A was approximately 5mg/L of culture using this method.

The UV/Vis absorption spectrum of purified recombinant sBVR-A revealed an absorption maximum at 260nm. This indicated the presence of a bound chromophore which absorbs at 260nm that co-purified with the enzyme. This was unique among all forms of BVR-A studied to date, none of which have been described with bound co-factor. This led to experiments to determine the nature of the 260nm chromophore. Reverse-phase HPLC tentatively identified one compound bound to sBVR-A as NADPH. The fluorescence spectrum lends support to this conclusion. This bound NADPH could have a structural role where it is involved in maintaining protein stability or quaternary structure or it could have a catalytic role with the protein acting as a transhydrogenase. Nicotinoproteins are proteins that act as transhydrogenases and use a bound co-factor as a prosthetic group. The bound co-factor is directly involved in the catalytic cycle. There are several examples of these proteins in the literature, eg. Human UDP-galactose-4-epimerase (Schulz *et al.*, 2004), formaldehyde dehydrogenase from *Pseudomonas putida* (Tanaka *et al.*, 2002) and methanol:NDMA oxidoreductase (Van Ophem *et al.*, 1993). Although it is highly likely that the bound co-factor leaves the active site and exchanges with NAD(P)H in the reaction medium it was important to rule out a transhydrogenase (no nucleotide exchange) mechanism for this enzyme. In this mechanism NAD(P)H binds to the enzyme-$NAD(P)^+$ complex and facilitates reduction of the $NAD(P)^+$ bound to the enzyme. The $NAD(P)^+$ then leaves the enzyme-NADPH complex, allowing biliverdin to bind and be reduced.

Experiments using 2'5' ADP-Sepharose affinity chromatography revealed that sBVR-A binds to this matrix and in doing so most probably interacts with the 2'5' ADP through the nucleotide binding site. If this is the case there must be some exchange between the 2'5' ADP and the nucleotide which is already bound to the protein. Reverse-phase HPLC analysis of the fraction which did not bind to the 2'5' ADP-Sepharose and flowed straight through revealed that only the protein bound and all other components were released into the flow through (see Fig. 3.13). HPLC

analysis of the eluted sBVR-A showed that there were no further components bound to the protein (see Fig 3.16). This result suggests that the bound nucleotide does exchange with free nucleotide during the reaction and it is therefore likely that the nucleotide which co-purifies with sBVR-A does exchange during the catalytic cycle and that sBVR-A from *Synechocystis* is not acting as a transhydrogenase. This conclusion is further supported by monitoring the A_{280}/A_{260} ratio during the 2'5' ADP-Sepharose affinity chromatography experiment. As sBVR-A binds to the matrix the A_{280}/A_{260} ratio of the effluent decreases, suggesting that the bound nucleotide has been exchanged and released from the protein while the sBVR-A which is eluted subsequently has a higher A_{280}/A_{260} ratio, suggesting that the nucleotide has been exchanged and is no longer bound to sBVR-A. Human liver biliverdin IXβ reductase (BVR-B) has also been shown to co-purify and co-crystallise with bound $NADP^+$ (Pereira *et al.*, 2001). However, work by Browne (2006) using ^{32}P-labelled $NADP^+$ suggests that the bound nucleotide does exchange with free nucleotide. Based on this evidence it is likely that the nucleotide bound to sBVR-A is exchanged during the reaction. It is therefore more likely that the nucleotide bound to sBVR-A serves both a structural and mechanistic role. There is evidence for this when sBVR-A is dialysed. During overnight dialysis the protein is very unstable and precipitates easily. This can be explained by the removal of the bound nucleotide during dialysis which causes the protein to become less stable and eventually precipitate. Although only one of the major peaks in Fig. 3.10 was identified (peak C as NADPH) it is possible that the remaining unidentified peaks are fragments of NADPH or are structurally similar as they are all competed off and released when sBVR-A binds the 2'5' ADP.

Phycocyanobilin ferredoxin oxidoreductase (PcyA) is an enzyme that is unique to photosynthetic bacteria and is responsible for converting biliverdin into the light harvesting tetrapyrrole of cyanobacteria and red algae, phycocyanobilin. Eukaryotic photosynthetic organisms such as plants have a direct descendent of this enzyme which they use to synthesise the chromophore phytochrome. This PcyA homologue is known as phytochromobilin synthase (HY2) and was cloned and characterised by Kohchi *et al.*, (2001). Both PcyA and HY2 obtain reducing equivalents from ferredoxin, which is maintained in its reduced state by ferredoxin $NADP^+$ reductase. PcyA was cloned as a GST fusion protein and was purified in a 4-step procedure, similar to HO1. The fusion protein was 70-80% pure following glutathione-Sepharose affinity chromatography and needed further purification as described below for raising antibodies (see Fig 3.26). In a mechanism similar to HO1, it is possible that contaminating negatively charged proteins bind to the positive patch of amino acids on the surface of PcyA where the acidic ferredoxin usually binds. PcyA was further purified by Ni^{2+} affinity chromatography, gel filtered and cleaved by thrombin on an S-hexyl glutathione Sepharose affinity column. At the end of the purification the recombinant PcyA protein was 90-100% pure (see Fig 3.18). Approximately 10mg

of purified recombinant protein was obtained per litre of culture. UV/Vis spectrometry revealed that in addition to the protein peak at 280nm there was absorbance between 300 and 500nm. This absorbance is characteristic of the absorbance spectrum for ferredoxin (see Fig. 3.20) and can possibly be explained by ferredoxin bound to PcyA. It is also possible that contaminating ferredoxin is seen on the SDS-PAGE gel in Fig. 3.26.

Frankenberg *et al.*, (2001) reported the cloning and overexpression of PcyA from *Synechocysytis sp.* PCC6803. They achieved between 1-10mg protein/litre of culture, using a similar expression system. They tested the activity of PcyA using a coupled apophytochrome assembly assay and HPLC analysis and showed that recombinant PcyA has the ability to catalyse the ferredoxin dependent reduction of biliverdin to phycocyanobilin. However, no activity for PcyA was observed in the present study when a continuous spectrophotometric assay was developed containing recombinant PcyA, ferredoxin, ferredoxin reductase, biliverdin IXα and NADPH. The pET.PcyA plasmid was sequenced and the PcyA insert was found to be consistent with the slr0116 gene encoding PcyA. For unknown reasons the recombinant PcyA did not exhibit biliverdin reductase activity in this assay.

Ferredoxin is an electron carrier and transfer protein and is kept in its reduced state by the transfer of electrons from NADPH in a reaction catalysed by ferredoxin $NADP^+$ reductase (FNR). The relationship between the two proteins is essential to photosynthesis in cyanobacteria and higher plants where it plays a role in redox metabolism. In addition to its role in photosynthesis, ferredoxin also transfers electrons to various enzymes, such as HO1 and PcyA, which then use these electrons during their catalytic cycle. Both ferredoxin and FNR were cloned and overexpressed as GST fusion proteins. Yields of holo GST-ferredoxin were approximately 5mg per 4 litres of culture. This yield was not particularly high due to the large amount of insoluble protein retained in inclusion bodies. Other groups have cloned and overexpressed recombinant ferredoxin, but not as a fusion protein, most likely as a result of the insolubility problems. Typical yields of between 5-7 mg per litre of culture have been described (Palma *et al.*, 2005, Guillouard *et al.* 2000, Piubelli *et al.* 1995). Commercially available ferredoxin is expensive and less pure. It was therefore decided to overexpress the protein in *E.coli*. The recombinant ferredoxin was not cleaved from its fusion partner as it was shown to be active as a GST fusion in the HO1 reaction at a concentration of 50μM. The purified GST-ferredoxin was red-brown, indicating the incorporation of the 2Fe-2S cluster into the protein. The final product was between 70-80% pure. The UV/Vis spectrum of the recombinant protein was identical to commercially available spinach ferredoxin.

of purified recombinant protein was obtained per litre of culture. UV/Vis spectrometry revealed that in addition to the protein peak at 280nm there was absorbance between 300 and 500nm. This absorbance is characteristic of the absorbance spectrum for ferredoxin (see Fig. 3.20) and can possibly be explained by ferredoxin bound to PcyA. It is also possible that contaminating ferredoxin is seen on the SDS-PAGE gel in Fig. 3.26.

Frankenberg *et al.,* (2001) reported the cloning and overexpression of PcyA from *Synechocysytis sp.* PCC6803. They achieved between 1-10mg protein/litre of culture, using a similar expression system. They tested the activity of PcyA using a coupled apophytochrome assembly assay and HPLC analysis and showed that recombinant PcyA has the ability to catalyse the ferredoxin dependent reduction of biliverdin to phycocyanobilin. However, no activity for PcyA was observed in the present study when a continuous spectrophotometric assay was developed containing recombinant PcyA, ferredoxin, ferredoxin reductase, biliverdin IXα and NADPH. The pET.PcyA plasmid was sequenced and the PcyA insert was found to be consistent with the slr0116 gene encoding PcyA. For unknown reasons the recombinant PcyA did not exhibit biliverdin reductase activity in this assay.

Ferredoxin is an electron carrier and transfer protein and is kept in its reduced state by the transfer of electrons from NADPH in a reaction catalysed by ferredoxin $NADP^+$ reductase (FNR). The relationship between the two proteins is essential to photosynthesis in cyanobacteria and higher plants where it plays a role in redox metabolism. In addition to its role in photosynthesis, ferredoxin also transfers electrons to various enzymes, such as HO1 and PcyA, which then use these electrons during their catalytic cycle. Both ferredoxin and FNR were cloned and overexpressed as GST fusion proteins. Yields of holo GST-ferredoxin were approximately 5mg per 4 litres of culture. This yield was not particularly high due to the large amount of insoluble protein retained in inclusion bodies. Other groups have cloned and overexpressed recombinant ferredoxin, but not as a fusion protein, most likely as a result of the insolubility problems. Typical yields of between 5-7 mg per litre of culture have been described (Palma *et al.,* 2005, Guillouard *et al.* 2000, Piubelli *et al.* 1995). Commercially available ferredoxin is expensive and less pure. It was therefore decided to overexpress the protein in *E.coli.* The recombinant ferredoxin was not cleaved from its fusion partner as it was shown to be active as a GST fusion in the HO1 reaction at a concentration of 50μM. The purified GST-ferredoxin was red-brown, indicating the incorporation of the 2Fe-2S cluster into the protein. The final product was between 70-80% pure. The UV/Vis spectrum of the recombinant protein was identical to commercially available spinach ferredoxin.

Ferredoxin $NADP^+$ reductase was purified as a GST fusion protein, followed by thrombin cleavage and removal of the GST moiety. Purified FNR was yellow indicating the presence of flavin adenine dinucleotide (FAD), which is required for activity of the enzyme. The spectrum of the recombinant FNR verified that it contained this flavin group and it was also shown to be active in the HO1 reaction. The final FNR product was between 90-100% pure. Other groups have cloned and overexpressed this enzyme before and report typical yields of between 1-10mg/litre of culture (Palma *et al.* 2005). Yields of purified FNR were similar using the expression system described in this chapter. The reason for cloning, overexpressing and purifying both ferredoxin and FNR in the context of this project was to use them in the study of the PcyA and HO1 reactions.

Antibodies were raised against the enzymes: HO1, sBVR-A and PcyA (see Fig 3.26 for purified proteins for antibodies).

Gene	Primer	Direction	$T_{m.}$ (^{O}C)	Size (bp)	Sequence
HO1	Oligo 1.	Forward	65	28	5' CGT.G GATCC.CATGAGTGTCAACTTAGCT 3' (BamH1)
HO1	Oligo 2.	Reverse	64.8	26	5' TAT.A AGCTT.CTAGCCTTCGGAGGTGG 3' (HindIII)
BVR-A	Oligo 3.	Forward	61.3	26	5' CGC.G GATCC.CATGTCTGAAAATTTTG 3' (BamH1)
BVR-A	Oligo 4.	Reverse	61.0	29	5' CGC.C TCGAG.CTAATTTTCAACCTTATATC 3' (Xho-1)
PcyA	Oligo 5.	Forward	66.7	30	5' CTT.G GATCC.CATGGCCGTCACTGATTTAAG 3' (BamH1)
PcyA	Oligo 6.	Reverse	65.8	31	5' CGG.CTGCA G.TTATTGGATAACATCAAATAAG 3' (Pst1)
Fer	Oligo 7.	Forward	61	25	5' CGC.G GATCC.CATGAATAATTGCGTA 3' (BamH1)
Fer	Oligo 8.	Reverse	57.1	23	5' GGC.A AGCTT.TCAAATTTCATCAC 3' (HindIII)
Fer.red	Oligo 9.	Forward	68	29	5' TCA.G GATCCC.ATGTACAGTCCCGGTTACG 3' (BamH1)
Fer.red	Oligo 10.	Reverse	68.1	28	5' CGC.A AGCTT.TTAGTAGGTTTCCACGTGC 3' (HindIII)

Table 3.1. Primers used for the amplification of protein coding regions of *Synechocystis* DNA

Direction, size and melting temperatures are indicated. Restriction sites are underlined. Restriction enzymes used are shown in red. Arrows indicate exact site of restriction. Start codons are shown in blue and stop codons (reverse complement) are shown in green

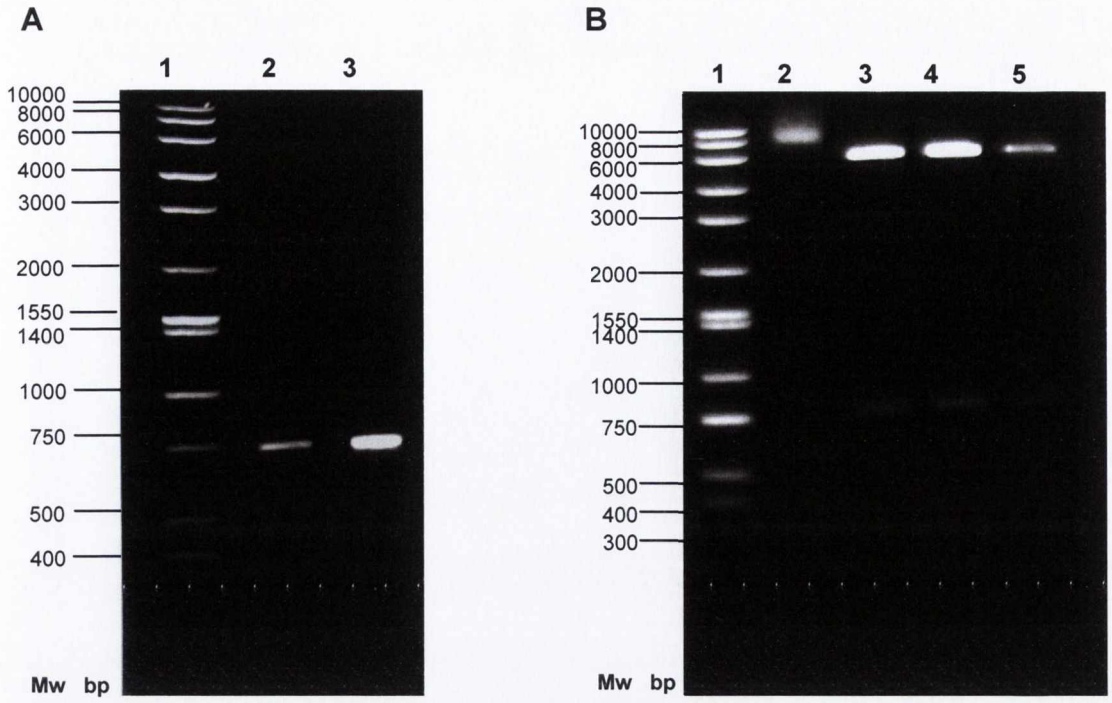

Figure 3.1 Cloning of *Synechocystis* HO1

A. PCR amplification of HO1 (723bp). Lane 1 contains molecular weight markers, Lane 2 contains 10µl of the PCR reaction (1/100 dilution of the DNA template), Lane 3 contains 10µl of the PCR reaction (1/10 dilution of the DNA template). **B**. Restriction digest of pET.HO1. Lane 1 contains molecular weight markers, Lane 2 contains undigested pET.HO1, Lanes 3-5 contain digested pET.HO1 showing HO1 insert

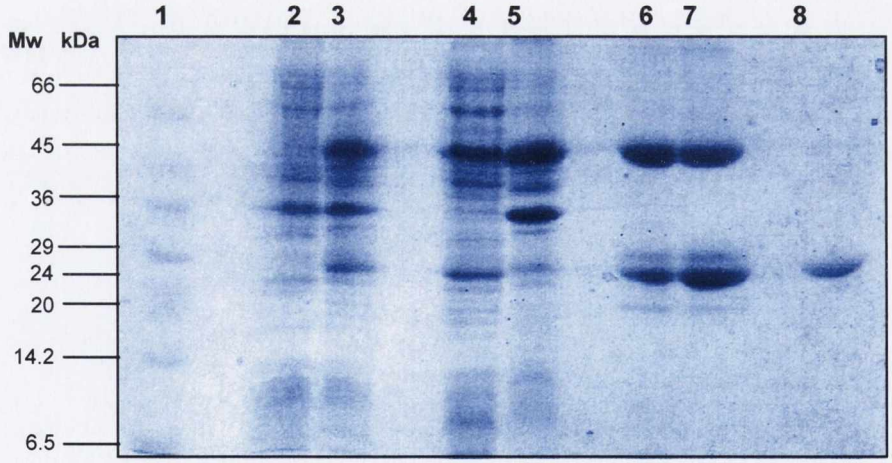

Figure 3.2 SDS-PAGE analysis of recombinant HO1

Lane 1 contains molecular weight markers, Lane 2 contains uninduced *E.coli,* Lane 3 contains IPTG induced *E.coli,* Lane 4 contains urea treated pellet, Lane 5 contains soluble supernatant fraction, Lane 6 contains glutathione-Sepharose purified GST-HO1, Lane 7 contains Ni^{2+} Sepharose purified GST-HO1, Lane 8 contains purified HO1 (24 kDa)

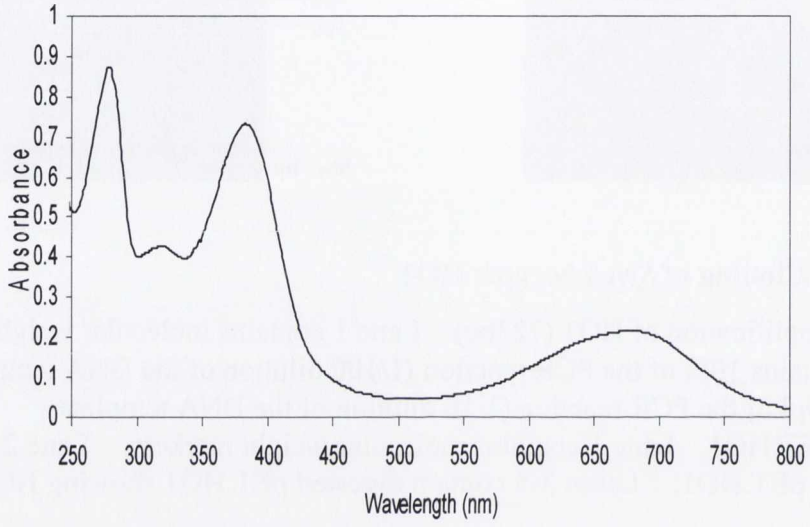

Figure 3.3 UV/Vis absorbance spectrum of recombinant *Synechocystis* HO1

The HO1 spectrum (in Tris buffer, pH7.5 containing 100mM NaCl) tentatively identifies the protein bound chromophore as biliverdin with characteristic absorbance maxima at 678nm and 378nm. Also present is the characteristic protein peak at 280nm

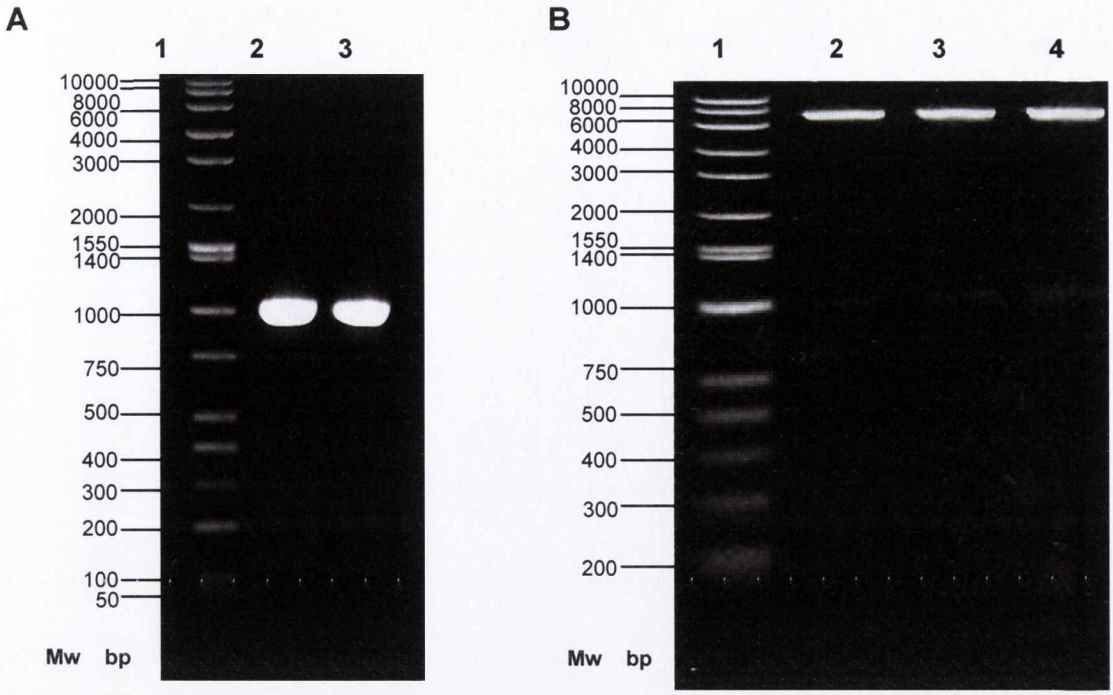

Figure 3.4 Cloning of *Synechocystis* BVR-A.

A. PCR amplification of BVR-A (953bp). Lane 1 contains molecular weight markers, Lane 2 contains 10µl of the PCR reaction (1/100 dilution of the DNA template), Lane 3 contains 10µl of the PCR reaction (1/10 dilution of the DNA template) **B**. Restriction digest of pET.BVR-A, Lane 1 contains molecular weight markers, Lanes 2-4 contain digested pET.BVR-A showing BVR-A insert

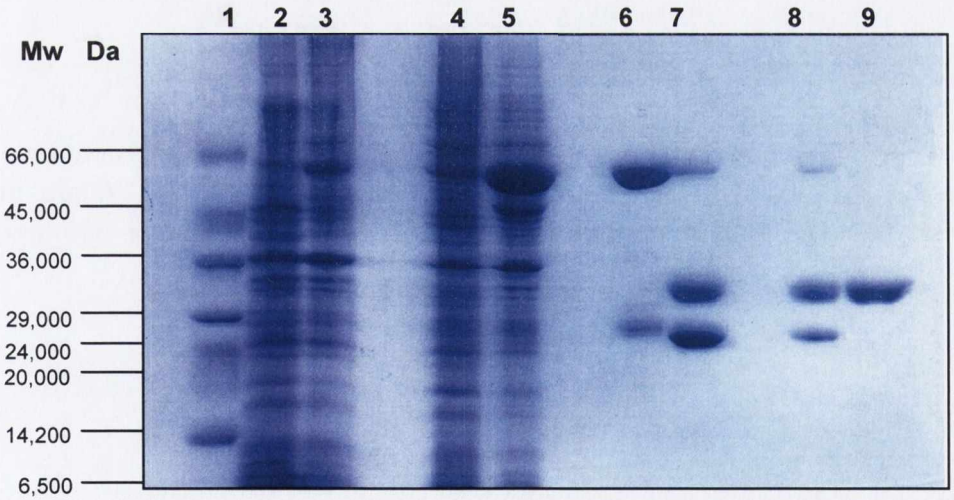

Figure 3.5 SDS-PAGE analysis of recombinant BVR-A

Lane 1 contains molecular weight markers, Lane 2 contains uninduced *E.coli,* Lane 3 contains IPTG induced *E.coli,* Lane 4 contains urea treated pellet, Lane 5 contains soluble supernatant fraction, Lane 6 contains glutathione-Sepharose purified GST-BVR-A, Lane 7 contains thrombin cleaved GST-BVR-A, Lane 8 contains partially purified BVR-A, Lane 9 contains purified BVR-A (34 kDa)

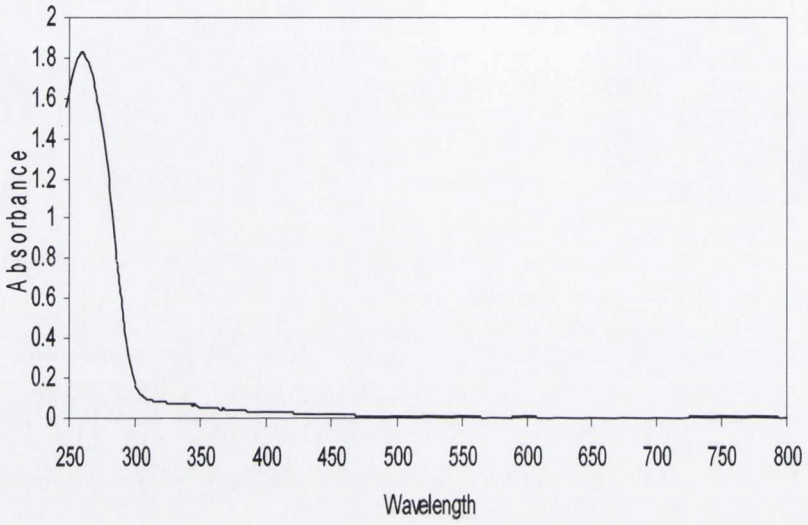

Figure 3.6 UV/Vis absorbance spectrum of recombinant *Synechocystis* BVR-A

The absorbance maximum of recombinant sBVR-A (in Tris buffer, pH7.5 containing 100mM NaCl) is shifted from the characteristic protein peak at 280nm to 260nm, indicating the presence of an additional bound component which absorbs at 260nm

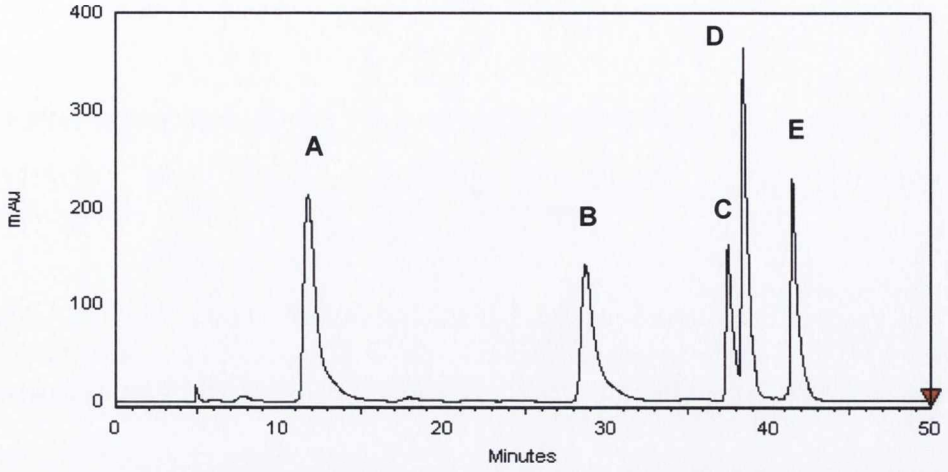
400
300
200
100
0
mAU
A
B
C
D
E
0
10
20
30
40
50
Minutes

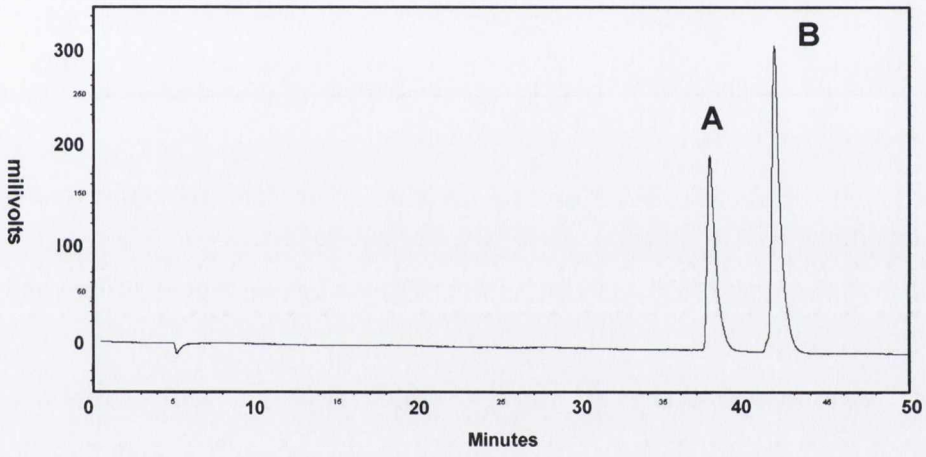
300
200
100
0
millivolts
A
B
0
10
20
30
40
50
Minutes

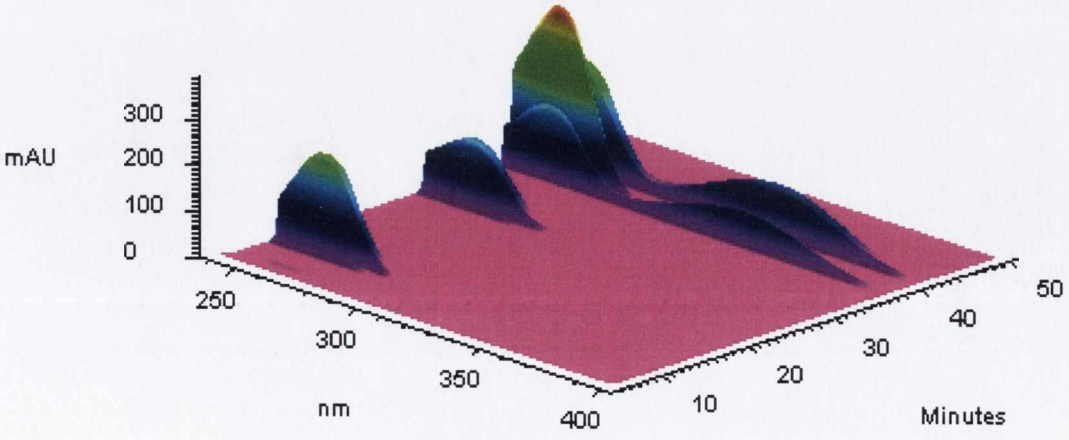
mAU
300
200
100
0
250
300
350
400
nm
10
20
30
40
50
Minutes

Figure 3.7 Separation of a mixture of nucleotides by reversed-phase HPLC

A. 100μM ATP (12min) **B**. 100μM $NADP^+$ (29min) **C**. 100μM NADPH (38min) **D**. 100μM NAD^+ (39min) **E**. 100μM NADH (42min) Detection was by absorbance was at 254nm

The HPLC column was equilibrated and the nucleotide standards (100μM of each) were prepared in potassium phosphate (100mM), pH6. Elution was achieved using a gradient of 40% methanol, 60% potassium phosphate (100mM), pH6 over a 50 minute period

Figure 3.8 Fluorescence detection of a mixture of nucleotides separated by reversed-phase HPLC

A. NADPH (38min) **B**. NADH (42min) Excitation was set at 340nm and emission at 460nm

Figure 3.9 Absorbance spectra of a mixture of nucleotides separated by HPLC

Spectrums were recorded by a photodiode array detector (PDA) set from 200-400nm

A. 100μM ATP (12min) **B**. 100μM NADP+ (29min)
C. 100μM NADPH (38min) **D**. 100μM NAD+ (39min)
E. 100μM NADH (42min)

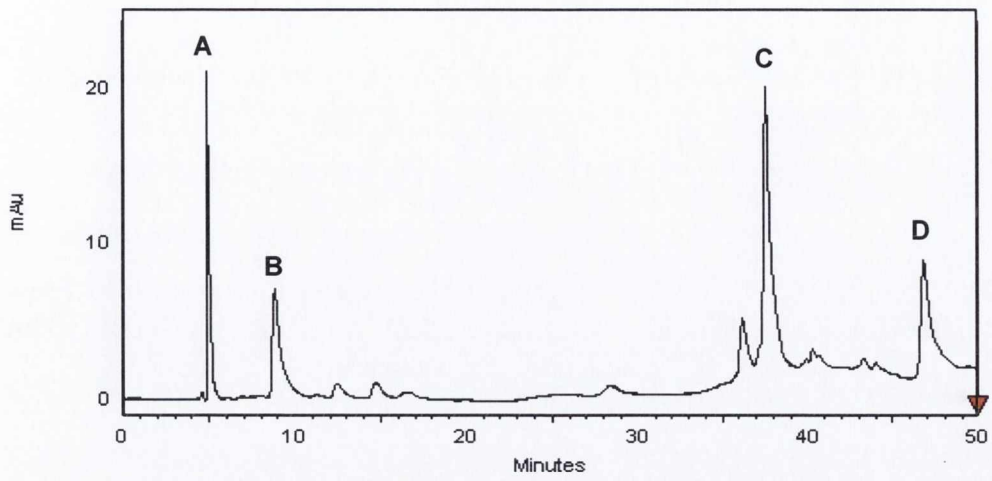
A
B
C
D
mAu
20
10
0
0
10
20
30
40
50
Minutes

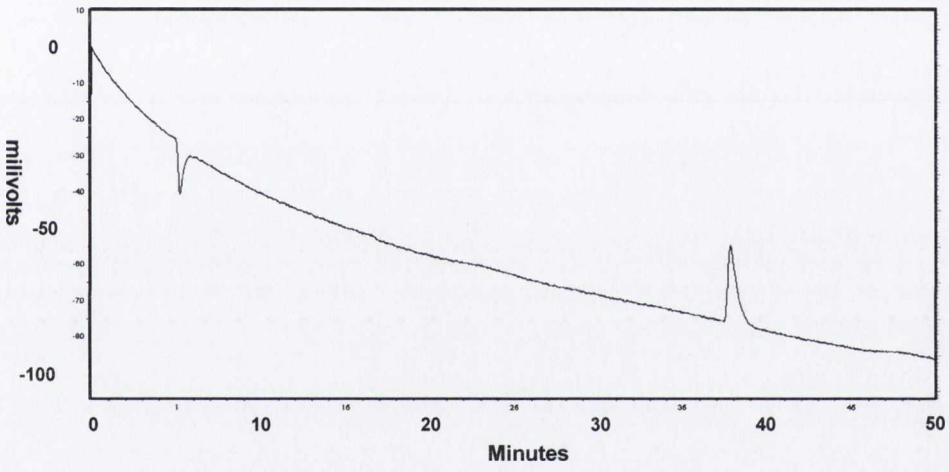
milivolts
0
-50
-100
0
10
20
30
40
50
Minutes

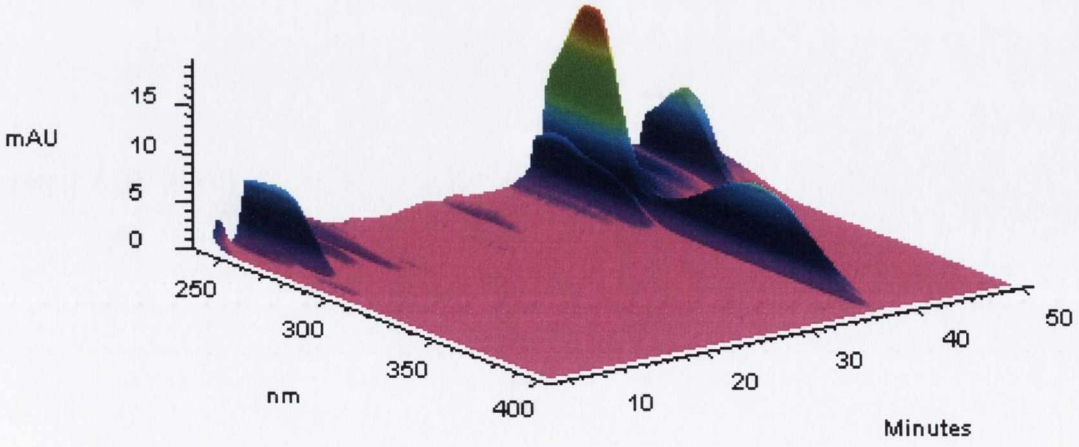
mAU
15
10
5
0
250
300
350
400
nm
10
20
30
40
50
Minutes

Figure 3.10 HPLC analysis of the nucleotide bound to sBVR-A, separated by reverse-phased HPLC

Major peaks shown are: **A**. protein (5min) **B**. unknown (9min)
C. NADPH (38min) **D**. unknown (47min)

The HPLC column was equilibrated in potassium phosphate (100mM), pH6. Elution was achieved using a gradient of 40% methanol, 60% potassium phosphate (100mM), pH6 over a 50 minute period. Detection was by absorbance at 254nm

Figure 3.11 Fluorescence detection of the nucleotide bound to sBVR-A separated by reverse-phased HPLC

The peak at 38min was tentatively identified as NADPH. Excitation was set at 340nm and emission at 460nm

Figure 3.12 Absorbance spectrum of the nucleotide bound to sBVR-A separated by reverse-phased HPLC

Spectra were recorded by a PDA set from 200-400nm. NADPH was tentatively identified at 38min

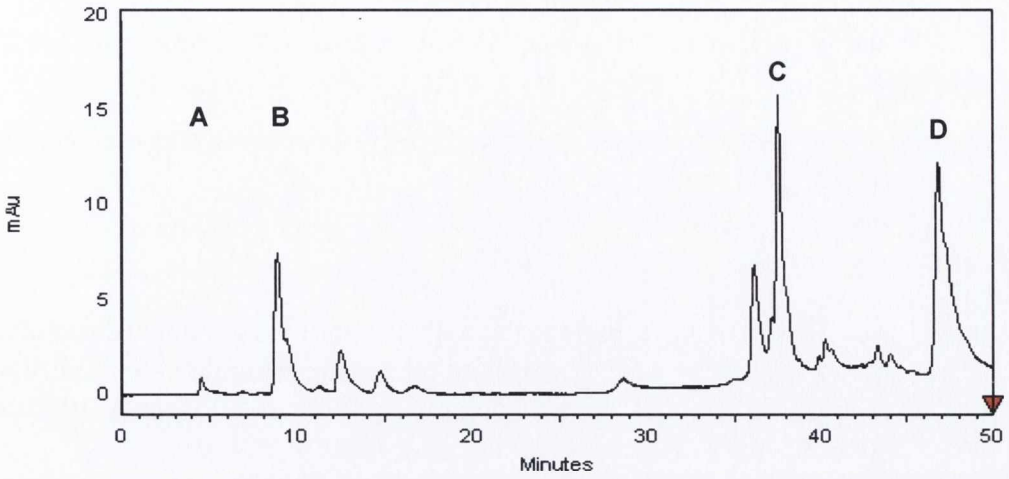
mAu
20
15
10
5
0
A
B
C
D
0
10
20
30
40
50
Minutes

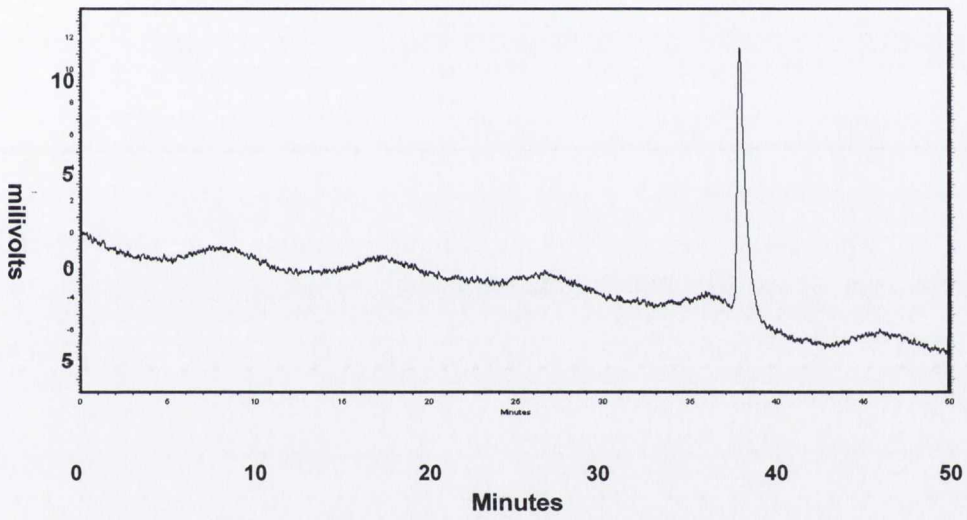
milivolts
10
5
0
5
0
10
20
30
40
50
Minutes

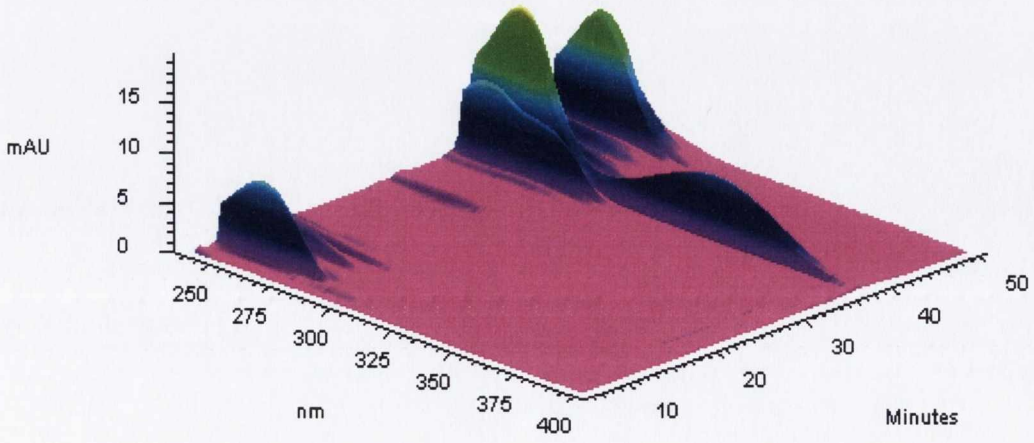
mAU
15
10
5
0
250
275
300
325
350
375
400
nm
10
20
30
40
50
Minutes

Figure 3.13 Reverse-phased HPLC analysis of the unbound fraction from the 2'5' ADP experiment

Shown is the fraction which did not bind to the 2'5' ADP-Sepharose and was released in the flow-through and analysed by reverse HPLC.
A. protein (5min) **B**. unknown (9min)
C. NADPH (38min) **D**. unknown (47min)

The unknown peaks B and D are consistent with 2'5' ADP or some related structure. The HPLC column was equilibrated in potassium phosphate (100mM), pH6. Elution was achieved using a gradient of 40% methanol, 60% potassium phosphate (100mM), pH6 over a 50 minute period. Detection was by absorbance at 254nm

Figure 3.14 Fluorescence analysis of the unbound fraction from the 2'5' ADP experiment separated by reverse-phased HPLC

The peak at 38min was tentatively identified as NADPH. Excitation was set at 340nm and emission at 460nm

Figure 3.15 Absorbance spectra of the compounds released from sBVR-A during the 2'5' ADP experiment and separated by reverse-phased HPLC

Spectra were recorded by a PDA set from 200-400nm. NADPH was tentatively identified at 38min

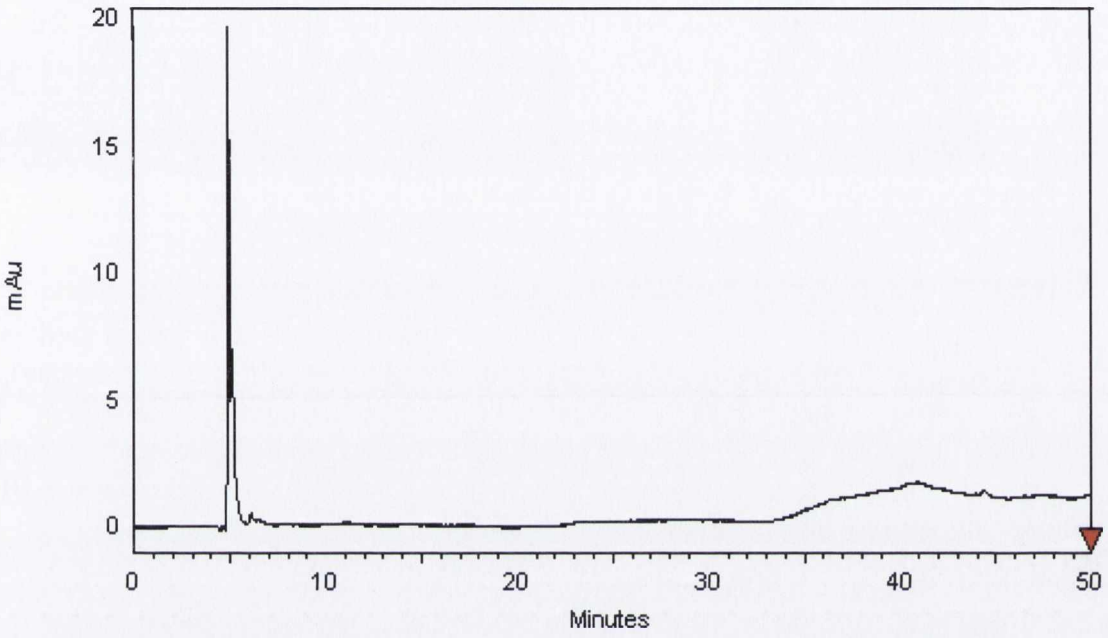

Figure 3.16 Reverse-phased HPLC analysis of the bound fraction from the 2`5` ADP-Sepharose experiment

The peak at 5min represents protein. No other compounds were detected. The HPLC column was equilibrated in potassium phosphate (100mM), pH6. Elution was achieved using a gradient of 40% methanol, 60% potassium phosphate (100mM), pH6 over a 50 minute period. Detection was by absorbance at 254nm.

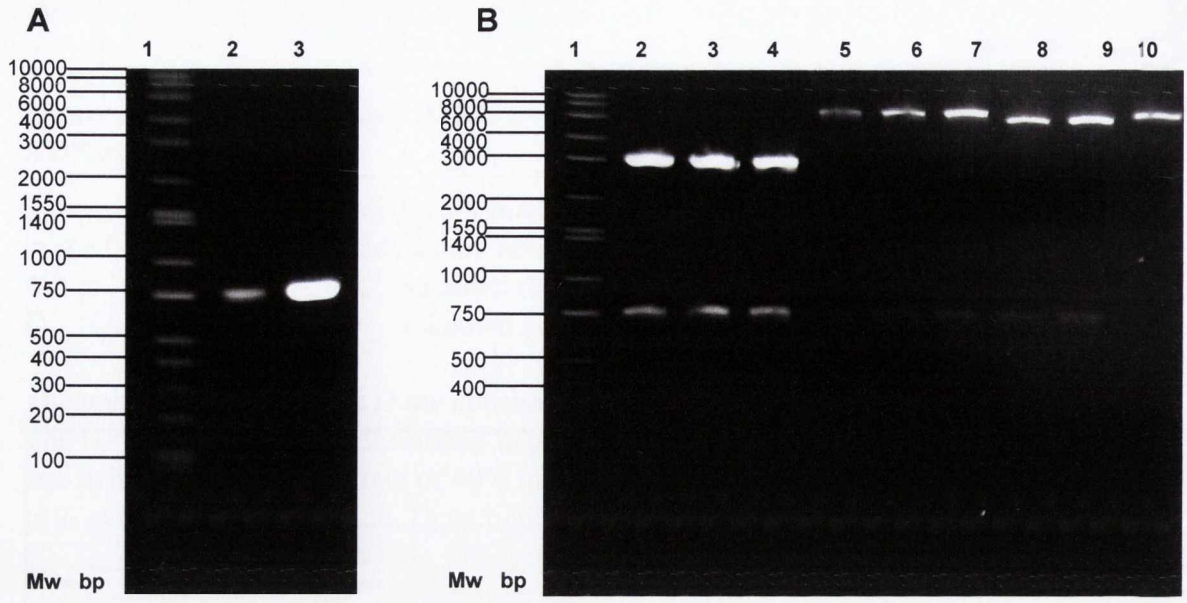

Figure 3.17 Cloning of *Synechocystis* PcyA

A. PCR amplification of PcyA (793bp). Lane 1 contains molecular weight markers, Lane 2 contains 10µl of the PCR reaction (1/100 v/v dilution of the DNA template), Lane 3 contains 10µl of the PCR reaction (1/10 v/v dilution of the DNA template) **B.** Restriction digests of pBlue.PcyA and pET.PcyA. Lane 1 contains molecular weight markers, Lanes 2-4 contain digested pBlue.PcyA showing PcyA insert, Lanes 5-10 contain digested pET.PcyA showing PcyA insert

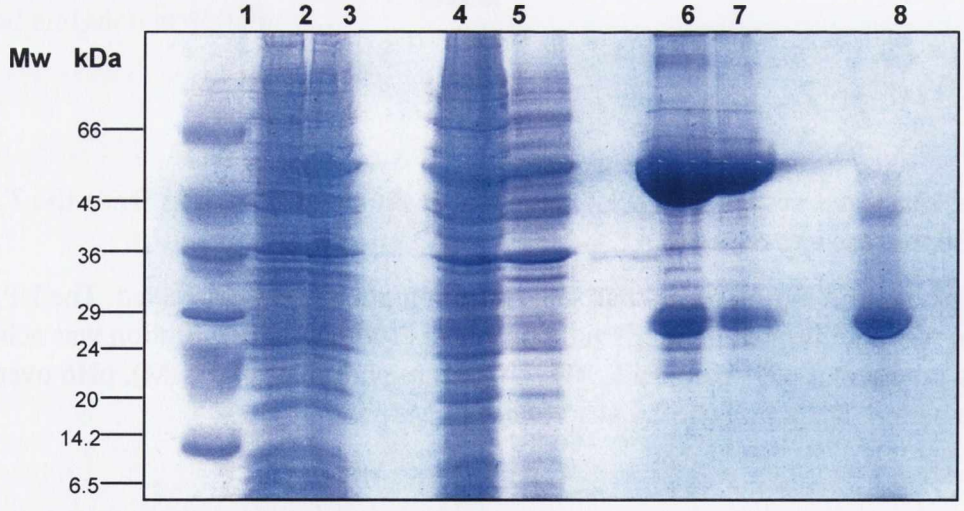

Figure 3.18 SDS-PAGE analysis of recombinant PcyA

Lane 1 contains molecular weight markers, Lane 2 contains uninduced *E.coli,* Lane 3 contains IPTG induced *E.coli,* Lane 4 contains urea treated pellet, Lane 5 contains soluble supernatant fraction, Lane 6 contains glutathione-Sepharose purified GST-PcyA, Lane 7 contains Ni^{2+} purified GST-PcyA, Lane 8 contains purified PcyA (24 kDa). It is also possible the lower band in lane 8 is ferredoxin which co-purified with PcyA

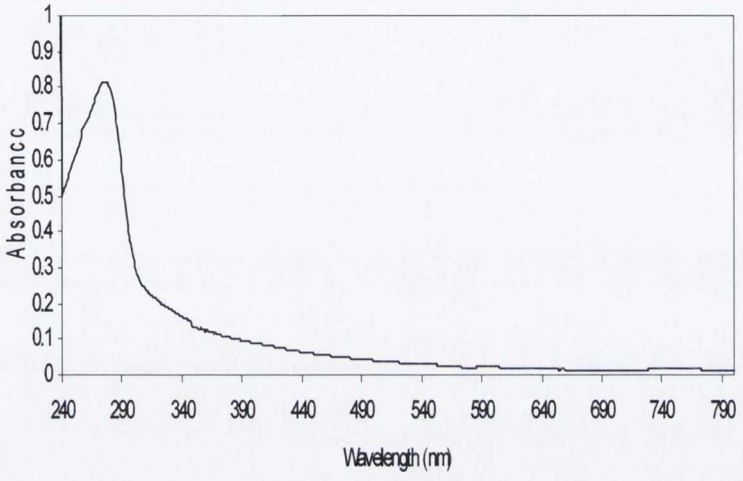

Figure 3.19 UV/Vis absorbance spectrum of recombinant *Synechocystis* PcyA

In addition to the protein peak at 280nm there is absorbance between 300-500nm which is characteristic of an absorbance associated with bound ferredoxin. The spectrum of recombinant PcyA was recorded in Tris buffer, ph 7.5, containing 100mM NaCl

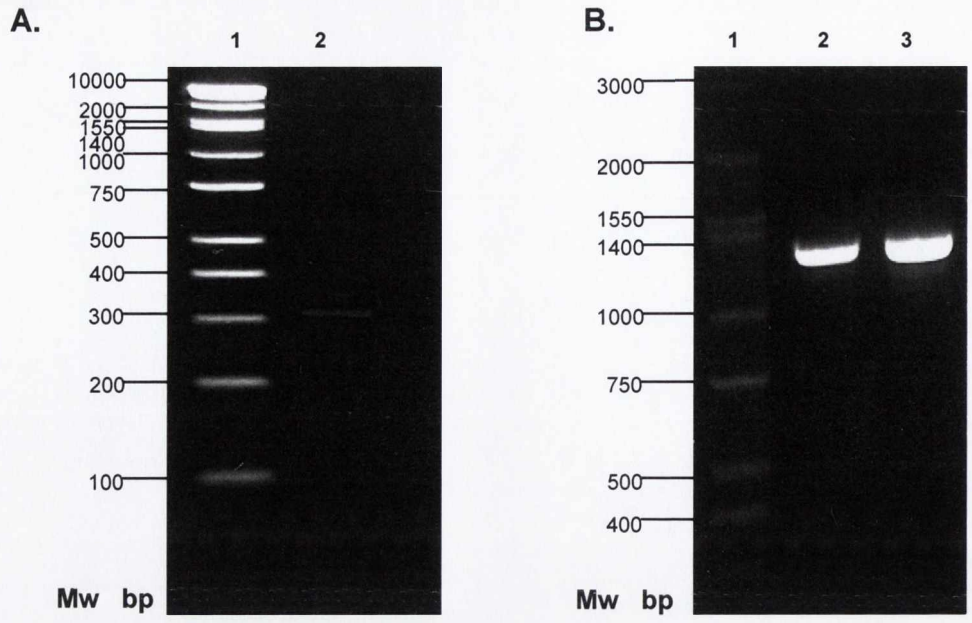

Figure 3.20 Cloning of *Synechocystis* Ferredoxin and Ferredoxin NADP$^+$ reductase.

A. PCR amplification of ferredoxin (293bp). Lane 1 contains molecular weight markers, Lane 2 contains 10µl of the PCR reaction (1/10 dilution of the DNA template). **B**. PCR amplification of Ferredoxin NADP$^+$ reductase (1242bp). Lane 1 contains molecular weight markers, Lane 2 contains 10µl of the PCR reaction (1/100 dilution of the DNA template), Lane 3 contains 10µl of the PCR reaction (1/10 dilution of the DNA template)

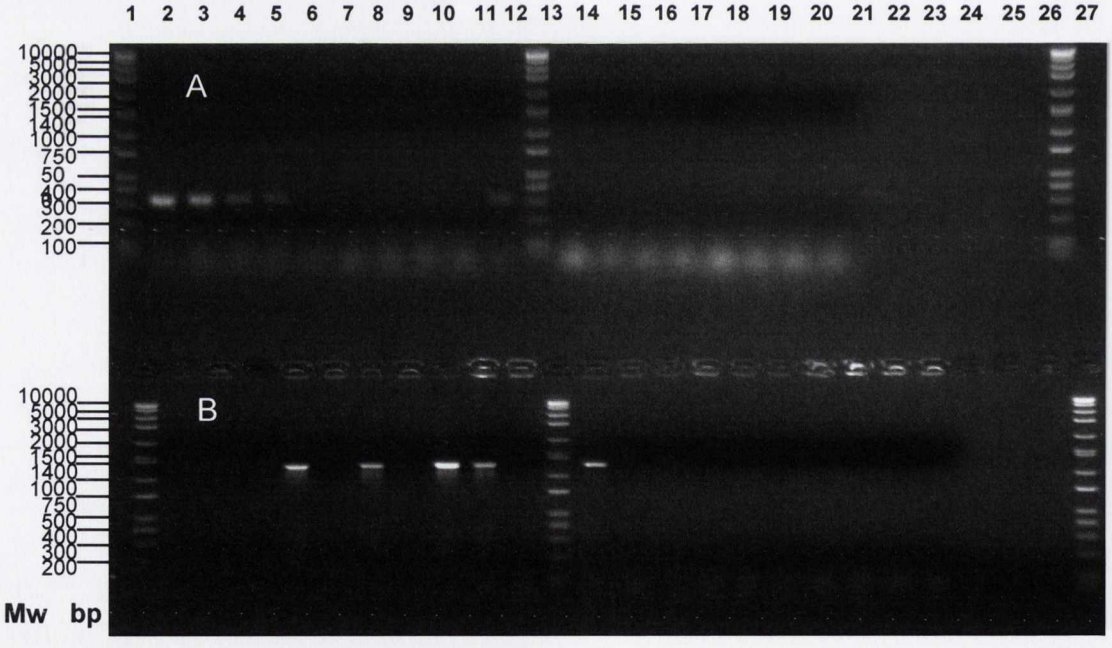

Figure 3.21 PCR screening of A. pET.fer and B. pET.FNR

Lanes 2, 3, 4, 5, 11, 12 in **A** contain PCR products (293bp) consistent with ferrededoxin and indicate that these clones are positive and contain the correct ferredoxin DNA fragment. Lanes 6, 8, 10, 11, 14 in **B** contain PCR products (1242bp) consistent with FNR and indicate that these clones are positive and contain the correct FNR DNA fragment. Lanes 1, 13 and 26 contain molecular weight markers

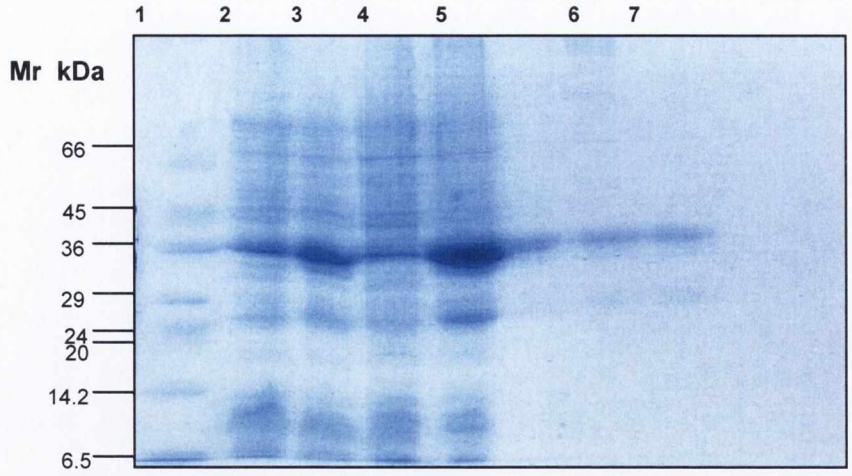

Figure 3.22 SDS-PAGE analysis of recombinant ferredoxin

Lane 1 contains molecular weight markers, Lane 2 contains uninduced *E.coli,* Lane *3* contains IPTG induced *E.coli,* Lane 4 contains urea treated pellet, Lane 5 contains soluble supernatant fraction, Lanes 6 and 7 contain GST-ferrexoxin (36 kDa)

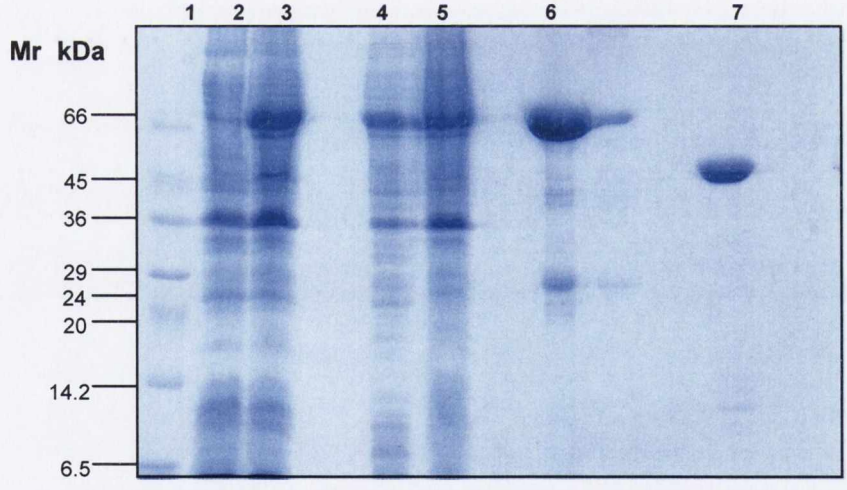

Figure 3.23 SDS-PAGE analysis of recombinant ferredoxin NADP$^+$ reductase

Lane 1 contains molecular weight markers, Lane 2 contains uninduced *E.coli,* Lane *3* contains IPTG induced *E.coli,* Lane 4 contains urea treated pellet, Lane 5 contains soluble supernatant fraction, Lane 6 contains glutathione-Sepharose purified GST-FNR, Lane 7 contains thrombin cleaved purified FNR (45 kDa)

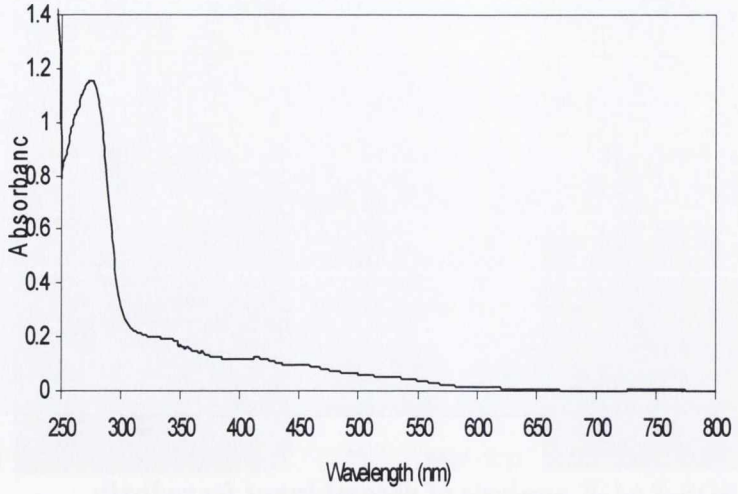

Figure 3.24 UV/Vis absorbance spectrum of recombinant GST-ferredoxin

The absorbance spectrum of recombinant GST-Ferredoxin (in Tris buffer, pH7.5 containing 100mM NaCl) shows the characteristic absorbance maxima for ferredoxin with peaks at 550nm, 450nm and 350nm. This indicates that recombinant GST-ferredoxin has folded correctly and has the iron-sulphur centre incorporated

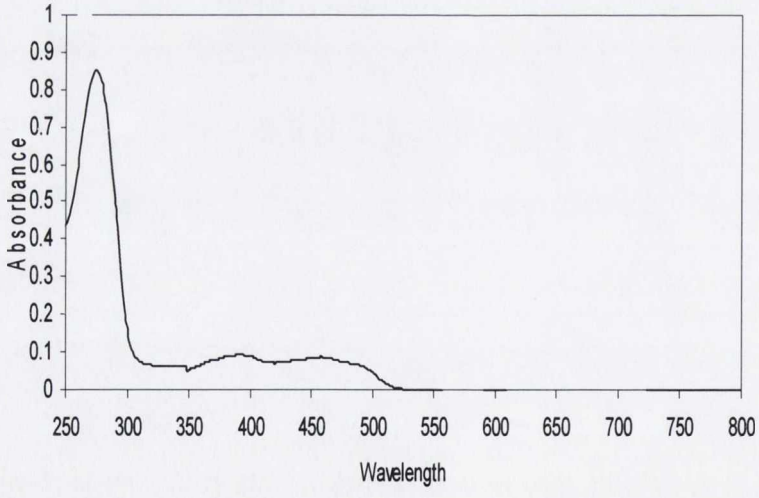

Figure 3.25 UV/Vis absorbance spectrum of recombinant *Synechocystis* FNR

The absorbance spectrum for recombinant FNR in Tris buffer (25mM), pH7.5 containing 100mM NaCl shows the characteristic absorbance maxima for FNR with peaks at 450nm and 450nm. This indicates that the protein has the required flavin prosthetic group

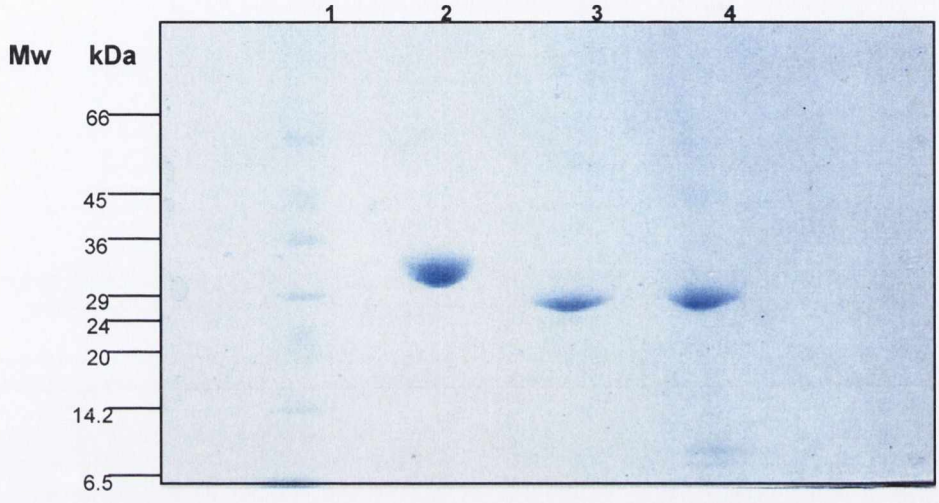

Figure 3.26 SDS-PAGE analysis of proteins injected into rabbits for the purpose of raising antibodies

Lane 1 contains molecular weight markers, Lane 2 contains purified sBVR-A (34kDa), Lane 3 contains purified HO1 (24kDa), Lane 4 contains purified PcyA (24 kDa)

CHAPTER 4

INITIAL RATE KINETICS OF *SYNECHOCYTIS* BILIVERDIN IXα REDUCTASE

4.1 Introduction

The initial rate kinetics of biliverdin IXα reductase have been examined in many different species, including human liver (Maines & Trakshel, 1993), rat kidney (Tenhunen *et al.,* 1970), guinea-pig liver (O'Carra & Colleran, 1971) salmon (Elliot, 1996) and ox kidney (Phillips, 1981; Rigney & Mantle, 1988). However, comprehensive kinetic studies and accurate determination of the kinetic parameters for mammalian BVR-As at physiological pH and in the absence of biliverdin binding proteins have proved refractory (Dunne, 2000). This is due to the profound substrate inhibition exhibited by mammalian BVR-As with biliverdin as the variable substrate together with the relative insolubility of the reaction product bilirubin IXα. The potent substrate inhibition has been shown to result from biliverdin binding to the enzyme-$NADP^+$ complex to form the catalytically unproductive enzyme-$NADP^+$-biliverdin ternary complex (Rigney & Mantle, 1988). Kinetic experiments are further complicated by the extreme insolubility of the reaction product bilirubin in aqueous solvents which have been reported as low as 7nM at pH7.4 (Brodersen, 1979). Generally BSA is included in the assay mix to bind bilirubin and thereby increase its relative solubility. However, the addition of BSA increases the extinction co-efficient of the product bilirubin and it also effectively decreases the concentration of free biliverdin.

The potent substrate inhibition exhibited by many BVR-As has also prevented full mechanistic studies of these enzymes as initial rate kinetics and product inhibition studies require both NAD(P)H and biliverdin at "non-saturating" and "saturating" levels for a complete mechanistic analysis. As a result only the mechanism of the ox kidney BVR-A at pH9 has been fully elucidated (Rigney & Mantle, 1988). At this pH it is possible to study the steady state kinetics of the ox enzyme in the absence of biliverdin binding proteins as the K_m for biliverdin is sufficiently high to obtain reliable initial rate measurements. These studies have revealed that the mechanism of ox kidney BVR-A is consistent with an ordered BiBi mechanism where NAD(P)H is the first substrate to bind to the enzyme, followed by biliverdin. Hydride transfer then occurs between NADPH and biliverdin and bilirubin is the first product to dissociate, followed by the oxidised co-factor (Rigney & Mantle, 1988; Rigney *et al.,* 1989).

With all known BVR-As studied to date NADPH has been shown to be the preferred co-factor for reduction of biliverdin, a fact which can easily be seen in the much lower K_m values for NADPH when compared with NADH (see Table 4.1). NADPH has also been suggested to promote tighter binding of biliverdin to the enzyme nucleotide complex (Dunne, 2000). The hydride ion transfer

has been shown to be stereospecific for all BVR-As studied to date. The human (Dunne, 2000), salmon liver (Elliot, 1996), rat kidney (Ennis, 1996) and *Synechocystis* (Walsh, unpublished data) enzymes have all been shown to exhibit B-face stereospecificity. During the reaction they have all been shown to remove the hydride from the B-face of the pyridine ring of NADH, in contrast to A-stereospecific enzymes which remove the hydride from the A-side of the pyridine ring. Although NADPH and NADH are structurally similar, they participate in different enzymatic processes with NADPH generally used for reductive biosynthesis and NAD^+ mainly used in oxidative reactions that ultimately yield ATP. The only difference between NADPH and NADH is the 2` phosphate on NADPH which increases its affinity for the enzyme. The presence of this phosphoester provides a discriminatory method which determines the nucleotide specificity of many pyridine nucleotide dependent enzymes (Carugo & Argos, 1997; Elmore *et al.*, 2002). In proteins which use NADH as co-factor there is usually an acidic residue (Asp or Glu) at the C-terminal edge of the β-2 strand of the Rossman fold where negatively charged residues can interact productively with the 2`OH group of the adenosine ribose of NADH and preclude the 2`phosphate. However, in proteins which preferentially use NADPH this site is usually occupied by small hydrophobic residues and positively charged residues (Lys or Arg) interact with the negatively charged 2` phosphate of the adenosine ribose of NADPH. Hydrogen bonds between phosphate moieties and ribose hydroxyl groups of the co-factors with the backbone amide groups of the protein are responsible for productive enzyme-cofactor interactions.

A complete kinetic analysis of *Synechocystis* BVR-A has not yet been reported. The cyanobacterial enzyme was the first BVR-A to appear in evolution and its characterisation should therefore provide information on the evolution of the mechanism of an enzyme from 3 billion years ago to the present day. However, before undertaking this study it was important to establish if the *Synechocystis* enzyme was subject to the same potent substrate inhibition as the mammalian enzymes as this behaviour complicates the gathering and interpretation of initial rate data.

4.2 Determination of the extinction co-efficient for bilirubin IXα

The extinction co-efficient for bilirubin at pH 4, 5, 6, 7, 8 and 9 was determined by recording the absorbance of known concentrations (0, 1, 2, 5, 10, 20μM) of bilirubin at 460nm and using the Beer-Lambert law ($A = \varepsilon.c.l$) to calculate the extinction co-efficient at each pH value. Fig. 4.1 shows that over the range of pH values studied and bilirubin concentrations used the graph is linear and there is a proportional increase in absorbance with concentration. The extinction co-efficient for bilirubin at any of the pH values used could therefore be accurately determined using the Beer-Lambert law. The extinction co-efficient for bilirubin remained relatively unchanged from pH4-5 with a small increase from pH5-6 and a further increase up to pH9 (see Table 4.2). It

is important to note that the stock solution of bilirubin was 1mM in DMSO (100%) and that the absorbance was measured immediately after dilution into buffer. With time the bilirubin precipitates and "coats" the walls of the cuvette (Phillips, 1981).

4.3 The effect of pH on enzyme activity

4.3.1 pH optimum for activity of sBVR-A

The effect of pH on the activity of sBVR-A was examined over a range of pH values and the optimum pH was established with both NADPH and NADH as co-factor. Fig. 4.2 shows that the optimum pH for activity with both co-factors was pH5. The activity of sBVR-A increased dramatically from pH4, peaked at pH5 and then decreased gradually as the pH was raised to pH7. This change in activity was seen with both co-factors. From this evidence it was concluded that the optimum pH for activity of sBVR-A was pH5 and all subsequent initial rate experiments were carried out at this pH. It should be noted that the enzyme was very stable between pH 5 to 7, however it exhibited dramatic instability at pH4 with a half life of only 30seconds at this pH (see below).

4.3.2 pH stability of *s*BVR-A

The experiments on pH stability were carried out to determine how stable the recombinant sBVR-A was over a range of pH values. Recombinant enzyme (5μg) was pre-incubated in buffers (100mM) ranging from pH4-9 for 10-180min and then assayed in 100mM sodium citrate, pH5. Fig. 4.3 shows that when NADPH is the co-factor sBVR-A is stable over most of the pH range used but loses activity at the extremes of pH: 4 and 9. It may be the case that at pH8 and 9 the enzyme is changing to an alkaline form which has lower activity (see Fig. 4.3). At pH4 the enzyme is completely inactive after 10min. A time course of inactivation of sBVR-A at pH4 shows that the enzyme loses 50% of its activity after 30sec, 90% after 1min and is completely inactive after 3 min at this pH (see Fig. 4.4). It should also be noted that the loss of activity between pH5 and 7 (in Fig. 4.2) is reversible but at pH4 the enzyme is irreversibly inactivated.

4.4 Initial rate kinetics of sBVR-A

4.4.1 Effect of enzyme concentration on initial rate

Fig 4.5 shows that at pH5 there is a linear relationship between initial rate and enzyme concentration over the range (0-10μg). Under these conditions true initial rates were being measured and all kinetic experiments were carried out within this range.

4.4.2 Effect of biliverdin concentration on initial rate kinetics of sBVR-A

These experiments were set up to determine whether the recombinant sBVR-A was effected by substrate inhibition by biliverdin at pH5. Both NADPH and NADH were used as co-factors and the biliverdin concentration was varied from 0.5-50μM. Fig. 4.6 clearly shows that with biliverdin as the variable substrate simple hyperbolic kinetics were observed up to 50μM biliverdin. It was therefore concluded that sBVR-A is not subject to substrate inhibition over the concentration range studied and that initial rate kinetics with biliverdin as the variable substrate could be conducted.

4.4.3 NADPH/NADH kinetics

Initial rate experiments with NADPH or NADH as the variable substrate were carried out by working at various fixed concentrations of biliverdin and varying the concentration of NADPH from 5-100μM or NADH from 50-1000μM. The "fixed" concentrations of biliverdin were also varied from 0.5-10μM to yield the 5 x 5 plot for NADPH seen in Fig 4.7. The curve fitting program "Wincurvefit" was used to fit the data to the Michaelis-Menten equation (equation 1). The apparent V_{max} values for NADPH were then replotted against the biliverdin concentration (see Fig. 4.9) to yield the true V_{max} and true K_m values for biliverdin with NADPH as co-factor (see Table 4.3). The initial rate measurements also yielded linear double reciprocal plots (see Fig. 4.8) and it was from these plots that the mechanism of sBVR-A was determined. The series of lines from these plots intersected behind the y-axis suggesting that the mechanism was sequential, where one of the substrates bound before the other and both must be present on the enzyme at the same time for catalysis to occur. However, these experiments could not tell which of the substrates bound first or if there was any particular order in their binding.

Experiments were repeated with NADH as the variable substrate and suggested that the mechanism at pH5 was also sequential with NADH. Results for NADH are shown in *Appendix II.* Fig. 1 in *Appendix II* shows the initial rates fitted to a hyperbola, Fig. 2 shows the double reciprocal plots and Fig. 3 shows the apparent V_{max} values plotted against the concentration of biliverdin. Kinetic parameters for biliverdin with NADH as co-factor are shown in Table 4.3.

4.4.4 Biliverdin kinetics

Initial rate experiments with biliverdin as the variable substrate were carried out similarly to those described for NADPH but now various "fixed" concentrations of NADPH were used and the biliverdin concentration was varied from 0.5-10μM. Curve fitting programs were used to fit the initial rate data to the Michaelis-Menten equation (see Fig. 4.10). The true V_{max} and K_m values for NADPH were calculated by re-plotting the apparent V_{max} values (obtained from the fits in Fig.

4.10) against the NADPH concentration (see Fig. 4.12) and the kinetic constants for NADPH are shown in Table 4.3. The initial rate data with biliverdin as the variable substrate also yielded linear intersecting double-reciprocal plots consistent with a sequential mechanism (see Fig. 4.11).

Experiments were repeated with biliverdin as the variable substrate and NADH as co-factor. Results for NADH are shown in *Appendix II.* Results were again consistent with those for NADPH. Fig. 4 in *Appendix II* shows the initial rates fit to a hyperbola; Fig. 5 shows the associated double reciprocal plot and Fig. 6 shows the apparent V_{max} values plotted against the NADH concentration. Kinetic parameters for NADH are shown in Table 4.3.

4.5 Effect of inorganic phosphate on the initial rate kinetics of sBVR-A

Inorganic phosphate anion has been shown to be an activator of human BVR-A (Franklin *et al.*, 2007). Experiments were set up to examine if inorganic phosphate had the same effect on the *Synechocystis* enzyme. Increasing amounts of sodium phosphate (0-100mM) were added to the sBVR-A assay under optimum conditions using both NADH and NADPH as co-factor and at both pH5 and pH7. The pH was monitored before and after the assay to ensure it did not change significantly when adding increasing amounts of phosphate. The effect of ionic strength was found to be minimal. Inorganic phosphate was found to have no effect on sBVR-A activity with either co-factor at either pH (see Fig. 4.13). It was therefore concluded that unlike the human enzyme inorganic phosphate was not an activator of sBVR-A. This is a major discriminating feature between the cyanobacterial enzyme and the vertebrate BVR-A family members.

4.6 Product inhibition studies

4.6.1 $NADP^+$/ NAD^+ inhibition

$NADP^+$ inhibition with NADPH as the variable substrate was carried out at saturating (10μM) levels of biliverdin. The inhibitory concentrations of $NADP^+$ ranged from 0-100μM while the concentration of NADPH was varied from 5-100μM. Curves were again fitted to the initial rate data set (see Fig. 4.20) and used to yield double reciprocal plots (see Fig. 4.14). The pattern of the double-reciprocal plots shows that $NADP^+$ exhibits competitive kinetics against NADPH (see Fig. 4.15). When the slope values of the double-reciprocal plots were re-plotted against the inhibitor concentration a linear relationship was obtained and used to determine the inhibitor constants K_{is} for $NADP^+$ (from the slope re-plot). The slope re-plot is shown in Fig. 4.16 and inhibitor values are shown in Table 4.4.

$NADP^+$ inhibition was also carried out with biliverdin as the variable substrate. These experiments were performed as described for NADPH but now the NADPH concentration was kept constant at

non-saturating levels (10μM) and saturating levels (1mM) of NADPH and the biliverdin concentration varied from 0.5-10μM. A concentration of 1mM was used for NADPH to ensure saturation. $NADP^+$ showed mixed inhibition against biliverdin at non-saturating levels of NADPH. Initial rate data was fitted to a rectangular hyperbola (see Fig 4.17) and the kinetic parameters used to generate double-reciprocal plots (see Fig. 4.18), slope re-plots (Fig. 4.19) and intercept re-plots (Fig 4.20) as described previously. When the experiment was repeated at saturating levels of NADPH no inhibition was observed (see Fig. 4.21) Inhibition constants (K_{is} from the slope re-plot and K_{ii} from the intercept re-plot) for $NADP^+$ with biliverdin as the variable substrate are shown in Table. 4.4.

Experiments with NAD^+ as the inhibitor against NADH as the variable substrate were carried out as described for $NADP^+$ with the NADH concentrations varied from 50-1000μM and the NAD^+ concentrations varied from 0-1000μM and are shown in *Appendix II*. Initial rate data at saturating levels of biliverdin is shown in *Appendix II* fitted to a rectangular hyperbola (Fig. 7), as the corresponding double-reciprocal plots (Fig. 8) and the corresponding slope re-plot (Fig. 9). NAD^+ showed competitive kinetics against NADH (see Fig. 9). Inhibitor constants for NAD^+ are shown in Table 4.4.

NAD^+ was a mixed inhibitor against biliverdin at non-saturating (100μM) levels of NADH (see *Appendix II*, Figs. 10, 11, 12 and 13).

4.6.2 Bilirubin inhibition

Bilirubin inhibition with biliverdin as the variable substrate was conducted at saturating (100μM) levels of NADPH. Bilirubin levels were increased from 0-10μM and biliverdin concentrations varied from 0.5-10μM. Initial rate data fitted to a rectangular hyperbola (Fig. 4.22), as the corresponding double-reciprocal plots (Fig. 4.23) and the corresponding slope (Fig 4.24) and intercept (Fig. 4.25) re-plots are shown in the figures indicated. Inhibition constants for bilirubin with biliverdin as the variable substrate are shown in Table 4.4. Fig. 4.23 shows that bilirubin is a mixed inhibitor against biliverdin at saturating levels of NADPH.

Product inhibition experiments with bilirubin as an inhibitor were also conducted with NADPH as the variable substrate (5-100μM) at non-saturating (1μM) and saturating (10μM) levels of biliverdin. Initial rate data for non-saturating levels of biliverdin fitted to a rectangular hyperbola is shown in Fig. 4.26 and as the corresponding double-reciprocal plots (Fig. 4.27) and slope (Fig 4.28) and intercept (Fig. 4.29) re-plots. Inhibition constants for bilirubin with NADPH as the variable substrate are shown in Table 4.4. Fig. 4.27 shows that bilirubin exhibits mixed inhibition

kinetics at non-saturating levels of biliverdin and when the experiment is repeated at saturating levels of biliverdin the inhibition becomes uncompetitive (see Fig. 4.31). The initial rate data set at saturating levels of biliverdin was fitted to a hyperbole (Fig. 4.30). The intercept re-plot from Fig. 4.31 is shown in Fig. 4.32.

Bilirubin exhibits mixed inhibition against NADH at non-saturating levels of biliverdin (see Appendix II, Figs. 14, 15, 16, and 17) and mixed inhibition against biliverdin at saturating levels of NADH (see Appendix II, Figs. 18, 19, 20, and 21). Inhibition constants are shown in Table 4.4.

A complete determination of the kinetic mechanism for *Synechocystis* BVR-A has not been described previously. Before embarking on this study a number of factors had to be taken into account. Most mammalian forms of BVR-A exhibit potent substrate inhibition so that the "linear" portion of double reciprocal space is limited severely. As much diagnostic information is obtained from double reciprocal patterns this severely restricts the interpretation of the initial rate kinetics. For example Rigney (1988) has shown that for the ox kidney enzyme as the biliverdin concentration approaches 10μM the enzyme becomes subject to potent substrate inhibition caused by biliverdin binding to an enzyme-$NADP^+$ complex and driving formation of a non-productive enzyme.$NADP^+$.biliverdin complex. Studies undertaken on the human enzyme by Dunne (2000) demonstrate an additional problem in many assays of BVR-A activity in the absence of a biliverdin binding protein (eg. BSA). Without BSA product time curves deviate from linearity very rapidly after initiation of the reaction. This makes it difficult to record reliable data. The addition of BSA gives stable initial rates, however it also introduces two factors that require correction. The first is an approximate doubling of the extinction co-efficient for bilirubin (at pH7.4) and the second is that the total biliverdin added is no longer "identical" to the free concentration. Previous work by Phillips (1981) and Rigney (1988) have tried to correct for these two complications but only with partial success. Phillips (1981) could only achieve a reasonable fit to the data with a physically unlikely number of biliverdin binding sites (N=10) with anomalously high dissociation constants (K_d=500mM). Therefore, it is far from ideal to include BSA in the assay for detailed kinetic studies. Indeed the ox kidney mechanism was elucidated in the absence of BSA (Rigney *et al.,* 1989), however the conditions were not optimal as the pH used was 9.

Schluchter & Glazer (1997) reported that *Synechocystis* BVR-A had an optimum of pH5.8, making it different to the mammalian enzymes which typically have optimums between pH7 and 8. However, the salmon enzyme has been described as having an optimum with NADH at pH6 (Elliot, 1996) and the *Xenopus tropicalis* enzyme has also been shown to exhibit significant activity at pH5 (Franklin, 2006). The pH optimum of sBVR-A determined in the present study was 5, a very acidic pH that may reflect an unusual location in the cell, possibly the intrathylakoid space. Interestingly both NADPH and NADH dependent activities showed the same pH dependent profiles, albeit that the NADPH activity was approximately 2-3 times that supported by NADH. The pH optimum described in the present study (pH5) is slightly different to that described by Schluchter & Glazer (1997). One difference between the two studies was in the way the recombinant proteins were cloned and heterologously produced. The sBVR-A described by Schluchter & Glazer (1997) was cloned with an N-terminal hexahistidine tag which facilitated

purification using Ni^{2+} affinity chromatography. However, the his-tag was not removed. The sBVR-A described in the present study was cloned as a GST-tagged protein and following purification the GST tag was removed. This may account for the different pH optimums observed. The sBVR-A purified in the present study has a pH optimum of 5 and all detailed initial rate studies were carried out at this pH. pH stability experiments were also conducted and revealed that sBVR-A was stable for at least 10 minutes at most of the pH values tested. At pH4 however, the enzyme was completely inactive after 10min and the time-course of inactivation revealed the half-life was 30sec. At pH5 the enzyme is relatively stable over a 3hour period. At pH9 there is some loss of activity, however, by following the time course of "inactivation" at both pH8 and pH9 the enzyme may be slowly transforming to an "alkaline form" with 80% of the specific activity.

A linear relationship was demonstrated between initial rate and enzyme concentration over the range 0-10μg and all the kinetic experiments described in this study were conducted within this range. It was also important to establish if sBVR-A was subject to substrate inhibition by biliverdin at its optimum pH of 5 as this would determine in how much detail the kinetic mechanism could be studied. The concentration of pyridine nucleotide was kept constant and the biliverdin concentration varied from 0.5-50μM. Concentration of biliverdin was not increased further as it precipitates at 100μM at pH5. Fig 4.6 clearly shows that at concentrations up to 50μM there was no decrease in the initial rate of sBVR-A with either NADPH or NADH as co-factor and both data sets gave good fits to a rectangular hyperbola. Under these conditions the *Synechocystis* enzyme is not subject to substrate inhibition and the complete kinetics with both NAD(P)H and biliverdin as the variable substrate could be completed at the optimum pH. It also allowed a complete mechanistic analysis to be undertaken.

Experiments varying NADPH and NADH revealed that NADPH was the preferred nucleotide for enzyme mediated reduction of biliverdin as the K_m for NADH is approximately 20 fold higher than that observed with NADPH as co-factor. The k_{cat} with NADPH as co-factor is approximately 2-3 times that observed with NADH. This difference is due to the 2' phosphate of NADPH which increases its affinity for the enzyme and possibly interacts with an arginine residue at or near the active site. Kikuchi *et al.,* (2001) have tentatively identified Arg 44 and Arg 45 as residues important in binding the 2' phosphate of NADPH. The *Synechocystis* enzyme, however, lacks both these arginine residues but does possess a lysine residue at position 44 which may be involved in NADPH binding. The *Synechocystis* enzyme does possess two arginine residues near the putative active site (Arg 34 and Arg 35) and there is an arginine residue conserved in all BVR-As at the putative active site (Arg 25 in the Synechocystis enzyme) which may be involved in binding the 2' phosphate of NADPH (see Fig. 5.12 for a multiple sequence alignment of all known BVR-As,

including the *Synechocystis* enzyme). It is likely that NADPH is the physiologically relevant co-factor. NADPH has a much higher affinity for all BVR-As and likely forms part of the binding pocket for biliverdin or results in a conformational change within the enzyme which then allows biliverdin to bind. The crystal structure of rat BVR-A reported by Kikuchi *et al.,* (2001) and Whitby *et al.,* (2002) suggest that BVR-A has only one nucleotide binding site, defined by a Rossman fold and composed of residues Gly 15, Val 16, Gly 17, Arg 18, Ala 19, and Gly 20 of the known rat crystal structures (see Fig. 4.33A). When carrying out detailed kinetic studies at pH5 it was important to note that pyridine nucleotides are particularly unstable at acidic pH values. Wu *et al.,* (1986) reported that at pH5 and 30°C the half life of NADPH was only 38min. Franklin (2006) reported that the rate of breakdown of these nucleotides is 2.6μM/min for NADPH and 1μM/min for NADH. In the kinetic experiments described in this chapter both nucleotides were freshly prepared each day in 10mM sodium phosphate, pH7 or 10mM Tris, pH7.5 and stored on ice prior to use to prevent degradation. All initial rates were measured during the first 30sec or less to avoid added complications of nucleotide breakdown.

BVR-A has been reported to be unique among all enzymes by having "dual co-factor/pH activity" (Kutty & Maines, 1981). This unusual property of the enzyme having two apparent pH optima, one at pH6.5-7 when using NADH as co-factor and another at pH8-9 with NADPH as co-factor has been reported for both the recombinant and native rat and human enzymes (Kutty & Maines, 1981; Maines *et al.,* 1996; Yamaguchi *et al.,* 1994), pig spleen enzyme (Noguchi *et al.,* 1979) and ox kidney enzyme (Rigney & Mantle, 1988). However, this effect has recently been shown to result from activation of BVR-A by inorganic phosphate anion which is the usual buffer system when assaying the enzyme with NADH at neutral pH values (Franklin *et al.,* 2007). Inorganic phosphate anion activates human BVR-A by mimicking the 2' phosphate of NADPH (Franklin *et al.,* 2007). For the human enzyme the activation effect of phosphate is due to its ability to enhance NADH binding as the apparent K_m for NADH is decreased over 100-fold with no change in the apparent V_{max} (Franklin *et al.,* 2007). In light of these observations phosphate was investigated as a potential activator of sBVR-A. Inorganic phosphate was found to have no effect on activity with NADPH or NADH as co-factor at either pH5 or pH7 (see Fig. 4.13). It was therefore concluded that unlike vertebrate BVR-As the *Synechocystis* enzyme was not activated by inorganic phosphate. In order to understand why vertebrate BVR-As are activated by phosphate and sBVR-A is not, the known crystal structures of the rat BVR-As were examined, as well as the amino acid sequences of all known BVR-As, including the *Synechocystis* enzyme. By examining the rat crystal structure of Whitby *et al.,* (2002) it was clear that the enzyme co-crystallized with three inorganic phosphate molecules, one of which occupies a site which is the proposed binding pocket for the 2' phosphate of NADPH (see Fig. 4.33). As shown in Fig 4.34 the proposed residues

involved in phosphate binding: Ser 43, Arg 44 and Arg 45 produce hydrogen bond interactions with the inorganic phosphate molecule. Site-directed mutagenesis studies by Franklin *et al.,* (2007) clearly showed that when Arg 44 was mutated to an alanine residue no phosphate activation was observed. Kikuchi *et al.,* (2000) also found, through a similar approach that Arg 44 played a significant role in promoting tighter binding of NADPH over NADH. Based on this evidence Arg 44 was identified as the putative residue involved in promoting tighter binding of NADPH and the phenomenon of phosphate activation in vertebrate BVR-As. Interestingly, by examination of the aminoacid sequences of all known BVR-As only the vertebrate forms of the enzyme have the equivalent of Arg 44 and Arg 45. The *Synechocystis* enzyme does not have arginine residues in these positions, resulting in the inability to bind the 2' phosphate at or near the NADPH binding pocket and this can possibly explain why no phosphate activation is observed with this enzyme. However, NADPH is the preferred co-factor so the absence of Arg 44 or Arg 45 is not responsible for determining the co-factor specificity of sBVR-A.

The initial rate studies produced a series of lines that intersected to the left of the ordinate when either substrate was varied at different fixed levels of the other substrate. This suggests that the mechanism of sBVR-A is sequential, where both substrates must be present on the enzyme prior to product release. However, this provided no evidence as to which of the substrates bound first or if there was any order to their binding. For this reason the mechanism was further investigated by conducting a complete product inhibition study. When $NADP^+$ was the inhibitor and NADPH the variable substrate competitive kinetics were observed at saturating levels of biliverdin. The same effect is observed at non-saturating levels of biliverdin. This suggested that $NADP^+$ could directly compete with NADPH for binding to the free enzyme and that there was a mutually exclusive nucleotide binding site on the enzyme. This also suggests that NADPH is the first substrate to bind and $NADP^+$ is the last product to leave. Attempts to demonstrate binding of pyridine nucleotide to the free enzyme using the quenching of protein fluorescence were thwarted by the tight binding NADPH described in Section 3.6.2. When $NADP^+$ was the inhibitor but this time NADPH fixed at non-saturating levels and biliverdin the variable substrate mixed inhibition was observed. This arises from $NADP^+$ binding to the free enzyme and biliverdin binding to the enzyme-NADPH complex. When this experiment was repeated at saturating levels of NADPH no inhibition was observed. The same patterns of inhibition were observed when NAD^+ was the inhibitor and NADH the variable substrate which suggests that the mechanism of sBVR-A is the same with NADPH and NADH.

When bilirubin was the inhibitor and biliverdin the variable substrate, at saturating and non-saturating levels of NADPH mixed inhibition was observed. Bilirubin can only bind to the

enzyme-$NADP^+$ complex and biliverdin binds the enzyme-NADPH complex. The inhibitor (bilirubin) and variable substrate (biliverdin) bind to different enzyme forms. At saturating levels of NADPH mixed inhibition was also observed. When bilirubin was the inhibitor but this time NADPH the variable substrate at non-saturating levels of biliverdin the inhibition pattern was again mixed. The inhibitor and variable substrate bind to different enzyme forms, bilirubin to the enzyme-$NADP^+$ complex and NADPH to the free enzyme. However, when NADPH was the variable substrate but this time at saturating levels of biliverdin, inhibition by bilirubin exhibited a different pattern and switched from mixed at non-saturating levels of biliverdin to uncompetitive at saturating levels. Because bilirubin binds to the enzyme-$NADP^+$ complex and biliverdin binds to the enzyme-NADPH complex, at saturating biliverdin levels bilirubin will be an uncompetitive inhibitor against NADPH which binds to the free enzyme. This change in inhibition patterns from mixed to uncompetitive is diagnostic for a strictly ordered sequential mechanism.

These experiments suggest that the mechanism of sBVR-A is consistent with an ordered sequential mechanism with NAD(P)H the first substrate to bind and bilirubin the first product to dissociate (see Fig. 4.35). The intersecting lines produced by the initial rate studies suggest a sequential mechanism and rule out a Ping Pong mechanism. Product inhibition studies then suggest an ordered sequential steady state mechanism. A rapid equilibrium random BiBi mechanism is ruled out because bilirubin is a mixed inhibitor against biliverdin as the variable substrate. If this was a random sequential mechanism where both products and both substrates could bind to free enzyme then both bilirubin and $NADP^+$ would be competitive inhibitors of NADPH when biliverdin is held constant and biliverdin when NADPH is held constant. This is clearly not the case. An equilibrium ordered mechanism is also ruled out because in this mechanism the binding of substrate NADPH and its product $NADP^+$ are assumed to be at equilibrium and $NADP^+$ is rapidly released from the enzyme-bilirubin-$NADP^+$ complex once it is formed. $NADP^+$ therefore cannot inhibit against NADPH or biliverdin when they are at saturating levels. A Theorell-Chance mechanism is also ruled out because in this mechanism no ternary complex is formed by the enzyme and substrates. If this was such a mechanism increasing biliverdin at saturating and non-saturating levels of NADPH would overcome the effect of bilirubin because no enzyme-NADPH-biliverdin complex is formed. There would therefore be competitive inhibition. These results are consistent with the mechanism of the ox kidney BVR-A at pH9 (Rigney & Mantle, 1988).

Substrate	Co-substrate	Guinea-pig liver (a)	Guinea-pig liver (b)	Rat kidney (c)	Rat liver (d)	Rat liver (e)	Ox kidney (f)	Pig spleen (d)	Human liver (h)
Biliverdin	**NADPH**	-	0.2	3.7	0.3	3	-	0.3	0.3
Biliverdin	**NADH**	0.6 – 1.4	1 - 2	-	3	5	5	1-2	-
NADPH	**Biliverdin**	-	2 - 5	-	3	3	-	0.5	13 - 36
NADH	**Biliverdin**	240	200 - 500	-	1500-2000	270	500	1500-2000	5600-8200

Table 4.1 Apparent K_m values for biliverdin and NADPH/NADH. Values indicated are in substrate concentration (μM)

(a) Singleton & Lancaster (1965)
(b) O'Carra & Colleran (1971)
(c) Tenhunen *et al.* (1970)
(d) Noguchi *et al.* (1979)
(e) Kutty & Maines (1981)
(f) Phillips (1981)
(g) Yamaguchi *et al.* (1994)

Adapted from Rigney (1986)

	V_{max} (µmoles/min/mg)	K_m (µM)	k_{cat} (s^{-1})	k_{cat}/K_m ($M^{-1}s^{-1}$)
NADH	0.29 +/- 0.04	207 +/- 66	0.17	825
NADPH	0.78 +/- 0.07	10.8 +/- 3.2	0.44	4.1×10^4
Biliverdin (NADH variable)	0.24 +/- 0.027	1.6 +/- 0.55	0.15	94×10^4
Biliverdin (NADPH variable)	0.79 +/- 0.07	2.3 +/- 0.59	0.45	196×10^4

Table 4.3 Kinetic parameters for sBVR-A at pH5

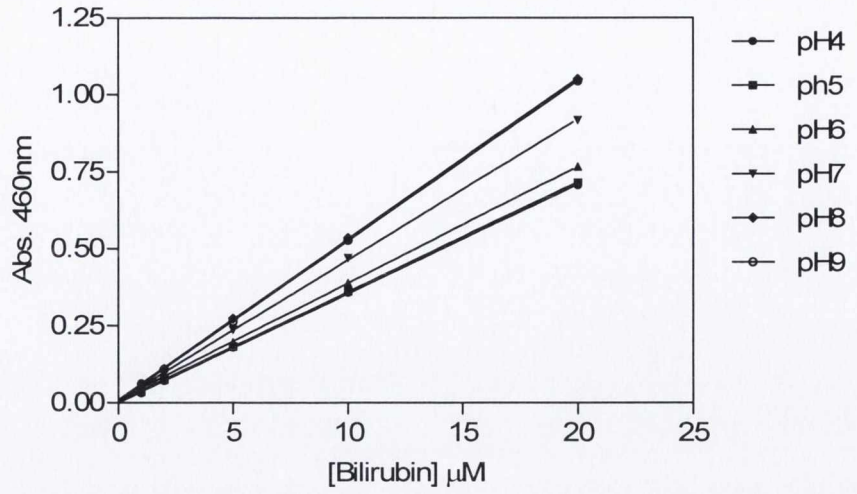

Figure 4.1 Determination of the extinction co-efficient for bilirubin IXα

The absorbance values of various concentrations of bilirubin IXα (0-20μM) at 460nm were used to calculate the extinction co-efficient using the Beer-Lambert law (A = ε.c.l). The buffers used (at a final concentration of 100mM) were sodium citrate (pH 4 and 5), sodium phosphate (pH 6 and 7) and Tris (pH 8 and 9).

pH	Extinction co-efficient (M^{-1} cm^{-1})
4	35.3×10^3
5	35.75×10^3
6	38.35×10^3
7	45.85×10^3
8	52.55×10^3
9	52.2×10^3

Table 4.2 Extinction co-efficients for bilirubin IXα at various pH values

Extinction co-efficients were calculated using the absorbance at 460nm of known concentrations of bilirubin IXα (0-20μM) and the Beer-Lambert law (A = ε.c.l). The buffers used were sodium citrate (pH 4 and 5), sodium phosphate (pH 6 and 7) and Tris (pH 8 and 9)

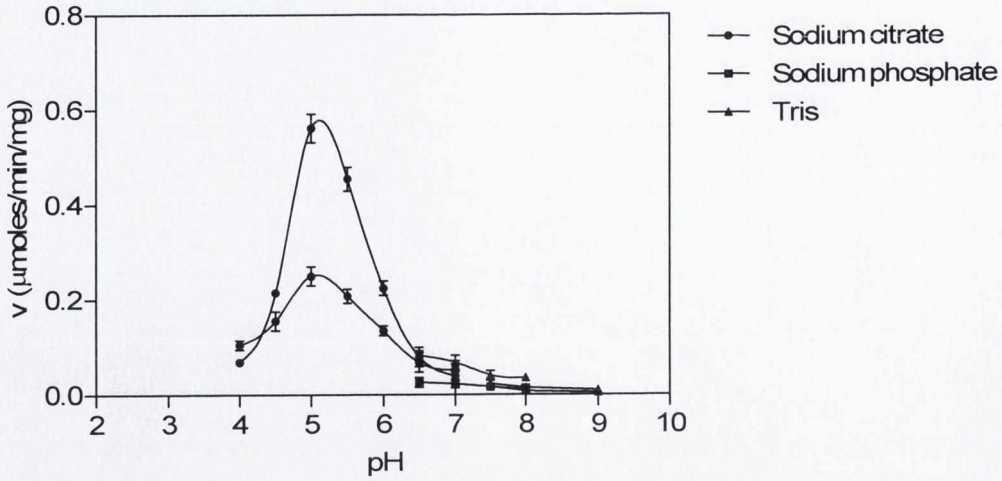
0.8
0.6
0.4
0.2
0.0
v (µmoles/min/mg)
2
3
4
5
6
7
8
9
10
pH
Sodium citrate
Sodium phosphate
Tris

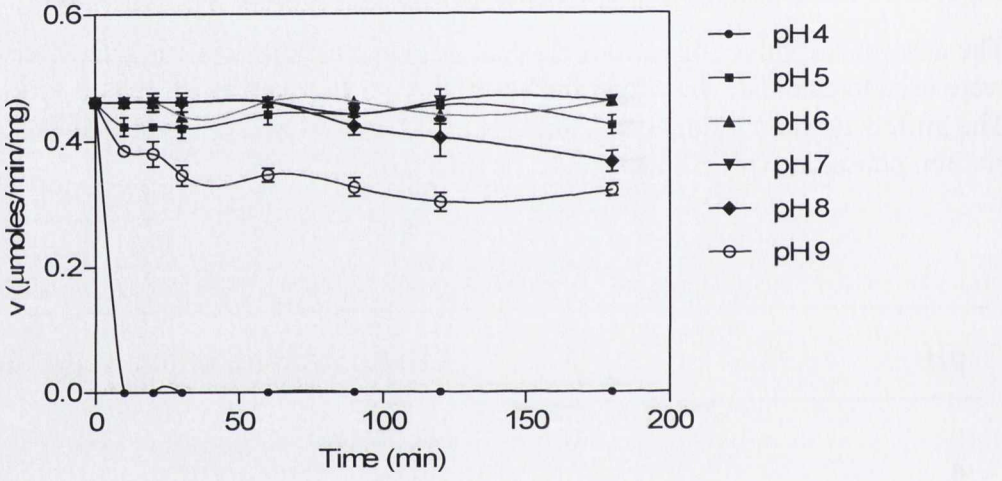
0.6
0.4
0.2
0.0
v (µmoles/min/mg)
0
50
100
150
200
Time (min)
pH4
pH5
pH6
pH7
pH8
pH9

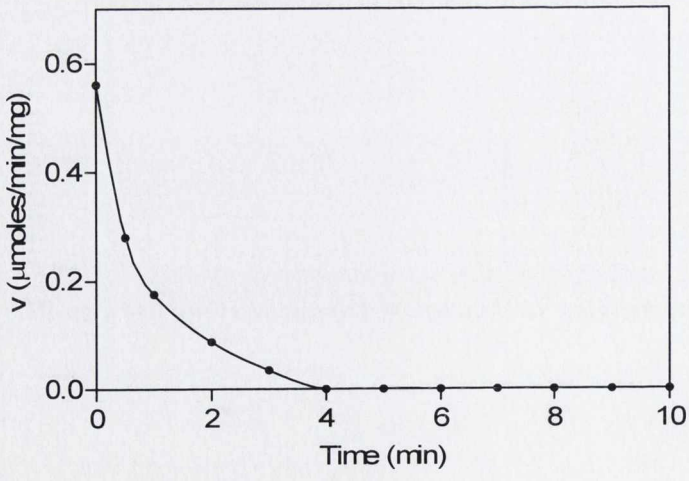
0.6
0.4
0.2
0.0
v (µmoles/min/mg)
0
2
4
6
8
10
Time (min)

Figure 4.2 pH profile of sBVR-A

Sodium citrate (100mM) was used to buffer in the range pH4-7 (pKs: 3.13, 4.76, 6.4). Sodium phosphate (100mM) was used from pH6-8 (pKs: 2.15, 7.2, 12.38). Tris-HCl (100mM) was used from pH8-9 (pK: 8.08). The pH profile shown in black is with NADPH as co-factor and in red is with NADH as co-factor. Experiments were performed in triplicate. Each datum point represents the mean and error bars represent the standard deviation of the triplicate values

Figure 4.3 pH stability of sBVR-A

5µg recombinant sBVR-A was incubated in buffers ranging from 4-9 for up to 3hours and assayed at the optimum pH (pH5). Sodium citrate (100mM) was used to buffer in the range pH4-7. Sodium phosphate (100mM) was used from pH6-8. Tris-HCl (100mM) was used from pH8-9. Experiments were performed in triplicate. Each datum point represents the mean and error bars represent the standard deviation of the triplicate values

Figure 4.4 Time dependence of the inactivation of sBVR-A at pH4

Experiments were conducted by incubating the enzyme (5µg) in sodium citrate (100mM), pH 4 for the indicated time periods and then assaying at pH5

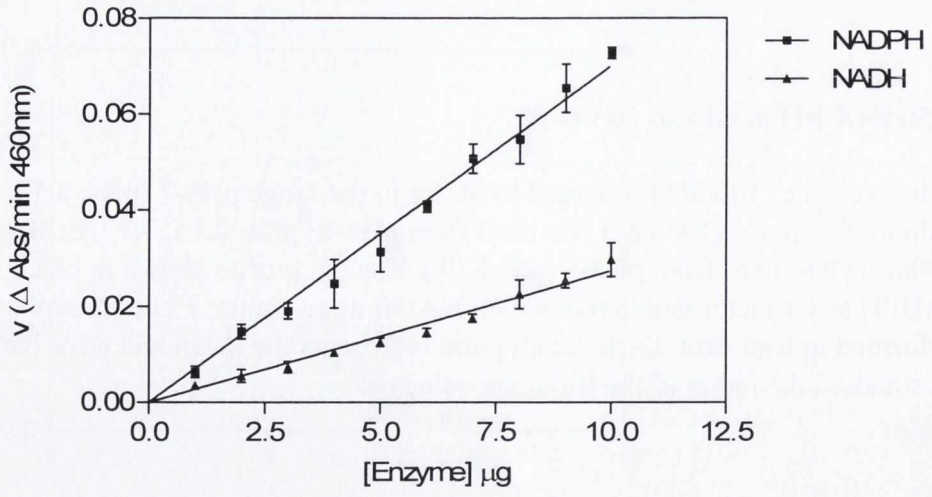

Figure 4.5 Effect of enzyme concentration on the initial rate of sBVR-A

Assays were performed in sodium citrate (100mM), pH5. Each assay (final volume 2ml) contained 0-10μg recombinant protein, 100μM NADPH or 1mM NADH and 10μM biliverdin IXα. The reaction was started by the addition of enzyme. Experiments were performed in triplicate. Each datum point represents the mean and error bars represent the standard deviation of the triplicate values. The solid lines are least squares fit to $y = mx+c$

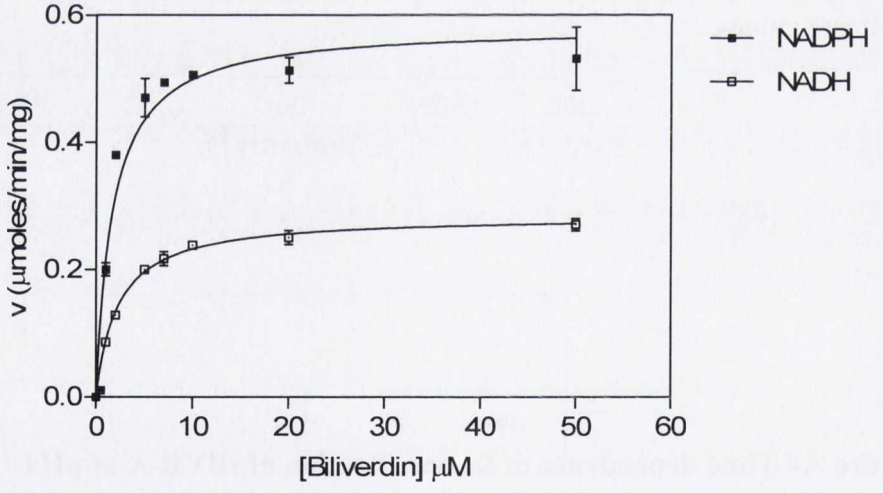

Figure 4.6 Effect of biliverdin concentration on the initial of sBVR-A

Assays were performed in sodium citrate (100mM), pH5. Each assay contained 5μg recombinant protein, 100μM NADPH or 1mM NADH and 0.5-50μM biliverdin IXα. Experiments were performed in triplicate. Each datum point represents the mean and error bars represent the standard deviation of the triplicate values. The curves are least squares fit to the Michaelis-Menten equation (equation 1).

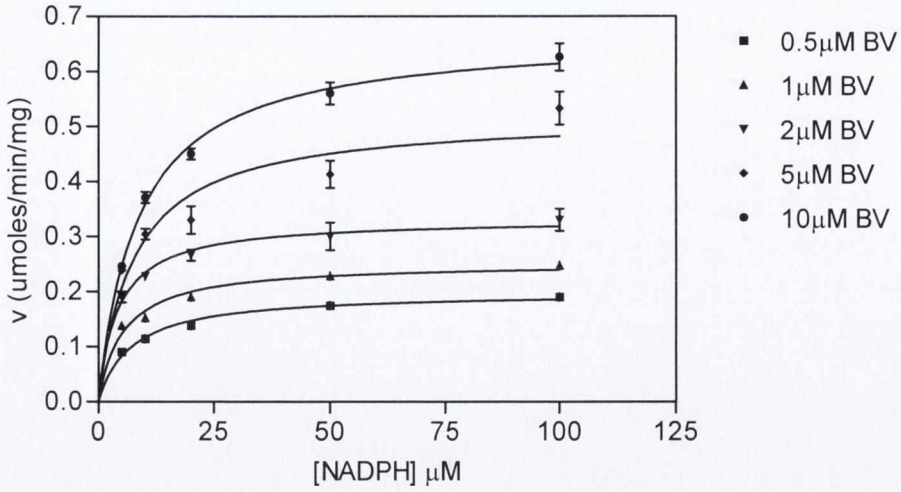
v (umoles/min/mg)
0.0
0.1
0.2
0.3
0.4
0.5
0.6
0.7
0
25
50
75
100
125
[NADPH] μM
0.5μM BV
1μM BV
2μM BV
5μM BV
10μM BV

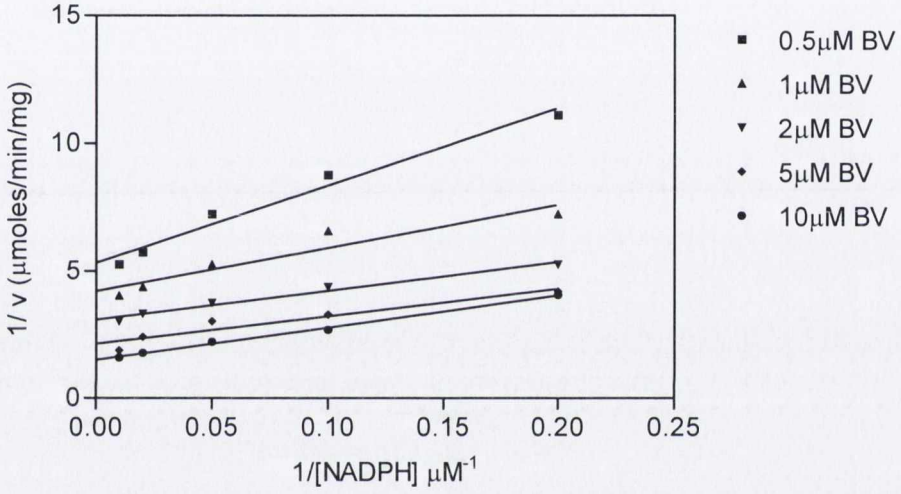
1/ v (μmoles/min/mg)
0
5
10
15
0.00
0.05
0.10
0.15
0.20
0.25
1/[NADPH] μM-1
0.5μM BV
1μM BV
2μM BV
5μM BV
10μM BV

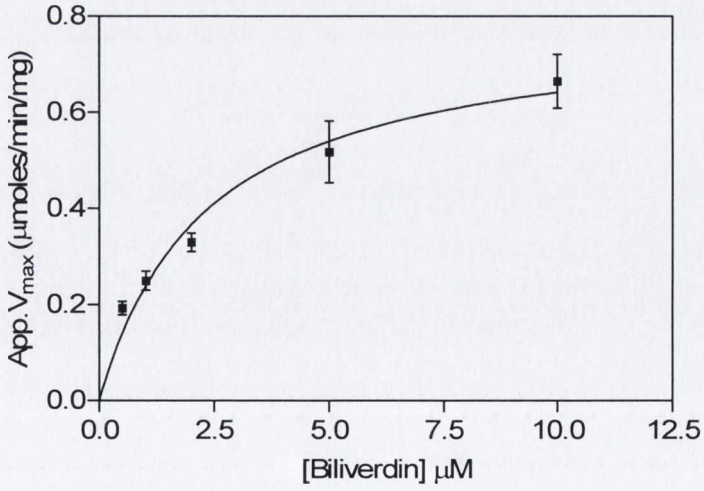
App. Vmax (μmoles/min/mg)
0.0
0.2
0.4
0.6
0.8
0.0
2.5
5.0
7.5
10.0
12.5
[Biliverdin] μM

Figure 4.7 Initial rate kinetics of sBVR-A with NADPH as the variable substrate

NADPH concentrations were varied from 5-100μM and biliverdin concentrations varied from 0.5-10μM. Reactions were performed in sodium citrate (100mM), pH5 and were initiated by the addition of sBVR-A (5μg). Experiments were performed in triplicate. Each datum point represents the mean and error bars represent the standard deviation of the triplicate values. The curves are least squares fit to the Michaelis-Menten equation (equation 1).

Figure 4.8 Double reciprocal plot with NADPH as the variable substrate

When the initial rates (see Fig. 4.7) were re-plotted as double reciprocals a pattern of linear intersecting lines was produced. These lines intersect to the left of the y-axis indicating a sequential mechanism. The solid lines are least squares fit to $y = mx+c$ and are for illustration purposes only. These were not used to determine kinetic parameters

Figure 4.9 Plot of apparent V_{max} *versus* biliverdin concentration

By re-plotting the apparent V_{max} values calculated against the various concentrations of the "fixed" substrate (biliverdin) it was possible to calculate the true V_{max} and true K_m for biliverdin (see Table 4.3). The curve is a least squares fit to the Michaelis-Menten equation (equation 1). Error bars represent the standard error

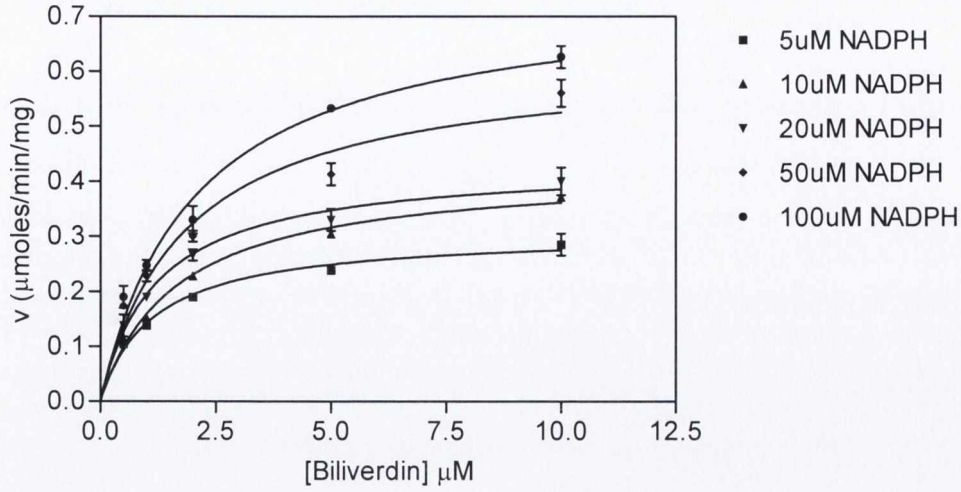
v (µmoles/min/mg)
0.0
0.1
0.2
0.3
0.4
0.5
0.6
0.7
0.0
2.5
5.0
7.5
10.0
12.5
[Biliverdin] µM
5uM NADPH
10uM NADPH
20uM NADPH
50uM NADPH
100uM NADPH

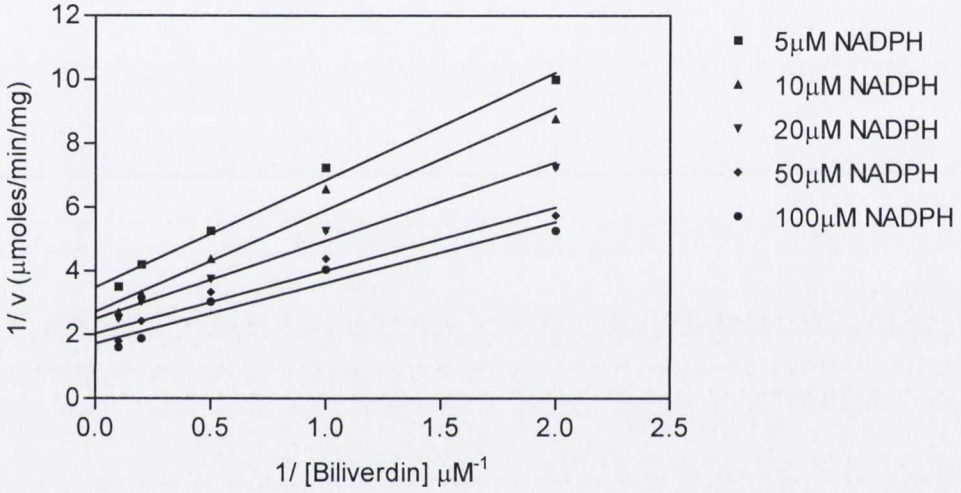
1/ v (µmoles/min/mg)
0
2
4
6
8
10
12
0.0
0.5
1.0
1.5
2.0
2.5
1/ [Biliverdin] µM-1
5µM NADPH
10µM NADPH
20µM NADPH
50µM NADPH
100µM NADPH

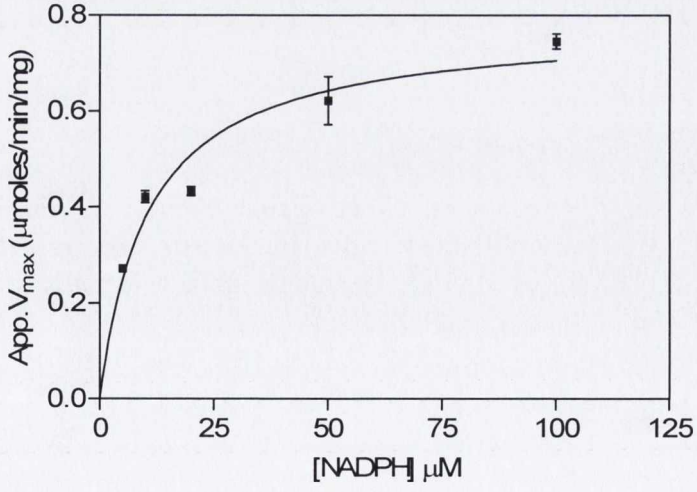
App. Vmax (µmoles/min/mg)
0.0
0.2
0.4
0.6
0.8
0
25
50
75
100
125
[NADPH] µM

Figure 4.10 Initial rate kinetics of sBVR-A with biliverdin as the variable substrate and NADPH as co-factor

Biliverdin concentrations were varied from 0.5-1μM and NADPH concentrations varied from 5-100μM. Reactions were performed in sodium citrate (100mM), pH5 and were initiated by the addition of sBVR-A (5μg). Experiments were performed in triplicate. Each datum point represents the mean and error bars represent the standard deviation of the triplicate values. The curves are least squares fit to the Michaelis-Menten equation (equation 1).

Figure 4.11 Double reciprocal plot with biliverdin as the variable substrate and NADPH as co-factor

When the initial rates (see Fig. 4.10) were re-plotted as double reciprocals a pattern of linear intersecting lines was produced. These lines intersect to the left of the y-axis indicating a sequential mechanism. The solid lines are least squares fit to $y = mx+c$ and are for illustration purposes only. These were not used to determine kinetic parameters

Figure 4.12 Plot of apparent V_{max} *versus* NADPH concentration

By re-plotting the apparent V_{max} values calculated against the various concentrations of the "fixed" substrate (NADPH) it was possible to calculate the true V_{max} and true K_m for NADPH (see Table 4.3). The curve is a least squares fit to the Michaelis-Menten equation (equation 1). Error bars represent the standard error

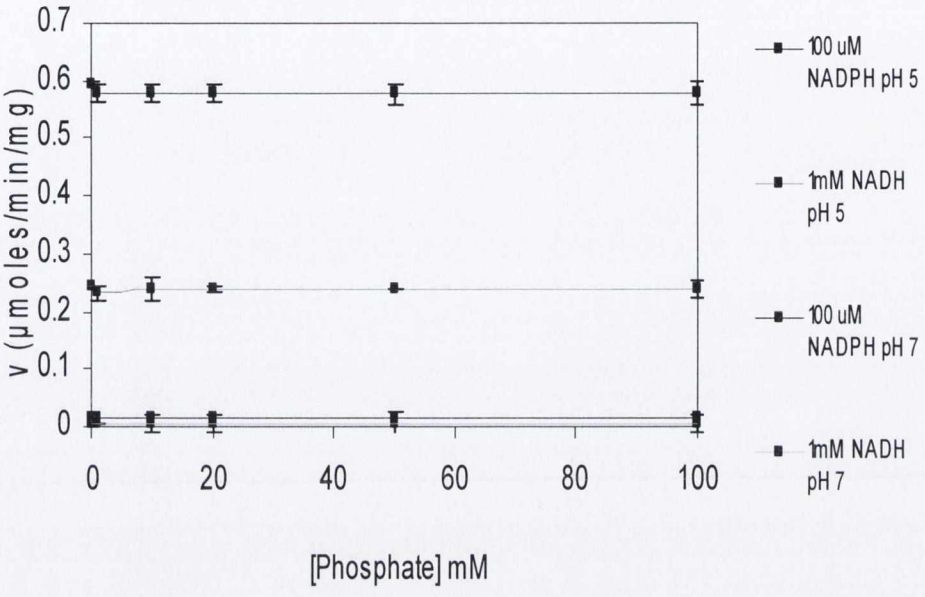

Figure 4.13 Effect of phosphate on the initial rate kinetics of sBVR-A

Sodium phosphate (0-100mM) was included in the sBVR-A assay as described in Section 4.5.

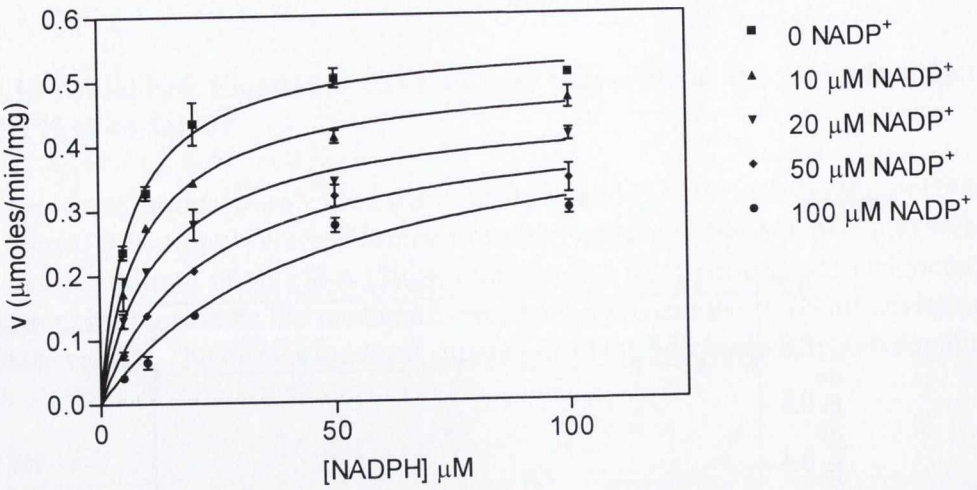
v (μmoles/min/mg)
0.6
0.5
0.4
0.3
0.2
0.1
0.0
0
50
100
[NADPH] μM
0 NADP+
10 μM NADP+
20 μM NADP+
50 μM NADP+
100 μM NADP+

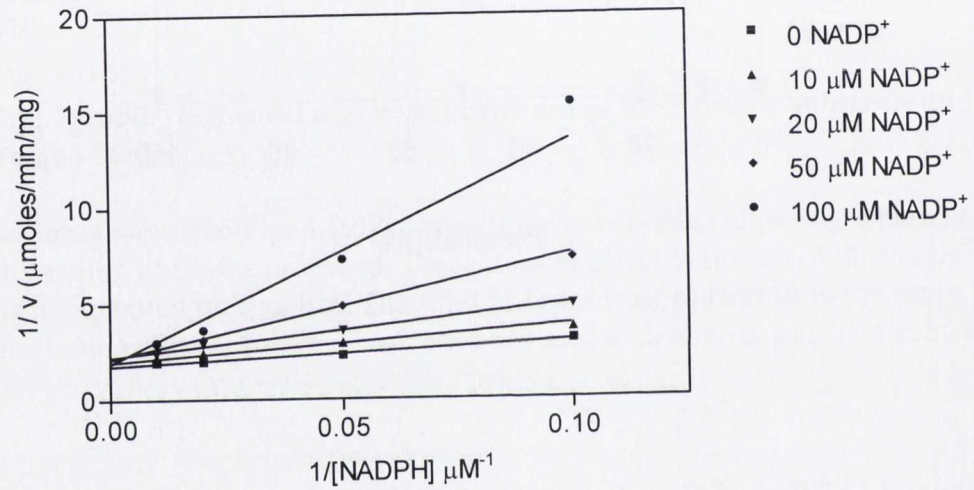
1/ v (μmoles/min/mg)
20
15
10
5
0
0.00
0.05
0.10
1/[NADPH] μM-1
0 NADP+
10 μM NADP+
20 μM NADP+
50 μM NADP+
100 μM NADP+

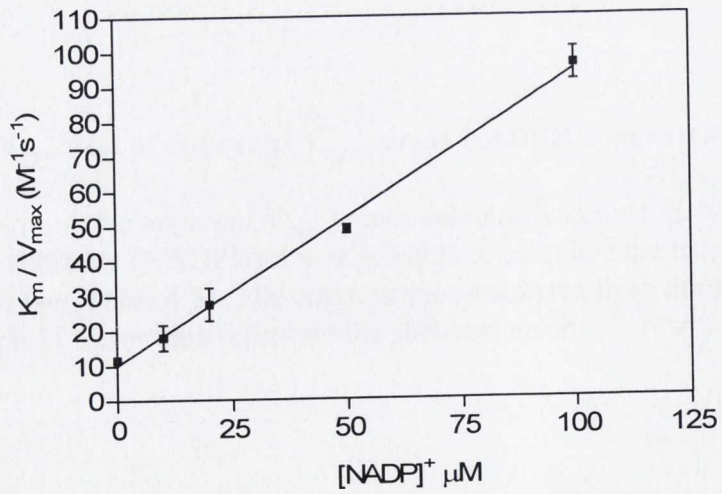
Km / Vmax (M-1s-1)
110
100
90
80
70
60
50
40
30
20
10
0
0
25
50
75
100
125
[NADP]+ μM

Figure 4.14 Initial rate kinetics of NADPH at varying concentrations of $NADP^+$ and saturating levels of biliverdin

NADPH was the variable substrate at concentrations ranging from 5-100μM. Biliverdin was held constant at saturating (10μM) levels. $NADP^+$ was increased from 0-100μM. Reactions were performed in sodium citrate (100mM), pH5 and were initiated by the addition of sBVR-A (5μg). Experiments were performed in triplicate. Each datum point represents the mean and error bars represent the standard deviation of the triplicate values. The curves are least squares fit to the Michaelis-Menten equation.

Figure 4.15 Double reciprocal plots with NADPH as the variable substrate at varying concentrations of $NADP^+$ and saturating levels of biliverdin

When the initial rates (see Fig. 4.14) were re-plotted as double reciprocals a pattern of linear intersecting lines was produced. These lines intersect at the y-axis indicating competitive kinetics.

Figure 4.16 Slope re-plot of $NADP^+$ inhibition with NADPH as the variable substrate and saturating levels of biliverdin

When the K_m / V_{max} (slope) values from the double-reciprocal plot shown in Fig. 4.15 were re-plotted against the concentration of $NADP^+$ a linear relationship was obtained where the line intersected the x-axis at $-K_{is}$. From this point the K_{is} value for $NADP^+$ against NADPH was calculated (see Table 4.4)

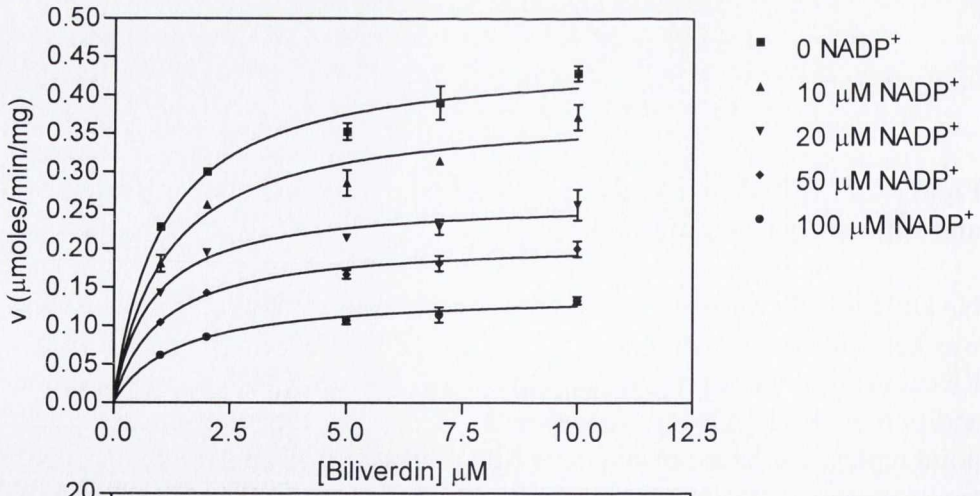
v (μmoles/min/mg)
[Biliverdin] μM
0 NADP+
10 μM NADP+
20 μM NADP+
50 μM NADP+
100 μM NADP+

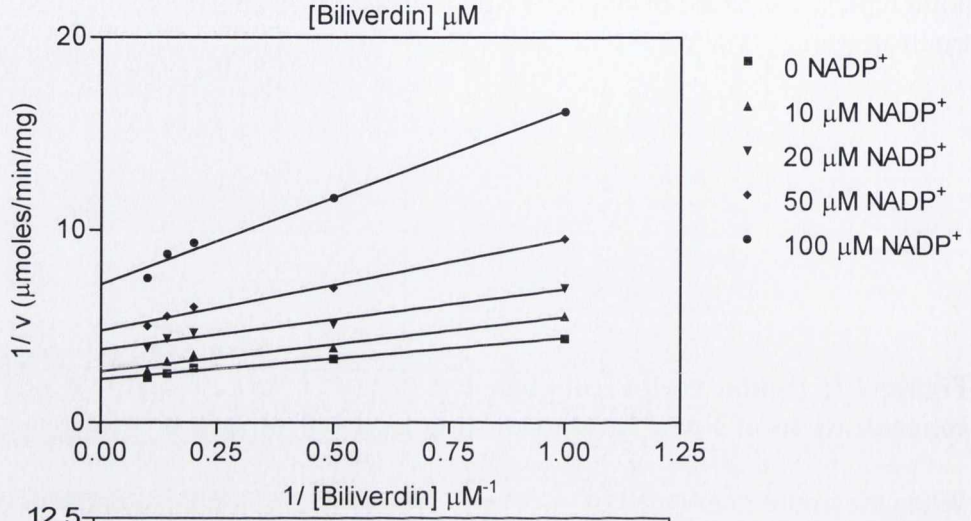
1/ v (μmoles/min/mg)
1/ [Biliverdin] μM-1
0 NADP+
10 μM NADP+
20 μM NADP+
50 μM NADP+
100 μM NADP+

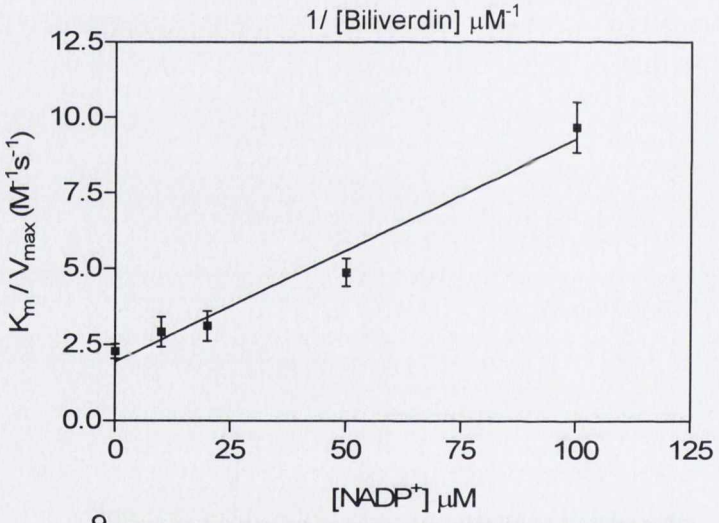
Km / Vmax (M-1s-1)
[NADP+] μM

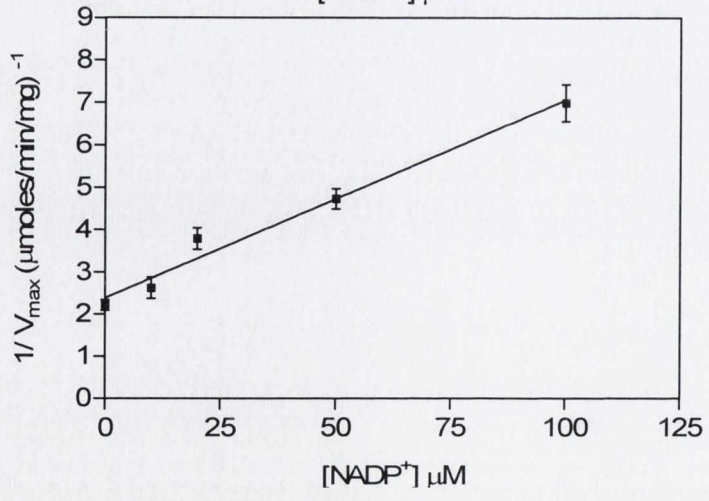
1/ Vmax (μmoles/min/mg) -1
[NADP+] μM

Figure 4.17 Product inhibition by $NADP^+$ with biliverdin as the variable substrate and non-saturating levels of NADPH

Biliverdin was the variable substrate at concentrations ranging from 0.5-10μM. NADPH was held constant at non-saturating levels (10μM). $NADP^+$ was increased from 0-100μM. Reactions were performed in sodium citrate (100mM), pH5 and were initiated by the addition of sBVR-A (5μg). Experiments were performed in triplicate. Each datum point represents the mean and error bars represent the standard deviation of the triplicate values. The curves are least squares fit to the Michaelis-Menten equation.

Figure 4.18 Double reciprocal plots of initial rate against biliverdin concentration at varying concentrations of $NADP^+$ and non-saturating levels of NADPH

When the initial rates (see Fig. 4.17) were re-plotted as double reciprocals a pattern of linear intersecting lines was produced. These lines intersect to the left of the y-axis indicating mixed inhibition.

Figure 4.19 Slope re-plot of $NADP^+$ inhibition with biliverdin as the variable substrate at non-saturating levels of NADPH

When the K_m / V_{max} (slope) values from the double-reciprocal plot shown in Fig. 4.18 were re-plotted against the concentration of $NADP^+$ a linear relationship was obtained where the line intersected the x-axis at $-K_{is}$. From this point the K_{is} value for $NADP^+$ against biliverdin was calculated (see Table 4.4) Error bars represent the standard error

Figure 4.20 Intercept re-plot of $NADP^+$ inhibition with biliverdin as the variable substrate at non-saturating levels of NADPH

When the 1/ V_{max} (intercept) values from the double-reciprocal plot shown in Fig.4.18 were re-plotted against the concentration of $NADP^+$ a linear relationship was obtained where the line intersected the x-axis at $-K_{ii}$. From this point the K_{ii} value for $NADP^+$ against biliverdin was calculated (see Table 4.4). Error bars represent the standard error

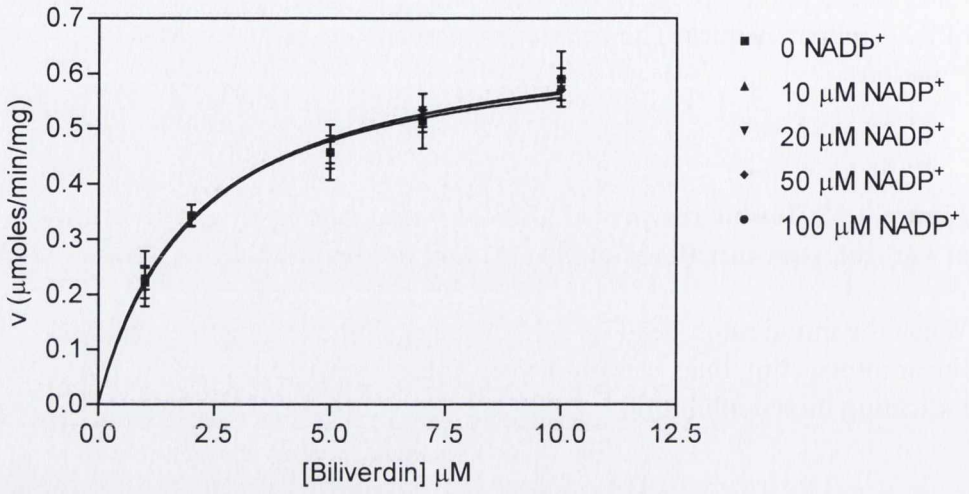

Figure 4.21 Initial rate kinetics of biliverdin at varying concentrations of $NADP^+$ and saturating concentrations of NADPH

Experiments were conducted at saturating levels of NADPH (1mM was used to ensure saturation). Biliverdin was the variable substrate at concentrations ranging from 1-10µM. $NADP^+$ was increased from 0-100µM. Reactions were performed in sodium citrate (100mM), pH5 and were initiated by the addition of sBVR-A (5µg). Experiments were performed in triplicate. Each datum point represents the mean and the error bars represent the standard deviation of the triplicate values. The curves are least squares fit to the Michaelis-Menten equation.

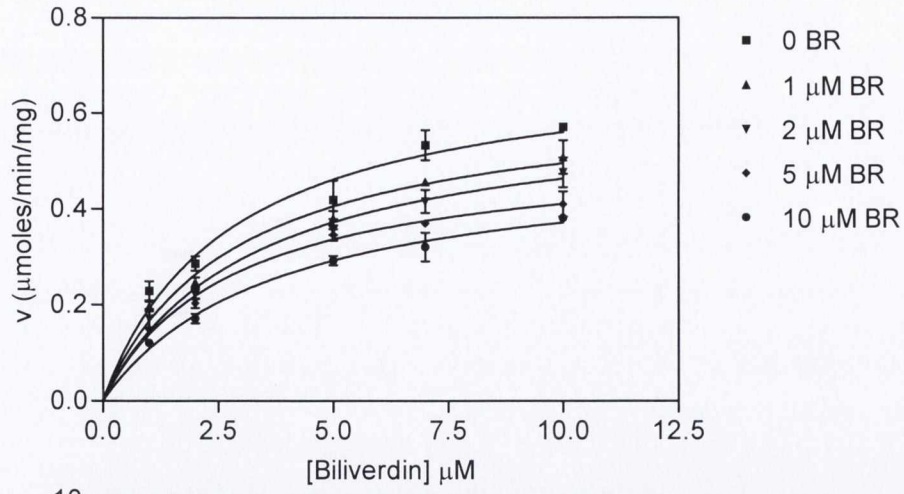
v (μmoles/min/mg)
[Biliverdin] μM
0 BR
1 μM BR
2 μM BR
5 μM BR
10 μM BR

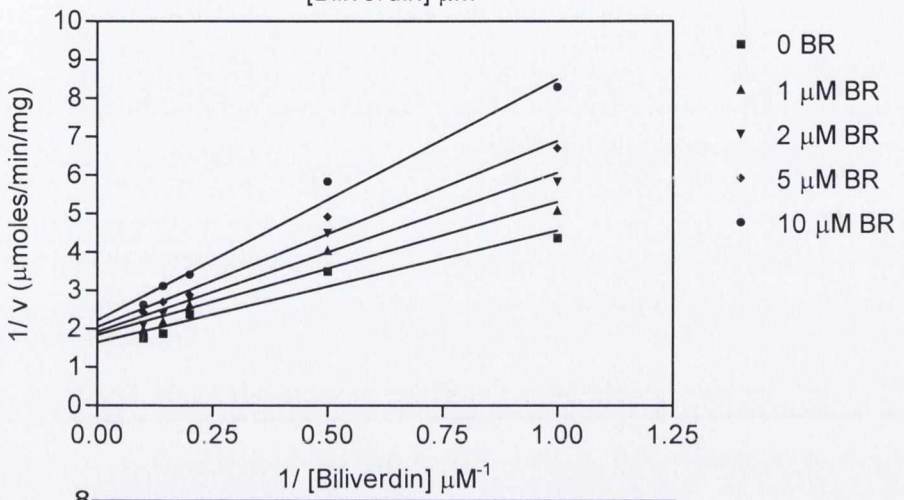
1/ v (μmoles/min/mg)
1/ [Biliverdin] μM-1
0 BR
1 μM BR
2 μM BR
5 μM BR
10 μM BR

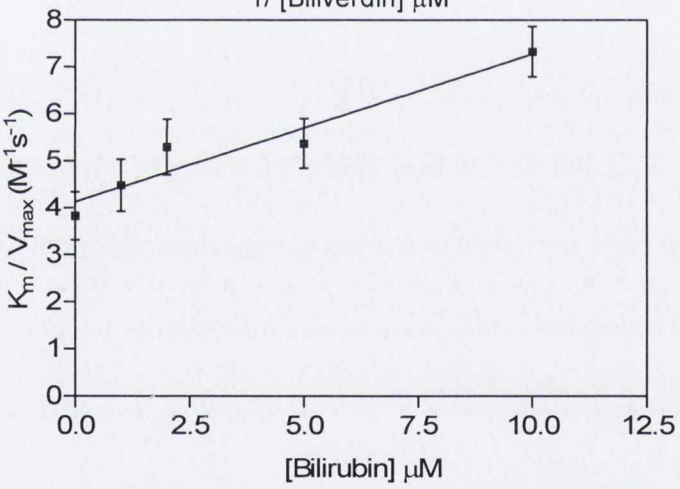
Km / Vmax (M-1s-1)
[Bilirubin] μM

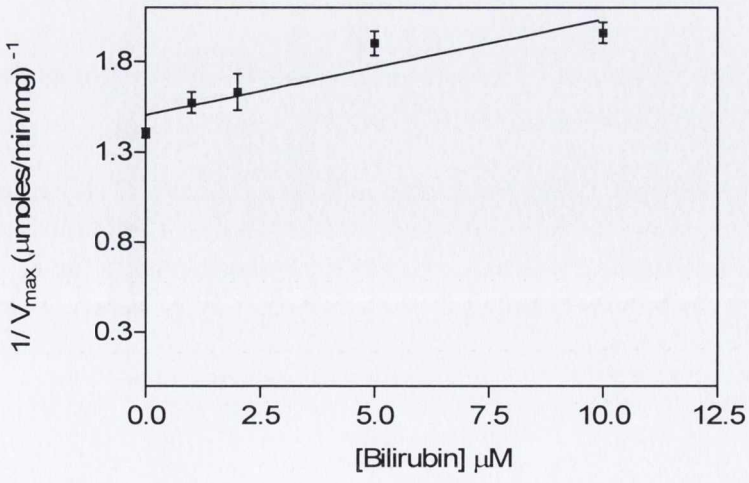
1/ Vmax (μmoles/min/mg) -1
[Bilirubin] μM

Figure 4.22 Product inhibition by bilirubin with biliverdin as the variable substrate at saturating levels of NADPH

Biliverdin was the variable substrate at concentrations ranging from 0.5-10μM. NADPH was held constant at saturating levels (100μM). Bilirubin was increased from 0-10μM. Reactions were performed in sodium citrate (100mM), pH5 and were initiated by the addition of sBVR-A (5μg). Experiments were performed in triplicate. Each datum point represents the mean and error bars represent the standard deviation of the triplicate values. The curves are least squares fit to the Michaelis-Menten equation.

Figure 4.23 Double reciprocal plots of initial rate against biliverdin concentration at varying concentrations of bilirubin

When the initial rates (see Fig. 4.22) were re-plotted as double reciprocals a pattern of linear intersecting lines was produced. These lines intersect to the left of the y-axis indicating mixed inhibition.

Figure 4.24 Slope re-plot of bilirubin inhibition with biliverdin as the variable substrate at saturating levels of NADPH

When the K_m / V_{max} (slope) values from the double-reciprocal plot shown in Fig. 4.23 were re-plotted against the concentration of bilirubin a linear relationship was obtained where the line intersected the x-axis at $-K_{is}$. From this point the K_{is} value for bilirubin against biliverdin was calculated (see Table 4.4) Error bars represent the standard error

Figure 4.25 Intercept re-plot of bilirubin inhibition with biliverdin as the variable substrate at saturating levels of NADPH

When the 1/ V_{max} (intercept) values from the double-reciprocal plot shown in Fig. 4.23 were re-plotted against the bilirubin concentrations a linear relationship was obtained where the line intersected the x-axis at $-K_{ii}$. From this point the K_{ii} value for bilirubin against biliverdin was calculated (see Table 4.4). Error bars represent the standard error

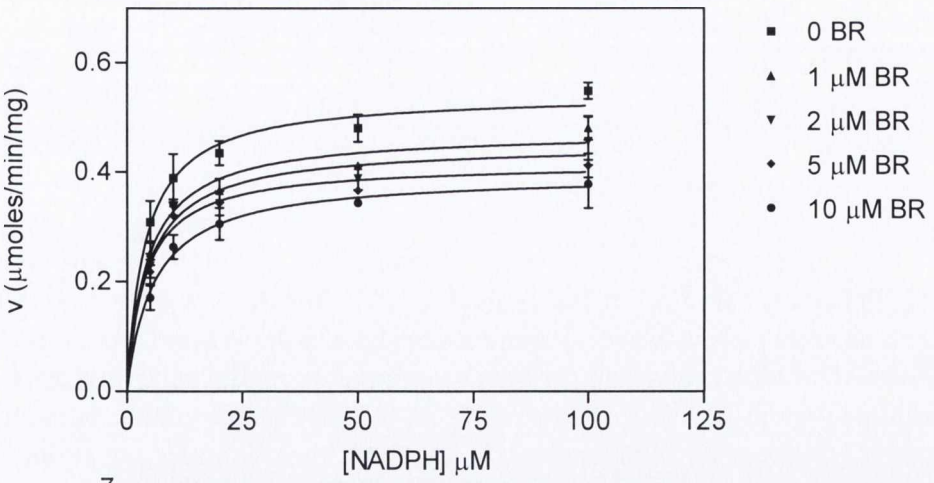
v (μmoles/min/mg)
0.0
0.2
0.4
0.6
0
25
50
75
100
125
[NADPH] μM
0 BR
1 μM BR
2 μM BR
5 μM BR
10 μM BR

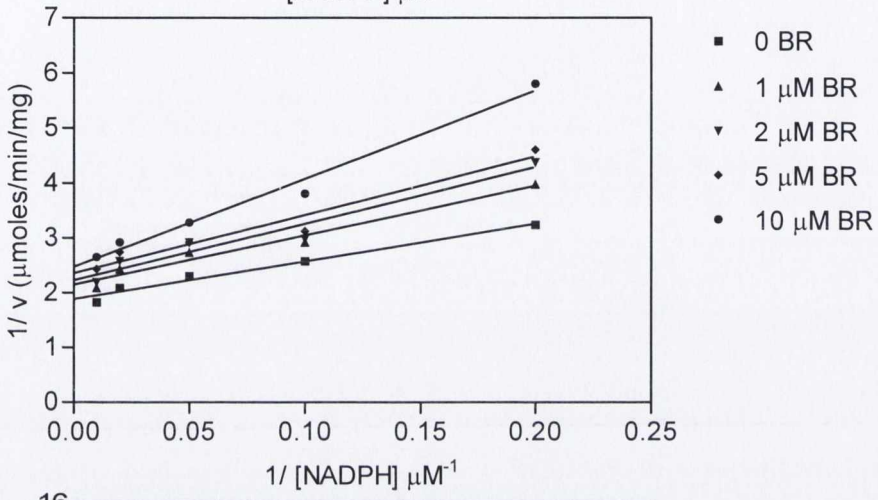
1/ v (μmoles/min/mg)
0
1
2
3
4
5
6
7
0.00
0.05
0.10
0.15
0.20
0.25
1/ [NADPH] μM-1
0 BR
1 μM BR
2 μM BR
5 μM BR
10 μM BR

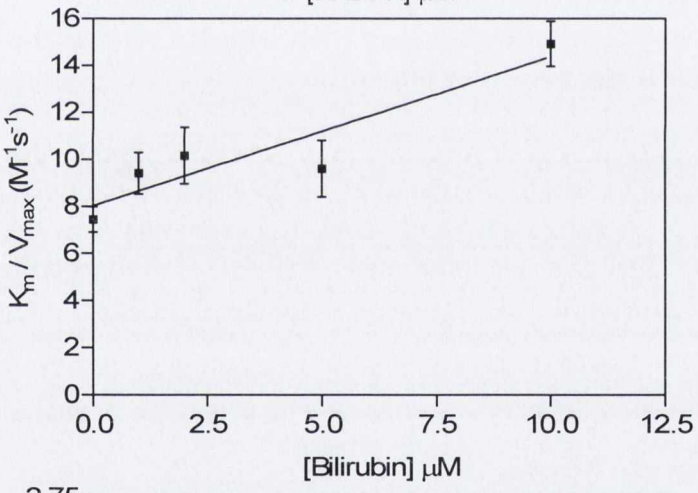
Km / Vmax (M-1s-1)
0
2
4
6
8
10
12
14
16
0.0
2.5
5.0
7.5
10.0
12.5
[Bilirubin] μM

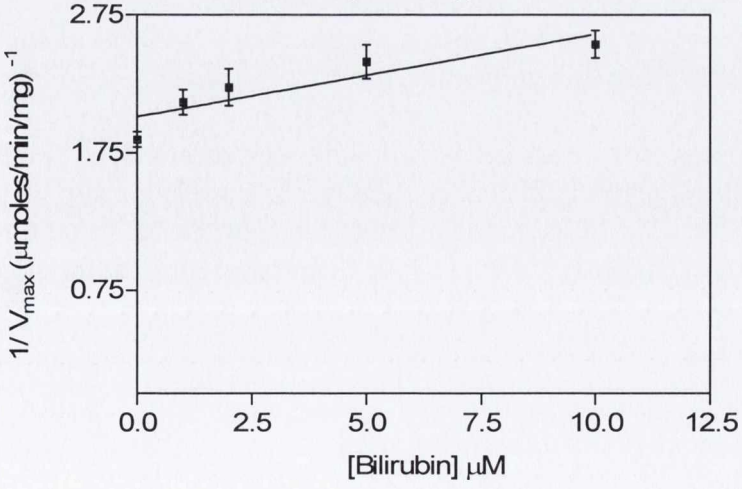
1/ Vmax (μmoles/min/mg) -1
0.75
1.75
2.75
0.0
2.5
5.0
7.5
10.0
12.5
[Bilirubin] μM

Figure 4.26 Product inhibition by bilirubin with NADPH as the variable substrate at non-saturating levels of biliverdin

NADPH was the variable substrate at concentrations ranging from 5-100μM. Biliverdin was held constant at non-saturating levels (1μM). Bilirubin was increased from 0-10μM. Reactions were performed in sodium citrate (100mM), pH5 and were initiated by the addition of sBVR-A (5μg). Experiments were performed in triplicate. Each datum point represents the mean and error bars represent the standard deviation of the triplicate values. The curves are least squares fit to the Michaelis-Menten equation.

Figure 4.27 Double reciprocal plots of initial rate against NADPH concentration at varying concentrations of bilirubin

When the initial rates (see Fig. 4.26) were re-plotted as double reciprocals a pattern of linear intersecting lines was produced. These lines intersect to the left of the y-axis indicating mixed inhibition.

Figure 4.28 Slope re-plot of bilirubin inhibition with NADPH as the variable substrate at non-saturating levels of biliverdin

When the K_m / V_{max} (slope) values from the double-reciprocal plot shown in Fig. 4.27 were re-plotted against the concentration of bilirubin a linear relationship was obtained where the line intersected the x-axis at $-K_{ii}$. From this point the K_{is} value for bilirubin against NADPH was calculated (see Table 4.4) Error bars represent the standard error

Figure 4.29 Intercept re-plot of bilirubin inhibition with NADPH as the variable substrate at non-saturating levels of biliverdin

When the 1/ V_{max} (intercept) values from the double-reciprocal plot shown in Fig. 4.27 were re-plotted against the bilirubin concentrations a linear relationship was obtained where the line intersected the x-axis at $-K_{ii}$. From this point the K_{ii} value for bilirubin against NADPH was calculated (see Table 4.4). Error bars represent the standard error

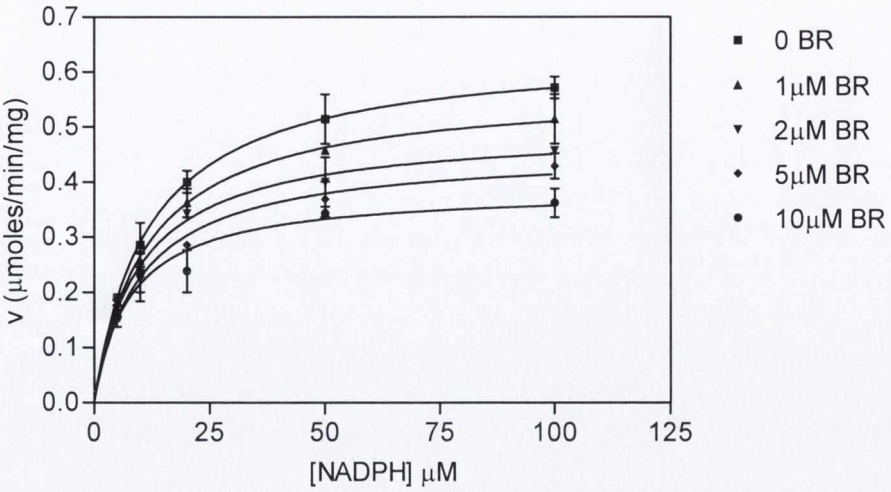
v (μmoles/min/mg)
0.0
0.1
0.2
0.3
0.4
0.5
0.6
0.7
0
25
50
75
100
125
[NADPH] μM
0 BR
1μM BR
2μM BR
5μM BR
10μM BR

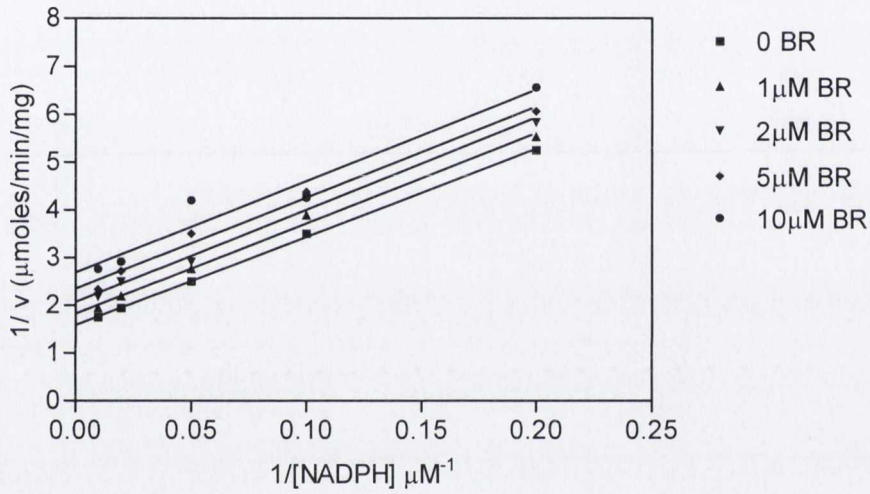
1/ v (μmoles/min/mg)
0
1
2
3
4
5
6
7
8
0.00
0.05
0.10
0.15
0.20
0.25
1/[NADPH] μM-1
0 BR
1μM BR
2μM BR
5μM BR
10μM BR

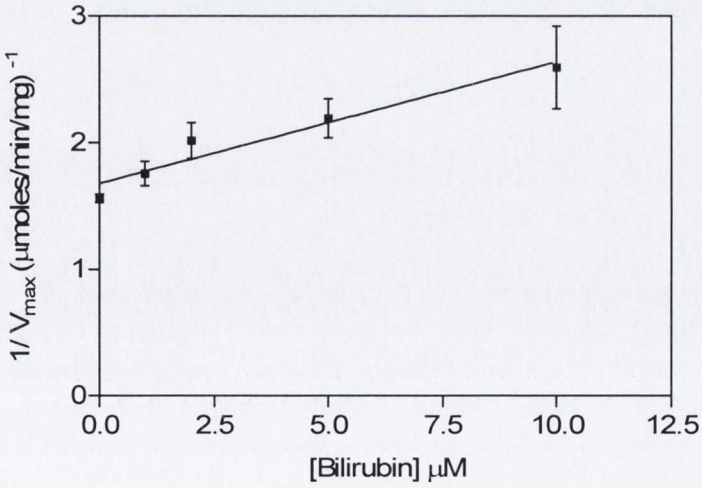
1/ Vmax (μmoles/min/mg) -1
0
1
2
3
0.0
2.5
5.0
7.5
10.0
12.5
[Bilirubin] μM

Figure 4.30 Product inhibition by bilirubin with NADPH as the variable substrate at saturating levels of biliverdin

NADPH was the variable substrate at concentrations ranging from 5-100μM. Biliverdin was held constant at saturating levels (10μM). Bilirubin was increased from 0-10μM. Reactions were performed in sodium citrate (100mM), pH5 and were initiated by the addition of sBVR-A (5μg). Experiments were performed in triplicate. Each datum point represents the mean and error bars represent the standard deviation of the triplicate values. The curves are least squares fit to the Michaelis-Menten equation.

Figure 4.31 Double reciprocal plots of initial rate against NADPH concentration at varying concentrations of bilirubin at saturating levels of biliverdin

When the initial rates (see Fig. 4.30) were re-plotted as double reciprocals a pattern of linear parallel lines was produced which indicates uncompetitive inhibition.

Figure 4.32 Intercept re-plot of bilirubin inhibition with NADPH as the variable substrate at saturating levels of biliverdin

When the $1/ V_{max}$ (intercept) values from the double-reciprocal plot shown in Fig. 4.31 were re-plotted against the bilirubin concentrations a linear relationship was obtained where the line intersected the x-axis at $-K_{ii}$. From this point the K_{ii} value for bilirubin against NADPH was calculated (see Table 4.4). Error bars represent the standard error

Figure 4.33 The nucleotide binding site of rat BVR-A and its interaction with inorganic phosphate.

Panel A; A cartoon diagram of BVR-A displaying the three phosphates in red which co-crystallised with the enzyme.

Panel B; A space-fill model of the enzyme showing the inorganic phosphate anion which is bound to the proposed NADPH 2' phosphate binding site. The active site Tyr97, above which the nicotinimide and biliverdin sit, is also highlighted.

Panel C and D; Space-filled models which show the nucleotide binding pocket with and without a bound phosphate anion.

Panel E and F; The residues which are involved in binding the 2' phosphate of NADPH and inorganic phosphate anions. The binding pocket consists of Ser43 and positively charged residues Arg44 and Arg45 which co-ordinate with the phosphate anion.

Panel G and H; The nucleotide binding domain of BVR-A (Panel G), is compared to the corresponding domain of glucose–fructose oxidoreductase (GFOR) from *Zymomonas mobilis* (Panel H). The Rossmann fold shown in red is located between the end of β1 and the start of α1 of BVR-A. The binding pocket consists of Ser43 and positively charged residues Arg44 and Arg45 which in conjunction with the Rossmann fold co-ordinate with NADPH and also with phosphate anions. A similar fold and the distribution of positively charged residues facilitating the interaction of the phosphate moiety of NADPH exist in the GFOR structure.

Adapted from Franklin (2006).

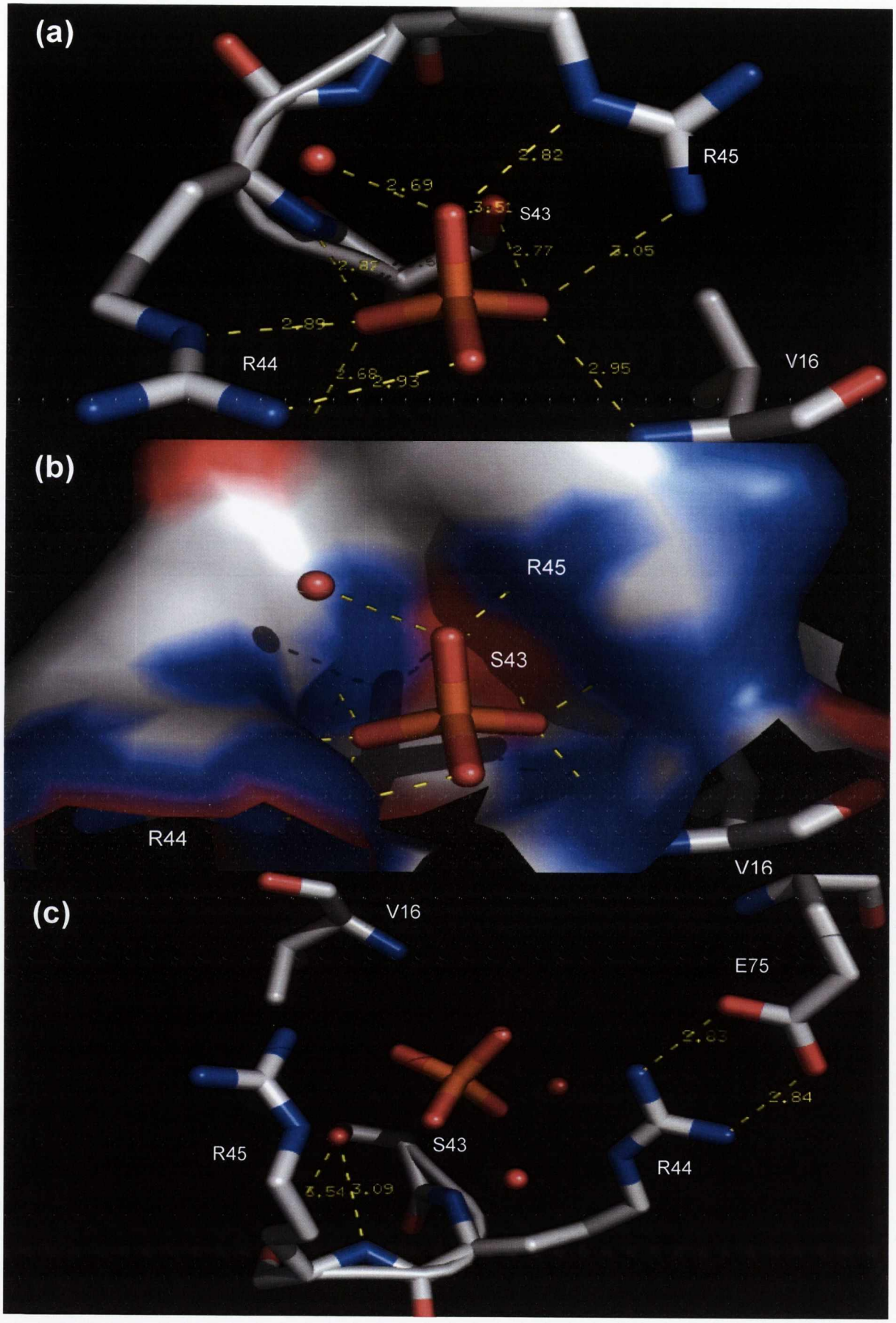
(a)
R45
S43
R44
V16
2.82
2.69
2.77
2.05
2.89
2.68
2.93
2.95
(b)
R45
S43
R44
V16
(c)
V16
E75
R45
S43
R44
2.84
3.09

Figure 4.34 The phosphate binding site of rat BVR-A

(a)

The residues which interact with the inorganic phosphate in rat BVR-A. Ionic contacts are represented by dotted lines (yellow). The numbers also in yellow correspond to the distances between interacting atoms. Red dots represent water molecules.

(b)

A surface diagram of the residues shown in (a). The phosphate pocket is clearly defined. There is a large distribution of positively charged residues along the walls of this pocket which co-ordinate with the phosphate anion.

(c)

Interactions of various residues within the phosphate binding pocket are highlighted. It is interesting to note that R44 and E75 form a salt bridge which connects the loop between B-sheets β2 and β3 with the αD helix in the rat crystal structure.

Adapted from Franklin *et al.,* (2007).

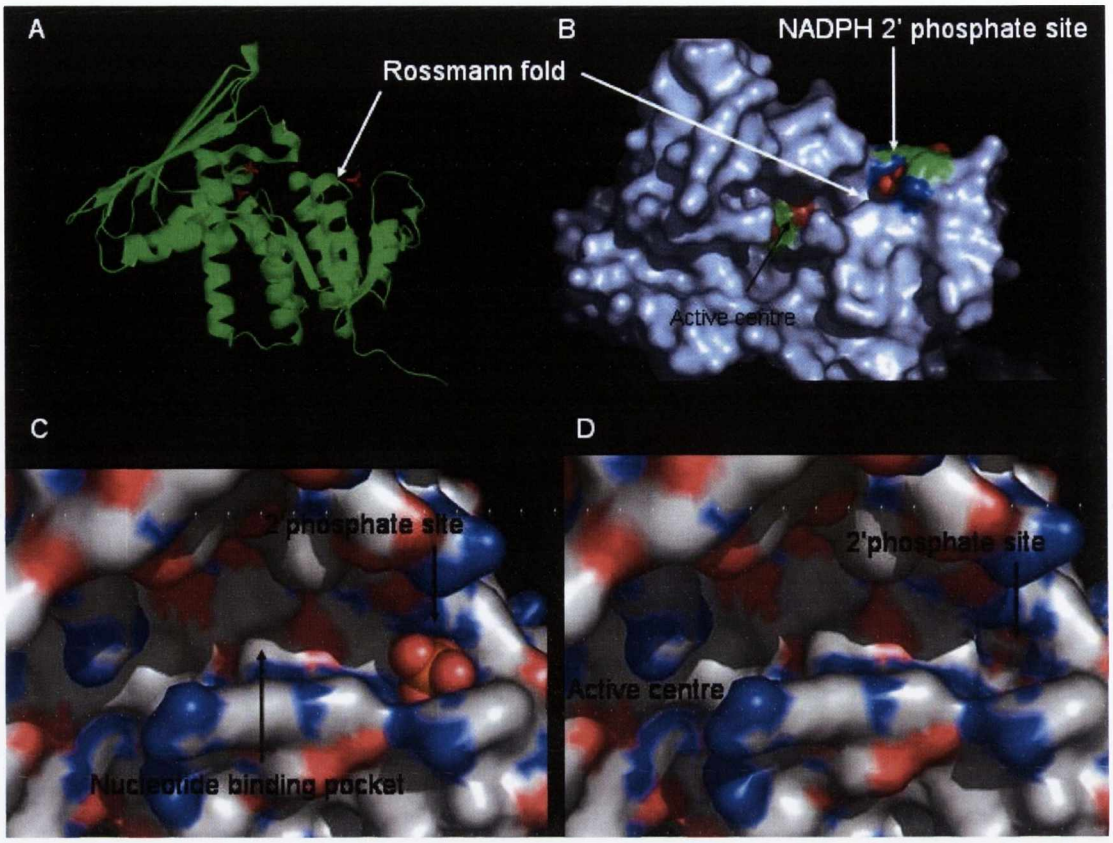
A
B
NADPH 2' phosphate site
Rossmann fold
Active centre
C
D
2'phosphate site
Nucleotide binding pocket
2'phosphate site
Active centre

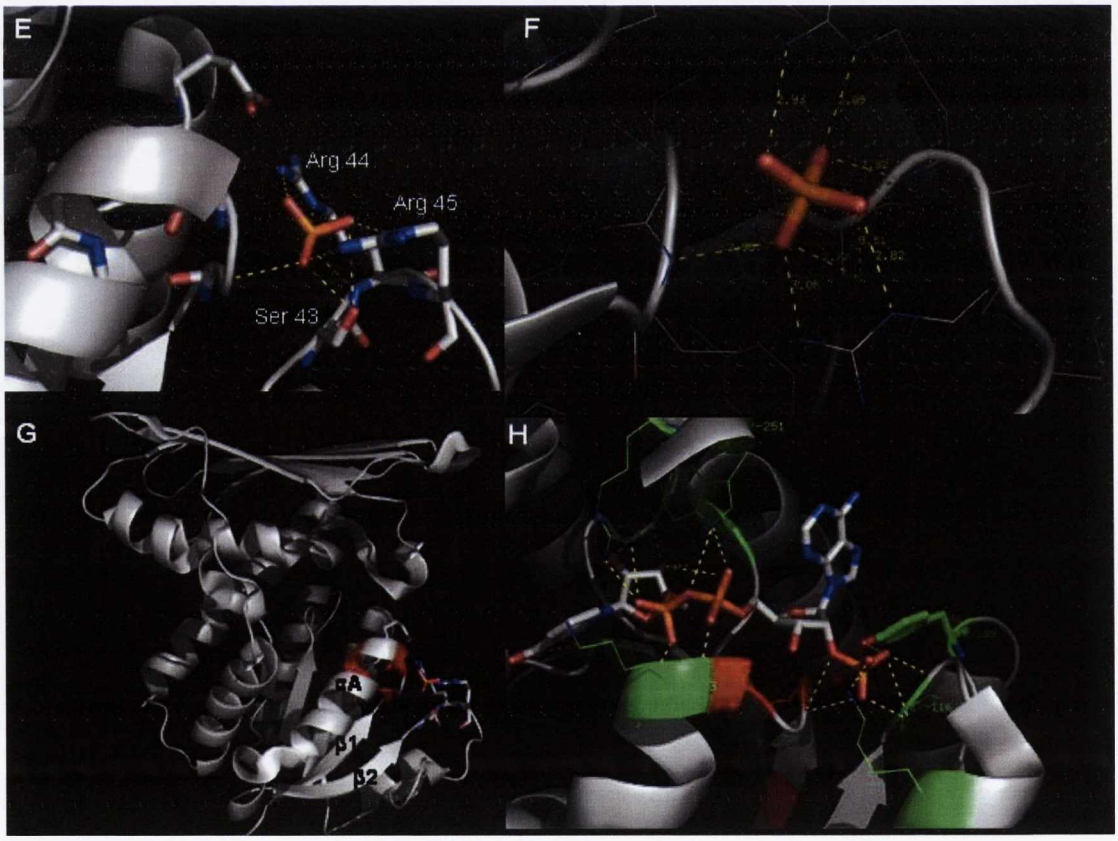
E
F
Arg 44
Arg 45
Ser 43
G
H

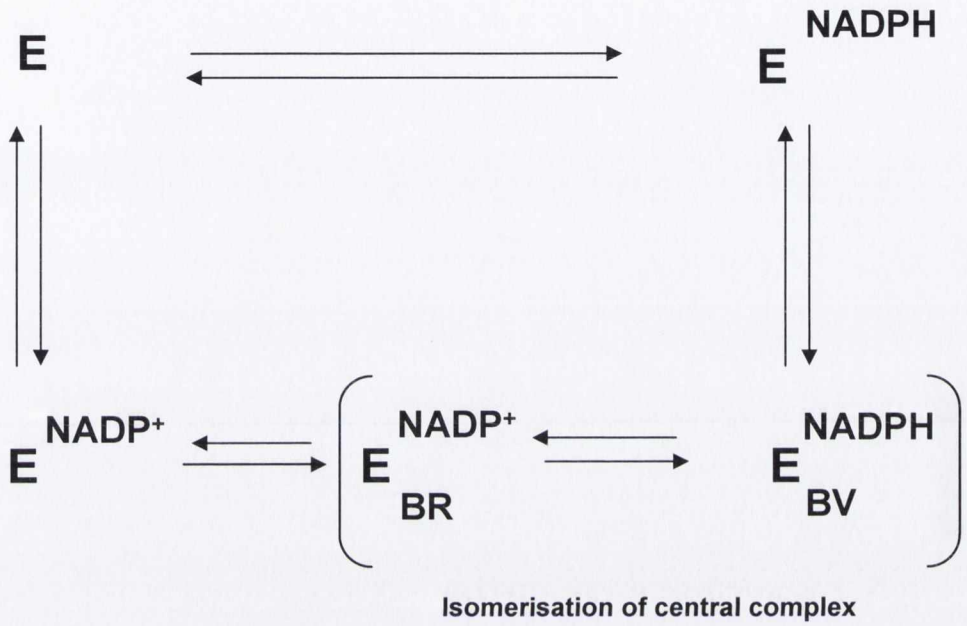

Figure 4.35 Proposed reaction mechanism for reduction of biliverdin by *s*BVR-A.

The proposed mechanism is a sequential ordered kinetic mechanism where NADPH binds, followed by biliverdin. Hydride transfer occurs between NADPH and the C10 bridge of biliverdin, reducing it to bilirubin. Bilirubin dissociates from the enzyme, followed by the reduced co-factor to yield free enzyme

CHAPTER 5

STUDIES ON THE ENZYMATIC MECHANISM OF *SYNECHOCYSTIS* BILIVERDIN IXα REDUCTASE

5.1 Introduction

The biliverdin reductase from *Synechocystis* has been shown to have an optimum pH for activity at pH5 with both NADH and NADPH as co-factor. This makes it unusual among the BVR-A family where the mammalian forms are active at more neutral pH values (typically pH7 to 9). However, an acidic pH optimum is not unique to the *Synechocystis* BVR-A as the salmon form of the enzyme shows optimal activity at pH6 (Elliot, 1996) and the *Xenopus tropicalis* enzyme also shows optimal activity at pH5 (Franklin, 2006). Preliminary studies revealed that the pH profile for sBVR-A shows a dramatic increase in activity as the pH is increased from 4 to 5, a peak at pH5 and then a gradual decrease in activity as the pH is raised to 7. The loss of activity in the pH region 5 to 7 was shown to be reversible, however, the loss of activity at pH4 was shown to be irreversible after only 30sec. This suggests that the enzyme is only active within a very narrow pH range (one pH unit above and below its optimum) and can be "switched on" and "switched off" by very small changes in pH on the "more acidic" limb of the pH curve. This is unlikely to be of physiological significance as the enzyme is extremely unstable at pH4 where it has a half life of only 30sec. However, in the context of this study the enzyme is stable over the pH range of interest (5 to 7) and unlike the mammalian BVR-As the *Synechocystis* enzyme is not substrate inhibited, making it possible to analyse in detail its activity as a function of pH over the entire range of pH stability. In light of this fact, together with the very acidic pH optimum (shared by both NADPH and NADH) and possible physiological implications of this pH optimum for the enzyme it was felt that a comprehensive study on the effect of pH on the activity of the *Synechocystis* enzyme would prove informative.

Detailed pH studies on *Synechocystis* BVR-A and particularly the effect of pH on the kinetic parameters can provide information on the kinetic and chemical mechanism of reduction of biliverdin by the enzyme using hydride from NAD(P)H. The study of the pH profile of the enzyme allows the prediction of the required protonation state of residues which may be involved in binding or catalysis or both and in this way it is possible to detect acid-base catalysis and gain information on the chemical mechanism of the enzymatic reaction. Although no crystal structure exists for *Synechocystis* BVR-A there are structures available for the rat and human enzymes. If these residues are conserved, examination of the putative active sites of the known rat and human BVR-A structures can provide further evidence that the residues identified through pH studies of sBVR-A are located at or near the active site and whether they play a role in catalysis. Initial rate studies of sBVR-A revealed a bell-shaped curve as a function of pH. This curve reflects the ionisations of possible amino acid residues which may be involved in the enzymatic reaction but

pH studies alone can only predict residues which may be involved in the reaction and they must be confirmed or ruled out by subsequent experiments.

5.2 The effect of pH on the kinetic parameters of sBVR-A

It is often the case that when determining the effect of pH on the kinetic parameters of a two substrate enzyme that one substrate is held at 10 x K_m (91% saturating) and the variation of initial rate with the concentration of the second substrate is then used to estimate V_{max}, k_{cat} and the K_m for the variable substrate. However, the assumption that a concentration that saturates at one pH will saturate at all the pH values studied is not without risk. All initial rate parameters reported in this thesis have been determined following classic 5 x 5 analysis using the method of Florini & Vestling (1957) to calculate K_m and V_{max}. The effect of pH on k_{cat} was investigated over the pH range 4.25 to 7 with NADPH and NADH. The full initial rate kinetics with NADPH, NADH and biliverdin as the variable substrate at each pH value are shown in *Appendix* III. The values measured for k_{cat} are shown when the data set is described with NADPH (Fig. 5.1A) or biliverdin (Fig. 5.1B) as the variable substrate. The same k_{cat} profile should be obtained (irrespective of which substrate is held as the variable) and this is clearly seen by overlaying Figs 5.1A and 5.1B (see Fig 5.1C). There is clearly a pK at 5.5 for the "less acidic" limb of the pH curve (see Section 5.4 for an approach to this calculation) defining a side-chain that must be protonated for catalysis to occur. There is no co-operativity for this protonation as the plot of log of k_{cat} *versus* pH gives a slope of approximately 1 (see Fig. 5.3A). On the "more acidic" limb of this curve there appears to be a co-operative pK (~ 4.8) and protonation of this group reduces the k_{cat} (but only by 50%). Great care has to be taken as the enzyme is highly unstable at the "more acidic" pH values, although the initial rates were obtained under conditions when at least 90% of the activity was retained. Kinetic parameters with NADPH variable are shown in Table 5.1 and with biliverdin variable are shown in Table 5.2. When the pyridine nucleotide is NADH the pK on the "less acidic" limb is clearly not co-operative and has a similar value (5.7) to that seen with NADPH (5.4). The plot of log of k_{cat} *versus* pH for NADH also gives a slope of approximately 1, similar to NADPH in the "less acidic limb" of the curve (see Fig. 5.3B). It is intriguing that the k_{cat} on the "more acidic" limb shows very little dependence on pH. A comparison of this behaviour with that seen when NADPH is the co-factor clearly suggests that protonation on the "more acidic" limb reduces (more so with NADPH) but does not abolish activity completely as the k_{cat} does not go to zero in this region whereas at the "less acidic" limb the k_{cat} tends to a low number (see Fig. 5.2). Kinetic parameters with NADH variable are shown in Table 5.3 and with biliverdin variable are shown in Table 5.4.

The effect of pH on the k_{cat}/K_m values for NADPH and NADH was also analysed. The values measured for k_{cat}/K_m are shown when the data set is manipulated with NADPH (Fig. 5.4A) and biliverdin (Fig. 5.4B) as the variable substrate and with NADH (Fig. 5.5A) and biliverdin (Fig. 5.5B) as the variable substrate. These parameters exhibit an optimum at approximately pH5 with both co-factors although there are significant errors for this parameter. When the data sets were plotted as log k_{cat}/K_m there is also an optimum at approximately pH5 and with NADPH there is a decrease at higher and lower pH with NADPH (Fig. 5.6A) and biliverdin (5.6B) as the variable substrate, consistent with the prediction that there are two ionisable groups involved in the enzymatic mechanism of the enzyme. Interestingly, with NADH (5.7A) and biliverdin (5.7B) as the variable substrate there is a decrease at higher pH but the decrease at lower pH which is evident with NADPH is not seen. The only difference between NADPH and NADH is the 2' phosphate on NADPH and there may be a pK of ~ 4.5-5 in effect seen in the "more acidic" limb with NADPH which is not in effect with NADH. This pK may be associated with an acidic residue which is involved or perturbed in binding the 2' phosphate of NADPH. A pK of ~ 5.5 is also in effect on the "less acidic" limb with the k_{cat}/K_m data with NADPH and NADH as co-factor, similar to the k_{cat} data. Also, as is the case with the k_{cat} data there appears to little dependence on pH with the k_{cat}/K_m data on the "more acidic" limb when NADH is the co-factor.

5.4 Treatment of pH data and prediction of pKs required for activity

The k_{cat} values for NADPH, NADH and biliverdin were plotted against pH and produced the bell-shaped curves shown in Figs. 5.1 and 5.2. It was felt that an accurate pK could not be determined from the "more acidic" limb of the k_{cat} *versus* pH curve because the enzyme was very unstable below pH5 and there appears to be co-operativity associated with this pK. The data for the "less acidic" limb of the pH curve is not affected by co-operativity (see Fig 5.3) and was fitted to the following equation (Richards generalised logistic function) for pK:

$$f(x) = \frac{a1 - c1}{1 + 10^{p1\,(-pH + pK1)}} + c1$$

In this expression a1 represents the upper limit of the sigmoid, c1 represents the lower limit of the sigmoid, p1 represents the Hill co-efficient and pH and pK represent the pH and pK of interest respectively. The data were fitted to this equation using the mathematical curve fitting program Wofram Mathematica. pK values were calculated for the enzyme activity with NADPH (Fig. 5.8) and biliverdin (Fig. 5.9) as the variable substrate and with NADH (Fig. 5.10) and biliverdin (Fig.

5.11) as the variable substrate and are shown in Table 5.5 below. Although it was felt that a pK value could not be determined from the "more acidic" limb of the pH curve due to enzyme instability and co-operativity it was also possible that there was a pK of ~4.8 in effect which may suggest that an acidic residue may be involved in the reaction (glutamic acid or aspartic acid with pK values of 3.9 and 4.07 respectively).

	pK
NADPH	5.43 +/- 0.01
NADH	5.65 +/- 0.059
Biliverdin (NADPH co-factor)	5.37 +/- 0.12
Biliverdin (NADH co-factor)	5.7 +/- 0.03

Table 5.5 pK values for sBVR-A activity determined from the k_{cat} data set

5.5 Identification of specific amino acid residues involved in substrate binding or catalysis or both

A pK value was predicted from the pH studies for each substrate which may reflect the ionisation of a particular amino acid residue which may be involved in the enzymatic reaction. The values determined are approximately the same for each substrate used with a pK of ~5.4 for NADPH and ~5.7 for NADH. This pK value suggests that a histidine residue (pK 6.04) is essential to the enzyme and at the optimum pH for the enzyme activity (pH5) must be protonated for substrates to bind or catalysis to occur. However, any particular residue or acid-base group is likely to be under the electrostatic influence of nearby charged groups and for this reason the identification of a particular amino acid with a kinetically characterised pK must be verified or ruled out through subsequent experiments.

5.5.1 Examination of the amino acid sequences and putative active sites of the known BVR-A family members

In order to identify residues which may be involved in the enzymatic mechanism of sBVR-A the amino acid sequences of all known and putative BVR-As and their equivalent positioning within the rat crystal structures of Kikuchi *et al.,* (2001) and Whitby *et al.,* (2002) were examined. The multiple sequence alignment of all known and putative BVR-As in Fig. 5.12 shows that there are a number of highly conserved motifs within the BVR-A family. These motifs are shown in more detail in Fig. 5.13. Region 1 in Fig. 5.13 is found between β1 and αA of the rat structure and comprises the Rossman fold and is relatively well characterised as the nucleotide binding site for members of the GFO/IDH/MOCA (of which BVR-A is a member). Of more interest to this study is region 2 which spans the αD helix and β6 sheet and is composed of a number of highly conserved residues (including H79 and H92 in the rat sequence) present in all BVR-As studied to date. Also present in this region is a highly conserved EYP motif present only in members of the BVR-A family. Region 3 in Fig. 5.13 is also of importance to this study and extends from β7 through to the 3_{10}F helix. This region contains the highly conserved, negatively charged glutamic acid residues: E96, E123 and E126 (from the rat sequence) and conserved histidine residues (H121 and H124). The last regions (4 and 5 in Fig. 5.13) also contain two conserved residues of interest to the present study, a positively charged arginine residue (R171) and a negatively charged aspartic acid (D253). Following the identification of conserved residues possibly involved in the enzymatic mechanism of sBVR-A it was important to establish if these residues were at or near the putative active site and if they could take part in the enzyme reaction. This was done by examining the rat BVR-A crystal structures of Kikuchi *et al.,* (2001) and Whitby *et al.,* (2002). By studying these structures it is clear that the important motifs shown in Fig. 5.13 and the conserved residues of interest are not widely distributed throughout the structure but are in very close proximity to each other and form a highly conserved region around the putative active site of the enzyme (see Fig. 5.14). It was therefore possible that any of the conserved residues described previously could be involved in the enzymatic mechanism of sBVR-A.

5.5.2 Inactivation of proposed active site residues involved in catalysis or binding or both through site-directed mutagenesis

Based upon the pH studies described previously and examination of the amino acid sequences of all known and putative BVR-As and the known rat BVR-A crystal structures it was decided to mutate the following residues in *Synechocystis* BVR-A: His 84 (His 79), His 97 (His 92), His 126 (His 121), His 129 (His 124), Glu 101 (Glu 96), Tyr 102 (Tyr 97), Arg 185 (Arg 171) and Asp 285

(Asp 252). Shown in brackets are the corresponding residues in rat BVR-A. These residues were all mutated to the relatively small and neutral amino acid alanine through site-directed mutagenesis.

5.5.2.1 Mutagenic primer design

Oligonucleotide primers incorporating the required mutation were designed individually according to the particular mutation. Mutagenic primers usually consisted of 40-45bps and had a GC content of at least 50%. The primers were designed to anneal to the same sequence on opposite strands of the target plasmid pETBVR-A, containing the sBVR-A gene. The desired mutation was designed in the middle of both the forward and reverse primers with 10-15bps of correct sequence on both sides. Individual mutagenic primers are shown in Table 5.6.

5.5.2.2 Mutagenesis reaction

Site-directed mutagenesis of the pETBVR-A plasmid was carried out according to the method of Fisher *et al.*, (1997) and is described in Section 2.2.11. Briefly, plasmid DNA (10-20ng), forward and reverse mutagenic primer (125ng of each), dNTPs (2.5mM of each of dCTP, dATP, dGTP and dTTP), 5µl 10 x P*fu* reaction buffer, 17µl nuclease free water and 1µl P*fu* polymerase were added to a 100µl PCR tube and mixed thoroughly. The reaction was carried out according to the modified PCR cycling conditions shown in Table 5.7 below. These cycling conditions were optimised for the mutagenesis of a single amino acid (one or two base pair changes depending on the mutant). When the reaction was complete DPN-1 restriction enzyme (1µl of 10U/ µl) was directly added to the tube, mixed well and incubated at 37°C for 1hour. DPN-1 digests methylated DNA and was therefore capable of digesting the parent plasmid DNA which was purified from *E.coli.* Following digestion the complete contents of the mutagenesis reaction was used to transform ultra-competent *E.coli* XL-1 blue cells as described in Section 2.2.9.2. Single colonies of successful kanamycin resistant transformants were streaked on agar plates, cultured and the plasmid DNA purified as described in Section 2.2.4. Purified plasmid DNA was sequenced as described in Section 2.2.12 to ensure the correct mutation had been inserted and no other mutations were present.

Step	Cycle name	Temperature (°C)	Time (min)
1	Hot start	95	30
2	Denaturation	95	30
3	Annealing	55	60
4	Elongation	68	420
5	No. Cycles	16 x step 2	
6	Hold & Cool	4	∞

Table 5.7 PCR cycling conditions for the site-directed mutagenenesis reaction for the mutation of a single amino acid

5.6 Purification of sBVR-A mutants

sBVR-A mutant plasmids, verified by sequencing were transformed into *E.coli* BL21 (DE3) cells and were cultured, induced and harvested as described in Sections 2.2.14. sBVR-A proteins containing the required amino acid changes were purified as described for the wild-type protein (see Section 3.4.3) without the 2'5' ADP Sepharose affinity chromatography step. In all cases the protein was expressed and could be purified using this method. SDS-PAGE analysis of the mutant sBVR-A proteins is shown in Fig. 5.15.

5.7 CD spectroscopy analysis of the sBVR-A mutants in the far UV region

Circular dichroism studies in the far UV region of the electromagnetic spectrum were carried out on the sBVR-A mutants and the wild-type protein in order to assess if any of the particular mutations had any effect on the structure or overall fold of sBVR-A (see Section 2.2.30 for CD protocol). In comparison to the wild-type protein (see Fig. 5.16a) the CD spectra of the mutants did not show any significant change, suggesting that the mutant proteins had folded up correctly and the overall structure was not greatly affected (see Figs 5.16 for CD spectra of the mutant sBVR-As). However, while most of the mutants had very similar CD spectra the spectrum of the H84A (Fig. 5.16C) and particularly the D285A (Fig. 5.16I) mutants exhibited slight changes which may suggest that the fold in these mutants is not be identical to the wild-type protein.

5.8 Kinetic analysis of the sBVR-A mutants

Each of the sBVR-A mutants was characterised kinetically to assess what effect, if any, the particular mutation had on the V_{max}, k_{cat} and K_m values for NADPH and biliverdin. Activity assays

and measurements were carried out as described in Section 2.2.23.1. Results of the activity measurements are shown in Table 5.8. The V_{max}, k_{cat} and K_m values for the H97A, H126A and H129A mutants were comparable to the wild-type (see Table 5.8) and it was concluded that these residues were not involved in substrate binding or catalysis or were not structurally important as the CD spectra of these mutants were also very similar to the wild-type protein (see *Appendix* IV, Figs. 1, 2, 3 for the initial rate kinetics of the H97A, H126A and H129A mutants respectively). However, a number of mutations appeared to affect the activity and binding of substrates to sBVR-A. The Y102A mutant exhibited a 2-3 fold decrease in the V_{max} and k_{cat} for both biliverdin and NADPH (see Table 5.8). The K_m for NADPH was decreased approximately 2-3 fold when compared to the wild-type and the K_m for biliverdin was increased approximately 8-fold to 16.19μM (see Fig 5.17). The E101A mutant showed a 3 fold decrease in the V_{max} and k_{cat} values (see Table 5.8). However, the errors are large on the values for biliverdin and the loss of activity is likely to be significantly less. This can also be seen in the initial rate data for the E101A mutant which does not fit well to a rectangular hyperbola (see Fig. 5.18B). The K_m value for NADPH is comparable to the wild-type but the K_m value for biliverdin is increased 10-fold to 21.66μM for this mutant (see Fig.5.18C). The R185A mutant exhibited a 10 fold decrease in the V_{max} and k_{cat} for the enzyme see Table 5.8. The K_m values for biliverdin and NADPH were not greatly affected (see Fig. 5.19). The D285A mutant also showed an 8-fold decrease in the V_{max} and k_{cat} (see Table 5.8). Although the K_m for NADPH appears to be decreased 10-fold to 1μM (see Fig. 5.20D) the K_m for biliverdin is not significantly affected. The most significant effects were exhibited by the H84A mutant. The apparent V_{max} values were decreased 100-fold approximately (see Table 5.8). The activity was too low to accurately determine the K_m or k_{cat} for this mutant and the data did not fit to a hyperbola (see Fig. 5.21).

5.9 Analysis of biliverdin IXα binding to sBVR-A mutants by CD spectroscopy

Biliverdin IXα and bilirubin IXα are optically active chromophores and give a characteristic CD spectrum when they "twist" into an unsymmetrical chromophore, usually when binding to certain proteins. They do not exhibit this CD spectrum when they are free in solution as both enantiomeric forms (plus and minus) of biliverdin IXα and bilirubin IXα are present in equimolar amounts (Nogales & Lightner, 1995). However, when it is bound to a protein and "locked" in a particular conformation optical rotation dispersion (ORD) maxima are evident at 380nm and 650nm. This makes circular dichroism a useful tool to study the binding of biliverdin to sBVR-A and its mutants. CD measurements with biliverdin were carried out as described in Section 2.2.30. Biliverdin (30μM) binding to wild-type sBVR-A (1 mg/ml) in the presence of 100μM $NADP^+$ is shown in Fig. 5.22A. The characteristic ORD maxima for biliverdin IXα are evident in this CD

spectrum where biliverdin binds in the plus (P) conformation. Each mutant at a concentration of 1mg/ml was incubated with 100μM $NADP^+$ and 30μM biliverdin IXα. The spectra of mutants H97A (Fig. 5.22B), H126A (Fig. 5.22C), H129A (Fig. 5.22D) and D285A (Fig. 5.22E) are comparable to the wild-type spectrum. However, the binding of biliverdin to mutant R185A appears to be slightly diminished as shown in Fig. 5.22F. Biliverdin binding to the E101A is almost completely ablated (see Fig. 5.22G) and binding to H84A is also severely diminished (see Fig. 5.22H). The inability of E101A to bind biliverdin effectively is reflected in its K_m value (8 times higher than the wild-type). Interestingly, the Y102A mutant appears to be capable of binding biliverdin but in the opposite conformation [(minus conformation (M)] to that bound by the wild-type (see Fig. 5.22I). Activity measurements suggest that the conformation bound by this mutant is less productive than that bound by the wild-type enzyme and this is also evident in the K_m values for the wild-type and Y102A mutant (approximately 10-fold higher for the Y102A mutant) (see Table. 5.8).

A comprehensive study on the effects of pH on *Synechocystis* BVR-A was undertaken to investigate the enzymatic mechanism of the enzyme and the effect of pH on the kinetic parameters. It was shown in Section 4.3 that sBVR-A exhibited a pH optimum of 5. This study was extended in the present chapter and confirmed that the optimum was approximately pH5 with both NADPH and NADH as co-factor. The stability of the enzyme was of particular importance during these studies as the enzyme was shown to be irreversibly inactivated at low pH with a half-life of only 30 seconds at pH4. For this reason it was decided to deal with the "less acidic" region (pH 5 to 7) of the pH curve and the pK associated with it. The enzyme was shown to be stable over this range, particularly during the first 30 seconds when initial rates were measured.

pH studies and the effect of pH on the kinetic parameters of sBVR-A have shown that both V_{max} and k_{cat} increase rapidly from pH4.25 to 5 and then decrease gradually up to pH7, particularly with NADPH where the enzyme exhibits 2-3 times more activity over NADH and the change in activity is seen more clearly. However, the effect of pH on the other kinetic parameters is more difficult to analyse. If k_{cat} which has an optimum at pH5 describes the measure of the release of product from the enzyme-substrate complex or reflects the chemical transformation of substrate into product then it would also be expected that the k_{cat}/K_m values for NADPH, NADH and biliverdin would follow the same pattern as V_{max} and k_{cat} and have an optimum at pH5. k_{cat} / K_m provides a measure of the rate of capture of substrate by enzyme into a productive enzyme-substrate complex which can later go on to form products. Therefore it would be expected that this parameter would also be optimal at pH5. This appears not to be the case (see Fig. 5.4 for NADPH and Fig. 5.5 for NADH). However, it may be the case that there is not sufficient reliability in the K_m data and this may explain why the k_{cat}/K_m value is not optimal at pH5. This is reflected in the large errors on some of the k_{cat}/K_m values. The log k_{cat}/K_m plots in Fig. 5.6 show that there is a decrease at both higher and lower pH when NADPH is the co-factor and the data exhibits a bell-shaped curve with an optimum at approximately pH5. Similar to the k_{cat} *versus* pH plots the log k_{cat}/K_m plot for NADPH indicate two groups are required in a given protonation state for binding or catalysis or both (one group protonated and the other group deprotonated). Interestingly, the log k_{cat}/K_m plot for NADH (Fig. 5.7) only shows a decrease at higher pH and the decrease at lower pH which is evident with NADPH is not observed. This may suggest that there is a pK of ~ 4.8 associated with binding the 2' phosphate of NADPH which is not associated with NADH and may indicate an acidic residue is involved. With both NADPH and NADH there are pK values of between 5.5-5.8 in the more acidic region of the pH curve, similar to the k_{cat} data.

The "less acidic" region of the k_{cat} *versus* pH data was fitted to a sigmoid using the equation for pK (equation 2) shown in Section 2.2.23.1. From the data a pK of 5.4 was predicted for NADPH and 5.7 for NADH dependent activity. Although only one pK was predicted from the pH studies without influence from another pK or co-operativity and because the enzyme was highly unstable in the "more acidic" region it was also possible that there could be another pK in effect in the "more acidic" region (one pK responsible for "switching" the enzyme on and the other for "switching" it off). Based on the pK determined from these studies it was predicted that a histidine residue may be involved in the enzymatic reaction. Following examination of the amino acid sequences of all known and predicted BVR-As and the two known rat BVR-A crystal structures it was decided to mutate possible residues which were at or near the putative active site of the enzyme and could possibly take part in the reaction.

In the search for a catalytically important histidine residue His84, His97, His126 and H129 were all converted to alanine residues through site directed mutagenesis. These residues are conserved in all the known and predicted BVR-A family members and modelling studies using the known rat BVR-A crystal structures have shown that they are located at or near the enzyme's active site and therefore capable of participating in the reaction (see Fig. 5.23 for a model of the substrate binding site of rat BVR-A showing the proposed catalytic residues). CD studies in the far UV region have shown that the overall structure and fold of H97A, H126A and H129A is very similar to the wild-type sBVR-A but the spectrum obtained with the H84A mutant is slightly different. This may suggest that there is a slight difference in the tertiary structure of the H84A mutant. By examination of the rat BVR-A crystal structure shown in Fig. 5.14 it can be seen that His84 (His79 in the rat enzyme) is located in the αD helix and may cause this helix to move slightly to allow access for the substrates to the active site or "clamp" the substrates in place to allow catalysis to take occur. Kinetic analysis suggests that the H97A, H126A and H129A mutants are similar to the wild-type enzyme and do not show any significant differences in the activity measurements or K_m values for NADPH or biliverdin. CD studies in the visible region of the spectrum investigating the binding of biliverdin to sBVR-A and its mutants also ruled out any possible role for His97, His126 and His129 in the reaction, binding of substrates or overall structure of sBVR-A. The H84A mutant, however, exhibited an approximately 100-fold decrease in activity when compared to the wild-type enzyme and CD studies investigating the binding of biliverdin also showed that the ability of the enzyme to bind biliverdin was severely diminished without this residue. These experiments suggest that His84 is essential to the enzyme and is likely to be the residue which is contributing the pK of 5.4 to the pH profile. The equivalent histidine residue in the rat BVR-A crystal structure (His79) is positioned in the αD segment in the active site and is seen to interact with the hydroxyl group of Ser74. The *Synechocystis* enzyme, however, has a threonine residue

(Thr79) in this position which could be interacting with His84. The experiments suggest that at pH5 this histidine residue may be protonated in order for biliverdin to bind. It is also possible that His84, acting as a general acid then donates the proton to the reaction and in the process protonating the pyrrole nitrogen of the tetrapyrrole substrate biliverdin IXα. Hydride transfer occurs between the C4 position of the pyridine nucleotide and the C10 position of biliverdin IXα (see Fig. 5.24). In this proposed mechanism it is not clear whether protonation of the pyrrole nitrogen of biliverdin IXα occurs before or after hydride transfer from NAD(P)H. However, QM/MM studies on the enzyme biliverdin IXβ reductase from human liver by Smith *et al.*, (2008) propose that protonation of the tetrapyrrole substrate occurs first to form an intermediate species followed by hydride transfer. The authors of this study also make a point of noting that mechanistically this serves as a good model for BVR-A. However, in this study QM/MM calculations together with site-directed mutagenesis propose that the proton is donated from bulk solvent whereas in the present study the proton is donated from a catalytically important histidine residue (see Fig. 5.24). Histidine residues have been implicated in many enzymatic mechanisms, including the catalytic triad of serine proteases (Blow *et al.*, 1969).

A number of other residues were mutated in order to investigate the enzymatic mechanism of sBVR-A. The pH studies may suggest that an acidic residue (Asp or Glu) may also be involved (although the equivalent pK could not be determined without influence from other factors). Following examination of the amino acid sequences of all known and predicted BVR-As and rat BVR-A crystal structures it was decided to mutate a conserved active site glutamic acid residue (Glu101) and a conserved aspartic acid residue (Asp285). This conserved Asp residue (Asp253 in the rat structure) forms ionic interactions with His120 (rat structure) which holds the β7 and αL segments in position (Kikuchi *et al.*, 2001). This view is supported by the CD spectrum of the D285A mutant in the far UV region. Absence of this Asp residue causes a change in the CD spectrum which can be attributed to destabilisation of this segment. Kinetic studies also indicate an important role for this residue with an approximate 10-fold decrease in the k_{cat} for the enzyme in its absence. When Glu101 was mutated to an alanine residue there was a considerable decrease in the activity of the enzyme (3-fold decrease approximately in the k_{cat}). This loss in activity is likely to be considerably less, however, as the error is quite large and the initial rate data did not fit well to a rectangular hyperbola. There was also an approximate 10-fold increase in the K_m for biliverdin and CD studies examining the binding of biliverdin to this mutant show that the ability of the enzyme to bind biliverdin is extremely diminished in its absence. An important substrate binding function and possible catalytic role is therefore proposed for Glu101. Experiments may suggest that this residue is deprotonated in order for biliverdin to bind. It may also be possible that this residue is acting as a proton acceptor during the reaction. Glu101 (Glu96 in the rat structure) is

located in the most conserved motif within BVR-A, the β6 sheet and the loop bridging the αE helix. Kikuchi *et al.*, (2001) mutated this residue in the rat enzyme and showed that the enzyme completely lost activity. They also described this residue and its similarity to the Glu128 residue in the glucose-fructose oxidoreductase enzyme (GFOR) of which there is much sequence similarity. In this enzyme the Glu residue hydrogen bonds to the amide group of the nicotinamide ring and they suggest that Glu96 in the rat enzyme may be carrying out the same function (Kikuchi *et al.*, 2001). Experiments described in this study suggest that the residue is directly involved in the reaction by binding biliverdin and possibly must be deprotonated in order to do so.

Tyr102 in the *Synechocystis* enzyme was also mutated to an alanine. This residue is located within the highly conserved EYP motif of BVR-As which makes this family unique among the GFO/IDH/MOCA (dehydrogenases having a lysine residue in place of the tyrosine). Interestingly, when this residue was mutated to an alanine the enzyme appeared to retain the capability of binding biliverdin but in a less productive conformation (as suggested by the activity measurements). The CD spectrum of biliverdin binding to the Y102A mutant showed that the enzyme could still bind biliverdin and lock it in a particular conformation, albeit the opposite conformation to the wild-type enzyme but kinetic analysis showed that it was a less productive conformation as the k_{cat} was approximately 3-fold lower and the K_m for biliverdin was approximately 8-fold higher. It appears that even in this less productive conformation hydride transfer can still occur between NAD(P)H and the C10 bridge of biliverdin, albeit at a lower rate. It therefore appears that the highly conserved Tyr102 residue is required for the binding of biliverdin in the correct orientation for efficient catalysis to occur.

Whitby *et al.*, (2002) suggested a catalytic role for Tyr97 in the rat enzyme but found that when they mutated it to a phenylalanine residue the enzyme retained 50% of the wild-type activity and when they mutated it to an alanine residue the mutant retained 64% activity. This result is consistent with the data obtained in this study for the equivalent mutation in the *Synechocystis* enzyme. The same authors also propose a substrate orientation role for Tyr97 (Whitby *et al.*, 2002). Results obtained in this study show that Tyr102 (Tyr97 in the rat enzyme) is required to orientate biliverdin into a position which is catalytically productive and that it is a histidine residue, His84 (His79 in the rat enzyme) is the proton donor to the reaction.

A highly conserved arginine residue (Arg185) was mutated to an alanine residue resulting in a 2-3 fold decrease in the k_{cat} for the enzyme. K_m values for NADPH and biliverdin were comparable to the wild-type and CD studies examining the structure and binding of biliverdin did not show any significant differences to the wild-type enzyme. Examination of the rat enzyme puts its equivalent

(Arg171) at the active site but its role is unclear. Hydrogen bonding occurs between Arg171, Ser170 and Tyr97 and it may be the case that Arg185 forms part of the substrate binding pocket (see Fig. 5.23). This basic arginine residue may form electrostatic interactions with the propionate side chains of biliverdin, orientating the substrate so that its C10 bridge is located above the pyridine nucleotide co-factor and ready for hydride transfer.

In conclusion, experiments based on the pH studies described in this chapter suggest a possible role for a histidine residue and maybe an acidic residue in the enzymatic mechanism of sBVR-A. Examination of the amino acid sequences of all the known and predicted BVR-As and the known rat BVR-A crystal structures identified a number of highly conserved histidine residues, as well as conserved glutamic and aspartic acid residues, a conserved tyrosine residue and a conserved lysine. It was decided to mutate these residues and examine their effect on the enzyme. This approach revealed a possible role for His84 in the binding of biliverdin to the enzyme and in proton transfer to the tetrapyrrole substrate during the reaction. A possible role in biliverdin binding was also uncovered for Glu101 which may also be acting as a proton acceptor during the reaction. Tyr102 was shown to be important for binding biliverdin in the orientation necessary for efficient catalysis. Structural roles, possibly in stabilising substrate binding or maintaining the structural integrity of certain domains was attributed to Asp285 and Arg185.

pH	V_{max} (µmoles/min/mg)	K_m^{NADPH} (µM)	k_{cat} (s^{-1})	k_{cat}/K_m^{NADPH} (M^{-1} s^{-1})
4.25	0.31 +/- 0.035	11.1 +/- 4.26	0.18 +/- 0.02	14,700 +/- 4,650
4.5	0.42 +/- 0.22	10.5 +/- 1.96	0.24 +/- 0.01	22,900 +/- 6,300
4.52	0.421 +/- 0.03	9.25 +/- 2.5	0.24 +/- 0.02	22,500+/- 68,00
4.6	0.6 +/- 0.15	13.7 +/- 1.1	0.34 +/- 0.01	26,060 +/- 7,800
4.65	0.66 +/- 0.02	23 +/- 2	0.38 +/- 0.01	16,190 +/- 5,720
4.75	0.78 +/- 0.03	7.07 +/- 1.04	0.44 +/- 0.02	61,700 +/- 16,400
4.87	0.77 +/- 0.044	8.051 +/- 1.8	0.43 +/- 0.03	53,840 +/- 14,000
5	0.781 +/- 0.06	10.78 +/- 3.2	0.44 +/- 0.03	41,000 +/- 10,600
5.12	0.77 +/- 0.07	9.57 +/- 3.2	0.43 +/- 0.04	39,300 +/- 12,390
5.13	0.72 +/- 0.03	5.05 +/- 1.04	0.40 +/- 0.02	76,300 +/- 16,390
5.25	0.55 +/- 0.01	4 +/- 0.7	0.31 +/- 0.01	77,900 +/- 8,090
5.37	0.52 +/- 0.016	5.28 +/- 0.73	0.29 +/- 0.01	55,700 +/- 12,400
5.5	0.37 +/- 0.004	1.06 +/- 0.15	0.21 +/- 0.01	168,400 +/- 15,600
6	0.26 +/- 0.01	1.04 +/- 0.44	0.15 +/- 0.01	141,300 +/- 12,900
6.5	0.089 +/- 0.005	5.1 +/- 1.5	0.05 +/- 0.01	9,800 +/- 1,900
7	0.053 +/- 0.002	2.3 +/- 1.7	0.03 +/- 0.01	13,050 +/- 678

Table 5.1 Kinetic parameters of sBVR-A as various pH values with NADPH as co-factor

pH	V_{max} (µmoles/min/mg)	$K_m^{Biliverdin}$ (µM)	k_{cat} (s^{-1})	$k_{cat}/K_m^{Biliverdin}$ (M^{-1} s^{-1})
4.25	0.29 +/- 0.07	2.98 +/- 1.68	0.16 +/- 0.04	54,900 +/- 21,925
4.5	0.43 +/- 0.05	2.74 +/- 0.78	0.24 +/- 0.03	88,231 +/- 34,873
4.52	0.41 +/- 0.02	0.39 +/- 0.09	0.24 +/- 0.01	604,384 +/- 120,574
4.6	0.63 +/- 0.04	0.69 +/- 0.17	0.36 +/- 0.02	517,222 +/- 133,341
4.65	0.66 +/- 0.04	2.12 +/- 0.4	0.37 +/- 0.02	175,623 +/- 56,670
4.75	0.77 +/- 0.05	1.41 +/- 0.27	0.44 +/- 0.03	309,474 +/- 96,549
4.87	0.77 +/- 0.04	1.39 +/- 0.22	0.44 +/- 0.04	310,994 +/- 103,036
5	0.79 +/- 0.07	2.32 +/- 0.59	0.45 +/- 0.02	194,971 +/- 67,235
5.12	0.66 +/- 0.04	2.3 +/- 0.6	0.38 +/- 0.02	163,604 +/- 38,033
5.13	0.68 +/- 0.03	1.4 +/- 0.33	0.39 +/- 0.02	27,5254 +/- 56,670
5.25	0.55 +/- 0.05	0.96 +/- 0.25	0.31 +/- 0.02	324,334 +/- 90,672
5.37	0.52 +/- 0.02	1.6 +/- 0.47	0.29 +/- 0.03	183,823 +/- 60,287
5.5	0.32 +/- 0.01	0.54 +/- 0.1	0.18 +/- 0.01	331,011 +/- 88,894
6	0.27 +/- 0.01	1 +/- 0.09	0.15 +/- 0.00	150,742 +/- 38,638
6.5	0.09 +/- 0.01	1.94 +/- 0.41	0.05 +/- 0.00	25,998 +/- 8,293
7	0.05 +/- 0.01	0.66 +/- 0.2	0.03 +/- 0.00	45,507 +/- 8,947

Table 5.2 Kinetic parameters of sBVR-A at various pH values with NADPH as co-factor and biliverdin as the variable substrate

pH	V_{max} (µmoles/min/mg)	K_m^{NADH} (µM)	k_{cat} (s^{-1})	k_{cat}/K_m^{NADH} (M^{-1} s^{-1})
4.25	0.228 +/- 0.015	26.9 +/- 12	0.13 +/- 0.01	3,973 +/- 723
4.5	0.24 +/- 0.04	165.3 +/- 20	0.14 +/- 0.2	833 +/- 1133
4.62	0.296 +/- 0.03	169.7 +/- 53	0.17 +/- 0.018	1,000 +/- 331
4.81	0.292 +/- 0.03	299 +/- 65	0.17 +/- 0.02	549 +/- 261
4.9	0.25 +/- 0.02	165 +/- 44	0.14 +/- 0.01	661 +/- 270
5	0.297 +/- 0.04	206.6 +/- 66	0.17 +/- 0.05	823 +/- 100
5.1	0.26 +/- 0.06	582 +/- 289	0.15 +/- 0.04	253 +/- 12.5
5.25	0.236 +/- 0.03	207 +/- 66	0.13 +/- 0.01	712 +/- 223
5.5	0.214 +/- 0.07	694 +/- 413	0.12 +/- 0.04	196 +/- 9.6
5.75	0.119 +/- 0.02	343 +/- 124	0.07 +/- 0.01	230 +/- 8.2
6.24	0.038 +/- 0.01	671 +/- 372	0.02 +/- 0.01	32 +/- 1.7
6.5	0.035 +/- 0.01	1183 +/- 897	0.019 +/- 0.01	24 +/- 0.69
6.75	0.02 +/- 0.00	1017 +/- 372	0.011 +/- 0.00	12.3 +/- 0.61

Table 5.3 Kinetic parameters of sBVR-A at various pH values with NADH as co-factor

pH	V_{max} (µmoles/min/mg)	$K_m^{Biliverdin}$ (µM)	k_{cat} (s^{-1})	$k_{cat}/K_m^{Biliverdin}$ (M^{-1} s^{-1})
4.25	0.19 +/- 0.02	0.68 +/- 1.3	0.107 +/- 0.011	156,692 +/- 8,721
4.5	0.24 +/- 0.04	1.24 +/- 0.57	0.138 +/- 0.022	111,234 +/- 37,792
4.62	0.3 +/- 0.05	4.94 +/- 1.78	0.17 +/- 0.028	34,415 +/- 15,923
4.81	0.29 +/- 0.01	0.98 +/- 0.11	0.164 +/- 0.006	167,697 +/- 51,536
4.9	0.28 +/- 0.04	2.24 +/- 0.38	0.159 +/- 0.022	70,837 +/- 56,689
5	0.26 +/- 0.02	1.6 +/- 0.55	0.15 +/- 0.011	93,750 +/- 13,826
5.1	0.28 +/- 0.04	1.11 +/- 0.5	0.158 +/- 0.02	132,740 +/- 39,682
5.25	0.26 +/- 0.04	1.054 +/- 0.5	0.147 +/- 0.02	139,793 +/- 40,492
5.5	0.24 +/- 0.05	1.9 +/- 1	0.136 +/- 0.03	71,583 +/- 30,315
5.75	0.14 +/- 0.03	0.67 +/- 0.5	0.079 +/- 0.014	117,569 +/- 28,344
6.24	0.038 +/- 0.01	2.5 +/- 1.4	0.022 +/- 0.005	8,613 +/- 3,239
6.5	0.05 +/- 0.01	8.3 +/- 2.5	0.028 +/- 0.005	3,413 +/- 2,040
6.75	0.022 +/- 0.01	6.9 +/- 3	0.0125 +/- 0.003	1806 +/- 1023

Table 5.4 Kinetic parameters of sBVR-A at various pH values with NADH as co-factor and biliverdin as the variable substrate

Mutation	Dir.	Base change	Sequence
H84A	for	CAT → GCT	5'- CACCATTAACCAACTCGCTGGGGCGATCGCCGAGG-3'
H84A	rev	GTA → CGA	5'- CCTCGGCGATCGCCCCAGCGAGTTGGTTAATGGTG-3'
H97A	for	CAT → GCT	5'- GCATTGCAAGCCGGTAAAGCTGTGGTGTTGGAATATC-3'
H97A	rev	GTA → GGA	5'- GATATTCCAACACCACAGCTTTACCGGCTTGCAATGC-3'
H126A	for	CAT → GCT	5'- CGGGAAAAAGGTAAATTACTGGCTGTGGAACATATTGAAC-3'
H126A	rev	GTA → GGA	5'- CAAGAATATGTTCCACAGCCAGTAATTTACCTTTTTCCCG-3'
H129A	for	CAT → GCT	5'- GTAAATTACTGCATGTGGAAGCTATTGAACTATTGGGGGG-3'
H129A	rev	GTA → GGA	5'- CCCCCCAATAGTTCAATAGCTTCCACATGCAGTAATTTAC-3'
E101A	for	GAA → GCA	5'- GCCGGTAAACATGTGGTGTTGGCATATCCTTTAGCGTTAACCTATG-
E101A	rev	CTT → CGT	5'- CATAGGTTAACGCTAAAGGATATGCCAACACCACATGTTTACCGGC-
Y102A	for	TAT → GCT	5'- CATGTGGTGTTGGAAGCTCCTTTAGCGTTAACCTATG-3'
Y102A	rev	ATA → CGA	5'- CATAGGTTAACGCTAAAGGAGCTTCCAACACCACATG-3'
R185A	for	CGC → GCC	5'- GTGGCGGCCTTGTCCGCCATCAGTCGCTTTACGG-3'
R185A	rev	GCG → CGG	5'- CCGTAAAGCGACTGATGGCGGACAAGGCCGCGAC-3'
D285A	For	GAC → GCC	5'- GAGGACTGTTCAGACAAGCCACGGAAGCAGTGTTGG-3'
D285A	rev	GTG → CGG	5'- CCAACACTGCTTCCGTGGCTTGTCTGAACAGTCCTC-3'

Table 5.6 Primers used in site-directed mutagenesis of sBVR-A

Shown in red are the mutated residues

Mutation	Variable substrate	V_{max} (µmoles/min/mg)	K_m (µM)	k_{cat} (s^{-1})
Wild-type	NADPH	0.78 +/- 0.06	10.78 +/- 3.2	0.44 +/- 0.034
	Biliverdin	0.79 +/- 0.07	2.32 +/- 0.59	0.45 +/- 0.02
Y102A	NADPH	0.33 +/- 0.06	3.55 +/- 3.2	0.18 +/- 0.034
	Biliverdin	0.33 +/- 0.022	16.19 +/- 1.62	0.18 +/- 0.012
R185A	NADPH	0.089 +/- 0.006	4.54 +/- 1.4	0.05 +/- 0.034
	Biliverdin	0.089 +/- 0.01	3.22 +/- 0.9	0.05 +/- 0.006
H129A	NADPH	0.68 +/- 0.01	4.53 +/- 0.32	0.39 +/- 0.006
	Biliverdin	0.68 +/- 0.055	1.3 +/- 0.34	0.39 +/- 0.03
H126A	NADPH	0.62 +/- 0.1	23.3 +/- 10	0.35 +/- 0.06
	Biliverdin	0.64 +/- 0.05	4.67 +/- 0.72	0.36 +/- 0.03
H97A	NADPH	0.58 +/- 0.05	5.81 +/- 2.3	0.33 +/- 0.03
	Biliverdin	0.58 +/- 0.026	2.26 +/- 0.28	0.33 +/- 0.015
H84A	NADPH	0.008	Unable to calculate	
	Biliverdin	0.008		
E101A	NADPH	0.27 +/- 0.034	8.8 +/- 4	0.15 +/- 0.02
	Biliverdin	0.25 +/- 0.22	21.66 +/- 24.55	0.14 +/- 0.13
D285A	NADPH	0.1 +/- 0.006	1 +/- 0.73	0.057 +/- 0.01
	Biliverdin	0.11 +/- 0.013	1.60 +/- 0.6	0.062 +/- 0.007

Table 5.8 Effect of mutations on the kinetic parameters of sBVR-A

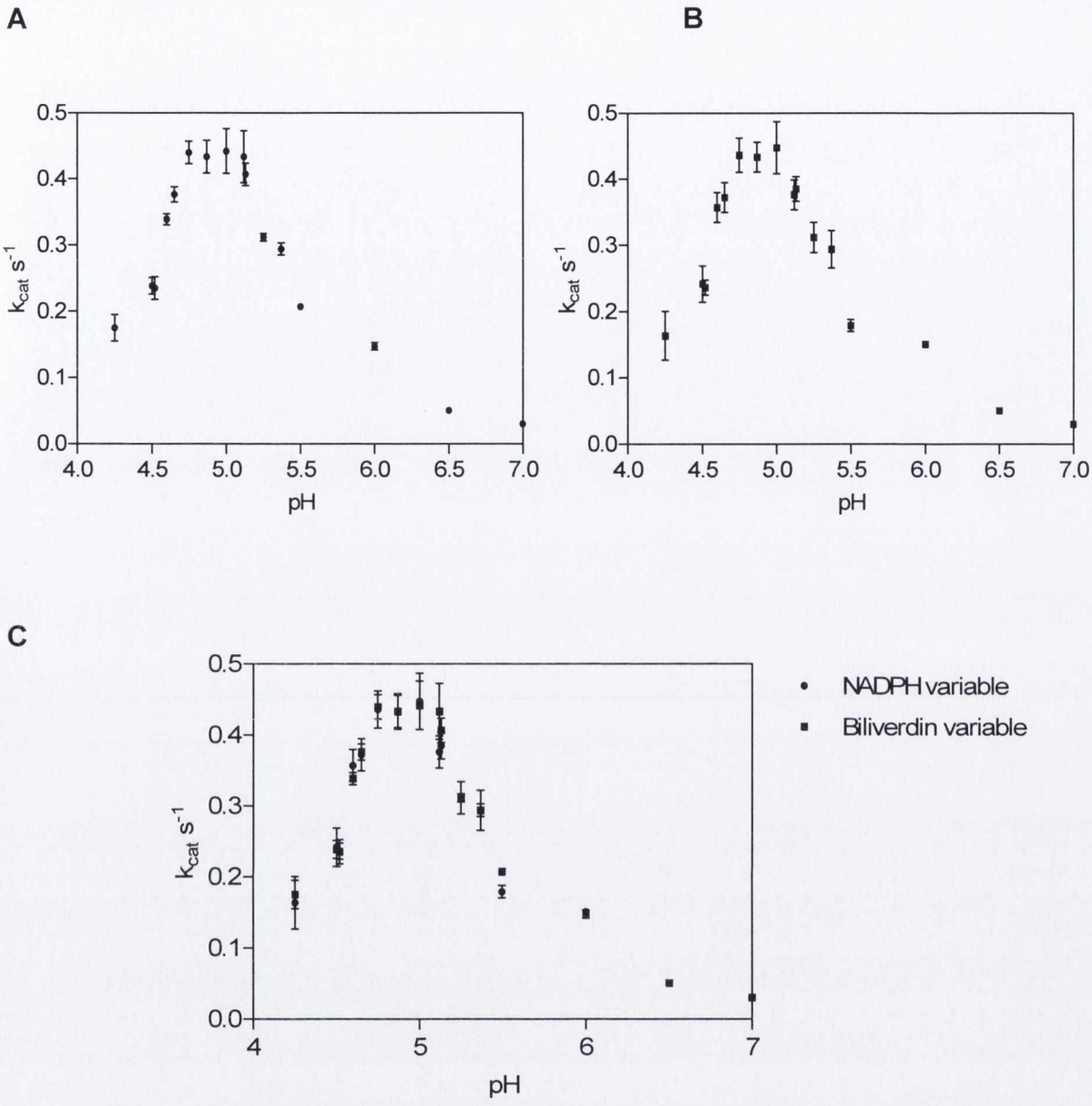

Figure 5.1 pH profiles of sBVR-A with NADPH as co-factor

A. k_{cat} *versus* pH with NADPH variable **B.** k_{cat} *versus* pH with biliverdin variable

C. Overlay of the k_{cat} *versus* pH data with NADPH and biliverdin variable

100mM Sodium citrate (pKs: 3.13, 4.76, 6.4) was used to buffer over the entire range pH4 to 7. Experiments were performed in triplicate. Each datum point represents the mean and error bars represent the standard deviation of the triplicate values

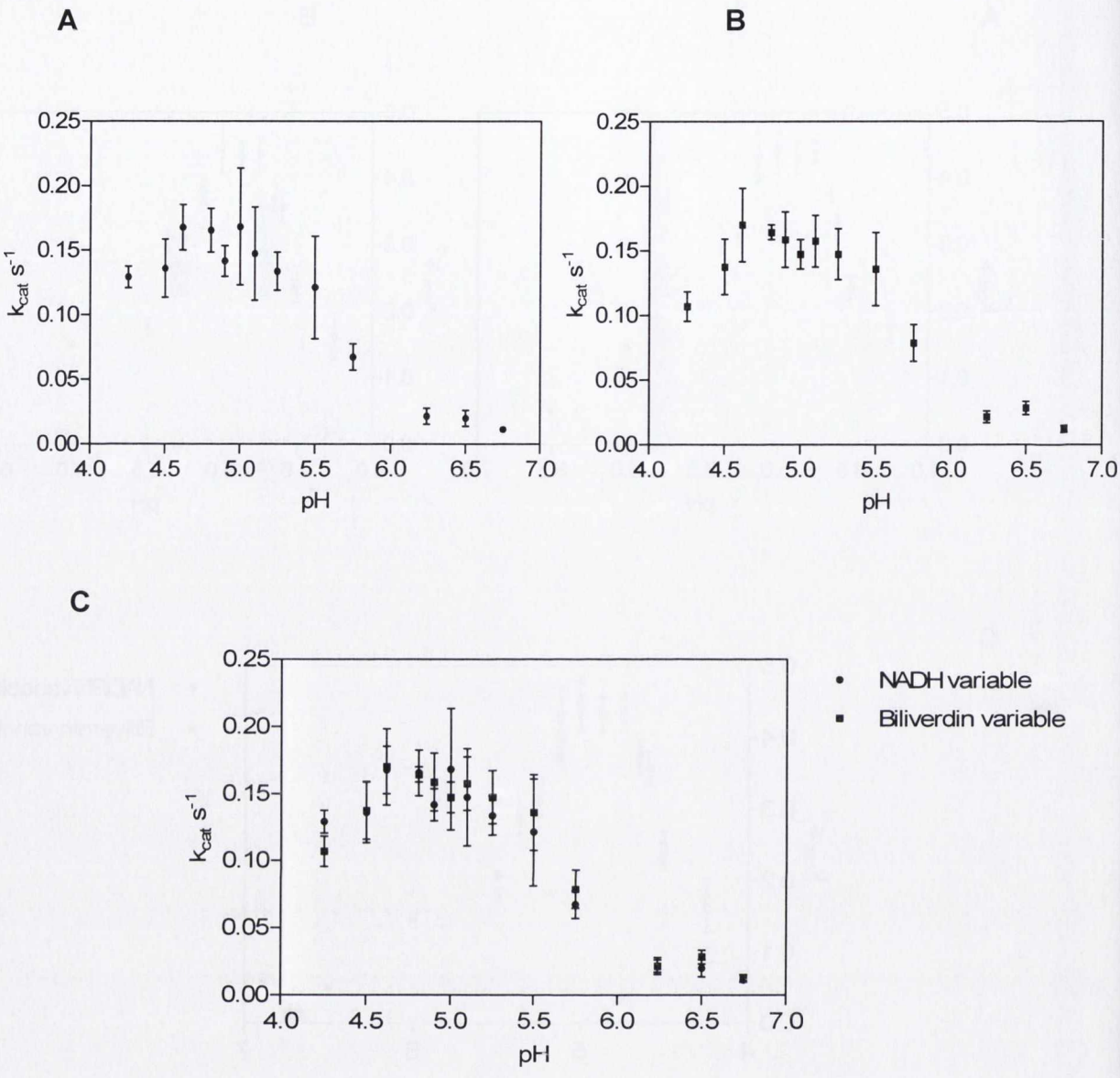

Figure 5.2 pH profiles of sBVR-A with NADH as co-factor

A. k_{cat} *versus* pH with NADH variable **B.** k_{cat} *versus* pH with biliverdin variable
C. Overlay of the k_{cat} *versus* pH data with NADH and biliverdin variable

100mM Sodium citrate (pKs: 3.13, 4.76, 6.4) was used to buffer over the entire range pH4 to 7. Experiments were performed in triplicate. Each datum point represents the mean and error bars represent the standard deviation of the triplicate values

A

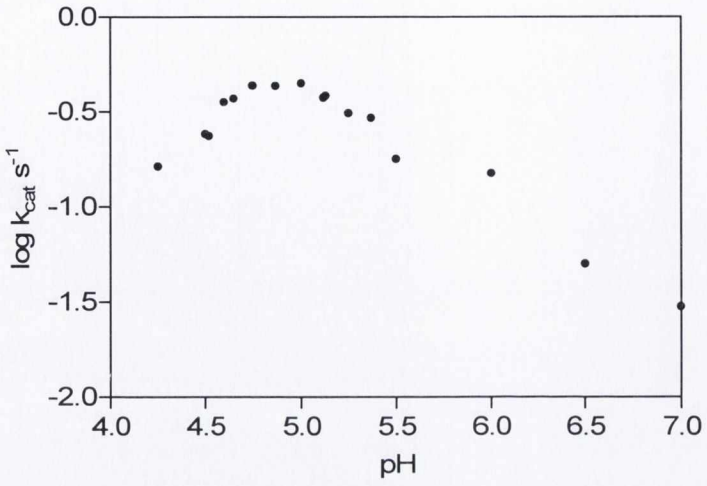

B

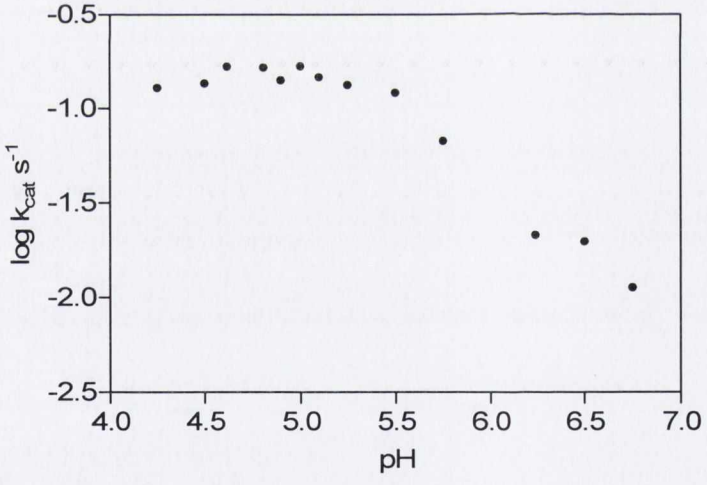

Figure 5.3 log k_{cat} *versus* pH for sBVR-A

A. NADPH as co-factor

B. NADH as co-factor

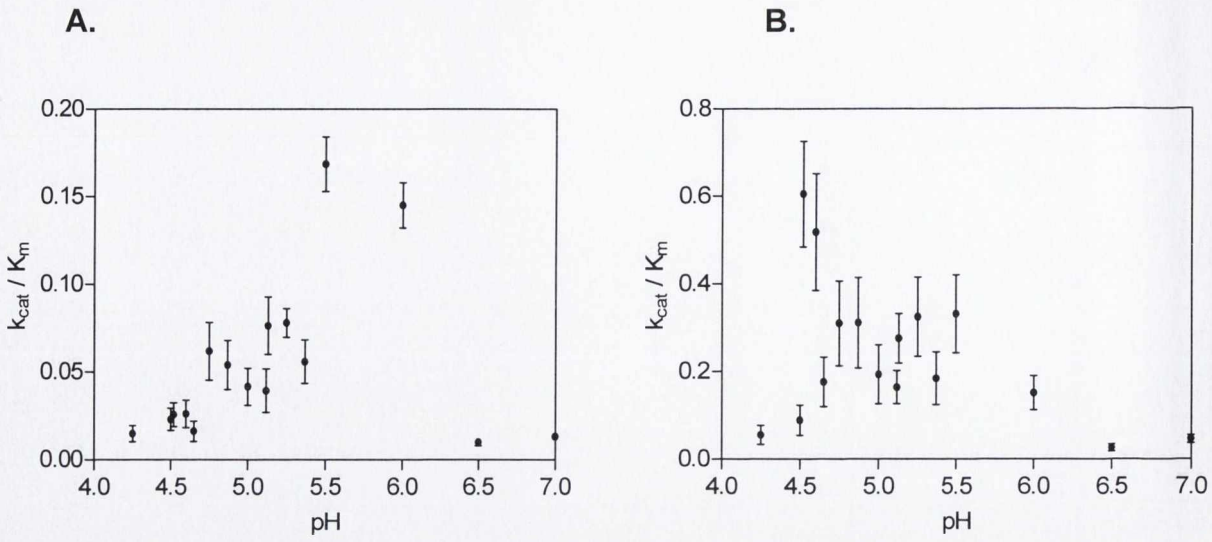

Figure 5.4 k_{cat}/ K_m *versus* pH with NADPH as co-factor

A. k_{cat}/ K_m *versus* pH with NADPH as the variable substrate **B.** k_{cat}/ K_m *versus* pH with biliverdin as the variable substrate

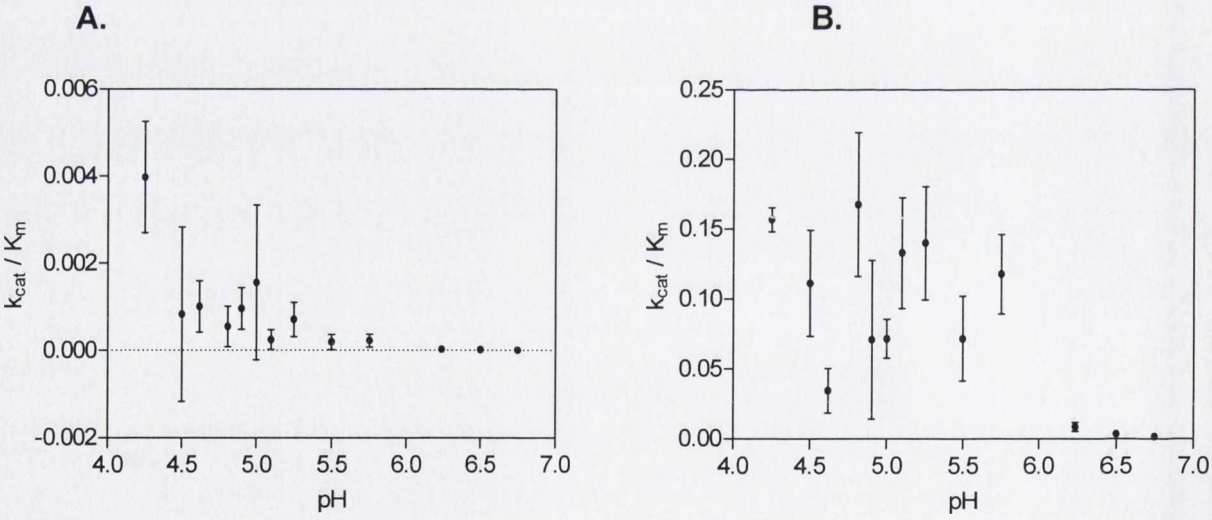

Figure 5.5 k_{cat}/ K_m *versus* pH with NADH as co-factor

A. k_{cat}/ K_m *versus* pH with NADH as the variable substrate **B.** k_{cat}/ K_m *versus* pH with biliverdin as the variable substrate

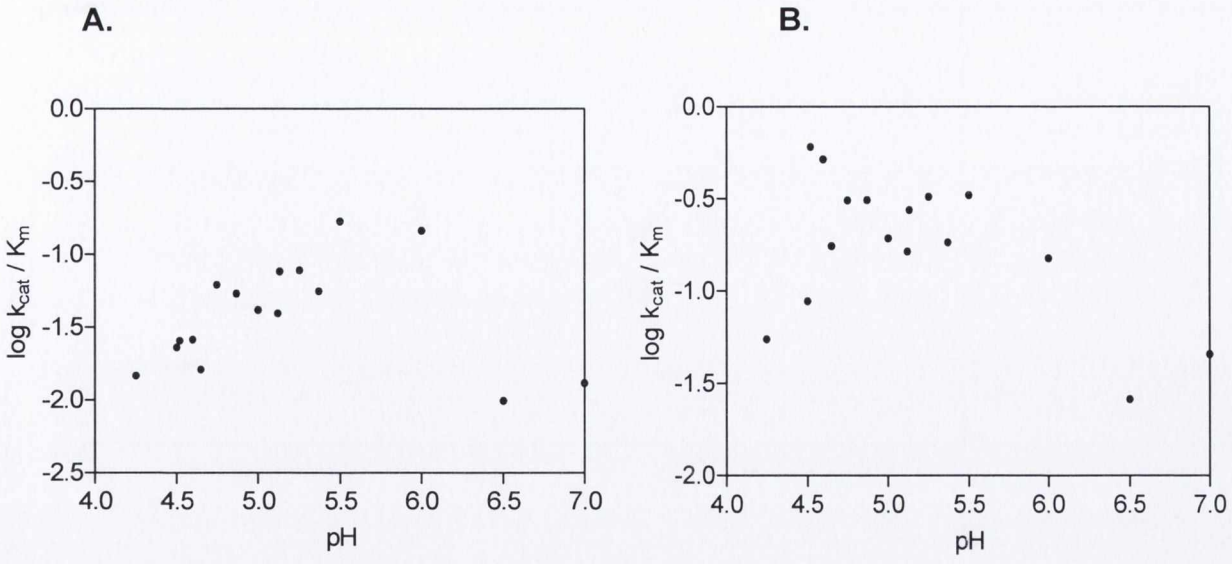

Figure 5.6 log k_{cat}/ K_m *versus* pH with NADPH as co-factor

A. Log k_{cat}/ K_m versus pH with NADPH as the variable substrate **B.** log k_{cat}/ K_m *versus* pH with biliverdin as the variable substrate

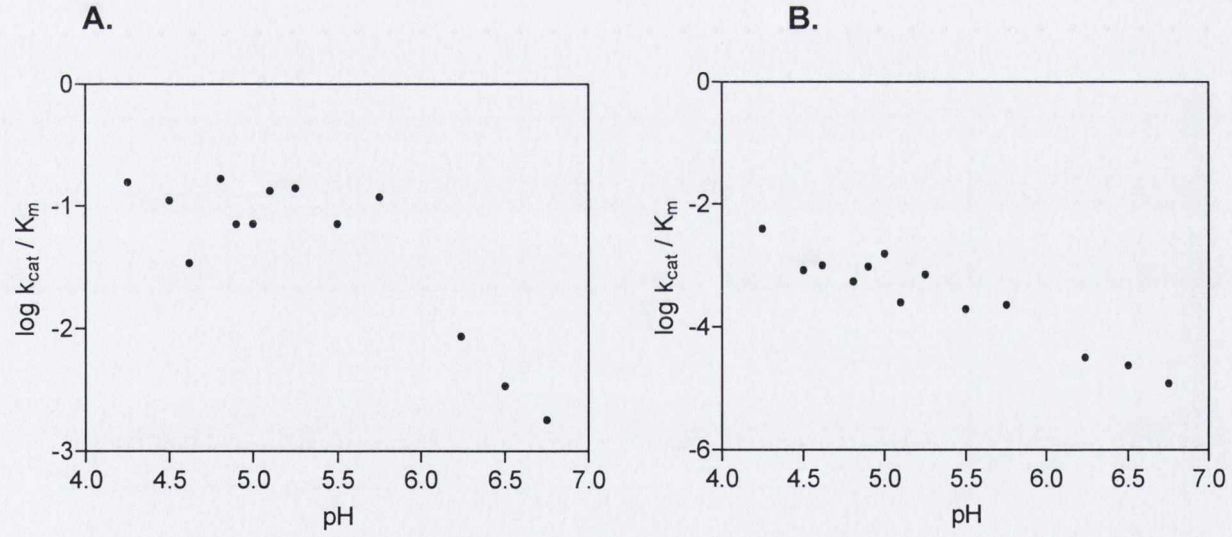

Figure 5.7 log k_{cat}/ K_m *versus* pH with NADH as co-factor

A. Log k_{cat}/ K_m versus pH with NADH as the variable substrate **B.** log k_{cat}/ K_m *versus* pH with biliverdin as the variable substrate

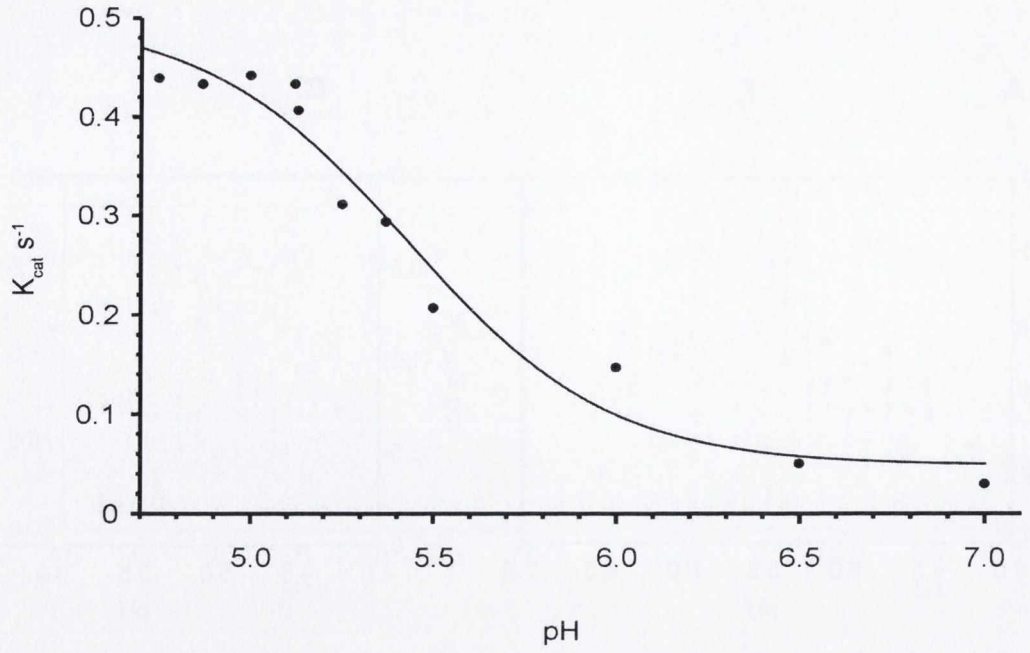

Figure 5.8 k_{cat} *versus* pH data for sBVR-A in the "less acidic" region with NADPH variable

The data were fit to the Richards generalised logistic function for pK shown in Section 5.4 and a pK of 5.43 +/- 0.01 was calculated

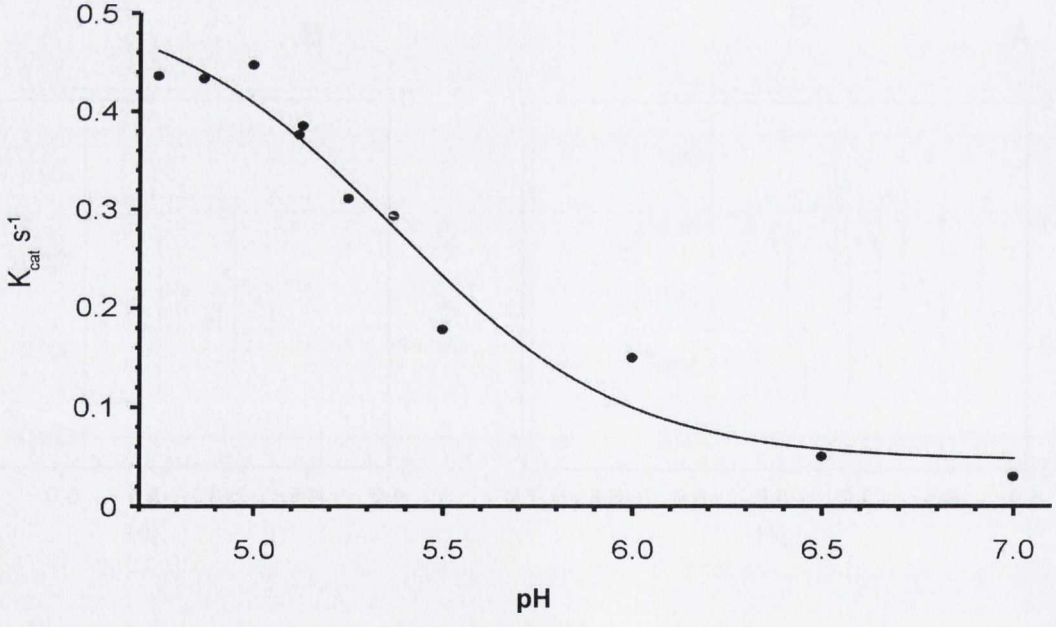

Figure 5.9 k_{cat} *versus* pH data for sBVR-A in the "less acidic" region with biliverdin variable substrate and NADPH as co-factor

The data were fit to the Richards generalised logistic function for pK shown in Section 5.4 and a pK of 5.37 +/- 0.12 was calculated

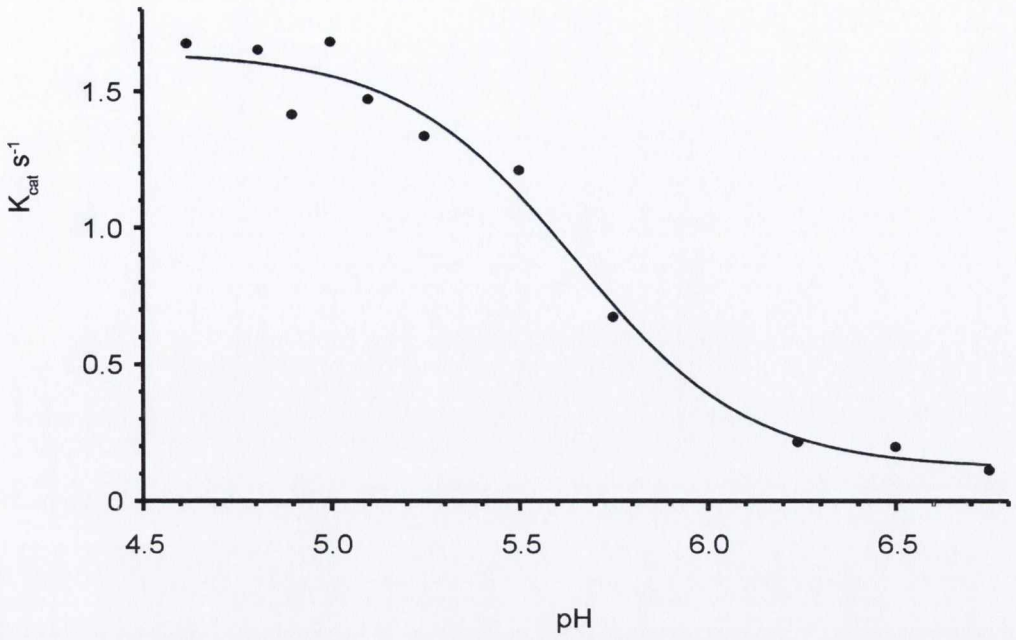

Figure 5.10 k_{cat} *versus* pH data for sBVR-A in the "less acidic" region with NADH variable

The data were fit to the Richards generalised logistic function for pK shown in Section 5.4 and a pK of 5.65 +/- 0.059 was calculated

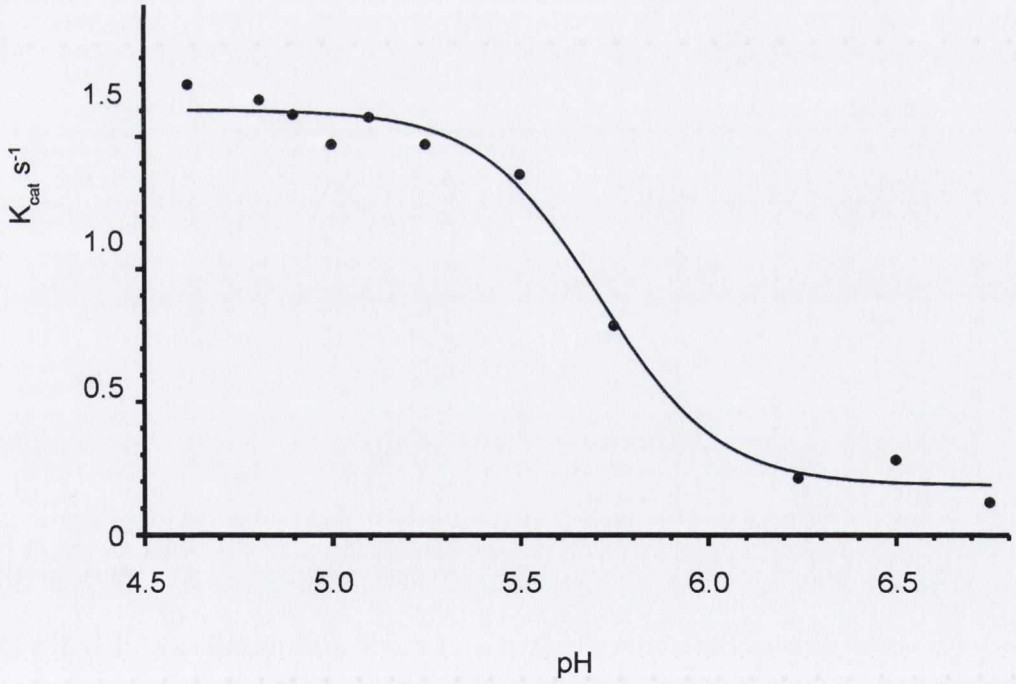

Figure 5.11 k_{cat} *versus* pH data for sBVR-A in the "less acidic" region with biliverdin variable and NADH as co-factor

The data were fit to the Richards generalised logistic function for pK shown in Section 5.4 and a pK of 5.7 +/- 0.03 was calculated

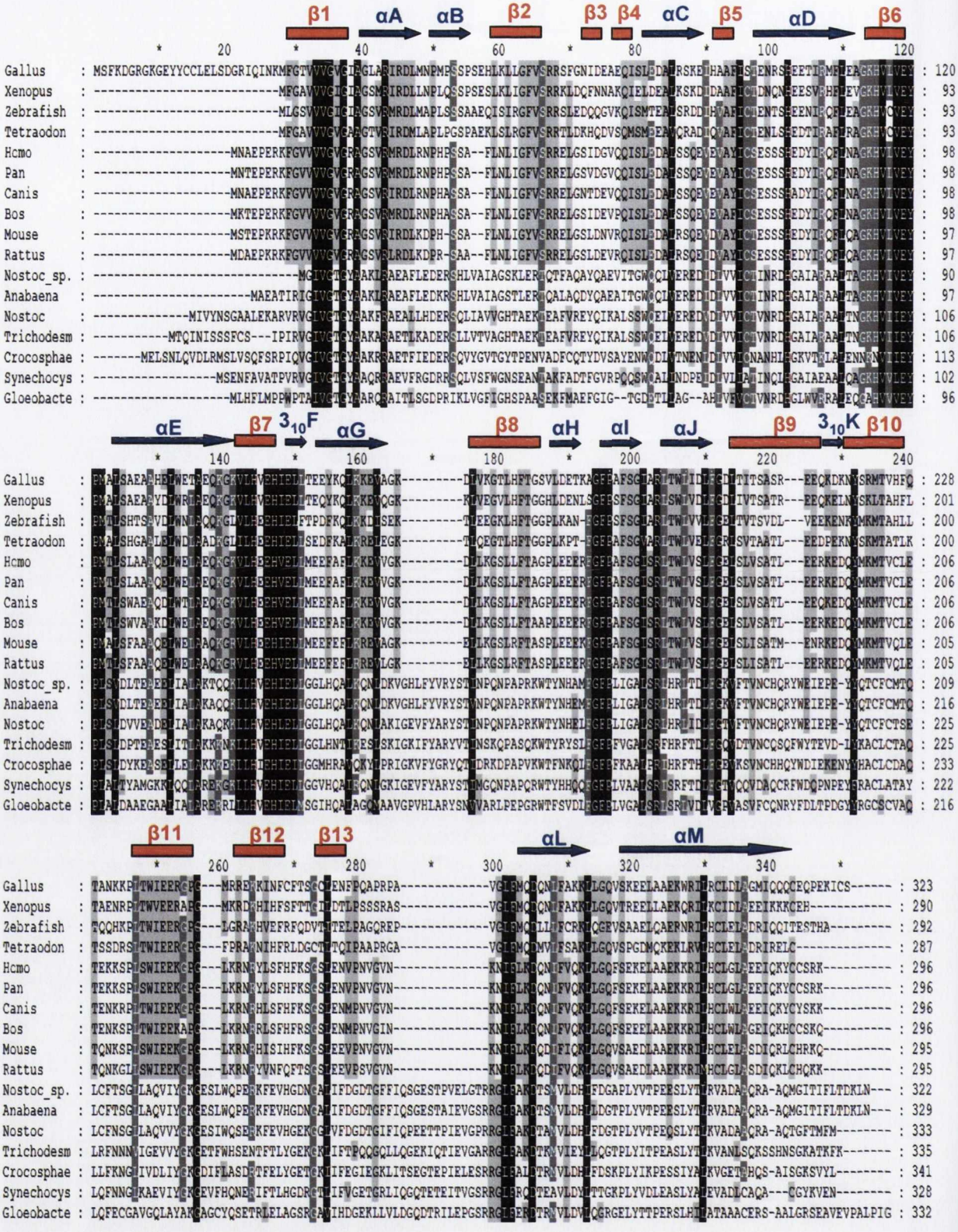

Figure 5.12 Multiple sequence alignment of all known and putative biliverdin IXα reductases

Sequences were retrieved using BlastP (NCBI) and aligned using ClustalW (EMBL). Features were added using Genedoc (Karl Nicholas, Pittsburg Supercomputing center). Conserved residues are shown in black, semi-conserved residues in dark grey and residues common to some sequences are shown in light grey. β-sheets are shown in red and α-helices in blue

Region 1.

The nucleotide binding domain between the β1 and αA segments in the rat structure which comprises the Rossman fold. This domain is common to all members of the GFO/IDH/MOCA family of which BVR-A is a member

VGVGRAG

Region 2.

The GFO/IDH/MOCA concensus sequence located at the end of the β6 in the rat structure. This region contains a number of highly conserved residues common to all BVR-As

H79 L87 H92 E96 Y97
LEDALRSQEIDVAYICSESSSHEDYIRQFLQAGKHVLVEYPMT

Region 3

The conserved sequence between the β7 sheet and 3_{10} helix F

L120
LHEEHVELL

Region 4.

The conserved sequence from αI to αJ

F161 R171
FGFPAFSGISRLTWLVSLFG

Region 5.

The conserved sequence beginning at the start of αL

D253
IFLKD

Figure 5.13 The most conserved regions of biliverdin IXα reductases

The five most conserved regions shown were identified through sequence analysis of all known and putative BVR-As. Regions of rat BVR-A sequence are shown and residues common to all BVR-As are shown in larger font. The tyrosine residue located within the EYP motif of BVR-As is shown in red

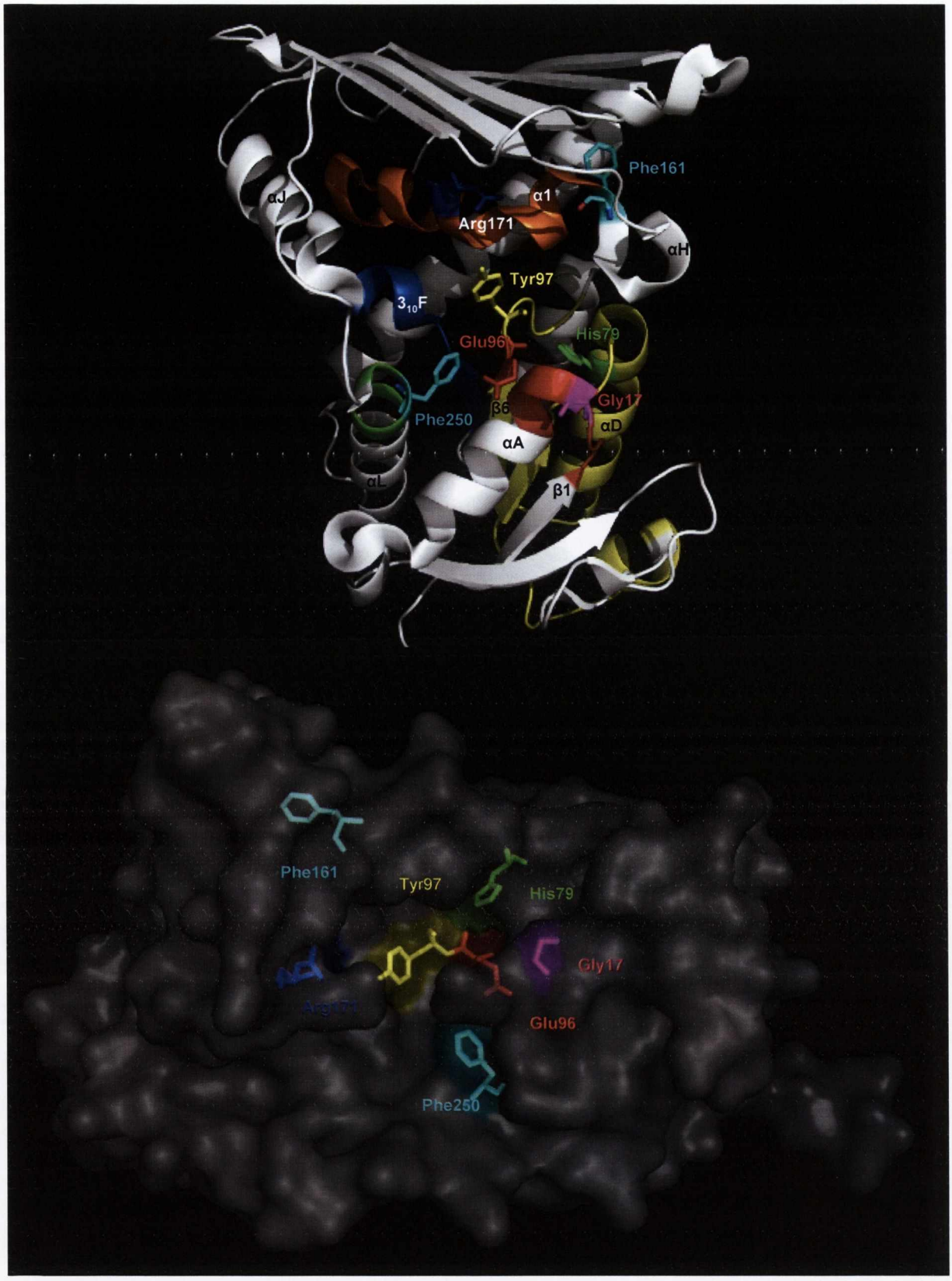

Figure 5.14 The most conserved residues of BVR-A
The 5 highly conserved motifs have been colour coded red, yellow, blue, orange and green. Similar colouring was used in the alignments of Figure 5.12. The ribbon diagram (top) shows the extent of conservation with many residues conserved deep at the core of the protein. The surface diagram (bottom) highlights the most conserved amino acids which are positioned around the active site and which are exposed at the surface

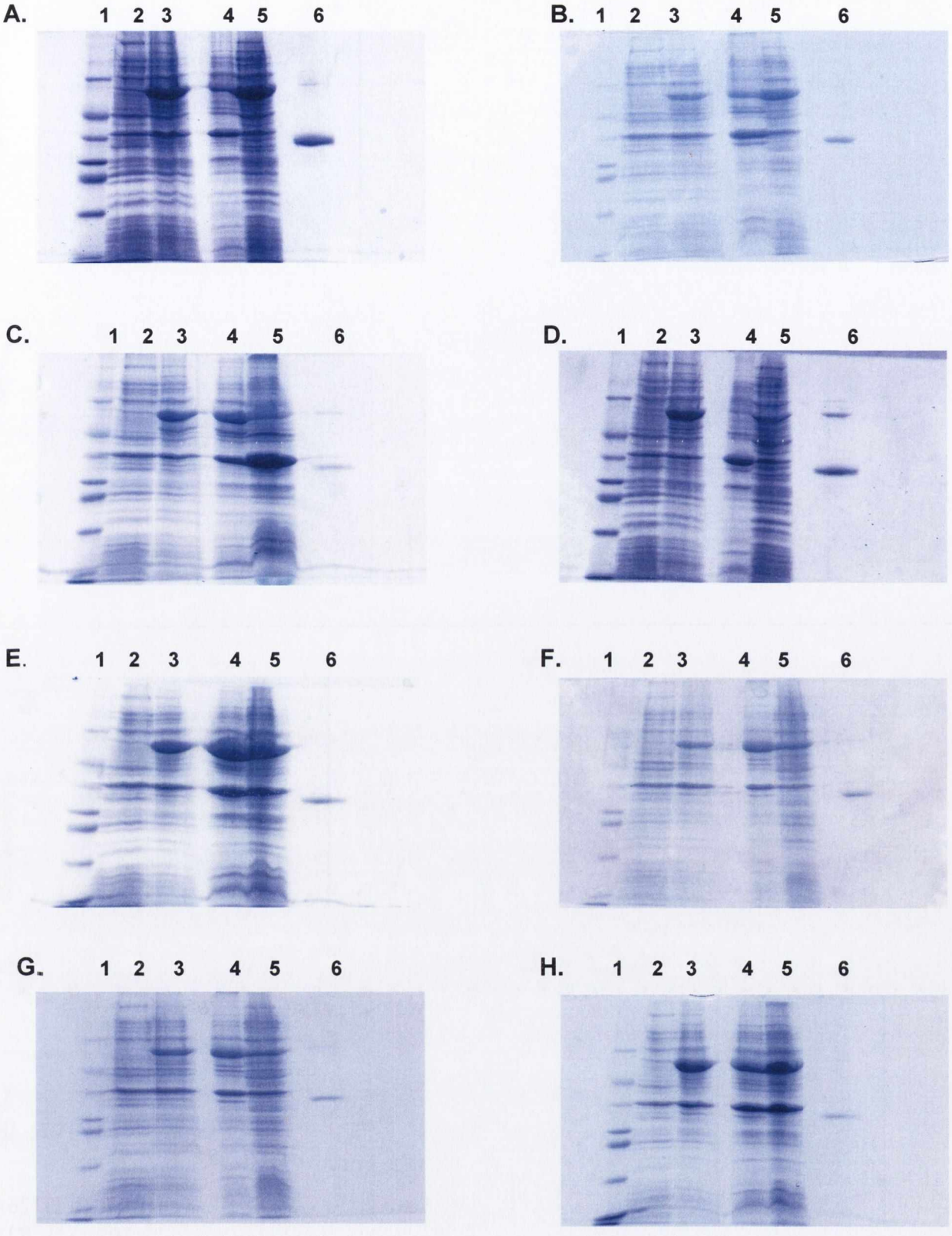

Figure 5.15 SDS-PAGE analysis of sBVR-A mutants

A. H84A **B**. H97A **C**. H126A **D**. H129A **E**. E101A. **F**. Y102A **G**. R185A **H**. D285A Lane 1 in all cases contains molecular weight markers (66, 45, 36, 24, 19, 14.5, 6.5 kDa), Lane 2 contains uninduced *E.coli*, Lane 3 contains IPTG induced *E.coli*, Lane 4 contains soluble supernatant fraction, Lane 5 contains urea treated pellet, Lane 6 contains glutathione-Sepharose purified sBVR-A mutant

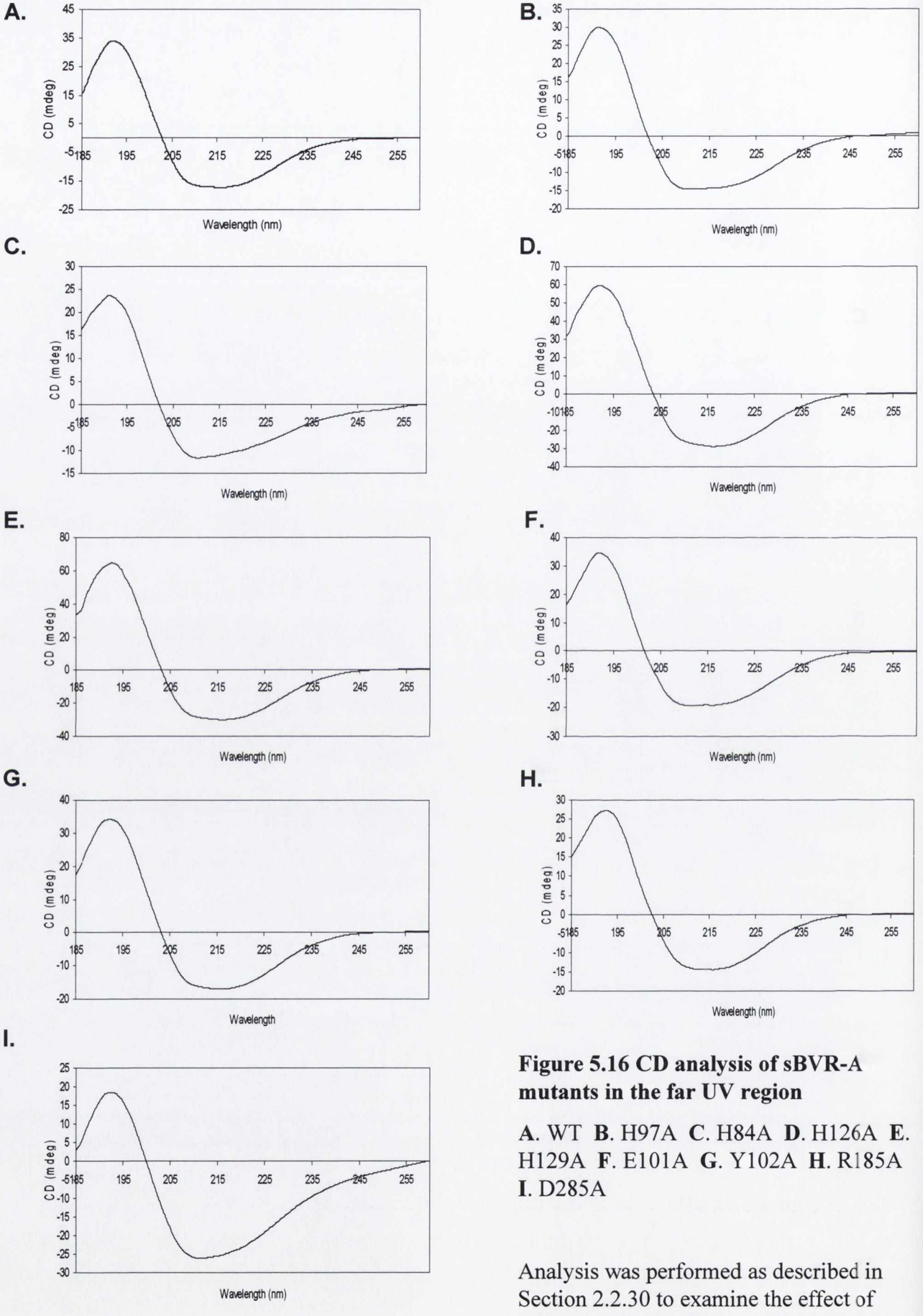

Figure 5.16 CD analysis of sBVR-A mutants in the far UV region

A. WT **B**. H97A **C**. H84A **D**. H126A **E**. H129A **F**. E101A **G**. Y102A **H**. R185A **I**. D285A

Analysis was performed as described in Section 2.2.30 to examine the effect of each mutation on the secondary structure of sBVR-A

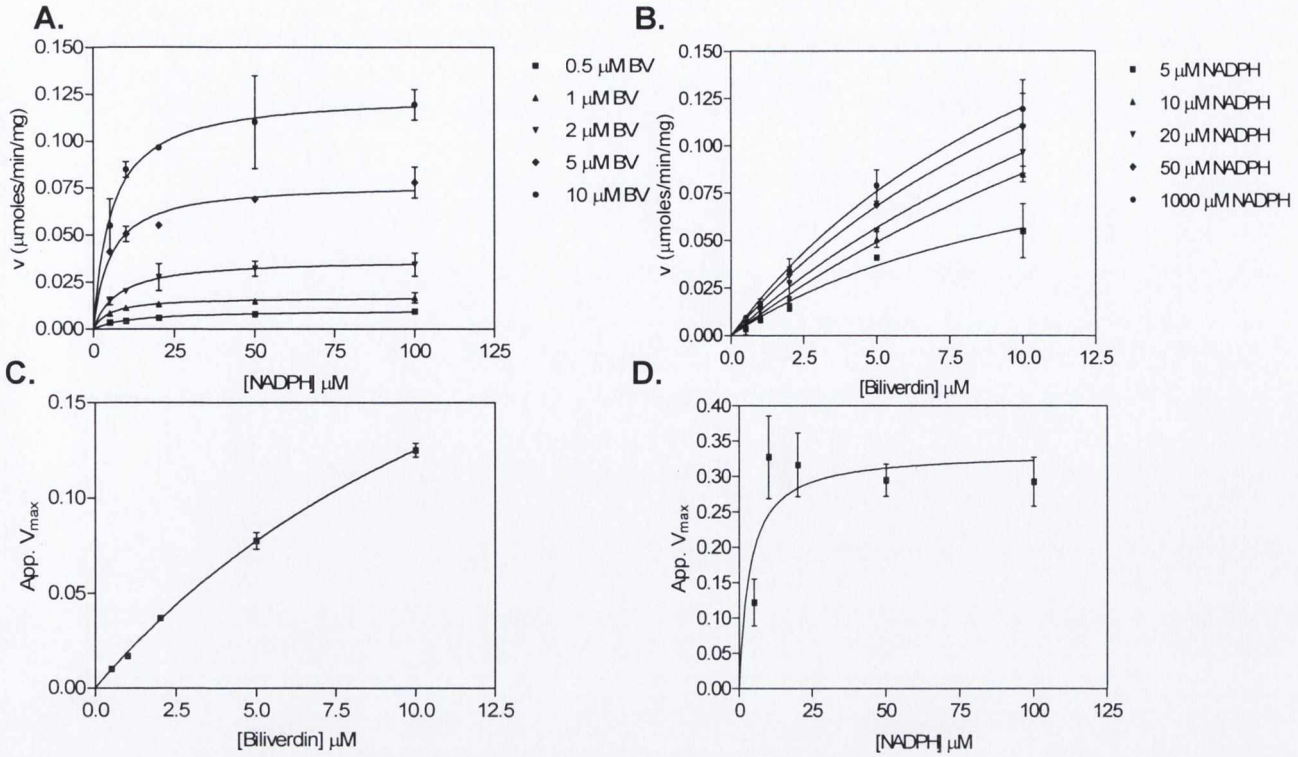

Figure 5.17 Kinetic analysis of the Y102A mutant

A. Initial rate kinetics of Y102AA with NADPH as the variable substrate **B**. Initial rate kinetics of Y102A with biliverdin as the variable substrate **C**. Plot of apparent V_{max} for NADPH versus biliverdin concentration **D**. Plot of apparent V_{max} for biliverdin versus NADPH concentration

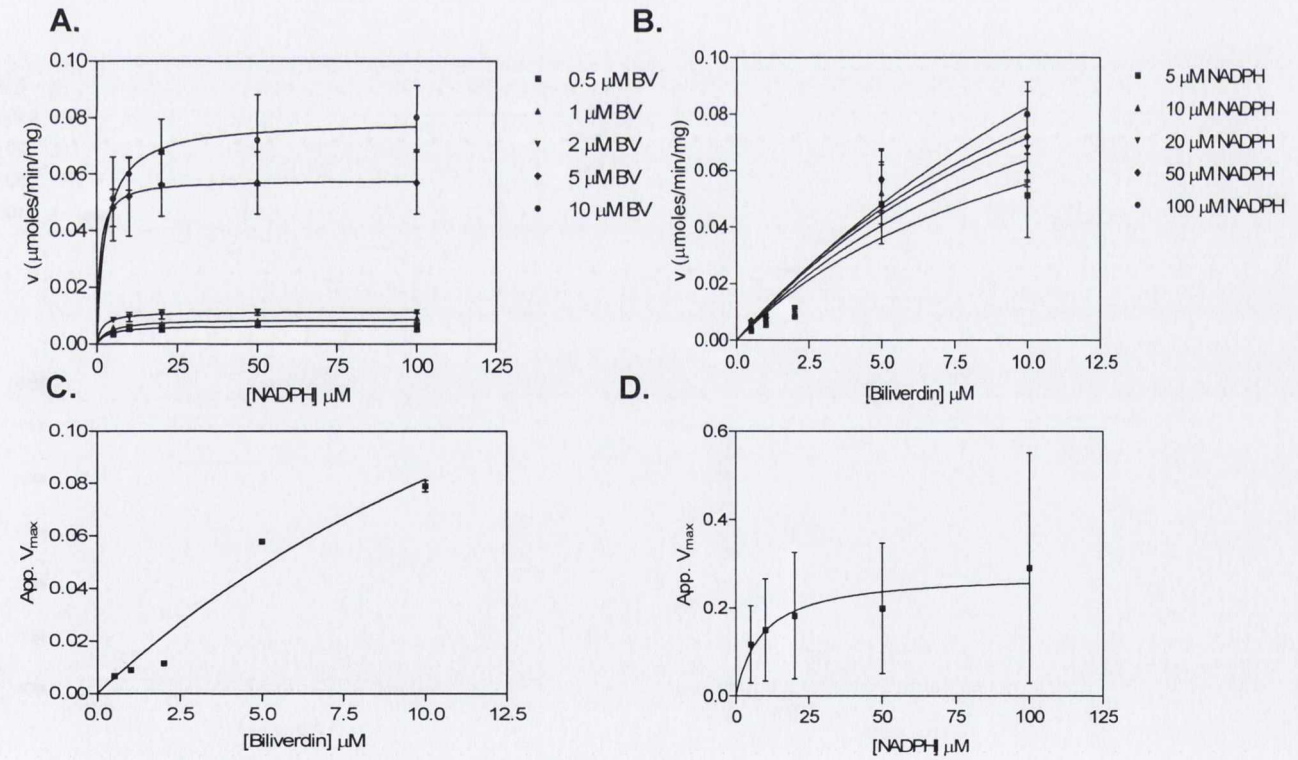

Figure 5.18 Kinetic analysis of the E101A mutant

A. Initial rate kinetics of E101A with NADPH as the variable substrate **B**. Initial rate kinetics of E101A with biliverdin as the variable substrate **C**. Plot of apparent V_{max} for NADPH versus biliverdin concentration **D**. Plot of apparent V_{max} for biliverdin versus NADPH concentration

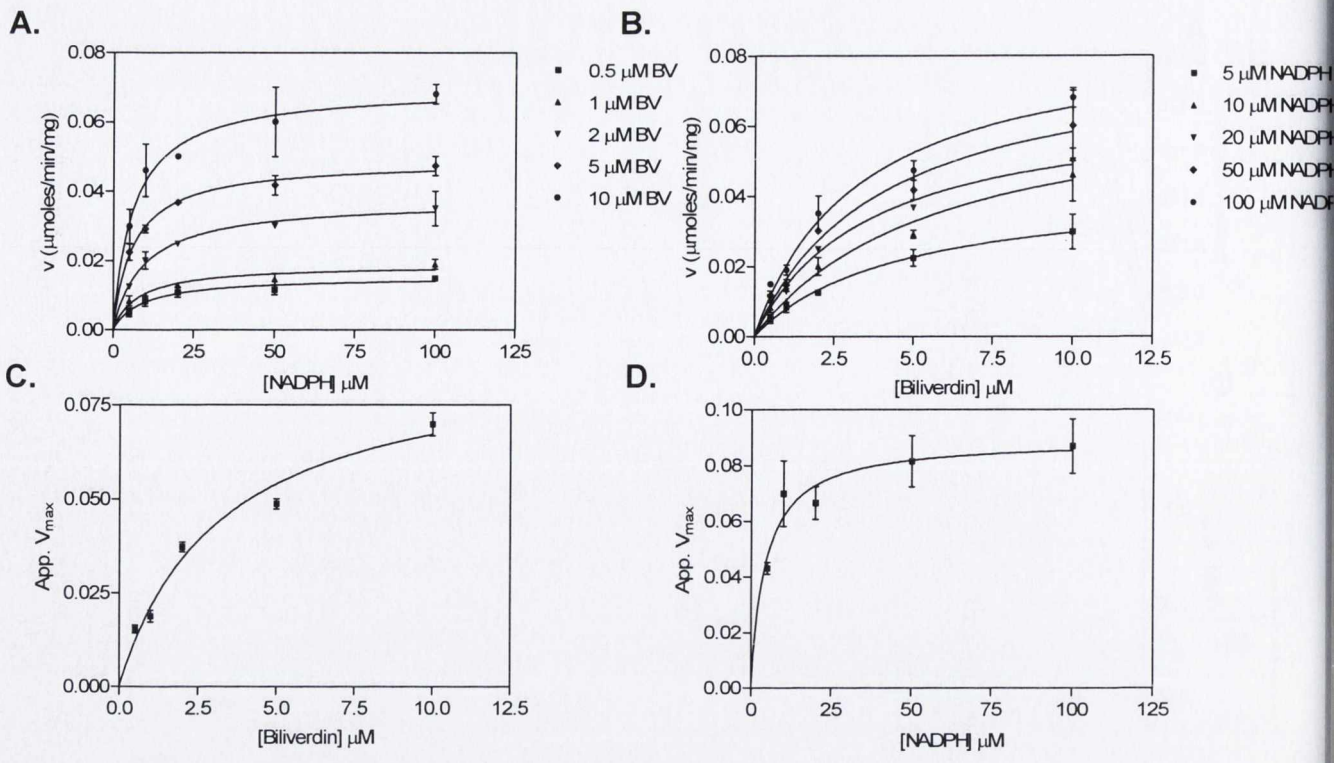

Figure 5.19 Kinetic analysis of the R185A mutant

A. Initial rate kinetics of R185A with NADPH as the variable substrate **B**. Initial rate kinetics of R185AA with biliverdin as the variable substrate **C**. Plot of apparent V_{max} for NADPH versus biliverdin concentration **D**. Plot of apparent V_{max} for biliverdin versus NADPH concentration

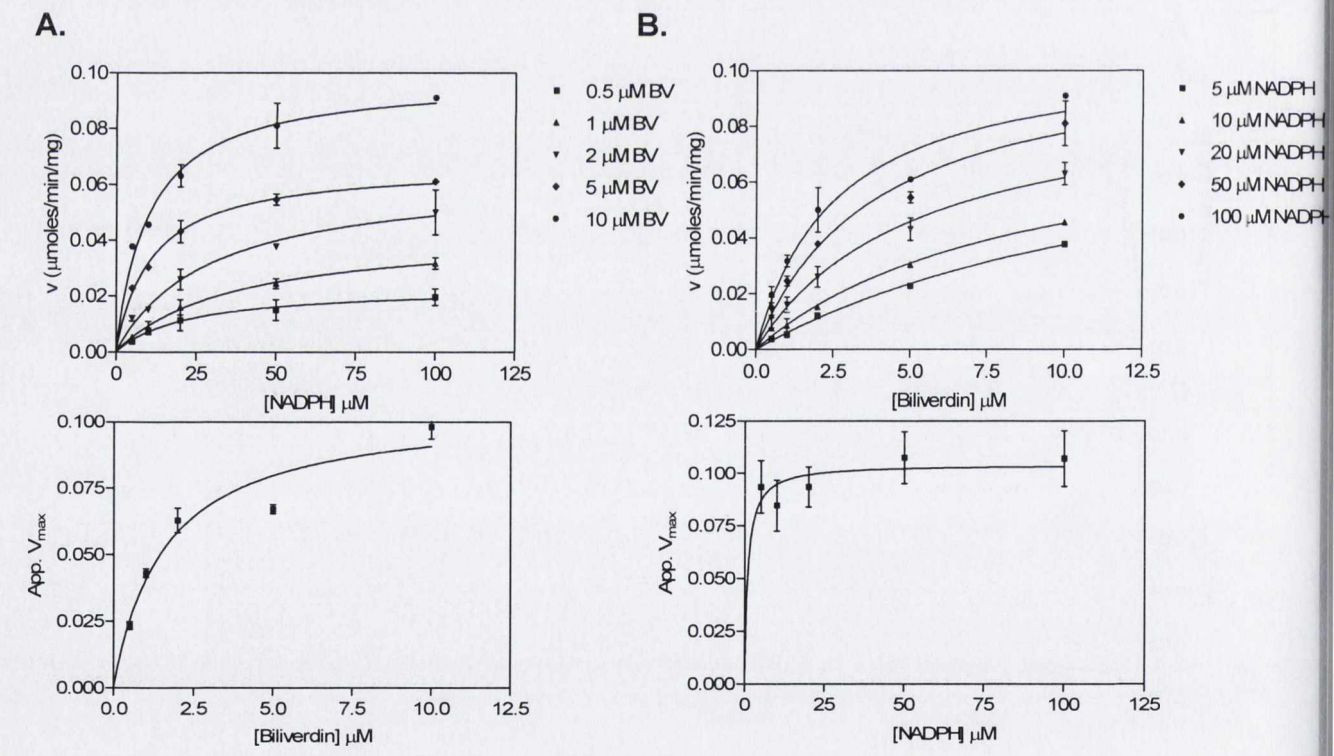

Figure 5.20 Kinetic analysis of the D285A mutant

A. Initial rate kinetics of D285A with NADPH as the variable substrate **B**. Initial rate kinetics of D285A with biliverdin as the variable substrate **C**. Plot of apparent V_{max} for NADPH versus biliverdin concentration **D**. Plot of apparent V_{max} for biliverdin versus NADPH concentration

A.

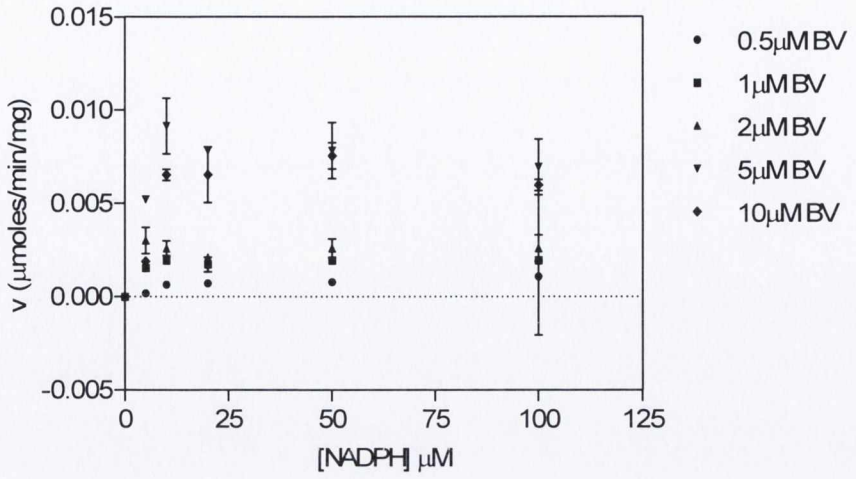

B.

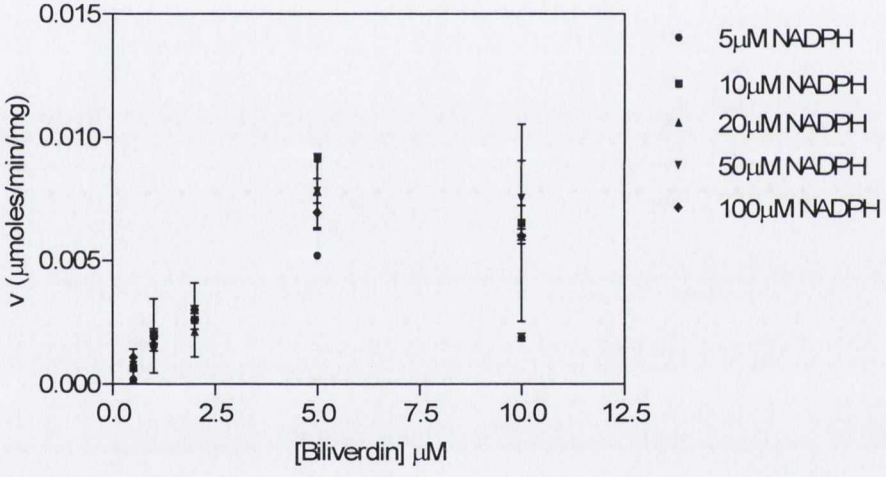

Figure 5.21 Kinetic analysis of the H84A mutant

A. Initial rate kinetics of H84A with NADPH as the variable substrate **B**. Initial rate kinetics of H84A with biliverdin as the variable substrate. Activity was severely affected and kinetic parameters could not be accurately determined. The data did not fit to a rectangular hyperbola

A.

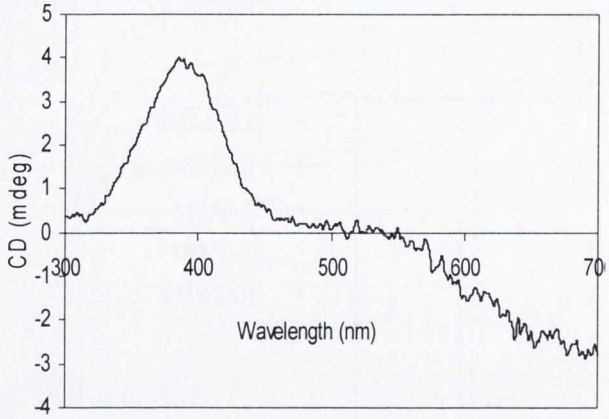
CD (mdeg)
Wavelength (nm)

B.

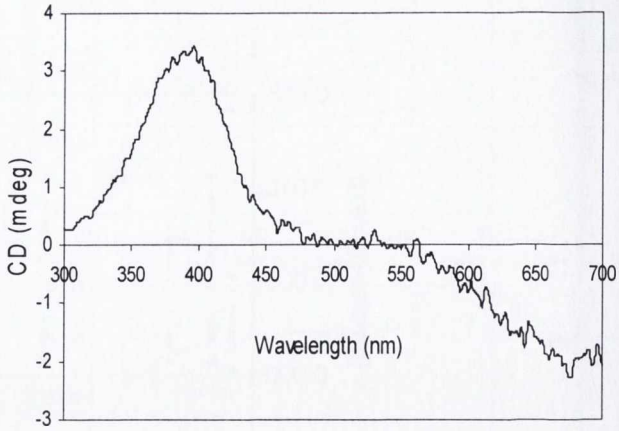
CD (mdeg)
Wavelength (nm)

C.

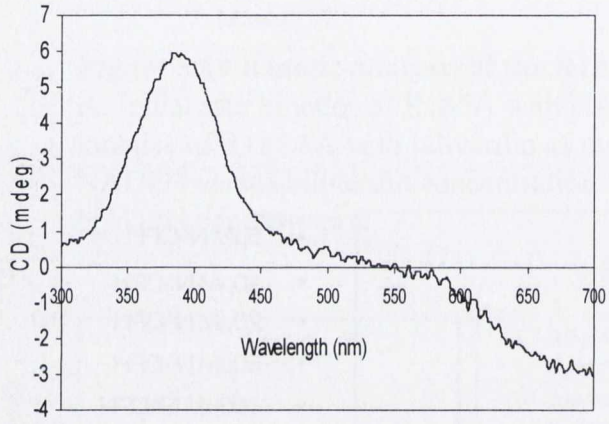
CD (mdeg)
Wavelength (nm)

D.

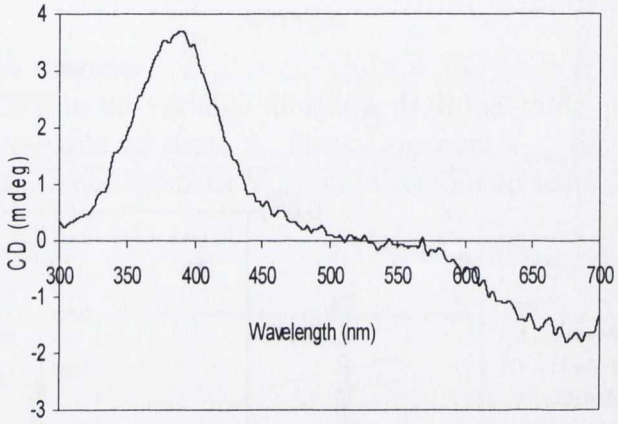
CD (mdeg)
Wavelength (nm)

E.

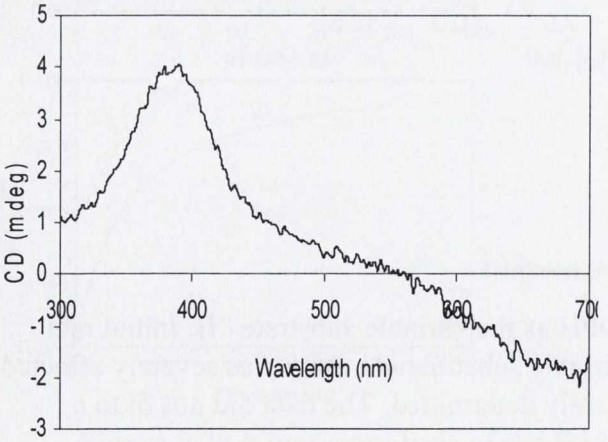
CD (mdeg)
Wavelength (nm)

F.

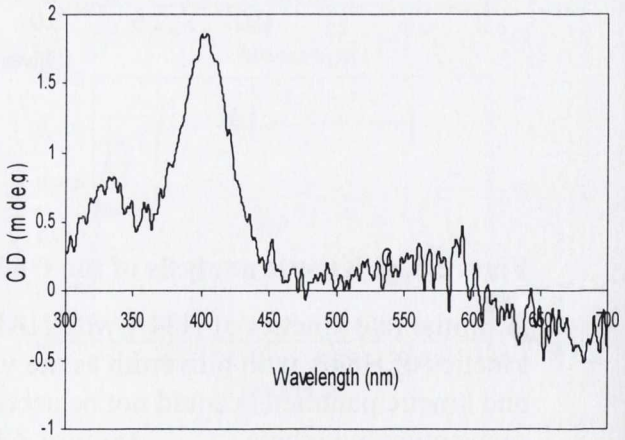
CD (mdeg)
Wavelength (nm)

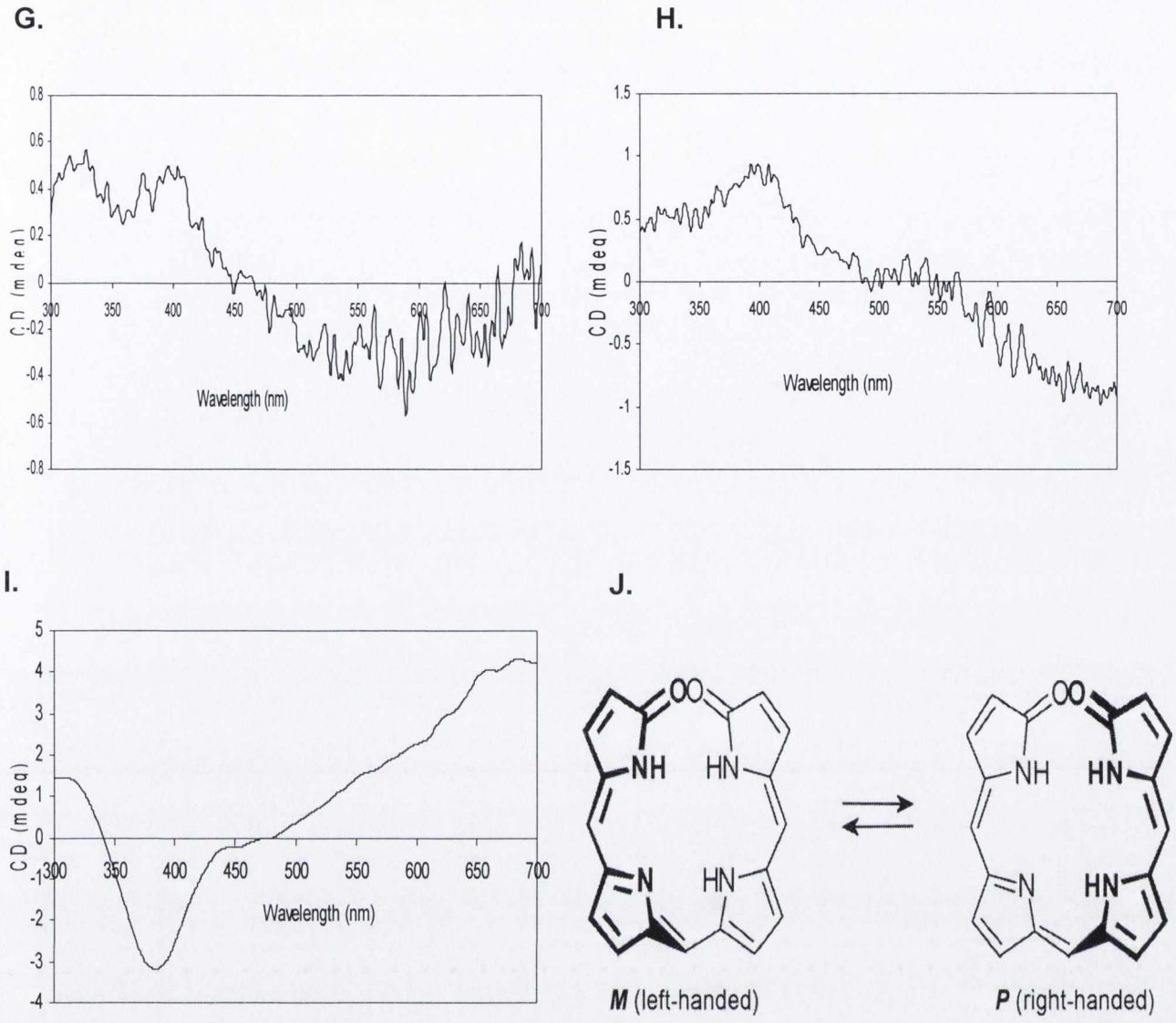

Figure 5.22 CD studies investigating the binding of biliverdin to wild-type sBVR-A and sBVR-A mutants

A. sBVR-A (1mg/ml) Biliverdin binds to sBVR-A in the plus (P) conformation
B. H97A (1mg/ml)
C. H126A (1mg/ml)
D. H129A (1mg/ml)
E. D285A (1mg/ml)
F. R185A. (1mg/ml) Biliverdin binding appears to be affected in this mutant
G. E101A (1mg/ml). Biliverdin binding to E101A is severely diminished
H. H84A (1mg/ml) . Biliverdin binding to H84A is severely diminished
I. Y102A (1mg/ml). Interestingly biliverdin binds to the Y102A mutant in the opposite conformation to the wild-type enzyme (in the minus conformation, M)
J. Two chiral enantiomeric forms of biliverdin IXα

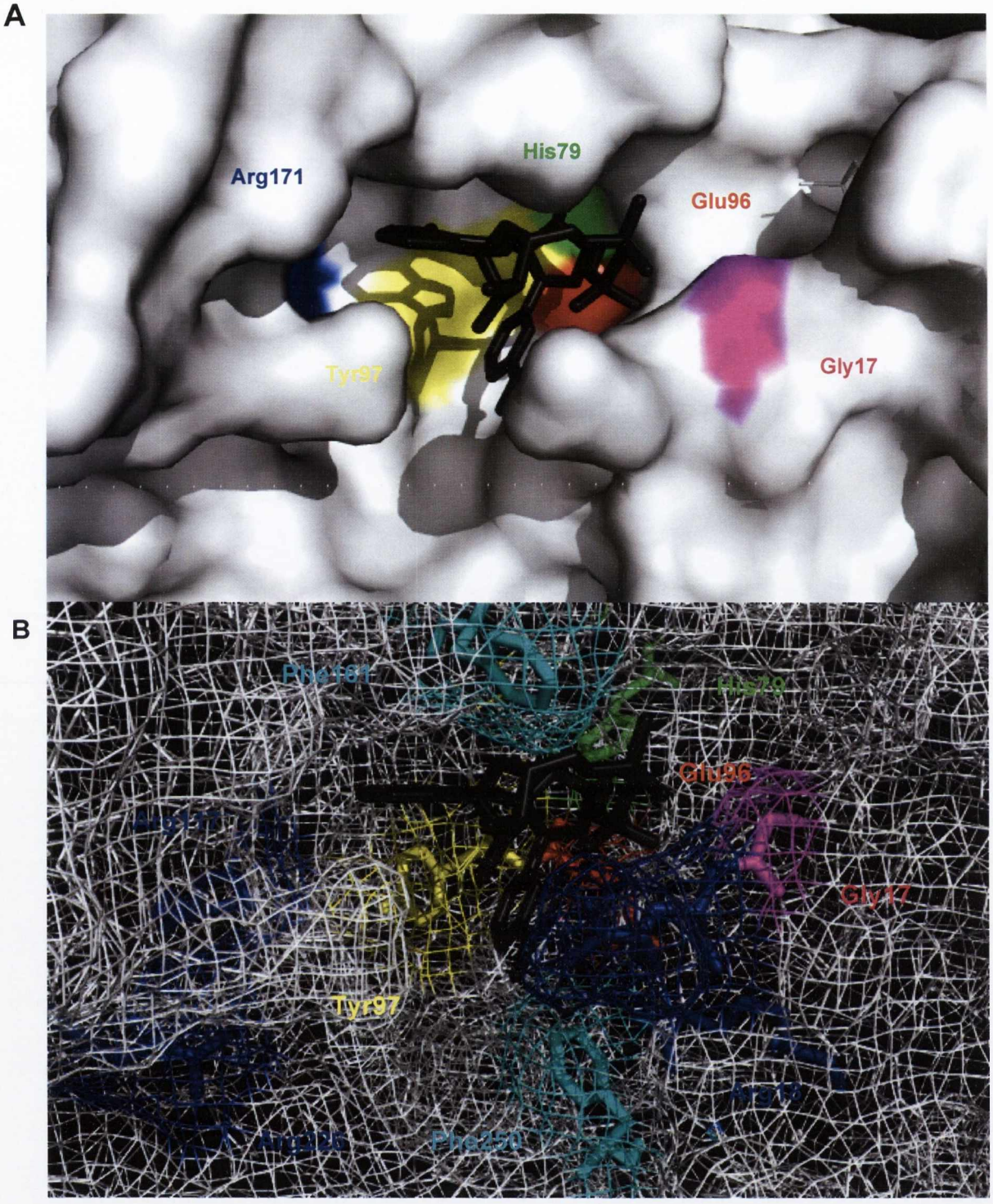

Figure 5.23 The substrate binding site of rat BVR-A showing the proposed active site catalytic residues

Figs. A and B show surface and mesh representations of the active site respectively with proposed catalytic and substrate binding residues indicated. In grey stick format is the pyrridine nucleotide. In this structure the adenine is stacked over the nicotinamide ring probably due to an artifact caused by Lys92 in a neighbouring subunit in the crystal lattice (Whitby *et al.,* 2002). The recently reported human BVR-A with $NADP^+$ bound shows the extended conformation (Kavanagh *et al.,* 2007). It is this extended conformation that is most likely adopted in solution by the rat enzyme. Y97, H79 and E96 correspond to Y102, H84 and E101 in *Synechocystis* BVR-A respectively

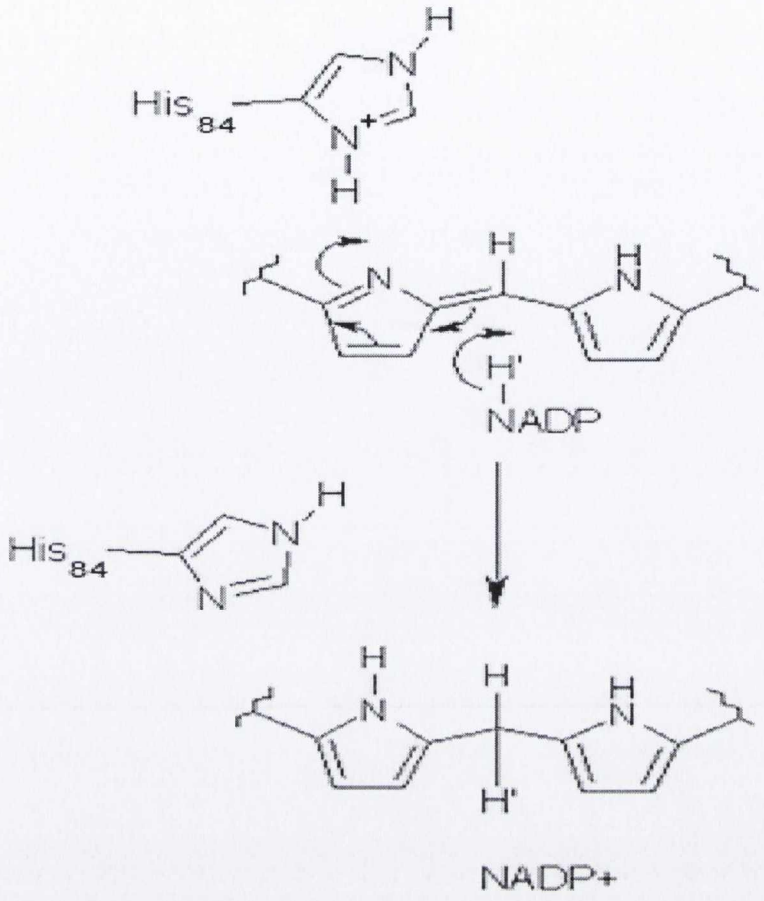

Figure 5.24 Proposed enzymatic mechanism of sBVR-A using hydride from NAD(P)H

NADPH binds to sBVR-A in the substrate binding pocket, followed by biliverdin IXα. Both His84, Glu101 and Tyr102 are needed for productive binding of biliverdin. His84 donates a H^+ to the pyrrole nitrogen of biliverdin IXα followed by hydride transfer from the C4 of NAD(P)H to the C10 bridge of biliverdin, reducing it to bilirubin IXα. It is not clear whether protonation of the pyrrole nitrogen precedes hydride transfer. Bilirubin then leaves the active site, followed by $NAD(P)^+$

CHAPTER 6

STRUCTURAL STUDIES ON *SYNECHOCYSTIS* BILIVERDIN IXα REDUCTASE

6.1 Introduction

Biliverdin IXα reductase has been described as a monomeric protein with a relative molecular mass (Mr) of approximately 34kDa in many species including pig spleen and rat liver (Noguchi *et al.*, 1979), rat liver (Kutty & Maines, 1981), human liver (Maines & Trakshel, 1993), ox kidney (Rigney, 1986) and salmon liver (Elliot, 1996). However, artificial dimers of rat BVR-A as GST fusions were described by Ennis *et al.*, (1997) and O'Carra & Colleran (1971) reported that partially purified guinea-pig liver BVR-A eluted from an S-200 gel-filtration chromatography column with a molecular weight of 70kDa. The theoretical molecular weight of a sBVR-A monomer is 36.64kDa, based on its amino acid composition (328 amino acids). Using electrospray mass-spectrometry Schluchter & Glazer, (1997) reported that a 6-histidine tagged sBVR-A had the appropriate molecular weight corresponding to its amino acid sequence (plus the six histidine residues). However, no detailed studies of the quaternary structure of sBVR-A have been described to date.

6.2 Initial rate kinetics of sBVR-A

The initial rate kinetics of recombinant sBVR-A described in Section 4.4 have shown that there is a linear relationship between initial rate and enzyme concentration over the range 0-10μg of enzyme in a final assay volume of 2ml (0-5μg/ml). This study was extended to investigate if the linear relationship was maintained at enzyme concentrations up to 100μg/ml. Enzyme assays were performed at pH5 as described in Section 2.2.23 with NADPH or NADH as co-factor and initiated by the addition of enzyme. Fig. 6.1 shows that when NADPH was the co-factor the initial rate begins to deviate from linearity at approximately 10-20μg/ml enzyme. The initial rate became progressively slower as the enzyme concentration reached 100μg/ml (see Fig. 6.1). Above this enzyme concentration it was felt that the data collected was unreliable as this was at the upper limits of the capacity of a regular UV/Vis spectrophotometer to measure reliable initial rates. Above this enzyme concentration by the time the enzyme was added to the assay and mixed thoroughly a significant proportion of the beginning of the reaction was not recorded. In order to overcome this problem the assays could be performed at a wavelength which is not the optimum for the production of bilirubin (e.g. 500nm) in order to obtain the linear portion of the initial rate for longer. A similar pattern was observed with NADH as co-factor with the initial rate beginning to deviate from linearity at approximately 20μg/ml (see Fig. 6.2). As with NADPH the initial rate became progressively slower as the enzyme concentration reached 100μg/ml. The pH of the assay was monitored before and after the reaction to ensure that it was not affected by adding increasing

amounts of enzyme, which was stored in 20mM Tris buffer, pH7.5. At the highest concentrations of enzyme used the substrates were only depleted by 5-10% so that genuine initial rates were measured.

6.3 Size exclusion chromatography using Sephadex-200

6.3.1 Calibration of the S-200 column

Individual S-200 columns (1 x 100cm) were equilibrated at pH5 (25mM sodium citrate, 100mM NaCl) at both 4°C and room temperature and pH7.5 (25mM Tris, 100mM NaCl) at both 4°C and room temperature as described in Section 2.2.15.4. Room temperature varied between 18 and 20°C. This purpose of this was to investigate if pH or temperature had any effect on the quaternary structure of sBVR-A. Briefly, Blue-dextran (2mg/ml) in a total volume of 500µl in equilibration buffer was applied to the gel-filtration column and its elution volume recorded and used to determine the void volume. Calibrating proteins [β-amylase (200kDa), alcohol dehydrogenase (150kDa), bovine serum albumin (66kDa), carbonic anhydrase (29kDa) and cytochrome C (12.4kDa)] were then individually applied to the column and their elution volumes were also recorded (see Fig. 6.3A for pH5, RT, *Appendix* V Fig. 1A for pH5, 4°C, *Appendix* V Fig. 2A for pH7.5, 4°C and *Appendix* V Fig. 3A for pH7.5, RT) and used to build the calibration curves which were then used to estimate the relative molecular mass (Mr) of sBVR-A. There is a linear relationship between the elution volume of a substance and the log of its relative molecular mass as confirmed in these calibration curves (see Fig. 6.3C, *Appendix* V, Figs, 1C, 2C and 3C).

6.3.2 Size-exclusion chromatography of recombinant sBVR-A

Recombinant sBVR-A (1mg/ml), purified as described in Section 3.4.3 was applied to each S-200 gel-filtration column in a total volume of 500µl in the relevant equilibration buffer. When the void column had eluted fractions (1ml) were collected and the protein detected by a positive reaction with Bradford reagent and by monitoring the absorbance at 280nm. An elution profile of sBVR-A was constructed for each gel-filtration experiment and the peak elution volume from these profiles was then used to determine the Mr of native sBVR-A under the conditions of the experiment by using the standard curves constructed from elution volumes of proteins of known Mr. At pH5 and room temperature the sBVR-A eluted from the gel-filtration column in a volume of 79.5ml (see Fig. 6.3B), corresponding to a relative molecular mass of 69kDa (see Fig. 6.3C). Samples of protein over the elution peak for sBVR-A were analysed by SDS-PAGE (see Fig. 6.3D) and confirmed that the protein subunit has an Mr of approximately 34kDa. sBVR-A activity assays were also performed on the samples from the peak of the elution profile and showed that the protein peak co-eluted with sBVR-A activity (see Fig. 6.3E). At pH5 and 4°C the protein eluted

from the gel-filtration column in a volume of 81ml corresponding to an Mr of 74kDa. SDS-PAGE analysis confirmed the Mr of the sBVR-A subunit as 34-36kDa. The protein peak also co-eluted with sBVR-A activity. Results for the gel-filtration experiments at pH5 and 4°C are shown in Fig. 1 in *Appendix* V. At pH7.5 and 4°C the protein eluted in a volume of 84ml corresponding to an Mr of 64kDa. SDS-PAGE analysis over the protein peak confirmed the subunit Mr as 34kDa and the protein peak also co-eluted with BVR-A activity. Results for the gel filtration experiments at pH7.5 and 4°C are shown in Fig. 2 in *Appendix* V. When the experiment was conducted at pH7.5 and room temperature the protein eluted in a volume of 90ml corresponding to an Mr of 66kDa. SDS-PAGE showed that the protein subunit has an Mr of 34kDa and the protein peak also co-eluted with sBVR-A activity. Results for the gel filtration experiments at pH7.5 and room temperature are shown in Fig. 3 in *Appendix* V. Table 6.1 shows the collated results of the gel-filtration experiments together with the results from light-scattering and analytical ultracentrifugation (see below).

6.4 Light scattering analysis of sBVR-A

Light scattering analysis of recombinant sBVR-A was carried out as described in Section 2.2.25. Briefly, purified recombinant sBVR-A (0.25mg/ml) was clarified using a 0.22μm filter and applied to an S-200 Superdex HR gel-filtration column (Amersham Biosciences) in a total volume of 1ml. The gel-filtration column was connected to an AKTA FPLC system (Amersham Biosciences) and the column was run at room temperature (18°C) and a flow rate of 0.5ml/min in the desired equilibration buffer. The gel-filtration column was connected online to the following flow detectors: a multiwavelength UV/Vis detector (Amersham biosciences), a miniDawn Tristar light scattering detector (Wyatt Technology) and an Optilab rEX Rayleigh interference detector (Wyatt Technology). The sBVR-A was fractionated according to its Mr on the S-200 HR gel-filtration column and the molecular mass then analysed from the absolute measurement of the laser scattered light intensity measured by the light scattering (LS) detector. The computer software Astra solved the equation based on Zimm's formalism (equation 7 in Section 2.2.25) that relates the excess scattered light to the concentration and weight-average molar mass of sBVR-A. Fig 6.4A shows the detection by the (LS) detector of a substance eluting from the S-200 HR gel-filtration column after 25min at pH5. The UV analysis (Fig. 6.4B) confirmed that this absorbed at 280nm and was therefore sBVR-A protein. Molar mass was determined using the Astra software which calculated a weight average molar mass of 73,232 g/mol +/- 1,173 for sBVR-A at pH5 and room temperature (Fig. 6.4C). The molar mass is calculated from the average mass of the entire peak shown in Fig. 6.4C. No other significant peaks were detected by the light scattering or UV/Vis detectors shown in these figures which suggest that the preparation is homogenous with a

molecular weight of 73kDa. SDS-PAGE clearly identified the subunit (Mr 34kDa) of the eluted protein and sBVR-A activity assays confirmed the identity of the peak fractions.

The experiment was also conducted at pH7.5 and room temperature. sBVR-A eluted from the gel-filtration column and was analysed by the LS detector at 30min. The UV/Vis analysis at 280nm confirmed that this substance was sBVR-A protein and Astra software calculated a molar mass of 66,210 g/mol +/- 4,635 for sBVR-A at pH7.5. SDS-PAGE analysis identified the subunit (Mr 34kDa) of the sBVR-A monomer and sBVR-A assays showed the protein peak co-eluted with sBVR-A activity. Results for the light scattering experiments at pH7.5 and room temperature are shown in Fig. 4 in *Appendix* V. Results from the light-scattering experiments are collated in Table 6.1.

6.5 Analytical ultracentrifugation (AUC)

6.5.1 Sedimentation velocity ultracentrifugation (SVU) analysis of sBVR-A

Recombinant sBVR-A was analysed by SVU as described in Section 2.2.24.1. sBVR-A samples (0.42ml of 0.1, 0.25 and 0.5mg/ml) were centrifuged at 50,000 rpm at 11°C or 20°C for 9hours. The reference cells contained samples of the buffers which did not contain protein. Changes in solute concentration were detected by Rayleigh interference and radial absorbance scans at 287nm. Scans (122) of each cell were collected during the 9 hour centrifugation period. Buoyancy, viscosity and density parameters for each buffer were calculated using the program Sednterp (Laue, *et al.*, 1992). The density (σ) and viscosity (η) of sodium citrate (25mM, pH5) at 11°C were calculated to be 1.00645 ml/g and 0.0010368 millipascals respectively. The partial specific volume (□) of sBVR-A under these conditions, based on the amino acid sequence was 0.7288 ml/g. Whole boundary profile analysis of sBVR-A was performed using the program Sedfit (Schuck, 2000) which modelled the data to the Lamm equation (equation 3 in Section 2.2.24.1). Results for pH5 at 11°C are shown in Fig. 6.5A. The sedimentation co-efficient (S) for sBVR-A was calculated from the sedimentation co-efficient distribution c (s) plot (Fig. 6.5B). A sedimentation co-efficient of 3.5 S was calculated for sBVR-A under these conditions. A molecular weight (Mr) of 71kDa was determined for sBVR-A by solving the Svedberg equation (equation 4).

SVU analysis of sBVR-A was also carried out at pH5 at 21°C. The density and viscosity of sodium citrate (25mM, pH5) at 21°C were calculated to be 1.00624 ml/g and 0.001009 millipascals respectively and the partial specific volume of sBVR-A under these conditions was 0.7360 ml/g. Whole boundary analysis of sBVR-A at pH5 and 21°C was again performed by Sedfit. The c (s) plot shows only one major peak with a sedimentation co-efficient of 3.92 S, corresponding to a

molecular weight of 80.1kDa and a root mean squared deviation of 0.0425. Results for SVU at pH5 and 21°C are shown in Fig. 5 in *Appendix* V.

sBVR-A was analysed at pH7.5 and both 11°C and 21°C in Tris buffer (25mM). The buoyancy parameters at 11°C were as follows: partial specific volume of sBVR-A was 0.7288 ml/g, buffer density was 1.00307 ml/g and buffer viscosity was 0.0010185 millipascals. Under these conditions sBVR-A sedimented with a co-efficient of 4.2 S, corresponding to a molecular weight of 80.4kDa and an rmsd of 0.029. Also present in this experiment was material of higher molecular weight, 126kDa. At 21°C the buoyancy parameters were as follows: partial specific volume of sBVR-A was 0.7360 ml/g, buffer density was 1.00307 ml/g and buffer viscosity was 0.0010185 millipascals. The sedimentation co-efficient for sBVR-A under these conditions was 4.18 Svedbergs, corresponding to a molecular weight of 80kDa. Also present in this experiment was material of lower molecular weight, 20kDa. Results for the SVU experiments at pH7.5 and 11°C and 21°C are shown in Figs. 6 and 7 in *Appendix* V respectively. Results of the SVU experiments on recombinant sBVR-A are collated in Table 6.1

6.5.2 Sedimentation equilibrium ultracentrifugation (SEU) analysis of sBVR-A

SEU experiments on recombinant sBVR-A were performed as described in Section 2.2.24.2 by collecting data at slower rotor speeds than in SVU experiments so that the sedimentation and diffusion forces in effect in the cell eventually balance and there is no net transport of molecules in the system. The molecular mass and dissociation constant for an associating system can be determined from such experiments. sBVR-A samples (0.1ml of 0.1, 0.3 and 1mg/ml in 3 different sectors of the analytical cell respectively) were centrifuged at 12,000, 15,000 and 18,000 rpm and a temperature of 4°C. The experiments were conducted in two different buffers: sodium citrate at pH5 or sodium phosphate at pH7. Radial absorbance scans at 275nm (10 replicates, radial step size 0.001 cm) and interference scans were performed at intervals of 5 hours. Buffer densities and viscosities were calculated using the program Sednterp as before and for 4°C, pH5 were as follows: the buffer density was 1.00645 ml/g and viscosity was 0.0010368 millipascals. The partial specific volume of sBVR-A under these conditions was 0.7288 ml/g. Scans were collected and judged to be at equilibrium by plotting radial offset versus time using the program Winmatch (David A. Yphantis). Winmatch analysis of the interference data for sBVR-A at 4°C and pH5 is shown in Fig. 6.6. Interference scans (one from each centrifuge speed) which were judged to be at equilibrium were then analysed using the program Sedanal V 4.34 (Stafford & Sherwood, 2004). Panels A to C in Fig. 6.7 show the analysis of the interference data from the 12,000 rpm rotor speed. This analysis fitted the data to a one species model allowing the molecular weight to "float" using the "simplex" fitting routine. The average molecular weight of sBVR-A under these

conditions was determined to be 69.2kDa. The Sedanal analysis of the interference data from the 15,000rpm rotor speed is shown in panels D to F in Fig. 6.7. The data were fitted to a one species model as before and produced a molecular weight of 63.9kDa. The data from the 18,000 rpm rotor speed (panels G to I in Fig. 6.7) produced a molecular weight of 55kDa .

The interference data from the experiment conducted at pH5 were also fitted to a self-associating monomer-dimer model (2A=A2) using Sedanal and used the "simplex" fitting routine to fit the data (see panels J to L in Fig. 6.7). In this case the monomer molecular weight was "fixed" at 34kDa and the equilibrium dissociation constant K_d was allowed to "float". Using this method an equilibrium dissociation constant of 45μM was calculated for the self-association of sBVR-A monomers under the conditions of the experiment. The best fit average of absolute deviations for the fitting of these data to the monomer-dimer model was 9.9×10^{-3}. Tight non-randomly dispersed residuals indicate a good fit to the model as is shown in panels J to L in Fig. 6.7.

SEU analysis of sBVR-A was also performed at pH7 in sodium phosphate buffer (20mM). Scans were again collected and judged to be at equilibrium by plotting radial offset versus time using the program Winmatch (see Fig. 6.8 for Winmatch analysis of interference scans at pH7). Interference scans which were judged to be at equilibrium were again analysed using Sedanal. The interference data analysed by Sedanal from the 12,000 rpm rotor speed is shown in panels A to C in Fig. 6.9. The data was fitted to a one species model using the "simplex" fitting routine and a molecular weight for sBVR-A of 73.8kDa was calculated under these conditions. The Sedanal analysis of the 15,000 rpm data is shown in panels D to F in Fig. 6.9. A molecular weight for sBVR-A under these conditions was calculated to be 77.7kDa at pH7. The data from the 18,000 rpm scan produced a molecular weight of 72kDa (see panels G to I in Fig 6.9).

The interference data from the experiment conducted at pH7 was also fitted to a self-associating monomer-dimer model using Sedanal and an equilibrium constant of 12.9μM was obtained (see panels J to L in Fig. 6.9) The best fit average of absolute deviations for the fitting of this data to the monomer-dimer model was 2.46×10^{-2}. The tight non-randomly dispersed residuals indicate a good fit to this model. Results from the SEU experiments are collated in Table 6.1.

6.6 Crystallization trials for sBVR-A

6.6.1 Preparation of protein for crystallization trials

sBVR-A was purified as described in Section 3.4.3 and further purified using 2'5' ADP-Sepharose affinity chromatography as described in Section 2.2.15.1d. Size-exclusion chromatography was employed to remove protein aggregates in preparation for initial crystallization screening trials as

described in Section 2.2.15.4. The protein was estimated by SDS-PAGE to be 95-100% pure following this purification procedure (see Fig. 6.10).

6.6.2 Initial crystallization screening trials

The sBVR-A purified in the previous section was concentrated to 2-5mg/ml as described in Section 2.2.17 in preparation for initial crystallization screening trials. Protein concentrations higher than this were not possible due to protein instability and precipitation. The screening trials used the "Wizard" crystallization screening kits according to the manufacturer's instructions and as described in Section 2.2.29.2. Briefly 2µl of sBVR-A protein was mixed with 2µl of precipitant and the "hanging drop" method was set up. The crystallization plates were kept at 4°C or room temperature and monitored every day using a stereomicroscope. BVR-A has not been successfully crystallized to date.

6.7 Homology modeling

This is a technique used to build a model of the 3D structure of a protein if it has not been solved by X-ray crystallography or NMR. It is based on the known structure of similar and related proteins and uses computer software to align the backbone of the sequence of the unknown protein to known structure templates. Homology modeling was used to build a model of sBVR-A as described in Section 2.3.31. Three homology modeling programs were used to predict the structure of *s*BVR-A. All three programs gave similar results showing two well defined domains with an overall structure similar to that of the known rat and human enzymes. Fig. 6.11 shows that there are two well defined β-sheet motifs and a similar arrangement of α-helices. There is also a clear Rossman-like fold motif. Some segments in sections of the predicted sBVR-A structure are less ordered with more loops and shorter α-helices (see Fig. 6.11).

Each of the three predicted *s*BVR-A structures were superimposed on the rat BVR-A structure of Kikuchi *et al.*, (2001). The Swissprot sBVR-A model superimposed on the rat structure is shown in Fig. 6.12A. The root mean squared deviation (rmsd) for the fit to the rat BVR-A template is 1.3 indicating a good fit. The surface representations in Figs. 6.12A and 6.12Bb show the substrate binding pocket of the sBVR-A model is similar to the rat BVR-A structure with the proposed catalytic residues described in Chapter 5 in similar positions and orientations within both structures.

6.8 Circular dichroism studies on the human and *Synechocystis* BVR-As and prediction of secondary structure

CD studies on sBVR-A in the far UV region of the electromagnetic spectrum were performed as described in Section 2.2.30. Results were analysed using the online secondary structure prediction server DICHROWEB (Whitmore & Wallace, 2004). This web-based server uses secondary structure prediction algorithms and compares the CD spectra from an unknown protein to the known CD spectra of a set of reference proteins of known structure. Predictions of secondary structure motifs of an unknown protein can be made in this way. The CD spectrum of recombinant sBVR-A was analyzed using the five algorithms available in DICHROWEB and the algorithm which gave the best fit with the lowest normalized root mean squared deviation (nrmsd) was employed. The CD spectra of sBVR-A in the region 185nm-240nm is shown in Fig. 6.13A and the DICHROWEB analysis using the algoritm CDSSTR and the variable selection method using protein reference set 6 is shown in Fig. 6.13B. This algorithm predicts that the overall secondary structure of sBVR-A consists of 20% α-helix, 23% β-sheet and 23% turns. The nrmsd is 0.013 indicating an excellent fit (see Fig. 6.13B). CD analysis of recombinant human BVR-A was also performed. Fig. 6.13C shows that the CD spectrum of human BVR-A is similar to sBVR-A, indicating that the overall structures and folds of both proteins are similar.

The initial rate kinetics of sBVR-A exhibited non-linear initial rate *versus* enzyme concentration curves when the range of enzyme concentration was extended from 10-100μg/ml with NADPH and NADH as co-factor. Above this concentration the linear relationship between initial rate and enzyme concentration is no longer maintained. This indicates that as the concentration of sBVR-A increases above 10-100μg/ml there is a change in the enzyme which results in a reduced initial rate. One mechanism consistent with this observation is that the enzyme may polymerise to a form with lower activity. This led to a thorough investigation of the quaternary structure of sBVR-A using various techniques. However, another mechanism which can be put forward to explain this phenomenon is that as increasing amounts of enzyme are assayed there may be increasing amounts of a possible inhibitor such as $NADP^+$ which may be present in the enzyme which results in the lower activity observed.

Gel-filtration using Sephadex-200 was performed at pH5 and pH7.5 and at both room temperature and 4°C. pH5 is likely to be the physiological pH for activity of the enzyme and room temperature (15-20°C) is likely to be the physiological temperature. Experiments at 4°C and pH7.5 were also performed to investigate if pH and temperature had any effect on the quaternary structure of sBVR-A. Under all the experimental conditions examined the Mr of sBVR-A was estimated to be 64-74kDa (see Table 6.1). The theoretical molecular weight of a sBVR-A monomer is 36.64kDa (based on its amino acid sequence) and it was therefore concluded that under the conditions of the experiments sBVR-A existed with an Mr approximately double the Mr of a monomer and suggests that sBVR-A was present as a dimer.

Laser light scattering was performed on recombinant sBVR-A to investigate its quaternary structure. This technique involves measuring the amount of light scattered by a substance e.g. protein, in solution at an angle relative to the incident laser beam. For globular proteins with a molecular weight of less than 500kDa the intensity of the scattered light is uniform in all directions and in theory the intensity of the scattered light is proportional to the product of the protein concentration multiplied by its molecular weight. Astra software (Wyatt, 1993) solves equation 7 in Section 2.2.25 which relates the excess scattered light to the concentration and weight-average molar mass and estimated an Mr for sBVR-A of between 66-73kDa depending on the conditions (see Table 6.1 for details). This technique also suggests that sBVR-A exists as a dimer under the conditions of the experiment. No other significant peaks were detected suggesting that sBVR-A existed as a homogenous preparation of dimers.

Analytical ultracentrifugation is a powerful technique for investigating the molecular weights of substances in solution and for examining self-associating systems. In the sedimentation velocity experiments on sBVR-A described in this chapter a uniform solution of sBVR-A at pH5 and pH7.5 and at 11°C and 21°C was placed in an analytical cell and centrifuged at a sufficiently high angular velocity to cause rapid sedimentation of solute towards the bottom of the cell. This results in depletion of sBVR-A at the meniscus and the rate of sedimentation of the boundary region is measured and modeled using the Lamm equation (equation 3 in Section 2.2.24.1) and used to determine the rate of sedimentation of sBVR-A (in Svedbergs, S). The value of S for sBVR-A depends on its mass and when converted to Mr by solving the Svedberg equation (equation 3 in Section 2.2.24.1) yields values of 70-80kDa (see Table 6.1). Under all of the pH and temperature conditions examined sBVR-A appears to behave as a dimer. Sedimentation equilibrium experiments were also carried out on sBVR-A at pH5 and pH7 at 4°C. From these experiments it was possible to determine the Mr of sBVR-A and the equilibrium dissociation constant (K_d) for the monomer-dimer equilibrium. The Mr for sBVR-A was estimated from these experiments to be between 55 and 75kDa suggesting that the major form of sBVR-A present is the dimer and the K_d describing the monomer-dimer equilibrium was approximately 10-50μM (see Table 6.1).

From the experiments described previously on the quaternary structure of sBVR-A it was concluded that the enzyme exists essentially as a dimer above a protein concentration of 50μg/ml. Crystallization of the enzyme and elucidation of its 3D structure would prove extremely informative for further investigations on the dimer interface and residues that may be involved in the dimerisation process. However, all attempts to crystallize the enzyme failed, including incubating the enzyme with $NADP^+$ and biliverdin. The likely reason for this is the high protein concentration generally required for crystallization (10mg/ml or higher). It was impossible to achieve this with sBVR-A due to protein instability and precipitation at concentrations above 2-5mg/ml. In the absence of a crystal structure for sBVR-A a model was built using homology modeling computer software and the known structures of a number of similar and related proteins as templates, including the human and rat BVR-As. The overall structure of the sBVR-A model was similar to the human and rat structures with two clearly defined β-sheet domains and a similar arrangement of α-helices. The secondary structure of sBVR-A was further investigated with circular dichroism spectroscopy and secondary structure prediction software. This technique predicted that sBVR-A consisted of 20% α-helix, 23% β-sheet and 23% turns. The known human enzyme consists of 40% α-helix and 26% β-sheet (Kavanagh *et al.*, unpublished data). In the models of sBVR-A shown in Fig. 6.11 it appears that there are more unordered regions with more loops and shorter α-helices. This is consistent with the CD data and secondary structure prediction obtained for sBVR-A.

A number of related and structurally similar proteins to BVR-A have been described as dimers and tetramers, including glucose-fructose oxidoreductase (GFOR) from *Zymomonas mobilis* (Lott *et al.*, 2000) and dihydrodiol dehydrogenase (DD) from the monkey *Macaca fascicularis* (Carbone *et al.*, 2008). The overall α-helix and β-sheet toplogy of BVR-A and the protein monomers of GFOR and DD are similar with the main differences existing in the length of some of the helices and sheets (see Fig. 6.14). Each protein also contains a dinucleotide binding domain. In fact, the authors of the dihydrodiol dehydrogenase dimer study make a point of noting the structural similarity between the rat BVR-A structure of Whitby *et al.*, (2002) and the monomer of dihydrodiol dehydrogenase (Carbone *et al.*, 2007). In this study the authors suggest that the dimer interface of monkey DD is comprised of the C-terminal anti-parallel β-sheet (Fig. 6.15B). The crystal structure of GFOR shows that the dimerisation of GFOR monomers is mediated through the interface of the same C-terminal β-sheet (see Fig. 6.15A). Indeed it is likely that the dimer interface of sBVR-A is comprised of the same C-terminal β-sheet (see Fig. 6.15C). The authors also show through site-directed mutagenesis that the dimerisation process of DD is mediated through two stacked and conserved arginine residues (see Fig. 6.15B); Carbone *et al.*, (2007). Interestingly, there are a number of conserved arginine residues in sBVR-A, including a semi-conserved arginine residue in the C-terminal β-sheet (Arg246 in sBVR-A, Arg226 in rat BVR-A and Arg227 in human BVR-A), which could be also mediating the dimerisation in sBVR-A (see Fig. 6.15d). This arginine residue is conserved in 65% of the known and putative BVR-As shown in the multiple sequence alignment in Fig. 5.12. However, there is another positively charged Lys residue in the remaining 23.5% of BVR-As shown in Fig. 5.12. There is another Arg residue (Arg215) in the C-terminal β-sheet of sBVR-A (see Fig. 6.15D) but this arginine residue is only present in one other BVR-A, gleobacter (also a bacterial BVR-A and more likely to be a dimer). Another point of similarity which Carbone *et al.*, (2007) discuss is the presence of a catalytic active site tyrosine residue in GFOR and DD and the presence of a catalytic active site histidine residue in another related and structurally similar protein 1,5-anhydro-D-fructose reductase (AFR) from *Sinorhizobium morelense* (Dambe *et al.*, 2006). Experiments described in Chapter 5 of the present study propose an active site tyrosine residue (Tyr102) in sBVR-A involved in substrate binding and a proposed catalytic active site His residue (His84) also involved in substrate binding. GFOR from *Zymomonas mobilis* was crystallized and found to have a tightly bound $NADP^+$ molecule present (Wiegert *et al.*, 1997). Also interesting is the fact that the sBVR-A described in this study was also found to have a tightly bound nucleotide which co-purified with the enzyme.

In conclusion, sBVR-A was found to exist with a molecular weight approximately double the molecular weight of a monomer, suggesting that the enzyme exists as a dimer under all of the experimental conditions examined. This dimerisation is concentration dependent, as indicated by

the initial rate kinetics of sBVR-A. It also appears that the dimer has lower activity than the monomer and may point to a regulatory mechanism for sBVR-A where as the enzyme concentration increases above 10μg/ml the activity decreases. Homology modeling and CD studies suggest that sBVR-A is structurally similar to the known crystal structures of the rat and human enzymes. There are also a number of examples in the literature of related and structurally similar enzymes to BVR-As which exist as dimers and tetramers, mediated through the interface of the C-terminal β-sheet (also present in sBVR-A) and through two stacked arginine residues (also possible for sBVR-A). There are also a number of other similarities between the proteins described in the previous paragraph and sBVR-A and it is proposed that sBVR-A exists as the dimer shown in Fig. 6.16 and is a member of a family of enzymes including GFOR and DD as suggested by the authors of these studies.

	pH	Temp (°C)	Mw (kDa)	K_d (μM)
Gel Filtration	5	18-20	69	
	5	4	74	
	7.5	18-20	66	
	7.5	4	64	
Light Scattering	5	18-20	73,232 +/- 1,173	
	7.5	18-20	66,210 +/- 4,635	
AUC velocity	5	11	71	
	5	21	80.1	
	7.5	11	80.4	
	7.5	21	80	
AUC equilibrium				
12,000 rpm	5	4	69.2	
15,000 rpm	5	4	63.9	45
18,000 rpm	5	4	55	
12,000 rpm	7	4	73.8	
15,000 rpm	7	4	77.7	12.9
18,000 rpm	7	4	72	

Table 6.1 Results of the experiments on the quaternary structure of sBVR-A

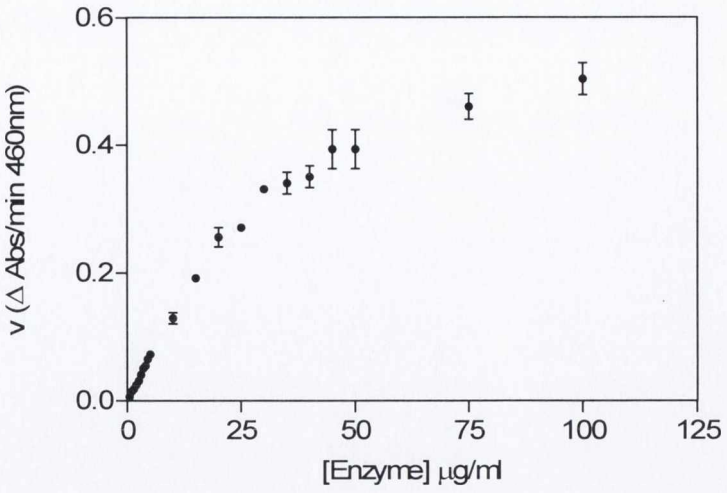

Figure 6.1 Initial rate kinetics of sBVR-A with NADPH as co-factor

Assays were performed in 100mM sodium citrate, pH5. Each assay contained 0-100µg/ml recombinant protein, 100µM NADPH and 10µM biliverdin IXα. The reaction was started by the addition of enzyme. Experiments were performed in triplicate. Each datum point represents the mean and error bars represent the standard deviation of the triplicate values.

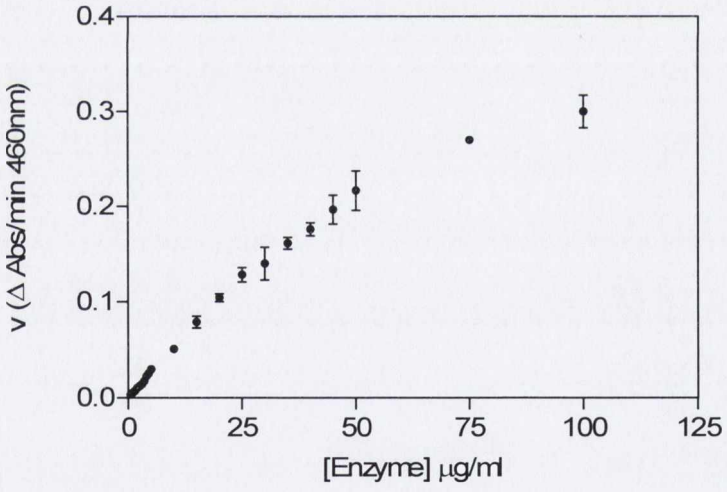

Figure 6.2 Initial rate kinetics of sBVR-A with NADH as co-factor

Assays were performed in 100mM sodium citrate , pH5. Each assay contained 0-100µg/ml recombinant protein, 1mM NADH and 10µM biliverdin IXα. The reaction was started by the addition of enzyme. Experiments were performed in triplicate. Each datum point represents the mean and error bars represent the standard deviation of the triplicate values.

A

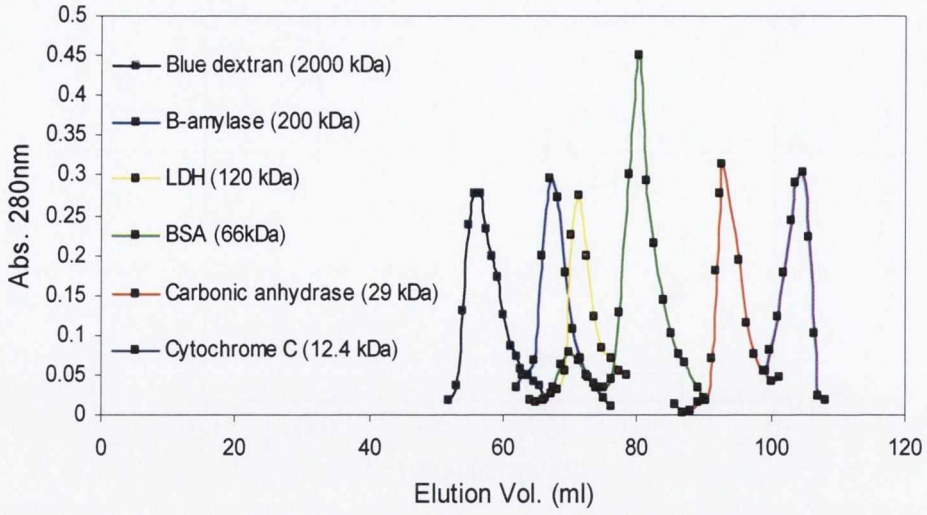
Blue dextran (2000 kDa)
B-amylase (200 kDa)
LDH (120 kDa)
BSA (66kDa)
Carbonic anhydrase (29 kDa)
Cytochrome C (12.4 kDa)
Abs. 280nm
Elution Vol. (ml)

B

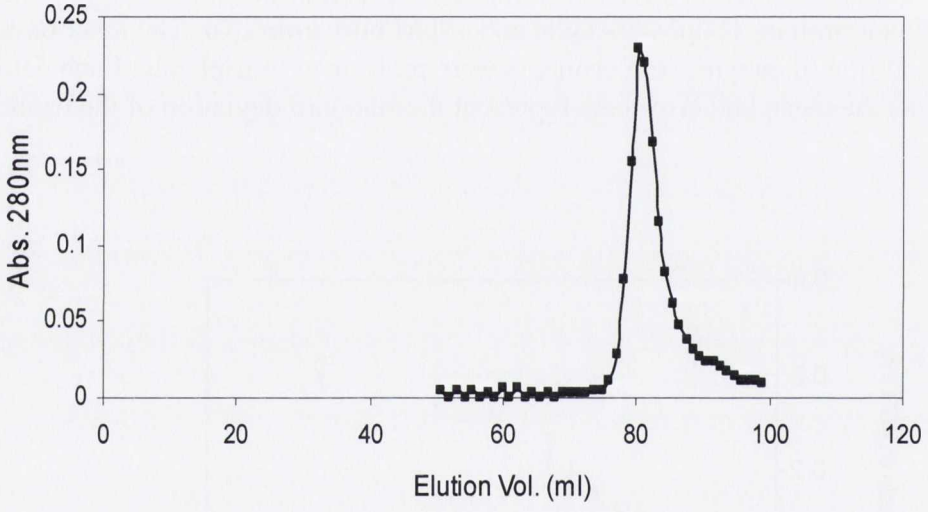
Abs. 280nm
Elution Vol. (ml)

C

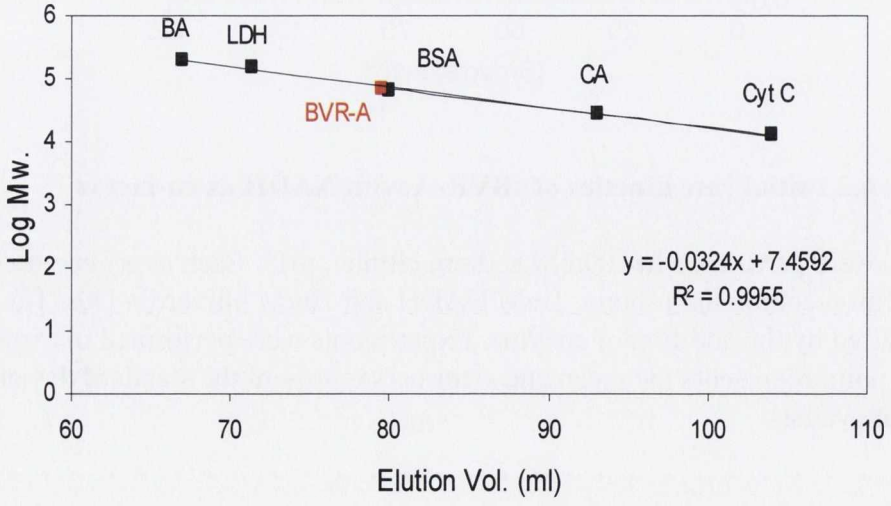
BA
LDH
BSA
CA
Cyt C
BVR-A
y = -0.0324x + 7.4592
R² = 0.9955
Log Mw.
Elution Vol. (ml)

D

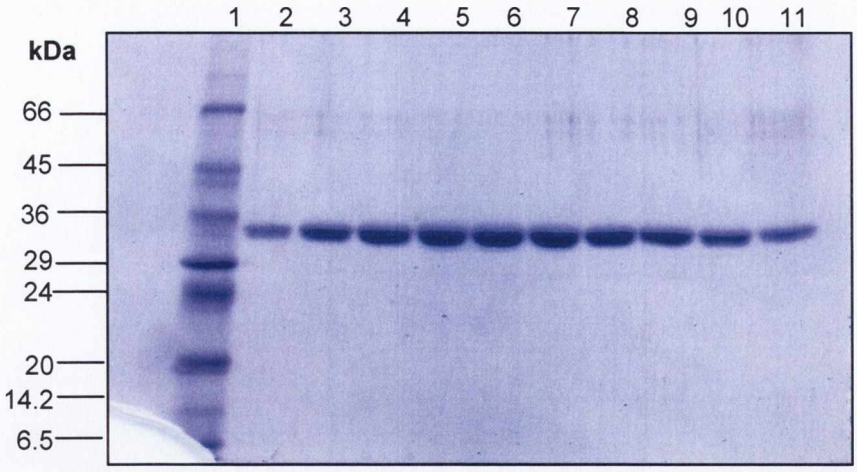

E

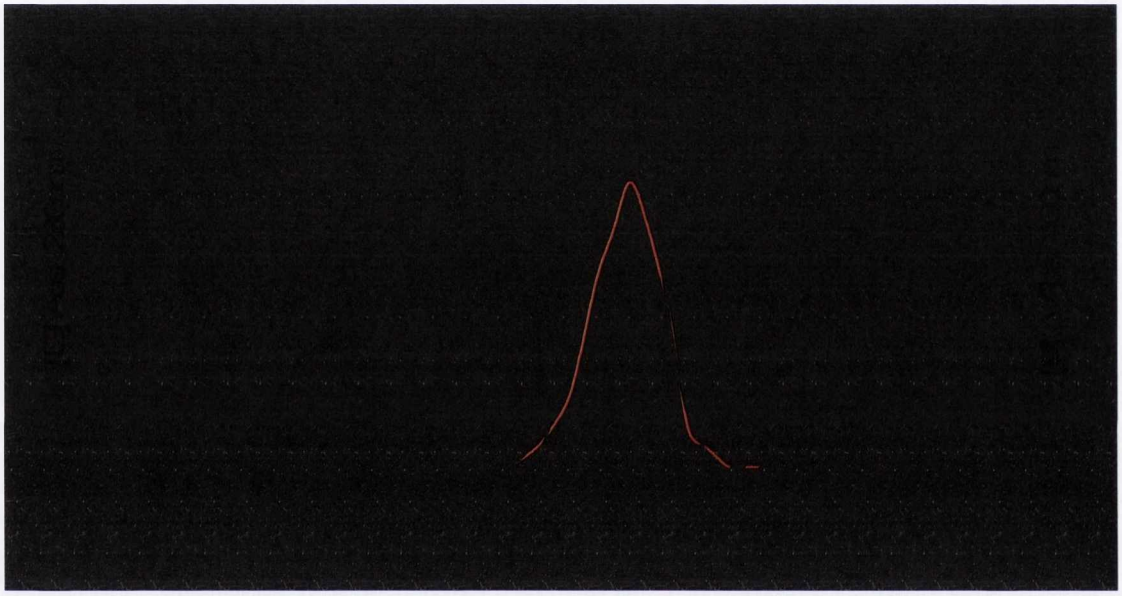

Figure 6.3 Size-exclusion chromatography of sBVR-A at pH 5 and room temperature (18-20°C)

A. Calibration of the S-200 column using various proteins of known molecular weight.

B. Elution profile of recombinant sBVR-A from the S-200 column. sBVR-A eluted in 79.5ml.

C. Calibration curve for the S-200 column at pH5 and room temperature and determination of the native molecular weight of sBVR-A. Under these conditions sBVR-A was shown to have an Mr of 69kDa

D. SDS-PAGE analysis of the protein which eluted from the S-200 column. The protein was shown to have a subunit molecular weight of approximately 34kDa.

E. sBVR-A activity assays on the protein which eluted from the S-200 column. The protein was shown to co-elute with sBVR-A activity. Assays were performed as described in Section 2.2.23. Shown in black is the A280 data and in red is the sBVR-A activity data

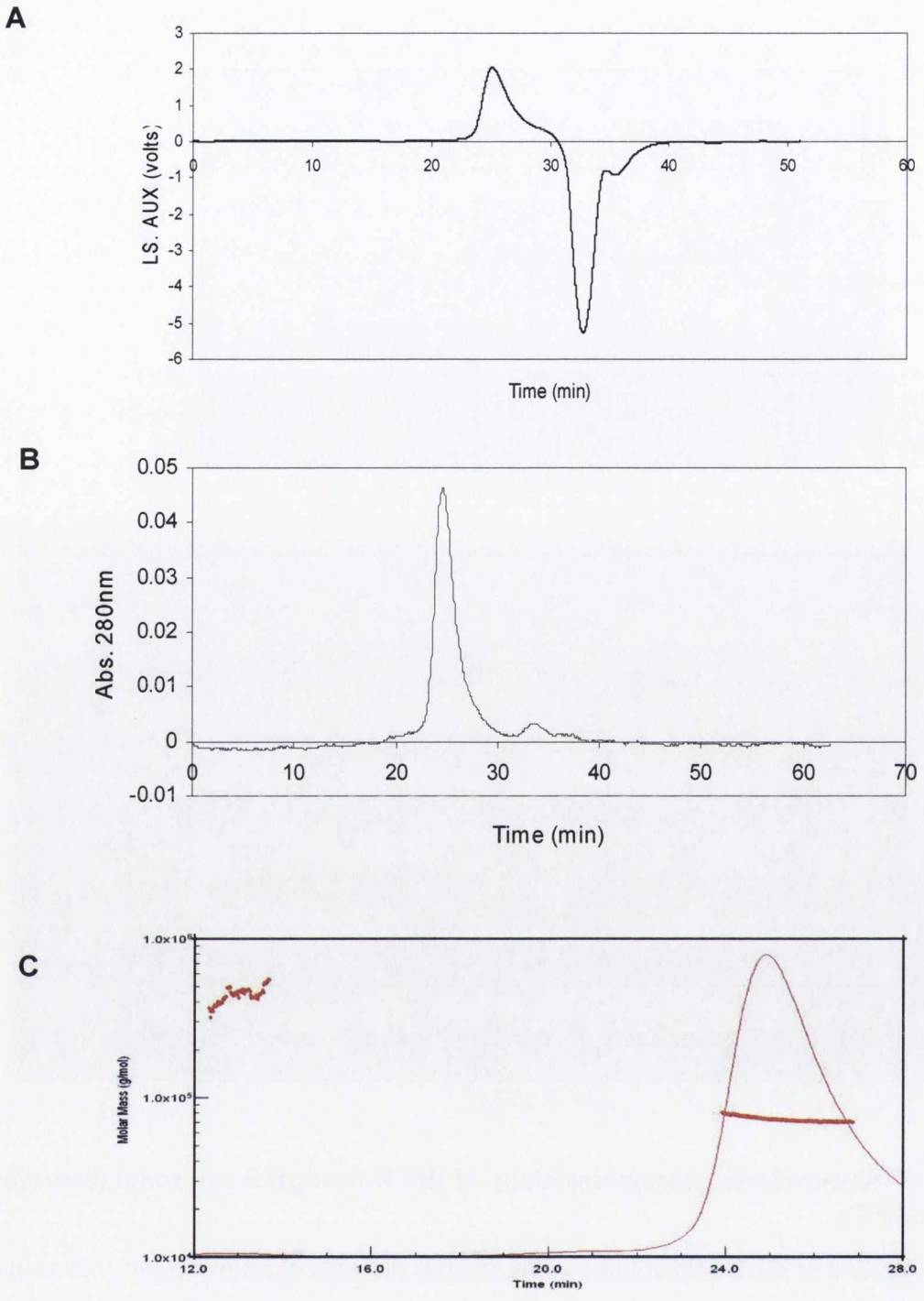

Figure 6.4 Light scattering analysis of sBVR-A at pH5 and room temperature (18-20°C)

A. Detection of sBVR-A by the light scattering detector following elution from the S-200 HR gel-filtration column. sBVR-A was detected following elution after 25min.

B. Detection of sBVR-A by the UV/Vis detector following elution from the S-200 HR gel-filtration column. sBVR-A was detected following elution after 25min.

C. Determination of the molar mass of sBVR-A at pH5 and room temperature. Mr determination was performed by Astra software which calculated an Mr of 73,232 g/mol for sBVR-A under these conditions.

A

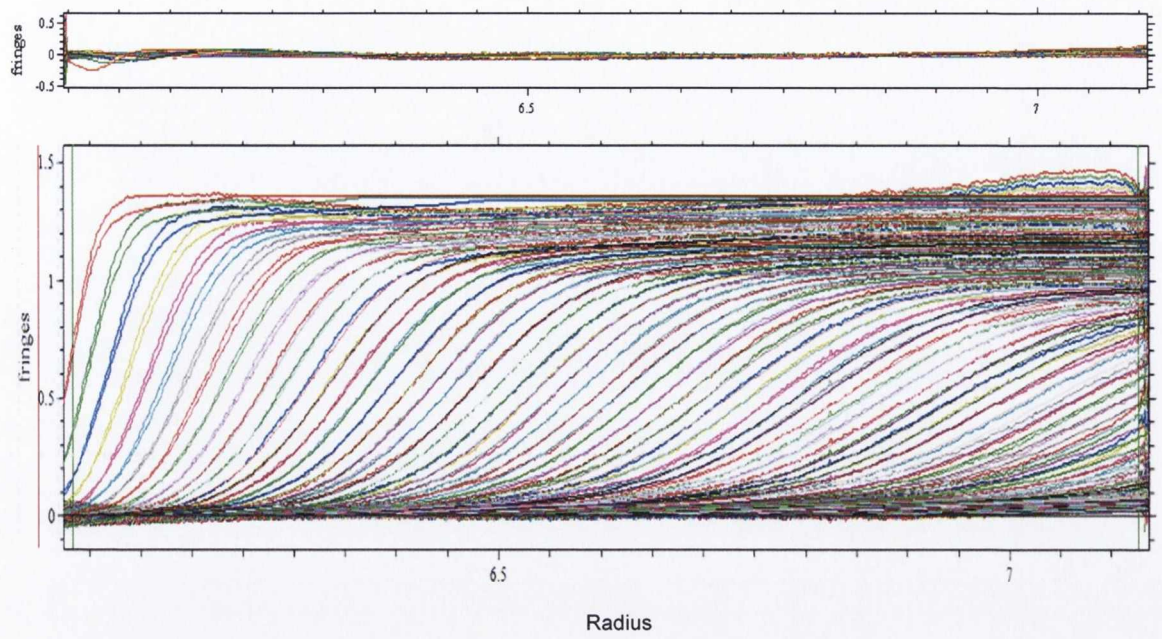

B

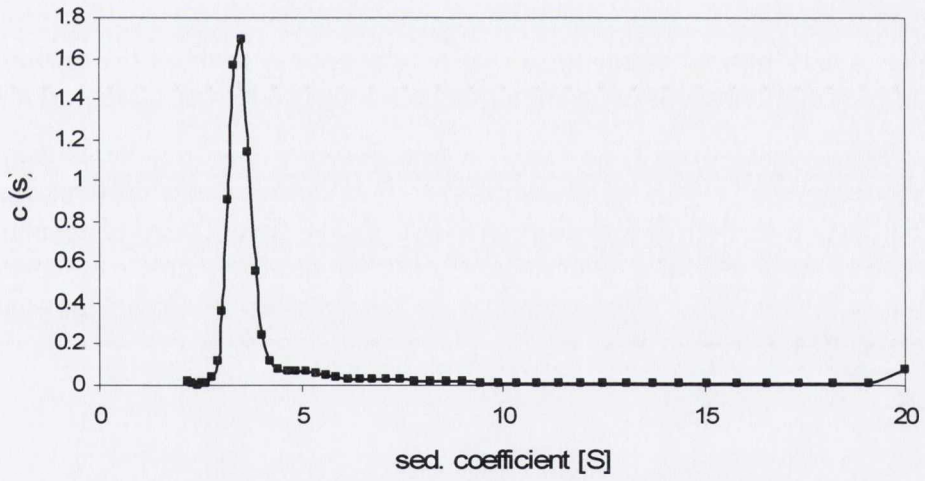

Figure 6.5 Sedimentation velocity analytical ultracentrifugation analysis of sBVR-A at pH5 and 11°C

A. Whole boundary analysis of sBVR-A. Changes in solute concentration were detected by Rayleigh interference. Experiments were performed as described in Section 2.2.24.1. Residuals are shown above the boundary analysis.

B. c (S) sedimentation co-efficient distribution analysis of sBVR-A. Whole boundary analysis was performed by Sedfit which produced a sedimentation co-efficient of 3.5S and a molecular weight of 71kDa for sBVR-A

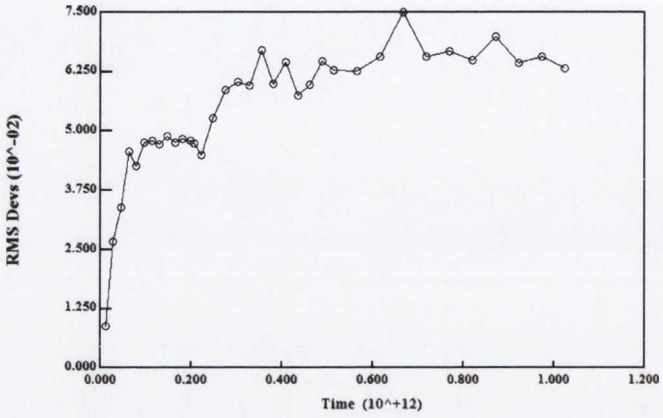

Figure 6.6 Winmatch analysis of the interference data from the sedimentation equilibrium ultracentrifugation experiment on sBVR-A at pH5 and 4°C

Interference scans were judged to be at equilibrium by plotting them against radial offset using the program Winmatch. sBVR-A at various concentrations was centrifuged at 12,000, 15,000, and 18,000 rpm. The first plateau in the above figure represents the equilibrium reached at 12,000rpm, the second plateau represents the equilibrium reached at 15,000 rpm and the third plateau represents the equilibrium reached at 18,000 rpm.

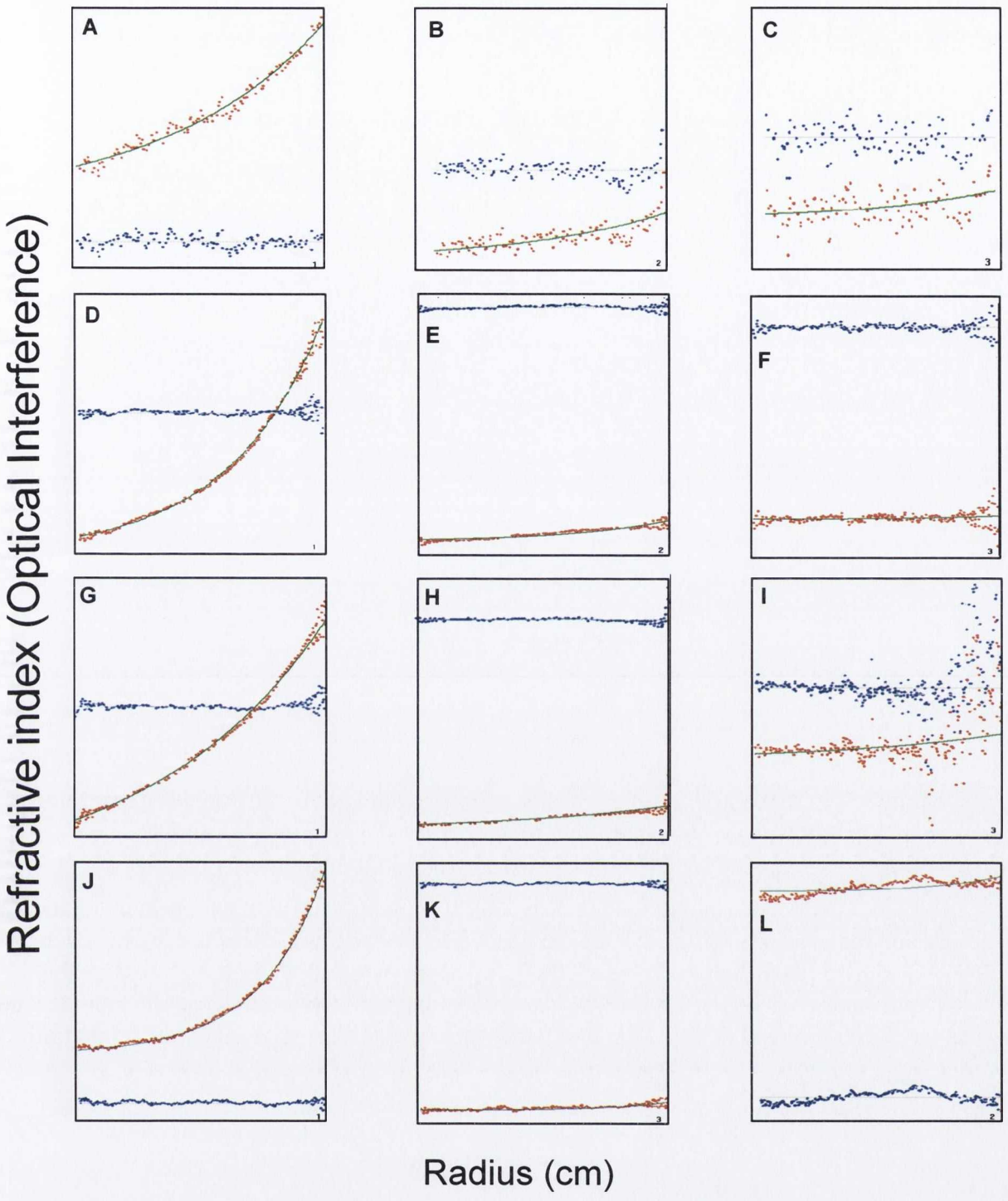

Figure 6.7 Sedimentation equilibrium ultracentrifugation analysis of sBVR-A at pH5 and 4°C

A. 1mg/ml, 12,000rpm, **B**. 0.3mg/ml, 12,000rpm, **C**. 0.1mg/ml, 12,000rpm
D. 1mg/ml, 15,000rpm, **E**. 0.3mg/ml, 15,000rpm, **F**. 0.1mg/ml, 15,000rpm
G. 1mg/ml, 15,000rpm, **H.** 0.3mg/ml, 15,000rpm, **I**. 0.1mg/ml, 15,000rpm
Figures **A-I** are sBVR-A data fit to a one species monomer model (see Table 6.1 for results) Figures **J-L** are fit to a 2 species self-associating dimer model (see Table 6.1 for results). In all cases interference data collected are shown in red and plotted against radial offset. The data were then fitted to the appropriate model which is shown in green. Residuals to the fit are shown in blue

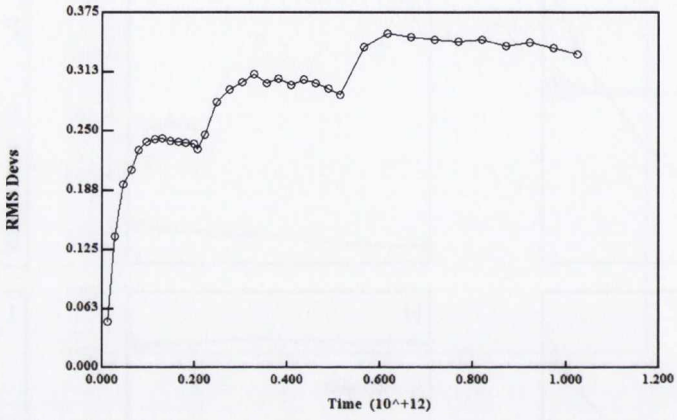

Figure 6.8 Winmatch analysis of the interference data from the sedimentation equilibrium ultracentrifugation experiment on sBVR-A at pH7 and 4°C

Interference scans were judged to be at equilibrium by plotting them against radial offset using the program Winmatch. sBVR-A at various concentrations was centrifuged at 12,000, 15,000, and 18,000 rpm. The first plateau in the above figure represents the equilibrium reached at 12,000rpm, the second plateau represents the equilibrium reached at 15,000 rpm and the third plateau represents the equilibrium reached at 18,000 rpm.

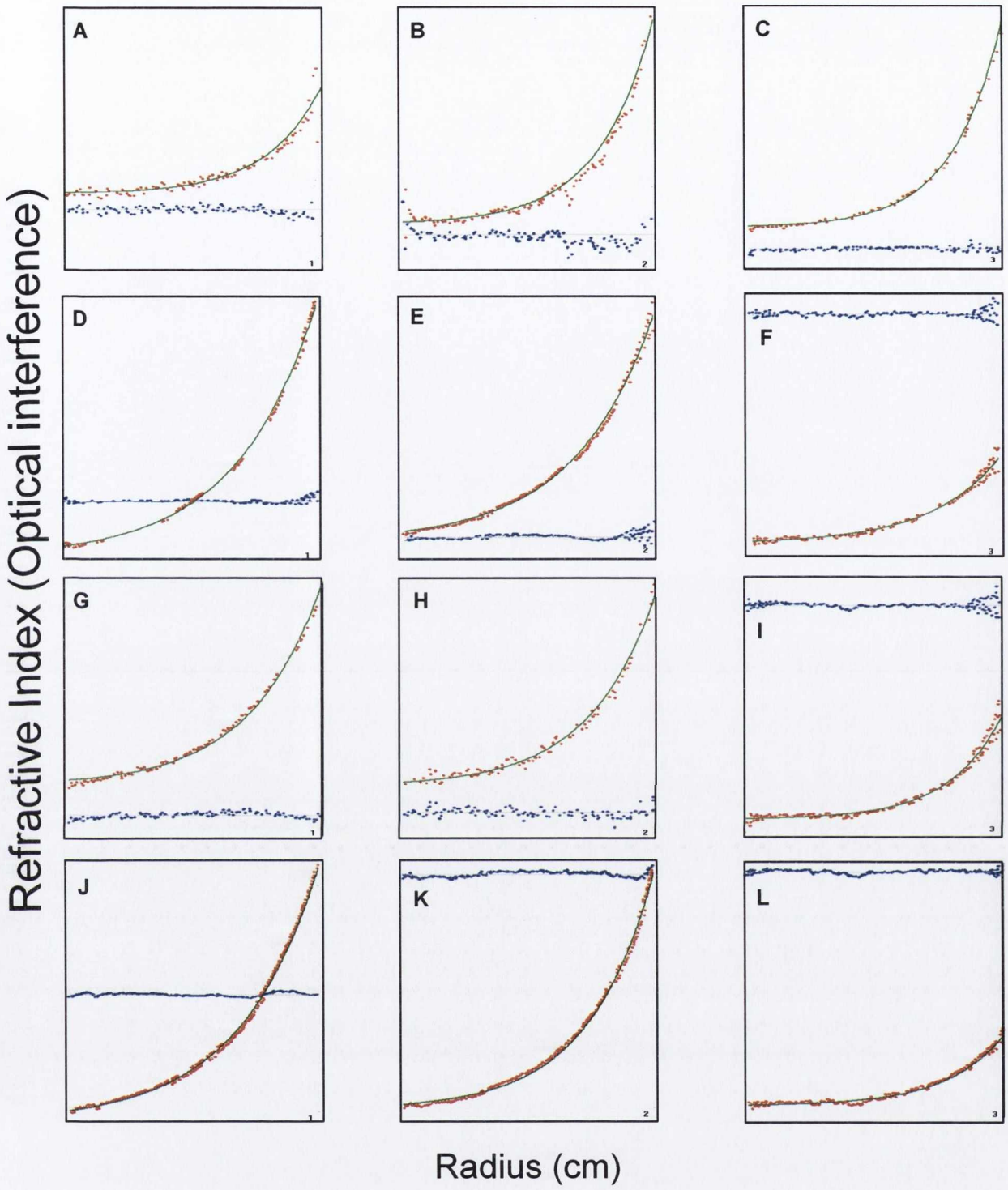

Figure 6.9 Sedimentation equilibrium ultracentrifugation analysis of sBVR-A at pH7 and 4°C

A. 1mg/ml, 12,000rpm, **B**. 0.3mg/ml, 12,000rpm, **C**. 0.1mg/ml, 12,000rpm
D. 1mg/ml, 15,000rpm, **E**. 0.3mg/ml, 15,000rpm, **F**. 0.1mg/ml, 15,000rpm
G. 1mg/ml, 15,000rpm, **H.** 0.3mg/ml, 15,000rpm, **I**. 0.1mg/ml, 15,000rpm
Figures **A-I** are sBVR-A data fit to a one species monomer model (see Table 6.1 for results) Figures **J-L** are fit to a 2 species self-associating dimer model (see Table 6.1 for results). In all cases interference data collected are shown in red and plotted against radial offset. The data were then fitted to the appropriate model and the fit to this model is shown in green. Residuals to the fit are shown in blue

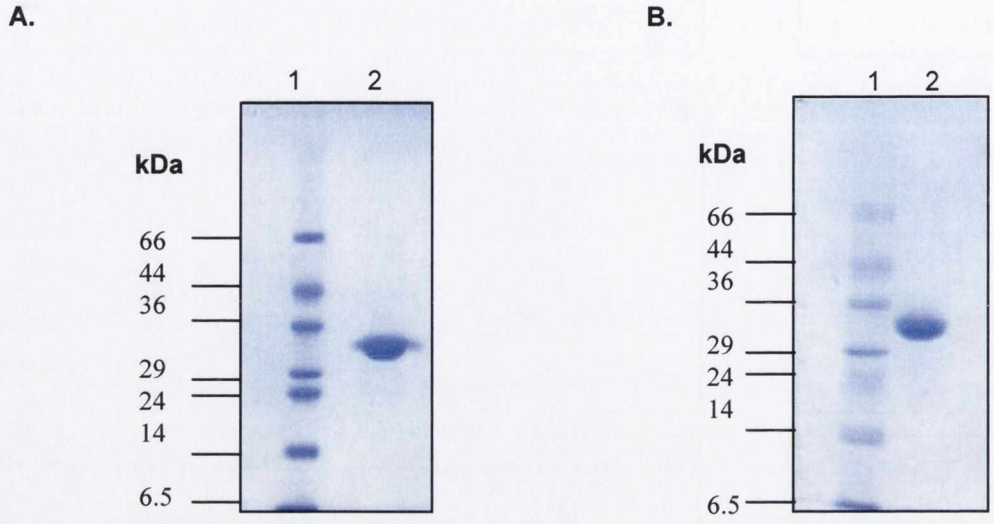

Figure 6.10 Purification of sBVR-A for crystallization trials

A. Purification of sBVR-A by 2'5' ADP-Sepharose affinity chromatography. Lane 1 contains molecular weight markers, Lane 2 contains purified sBVR-A

B. Purification of sBVR-A by S-200 gel-filtration chromatography. Following Purification of sBVR-A by 2'5' ADP-Sepharose affinity chromatography the protein was further purified by gel-filtration to remove protein aggregates. Lane 1 contains molecular weight markers. Lane 2 contains purified sBVR-A

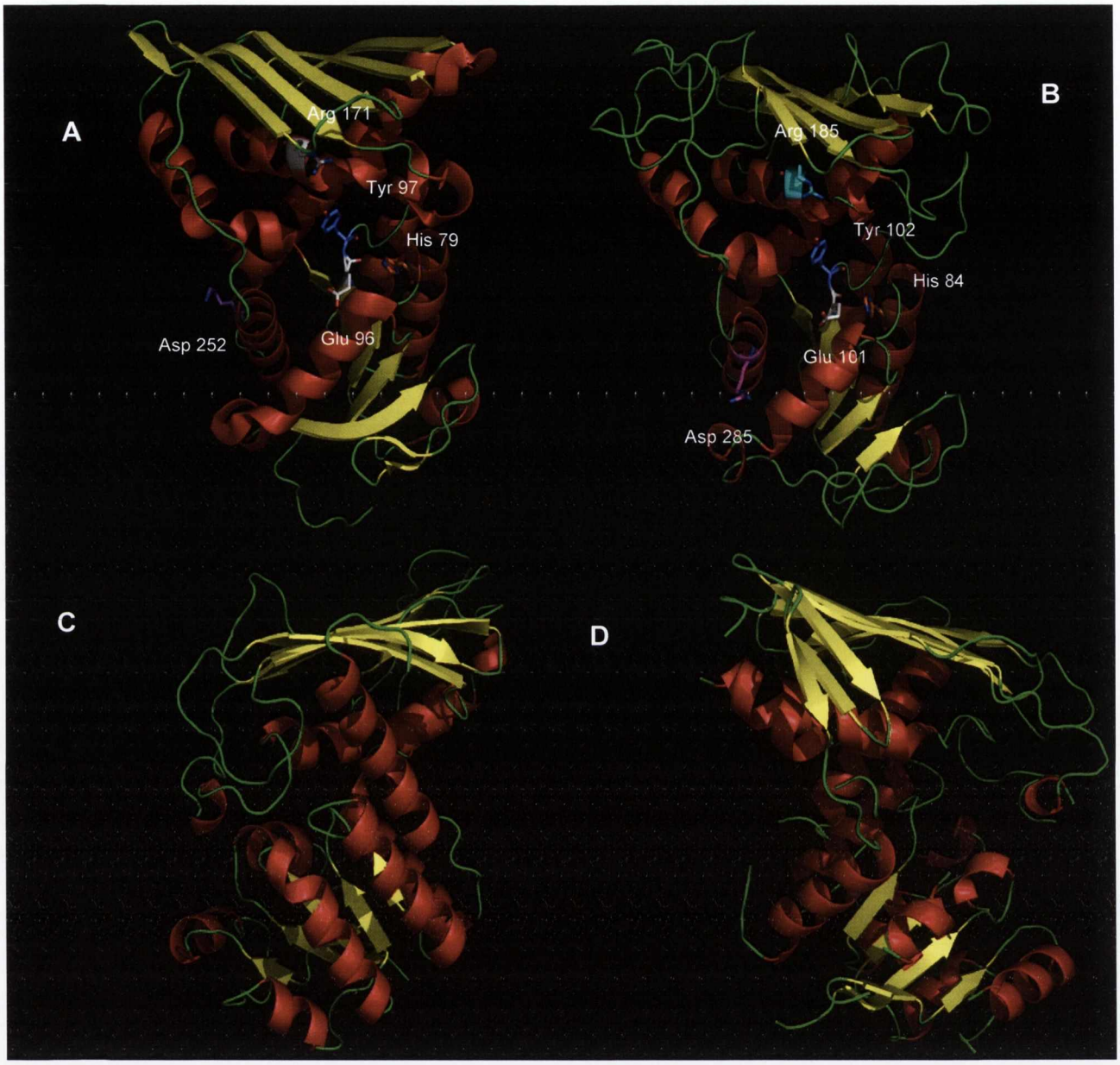

Figure 6.11 Homology modelling of *s*BVR-A.

The 3D models of sBVR-A was constructed using 3 homology modelling programs as described in Section 2.24. **A**. Known rat BVR-A crystal structure. **B**. Swissprot sBVR-A model. **C**. Easypred 3D sBVR-A model. **D**. Phyre sBVR-A model

Shown in red are α -helices, in yellow are β -sheets and in green are loops. Also shown in the rat BVR-A structure and Swisprot sBVR-A model are residues proposed to be important in substrate binding and catalysis. These residues are also in the equivalent positions in the sBVR-A models as they are in the known rat BVR-A crystal structure. Structures were modelled using Pymol (Delano Scientific, 2002)

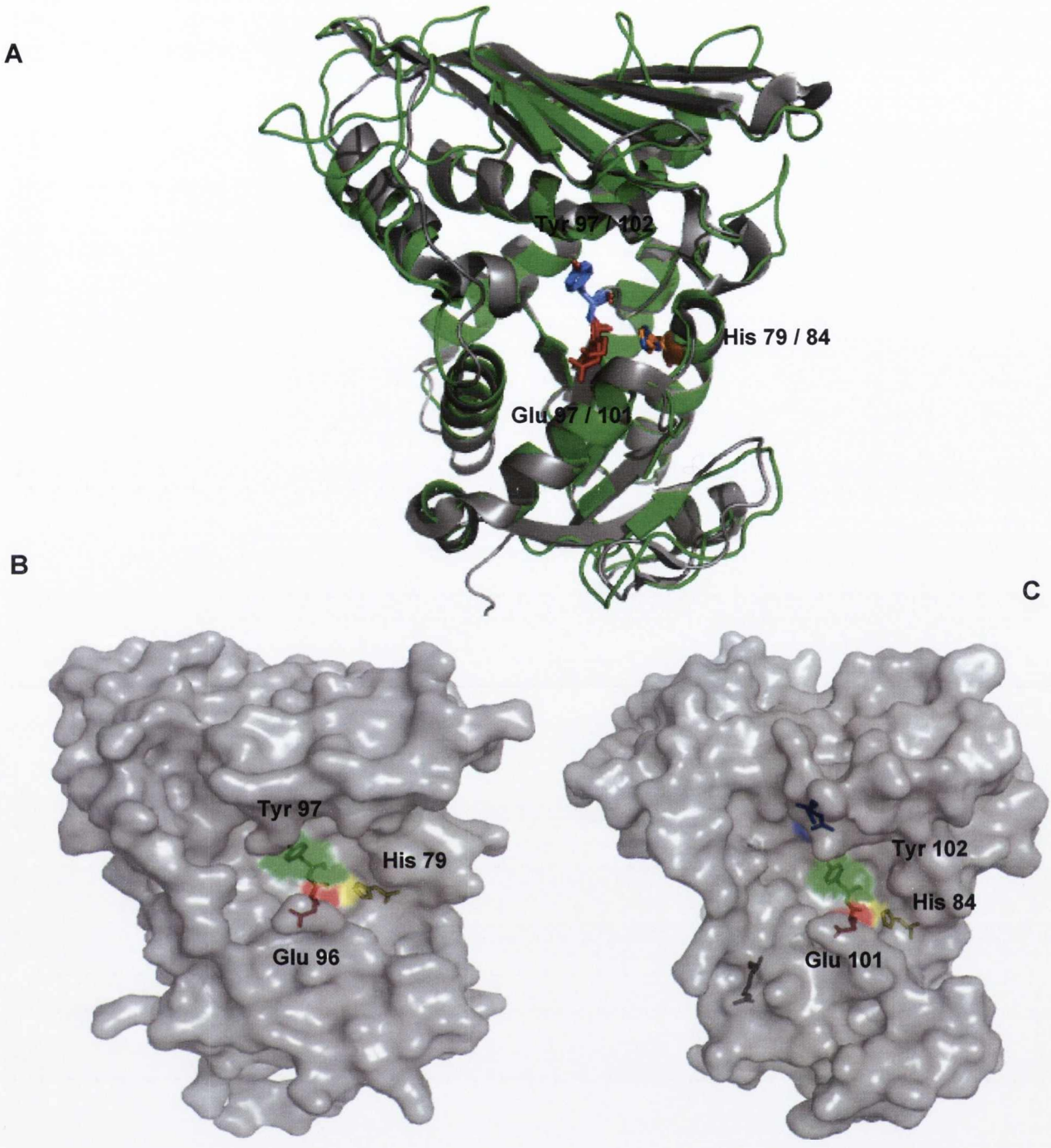

Figure 6.12 Molecular modelling of rat and *Synechocystis* BVR-A

A. Known rat BVR-A crystal structure (grey) and Swissprot sBVR-A model (green) superimposed. Overall structures are very similar with 2 clear domains. The goodness of fit parameter (rmsd) is 1.3 indicating a good fit for the model to the rat BVR-A template. Also shown are proposed active site residues. The position of these residues are very similar positions in the active sites of both enzymes

B. Surface representation of rat BVR-A showing proposed active site residues

C. Surface representation of sBVR-A model showing proposed active site residues.

Structures were modelled using Pymol (Delano Scientific, 2002).

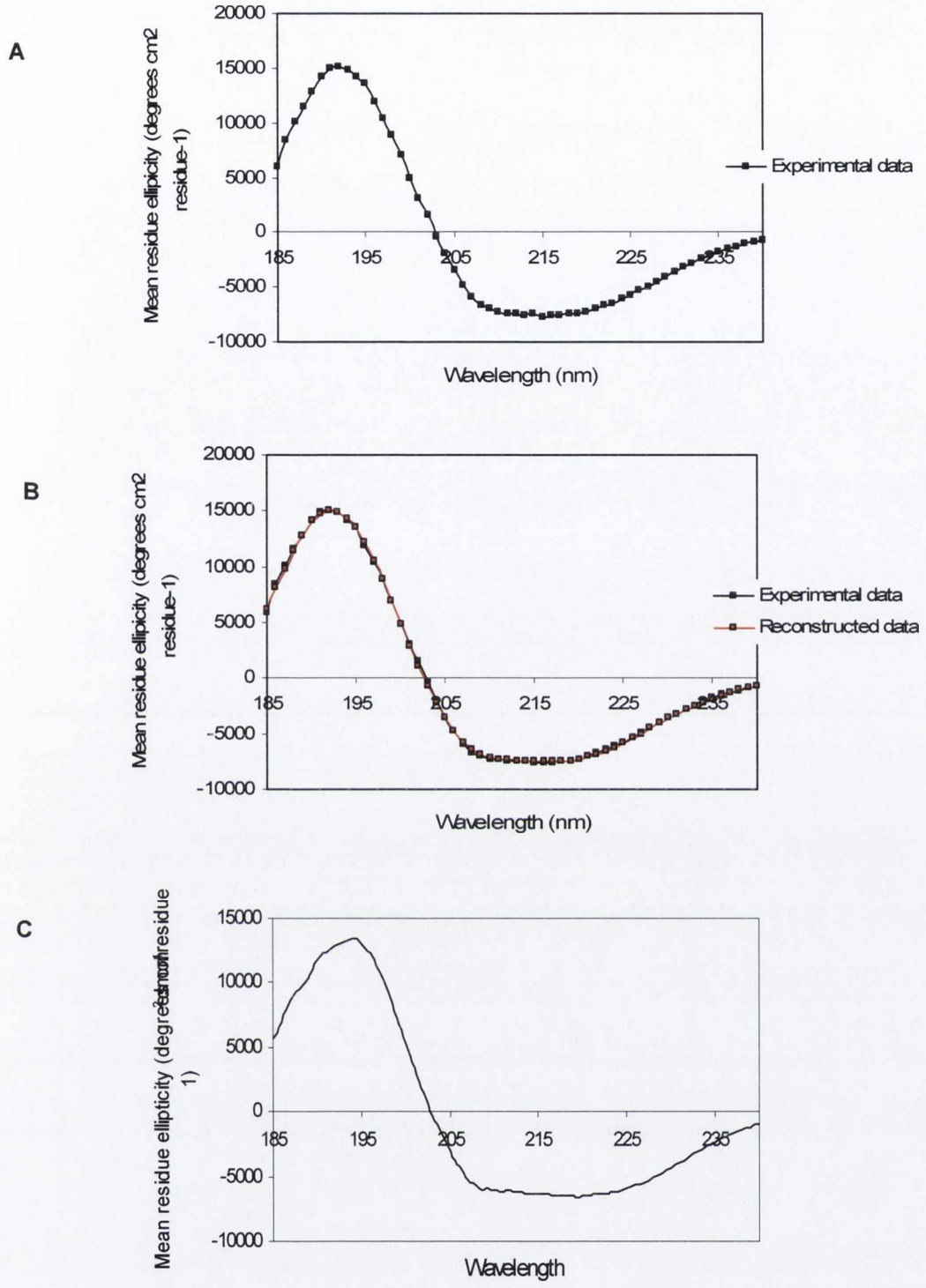

Figure 6.13 CD analysis of sBVR-A and human BVR-A and prediction of secondary structure

A. CD spectrum of sBVR-A in the far UV region

B. DICHROWEB analysis of sBVR-A. Shown in black is the experimentally determined data and in red is the data constructed by comparison of the CD data to the CD spectrums of the set of reference proteins of known structure

C. CD spectrum of human BVR-A in the far UV region

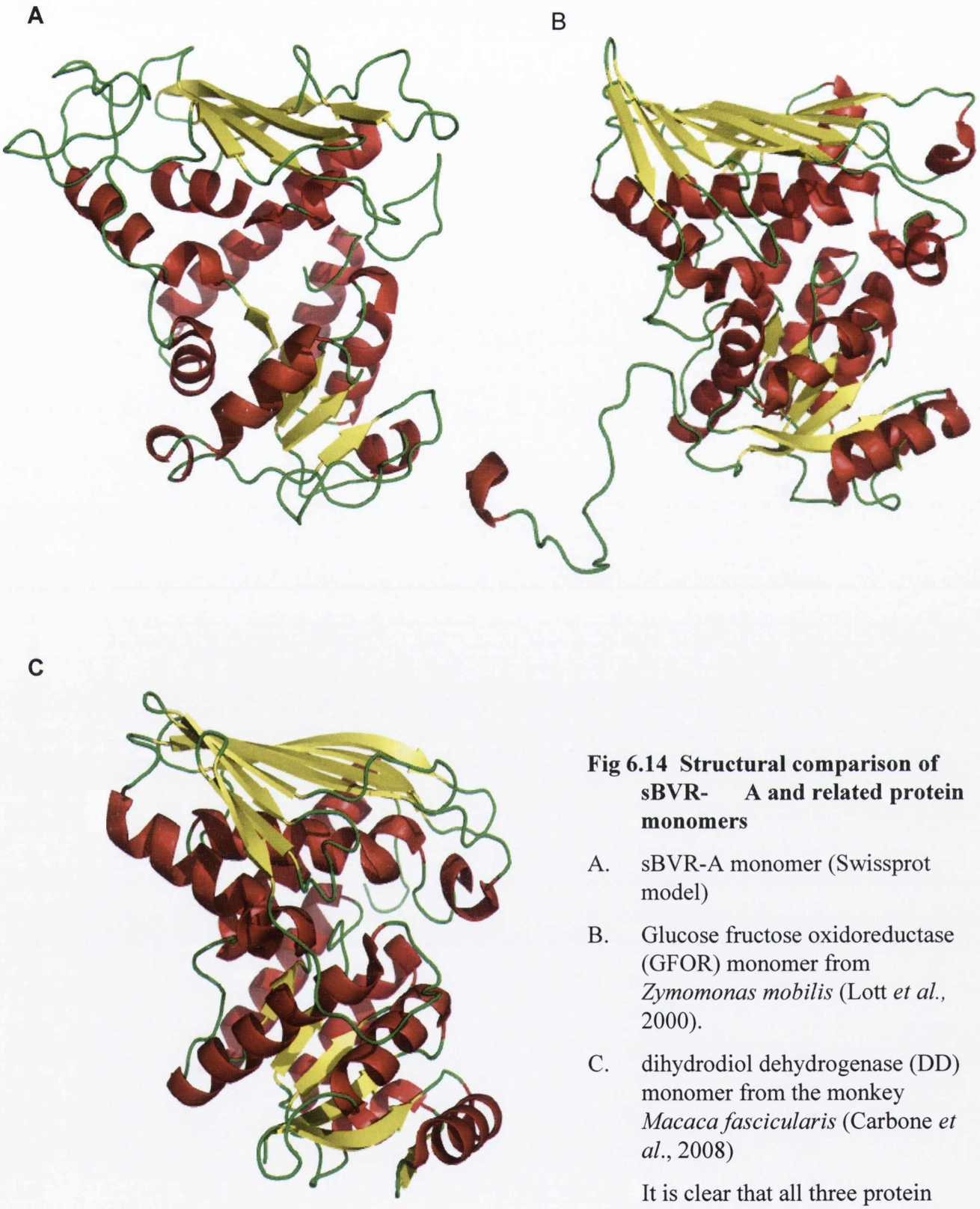

Fig 6.14 Structural comparison of sBVR- A and related protein monomers

A. sBVR-A monomer (Swissprot model)

B. Glucose fructose oxidoreductase (GFOR) monomer from *Zymomonas mobilis* (Lott *et al.*, 2000).

C. dihydrodiol dehydrogenase (DD) monomer from the monkey *Macaca fascicularis* (Carbone *et al.*, 2008)

It is clear that all three protein monomers have a similar overall shape with two β-sheet domains (including a C-terminal β-sheet) and a similar overall arrangement of α-helices, including a Rossman-like fold domain

Structures were modelled using Pymol (Delano Scientific, 2002)

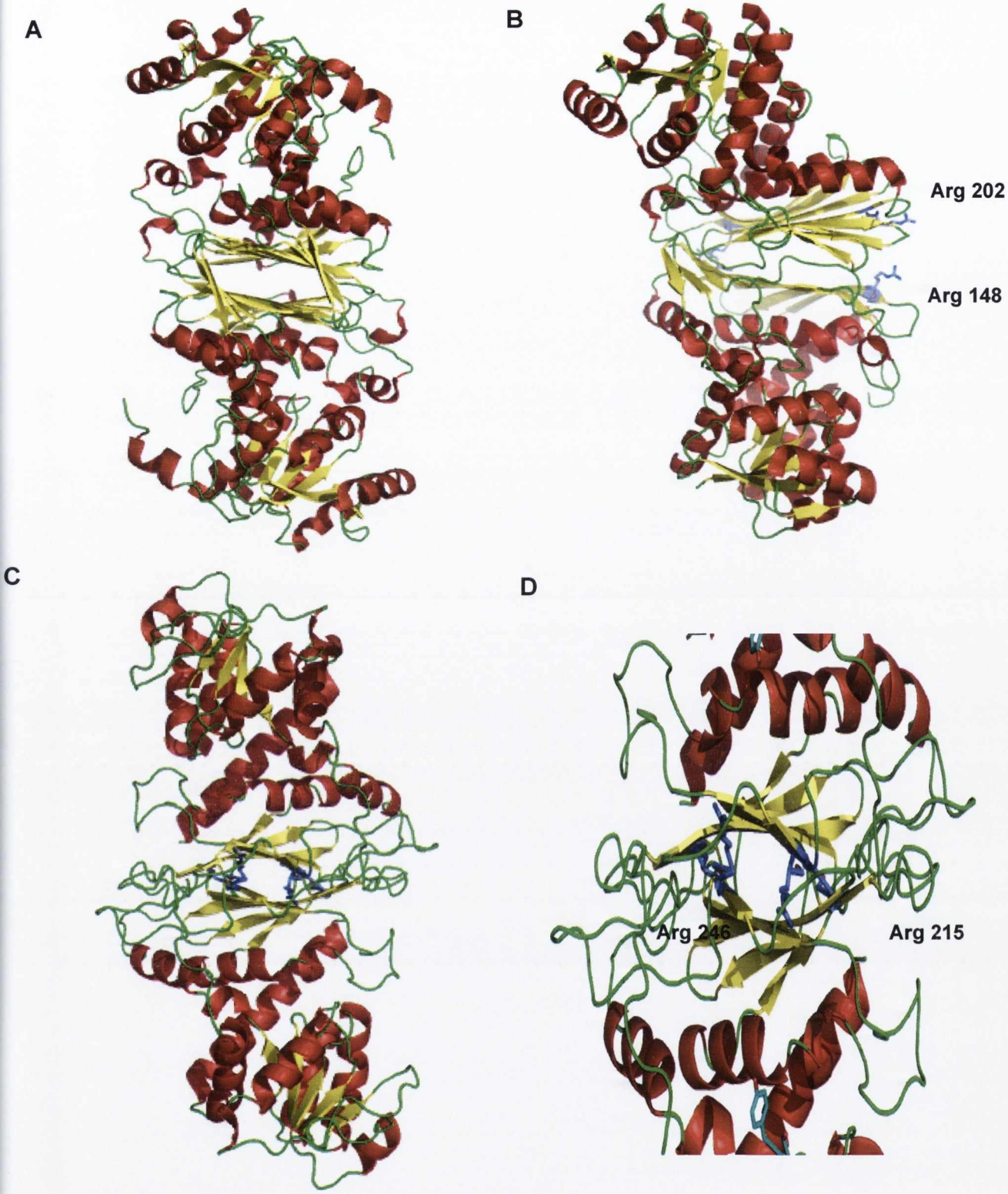

Figure 6.15 sBVR-A and related protein dimers

A. Crystal structure of the GFOR dimer (Lott *et al.*, 2000) **B.** DD dimer showing arginine residues involved in the dimerisation process (Carbone *et al.*, 2008) **C.** Proposed sBVR-A dimer **D.** Close up view of the proposed sBVR-A dimer interface showing arginine residues possibly involved in the dimerisation process. In all cases dimerisation is mediated through the interface of the C-terminal β-sheet

Structures were modelled using Pymol (Delano Scientific, 2002).

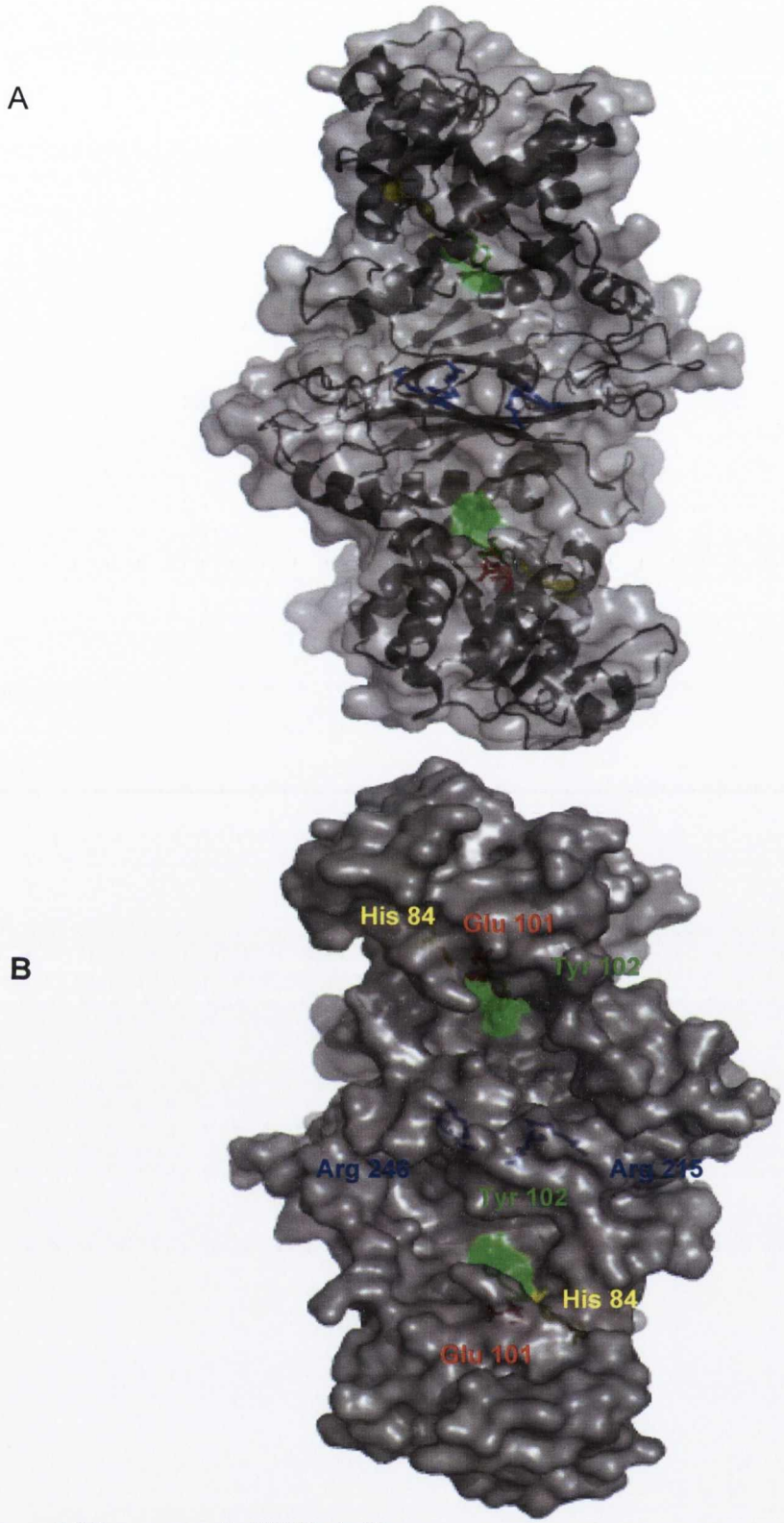

Figure 6.16 proposed sBVR-A dimer

A. Transparent surface representation of the proposed sBVR-A dimer mediated through the interface of the C-terminal β-sheet. Shown are the secondary structures and arginine residues in the interface which are possibly involved in the dimerisation process **B.** Surface representation of the proposed sBVR dimer showing the proposed active site catalytic and substrate binding residues. In this figure it is clear that both proposed active sites are accessible to substrates.
Structures were modelled using Pymol (Delano Scientific, 2002).

CHAPTER 7

FUNCTIONAL STUDIES ON *SYNECHOCYSTIS* BILIVERDIN IXα REDUCTASE

7.1 Introduction

Cyanobacteria use linear tetrapyrroles (phycoerthrobilin and phycocyanobilin) to harvest light energy from the sun. These photosynthetic accessory pigments are covalently attached to water soluble proteins to form phycobiliproteins. In *Synechocystis sp.* PCC 6803 the phycobiliproteins are arranged in a highly ordered multi-protein complex on the exterior of the thylakoid membrane known as phycobilisomes. Light energy in the yellow, green, orange or red portion of the visible spectrum is absorbed by these linear tetrapyrrole chromophores (phycobilins) and transferred to chlorophyll *a* in the thylakoid membrane with more than 90% efficiency, thereby facilitating efficient photosynthesis in these organisms. The phycobilins are synthesised from heme by heme oxygenase (HO) which converts heme to biliverdin IXα which is in turn converted to phycocyanobilin (PCB) or bilirubin IXα by phycocyanobilin ferredoxin oxidoreductase (PcyA) and biliverdin IXα reductase (sBVR-A) respectively. This simple system is found in *Synechocystis* sp. PCC6803, however other cyanobacteria also reduce biliverdin IXα to phycoerythrobilin in a four electron transfer process from individual reduced ferredoxin molecules. Biliverdin IXα therefore represents a branch point in the metabolism of heme. PCB is incorporated into the phycobiliprotein phycocyanin followed by incorporation of phycocyanin into the phycobilisome for use in light harvesting. It is relatively well understood that the function of PCB is to absorb light and pass the energy onto chlorophyll *a* in the thylakoid membrane thereby facilitating efficient photosynthesis in these organisms. However, the function of sBVR-A or bilirubin IXα in cyanobacteria is less clear and it is a major aim of this study to investigate their physiological function.

The genome of *Synechocystis sp.* PCC6803 has been completely sequenced and published (Kazusa DNA research Institute) and consists of a 3.5mb circular chromosome (see Fig. 7.1). Every *Synechocystis* cell contains up to 12 copies of this genome so that all 12 copies of the gene must be targeted and disrupted when constructing knock-out strains. The procedure outlined in the present study for gene targeting has been adapted from protocols described by Eaton-Rye, (2004). The sBVR-A gene was targeted by transforming wild-type glucose-tolerant *Synechocystis sp.* PCC6803 cells with a specially designed knock-out construct consisting of the wild-type gene with a kanamycin resistance cassette inserted into a unique Hpa-1 restriction site. This cassette is designed to disrupt the gene, separating essential catalytic domains in the protein and create a strain of *Synechocystis* lacking a functional biliverdin IXα reductase.

7.2 Design and construction of the sBVR-A knock-out construct

The sBVR-A knock-out construct was designed as described in Section 2.2.32. The wild-type sBVR-A allele consists of the 987bp sBVR gene (see Fig. 7.2). Homology regions (250bp upstream and 263bp downstream of the sBVR-A gene) are also required for recombination (see the wild-type sBVR-A sequence file in Fig. 7.4). The sBVR-A knock-out allele consists of the wild-type allele with a 1550bp kanamycin resistance cassette inserted into a unique Hpa-1 restriction site within the sBVR-A gene (see Fig. 7.3). It is this antibiotic resistance cassette that disrupts the sBVR-A gene and confers kanamycin resistance thereby allowing for selection of cells with the disrupted sBVR-A gene (see Fig. 7.5 for the sequence file of the sBVR-A knock-out allele). A 1500bp DNA fragment, consisting of the sBVR-A gene (987bp) and homology regions (513bp) was amplified from *Synechocystis sp.* PCC 6803 genomic DNA using specific primers that incorporated a BamH1 site in the forward primer (oligo 1 in Table 7.1) and an EcoR1 site in the reverse primer (oligo 2 in Table 7.1). Fig. 7.6A shows the PCR product obtained is approximately 1500bps and corresponds to the required fragment. This fragment was cloned into the BamH1 and EcoR1 sites of the cloning vector pBluescipt SK+ to create the plasmid pBBVR-A. Following ligation of the 1500bp fragment into pBluescript SK+ the complete contents of the ligation reaction were transformed into competent *E.coli* XL-1 blue cells as described in Section 2.2.9.2 and screened by restriction analysis as described in Section 2.2.10.1. Fig. 7.6B shows that of the 8 clones selected one had the correct insert present (see lane 7, indicated by an arrow). This clone was re-plated onto ampicillin resistant master plates and the plasmid DNA was purified as described in Section 2.2.4. The kanamycin resistance cassette (1550bp) was digested and excised from the plasmid vector pUK4K (Amersham Biosciences) using the restriction enzyme Pvu-II (see Fig. 7.6C). Following excision of the fragment from the agarose gel and purification the kanamycin resistance cassette was "blunt-end" cloned into the unique Hpa-1 site in the previously digested pBBVR-A plasmid (see Fig. 7.6D) to create the knock-out plasmid pBBVR-AKan as described in Section 2.2.32.2. Positive clones were isolated and the orientation of the cassette was screened for by restriction analysis. Fig. 7.6E shows that in all the clones selected the cassette was cloned in the forward direction. This construct was sequenced (see Fig. 7.5) as described in Section 2.2.12, purified and transformed into wild-type glucose-tolerant *Synechocystis sp.* PCC6803 cells as described in Section 2.2.32.4.

7.3 Genomic screening for positive *Synechocystis sp.* PCC6803 knock-out clones

7.3.1 Genomic screening for recombination of the knock-out construct into the correct location in the *Synechocystis* genome

Screening was carried out by PCR as described in Section 2.2.32.5a. A schematic of the PCR screening and the regions of DNA where the primers anneal is shown in Fig. 7.7. Individual kanamycin resistant clones (100) were picked from the original Bg11 transformation plates and re-plated on kanamycin resistant master plates. These clones were then picked and re-plated for 10 successive generations on Bg11 agar containing 5mM glucose and 25μg/ml kanamycin and screened. Although these clones were kanamycin resistant it was a possibility that the knock-out construct could have recombined anywhere in the *Synechocystis* genome. The first screen was therefore to verify that the sBVR-A knock-out construct had recombined in the correct location in the *Synechocystis* genome. Oligonucleotide primers were designed to anneal to a region of genomic DNA 430bp upstream of the sBVR-A gene and outside the region used for homologous recombination (oligo 3 in Table. 7.1) and to a region 793bp into the kanamycin resistance cassette (oligo 4 in Table 7.1). The regions of DNA where these primers anneal are shown in yellow in the sequence file shown in Fig. 7.5. A PCR product of the correct size (1823bp) would verify that the construct had been inserted into the correct place in the genome. Fig. 7.8A shows the results of the PCR screening from 20 clones. It is shown in this figure that the 1823bp PCR product is obtained from the majority of the clones, suggesting that these clones have the knock-out construct correctly inserted. No PCR product was obtained from wild-type genomic DNA as there is no knock-out construct present in the wild-type cells.

7.3.2 Genomic screening for segregation of the wild-type and sBVR-A knock-out alleles

Initial genomic screening verified that the sBVR-A knock-out construct had recombined in the correct place in the *Synechocystis* genome. However, this strain of *Synechocystis* contains numerous copies of its genome in every cell and a method for estimating the degree of segregation or how many copies of the wild-type gene had been replaced with the disrupted gene was required. PCR conditions were developed to estimate the degree of segregation of wild-type alleles from knock-out alleles. Primers were designed to bind to specific sites upstream (oligo 5 in Table 7.1) and downstream of the sBVR-A gene (oligo 6 in Table 7.1) and outside the homologous regions used for recombination (see Fig. 7.5 and 7.7). Using these primers it was possible to estimate how many copies of the wild-type allele had been replaced with the knock-out allele because the knock-out allele has an extra 1550bp kanamycin resistance cassette inserted into the gene which can be visualized on an agarose gel using this PCR protocol. However, after 10 generations none

of the 20 clones selected had shown any significant signs of segregation (see Fig. 7.8B). The wild-type PCR product using these primers consists of 2320bp (see Fig. 7.4).

The method used to segregate the alleles in the selected clones was modified in an effort to force their segregation. The antibiotic concentration was increased to 50μg/ml and the light output of the growth chamber was decreased from 447 to 224 μEinsteins m^{-2} s^{-1} and the light-dark cycle was changed from 16 hours light, 8 hours dark to 8 hours light, 16 hours dark. The kanamycin concentration was increased to 50μg/ml to increase the selective pressure on the knock-out allele and try to force segregation. Each clone was also "split" and grown completely in the dark with only 15 minutes light per day. The clones were picked and re-plated for another 10 generations under these conditions and screened again for signs of segregation by PCR as described above. The 4 selected clones shown in Fig. 7.9A now exhibited signs of allele segregation. The wild-type genomic DNA (lane 2 in Fig. 7.9A) shows the wild-type allele plus the homology regions and extra DNA upstream and downstream where the primers anneal at 2320bps but in the targeted clones the major PCR product was now seen at 3870bps (see lanes 2-5 in Fig. 7.9A). The 1550bp difference in size between the wild-type allele and the knock-out allele was due to the 1550bp kanamycin cassette inserted into the sBVR-A gene.

In order to completely segregate the alleles the kanamycin concentration was further increased to 100μg/ml and the sBVR-A knock-out clones were picked and re-plated for approximately 30 further generations. A further screening protocol was also developed to distinguish between the wild-type and knock-out alleles as described in Section 2.2.32.5a. This method developed a PCR reaction that was specific to the knock-out allele. It utilised a Xho-1 restriction site that was located within the kanamycin cassette but nowhere else within the sBVR-A gene or the homologous regions. Digestion of wild-type genomic DNA with Xho-1 would have no effect on the PCR product formed because there was no Xho-1 restriction site within this region but digestion of genomic DNA from the knock-out clones would result in no PCR product formed because the priming sites were now on regions of DNA that were separated by digestion with Xho-1 (see Fig. 7.7). The primers and PCR conditions were the same as those used to estimate the levels of segregation. Fig. 7.9B shows that digestion with Xho-1 has no effect on the wild-type allele because there is no Xho-1 restriction site within this allele but no PCR product is obtained from the knock-out clones because the priming sites are now separated by digestion with Xho-1. This result suggested that the alleles were completely segregated and no wild-type copies of the sBVR-A gene remained in these clones.

7.4 Western blotting analysis of the sBVR-A knock-out clones

sBVR-A clones (10) verified in the previous section as having no copies of the wild-type sBVR-A gene remaining were analysed by western blotting to ensure no sBVR-A protein was present. Western blotting of *Synechocystis* cytosol was carried out as described in Section 2.2.19.1c. Briefly, 50ml cultures of each sBVR-A knock-out clone were grown in Bg11 medium containing 5mM glucose and 100μg/ml kanamycin as described in Section 2.2.2. A 50ml culture of the wild-type cells was also grown but in the absence of kanamycin. When the cultures were in the exponential log phase (OD_{730} = 0.7-0.9) the cells were harvested by centrifugation at 4000 x g at 4°C and stored at -20°C overnight. The cells were washed 3 times in 20mM sodium phosphate, pH7 by repeated resuspension and centrifugation and finally resuspended in 50mM Tris-HCl pH7.5, 50mM NaCl, 5mM EDTA and 10μl complete protease inhibitor cocktail (Sigma). Acid-washed glass beads (2μm diameter) were added to the cell suspension to 1cm below the surface and the cells were disrupted by 3 cycles of vortexing for 1min followed by 1min on ice. Cell debris and glass beads were removed by centrifugation at 2,000 x g for 2min at 4°C. The cell supernatant containing soluble protein and cell membranes were transferred to a fresh 1.5ml tube and a Bradford assay was performed as described in Section 2.2.18.3 to determine the protein concentration.

SDS-PAGE of *Synechocystis* total cell lysate was performed as described in Section 2.2.19.1. Protein (100μg) from each clone, including wild-type cells was fractionated using a 20 x 15cm SDS-PAGE gel apparatus and the proteins transferred to Immobilon P membrane (Millipore) as described in Section 2.2.19.3. Anti-sBVR-A antibodies were then used to detect the presence of sBVR-A protein as described in Section 2.2.19.4. A second SDS-PAGE gel was also used to ensure equal loading of protein samples into each well and this gel was stained and visualised as described in Section 2.2.19.2. sBVR-A protein was detected in the wild-type cells but in each of the knock-out clones no sBVR-A protein was detected, verifying that the gene had been disrupted and no sBVR-A protein was present (see Fig. 7.10).

7.5 Analysis of the sBVR-A mutant phenotype

7.5.1 Analysis of the growth characteristics of the sBVR-A mutant cells

The growth characteristics of the sBVR-A knock-out cells were evaluated under low levels of light (224 μEinsteins m^{-2} s^{-1}) in three knock-out clones (2, 3 and C2) and then compared to the growth characteristics of the wild-type cells. The mutant and wild-type cells were cultured in identical conditions. Cells (50ml) were cultured as described in Section 2.2.2 in the absence of glucose and kanamycin and the growth characteristics evaluated based on cell number by counting the cells or

recording the OD_{730} every 24 hours as described in Section 2.2.33.1. The data were then used to construct the growth curves shown in Fig. 7.11. There appears to be a slight difference between the wild-type cells and the three knock-out clones up to 80 hours culturing time, where the knock-out cells lag slightly behind the wild-type cells. However, from 300 hours onwards the rate of growth appears to be similar for the wild-type and knock-out cells, although the number of cells in the three knock-out cultures remains approximately 200 x 10^6 behind the wild-type.

The growth characteristics of the mutant cells were also evaluated under conditions of high light (895 μEinsteins m^{-2} s^{-1}). Growth curves were again constructed and are shown in Fig. 7.12. The effect on growth in the sBVR-A mutants now appears to be more severely affected, particularly during the log phase of cell growth (24-96 hours) where the wild-type cells are dividing and growing much more rapidly than the mutant cells (see Fig. 7.12). The cell density of the knock-out cultures reaches only approximately 70% of that of the wild-type (see Fig. 7.12) and the cells appear yellow (see Fig. 7.13), possibly due to "chlorosis" or bleaching.

7.5.1.1 Analysis of the growth characteristics of the sBVR-A mutant cells in the presence of bilirubin IXα

The sBVR-A mutant and wild-type cells were cultured in Bg11 medium supplemented with bilirubin IXα (0.1-1μM) under high light conditions as described in Section 2.2.33.1. The purpose of this was to investigate if the product of the sBVR-A reaction, bilirubin IXα, had any effect on the growth of the mutant cells and if it could return the mutant cells to the wild-type phenotype. Wild-type cells were also cultured in the presence and absence of bilirubin. When bilirubin was included in the growth medium of the mutant cells the growth rate was comparable to the wild-type cells which were cultured in its absence (see Fig. 7.14). In this case bilirubin appears to be having an effect as the mutant cells now grow at the same rate as the wild-type cells. However, when bilirubin was included in the growth medium of the wild-type cells under these conditions, growth rate is further increased (see Fig. 7.14). Bilirubin appears to be able to enhance growth of the wild-type cells under high light conditions. The chlorotic effect on the cells also appears to be less severe in the presence of bilirubin.

7.5.2 Analysis and identification of the photosynthetic and carotenoid pigments from wild-type and sBVR-A knock-out cells

7.5.2.1 HPLC separation and initial analysis of pigments

Pigments such as chlorophyll and carotenoids were analysed from wild-type and mutant sBVR-A cells by reverse-phase HPLC using the method of Mohamed & Vermass (2004) as described in

Section 2.2.33.2. Wild-type and mutant (2, 3 and C2) cells were cultured under medium levels of light (447 μEinsteins m^{-2} s^{-1}) until the OD_{730} was exactly 0.5 and then harvested by centrifugation at 4000 x g for 10min at 4°C. If the OD_{730} was slightly above 0.5 the culture was diluted with fresh Bg11 medium to achieve an OD_{730} of exactly 0.5. Cells were then "snap-frozen" in liquid nitrogen and freeze-dried overnight. Pigments were extracted by resuspending the cells in 100% methanol containing 0.1% NH_4OH in the dark and on ice. Three successive resuspensions followed by incubation on ice was carried out. Depending on the amount of pigments obtained they were either concentrated by evaporating under a stream of nitrogen or diluted in 100% methanol containing 0.1% NH_4OH prior to analysis. Samples (50μl) were centrifuged at 13,000 x g at 4°C for 10min and immediately loaded onto a "Supelco Discovery" C18 reversed phase HPLC column (4mm x 25mm) at a flow rate of 1ml/min. The mobile phase consisted of 90% acetonitrile, 10% H_20 and 0.01% triethylamine. Pigments were eluted using a linear 18min gradient of 0-95% ethyl acetate and the absorption spectra of the eluted pigments were recorded continuously by an online photodiode array detector in the 300-700-nm range. By comparison of the elution profiles of the pigments from the wild-type (Fig. 7.15) and mutant cells (Figs. 7.16) it appears that there is decreased levels of chlorophyll *a* (peak C) in the sBVR-A knock-out cells, possibly coupled with an increase in the levels of certain carotenoids (peaks A and E in Figs 7.15 and 7.16). Chlorophyll and carotenoids were tentatively identified by their absorbance spectra and through the published results of Mohamed & Vermass (2004).

7.5.2.2 Mass spectrometry analysis of the eluted pigments

The peak fractions of the various pigments which were analysed in the previous section were collected (100-500μl fractions) following elution from the HPLC column (see Fig. 7.15) In order to obtain sufficient quantities of each pigment for mass spectrometry analysis this procedure was repeated several times. The pigments were concentrated under a stream of nitrogen in the dark and stored at -80°C. Samples (10μl) were added to 100% HPLC grade methanol (90μl) as the solvent and mass spectra were obtained by matrix-assisted laser desorption ionization time of flight (MALDI-TOF)-mass spectrometry using a Waters Q-TOF premier mass spectrometer in electrospray + mode. The molecular weight of the compound represented by peak B in Fig. 7.15 was determined to be 568 g/mol (see Fig. 7.17A). Although a number of compounds were detected with different molecular weights, the major compound has a molecular weight of 568 g/mol, corresponding to a molecular formula of $C_{40}H_{56}O_2$ and the carotenoid zeaxanthin. No other compounds were detected which had molecular weights corresponding to other carotenoids and based on the absorbance spectrum it was concluded that peak B was zeaxanthin. The compound represented by peak C in Fig. 7.15 has a molecular weight of 893 g/mol (Fig. 7.17B),

corresponding to a molecular formula of $C_{55}H_{72}MgN_4O_5$ and to chlorophyll *a*. The compound represented by peak E in Fig. 7.15 has a molecular weight of 536 g/mol (Fig. 7.17C) corresponding to a molecular formula of $C_{40}H_{56}$ and to β-carotene. Based on the absorbance spectra peak A was the carotenoid myxoxanthophyll and peak D was the remaining carotenoid echinenone. The carotenoids of *Synechocystis* were therefore identified based on their spectral properties, retention times and molecular masses in some cases.

7.5.2.3 Analysis of pigments under various growth conditions

Wild-type and sBVR-A knock-out cells were cultured as described in Section 2.2.2 in the presence of 5mM glucose under low (224 μEinsteins m^{-2} s^{-1}), medium (447 μEinsteins m^{-2} s^{-2}) or high (895 μEinsteins m^{-2} s^{-1}) levels of light until the OD_{730} was exactly 0.5. The cells were then harvested and the pigments analysed as described in Section 7.5.2.1. When the wild-type cells were grown under low light, levels of chlorophyll are high and levels of carotenoids are low (see Fig. 7.18A). Wild-type cells grown under medium levels of light show a small increase in the levels of carotenoids (see Fig. 7.18C) and cells grown under high light show a greater increase in the levels of carotenoids with a possible decrease in the levels of chlorophyll (see Fig. 7.18D). Myxoxanthophyll (peak A) shows the greatest increase. When the mutant cells were grown under low light chlorophyll levels are high and carotenoid levels are low (see Fig. 7.19A). However, although levels of carotenoids are low it appears that they are slightly higher when compared to the levels of carotenoids from the wild-type cells grown under the same conditions. When the cells are grown under medium light there also appears to be a slight increase in the levels of carotenoids, particularly myxoxanthophyll (see Fig. 7.19C). Levels of carotenoids also appear to be slightly higher in the mutant cells than in the wild-type and chlorophyll may be slightly lower. However, the greatest change is seen when the mutant cells are grown under high light. Chlorophyll levels now appear to be decreased and there may be a further increase in the levels of carotenoids, particularly myxoxanthophyll (see Fig. 7.19D).

7.6 Analyis of the expression levels of HO1, PcyA and sBVR-A in wild-type *Synechocystis* cells under various conditions

7.6.1 Effect of glucose on the levels of HO1, PcyA and sBVR-A

A glucose tolerant strain of *Synechocystis* sp. PCC6803 was used in many of the studies described in this work. It was felt necessary therefore to investigate if glucose had an affect on the enzymes required for the light harvesting pigment phycocyanobilin (HO1 and PcyA) or sBVR-A. *Synechocystis* cells were cultured (250ml) as described in Section 2.2.2 in the absence of glucose until the OD_{730} was approximately 0.7. At this point a 50ml sample was taken and the cells

harvested by centrifugation as described previously and stored at -20°C. Sterile glucose was added to the culture at a final concentration of 5mM and samples were extracted and harvested after 3, 6, 12 and 24 hours. Preparation of protein samples from each time point, SDS-PAGE and western blotting were performed as described in Section 2.2.19. Fig. 7.20 shows that glucose had no effect on the expression of HO1, PcyA or sBVR-A under these conditions.

7.6.2 Effect of bilirubin IXα on the levels of HO1, PcyA and sBVR-A

Bilirubin was shown to effect the growth of both wild-type and mutant sBVR-A cells (see Section 7.5.1.1). The effect of bilirubin on the levels of HO1, PcyA and sBVR-A was investigated by growing wild-type *Synechocystis* (250ml) cells to an OD_{730} of approximately 0.7. At this point all traces of glucose and antibiotics were removed as described in Section 2.2.33.1. A 50ml sample was extracted and stored and bilirubin IXα was added to the culture at a final concentration of 10μM. Samples were taken after 3, 6, 12 and 24 hours. Preparation of protein samples from each time point, SDS-PAGE and western blotting were performed as described in Section 2.2.19. Fig. 7.21A shows that the levels of HO1 appear to increase after 3hours in the presence of bilirubin but no effect was observed on the levels of PcyA or sBVR-A protein under these conditions.

7.6.3 Effect of light on the levels of HO1, PcyA and sBVR-A

7.6.3.1 Effect of low levels of light

The effect of low levels of light (224μEinsteins m^{-2} s^{-1}) on the levels of HO1, PcyA and sBVR-A was investigated by growing *Synechocystis* cells (250ml) under low light to an OD_{730} of approximately 0.7. At this point all traces of glucose and antibiotics were removed as described in Section 2.2.33.1 and the culture was covered with tin foil for 24hours to ensure the culture was dark adapted. After 24hours a 50ml sample was removed and stored. The tin foil was then removed and the culture exposed to low levels of light and samples were extracted after 3, 6, 12 and 24hours. Preparation of protein samples from each time point, SDS-PAGE and western blotting were performed as described in Section 2.2.19. Fig. 7.22 shows that low levels of light had no effect on the levels of HO1, PcyA or sBVR-A protein under these conditions.

7.6.3.2 Effect of high levels of light

The effect of high levels of light (895 μEinsteins m^{-2} s^{-1}) on the enzymes was investigated as described in the previous section with one modification. *Synechocystis* cells (250ml) were grown under low light (224 μEinsteins m^{-2} s^{-1}) to an OD_{730} of approximately 0.7 as described in Section 2.2.2. At this point all traces of glucose and antibiotics were removed as described in Section 2.2.33.1 and the culture was covered with tin foil for 24hours. After 24hours a 50ml sample was

removed and the cells were harvested and stored as described previously. The tin foil was then removed and the culture exposed to high levels of light (895 μEinsteins m^{-2} s^{-1}) and samples were extracted after 3, 6, 12 and 24 hours. Preparation of protein samples from each time point, SDS-PAGE and western blotting were performed as described in Section 2.2.19. Fig. 7.23A shows that the levels of HO1 appear to decrease slightly after 3 hours. There is no effect on PcyA (Fig 7.23B) but the levels of sBVR-A protein appear to increase after 3hours and continue to increase up to 24hours under these conditions (see Fig. 7.23C).

7.6.4 Effect of H_2O_2 on the levels of HO1, PcyA and sBVR-A

The effect of H_2O_2 was investigated as an inducer of oxidative stress in cyanobacteria and its effect on the levels of HO1, PcyA and sBVR-A was investigated by western blotting. Cultures of *Synechocystis* cells (250ml) were grown under low light (224 μEinsteins m^{-2} s^{-1}) until the OD_{730} was approximately 0.7 as described in Section 2.2.2. At this point all traces of glucose and antibiotics were removed as described in Section 2.2.33.1. H_2O_2 was added to the culture at final concentrations of 1mM, 10mM and 100mM and samples (50ml) were taken after 3, 6, 12 and 24 hours. Preparation of protein samples from each time point, SDS-PAGE and western blotting were performed as described in Section 2.2.19. Hydrogen peroxide (1mM) has no effect on HO1 (Fig. 7.24A) or PcyA (Fig. 7.24B) but levels of sBVR-A appear to increase slightly after 3 hours (Fig. 7.24C). At 10mM H_2O_2 concentration the levels of HO1 decrease dramatically after 3hours and remain low up to 24hours (see Fig. 7.25A). The levels of PcyA remain constant (Fig. 7.25B) and the levels of sBVR-A appear to increase slightly form 3-24 hours (see Fig. 7.25C). At 100mM H_2O_2 concentration the levels of HO1 decrease dramatically after 3 hours (Fig. 7.26A), PcyA decreases from 6-24 hours (Fig. 7.26B) and sBVR-A appears to increase after 3 hours and then decreases up to 24 hours (see Fig. 7.26C).

7.6.5 Effect of norflurazon on the levels of HO1, PcyA and sBVR-A

Norflurazon is an inhibitor of phytoene desaturase and blocks formation of ε-carotene from phytoene and therefore inhibits carotenoid biosynthesis in plants and cyanobacteria. The effect of norflurazon on HO1, PcyA and sBVR-A was investigated by growing cultures of *Synechocystis* cells (250ml) under low light (224 μEinsteins m^{-2} s^{-1}) until the OD_{730} was approximately 0.7 as described in Section 2.2.2. At this point all traces of glucose and antibiotics were removed as described in Section 2.2.33.1. Norflurazon was added to the culture at a final concentration of 25μM and samples (50ml) were taken after 3, 6, 12 and 24 hours. Preparation of protein samples from each time point, SDS-PAGE and western blotting were performed as described in Section 2.2.19. In the presence of norflurazon and subsequently in the absence of protective carotenoids

the levels of HO1 decrease after 6 hours treatment (see Fig. 7.27A). The levels of PcyA remain constant (see Fig. 7.27B) and the levels of sBVR-A appear to increase after 3hours and a significant increase in protein levels is observed after 24 hours (Fig. 7.27C) under these conditions.

It is a major aim of this study to investigate the role of sBVR-A in cyanobacteria. This was done by disrupting the sBVR-A gene by inserting a kanamycin resistance cassette into it by homologous recombination. This separated vital domains required for catalytic activity and effectively resulted in a strain of *Synechocystis* sp. PCC6803 which lacked the enzyme biliverdin IXα reductase. As wild-type *Synechocystis* cells have up to 12 copies of their genome a protocol was developed to segregate the wild-type copies of the sBVR-A gene and result in a completely segregated sBVR-A knock-out strain. This proved difficult and it required approximately 50 generations and relatively low levels of light and high antibiotic concentrations to increase the selective pressure on the knock-out allele and force segregation. It should be noted that if a gene is targeted which is essential to survival, the organism will retain the gene as the gene product is required to survive and creating a fully segregated mutant will prove impossible. When targeting the sBVR-A gene, creating a fully segregated mutant proved difficult, suggesting that the product of the sBVR-A gene was important for the survival of *Synechocystis* sp. PCC6803.

Photosynthetic organisms, including cyanobacteria use oxygen as a powerful electron acceptor. However, reactive oxygen species (ROS), including singlet oxygen ($^1O_2$), hydrogen peroxide (H_2O_2), superoxide anion (O_2^-) and hydroxyl radical (OH^-) are generated as intermediates of oxygen reduction and are powerful oxidizing agents, damaging DNA, proteins and lipids. *Synechocystis* sp. PCC6803 generates large amounts of ROS and is subject to oxidative stress generated from both photosynthesis and respiration and must have developed powerful anti-oxidative systems to survive and to deal with this stress. The major effects of oxidative stress in cyanobacteria are the photoinactivation of photosystem II (PSII) and degradation of chlorophyll, a process known as "chlorosis". This process (chlorophyll and phycobilin depletion) appears to be evident in *Synechocystis* cells lacking sBVR-A and can occur in response to light induced oxidative damage or nutrient deprivation and is visible in the cells as a colour change from blue-green to green-yellow resulting from the "bleaching" of chlorophyll in response to oxidative damage or degradation of the phycobilisome in response to nutrient deprivation. This process appears to be evident in Fig. 7.13 where there is a colour change from green to yellow possibly due to the depletion or degradation of chlorophyll and phycobilisomes in response to oxidative damage. In *Synechocystis* phycobilisome degradation is an ordered proteolytic process where a small polypeptide nblA is expressed upon nitrogen deprivation and results in phycobilisome degradation (Baier *et al.*, 2001). It is possible that nblA is upregulated in the sBVR-A knock-out cells leading to phycobilisome degradation.

Analysis of the growth characteristics of the sBVR-A mutants suggest that sBVR-A is required for normal growth. This is particularly evident under conditions of light stress. In medium light conditions there is a slightly lower rate of cell growth and cell density is decreased by approximately 200 x 10^6 cells at the end of the time course but there is a severely decreased rate of cell growth, particularly in the log phase under conditions of light stress with cell density of the sBVR-A mutant cultures reaching only 70% of the wild-type culture. The appearance of the mutant cells also differs from the wild-type cells under these conditions (see Fig. 7.13) and suggests that the levels of the photosynthetic pigments (chlorophyll *a*) and protective carotenoids are different in the mutant cells. This led to analysis of the chlorophyll and carotenoid content of the cells under various growth conditions. A preliminary analysis of the pigments under normal growth conditions (447 μEinsteins m^{-2} s^{-1}, 12 hours light/12 hours dark) suggested that there were decreased levels of chlorophyll possibly coupled with increased carotenoids in the mutant cells. Pigments were identified based on their spectral properties, retention times and molecular mass in some cases. Preliminary analysis led to a more detailed investigation of the pigment levels under different growth conditions. In both the wild-type and sBVR-A mutant cells grown under low light the levels of chlorophyll are high and carotenoids are low. As the level of light increases the differences between the wild-type and mutant cells become more obvious. Under medium levels of light the increase in the levels of carotenoids, particularly myxoxanthophyll is more obvious, coupled with a slight decrease in the level of chlorophyll but under high levels of light the differences are most obvious. Now chlorophyll levels appear to be noticeably decreased in the sBVR-A mutant cells and levels of carotenoids are possibly higher. Interestingly, it appears that the carotenoid which shows the greatest change is myxoxanthophyll.

Mutant sBVR-A cells do not have the ability to make bilirubin IXα. As a result bilirubin IXα was included in the growth medium of both wild-type and mutant sBVR-A cells to investigate what effect, if any, it had on the growth of these cells. Interestingly, under conditions of light stress growth appears to be enhanced in the wild-type cells when bilirubin is present. Differences were also observed in the mutant cells when bilirubin was present. These cells were able to grow "normally" when compared to the wild-type cells grown without bilirubin. Although bilirubin appears to be having an effect more work is needed to investigate how bilirubin is causing this effect. It should also be noted that sBVR-A has the ability to reduce phycocyanobilin to the corresponding rubin (phycocyanorubin) *in vitro*. This means that phycocyanobilin which is used for light harvesting may be diverted from this important function. There is no evidence that this occurs *in vivo* and it is likely that sBVR-A is segregated and does not encounter phycocyanobilin within cells but it is also a possibility that phycocyanorubin is having an important physiological

effect. As discussed previously sBVR-A is most active at pH5 and therefore likely to be located in the intrathylakoid space. PcyA however has been shown to be active at pH7 and is likely to be located in the cytosol. It is unlikely therefore that sBVR-A encounters phycocyanobilin within the cell. Further work is needed to determine unambiguously the location of these enzymes within the cell using electron microscopy and to determine if *Synechocystis* make phycocyanorubin.

The analysis of the growth characteristics and levels of chlorophyll and protective carotenoids under various conditions suggests an important role for sBVR-A in *Synechocystis* sp. PCC6803. It would therefore prove informative to investigate if the expression levels of the enzymes responsible for the synthesis of the light harvesting pigment phycocyanobilin (HO1 and PcyA) or the apparently protective sBVR-A varied under different conditions, particularly stress conditions. This was done by growing cultures of wild-type *Synechocystis* cells, treating them under various conditions of light or with various chemicals and examining the effect on HO1, PcyA and sBVR-A levels using western-blotting. *Synechocystis* sp. PCC6803 has the ability to carry out respiration as well as photosynthesis. The main source of NADPH in the dark is the oxidative pentose phosphate pathway and an exogenous sugar such as glucose can serve as the source of electrons. The glucose tolerant strain of *Synechocystis* sp. PCC6803 used in this study can grow myxotrophically in the presence of glucose and because glucose was used in many of the experiments it was felt necessary to investigate if it had any effect on the levels of HO1, PcyA or sBVR-A. Glucose was found to have no effect on any of these enzymes. The product of the sBVR-A reaction, bilirubin IXα was found to increase the levels of HO1 slightly after 3hours and had little effect on the levels of sBVR-A or PcyA. The effect of light (low light and high light) on the levels of the enzymes was also investigated. Low levels of light were found to have little effect on the levels of HO1, PcyA or sBVR-A but high levels of light were found to decrease the levels of HO1 after 6 hours and increase the levels of sBVR-A after 6 hours, continuing up to 24 hours. No effect was obsered with PcyA. Hydrogen peroxide at various concentrations was used as an inducer of oxidative stress and at 1mM concentration was found to have little effect on HO1, PcyA or sBVR-A but at 10mM was found to decrease the levels of HO1 dramatically after 3hours and increase the levels of sBVR-A slightly after 3hours. Levels of PcyA remained unchanged. At 100mM H_2O_2 the levels of HO1 also decreased after 3hours, PcyA levels decreased after 6hours and sBVR-A levels appear to be increased slightly after 3hours and then decrease after 12hours. These are extremely harsh conditions and likely resulted in cell death. Norflurazon is an inhibitor of carotenoid biosynthesis in plants and cyanobacteria. It may be the case that sBVR-A effects the levels of certain carotenoids and there is likely to be much oxidative stress in these cells in the absence of carotenoids. In the presence of norflurazon HO1 levels decrease after 6hours and sBVR-A levels show a slight increase after 3 hours with the greatest increase in protein levels observed after 24

hours. Levels of PcyA remain unchanged. A pattern is observed through these experiments. In conditions of stress, induced by high light, H_2O_2 or a carotenoid inhibitor, levels of HO1 go down and levels of sBVR-A go up. Levels of PcyA remain unchanged and PcyA can therefore act as a protein loading control in most cases. It is also interesting that in conditions of stress a second immuno-reactive band appears to be present with the sBVR-A band which may suggest that sBVR-A is modified under these conditions. These results also suggest a possible protective role for sBVR-A. Also interesting is the fact that HO1 levels appear to go up after treatment with bilirubin. If bilirubin itself is having an anti-oxidative effect then a reduction in oxidative stress may cause an increase in HO1 levels. It is a possibility that under stress conditions there is a signaling mechanism leading to the repression of HO1 transcription. This mechanism may lead to down-regulation of light harvesting (a source of more reactive oxygen species) through the repression of phycocyanobilin synthesis. This mechanism will also lead to a reduction in biliverdin IXα and subsequently phycocyanobilin and maybe bilirubin IXα also. However experiments described in the present work suggest that only very low levels of bilirubin are required to have a significant effect.

Schluchter & Glazer, (1997) inactivated the sBVR-A gene in *Synechocystis* sp. PCC6803 and described a phenotype characterized by a decrease in protein bound phycocyanobilin by 83% and no complete phycobilisomes. The authors therefore suggest that inactivation of the sBVR-A gene suppresses but does not prevent synthesis of phycocyanobilin and phycobilisomes and suggest a regulatory role for sBVR-A where conversion of biliverdin to bilirubin directly modulates the flux of biliverdin into the phycocyanobilin biosynthesis pathway (Schluchter & Glazer, 1997). However, through personal communication with Dr. Wendy Schluchter (University of California, Berkley) we were informed that they inadvertently disrupted a gene required for incorporation of phycocyanobilin into the light harvesting complex. It is highly unlikely that a spontaneous or secondary mutation is responsible for the effects described in this work as multiple different mutants were created which show similar behaviour and it is unlikely that the same secondary mutation is responsible for the effects observed.

Experiments described in the present work using a strain of *Synechocystis* sp. PCC6803 which lacks sBVR-A and examining the effect of various conditions, as well as chemical agents suggest a protective role for biliverdin IXα reductase in *Synechocystis* sp. PCC6803. However, at this stage it is unclear how sBVR-A exerts this protective effect and more work is needed to investigate and clarify the effect. One possibility is that bilirubin IXα is a scavenger of reactive oxygen species (ROS), particularly singlet oxygen. There is evidence in mammals that bilirubin is carrying out this function (Stocker *et al.* 1987). Using RNA interference it was shown that cells depleted in

human BVR-A exhibited a 3-fold increase in the levels of ROS (Sedlak & Snyder, 2004). Cells which were depleted in the main physiological anti-oxidant glutathione by 95% only exhibited a 50% increase in ROS, suggesting that bilirubin is acting as a significant physiological anti-oxidant in these cells. Sedlak & Snyder (2004) propose a biliverdin reductase cycle to explain how bilirubin concentrations as low as 10nM can protect cultures from the oxidative stress caused by 10,000 times higher concentrations of H_2O_2. In this cycle lipophilic reactive oxygen species act directly on bilirubin causing it to re-oxidise to biliverdin. BVR-A then catalyzes the re-conversion of biliverdin to bilirubin in a BVR-A mediated biliverdin bilirubin redox cycle, thereby allowing bilirubin to detoxify a 10,000 fold excess of ROS (Sedlak & Snyder, 2004). It is possible that a similar cycle is operating in *Synechocystis.* However, in the absence of sBVR-A in Synechocystis bilirubin also appears to be having a affect which rules out the possibility of a BVR-A mediated redox cycle in these cells. In the sBVR-A knock-out strain described in this work the carotenoid myxoxanthophyll appears to be the carotenoid which is elevated the most under light stress conditions. Interestingly, myxoxanthophyll has been shown to be the carotenoid which has the highest induction in response to oxidative stress in four freshwater cyanobacteria (Schlagerl & Muller, 2006). In addition the same carotenoid has been shown to be the most effective in protection against peroxidation in *Synechocystis* sp. PCC6803 (Steiger *et al.,* 1999). Bilirubin has previously been shown to be an even more effective protectant against lipid peroxidation than vitamin E in mammals (Stocker *et al.,* 1987). This also lends support to the observation that sBVR-A is an anti-oxidative stress enzyme in cyanobacteria.

It is also a possibility that bilirubin is exerting an effect through a signalling mechanism leading to the induction of gene expression of antioxidative proteins in *Synechocystis.* In mammals bilirubin has been shown to bind to the aryl-hydrocarbon receptor (Ahr receptor) which is a ligand-dependent transcription factor that mediates many of the biological and toxicological actions of 2,3,7,8-tetrachlorodibenzo-*p*-dioxin (TCDD, dioxin) and related chemicals (Phelan *et al.* 1998). Bilirubin may be exerting a similar effect by binding to a protein within *Synechocystis* cells leading to transcription of certain anti-stress genes. In mammalian cells BVR-A has been shown to be translocated to the nucleus where it is involved in the regulation of the transcription factor ATF-2 and cAMP regulated genes and cell signalling leading to upregulation of anti-oxidative proteins, including HO1 (Kravets *et al.,* 2004). It is also possible that phycocyanorubin may be exerting the same effect and more work needs to be done to define the effect. Bilirubin or phycocyanorubin may also be acting in a signalling capacity as photoreceptors. Plants and cyanobacteria use visible light to sense their environmental conditions. Plants use phytochrome, a soluble chromoprotein with a bound linear tetrapyrrole (phytochromobilin) and use this photo sensor to mediate processes such as seed germination and flower induction. In *Synechocystis*

phycocyanobilin has been shown to be the linear tetrapyrrole chromophore for the bacteriophytochrome Cph1 (Hubschmann *et al.,* 2001). Biliverdin has also been shown to be the photoreceptor for the phytochrome BphP from *Bradyrhizobium* (Jorissen *et al.,* 2002). Recently another photoreceptor has been discovered in *Synechocystis*, PixJ1 which mediates positive phototactic motility (Yoshihara *et al.,* 2006). The authors of this study suggest that phycocyanobilin is also the chromophore of this photoreceptor but also suggest that phycocyanorubin could be carrying out the same effect.

Although effects are observed in *Synechocystis* sp. PCC6803 cells when the sBVR-A gene is disrupted, on protein levels under stress conditions and when bilirubin IXα is included in the growth medium of cells under high light conditions, why this effect is observed is presently unclear. More work is needed to define the effect, what exactly is causing the effect, is bilirubin directly causing the effect by scavenging ROS or binding to an intracellular protein or initiating a signaling mechanism. It is also possible, although unlikely that phycocyanorubin is the physiologically important product of the sBVR-A reaction and future work is needed to clarify the relationship between sBVR-A and the apparent oxidative stress observed in *Synechocystis* sp. PCC6803 in the present work (see Fig. 5.28 for a model of oxidative stress in cyanobacteria and a possible role for sBVR-A.

Gene	Primer	Direction	$T_{m.}$ (^{O}C)	Size (bp)	Sequence
sBVR-A	Oligo 1.	Forward	66.3	25	5' TAT.G GATCC.TACCCCCAGGGAACA 3' (BamH1)
sBVR-A	Oligo 2.	Reverse	66.3	25	5' TGT.G AATTCGTCCCCTTTCCGGCAG 3' (EcoR1)
Genomic screening primers					
S.P 1	Oligo 3.	Forward	66.7	29	5' GTGGTGATTTTAAGGTGGATTTAGCGGGG 3'
S.P 1	Oligo 4	Reverse	66.7	29	5' CGCTCGTCATCAAAATCACTCGCATCAAC 3'
S.P 2	Oligo 5	Forward	72.2	30	5' TCCAGTCGTTGCCGGTGGTGTTTCTCACGG 3'
S.P 2	Oligo 6	Reverse	72.4	28	5' ACGGTGGTGGGTTTAATGGGGACGGCGG 3'

Table 7.1 Primers used for the construction of the sBVR-A knock-out construct and for genomic screening of sBVR-A knock-out clones

Direction, size and melting temperatures are indicated. Restriction sites where applicable are underlined. Restriction enzymes used are shown in red. Arrows indicate exact site of restriction. The set of sBVR-A primers were used to amplify the sBVR-A gene plus 513bp homology regions from *Synechocystis* sp. PCC6803 genomic DNA.
The S.P1 primers indicate the set of screening primers used to verify the location of the knock-out construct in the *Synechocystis* genome and are shown in yellow in the sequence file shown in Fig. 7.5. The S.P2 primers indicate the set of screening primers used to estimate the degree of segregation of the wild-type and knock-out alleles and are shown in green in the sequence files shown in Figs. 7.4 and 7.5

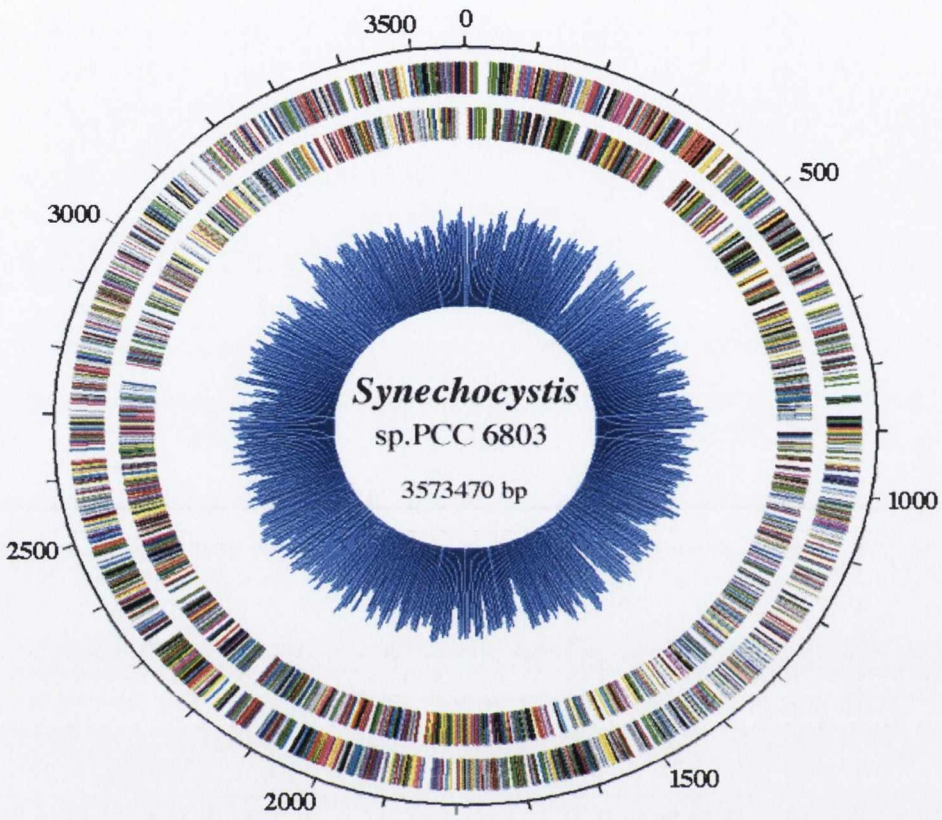

Figure. 7.1 Genome of *Synechocystis* sp. PCC6803

Every *Synechocystis* cell contains up to 12 copies of this 3.5mb circular chromosome. There are a predicted 3168 protein coding genes contained within this genome. The sBVR-A gene is annotated as slr1784 and is located from 243158-244144

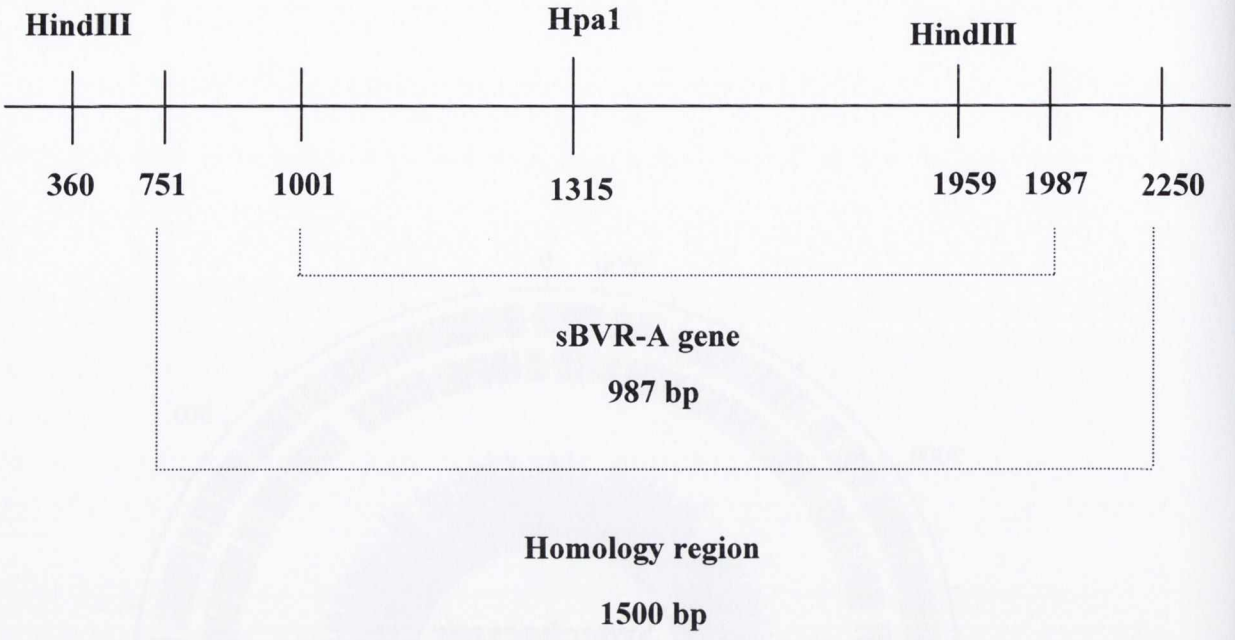

Figure 7.2 A physical map of the wild-type sBVR-A allele

Shown are restriction sites used for insertion of the kanamycin resistance cassette and for possible Southern blotting. Numbers correspond to the sequence file shown in Fig. 7.4

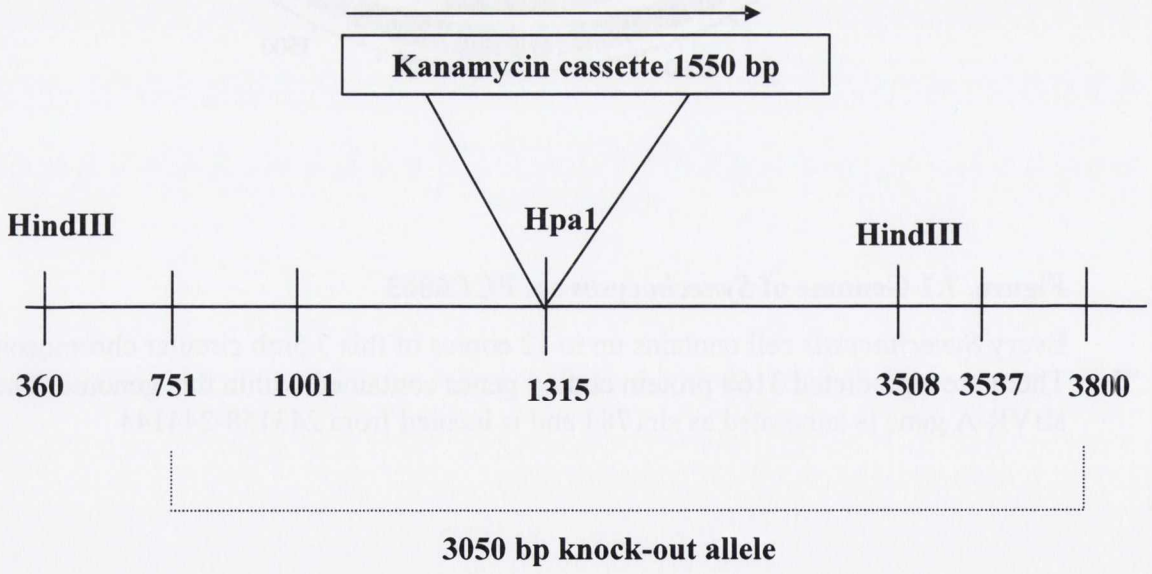

Figure 7.3 A physical map of the sBVR-A knock-out allele

Shown is the kanamycin resistance cassette inserted into the unique Hpa-1 site. Numbers correspond to the sequence file shown in Fig. 7.5. The arrow represents the direction of transcription of the kanamycin resistance gene

Upstream Sequence

```
     1 TTGTGGGCAA TAGACTAGCC CAAGCAAACT TGGGGGCCGG AGTGGGAGTT
    51 GCCGAACGGT TTCTTGGGAT GGATTGACTC AACCCCGGGT GGGCTTGAGT
   101 TTGCTGCGCC CCAGGCTAGT TTTTCTTGAG TTTATCCCCC GTGATAGGCT
   151 GATGGGGGGA GGAATCAGCC AGTCTGGCAA CCTGCTACGA TCGCCTCCTA
   201 CTAAACCGCC CTATTTACCT TTGCACGACT GCATTACCGC CATGGCAGAA
   251 CCCATTTCCC TATTGTTAGT TGATGATGAA CCCGGTGTAC GGGAATCCGT
   301 GCAGGCGTTC CTAGAAGATA GTGGTGATTT TAAGGTGGAT TTAGCGGCCA
   351 ATGCCACGGA AGCTTGGGAT TATCTTCAGC ACCATTTGCC GGCTTTGGTC
   401 ATTTCCGACA TTATGATGCC CCAGGTGGAC GGTTATCAGT TTTTGCAAAA
   451 GCTCCGGGAG GATGCCCGCT TCCAGTCGTT GCCGGTGGTG TTTCTCACGG
   501 CCCGGGGGAT GACTGGCGAT CGCATTCAAG GTTATCAAAC TGGCTGTGAC
   551 GCTTTTTTAT CCAAGCCCTT TGACCCCGAT GAATTGGAGG CGATCGTCCG
   601 TAATTTATTA GCTCGTCAAC AGGCCAGTAG CGATGCGGGC AGTGAATCGG
   651 CTAAGTTACA GGAAATTTAC CAGGAAATCC GGGCTTTAAA GGAGCAAATT
   701 GGCCAACCCA GCGGTATCCA CACCACTCCG TCGCCGATCA AGCTGGATTT
```

Homology Region 1

```
   751 TACCCCCAGG GAACAGAGCG TTTTAGATTT GGTTTCCCAG GGCTTAATGA
   801 ACAAAGAAAT TGCGGCCCAG TTGAAGACCA GTGTCCGCAA CGTGGAAAAG
   851 TATGTCAGTC GTTTATTTAC CAAAACTGGG ACTAATAGCC GCACTGAATT
   901 AGTTCGTTTT GCCCTGCAAC ACGGCTTAAC AGAATAACTA TGACAAGTTC
   951 GCAGCAATTA TTTGGTTGAG CCAGTCTTTT TTGATTTTTC CCAAGGTACT
  1001 ATGTCTGAAA ATTTTGCAGT TGCTACGCCG GTGCGGGTCG GAATTGTCGG
  1051 TACTGGTTAT GCGGCCCAAC GTCGGGCGGA AGTTTTCCGG GGCGATCGCC
  1101 GTAGTCAATT GGTTAGTTTT TGGGGCAATA GTGAAGCCAA TACAGCTAAA
  1151 TTTGCCGATA CTTTTGGAGT TAGACCCCAG CAATCTTGGC AGGCATTAAT
  1201 TAATGATCCA GAGATAGATT TAGTGCTCAT TGCCACCATT AACCAACTCC
  1251 ATGGGGCGAT CGCCGAGGCG GCATTGCAAG CCGGTAAACA TGTGGTGTTG
  1301 GAATATCCTT TAGCGTTAAC CTATGCCATG GGCAAAAAAC TACAACAGTT
  1351 AGCCCGGGAA AAAGGTAAAT TACTGCATGT GGAACATATT GAACTATTGG
  1401 GGGGAGTACA CCAAGCCATT CGCCAGAACC TAGGCAAAAT TGGTGAGGTT
  1451 TTTTACGCCC GCTATAGCAC CATCATGGGA CAAAATCCCG CTCCCCAACG
  1501 TTGGACCTAT CACCATCAGC AATTTGGCTT TCCTTTAGTG GCGGCCTTGT
  1551 CCCGCATCAG TCGGTTTACG GATTTATTCG GTACAGTACA GCAGGTGGAT
  1601 GCCCAATGTC GTTTTTGGGA TCAGCCTAAT CCGGAATATT TTCGGGCTTG
  1651 TTTAGCCACC GCCTATCTCC AGTTTAATAA TGGTCTTAAA GCGGAGGTTA
  1701 TCTATGGCAA AGGGGAAGTT TTTCACCAGA ATGAACGGAT TTTTACCCTC
  1751 CATGGCGATC GAGGCACCTT AATTTTTGTC GGGGAAACAG GTAGGTTAAT
  1801 TCAGGGACAA ACGGAAACTG AAATTACCGT TGGTAGTCGT CGAGGACTGT
  1851 TCAGACAAGA CACGGAAGCA GTGTTGGATT ATCTAACCAC TGGTAAGCCC
  1901 CTTTATGTGG ATTTAGAAGC TAGTTTATAT GCTTTAGAAG TGGCGGATCT
  1951 CTGTGCCCAA GCTTGTGGAT ATAAGGTTGA AAATTAGCGG AAATATCGGC
```

Homology Region 2

```
  2001 AGTTAGCCAA ACAAAAATTG GCAGATATAA ACTGCTGAAA AAATCCCCAC
  2051 TACATCGGCC GTCAGCCCGG CCAGAAGGGC ATAGCGAATT TTTTTAATGC
  2101 CCACTGAACC AAAATAAACC GCCAGTACGT AAAATGTGGT TTCCGTAGAA
  2151 CCAAACATGG TGGCCGCAGT TTTCGCAATC AAGGAATCGG GGCCATGTTG
  2201 TTCTACCAAG TCAGCAAACA AACCAAAGGA ACCACTGCCG GAAAGGGGAC
  2251 GCATTAGGGC CAACAGTAAG TTCTCCGGCG GAAAATTGAC CAAACTCAAC
  2301 ACTGGGCTAA GCACCGTCAG CAATAAATCC AGCATGCCAG AAGCCCGAAA
  2351 CATGGCGATC GCCACTAGCA TAGCCACTAG GAAAGGAATA ATCCTCACGG
  2401 CAATGGTGAA ACCTTCCTGG GCTCCGTCCA CAAAAACTTC GTAAACTTTA
  2451 ACTTTTTTGA CCACCAGGCC ATAAAAGGGA ATGCCACAGA GCAAAAAGGG
```

```
2501 AATAACATAT TTTGCTCCAG CATTAAAAAT ATCAGCGACG GATTCGAGCA
2551 TTATTTTTCT ATATCCTGGG GGAAGTAAAA AGCACTAACA ATTAGTTCTT
2601 ATAGTTTTTA TATTTATCAA ACAAGTTAAT TAAATTCTTC TTCTGGTTCC
2651 ACCGTAGCAG GCAAAGCAAA TATCTTAAGT CGGGCTAAAA GTTTAGCTGC
2701 AATAATGGCT GTTGCCGTGG AACAAGTAGT AGCCAAAATT GTTGAGAAAA
2751 AAATGTCATT GGCCGCCGTC CCCATTAAAC CCACCACCGT AGCAGGCAAA
2801 ATTAATTGCA CACTGGAAGT ATTAATAGCT AAAAACATAC ACATGGCATC
2851 GGTGGCGATA CTTTTATTGG GATTGATTTC CTCCAACTCC TGCATCGCTT
2901 TTAAGCCCAA AGGGGTGGCC GCATTACCTA GTCCCAAAAT ATTGGCGGAC
2951 ATATTCAACA CAATGGAACC GATCGCCGGA TGCTCTG

Downstream Sequence
```

Figure 7.4 Sequence file of the sBVR-A wild-type allele

Shown in red is the sBVR-A gene, homology regions (shown in blue) and upstream and downstream sequence. Also shown is the unique Hpa-1 restriction site in yellow. Shown in green are the screening primers used to estimate the degree of segregation of the wild-type and knock-out alleles

Upstream Sequence

```
   1 TTGTGGGCAA TAGACTAGCC CAAGCAAACT TGGGGGCCGG AGTGGGAGTT
  51 GCCGAACGGT TTCTTGGGAT GGATTGACTC AACCCCGGGT GGGCTTGAGT
 101 TTGCTGCGCC CCAGGCTAGT TTTTCTTGAG TTTATCCCCC GTGATAGGCT
 151 GATGGGGGGA GGAATCAGCC AGTCTGGCAA CCTGCTACGA TCGCCTCCTA
 201 CTAAACCGCC CTATTTACCT TTGCACGACT GCATTACCGC CATGGCAGAA
 251 CCCATTTCCC TATTGTTAGT TGATGATGAA CCCGGTGTAC GGGAATCCGT
 301 GCAGGCGTTC CTAGAAGATA GTGGTGATTT TAAGGTGGAT TTAGCGGCCA
 351 ATGCCACGGA AGCTTGGGAT TATCTTCAGC ACCATTTGCC GGCTTTGGTC
 401 ATTTCCGACA TTATGATGCC CCAGGTGGAC GGTTATCAGT TTTTGCAAAA
 451 GCTCCGGGAG GATGCCCGCT TCCAGTCGTT GCCGGTGGTG TTTCTCACGG
 501 CCCGGGGGAT GACTGGCGAT CGCATTCAAG GTTATCAAAC TGGCTGTGAC
 551 GCTTTTTTAT CCAAGCCCTT TGACCCCGAT GAATTGGAGG CGATCGTCCG
 601 TAATTTATTA GCTCGTCAAC AGGCCAGTAG CGATGCGGGC AGTGAATCGG
 651 CTAAGTTACA GGAAATTTAC CAGGAAATCC GGGCTTTAAA GGAGCAAATT
 701 GGCCAACCCA GCGGTATCCA CACCACTCCG TCGCCGATCA AGCTGGATTT
```

Homology Region 1

```
 751 TACCCCCAGG GAACAGAGCG TTTTAGATTT GGTTTCCCAG GGCTTAATGA
 801 ACAAAGAAAT TGCGGCCCAG TTGAAGACCA GTGTCCGCAA CGTGGAAAAG
 851 TATGTCAGTC GTTTATTTAC CAAAACTGGG ACTAATAGCC GCACTGAATT
 901 AGTTCGTTTT GCCCTGCAAC ACGGCTTAAC AGAATAACTA TGACAAGTTC
 951 GCAGCAATTA TTTGGTTGAG CCAGTCTTTT TTGATTTTTC CCAAGGTACT
1001 ATGTCTGAAA ATTTTGCAGT TGCTACGCCG GTGCGGGTCG GAATTGTCGG
1051 TACTGGTTAT GCGGCCCAAC GTCGGGCGGA AGTTTTCCGG GGCGATCGCC
1101 GTAGTCAATT GGTTAGTTTT TGGGGCAATA GTGAAGCCAA TACAGCTAAA
1151 TTTGCCGATA CTTTTGGAGT TAGACCCCAG CAATCTTGGC AGGCATTAAT
1201 TAATGATCCA GAGATAGATT TAGTGCTCAT TGCCACCATT AACCAACTCC
1251 ATGGGGCGAT CGCCGAGGCG GCATTGCAAG CCGGTAAACA TGTGGTGTTG
1301 GAATATCCTT TAGCGTTGGC ACGACAGGTT TCCCGACTGG AAAGCGGGCA
```

Kanamycin Cassette

```
1351 GTGAGCGCAA CGCAATTAAT GTGAGTTAGC TCACTCATTA GGCACCCCAG
1401 GCTTTACACT TTATGCTTCC GGCTCGTATG TTGTGTGGAA TTGTGAGCGG
1451 ATAACAATTT CACACAGGAA ACAGCTATGA CCATGATTAC GAATTCCCCG
1501 GATCCGTCGA CCTGCAGGGG GGGGGAAAGC CACGTTGTGT CTCAAAATCT
1551 CTGATGTTAC ATTGCACAAG ATAAAAATAT ATCATCATGA ACAATAAAAC
1601 TGTCTGCTTA CATAAACAGT AATACAAGGG GTGTTATGAG CCATATTCAA
1651 CGGGAAACGT CTTGCTCGAG GCCGCGATTA AATTCCAACA TGGATGCTGA
1701 TTTATATGGG TATAAATGGG CTCGCGATAA TGTCGGGCAA TCAGGTGCGA
1751 CAATCTATCG ATTGTATGGG AAGCCCGATG CGCCAGAGTT GTTTCTGAAA
1801 CATGGCAAAG GTAGCGTTGC CAATGATGTT ACAGATGAGA TGGTCAGACT
1851 AAACTGGCTG ACGGAATTTA TGCCTCTTCC GACCATCAAG CATTTTATCC
1901 GTACTCCTGA TGATGCATGG TTACTCACCA CTGCGATCCC CGGGAAAACA
1951 GCATTCCAGG TATTAGAAGA ATATCCTGAT TCAGGTGAAA ATATTGTTGA
2001 TGCGCTGGCA GTGTTCCTGC GCCGGTTGCA TTCGATTCCT GTTTGTAATT
2051 GTCCTTTTAA CAGCGATCGC GTATTTCGTC TCGCTCAGGC GCAATCACGA
2101 ATGAATAACG GTTTGGTTGA TGCGAGTGAT TTTGATGACG AGCGTAATGG
2151 CTGGCCTGTT GAACAAGTCT GGAAAGAAAT GCATAAGCTT TTGCCATTCT
2201 CACCGGATTC AGTCGTCACT CATGGTGATT TCTCACTTGA TAACCTTATT
2251 TTTGACGAGG GGAAATTAAT AGGTTGTATT GATGTTGGAC GAGTCGGAAT
2301 CGCAGACCGA TACCAGGATC TTGCCATCCT ATGGAACTGC CTCGGTGAGT
2351 TTTCTCCTTC ATTACAGAAA CGGCTTTTTC AAAAATATGG TATTGATAAT
2401 CCTGATATGA ATAAATTGCA GTTTCATTTG ATGCTCGATG AGTTTTTCTA
2451 ATCAGAATTG GTTAATTGGT TGTAACACTG GCAGAGCATT ACGCTGACTT
```

2501 GACGGGACGG CGGCTTTGTT GAATAAATCG AACTTTTGCT GAGTTGAAGG
2551 ATCAGATCAC GCATCTTCCC GACAACGCAG ACCGTTCCGT GGCAAAGCAA
2601 AAGTTCAAAA TCACCAACTG GTCCACCTAC AACAAAGCTC TCATCAACCG
2651 TGGCTCCCTC ACTTTCTGGC TGGATGATGG GGCGATTCAG GCCTGGTATG
2701 AGTCAGCAAC ACCTTCTTCA CGAGGCAGAC CTCAGCGCCC CCCCCCCCCT
2751 GCAGGTCGAC GGATCCGGGG AATTCACTGG CCGTCGTTTT ACAACGTCGT
2801 GACTGGGAAA ACCCTGGCGT TACCCAACTT AATCGCCTTG CAGCGTGTTG
2851 GAATATCCTT TAGCGTTAAC CTATGCCATG GGCAAAAAAC TACAACAGTT
2901 AGCCCGGGAA AAAGGTAAAT TACTGCATGT GGAACATATT GAACTATTGG
2951 GGGGAGTACA CCAAGCCATT CGCCAGAACC TAGGCAAAAT TGGTGAGGTT
3001 TTTTACGCCC GCTATAGCAC CATCATGGGA CAAAATCCCG CTCCCCAACG
3051 TTGGACCTAT CACCATCAGC AATTTGGCTT TCCTTTAGTG GCGGCCTTGT
3101 CCCGCATCAG TCGGTTTACG GATTTATTCG GTACAGTACA GCAGGTGGAT
3151 GCCCAATGTC GTTTTTGGGA TCAGCCTAAT CCGGAATATT TTCGGGCTTG
3201 TTTAGCCACC GCCTATCTCC AGTTTAATAA TGGTCTTAAA GCGGAGGTTA
3251 TCTATGGCAA AGGGGAAGTT TTTCACCAGA ATGAACGGAT TTTTACCCTC
3301 CATGGCGATC GAGGCACCTT AATTTTTGTC GGGGAAACAG GTAGGTTAAT
3351 TCAGGGACAA ACGGAAACTG AAATTACCGT TGGTAGTCGT CGAGGACTGT
3401 TCAGACAAGA CACGGAAGCA GTGTTGGATT ATCTAACCAC TGGTAAGCCC
3451 CTTTATGTGG ATTTAGAAGC TAGTTTATAT GCTTTAGAAG TGGCGGATCT
3501 CTGTGCCCAA GCTTGTGGAT ATAAGGTTGA AAATTAGCGG AAATATCGGC

Homology Region 2

3551 AGTTAGCCAA ACAAAAATTG GCAGATATAA ACTGCTGAAA AAATCCCCAC
3601 TACATCGGCC GTCAGCCCGG CCAGAAGGGC ATAGCGAATT TTTTTAATGC
3651 CCACTGAACC AAAATAAACC GCCAGTACGT AAAATGTGGT TTCCGTAGAA
3701 CCAAACATGG TGGCCGCAGT TTTCGCAATC AAGGAATCGG GGCCATGTTG
3751 TTCTACCAAG TCAGCAAACA AACCAAAGGA ACCACTGCCG GAAAGGGGAC
3801 GCATTAGGGC CAACAGTAAG TTCTCCGGCG GAAAATTGAC CAAACTCAAC
3851 ACTGGGCTAA GCACCGTCAG CAATAAATCC AGCATGCCAG AAGCCCGAAA
3901 CATGGCGATC GCCACTAGCA TAGCCACTAG GAAAGGAATA ATCCTCACGG
3951 CAATGGTGAA ACCTTCCTGG GCTCCGTCCA CAAAAACTTC GTAAACTTTA
4001 ACTTTTTTGA CCACCAGGCC ATAAAAGGGA ATGCCACAGA GCAAAAAGGG
4051 AATAACATAT TTTGCTCCAG CATTAAAAAT ATCAGCGACG GATTCGAGCA
4101 TTATTTTTCT ATATCCTGGG GGAAGTAAAA AGCACTAACA ATTAGTTCTT
4151 ATAGTTTTTA TATTTATCAA ACAAGTTAAT TAAATTCTTC TTCTGGTTCC
4201 ACCGTAGCAG GCAAAGCAAA TATCTTAAGT CGGGCTAAAA GTTTAGCTGC
4251 AATAATGGCT GTTGCCGTGG AACAAGTAGT AGCCAAAATT GTTGAGAAAA
4301 AAATGTCATT GGCCGCCGTC CCCATTAAAC CCACCACCGT AGCAGGCAAA
4351 ATTAATTGCA CACTGGAAGT ATTAATAGCT AAAAACATAC ACATGGCATC
4401 GGTGGCGATA CTTTTATTGG GATTGATTTC CTCCAACTCC TGCATCGCTT
4451 TTAAGCCCAA AGGGGTGGCC GCATTACCTA GTCCCAAAAT ATTGGCGGAC
4501 ATATTCAACA CAATGGAACC GATCGCCGGA TGCTCTG

Downstream Sequence

Figure 7.5 Sequence file of the sBVR-A knock-out allele

Shown in red is the sBVR-A gene disrupted by the 1550bp kanamycin resistance cassette (shown in pink), homology regions are shown in blue, screening primers used to determine the location of the construct in the *Synechocystis* genome are shown in yellow, screening primers used to determine the degree of segregation are shown in green and the unique Xho-1 restriction within the kanamycin cassette is shown in turquoise.

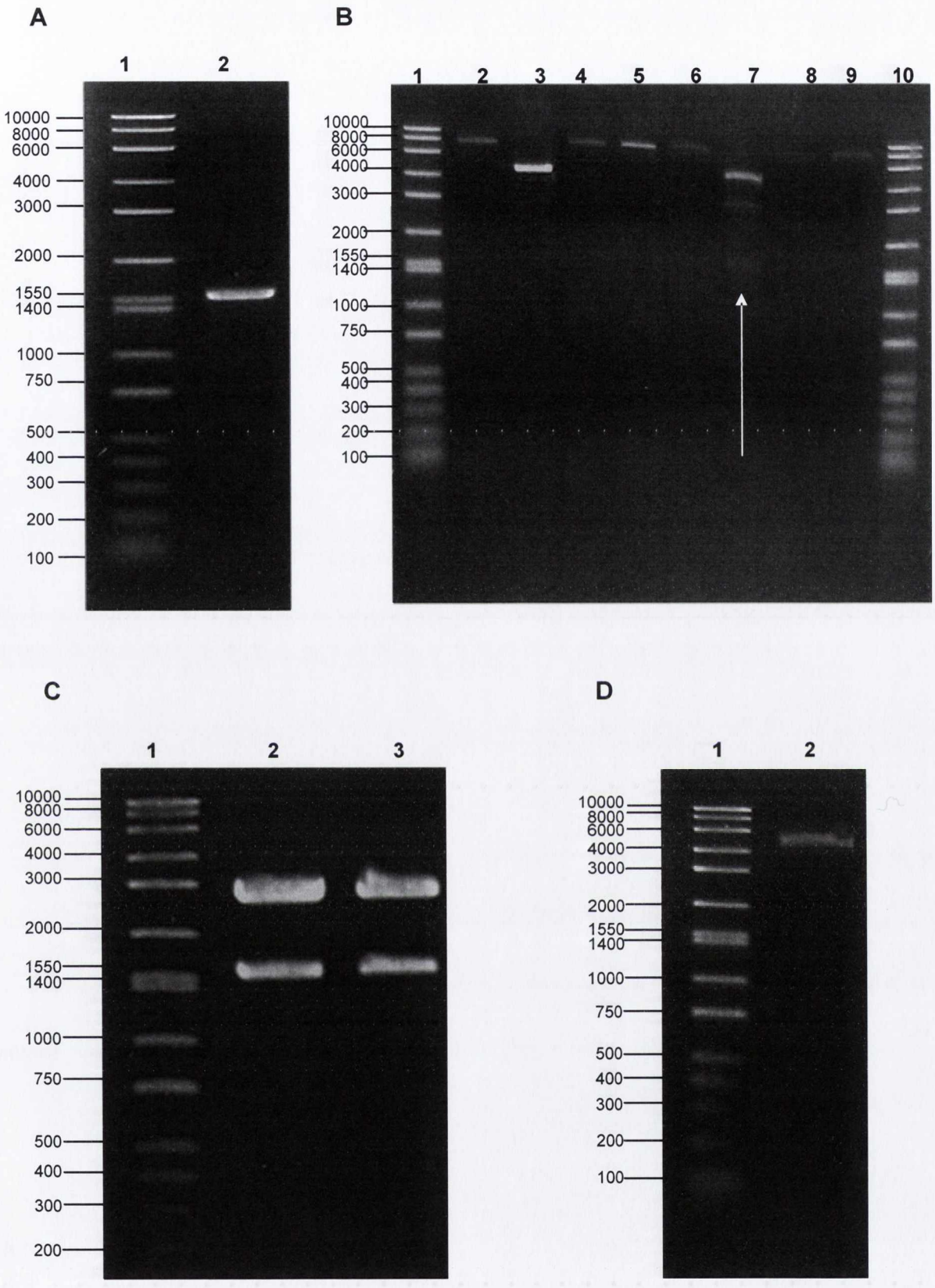
A
1
2
10000
8000
6000
4000
3000
2000
1550
1400
1000
750
500
400
300
200
100
B
1
2
3
4
5
6
7
8
9
10
10000
8000
6000
4000
3000
2000
1550
1400
1000
750
500
400
300
200
100
C
1
2
3
10000
8000
6000
4000
3000
2000
1550
1400
1000
750
500
400
300
200
D
1
2
10000
8000
6000
4000
3000
2000
1550
1400
1000
750
500
400
300
200
100

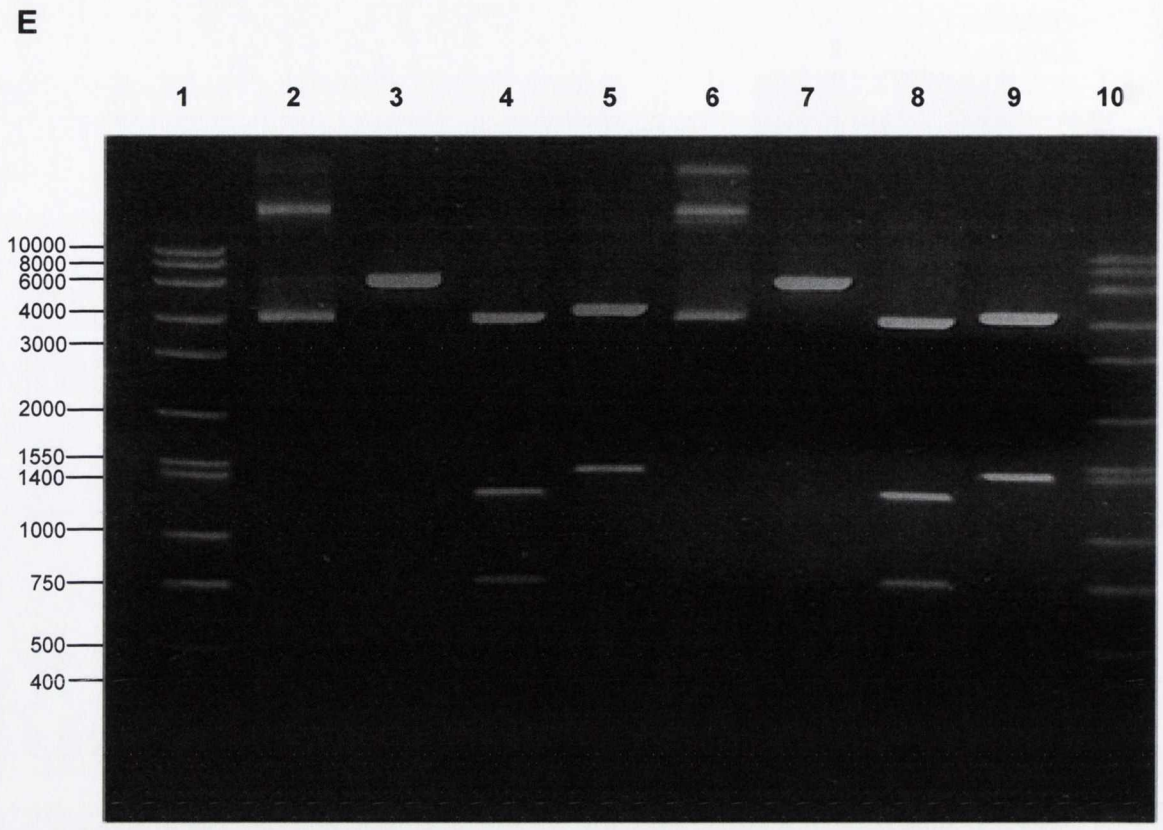

Fig. 7.6 Construction of the sBVR-A knock-out construct

A. PCR amplification of the 1500bp sBVR-A gene plus homology regions

B. Restriction digest (BamH1/EcoR1) of pBBVR-A showing the 1500bp DNA fragment in lane 7

C. Kanamycin resistance cassette digested from the pUC4K vector using Pvu-II

D. pBBVR-A digested with Hpa-1

E. Restriction analysis of 2 pBBVR-Akan clones verifying the orientation of the kanamycin resistance cassette. Lanes 2 and 6 are digested with Hpa-1 which does not cut the plasmid, lanes 3 and 7 are digested with Not-1 which cuts the plasmid once, lanes 4 and 8 are digested with Bam-H1 which digests the plasmid 3 times and lanes 5 and 9 are digested with Hind-III which digests the plasmid 3 times. The restriction digests confirm that the kanamycin cassette is cloned in the forward direction.

Lane 1 in all cases contains molecular weight markers

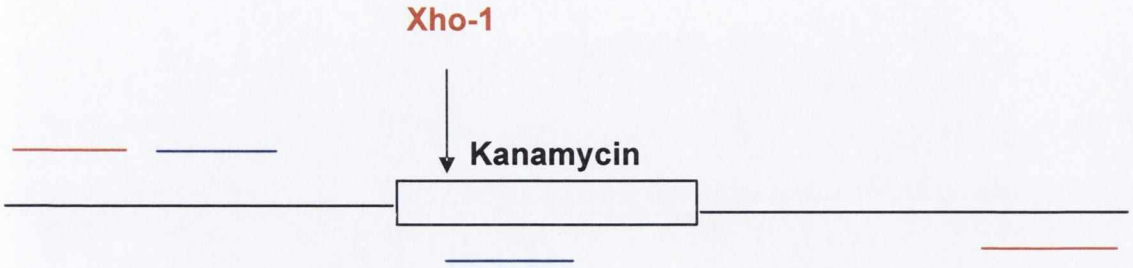

Figure 7.7 Schematic representation of the sBVR-A knock-out allele, showing the regions of DNA where the screening primers anneal.

Shown in blue are the set of screening primers shown in Fig. 7.5 and Table 7.1 used to verify the location of the knock-out construct in the *Synechocystis* genome and in red are the set of screening primers shown in Figs. 7.4 and 7.5 and Table 7.1 used to estimate the degree of segregation of the wild-type and knock-out alleles. The unique Xho-1 restriction site within the kanamycin resistance cassette is indicated by the arrow.

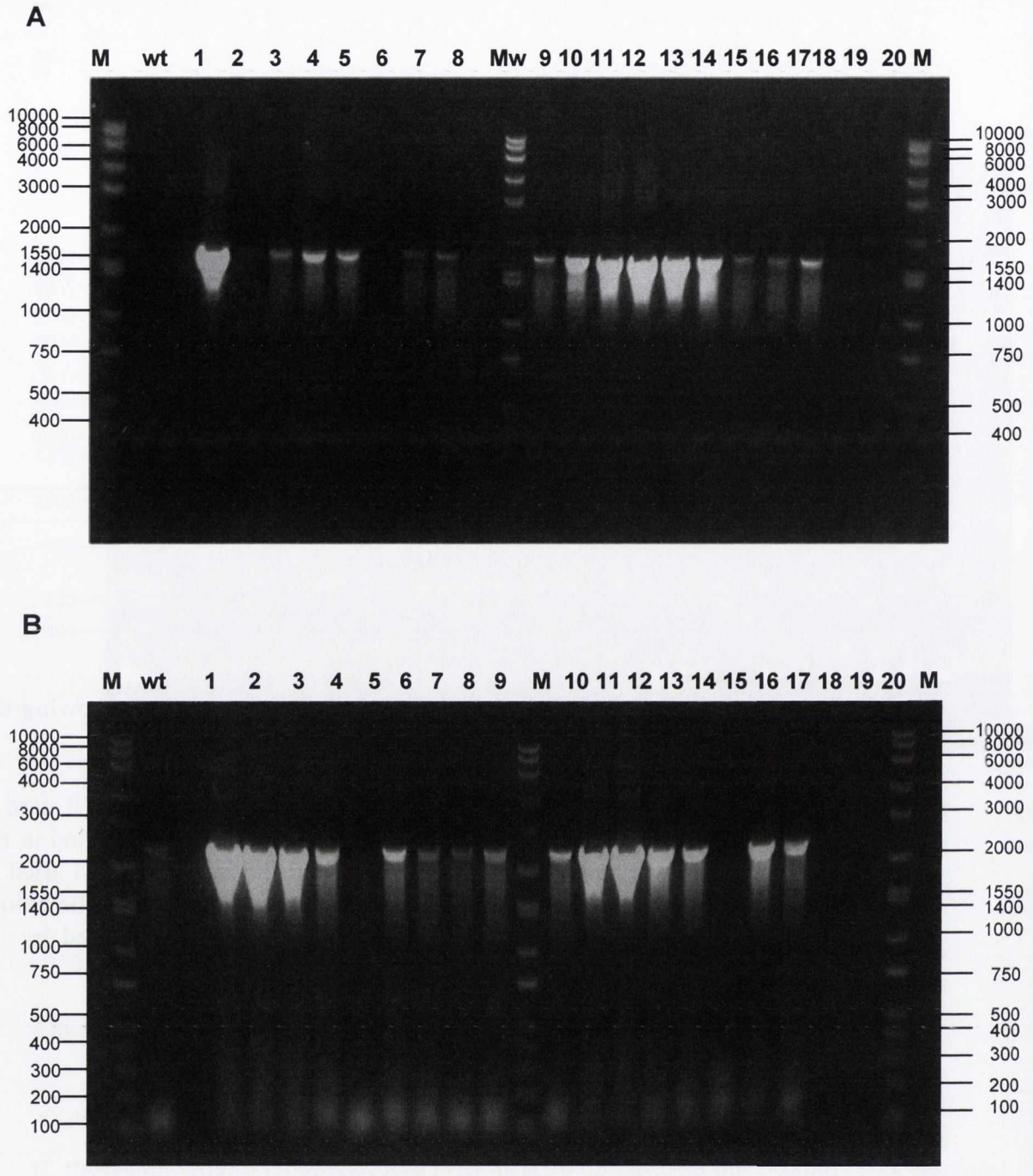

Figure 7.8 Genomic screening of sBVR-A knock-out clones

A. Screening for recombination of the knock-out construct in the correct location in the *Synechocystis* genome. The PCR product (1823bp) indicates that the construct has been correctly recombined. The wild-type (wt) lane contains no product as no knock-out construct is present in these cells. Different clones are numbered 1-20 and molecular weight markers are represented by M.

B. Screening for segregation of the wild-type and knock-out alleles. The wild-type (wt) PCR product consists of 2300bp. The knock-out allele consists of 3850bp. It is shown in all the clones (1-20) that the wild-type allele is present and in the majority of copies and no segregation has occurred in any of the clones tested

A

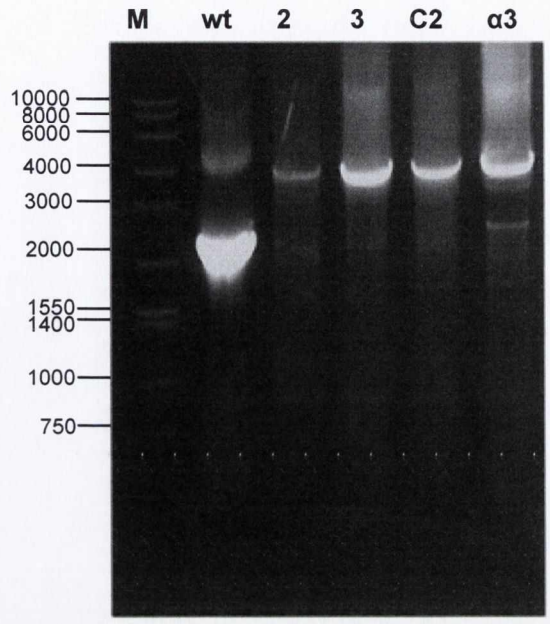

B

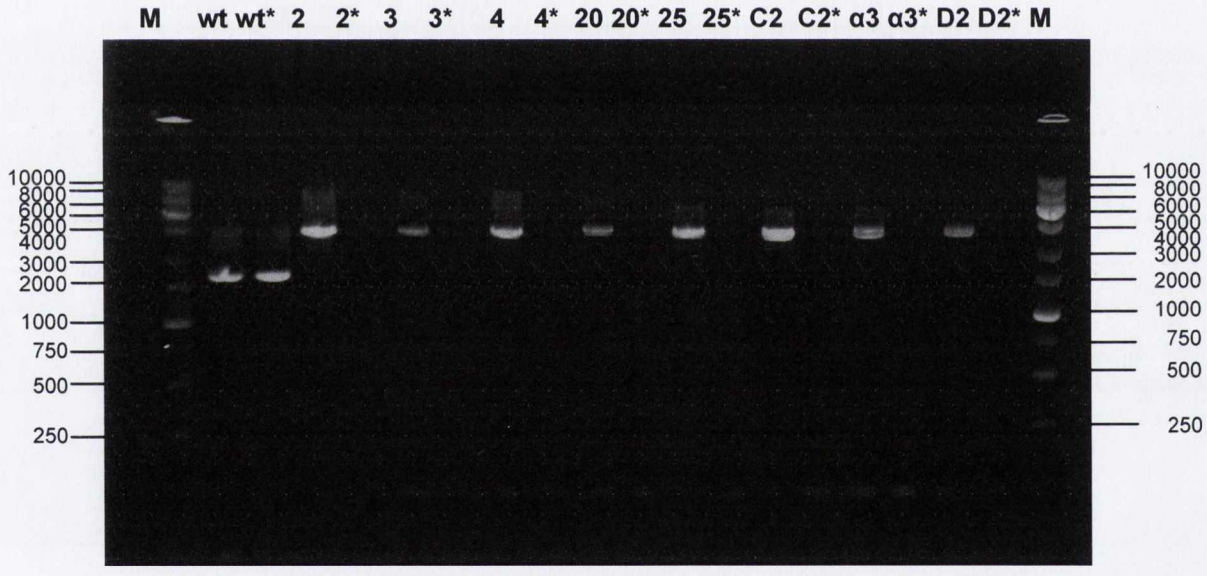

Figure 7.9 Segregation of the wild-type and sBVR-A knock-out alleles

A. Signs of segregation of the wild-type (wt) allele (2320bp) and the knock-out allele (3780bp) in the selected clones 2, 3, C2 and α3. M represents molecular weight markers.

B. Completely segregated sBVR-A knock-out mutants. Mutant names are indicated in each lane. * represents genomic DNA from wild-type or knock-out cells digested with Xho-1 which results in no PCR product formed for the knock-out cells. Xho-1 has no effect on wild-type DNA. Mw represents molecular weight markers.

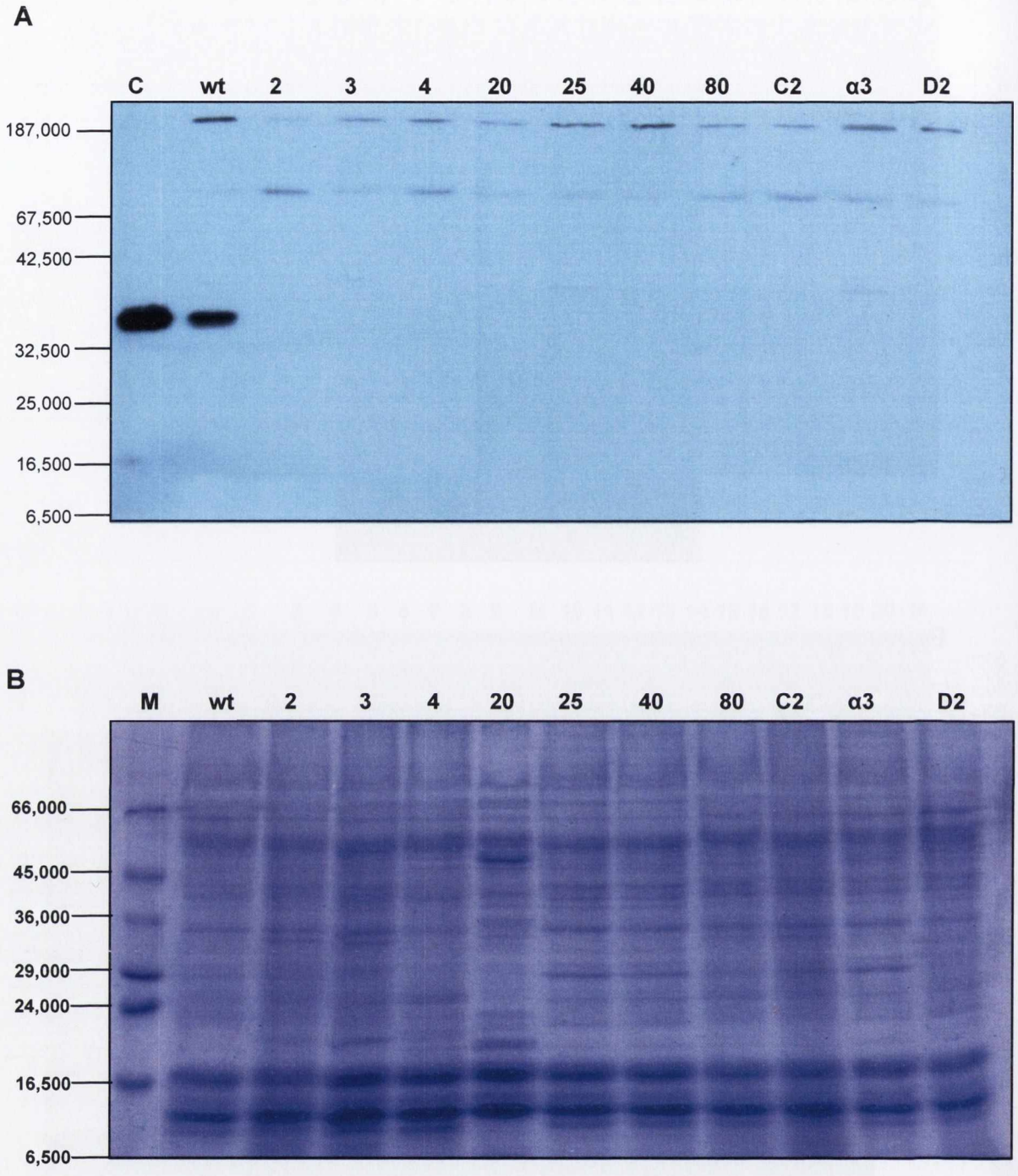

Figure 7.10 Detection of sBVR-A protein in wild-type and sBVR-A knock *Synechocystis* cells by western blotting

A. Western blot of wild-type (wt) and sBVR-A knock-out cells. C represents a 20rg recombinant sBVR-A protein control. The name of each clone is shown at the tip of each well. Mobility of molecular weight standards is indicated

B. SDS-PAGE loading control

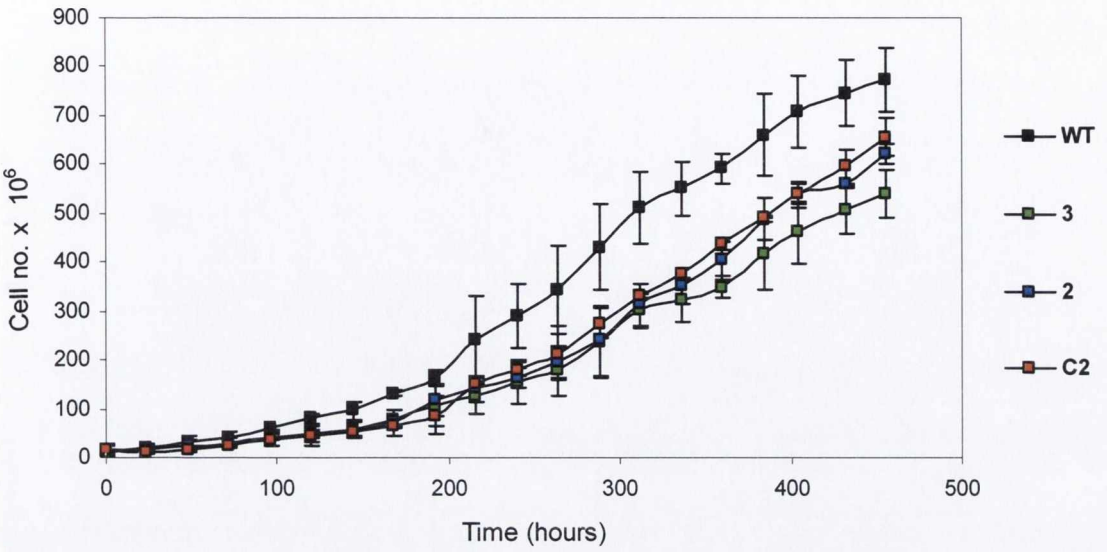

Figure 7.11 Analysis of the growth characteristics of the wild-type *Synechocystis* and sBVR-A knock-out cells under low light conditions (224 µEinsteins m^{-2} s^{-1}), 8 hours light, 16 hours dark

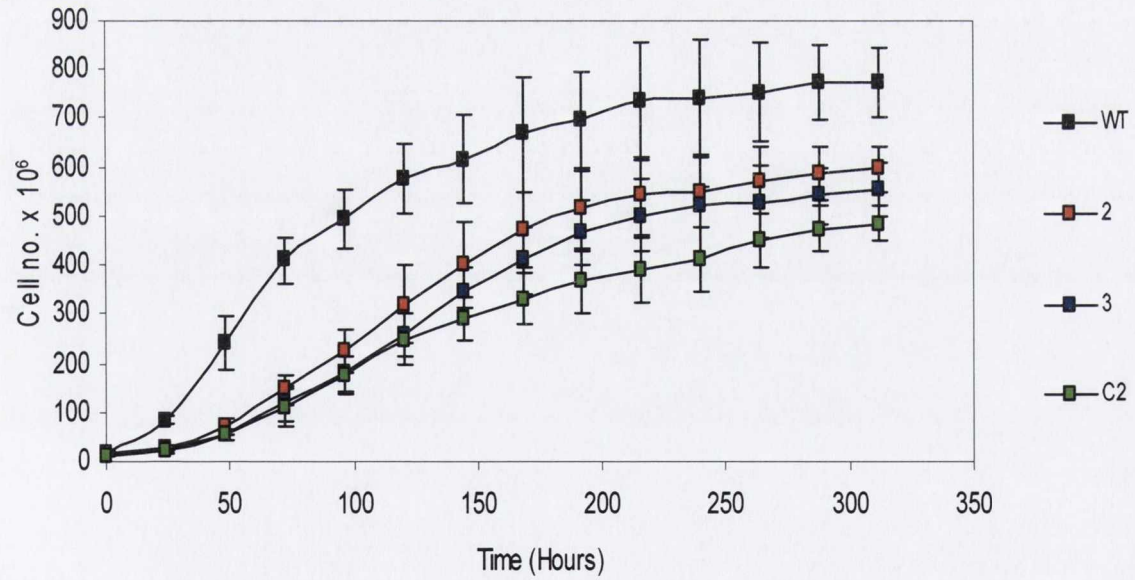

Figure 7.12 Analysis of the growth characteristics of the wild-type *Synechocystis* and sBVR-A knock-out cells under high light conditions (895 µEinsteins m^{-2} s^{-1}), 24 hours light

A

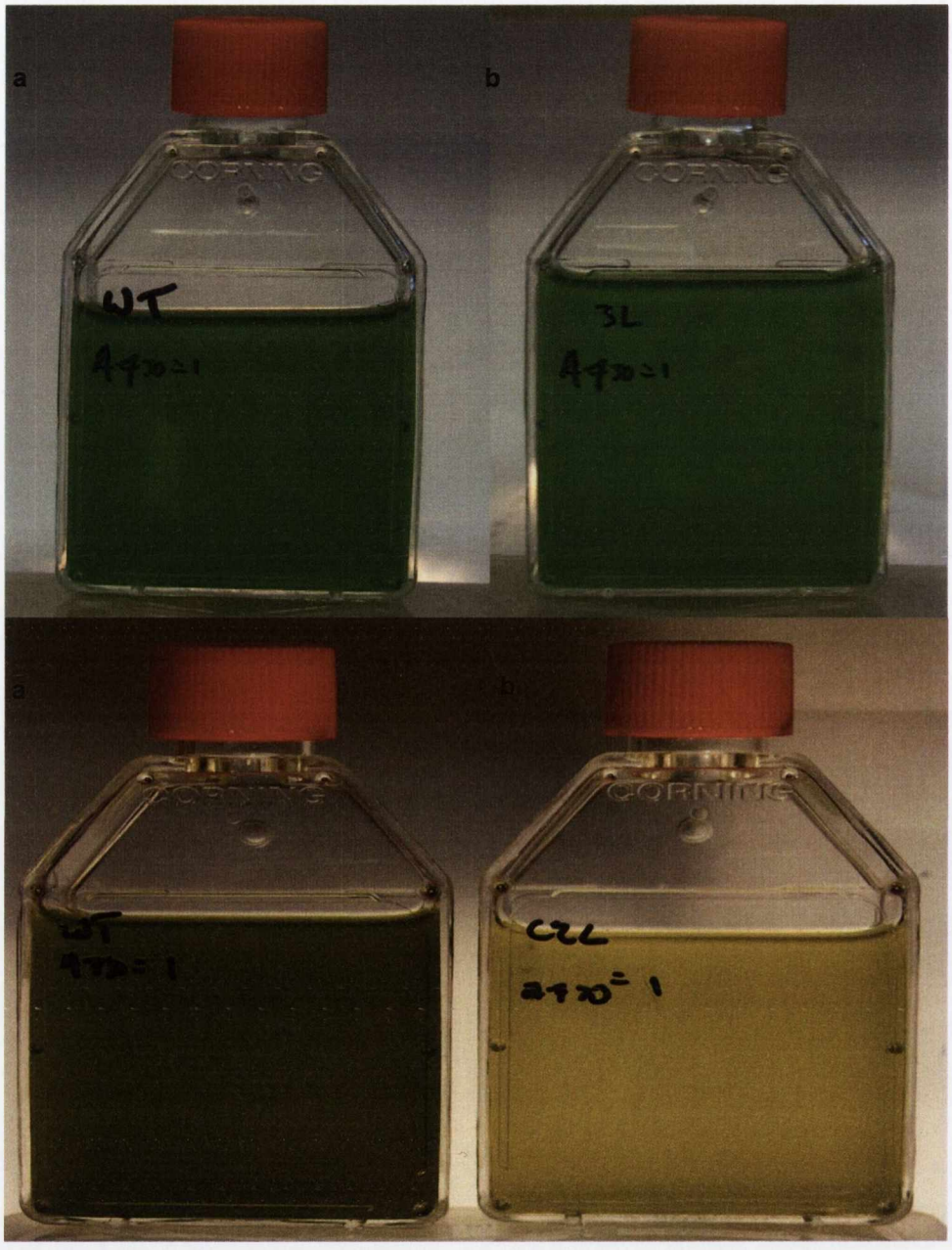

Figure 7.13 Appearance of the wild-type *Synechocystis* and sBVR-A knock-out cells

A. Cells grown under low light conditions (224 μEinsteins m^{-2} s^{-1}), 8 hours light, 16 hours dark

B. Cells grown under high light conditions (895 μEinsteins m^{-2} s^{-1}) 24 hours light

a in both cases represents wild-type cells and b represents sBVR-A knock-out cells

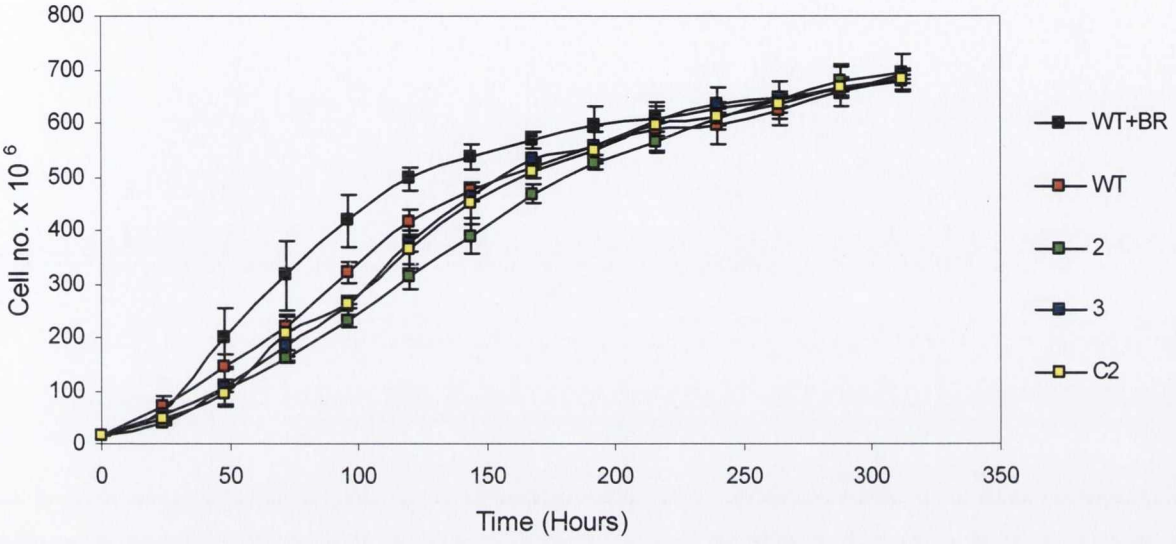

Figure 7. 14 Effect of bilirubin IXα on the growth characteristics of wild-type *Synechocystis* and sBVR-A knock-out cells

Cells were grown under high light conditions (895 μEinsteins m^{-2} s^{-2}), 24 hours light. Bilirubin (100nM) was added to the growth medium every 24 hours and the cultures were left in the dark for one hour until the OD_{730} reached 0.3. The bilirubin concentration was then increased to 1μM for the remainder of the growth period

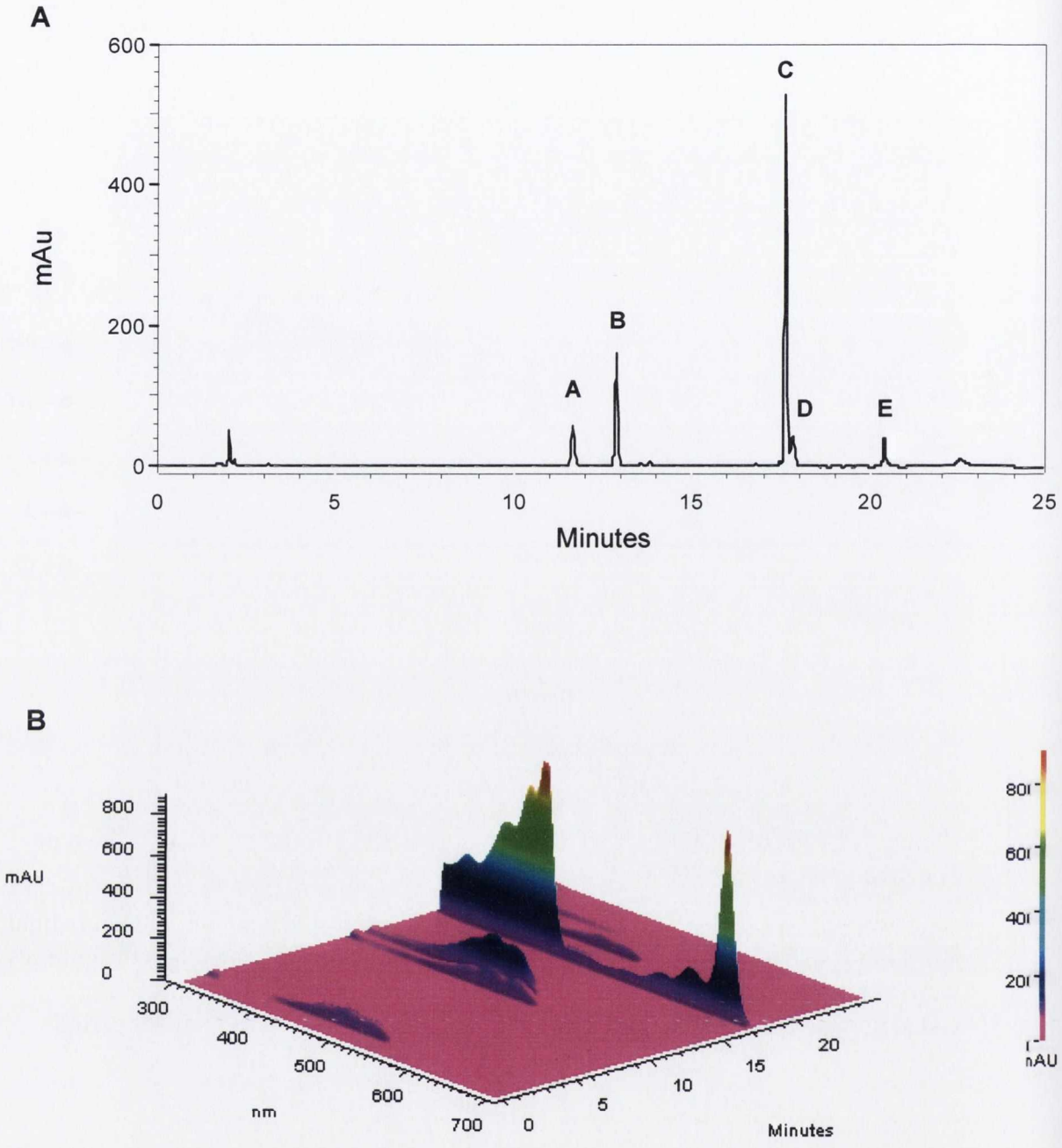

Figure 7.15 Pigment analysis of wild-type *Synechocystis* sp. PCC6803 cells

A. Reverse phase HPLC analysis of wild-type *Synechocystis* cells. Detection was by absorbance at 440nm. Peak A (retention time: 11.6 min), peak B (retention time: 12.9 min), peak D (retention time 17.8 min) and peak E (retention time: 20.5 min) were tentatively identified as carotenoids. Peak C (retention time 17.5 min) was tentatively identified as chlorophyll *a*. Cells were cultured as described in Section 2.2.2 in the presence of 5mM glucose and medium levels of light (224 μEinsteins m^{-2} s^{-1})

B. Absorbance spectra of the pigments separated by reverse-phase HPLC. Spectra were recorded by an online photo-diode array detector in the 300-700nm range.

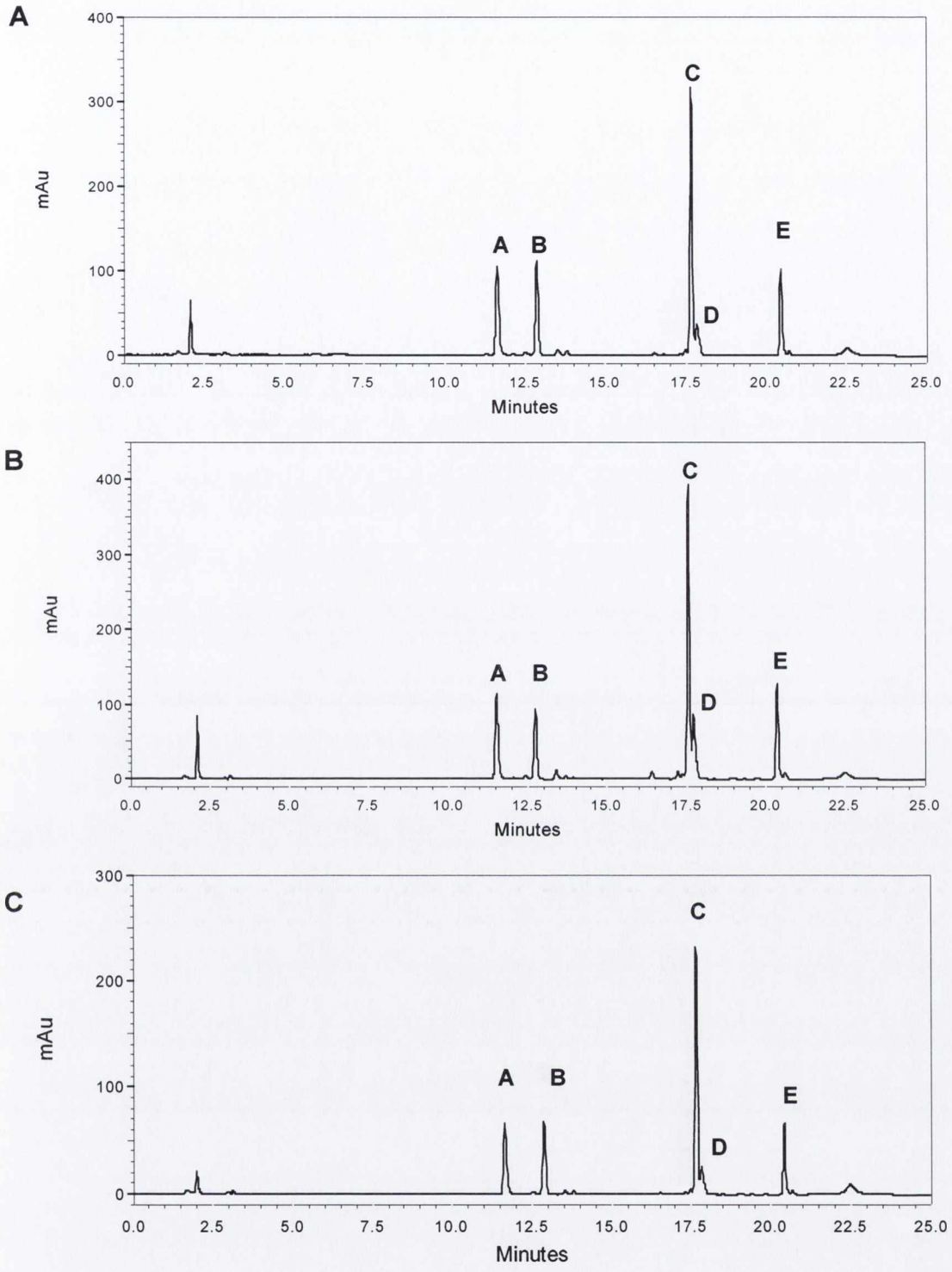

Figure 7.16 Pigment analysis of sBVR-A knock-out cells

A. Reverse phase HPLC analysis of sBVR-A mutant 2. **B.** Reverse phase HPLC analysis of sBVR-A mutant 3 **C.** Reverse phase HPLC analysis of sBVR-A mutant C2. Cells were cultured as described in Section 2.2.2 in the presence of 5mM glucose and medium levels of light (224 μEinsteins m^{-2} s^{-1}). Detection was by absorbance at 440nm. Peak A (retention time: 11.6 min), peak B (retention time: 12.9 min), peak D (retention time 17.8 min) and peak E (retention time: 20.5 min) were tentatively identified as carotenoids. Peak C (retention time 17.5 min) was tentatively identified as chlorophyll *a*

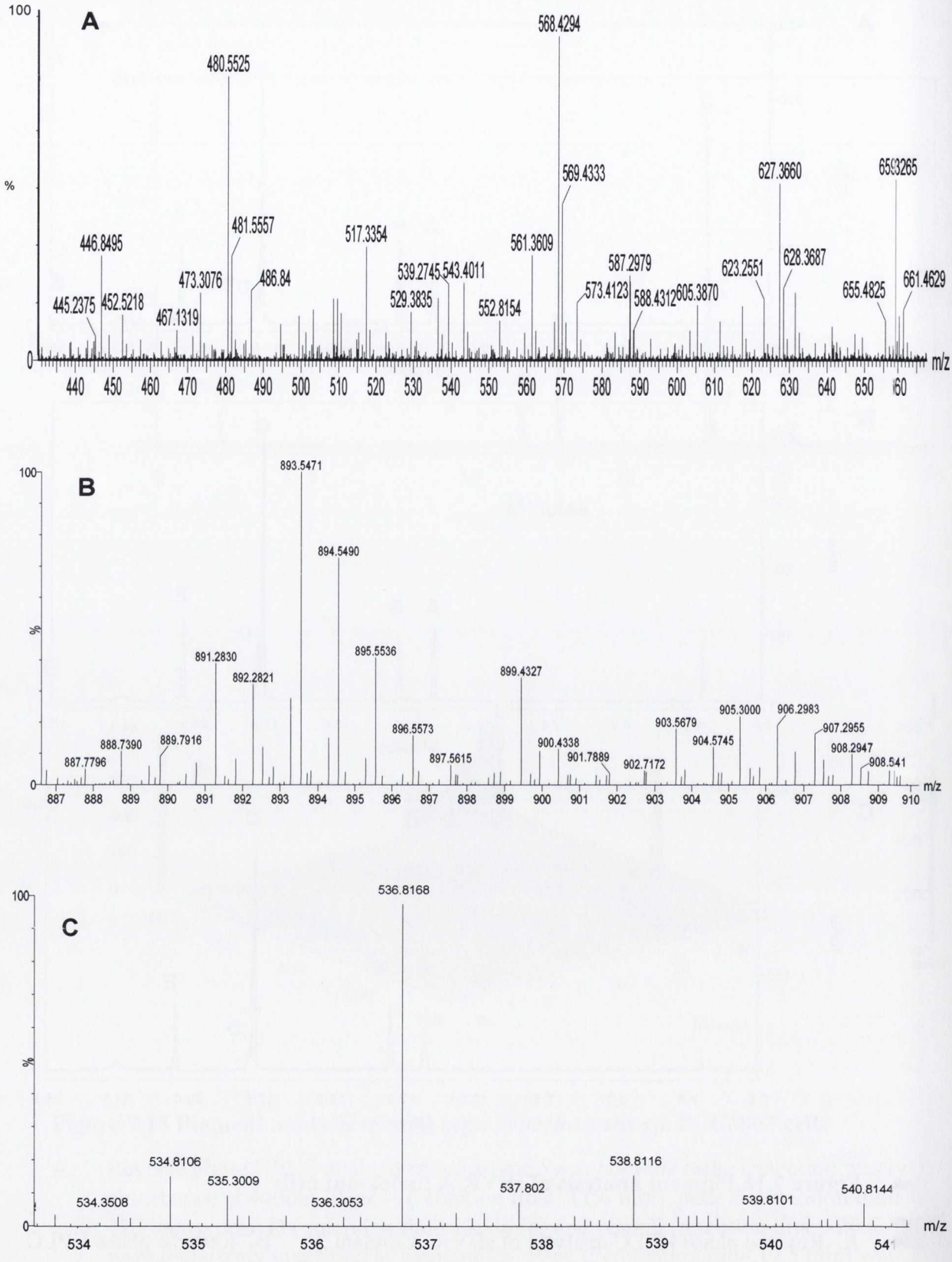

Figure 7.17 Mass spectrometry analysis of the HPLC purified pigments

A. Mass spectrometry analysis of peak B (retention time: 11.6 min) in Fig. 7.15. B. Mass spectrometry analysis of peak C (retention time: 17.6 min) in Fig. 7.15. C. Mass spectrometry analysis of peak E (retention time: 20 min) in Fig. 7.15

A

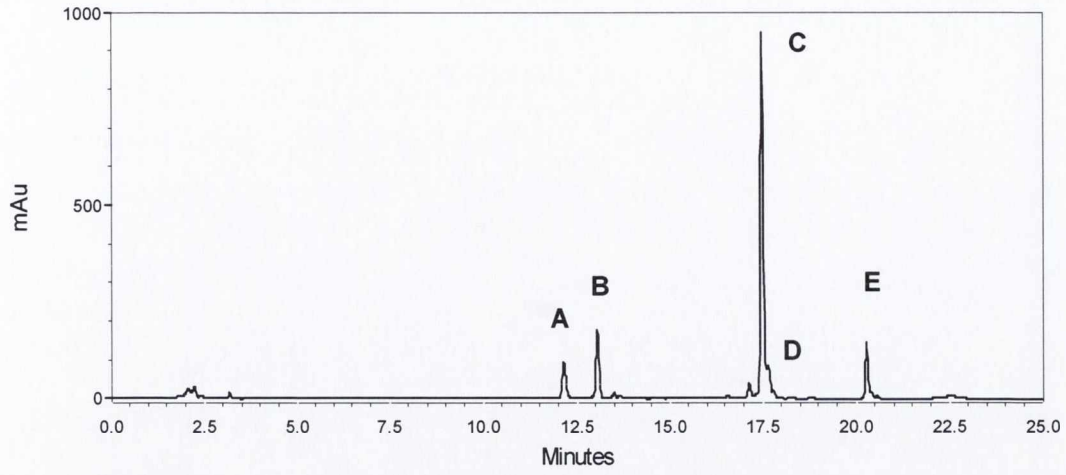
1000
500
0
mAu
A
B
C
D
E
0.0
2.5
5.0
7.5
10.0
12.5
15.0
17.5
20.0
22.5
25.0
Minutes

B

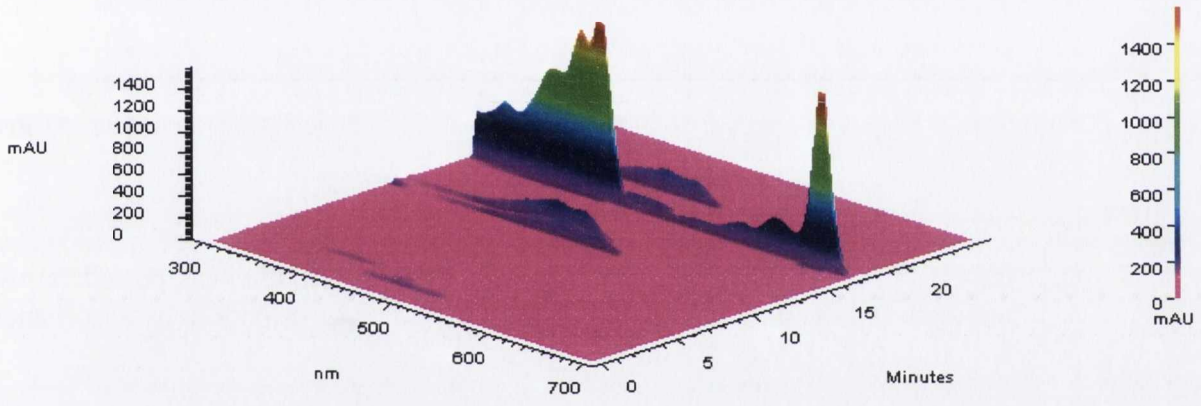
mAU
1400
1200
1000
800
600
400
200
0
300
400
500
600
700
nm
0
5
10
15
20
Minutes
1400
1200
1000
800
600
400
200
0
mAU

C

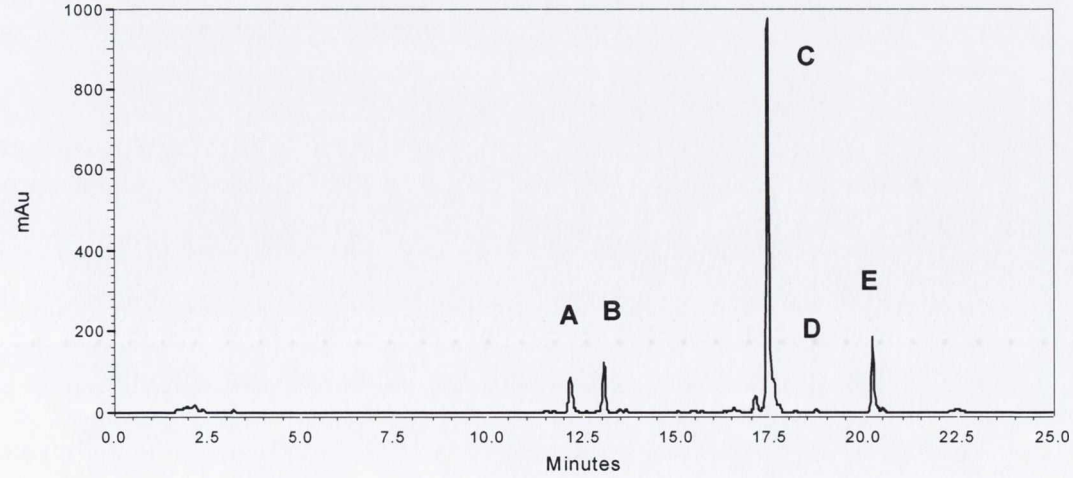
1000
800
600
400
200
0
mAu
A
B
C
D
E
0.0
2.5
5.0
7.5
10.0
12.5
15.0
17.5
20.0
22.5
25.0
Minutes

D

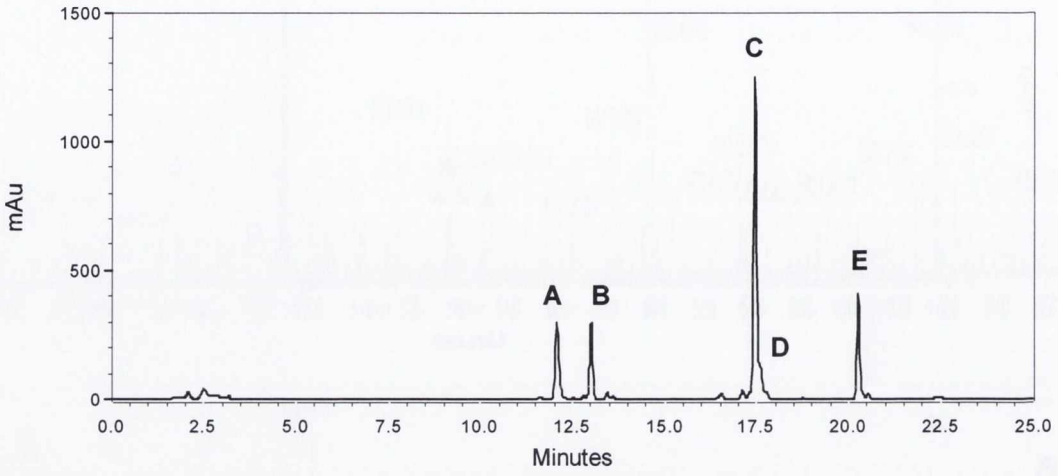

Figure 7.18 Pigment analysis of wild-type *Synechocystis* cells under different growth conditions

A. Reverse phase HPLC analysis of pigments extracted from wild-type cells grown under low light conditions (224 Einsteins m^{-2} s^{-1}). Detection was by absorbance at 440nm

B. Absorbance spectra of the eluted pigments extracted from wild-type cells grown under low light conditions. Spectra were recorded by an online photo-diode array detector in the 300-700nm range.

C. Reverse phase HPLC analysis of pigments extracted from wild-type cells grown under medium light conditions (447 Einsteins m^{-2} s^{-1}). Detection was by absorbance at 440nm

D. Reverse phase HPLC analysis of pigments extracted from wild-type cells grown under high light conditions. (895 Einsteins m^{-2} s^{-1}). Detection was by absorbance at 440nm

Absorbance spectra were recorded in all cases with an online online photo-diode array detector in the 300-700nm range. However, for clarity the absorbance spectra for the cells grown under medium and high light have been ommitted.

Peaks A, B, C, D and E were tentatively identified as myxoxanthophyll, zeaxanthin, chlorophyll *a*, echinenone and β-carotene respectively

A

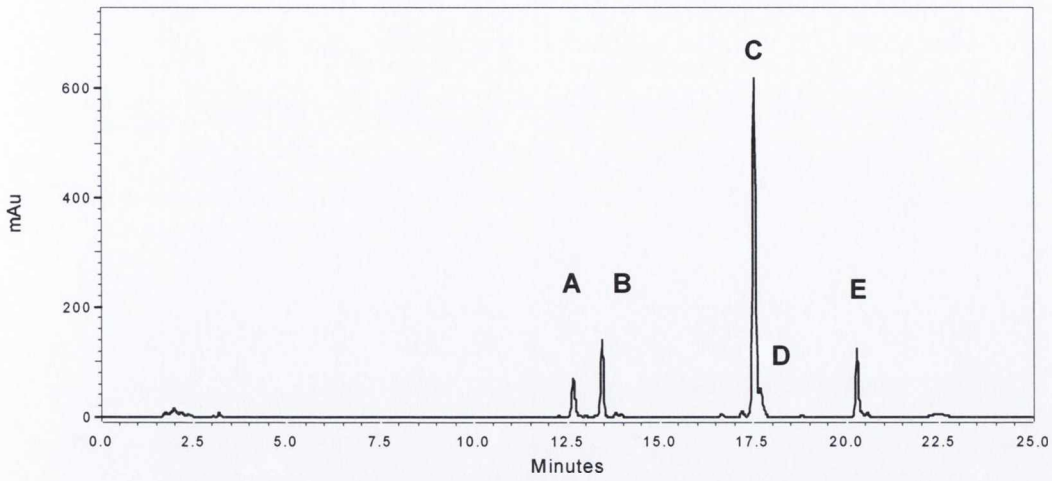
C
A
B
D
E
mAu
600
400
200
0
0.0
2.5
5.0
7.5
10.0
12.5
15.0
17.5
20.0
22.5
25.0
Minutes

B

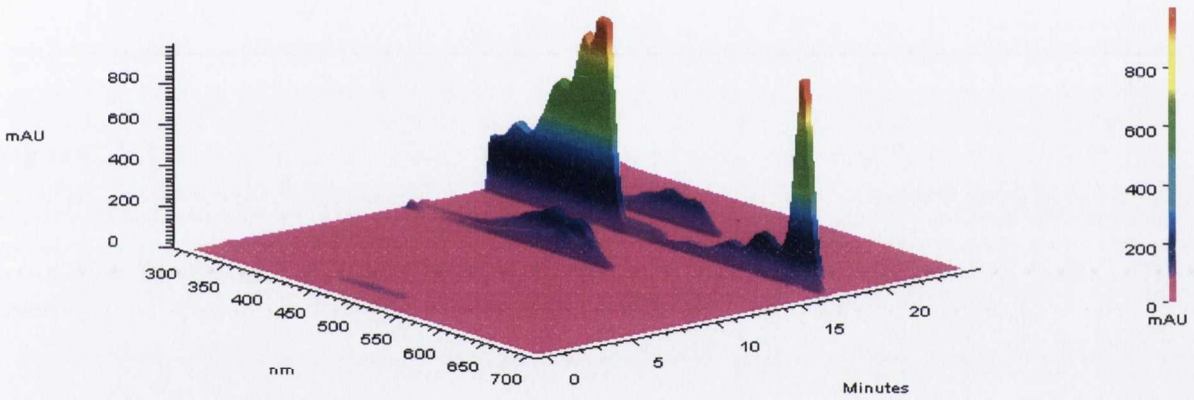
mAU
800
600
400
200
0
300
350
400
450
500
550
600
650
700
nm
0
5
10
15
20
Minutes
800
600
400
200
0
mAU

C

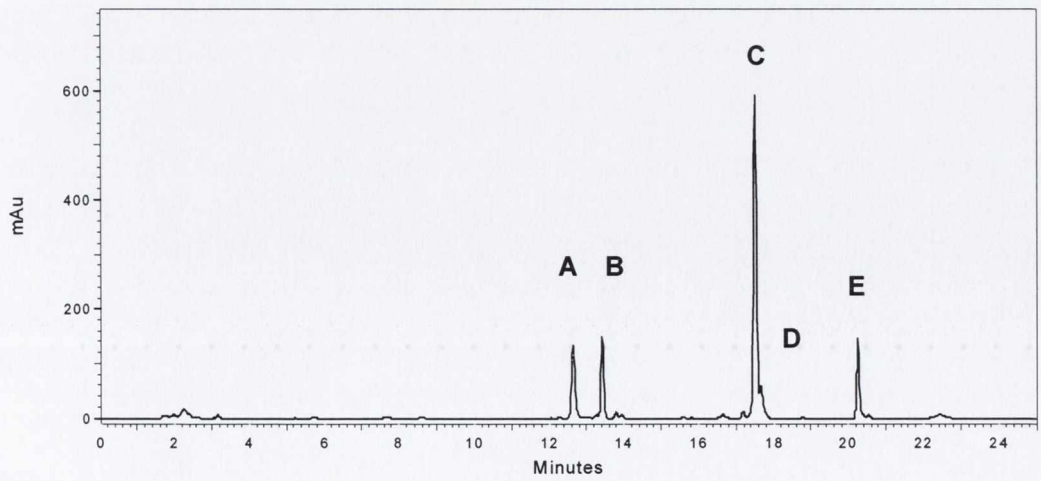
C
A
B
E
D
mAu
600
400
200
0
0
2
4
6
8
10
12
14
16
18
20
22
24
Minutes

D

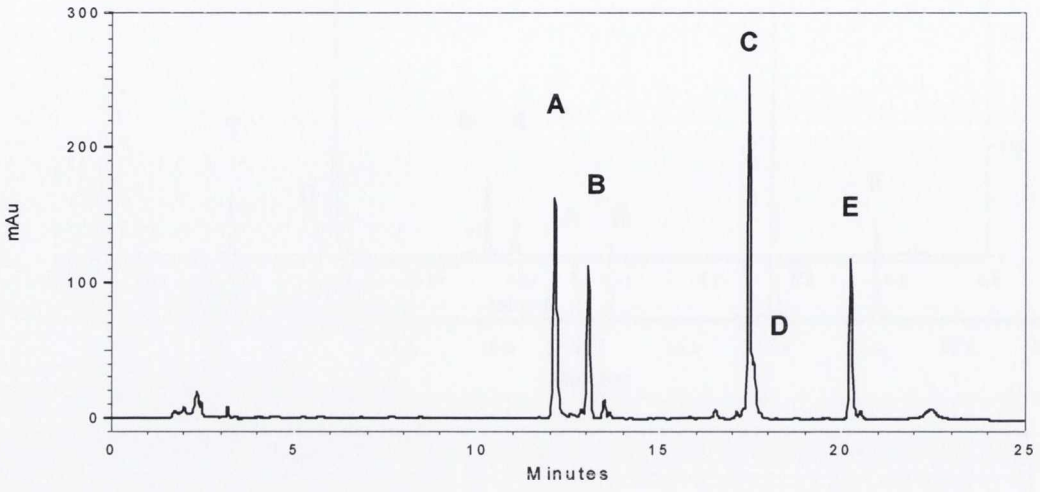

Figure 7.19 Pigment analysis of the sBVR-A knock-out cells under different growth conditions

A. Reverse phase HPLC analysis of pigments extracted from knock-out cells grown under low light conditions (224 Einsteins m^{-2} s^{-1}). Detection was by absorbance at 440nm

B. Absorbance spectra of the eluted pigments extracted from knock-out cells grown under low light conditions. Spectra were recorded by an online photo-diode array detector in the 300-700nm range.

C. Reverse phase HPLC analysis of pigments extracted from knock-out cells grown under medium light conditions (447 Einsteins m^{-2} s^{-1}). Detection was by absorbance at 440nm

D. Reverse phase HPLC analysis of pigments extracted from knock-out cells grown under high light conditions. (895 Einsteins m^{-2} s^{-1}). Detection was by absorbance at 440nm

Absorbance spectra were recorded in all cases with an online online photo-diode array detector in the 300-700nm range. However, for clarity the absorbance spectra for the cells grown under medium and high light have been ommitted.

Peaks A, B, C, D and E were tentatively identified as myxoxanthophyll, zeaxanthin, chlorophyll *a*, echinenone and β-carotene respectively

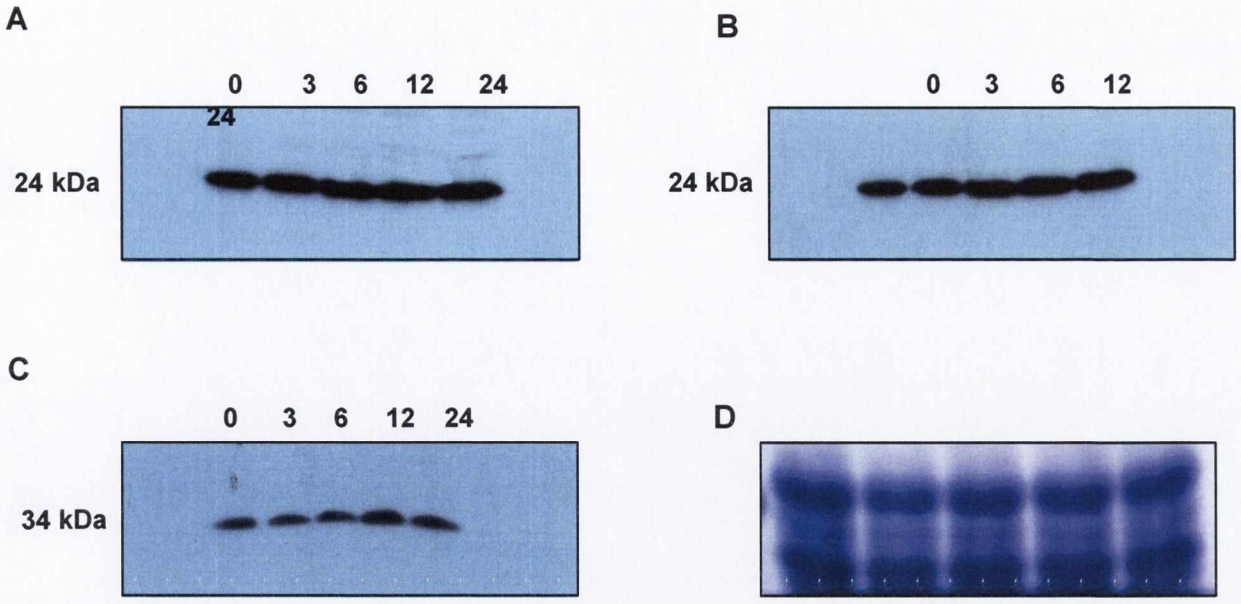

Figure 7.20 Effect of glucose on the expression levels of HO1, PcyA and sBVR-A

A. HO1 **B**. PcyA **C**. sBVR-A **D**. SDS-PAGE loading control.
Cell number was normalised as described in Section 2.2.19.1c. The 50ml sample contained approximately 7.5 x 10^9 cells. 100µg of *Synechocystis* protein was loaded in each well as determined by the Bradford assay. The primary antibody was diluted 1/1,000 (v/v) and the secondary antibody diluted 1/20,000 (v/v)

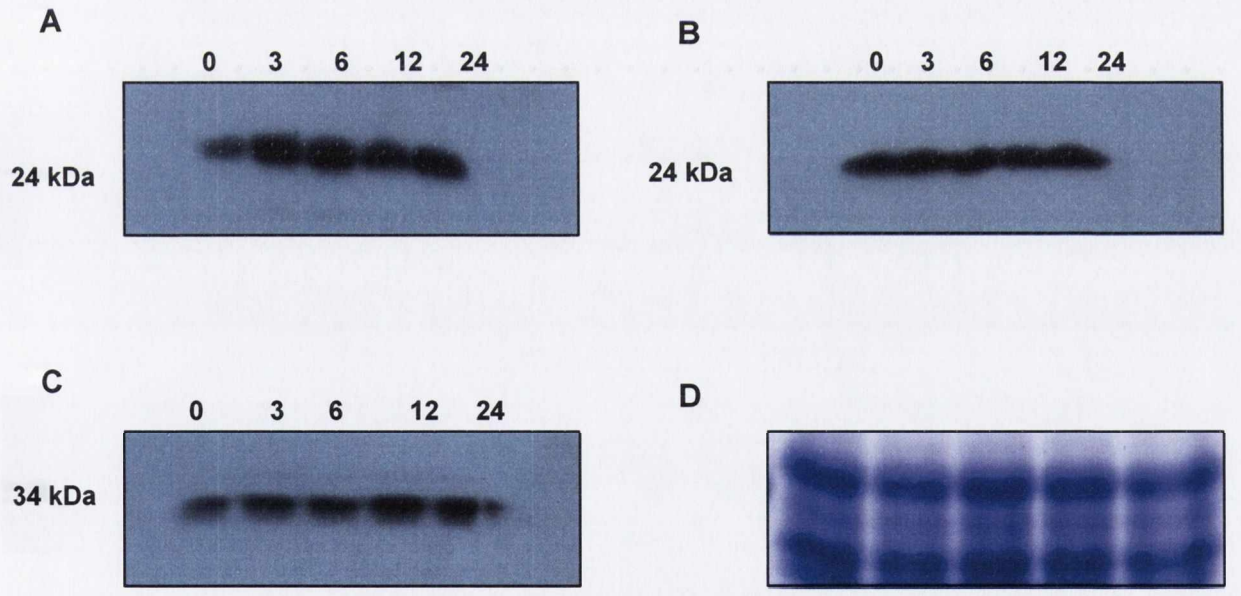

Figure 7.21 Effect of bilirubin IXα on the expression levels of HO1, PcyA and sBVR-A

A. HO1 **B.** PcyA **C**. sBVR-A **D**. SDS-PAGE loading control
Cell number was normalised as described in Section 2.2.19.1c. The 50ml sample contained approximately 7.5 x 10^9 cells. 100µg of *Synechocystis* protein was loaded in each well as determined by the Bradford assay. The primary antibody was diluted 1/1,000 (v/v)and the secondary antibody diluted 1/20,000 (v/v)

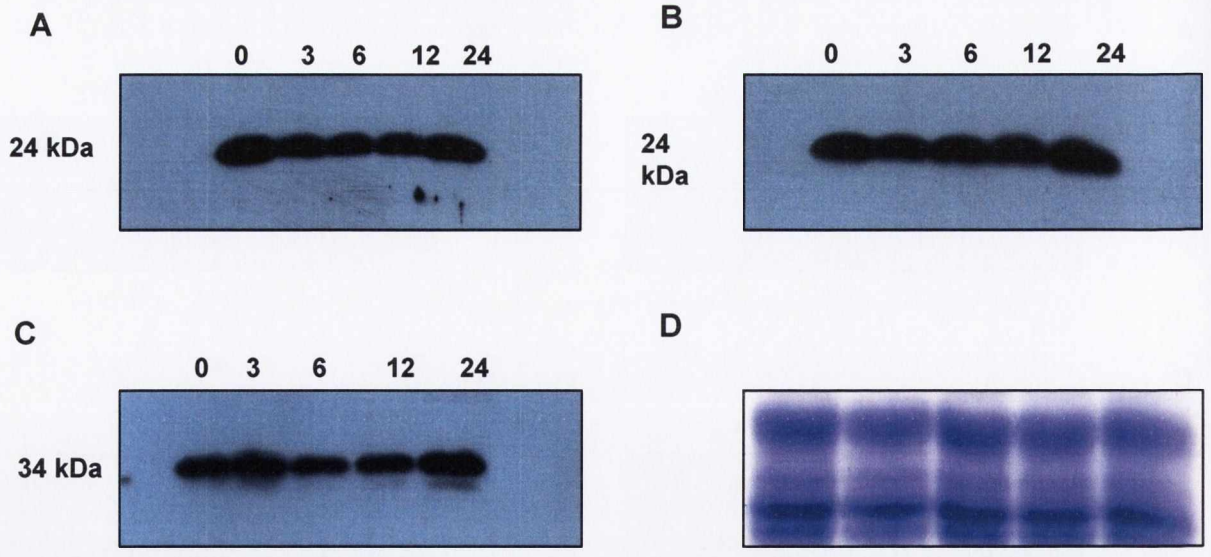

Figure 7.22 Effect of low levels of light on the expression levels of HO1, PcyA and sBVR-A

A. HO1 **B**. PcyA **C**. sBVR-A **D**. SDS-PAGE loading control
Cell number was normalised as described in Section 2.2.19.1c. The 50ml sample contained approximately 7.5 x 10^9 cells. 100µg of *Synechocystis* protein was loaded in each well as determined by the Bradford assay. The primary antibody was diluted 1/1,000 (v/v) and the secondary antibody diluted 1/20,000 (v/v)

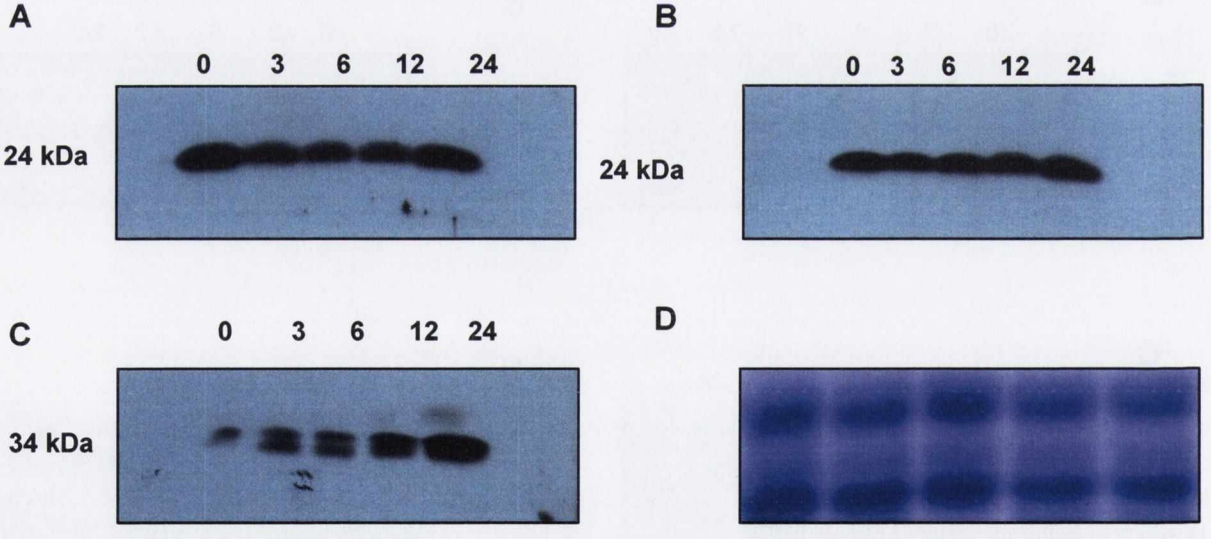

Figure 7.23 Effect of high levels of light on the expression levels of HO1, PcyA and sBVR-A

A. HO1 **B**. PcyA **C**. sBVR-A **D**. SDS-PAGE loading control
Cell number was normalised as described in Section 2.2.19.1c. The 50ml sample contained approximately 7.5 x 10^9 cells. 100µg of *Synechocystis* protein was loaded in each well as determined by the Bradford assay. The primary antibody was diluted 1/1,000 (v/v) and the secondary antibody diluted 1/20,000 (v/v)

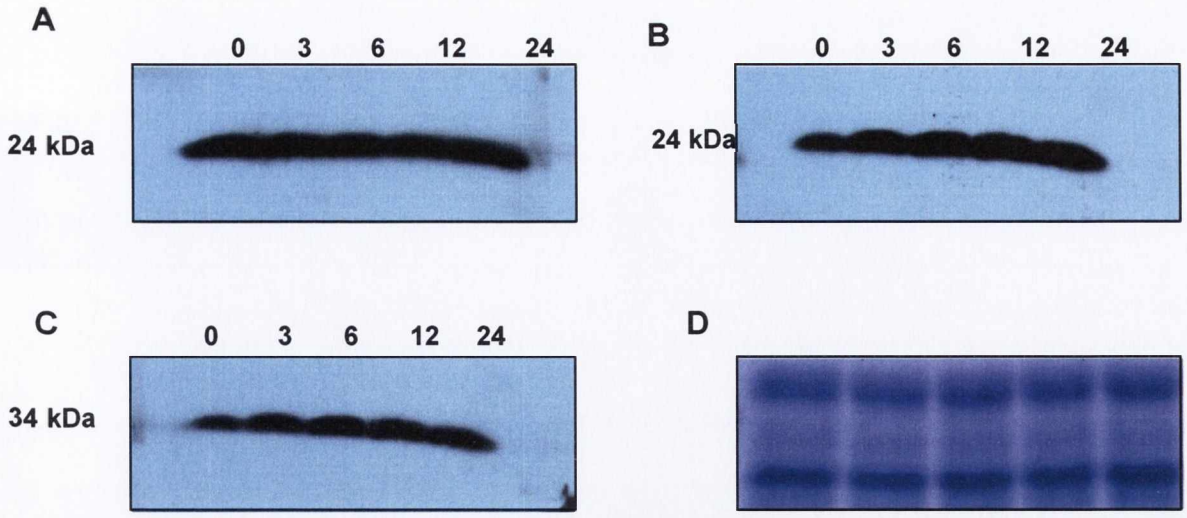

Figure 7.24 Effect of H_20_2 (1mM) on the expression levels of HO1, PcyA and sBVR-A

A. HO1 **B**. PcyA **C**. sBVR-A **D**. SDS-PAGE loading control
Cell number was normalised as described in Section 2.2.19.1c. The 50ml sample contained approximately 7.5 x 10^9 cells. 100µg of *Synechocystis* protein was loaded in each well as determined by the Bradford assay. The primary antibody was diluted 1/1,000 (v/v) and the secondary antibody diluted 1/20,000 (v/v)

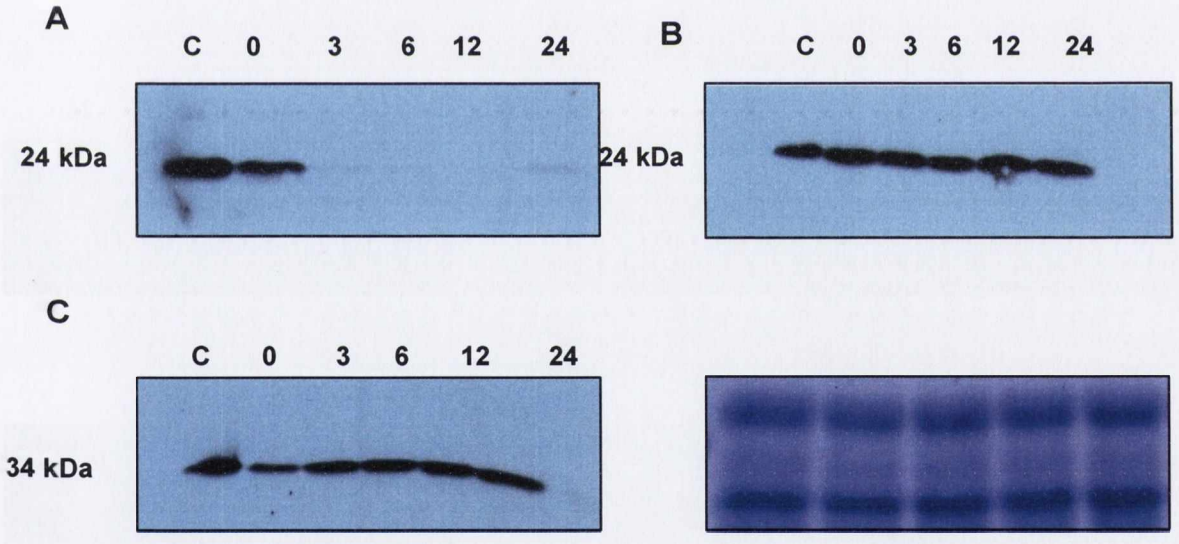

Figure 7.25 Effect of H_20_2 (10mM) on the expression levels of HO1, PcyA and sBVR-A

A. HO1 **B**. PcyA **C**. sBVR-A **D**. SDS-PAGE loading control
C represents a 20ng recombinant protein control in each case. Cell number was normalised as described in Section 2.2.19.1c. The 50ml sample contained approximately 7.5 x 10^9 cells. 100µg of *Synechocystis* protein was loaded in each well as determined by the Bradford assay. The primary antibody was diluted 1/1,000 (v/v) and the secondary antibody diluted 1/20,000 (v/v)

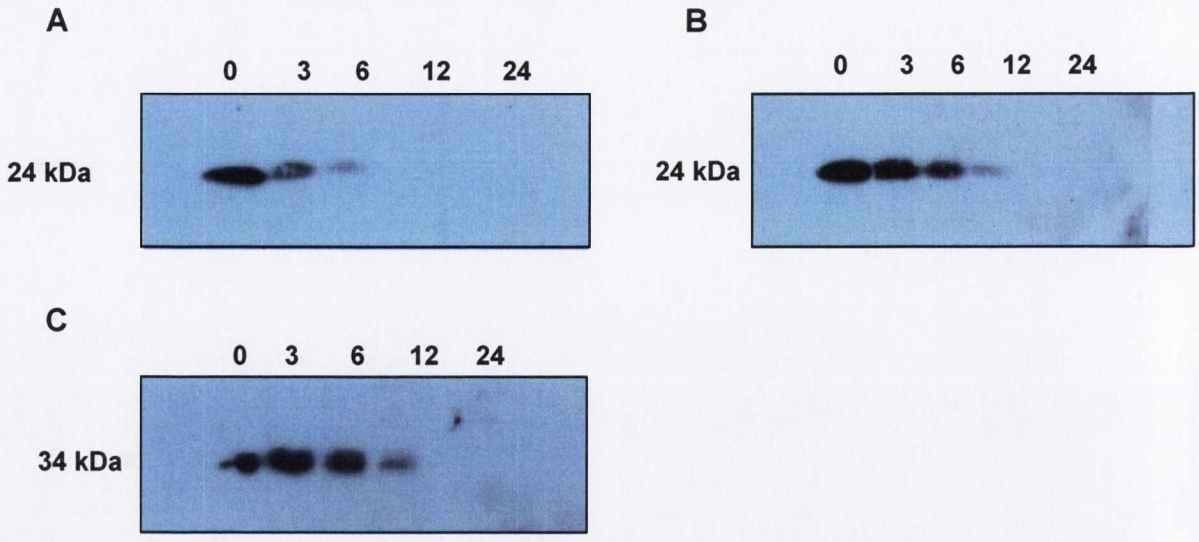

Figure 7.26 Effect of H_2O_2 (100mM) on the expression levels of HO1, PcyA and sBVR-A

A. HO1 **B**. PcyA **C**. sBVR-A
Cell number was normalised as described in Section 2.2.19.1c. The 50ml sample contained approximately 7.5 x 10^9 cells. 100µg of *Synechocystis* protein was loaded in each well as determined by the Bradford assay. The primary antibody was diluted 1/1,000 (v/v) and the secondary antibody diluted 1/20,000 (v/v)

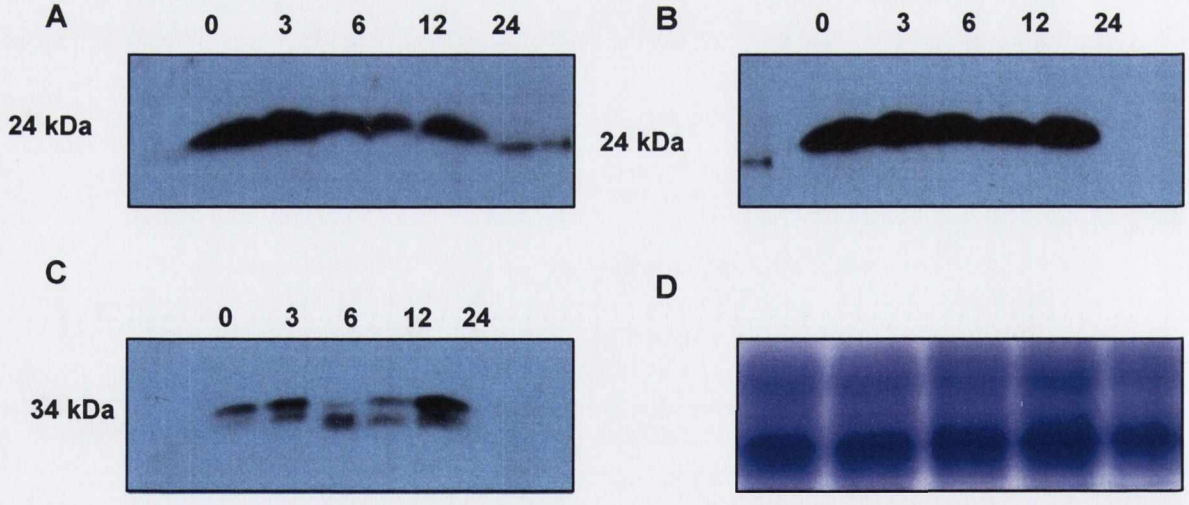

Figure 7.27 Effect of norflurazon (25µM) on the expression levels of HO1, PcyA and sBVR-A

A. HO1 **B**. PcyA **C**. sBVR-A **D**. SDS-PAGE loading control
Cell number was normalised as described in Section 2.2.19.1c. The 50ml sample contained approximately 7.5 x 10^9 cells. 100µg of *Synechocystis* protein was loaded in each well as determined by the Bradford assay. The primary antibody was diluted 1/1,000 (v/v) and the secondary antibody diluted 1/20,000 (v/v)

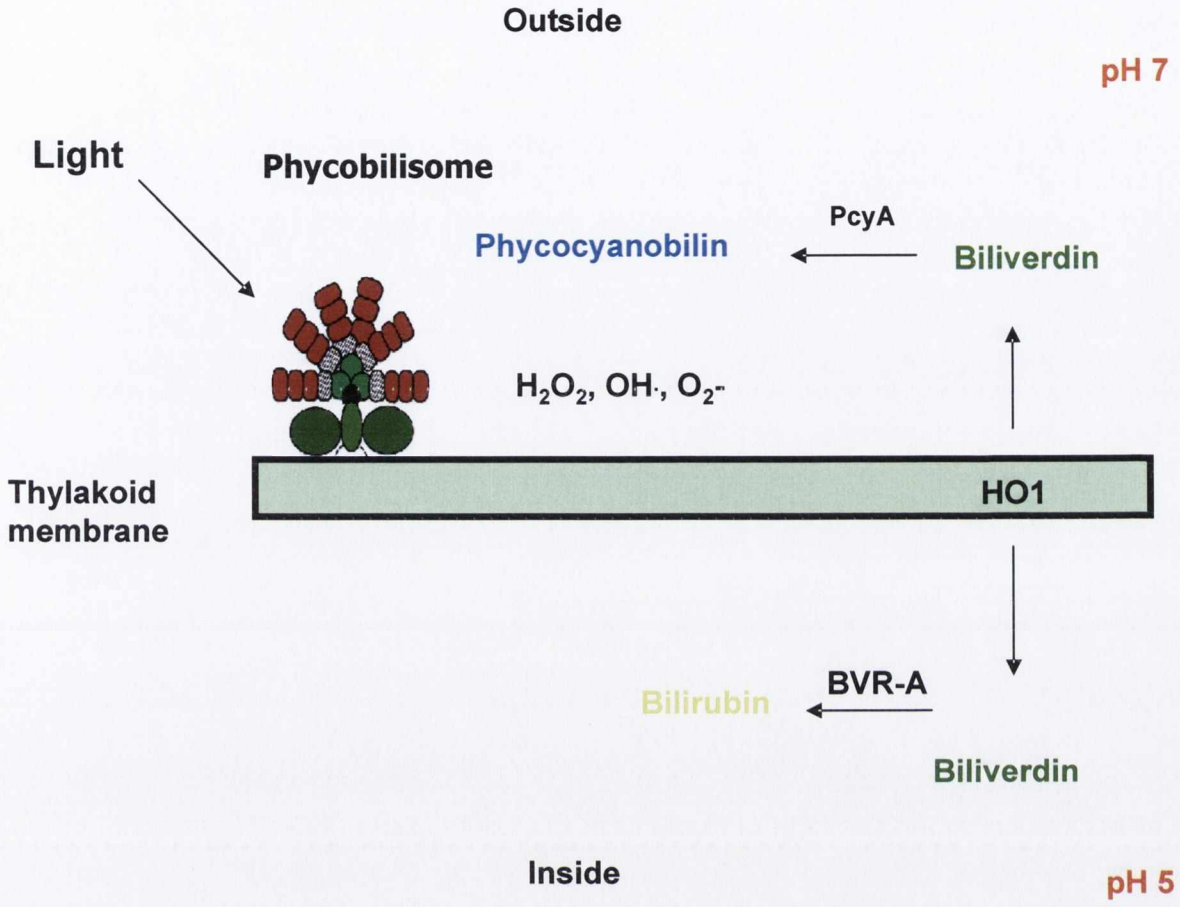

Figure 7.28 Model of light induced oxidative stress and a possible role for sBVR-A

Under conditions of light stress reactive oxygen species are generated. Light harvesting is decreased by down-regulating heme oxygenase and up-regulating sBVR-A. Bilirubin serves to combat the stress by acting as an anti-oxidative molecule or leading to transcription of anti-oxidative enzymes.

CHAPTER 8

GENERAL DISCUSSION

To date the literature on the biliverdin IXα reductase from *Synechocystis* sp. PCC6803 and indeed cyanobacteria as a whole extends to the one study performed by Schluchter & Glazer (1997). As a result there is no information on the kinetic or enzymatic mechanism of the enzyme, its sub-cellular localization or the function of bilirubin IXα in this ancient organism. To this end it was decided to extend the original study of Schluchter & Glazer and delve deeper into the world of biliverdin reduction in cyanobacteria with particular focus on the NAD(P)H dependent BVR-A and its metabolite bilirubin IXα.

In cyanobacteria and higher eukaryotes heme is broken down to biliverdin IXα by heme oxygenase and is further metabolised to bilirubin IXα by biliverdin IXα reductase. In cyanobacteria biliverdin is also reduced to the light harvesting pigments of these organisms, the phycobilins (phycocyanobilin and phycoerythrobilin). The protein coding DNA for heme oxygenase 1, biliverdin IXα reductase and phycocyanobilin ferredoxin oxidoreductase was successfully amplified from *Synechocystis* genomic DNA and cloned into a modified pET-41a expression vector for production of recombinant GST tagged protein. These recombinant proteins displayed the appropriate molecular weights on SDS-PAGE, following cleavage of the GST moiety using thrombin. Following purification of each protein to homogeneity antibodies were raised against the respective proteins. These antibodies were used to examine the expression levels of their respective proteins under various conditions and to set up preliminary conditions for the elucidation of their sub-cellular locations using immuno-gold labeled antibodies and electron microscopy. Although the latter has not yet been successfully accomplished preliminary conditions have been established involving the determination of the optimum concentration of primary and secondary antibodies and incubation times and hopefully in the near future this aim will be achieved (see Fig. 8.1 for a section of a *Synechocystis* cell probed with anti-sBVR-A antibodies and visualized by electron microscopy using the protocol described in Section 2.2.34).

As described in Section 4.1 the kinetic mechanism of any BVR-A under optimum conditions has not been previously determined, mainly due to the potent substrate inhibition by biliverdin above concentrations of approximately 10μM. It was a major aim of this study therefore to examine if the *Synechocystis* enzyme was subject to the same inhibition by biliverdin and if not to perform the initial rate kinetics with both NAD(P)H and biliverdin as the variable substrates. Together with a complete product inhibition study this allowed the kinetic mechanism of sBVR-A to be determined under optimum conditions. It was shown that sBVR-A was not inhibited by biliverdin up to concentrations even as high as 50μM and the complete kinetic mechanism was determined to

be a classic compulsory ordered mechanism with NAD(P)H the first substrate to bind and bilirubin IXα the first product to leave. This is in agreement with the kinetic mechanism determined by Rigney & Mantle (1988) for the ox kidney enzyme at pH9. The optimum pH was determined to be 5 with all substrates which may indicate a particular location within the cell such as the intrathylakoid space. The pH within this compartment is known to be approximately pH 5 while the pH in the cytosol is known to be approximately pH 7 (Lawrence *et al.*, 1997). The *Synechocystis* BVR-A retains approximately 10% activity at pH 7 which suggests that if the enzyme is located in the cytosol it is not very active and possibly not very important in this environment. At pH 7 the k_{cat} is very low and if BVR-A plays an important role in *Synechocystis* it is likely to be located within a compartment in the cell which has a pH of 5, where the enzyme is most active and therefore the intrathylakoid space. Efforts are ongoing to determine if this assumption is correct.

The chemical mechanism of *Synechocystis* biliverdin IXα reductase was also investigated in this study. This began with a full pH study and the effect of pH on the kinetic parameters of the enzyme. When the k_{cat} data was analysed as a function of pH with NADPH and NADH as co-factors a clear pK of approximately 5.5 was determined from the "less acidic" limb of the pH curve which suggests that a histidine residue may be essential to the enzyme and must be protonated in order for substrates to bind or catalysis to occur. There was no co-operativity associated with this protonation. On the "more acidic" limb of the curve there appears to be a co-operative pK in effect and protonation of this group decreases the k_{cat} by approximately 50%. This may suggest that the enzyme is highly regulatory as the enzyme loses 50% of its activity over a very small pH change (0.5 pH units). However, the enzyme was shown to be extremely unstable and irreversibly inactivated at low pH with a half-life of only 30 sec at pH 4. The enzyme was reversibly inactivated at higher pH values and for this reason it was decided to deal with the "less acidic" limb of the curve and the pK of 5.5 associated with it. This led to a search for catalytically important histidine residues and other important residues which may be involved in substrate binding or catalysis. Following examination of the multiple sequence alignment and active sites of the known rat and human BVR-A crystal structures it was decided to mutate a series of residues. Of these residues His84 is proposed to be involved in the binding of biliverdin to the enzyme and proton transfer to the reaction and must be protonated at pH5 in order to do so. Glu101 is proposed to be involved in the binding of biliverdin to the enzyme and possibly must be deprotonated at pH5 and Tyr102 is involved in binding of biliverdin in the correct orientation and positioning of the C10 bridge above the C4 of NAD(P)H for efficient hydride transfer and reduction of biliverdin to occur. These residues are highly conserved across all BVR-As, including mammals and it is

proposed that they may carry out the same function in others organisms also. These functions have not been previously attributed to these particular amino acids.

Non-linear initial rate versus enzyme concentration curves for sBVR-A above protein concentrations of approximately 20-30μg/ml led to an investigation of the quaternary structure of the enzyme under various conditions of pH and temperature. Analytical ultracentrifugation (sedimentation velocity and sedimentation equilibrium), size-exclusion chromatography and laser light scattering all produced a molecular weight for the enzyme of approximately 70kDa. The theoretical molecular weight, based on the amino acid sequence is 36kDa which suggests that sBVR-A exists as a stable dimer in solution. This is the first BVR-A to be described as a dimeric protein. The initial rate *versus* enzyme concentration curves suggest that the dimer has lower activity than the monomer. This may suggest a further regulatory mechanism for the enzyme, where the activity decreases as the enzyme concentration increases above 20-30μg/ml. It should be noted that all of the initial rate studies described in this work were performed at 2-5μg/ml, where there is a linear relationship between initial rate and enzyme concentration and true initial rates are being measured. The initial rate studies performed here therefore represent the kinetics of the sBVR-A monomer. There are a number of proteins described in the literature which are highly similar monomerically to BVR-As, including glucose-fructose oxidoreductase and dihydrodiol dehydrogenase. The crystal structures of these enzymes show that they are dimers and that the dimerisation interface consists of a C-terminal β-sheet which is present in both monomers. sBVR-A also contains a similar C-terminal β-sheet and it is proposed that the enzyme also dimerises through the interface of this β-sheet. The authors of the dihydriol dehydrogenase study suggest that these structurally similar enzymes which dimerise through this interface should form their own family of enzymes and include BVR-A in this family, even though no BVR-A enzyme was previously shown to form dimers. It should be noted however that although the experiments described in this study suggest that sBVR-A exists as a dimer at concentrations above 20-30 μg/ml *in vitro* this may not be the case *in vivo* as we do not know the exact concentration of the enzyme within the cell. However a rough estimate of the BVR-A concentration, based on western blotting is approximately 200-500ng/ml which would suggest that the enzyme is a monomer under normal physiological conditions.

The studies described here on the kinetic and enzymatic mechanism and structure of sBVR-A led to a functional study of the enzyme and its metabolite bilirubin IXα in cyanobacteria and what could be learned about the system in higher eukaryotes. Schluchter & Glazer (1997) first reported that the function of biliverdin IXα reductase in *Synechocystis* was in normal phycobiliprotein biosynthesis and in controlling the flux of biliverdin into the phycobilin biosynthetic pathway. It

was felt that a further study on the function of sBVR-A and bilirubin in *Synechocystis* would prove informative, not just in cyanobacteria but in eukaryotes also. The gene encoding sBVR-A was disrupted by interposon mutagenesis and the lack of sBVR-A was verified by western blotting. Preliminary evidence suggests that there is a chlorotic or bleaching phenotype, characterized by a decrease in chlorophyll levels, possibly coupled with an increase in certain carotenoids, particularly under stress conditions generated by high light. However, at this point more work is needed to verify this phenotype and characterize how the response is mediated. The product of the sBVR-A reaction, bilirubin IXα and possibly phycocyanorubin also (sBVR-A can reduce phycocyanobilin to phycocyanorubin *in vitro*) appear to be required for normal growth, particularly under conditions of light stress as growth is decreased in their absence. Interestingly the presence of bilirubin IXα in the growth medium under light stress conditions appears to return the sBVR-A mutant cells to the wild-type phenotype and enhance the growth of wild-type cells under the same conditions. At present it is also unclear how this effect is mediated. Examination of the expression levels of HO1, PcyA and sBVR-A under various conditions suggests that under conditions of stress, induced by hydrogen peroxide or high light the levels of HO1 decrease and sBVR-A increase. PcyA levels remain largely unchanged. This may suggest that *Synechocystis* cells under conditions of stress down-regulate light harvesting, a source of more reactive oxygen species by decreasing the levels of HO1 and increasing the levels of sBVR-A. However, at this point there are many unanswered questions and these will be the focus of much of the future work on BVR-A and bilirubin in cyanobacteria. We still do not know if cyanobacteria make bilirubin IXα or phycocyanorubin and although attempts were made to detect these metabolites through HPLC and specific colorimetric assays they were not detected. The likely reason for this is that they are present in concentrations too low to detect using these methods. In addition to its recognized enzymatic and reductive role in heme metabolism BVR-A and its metabolite bilirubin have been implicated to be involved in a significant anti-oxidant mechanism in mammals through a BVR-A mediated biliverdin bilirubin redox cycle. This theory however is still controversial. Other theories suggest that BVR-A is a signalling protein and can act as a transcription factor. This study in cyanobacteria may suggest an ancient anti-oxidative role for BVR-A and bilirubin which does not involve bilirubin cycling and it is hoped that through further investigation of this system in *Synechocystis* we can gain some useful insight and clues about the role of the system in mammals.

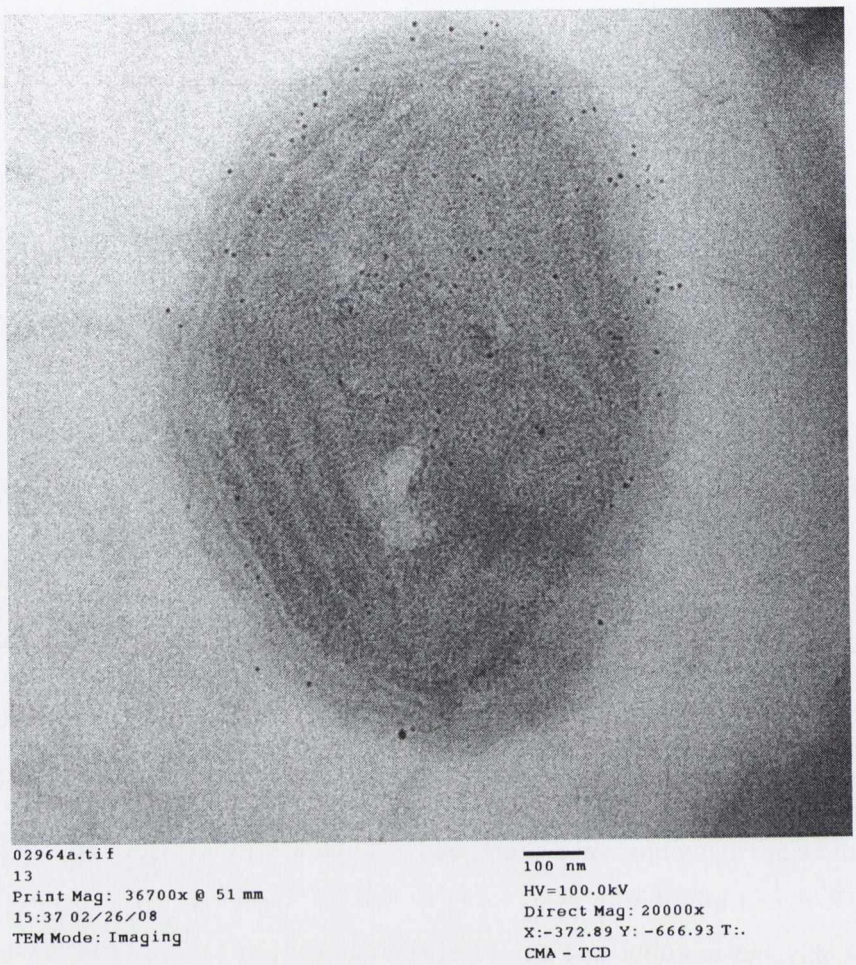

Figure 8.1 Cross section of a *Synechocystis* cell visualized by electron microscopy

sBVR-A antibodies were used at a dilution of 1/5000 (v/v), secondary anti-rabbit immuno-gold labeled antibodies were used at a concentration of 1/100 (v/v) as described in Section 2.2.34. It should be noted that in the control experiment where pre-immune serum replaced the anti-sBVR-A antibodies the cells had the same localization of immuno-gold. It was therefore concluded that the above localization was non-specific. However in these experiment the dilutions of anti-bodies, incubation times and thickness of sections was optimized for further determination of the subcellular localization of sBVR-A

Appendix I

***E. Coli* Strain**	**Genotype**
BL21 (DE3) (Novagen)	*F^- ompT gal dcm lon hsdS_B(r_B^- m_B^-) λ(DE3 [lacI lacUV5-T7 gene 1 ind1 sam7 nin5])*
BL21 (DE3) RIL (Novagen)	*Strain[a]: E. coli B F-ompT hsdS_B(r_B^- m_B^-)dcm+ Tet^r galλ (DE3) endA The [argU ileY leuW cam^r]**
Top10 (Invitrogen)	*F- mcrA Δ(mrr-hsdRMS-mcrBC) φ80lacZΔM15 ΔlacX74 nupG recA1 araD139 Δ(ara-leu)7697 galE15 galK16 rpsL(Str^R) endA1 $λ^-$*
XL-1 Blue (Stratagene)	*endA1 gyrA96(nal^R) thi-1 recA1 relA1 lac glnV44 F'[::Tn10 proAB$^+$ $lacI^q$ Δ(lacZ)M15] hsdR17(r_K^- m_K^+)*

Appendix II

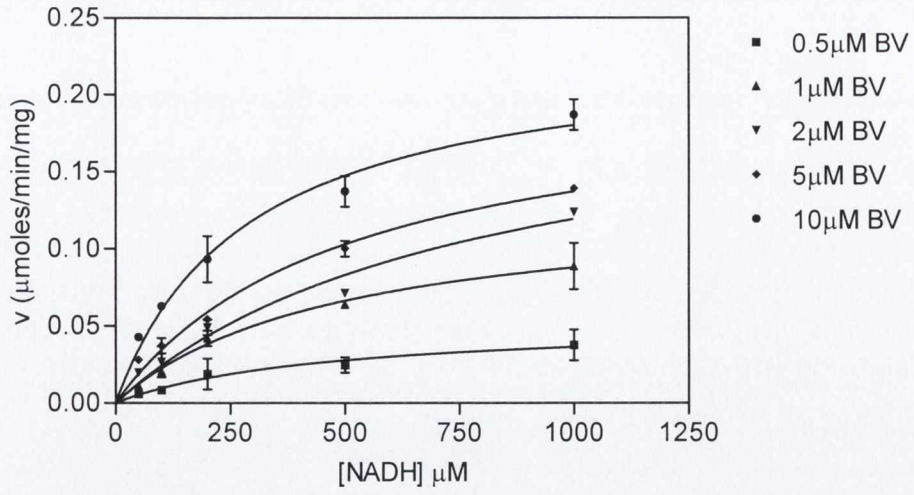
0.25
0.20
0.15
0.10
0.05
0.00
v (µmoles/min/mg)
0
250
500
750
1000
1250
[NADH] µM
0.5µM BV
1µM BV
2µM BV
5µM BV
10µM BV

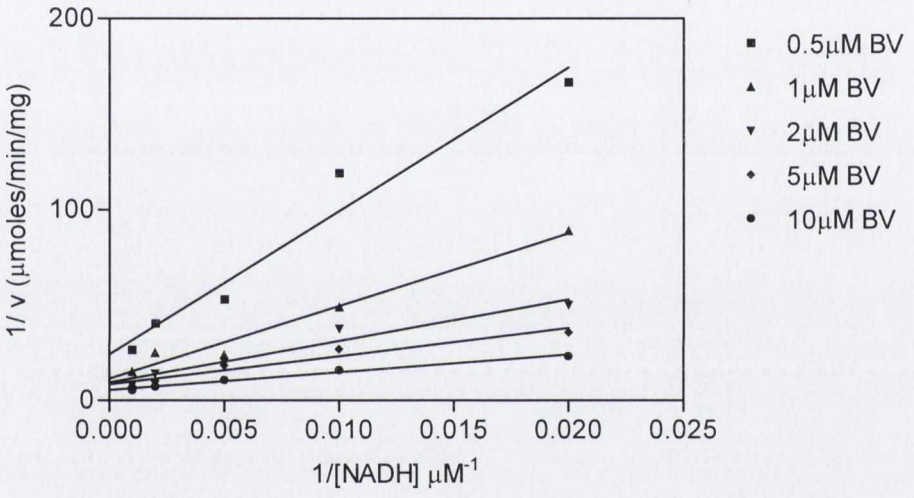
200
100
0
1/ v (µmoles/min/mg)
0.000
0.005
0.010
0.015
0.020
0.025
1/[NADH] µM-1
0.5µM BV
1µM BV
2µM BV
5µM BV
10µM BV

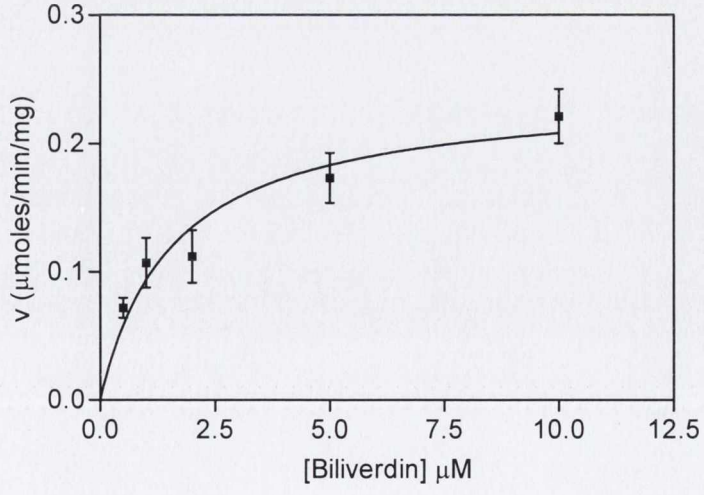
0.3
0.2
0.1
0.0
v (µmoles/min/mg)
0.0
2.5
5.0
7.5
10.0
12.5
[Biliverdin] µM

Figure 1. Initial rate kinetics of sBVR-A with NADH as the variable substrate

NADH concentrations were varied from 50-1000μM and biliverdin concentrations varied from 0.5-1μM. Reactions were performed in sodium citrate (100mM), pH5 and were initiated by the addition of sBVR-A (5μg). Experiments were performed in triplicate. Each data point represents the mean and error bars represent the standard deviation of the triplicate values. The curves are least squares fit to the Michaelis-Menten equation (see Section X).

Figure 2. Double reciprocal plot with NADH as the variable substrate

When the initial rates (see Fig. 1) were re-plotted as double reciprocals a pattern of linear intersecting lines was produced. These lines intersect to the left of the y-axis indicating a sequential mechanism. The solid lines are least squares fit to $y = mx+c$ and are for illustration purposes only. These were not used to determine kinetic parameters.

Figure 3. Plot of apparent V_{max} versus biliverdin concentration

By re-plotting the apparent V_{max} values calculated against the various concentrations of the "fixed" substrate (biliverdin) it was possible to calculate the true V_{max} and true K_m for biliverdin (see Table 4.3). The curve is a least squares fit to the Michaelis-Menten equation (equation 1). Error bars represent the standard error

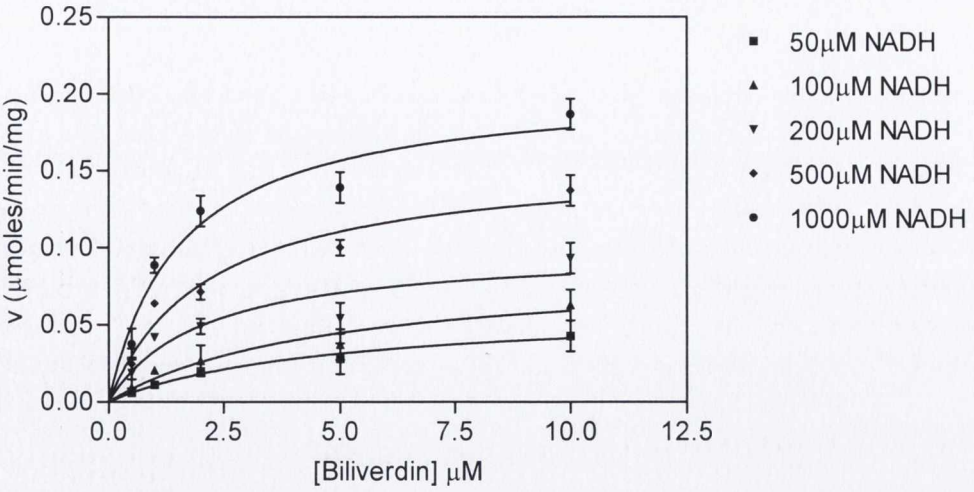
0.25
0.20
0.15
0.10
0.05
0.00
v (µmoles/min/mg)
0.0
2.5
5.0
7.5
10.0
12.5
[Biliverdin] µM
50µM NADH
100µM NADH
200µM NADH
500µM NADH
1000µM NADH

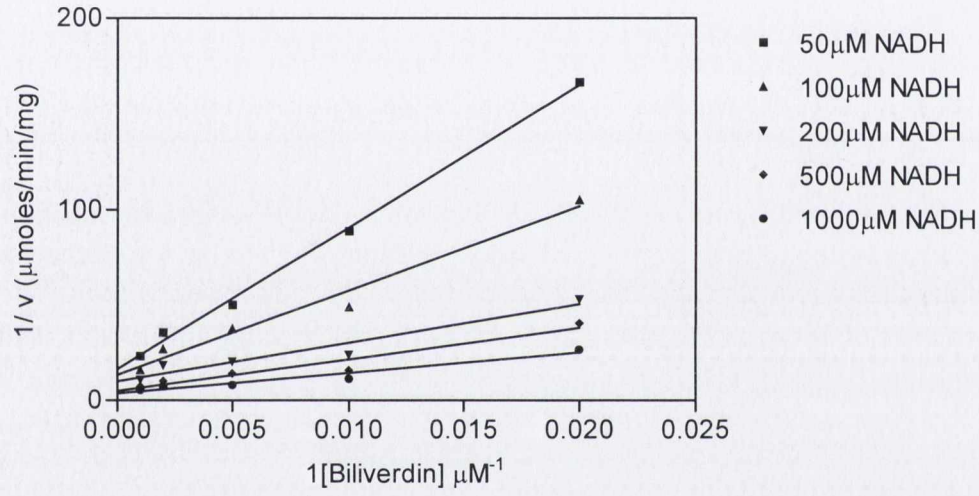
200
100
0
1/ v (µmoles/min/mg)
0.000
0.005
0.010
0.015
0.020
0.025
1[Biliverdin] µM-1
50µM NADH
100µM NADH
200µM NADH
500µM NADH
1000µM NADH

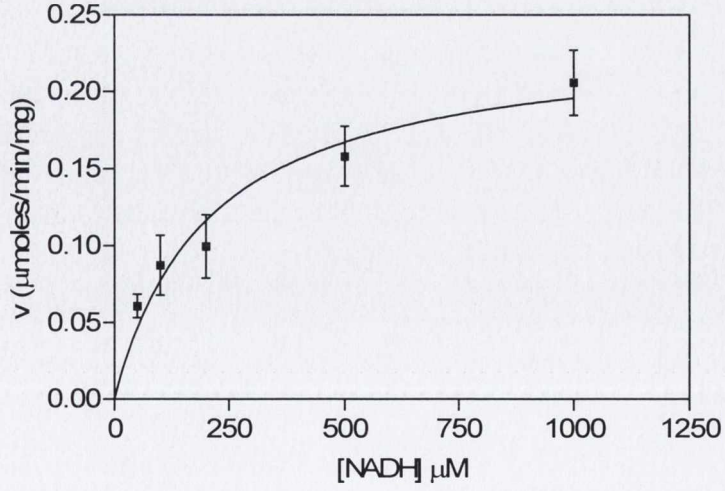
0.25
0.20
0.15
0.10
0.05
0.00
v (µmoles/min/mg)
0
250
500
750
1000
1250
[NADH] µM

Figure 4. Initial rate kinetics of sBVR-A with biliverdin as the variable substrate and NADH as co-factor

Biliverdin concentrations were varied from 0.5-10μM and NADH concentrations varied from 50-1000μM. Reactions were performed in sodium citrate (100mM), pH5 and were initiated by the addition of sBVR-A (5μg). Experiments were performed in triplicate. Each data point represents the mean and error bars represent the standard deviation of the triplicate values. The curves are least squares fit to the Michaelis-Menten equation (equation 1).

Figure 5. Double reciprocal plot with biliverdin as the variable substrate and NADH as co-factor

When the initial rates (see Fig. 4) were re-plotted as double reciprocals a pattern of linear intersecting lines was produced. These lines intersect to the left of the y-axis indicating a sequential mechanism. The solid lines are least squares fit to $y = mx+c$ and are for illustration purposes only. These were not used to determine kinetic parameters

Figure 6. Plot of apparent V_{max} *versus* NADH concentration

By re-plotting the apparent V_{max} values calculated against the various concentrations of the "fixed" substrate (NADH) it was possible to calculate the true V_{max} and true K_m for NADH (see Table 4.3). The curve is a least squares fit to the Michaelis-Menten equation (equation 1). Error bars represent the standard error

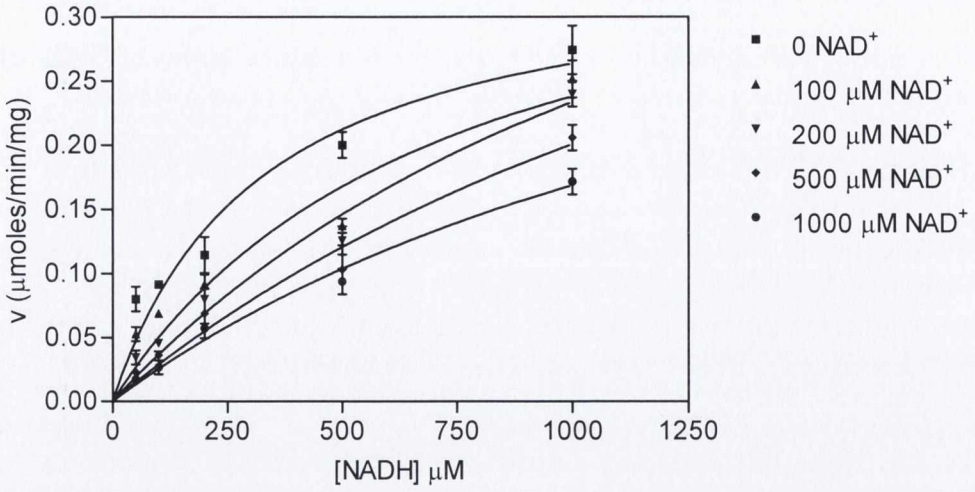
v (μmoles/min/mg)
[NADH] μM
0 NAD+
100 μM NAD+
200 μM NAD+
500 μM NAD+
1000 μM NAD+

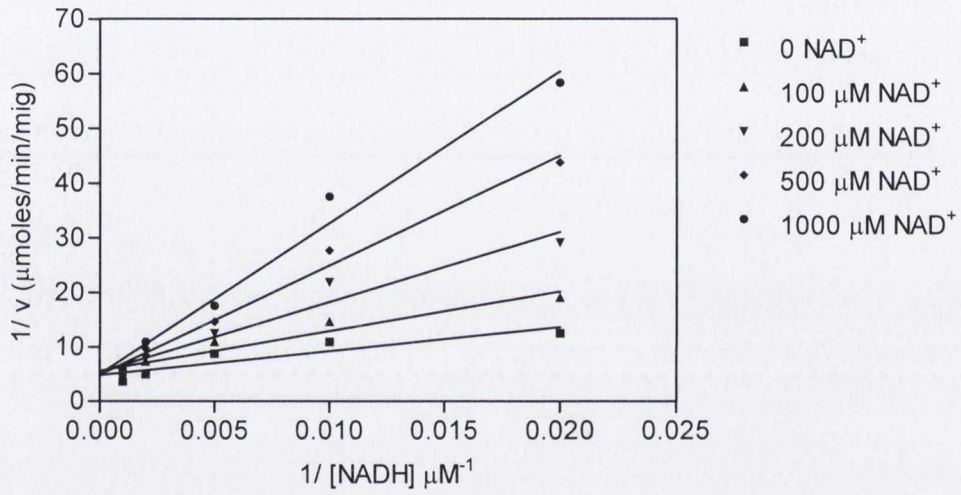
1/ v (μmoles/min/mig)
1/ [NADH] μM-1
0 NAD+
100 μM NAD+
200 μM NAD+
500 μM NAD+
1000 μM NAD+

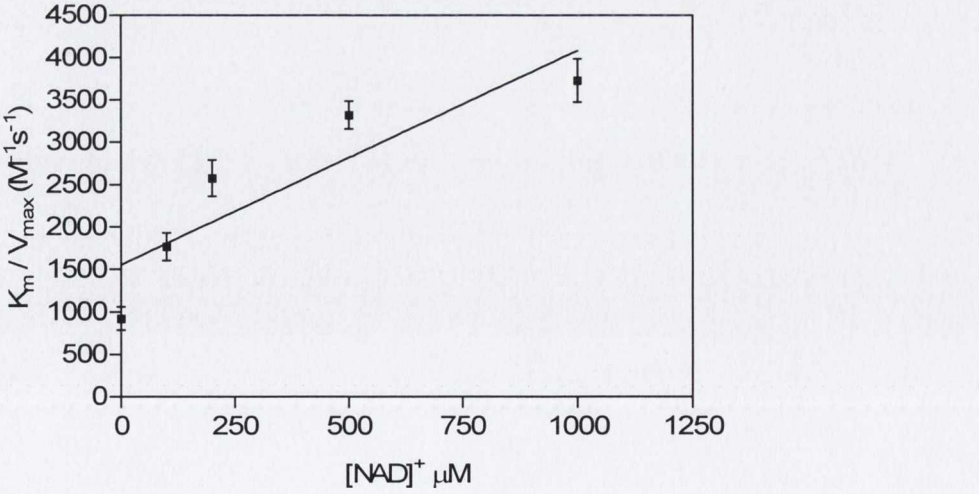
Km / Vmax (M-1s-1)
[NAD]+ μM

Figure 7. Initial rate kinetics of NADH at varying concentrations of NAD^+ and saturating biliverdin

NADH was the variable substrate at concentrations ranging from 50-1000μM. Biliverdin was held constant at saturating (10μM) levels. NAD^+ was increased from 0-1000μM. Reactions were performed in sodium citrate (100mM), pH5 and were initiated by the addition of sBVR-A (5μg). Experiments were performed in triplicate. Each data point represents the mean and error bars represent the standard deviation of the triplicate values. The curves are least squares fit to the Michaelis-Menten equation.

Figure 8. Double reciprocal plots with NADH as the variable substrate at varying concentrations of NAD^+

When the initial rates (see Fig. 7) were re-plotted as double reciprocals a pattern of linear intersecting lines was produced. These lines intersect at the y-axis indicating competitive kinetics.

Figure 9. Slope re-plot of NAD^+ inhibition with NADPH as the variable substrate

When the K_m / V_{max} (slope) values from the double-reciprocal plot shown in Fig. 8 were re-plotted against the concentration of NAD^+, the K_{is} value for NAD^+ against NADH was calculated from the $-K_{is}$ intersect point on the x-axis point (see Table 4.4)

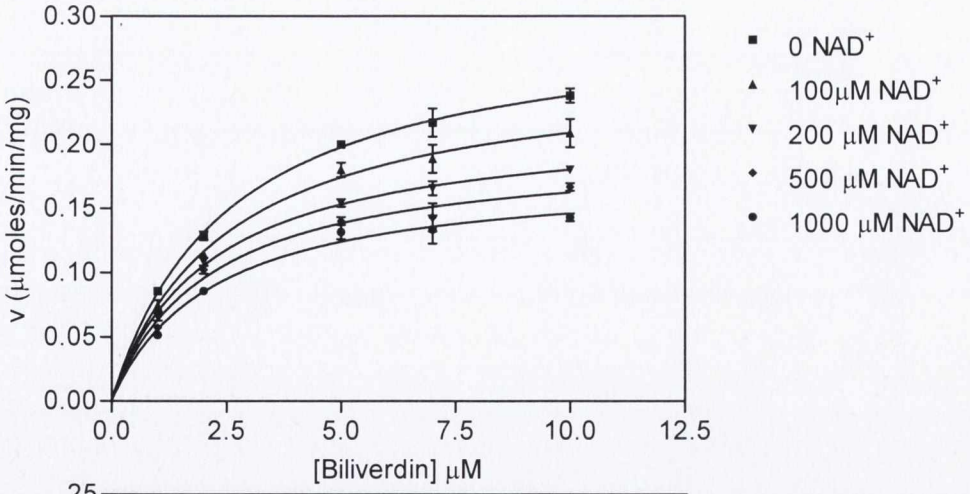
v (µmoles/min/mg)
[Biliverdin] µM
0 NAD+
100µM NAD+
200 µM NAD+
500 µM NAD+
1000 µM NAD+

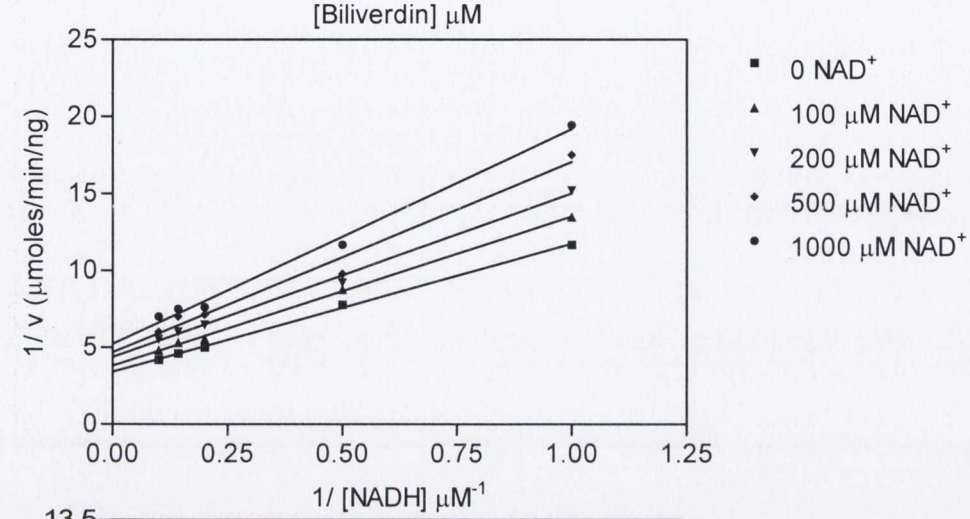
1/ v (µmoles/min/ng)
1/ [NADH] µM-1
0 NAD+
100 µM NAD+
200 µM NAD+
500 µM NAD+
1000 µM NAD+

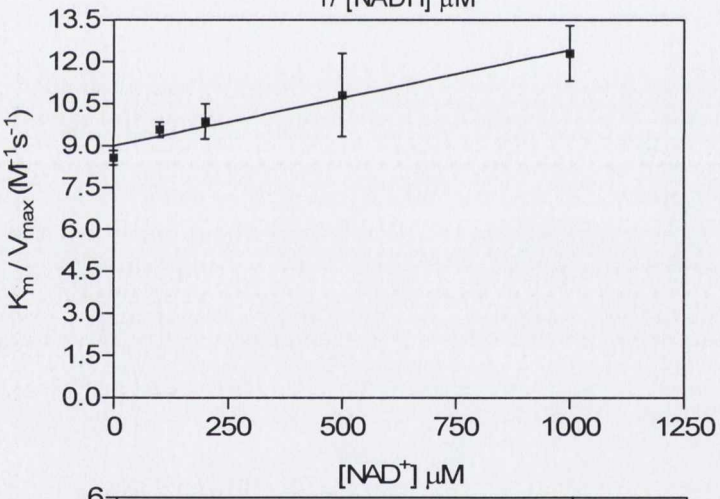
Km / Vmax (M-1s-1)
[NAD+] µM

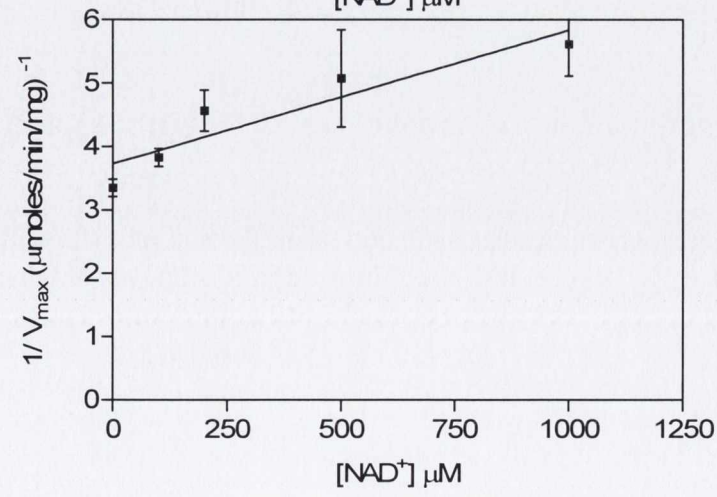
1/ Vmax (µmoles/min/mg) -1
[NAD+] µM

Figure 10. Product inhibition by NAD^+ with biliverdin as the variable substrate and non-saturating levels of NADH

Biliverdin was the variable substrate at concentrations ranging from 0.5-10μM. NADH was held constant at non-saturating levels (100μM). NAD^+ was increased from 0-1000μM. Reactions were performed in sodium citrate (100mM), pH5 and were initiated by the addition of sBVR-A (5μg). Experiments were performed in triplicate. Each data point represents the mean and error bars represent the standard deviation of the triplicate values. The curves are least squares fit to the Michaelis-Menten equation.

Figure 11. Double reciprocal plots of initial rate against biliverdin concentration at varying concentrations of NAD+

When the initial rates (see Fig. 10) were re-plotted as double reciprocals a pattern of linear intersecting lines was produced. These lines intersect to the left of the y-axis indicating mixed inhibition.

Figure 12. Slope re-plot of NAD^+ inhibition with biliverdin as the variable substrate at non-saturating levels of NADH

When the K_m / V_{max} (slope) values from the double-reciprocal plot shown in Fig. 11 were re-plotted against the concentration of NAD^+ a linear relationship was obtained where the line intersected the x-axis at $-K_{is}$. From this point the K_{is} value for NAD^+ against biliverdin was calculated (see Table 4.4) Error bars represent the standard error

Figure 4.13 Intercept re-plot of NAD^+ inhibition with biliverdin as the variable substrate at non-saturating levels of NADH

When the 1/ V_{max} (intercept) values from the double-reciprocal plot shown in Fig. 4.11 were re-plotted against the NAD^+ concentrations a linear relationship was obtained where the line intersected the x-axis at $-K_{ii}$. From this point the K_{ii} value for NAD^+ against biliverdin was calculated (see Table 4.4). Error bars represent the standard error

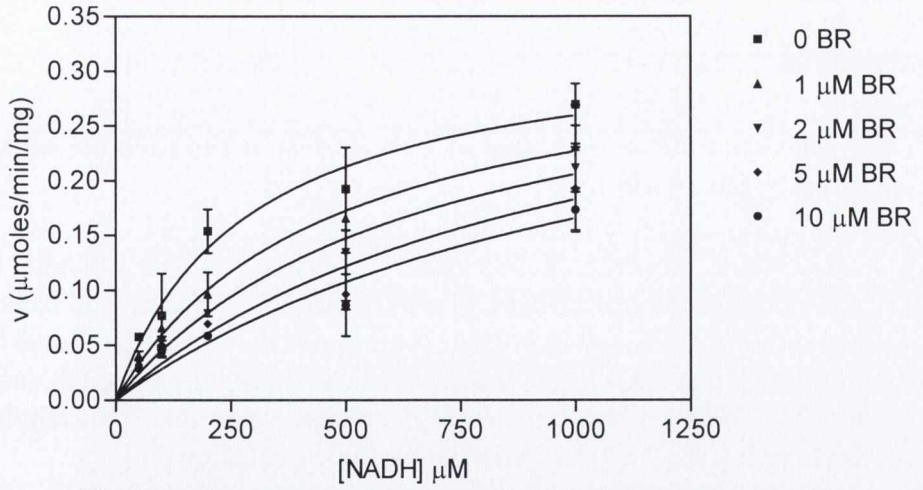
v (μmoles/min/mg)
[NADH] μM
0 BR
1 μM BR
2 μM BR
5 μM BR
10 μM BR

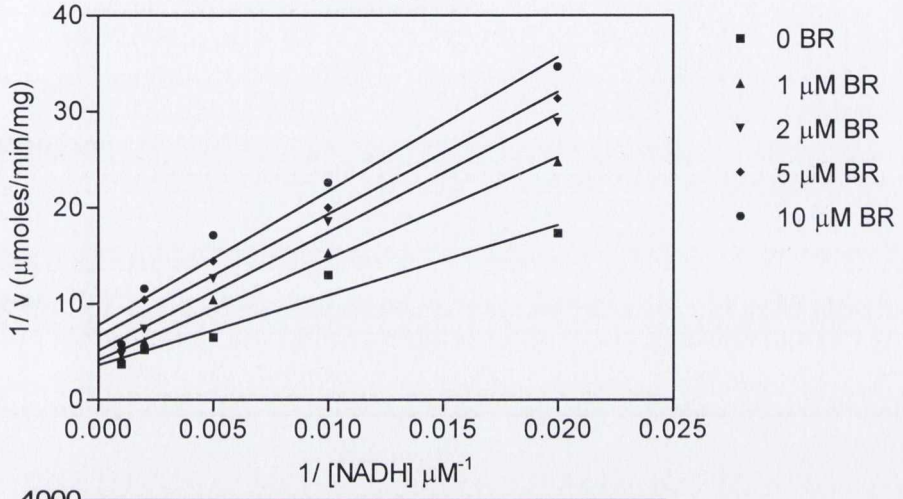
1/ v (μmoles/min/mg)
1/ [NADH] μM-1
0 BR
1 μM BR
2 μM BR
5 μM BR
10 μM BR

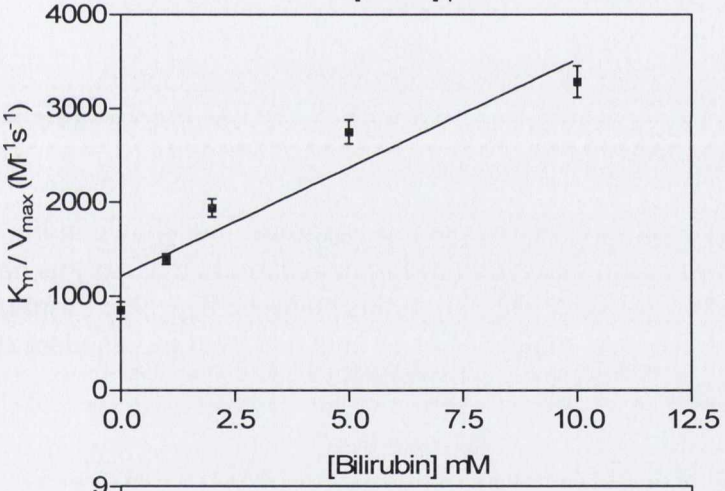
Km / Vmax (M-1s-1)
[Bilirubin] mM

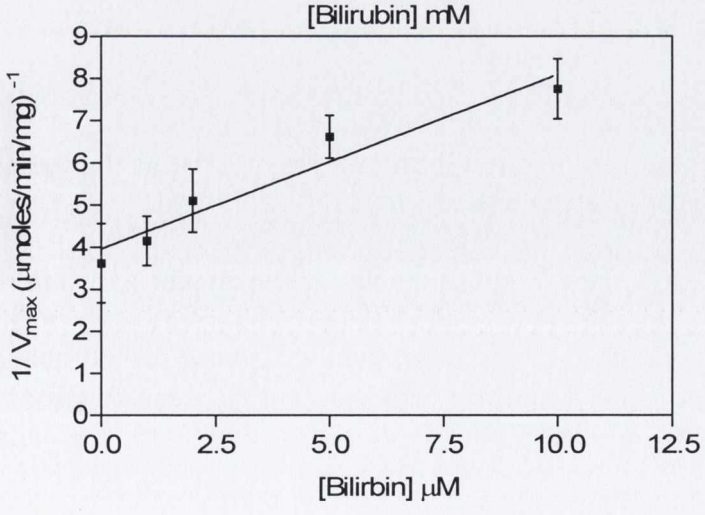
1/ Vmax (μmoles/min/mg) -1
[Bilirbin] μM

Figure 14. Product inhibition by bilirubin with NADH as the variable substrate at non-saturating levels of biliverdin

NADH was the variable substrate at concentrations ranging from 50-1000μM. Biliverdin was held constant at non-saturating levels (1μM). Bilirubin was increased from 0-10μM. Reactions were performed in sodium citrate (100mM), pH5 and were initiated by the addition of sBVR-A (5μg). Experiments were performed in triplicate. Each data point represents the mean and error bars represent the standard deviation of the triplicate values. The curves are least squares fit to the Michaelis-Menten equation.

Figure 15. Double reciprocal plots of initial rate against NADH concentration at varying concentrations of bilirubin

When the initial rates (see Fig. 14) were re-plotted as double reciprocals a pattern of linear intersecting lines was produced. These lines intersect to the left of the y-axis indicating mixed inhibition.

Figure 16. Slope re-plot of bilirubin inhibition with NADH as the variable substrate at non-saturating levels of biliverdin

When the K_m / V_{max} (slope) values from the double-reciprocal plot shown in Fig. 15 were re-plotted against the concentration of bilirubin a linear relationship was obtained where the line intersected the x-axis at $-K_{is}$. From this point the K_{is} value for bilirubin against NADH was calculated (see Table 4.4) Error bars represent the standard error

Figure 17. Intercept re-plot of bilirubin inhibition with NADH as the variable substrate at non-saturating levels of biliverdin

When the 1/ V_{max} (intercept) values from the double-reciprocal plot shown in Fig. 15 were re-plotted against the concentration of bilirubin a linear relationship was obtained where the line intersected the x-axis at $-K_{ii}$. From this point the K_{ii} value for bilirubin against NADH was calculated (see Table 4.4). Error bars represent the standard error

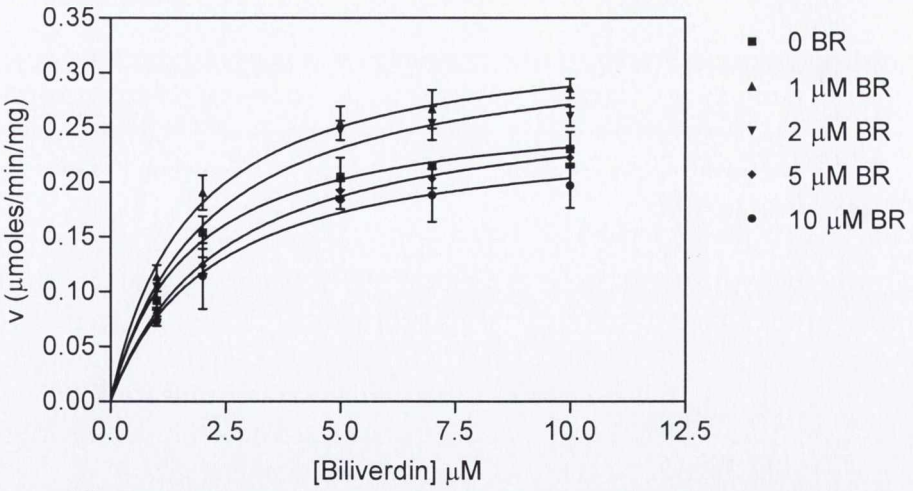
v (μmoles/min/mg)
[Biliverdin] μM
0 BR
1 μM BR
2 μM BR
5 μM BR
10 μM BR

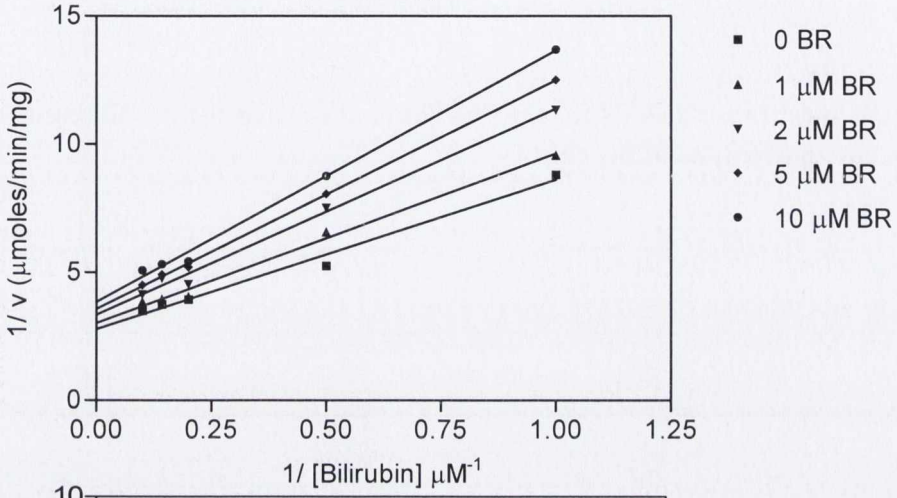
1/ v (μmoles/min/mg)
1/ [Bilirubin] μM-1
0 BR
1 μM BR
2 μM BR
5 μM BR
10 μM BR

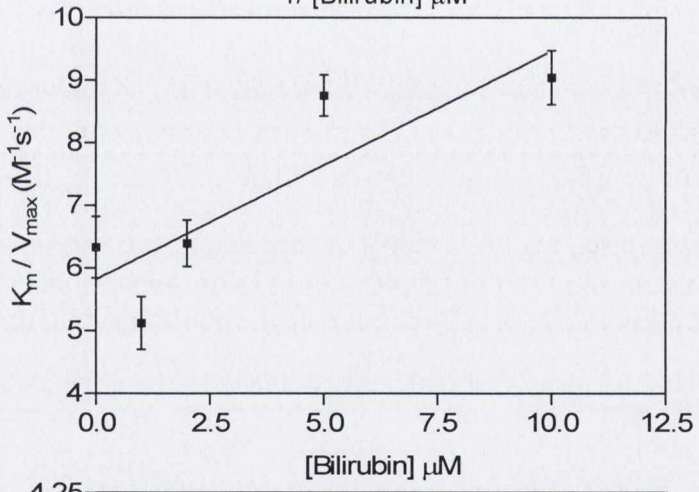
Km / Vmax (M-1s-1)
[Bilirubin] μM

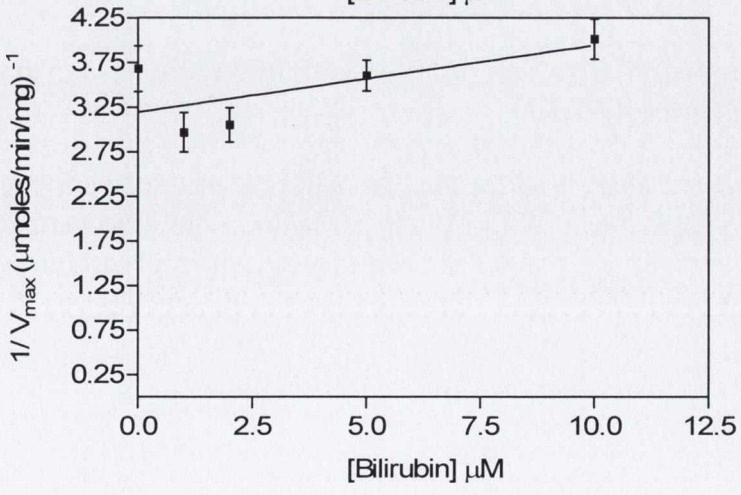
1/ Vmax (μmoles/min/mg) -1
[Bilirubin] μM

Figure 18. Product inhibition by bilirubin with biliverdin as the variable substrate at saturating levels of NADH

Biliverdin was the variable substrate at concentrations ranging from 0.5-10μM. NADH was held constant at saturating levels (1000μM). Bilirubin was increased from 0-10μM. Reactions were performed in sodium citrate (100mM), pH5 and were initiated by the addition of sBVR-A (5μg). Experiments were performed in triplicate. Each data point represents the mean and error bars represent the standard deviation of the triplicate values. The curves are least squares fit to the Michaelis-Menten equation.

Figure 19. Double reciprocal plots of initial rate against biliverdin concentration at varying concentrations of bilirubin

When the initial rates (see Fig. 18) were re-plotted as double reciprocals a pattern of linear intersecting lines was produced. These lines intersect to the left of the y-axis indicating mixed inhibition.

Figure 20. Slope re-plot of bilirubin inhibition with biliverdin as the variable substrate at saturating levels of NADH

When the K_m / V_{max} (slope) values from the double-reciprocal plot shown in Fig. 19 were re-plotted against the concentration of bilirubin a linear relationship was obtained where the line intersected the x-axis at $-K_{is}$. From this point the K_{is} value for bilirubin against biliverdin was calculated (see Table 4.4) Error bars represent the standard error

Figure 21. Intercept re-plot of bilirubin inhibition with biliverdin as the variable substrate at saturating levels of NADH

When the 1/ V_{max} (intercept) values from the double-reciprocal plot shown in Fig. 19 were re-plotted against the concentration of bilirubin a linear relationship was obtained where the line intersected the x-axis at $-K_{ii}$. From this point the K_{ii} value for bilirubin against biliverdin was calculated (see Table 4.4). Error bars represent the standard error

Appendix III

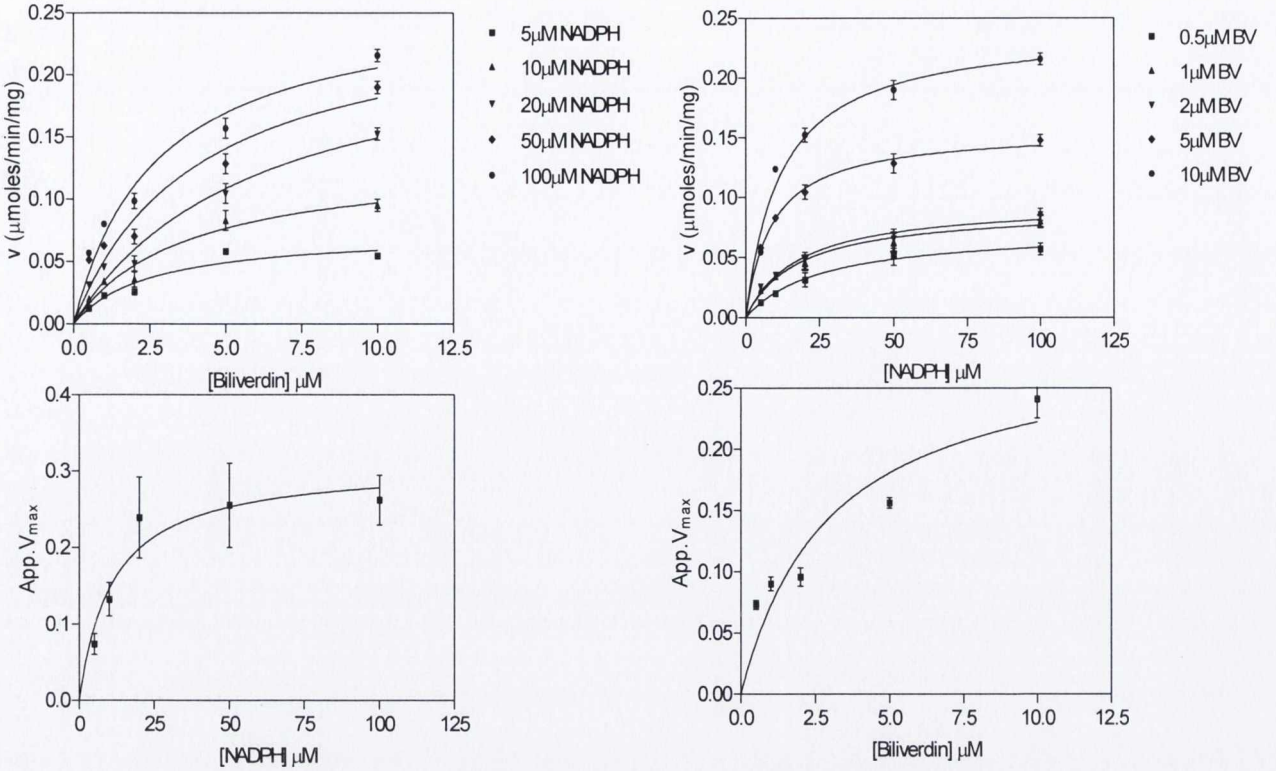

Figure 1. Initial rate kinetics of sBVR-A with NADPH as co-factor at pH 4.25

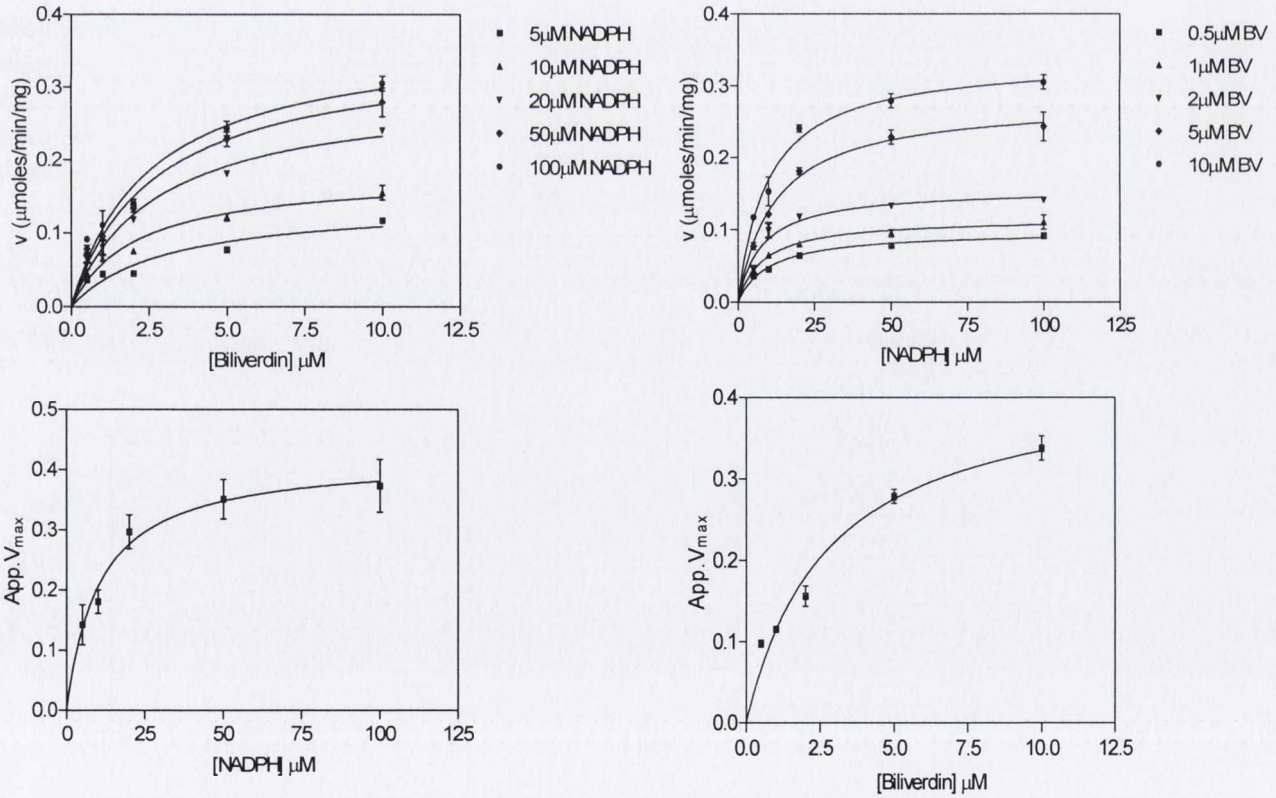

Figure 2. Initial rate kinetics of sBVR-A with NADPH as co-factor at pH 4.5

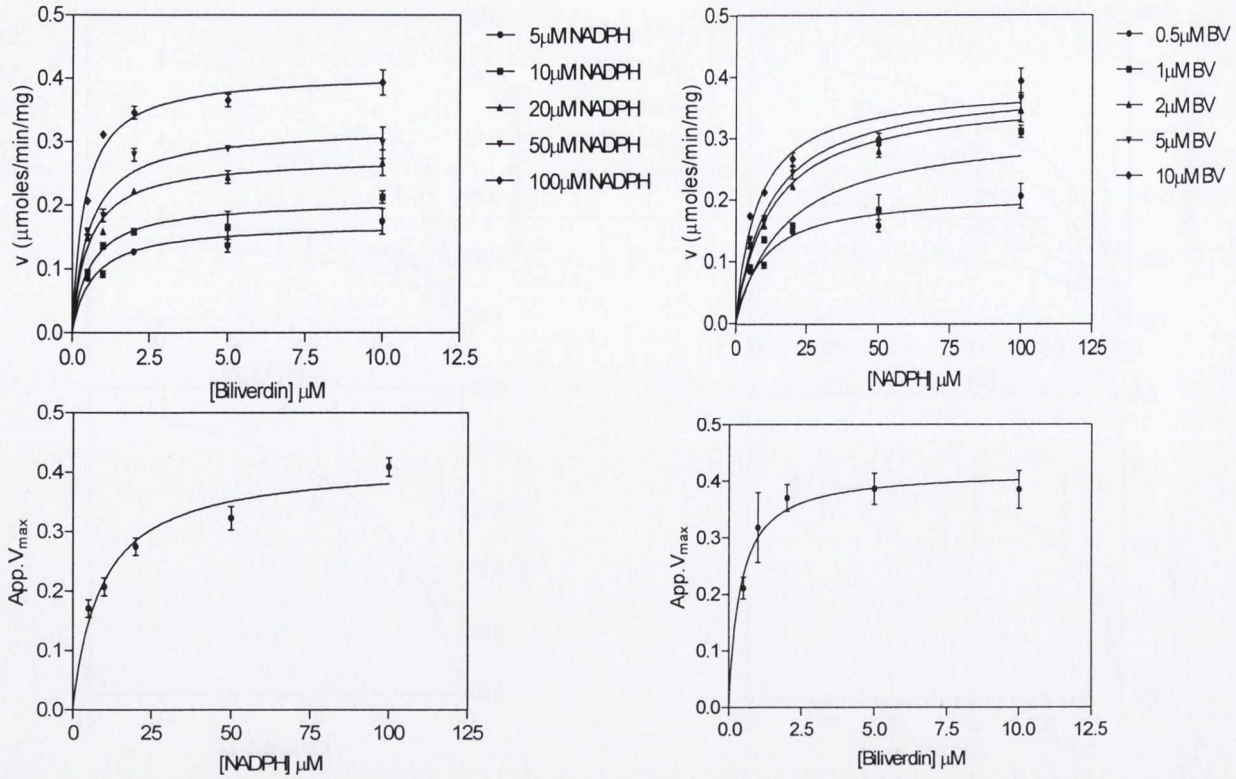

Figure 3. Initial rate kinetics of sBVR-A with NADPH as co-factor at pH 4.52

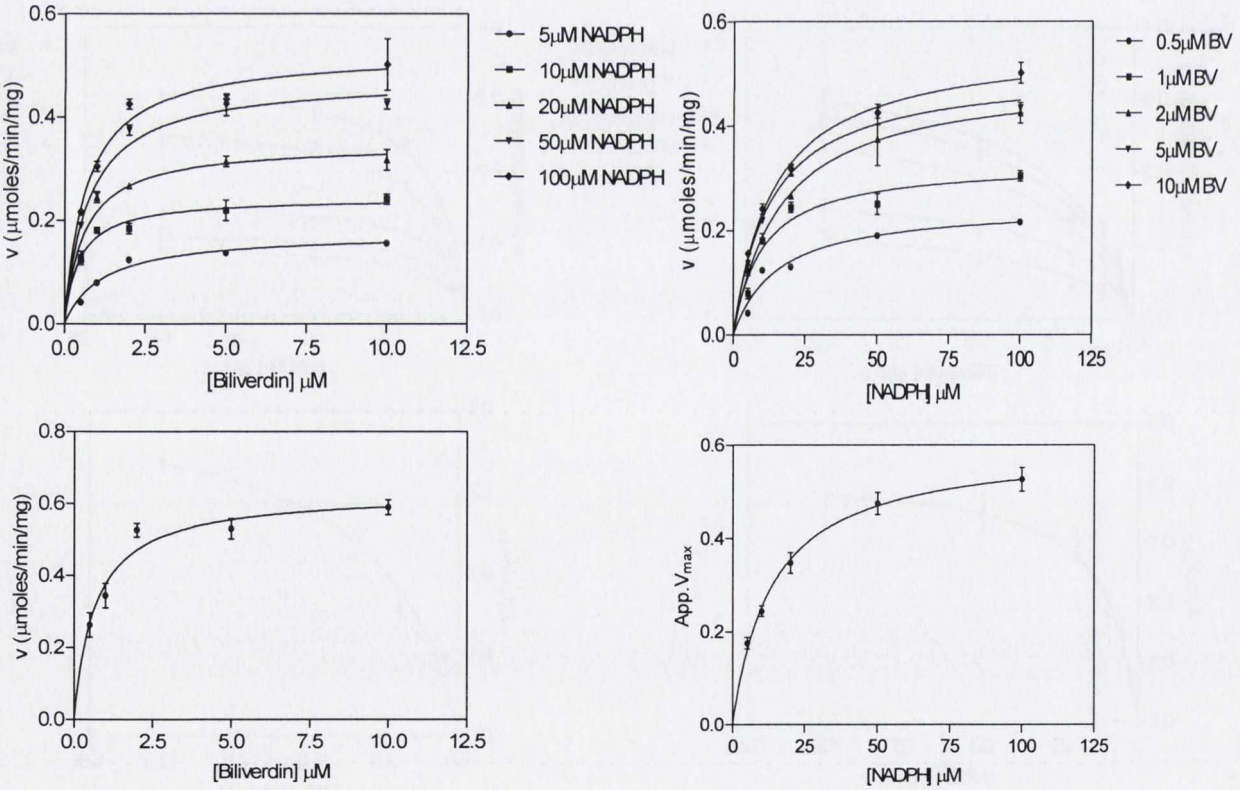

Figure 4. Initial rate kinetics of sBVR-A with NADPH as co-factor at pH 4.6

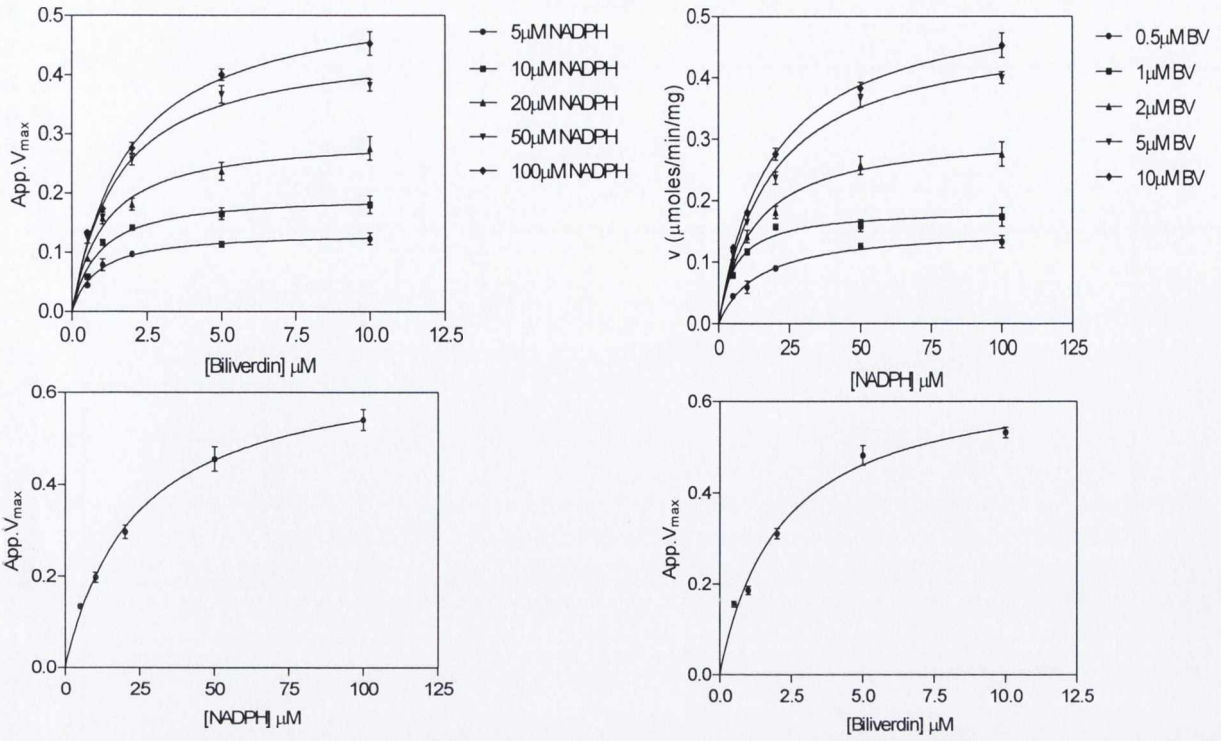

Figure 5. Initial rate kinetics of sBVR-A with NADPH as co-factor at pH 4.65

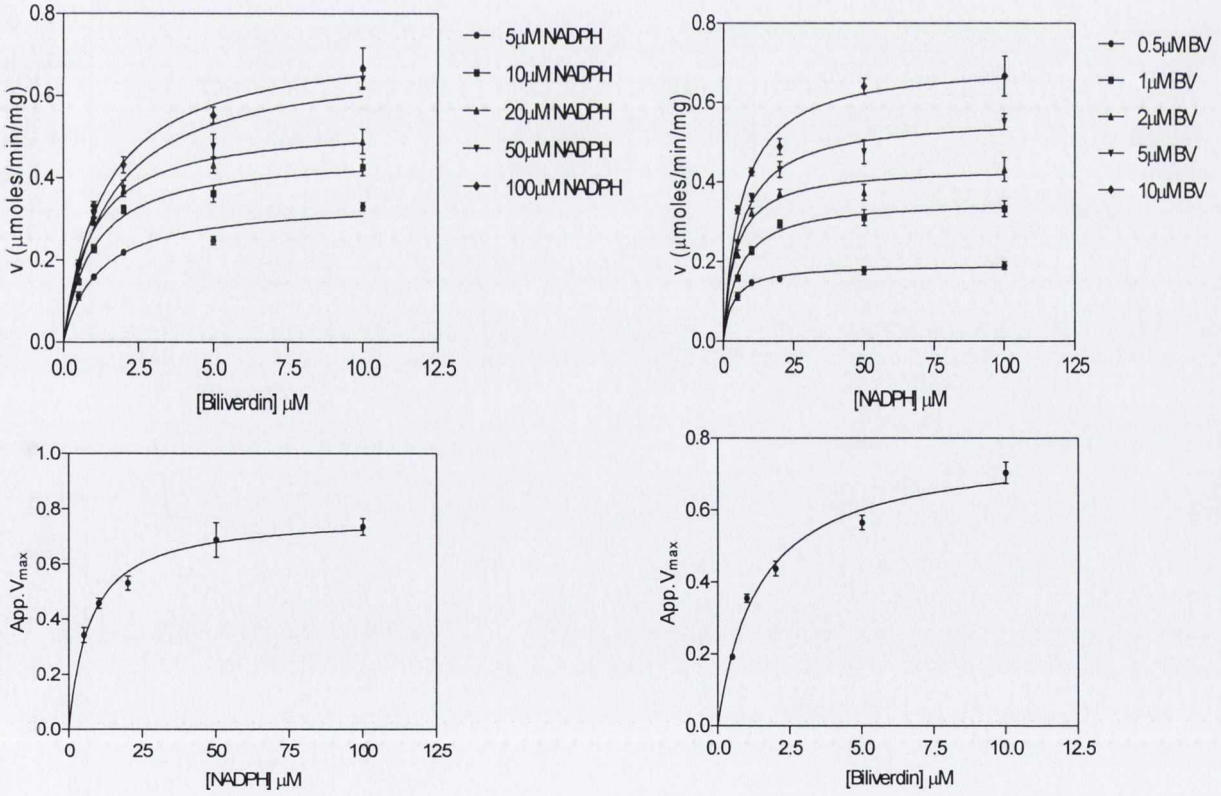

Figure 6. Initial rate kinetics of sBVR-A with NADPH as co-factor at pH 4.75

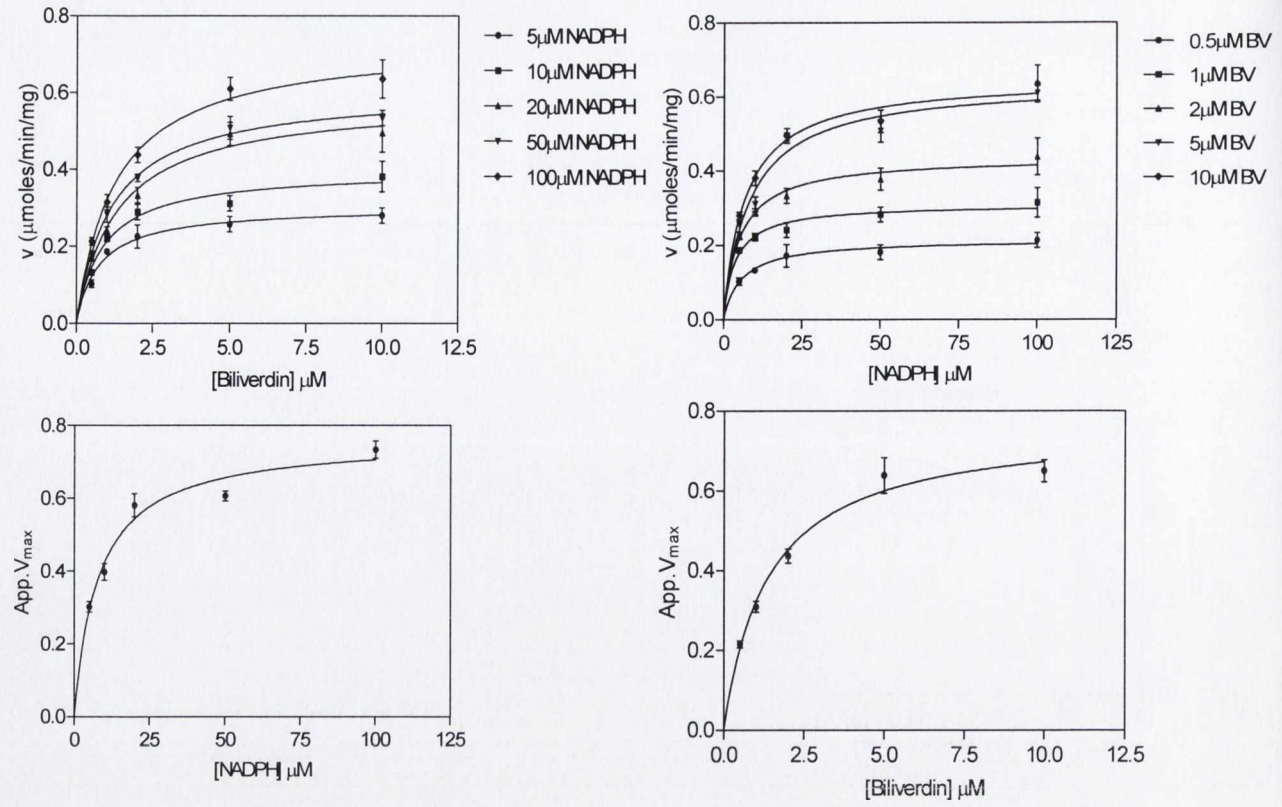

Figure 7. Initial rate kinetics of sBVR-A with NADPH as co-factor at pH 4.87

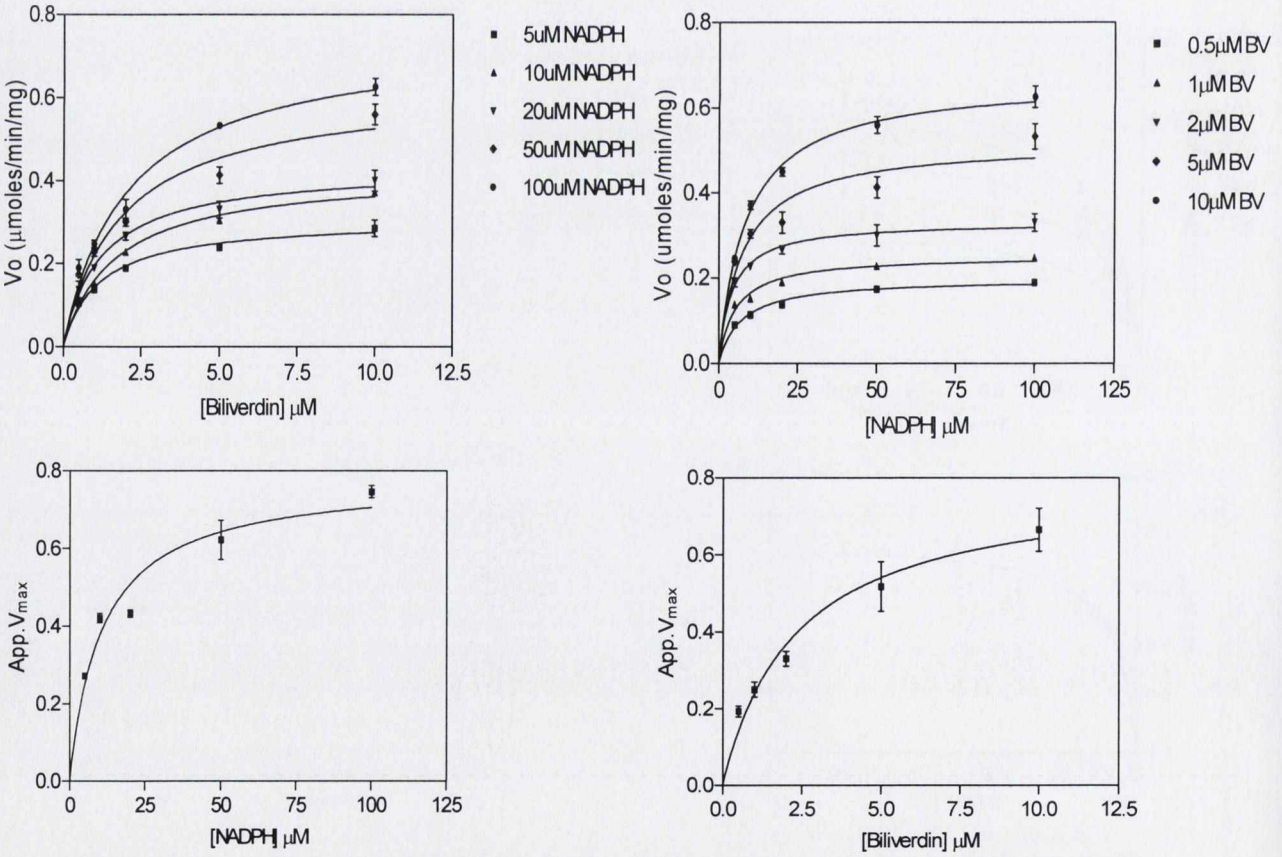

Figure 8. Initial rate kinetics of sBVR-A with NADPH as co-factor at pH 5

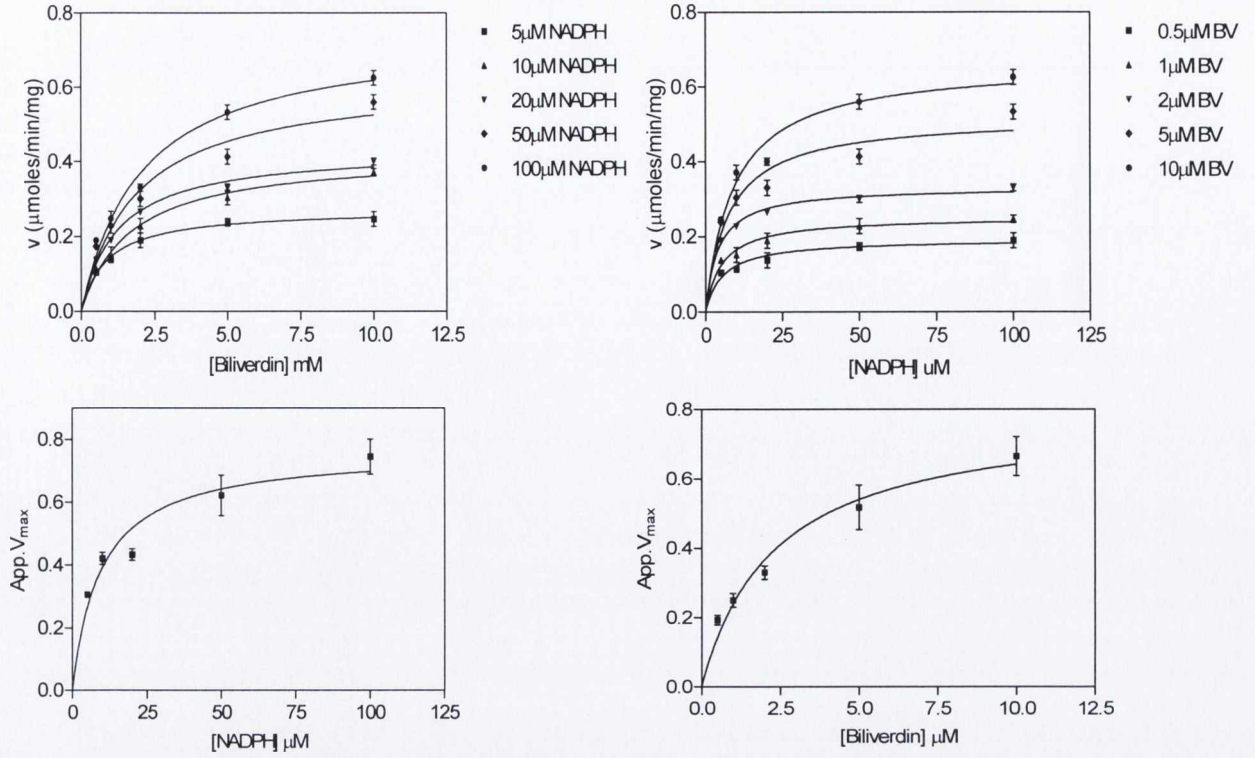

Figure 9. Initial rate kinetics of sBVR-A with NADPH as co-factor at pH5.12

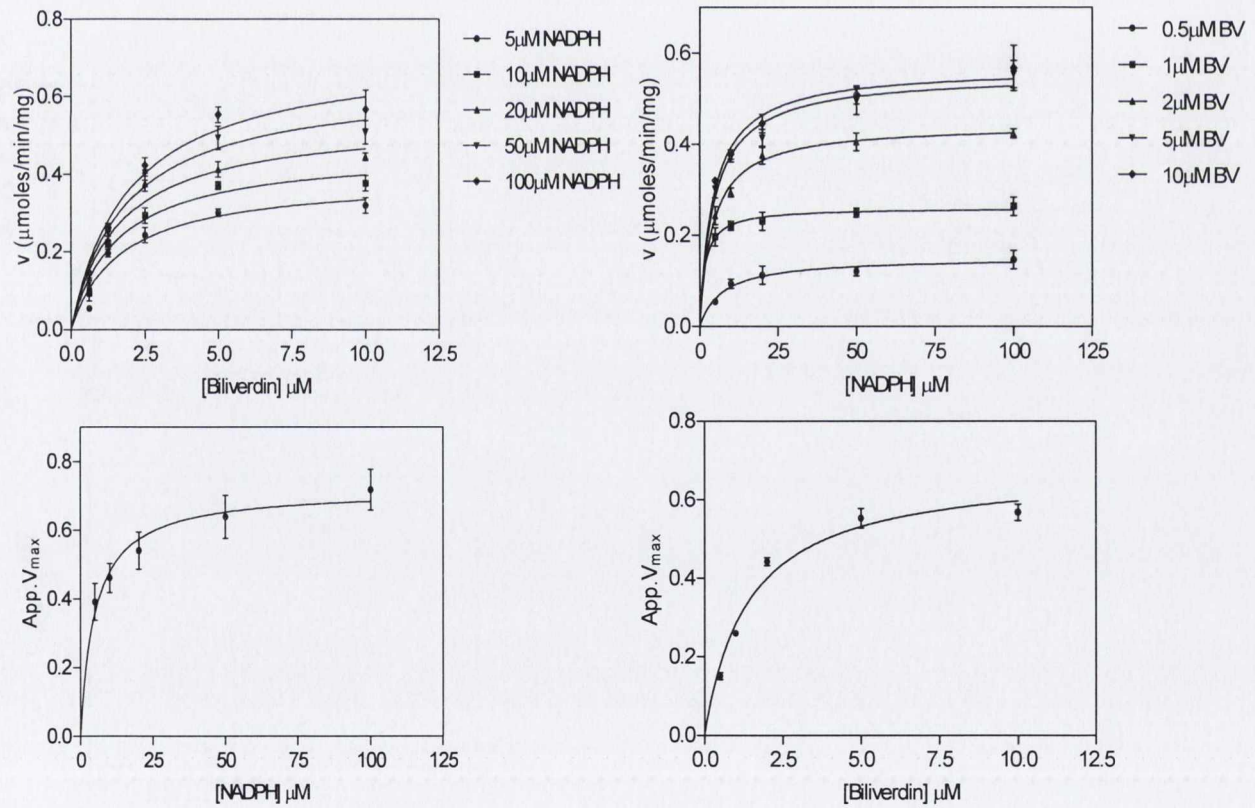

Figure 10. Initial rate kinetics of sBVR-A with NADPH as co-factor at pH 5.13

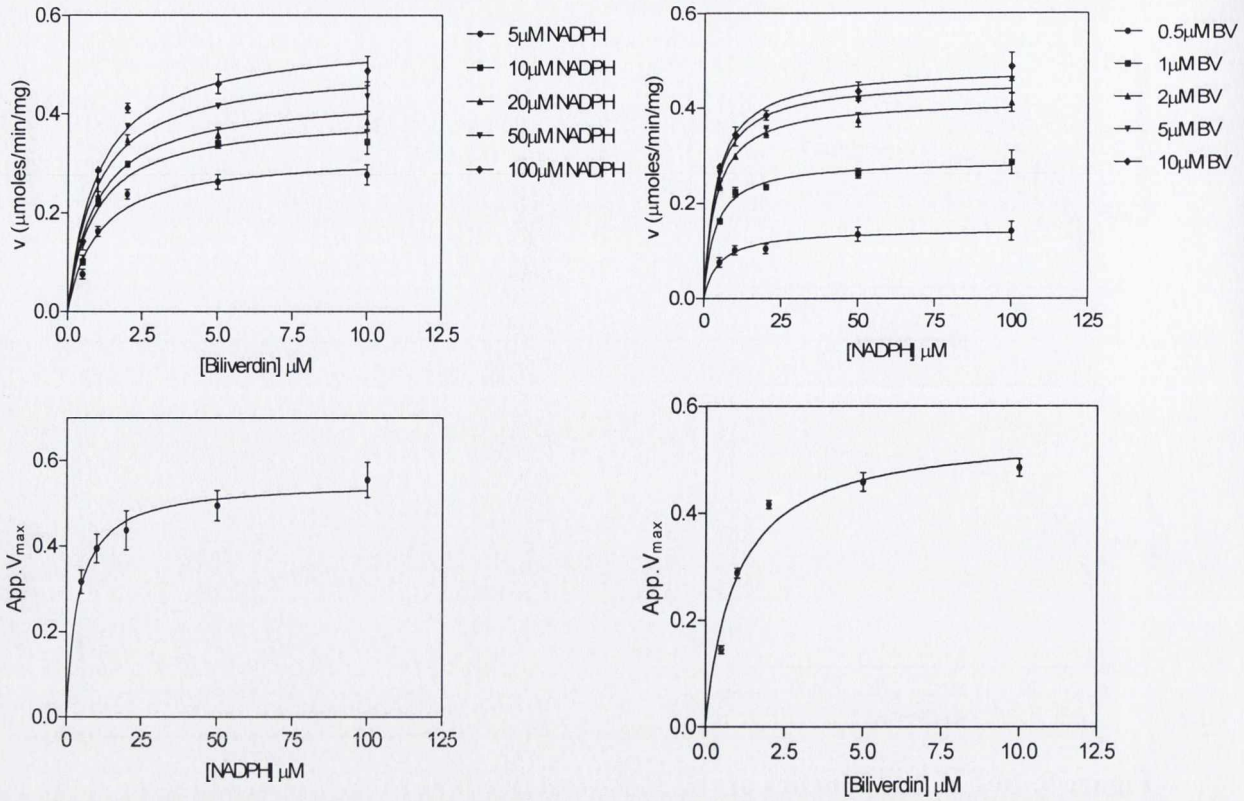

Figure 11. Initial rate kinetics of sBVR-A with NADPH as co-factor at pH 5.25

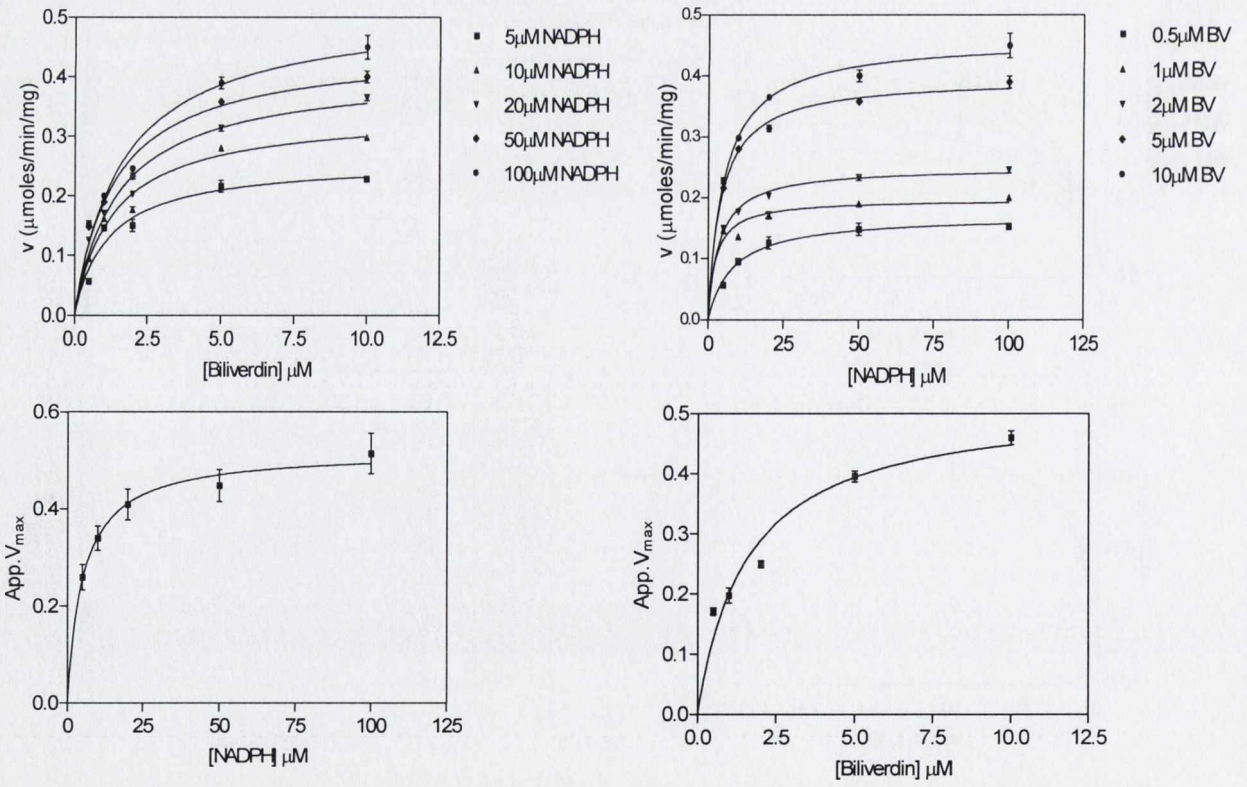

Figure 12. Initial rate kinetics of sBVR-A with NADPH as co-factor at pH 5.37

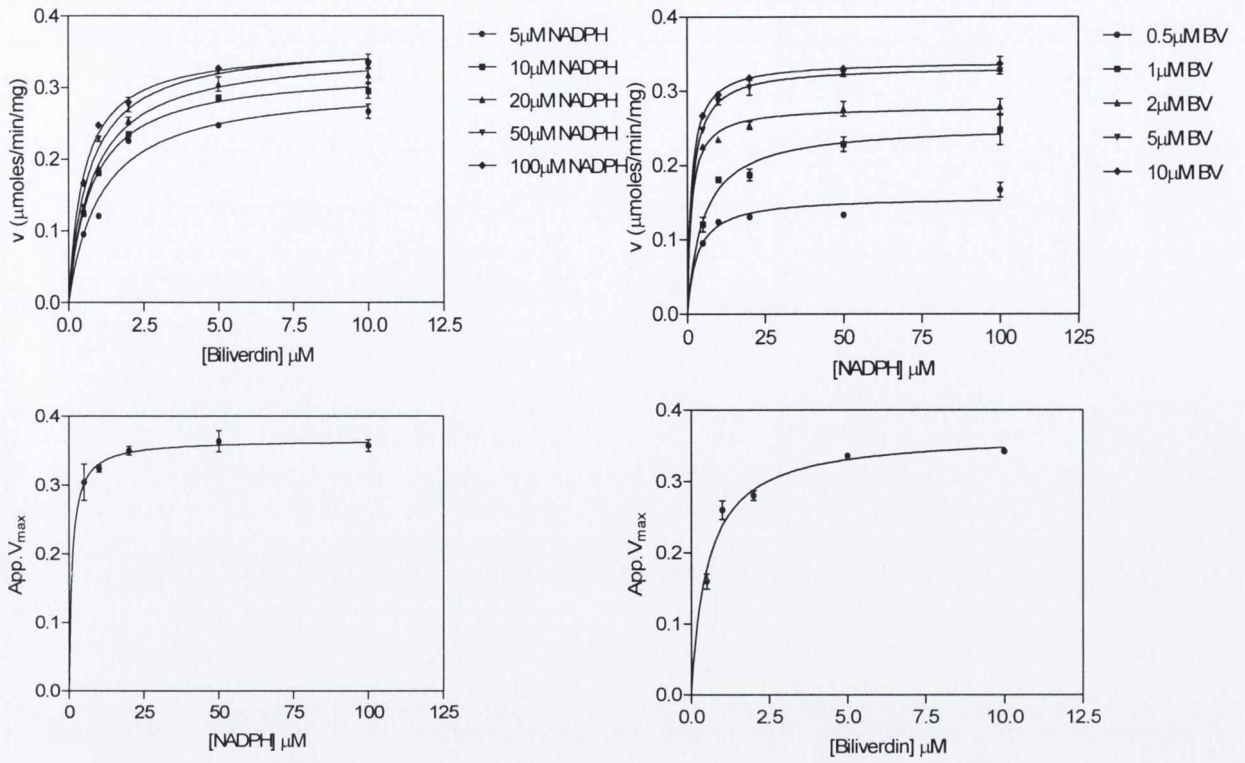

Figure 13. Initial rate kinetics of sBVR-A with NADPH as co-factor at pH 5.5

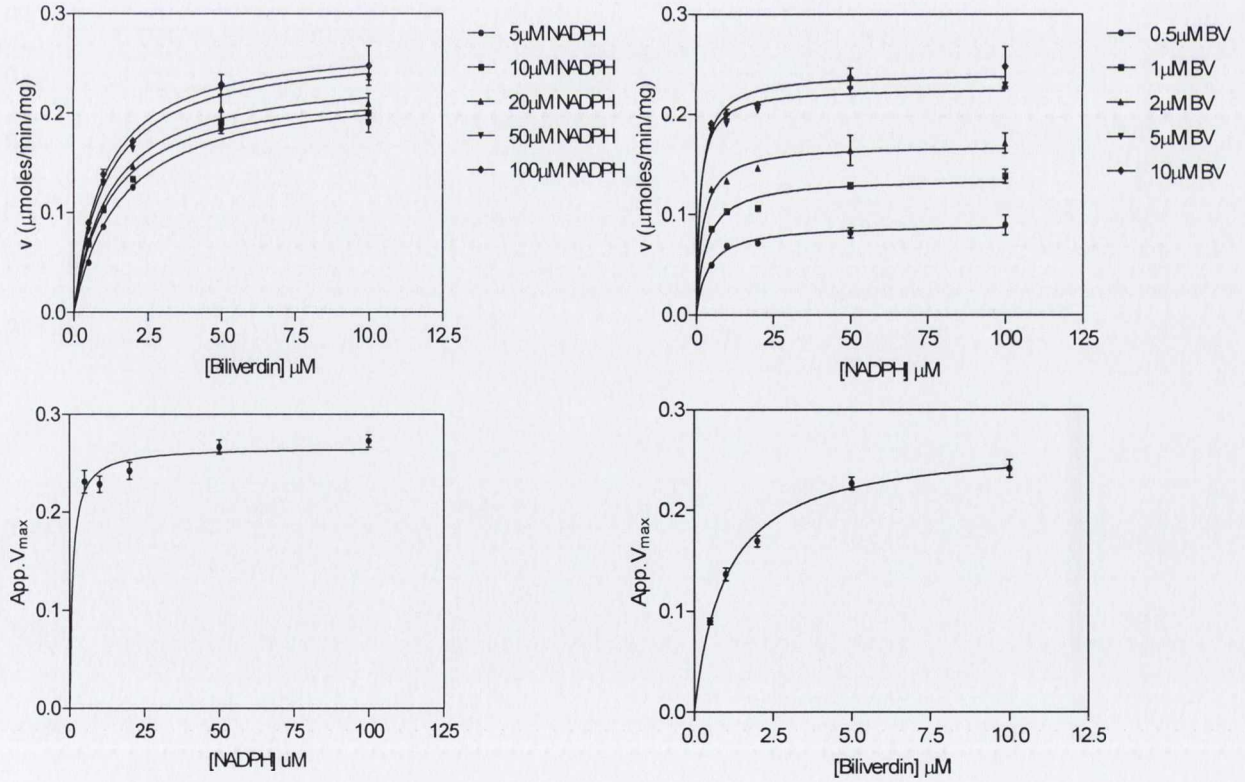

Figure 14. Initial rate kinetics of sBVR-A with NADPH as co-factor at pH 6

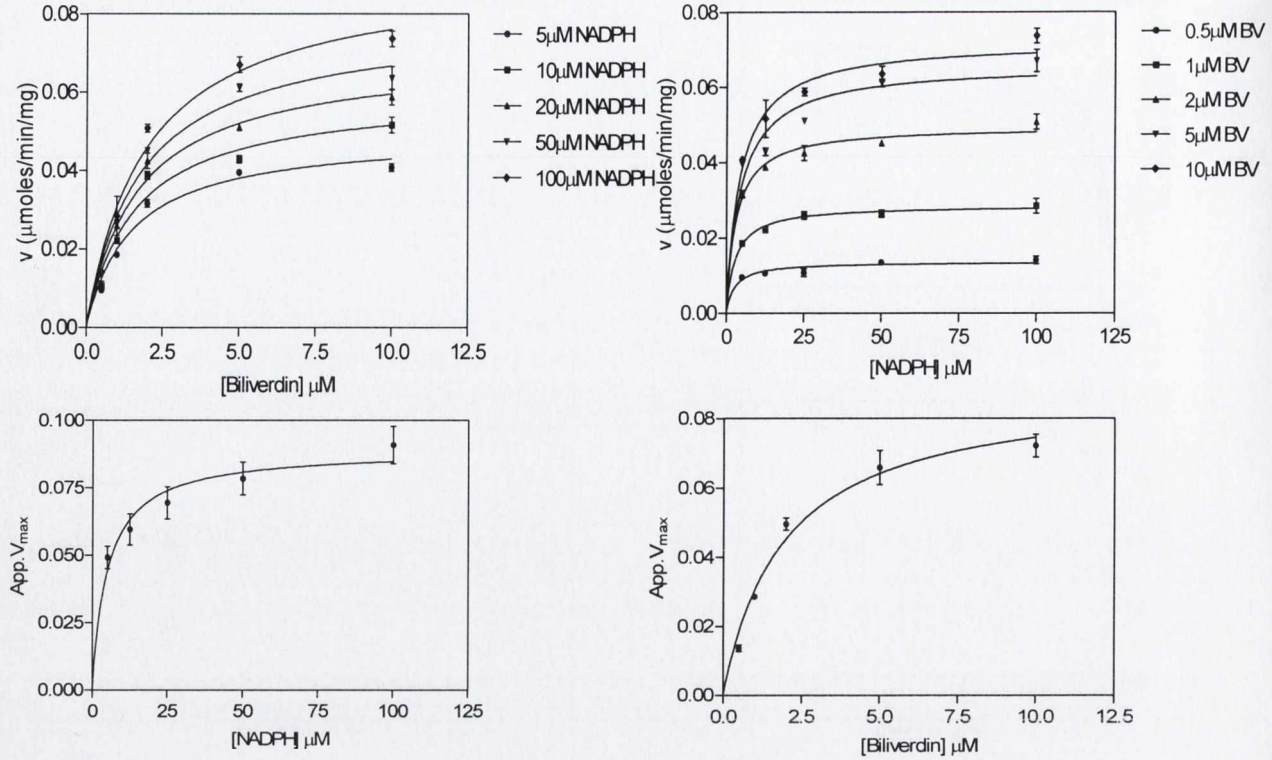

Figure 15. Initial rate kinetics of sBVR-A with NADPH as co-factor at pH 6.5

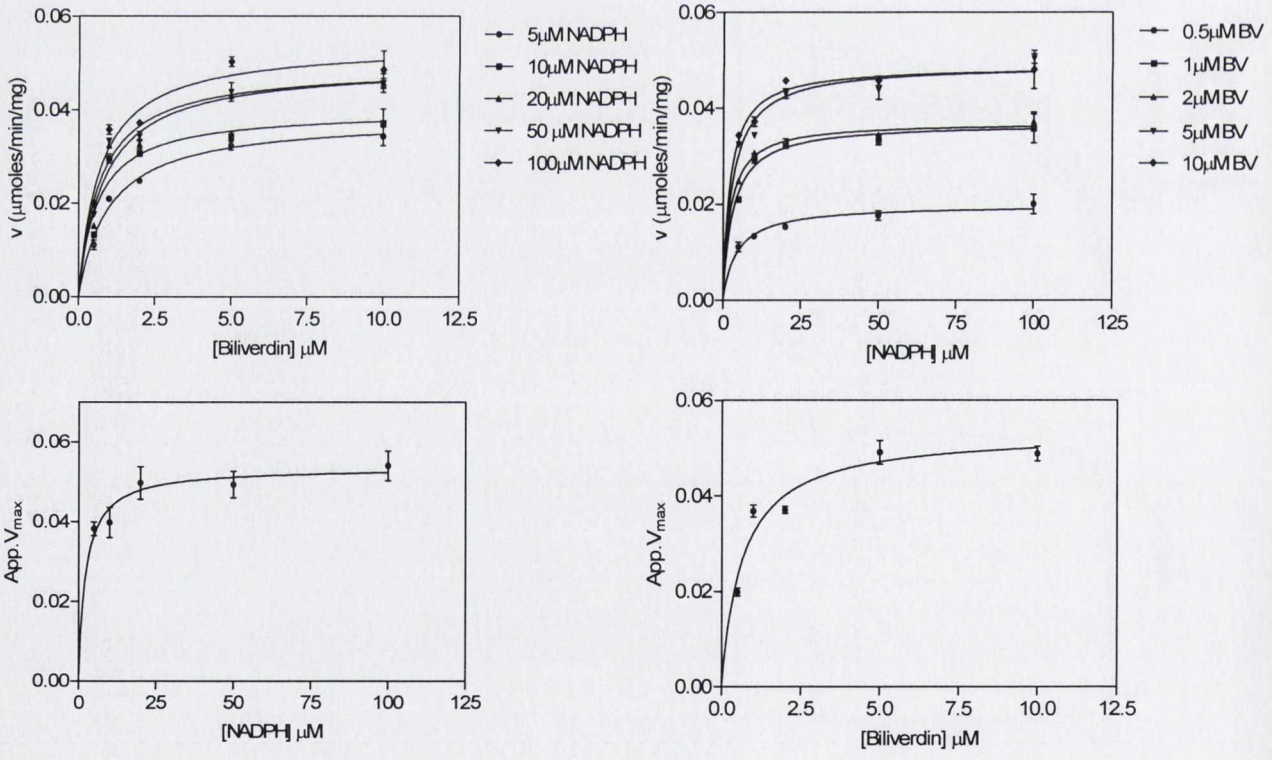

Figure 16. Initial rate kinetics of sBVR-A with NADPH as co-factor at pH 7

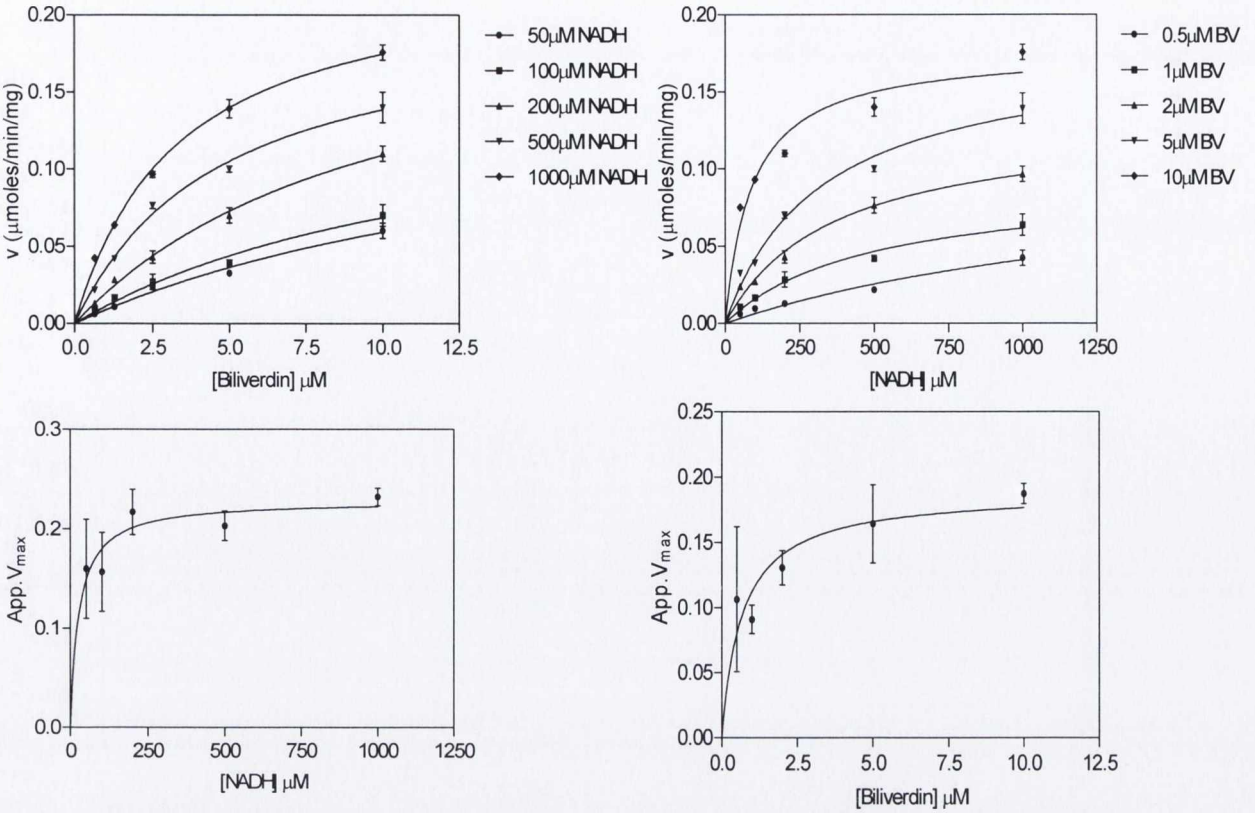

Figure 17. Initial rate kinetics of sBVR-A with NADH as co-factor at pH 4.25

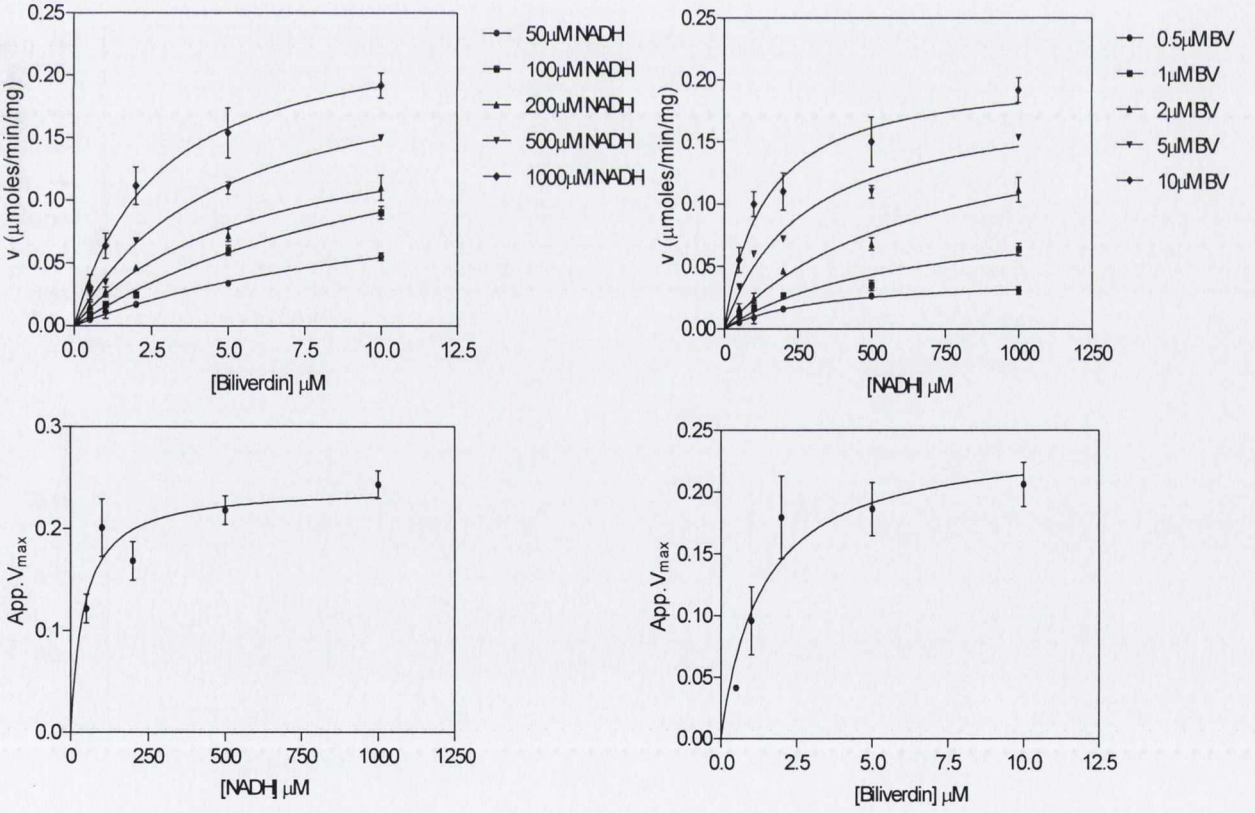

Figure 18. Initial rate kinetics of sBVR-A with NADH as co-factor at pH 4.5

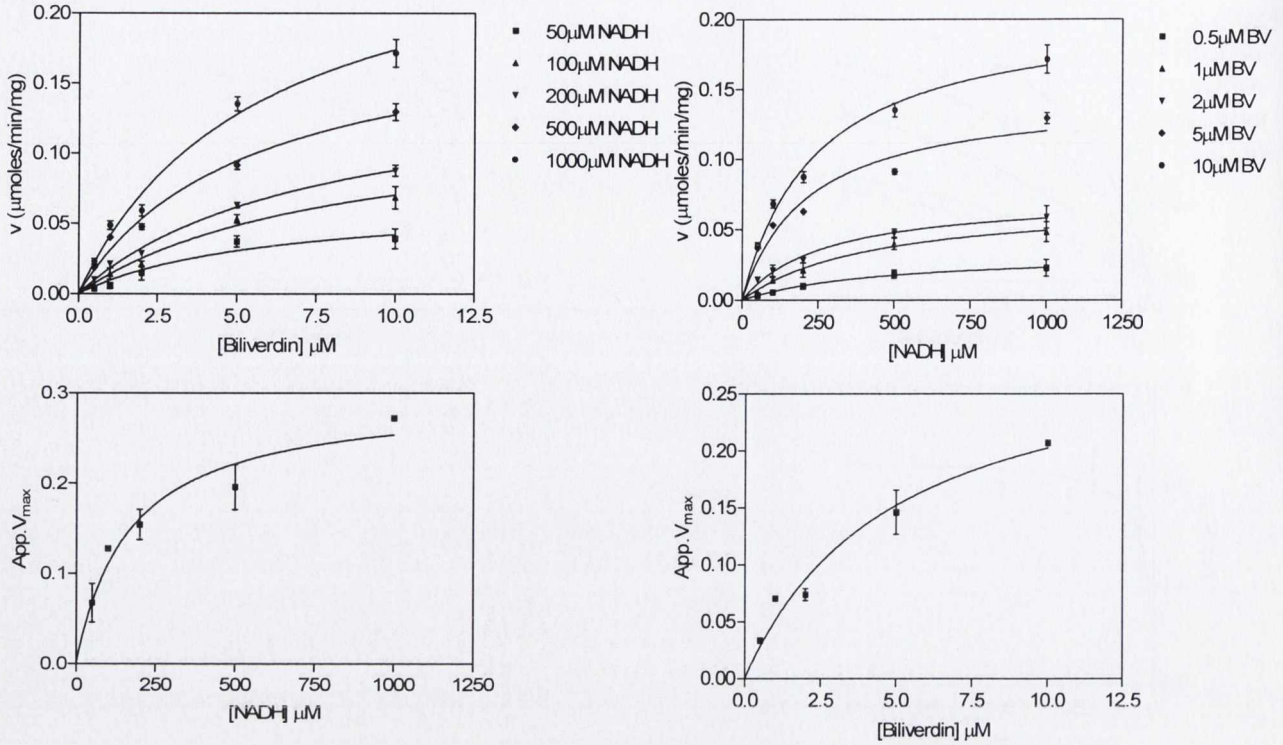

Figure 19. Initial rate kinetics of sBVR-A with NADH as co-factor at pH 4.62

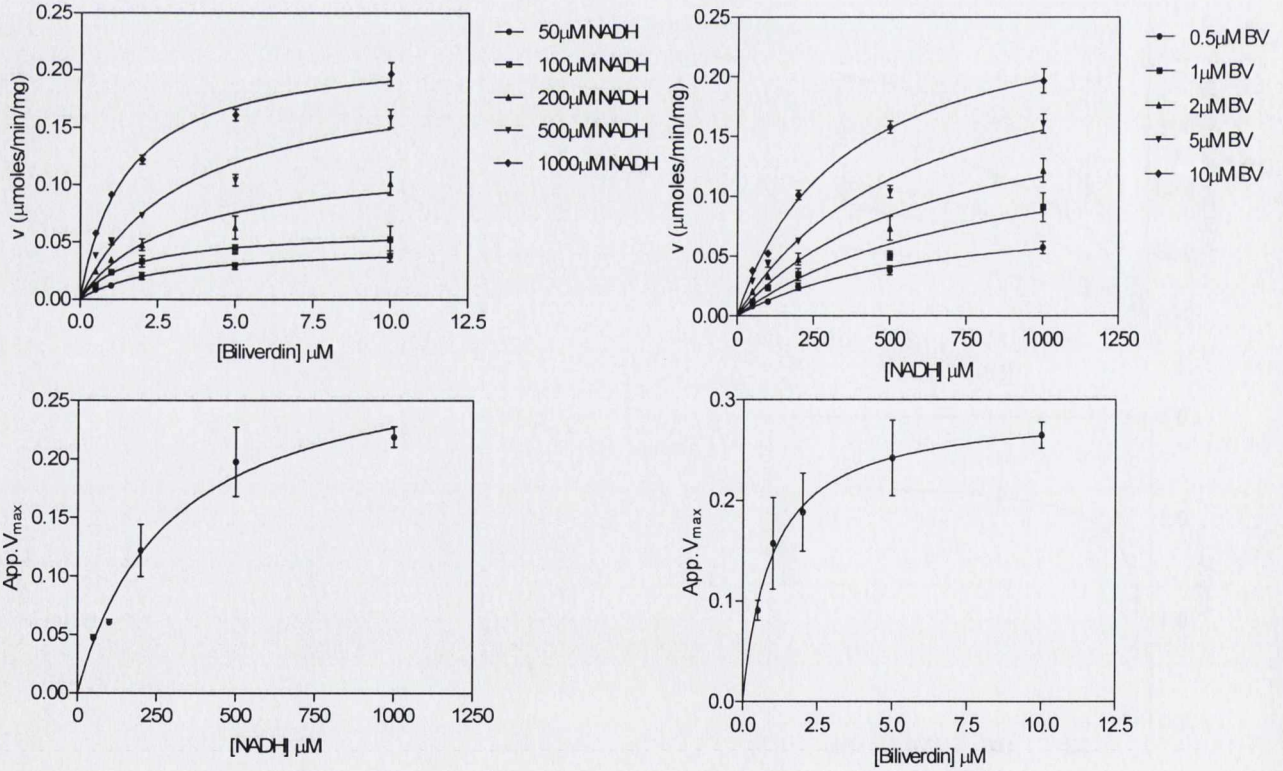

Figure 20. Initial rate kinetics of sBVR-A with NADH as co-factor at pH 4.81

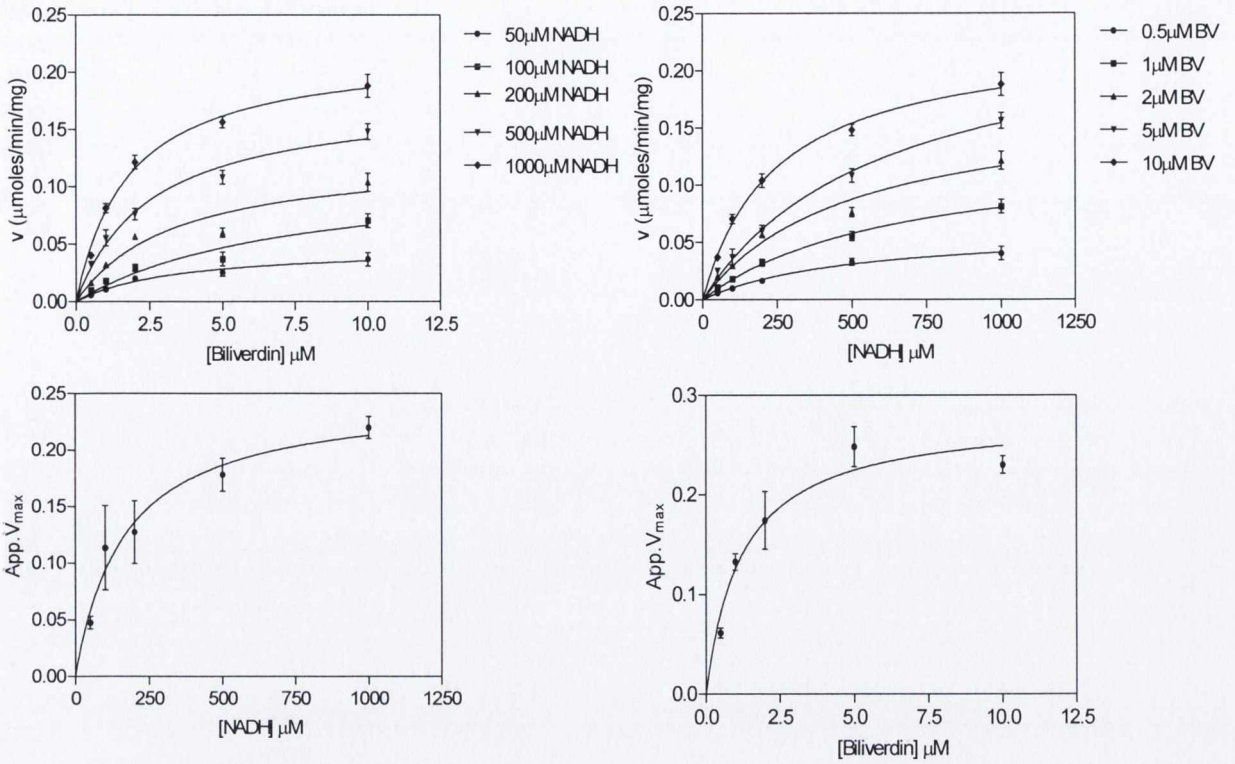

Figure 21. Initial rate kinetics of sBVR-A with NADH as co-factor at pH 4.9

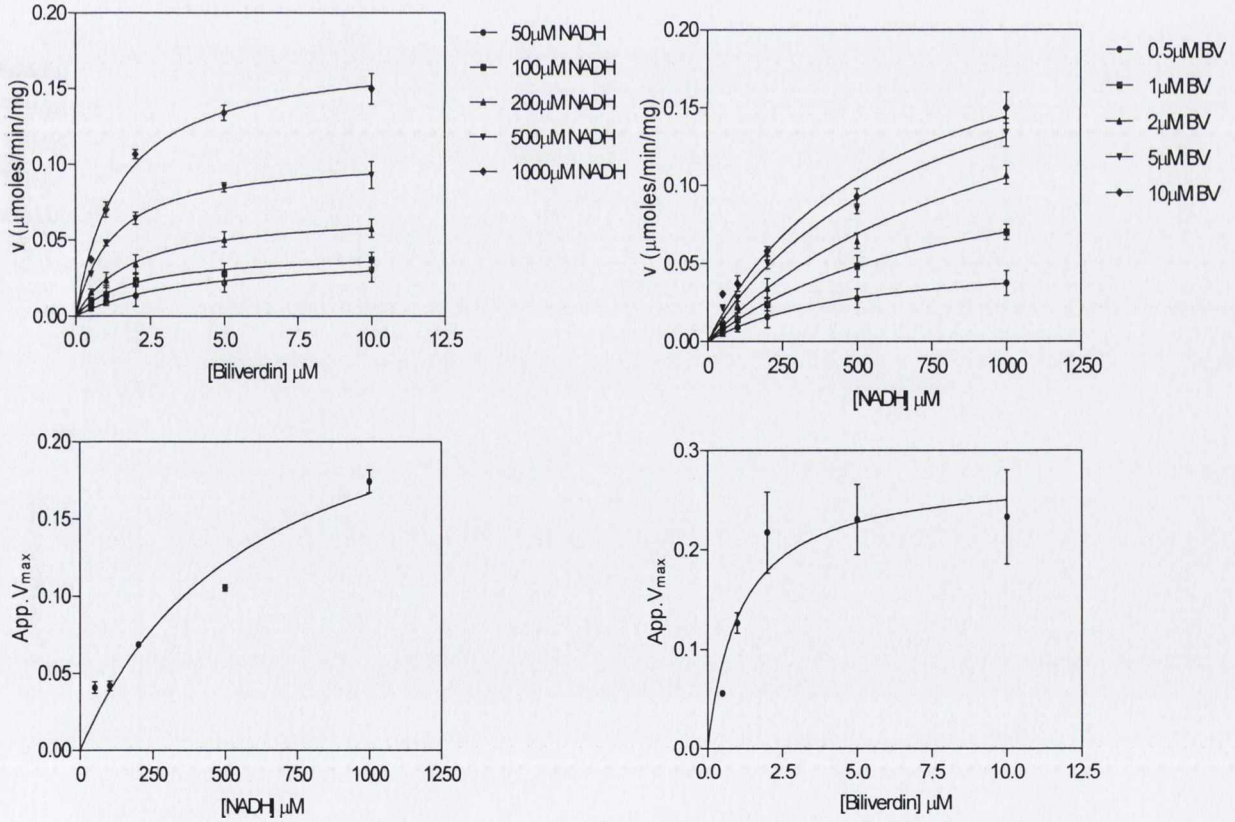

Figure 22. Initial rate kinetics of sBVR-A with NADH as co-factor at pH 5.1

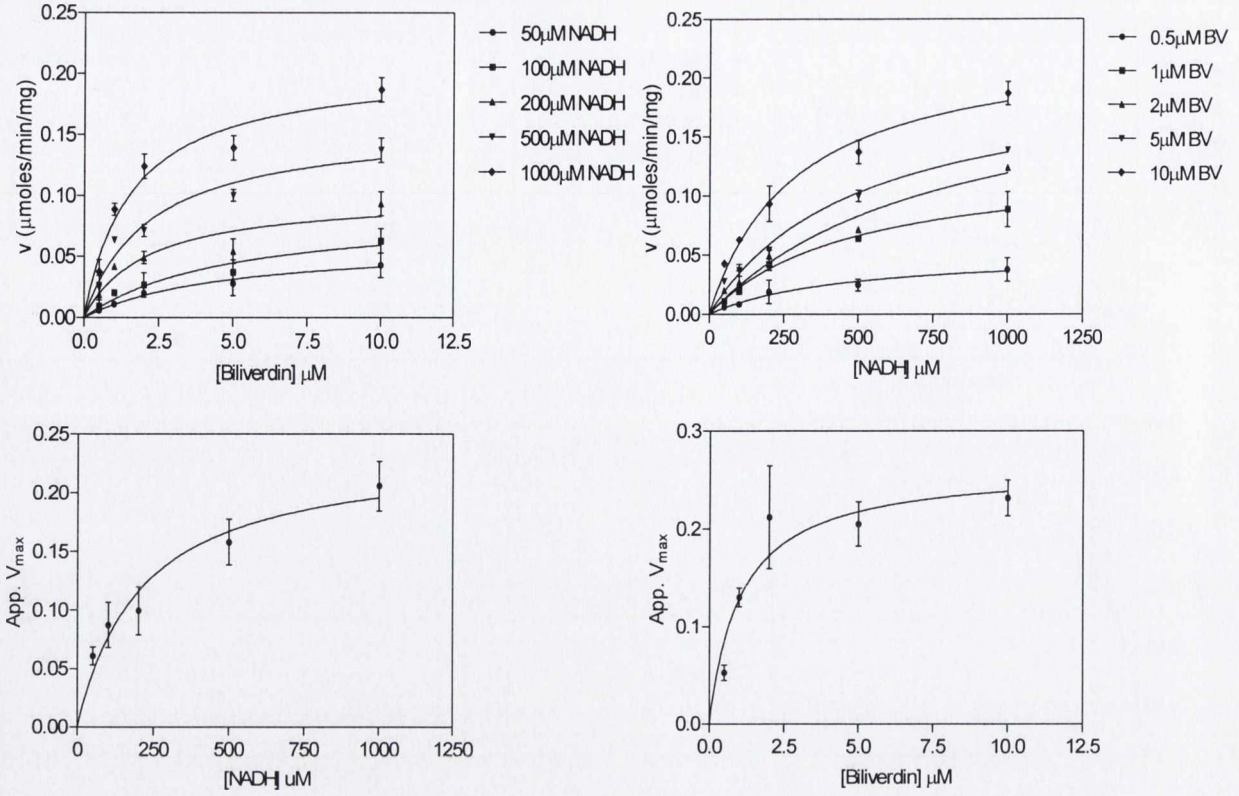

Figure 23. Initial rate kinetics of sBVR-A with NADH as co-factor at pH 5.25

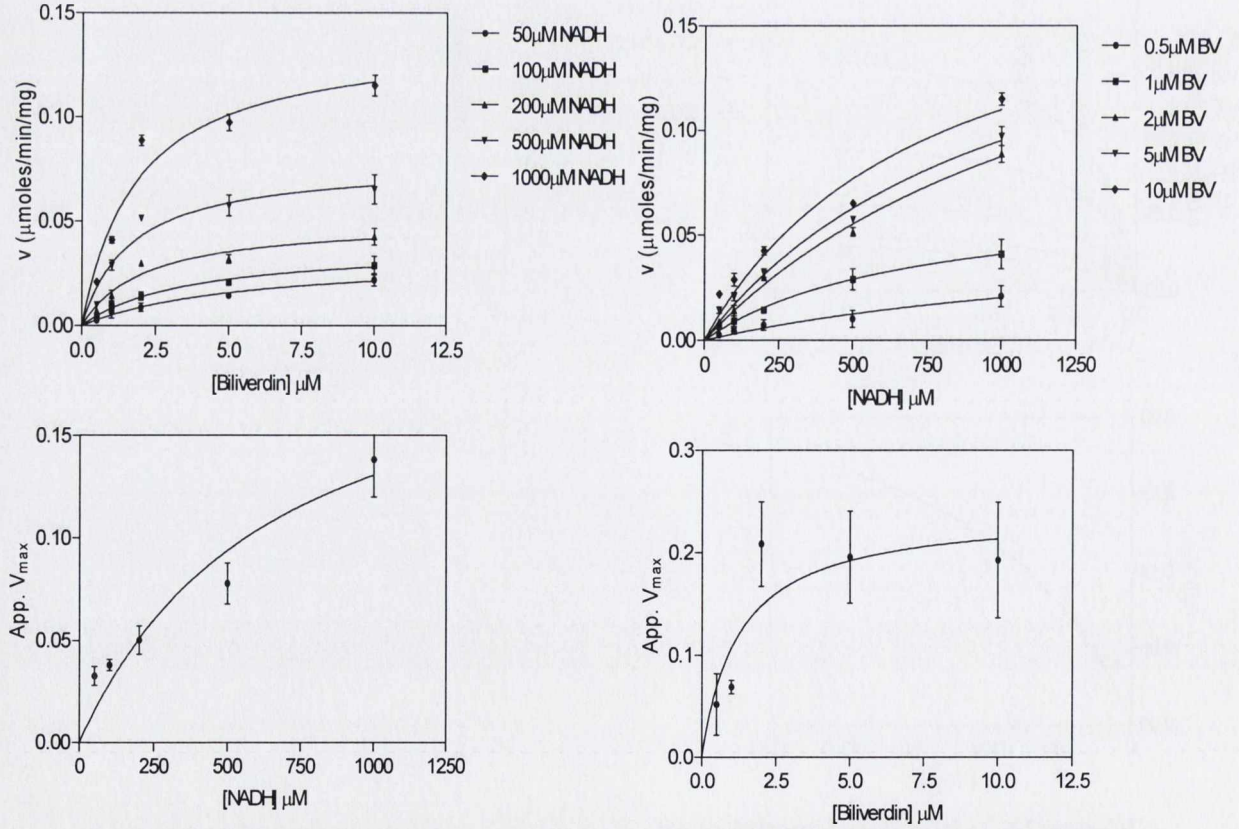

Figure 24. Initial rate kinetics of sBVR-A with NADH as co-factor at pH 5.5

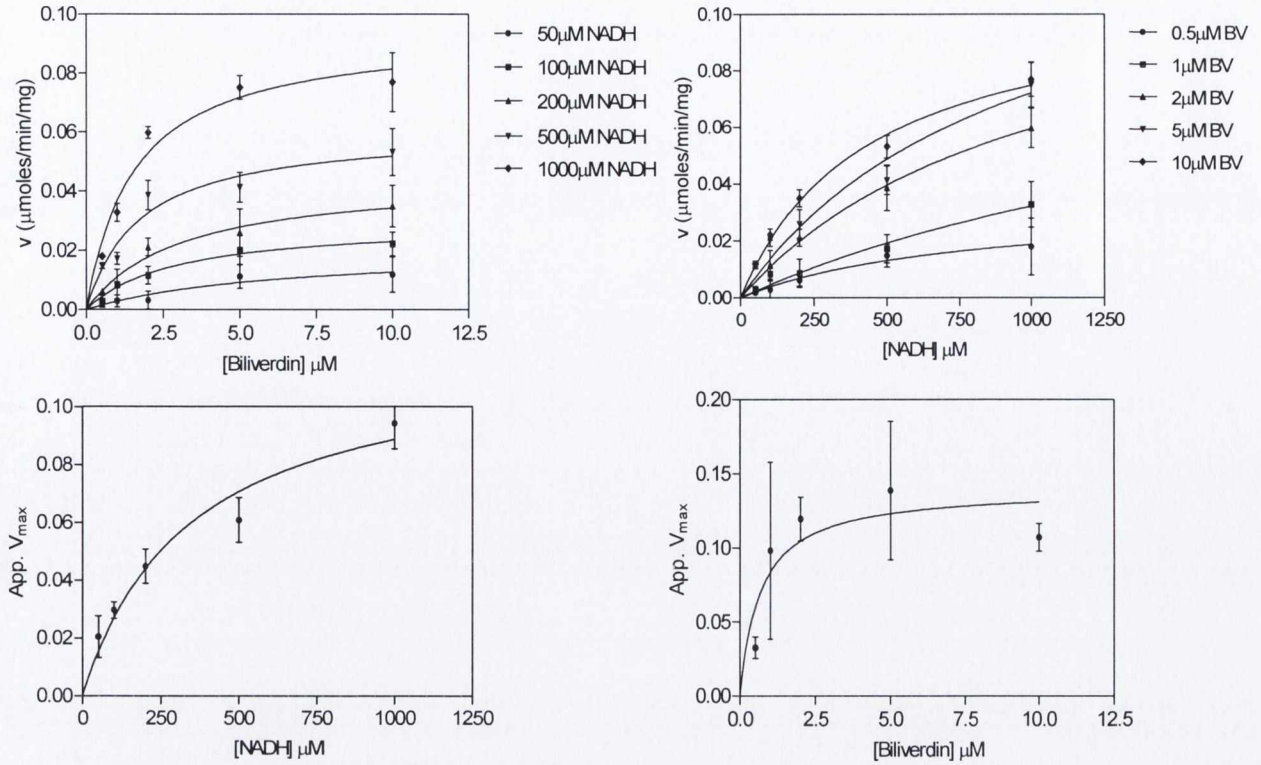

Figure 25. Initial rate kinetics of sBVR-A with NADH as co-factor at pH 5.75

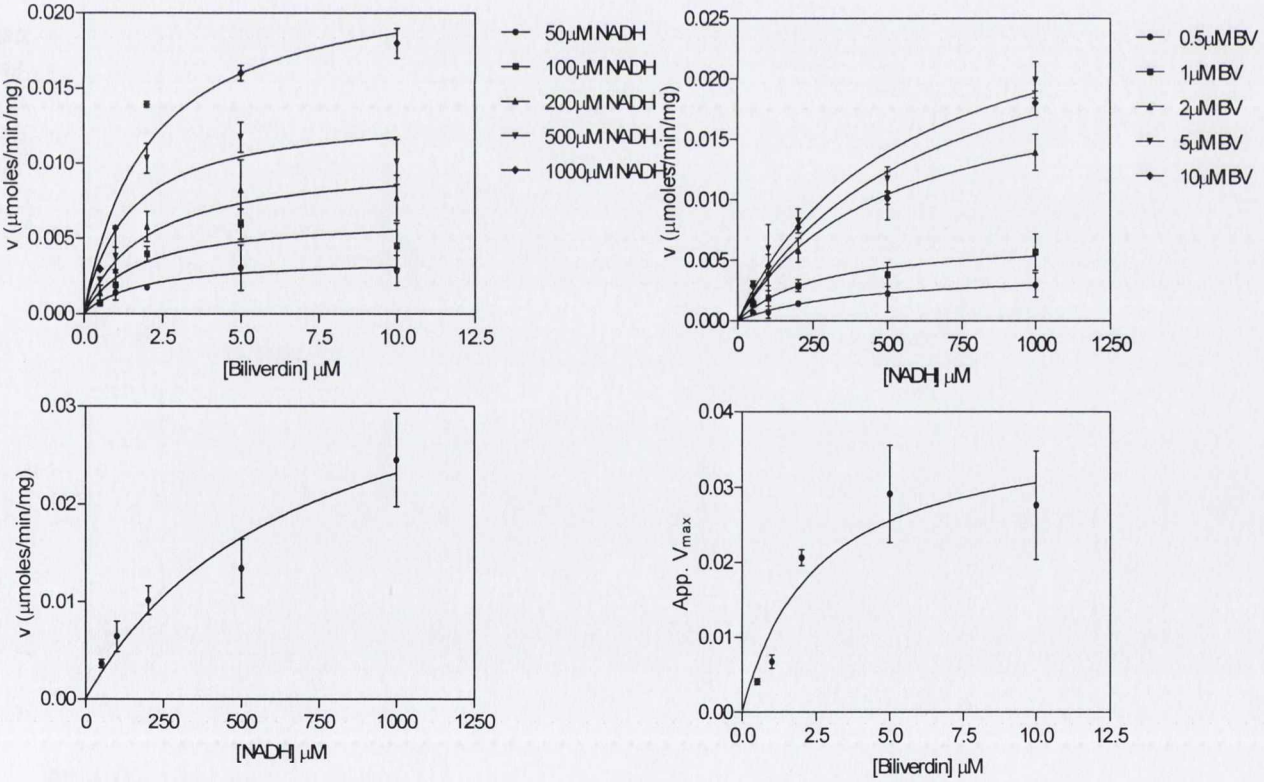

Figure 26. Initial rate kinetics of sBVR-A with NADH as co-factor at pH 6.24

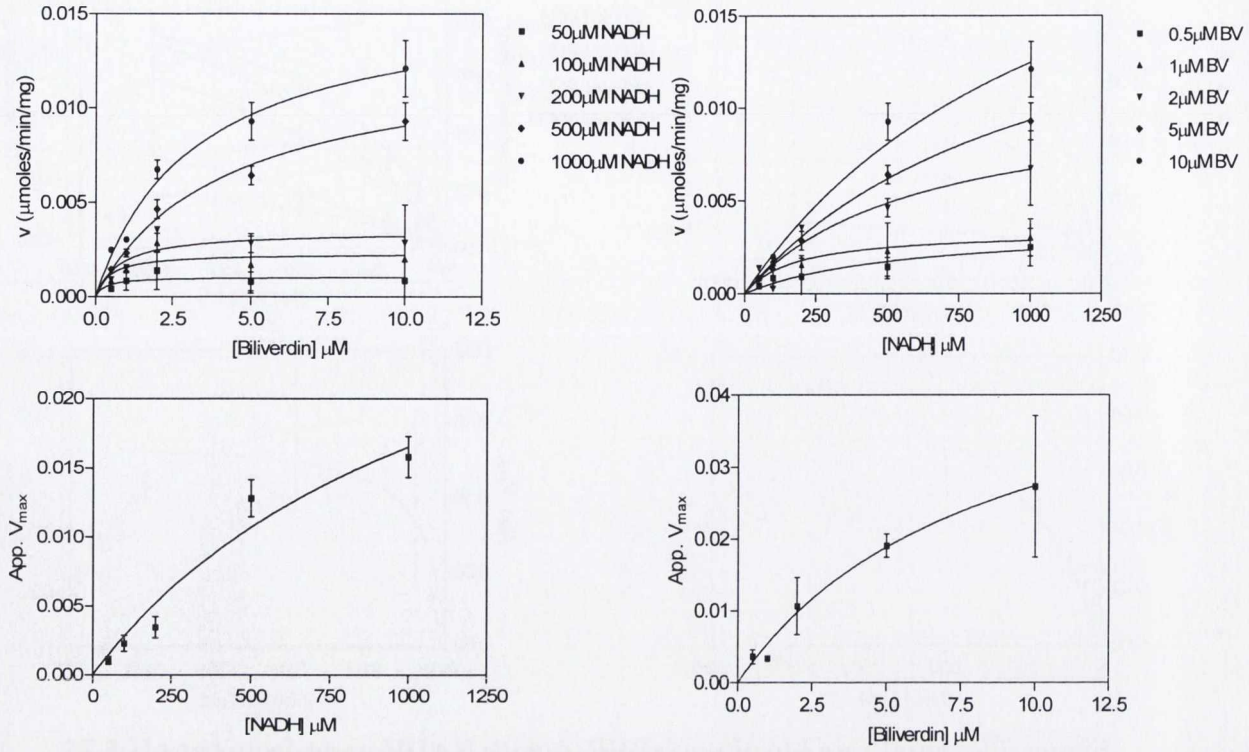

Figure 27. Initial rate kinetics of sBVR-A with NADH as co-factor at pH 6.5

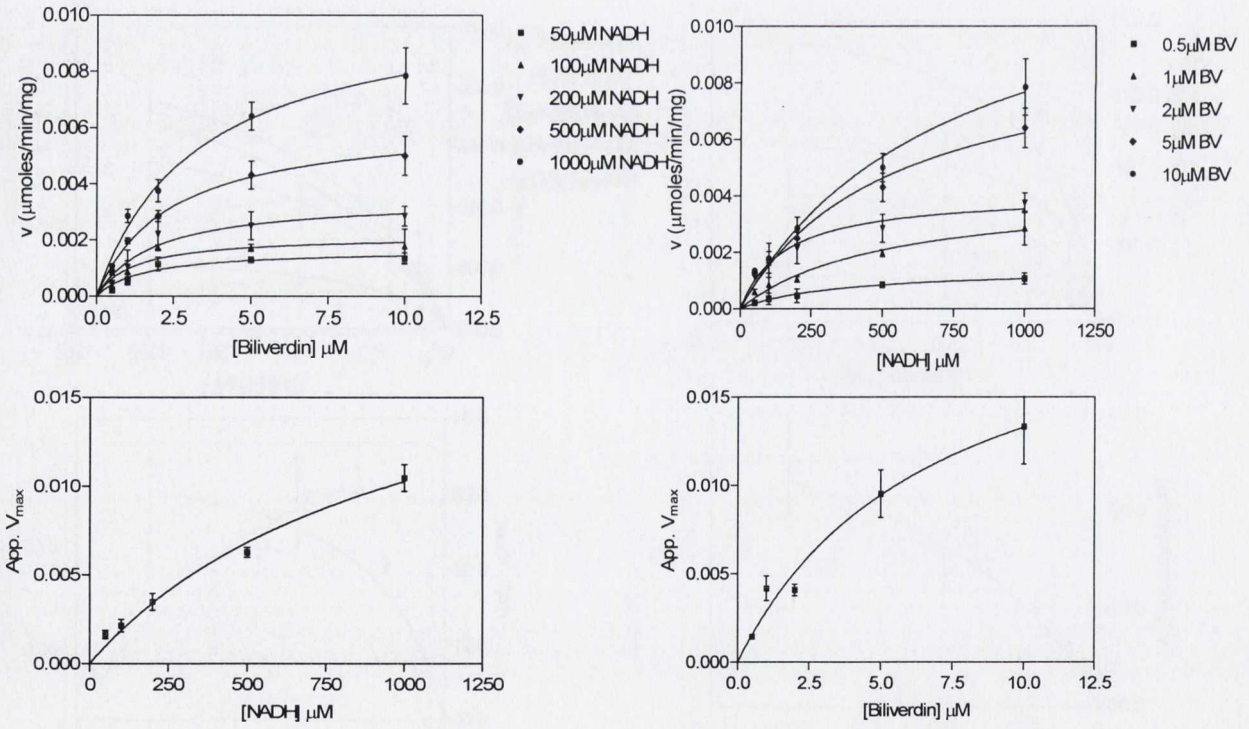

Figure 28. Initial rate kinetics of sBVR-A with NADH as co-factor at pH 6.75

Appendix IV

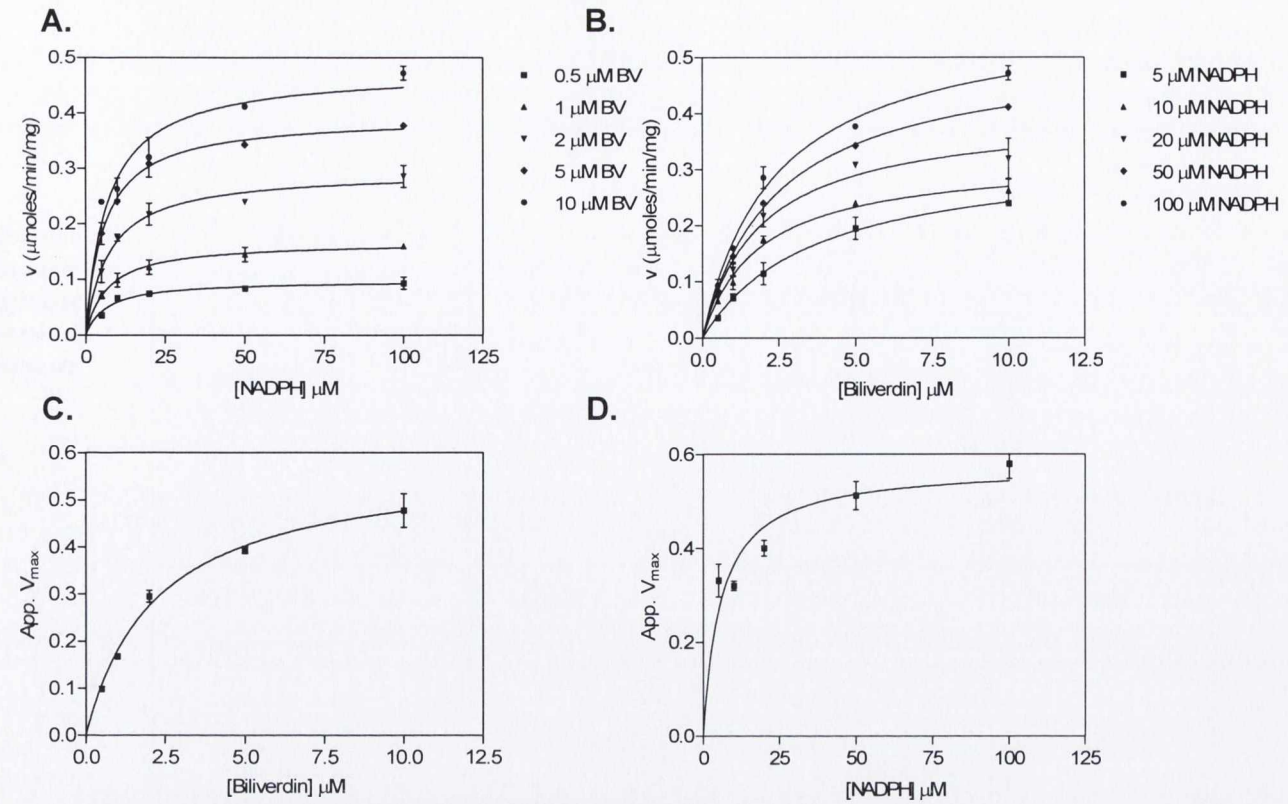

Figure 1. Kinetic analysis of the H97A mutant

A. Initial rate kinetics of H97A with NADPH as the variable substrate **B**. Initial rate kinetics of H97A with biliverdin as the variable substrate **C**. Plot of apparent V_{max} for NADPH versus biliverdin concentration **D**. Plot of apparent V_{max} for biliverdin versus NADPH concentration

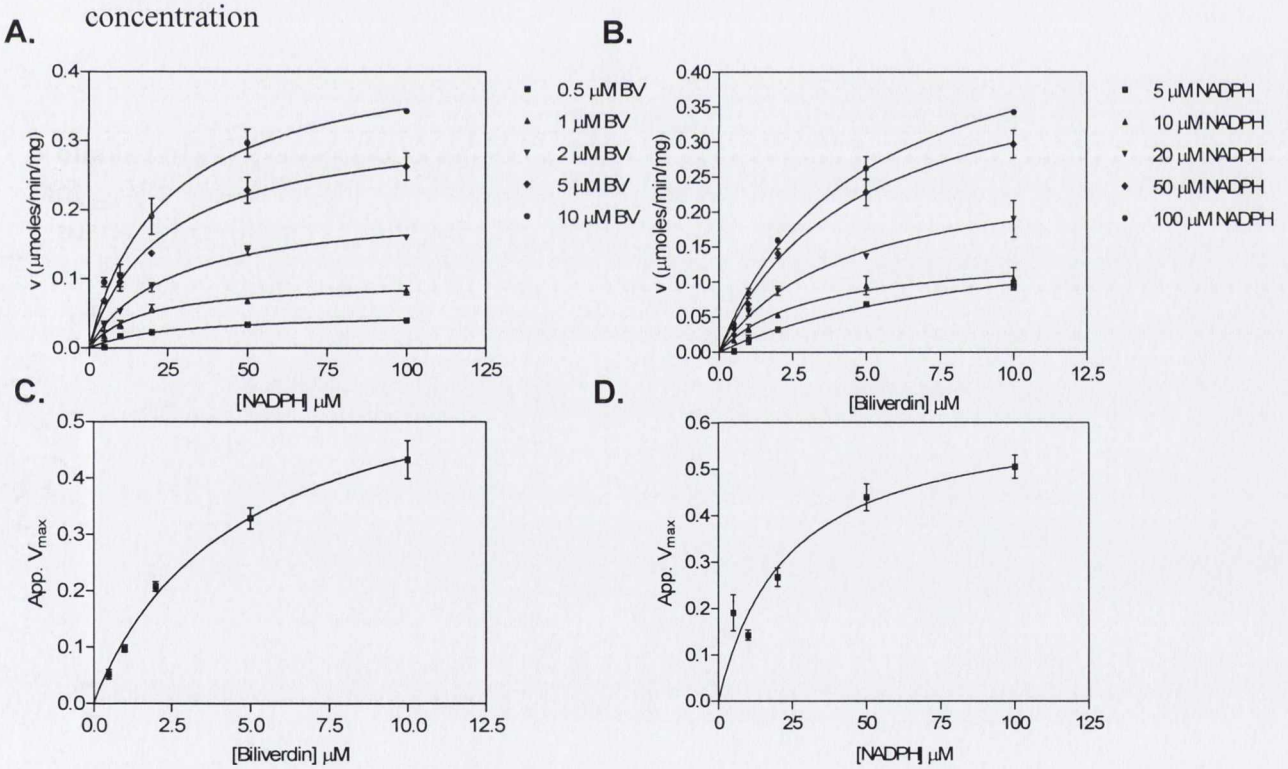

Figure 2. Kinetic analysis of the H126A mutant

A. Initial rate kinetics of H126A with NADPH as the variable substrate **B**. Initial rate kinetics of H126A with biliverdin as the variable substrate **C**. Plot of apparent V_{max} for NADPH versus biliverdin concentration **D**. Plot of apparent V_{max} for biliverdin versus NADPH concentration

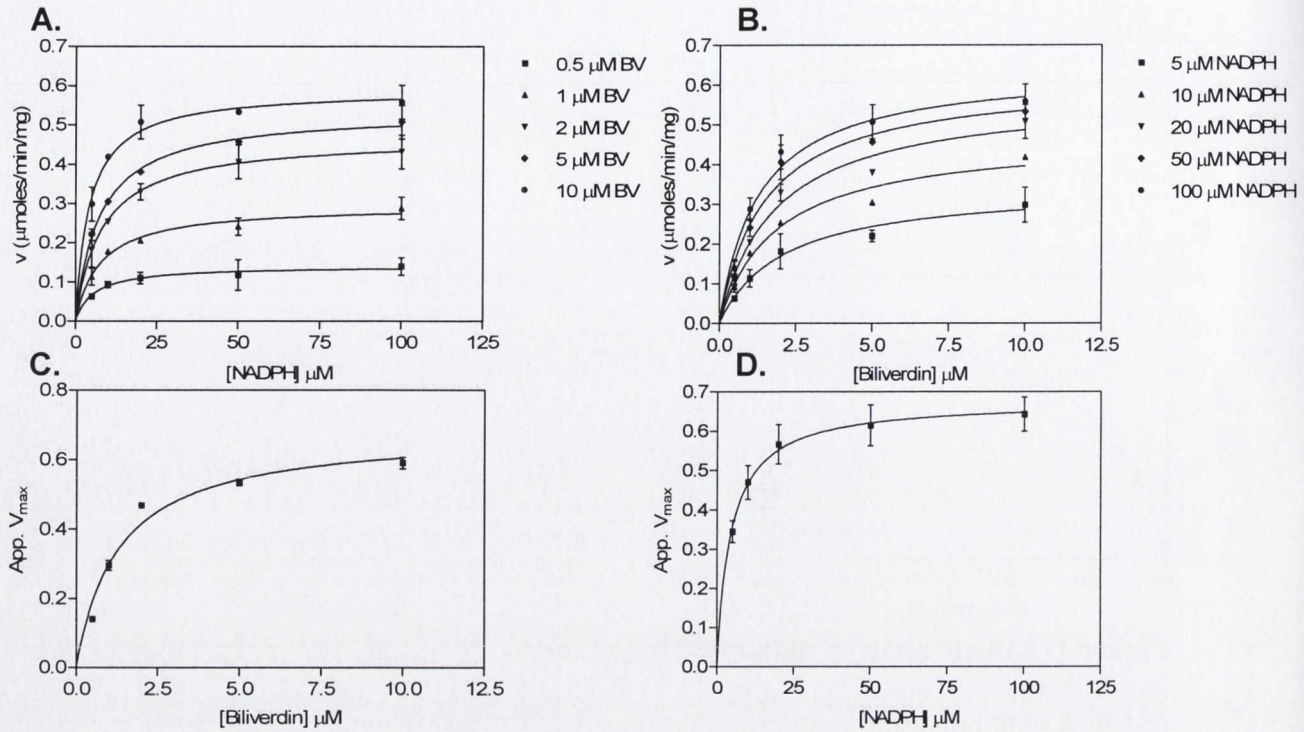

Figure 3. Kinetic analysis of the H129A mutant

A. Initial rate kinetics of H129A with NADPH as the variable substrate **B**. Initial rate kinetics of H129A with biliverdin as the variable substrate **C**. Plot of apparent V_{max} for NADPH versus biliverdin concentration **D**. Plot of apparent V_{max} for biliverdin versus NADPH concentration

Appendix V

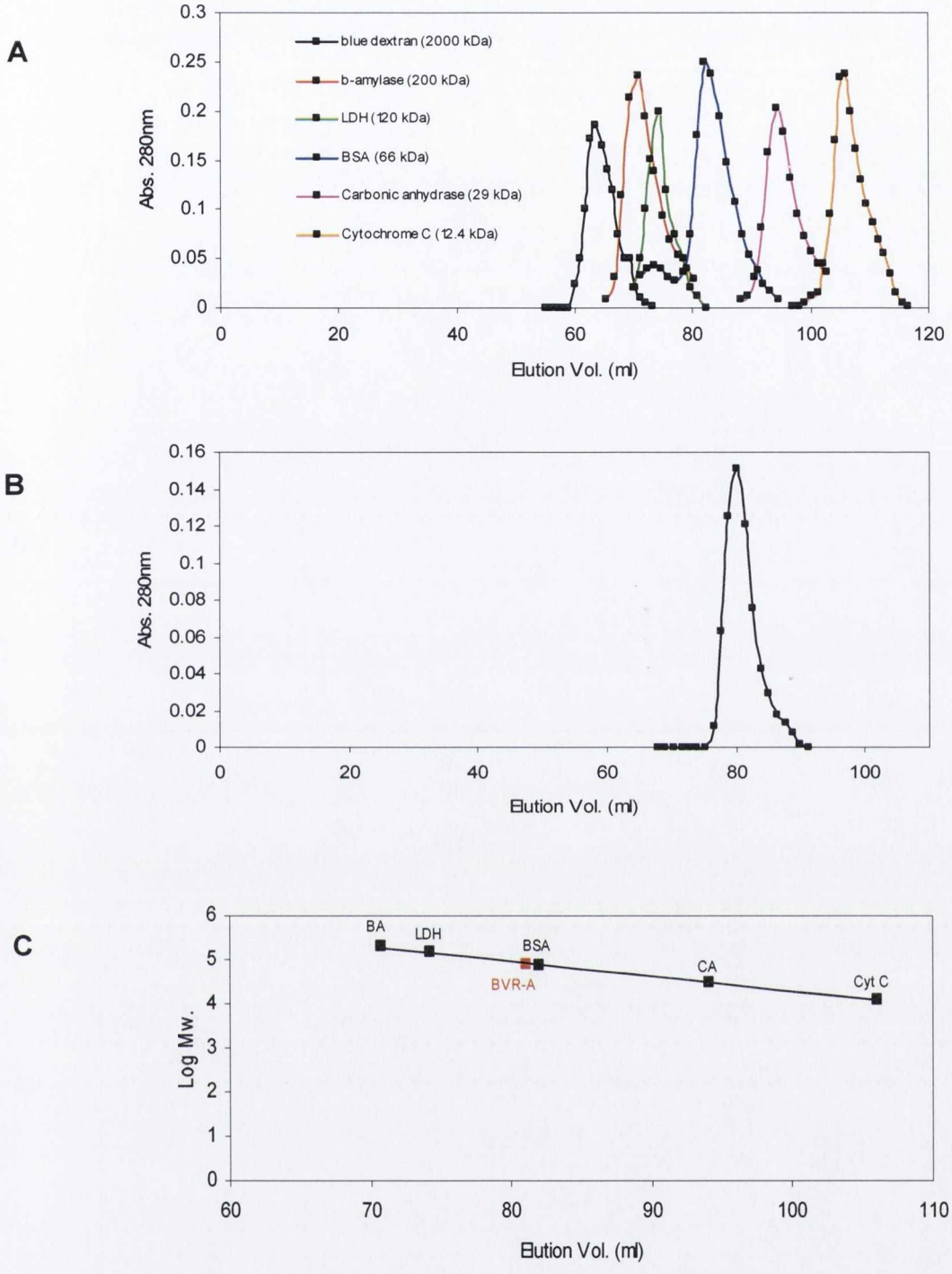

Figure 1 Size-exclusion chromatography of sBVR-A at pH5 and 4°C)

A. Calibration of the S-200 column using various proteins of known molecular weight.
B. Elution profile of recombinant sBVR-A from the S-200 column. sBVR-A eluted in 81ml.
C. Calibration curve for the S-200 column at pH5 and room temperature and determination of the native molecular weight of sBVR-A. Under these conditions sBVR-A was shown to have an Mr of 74kDa

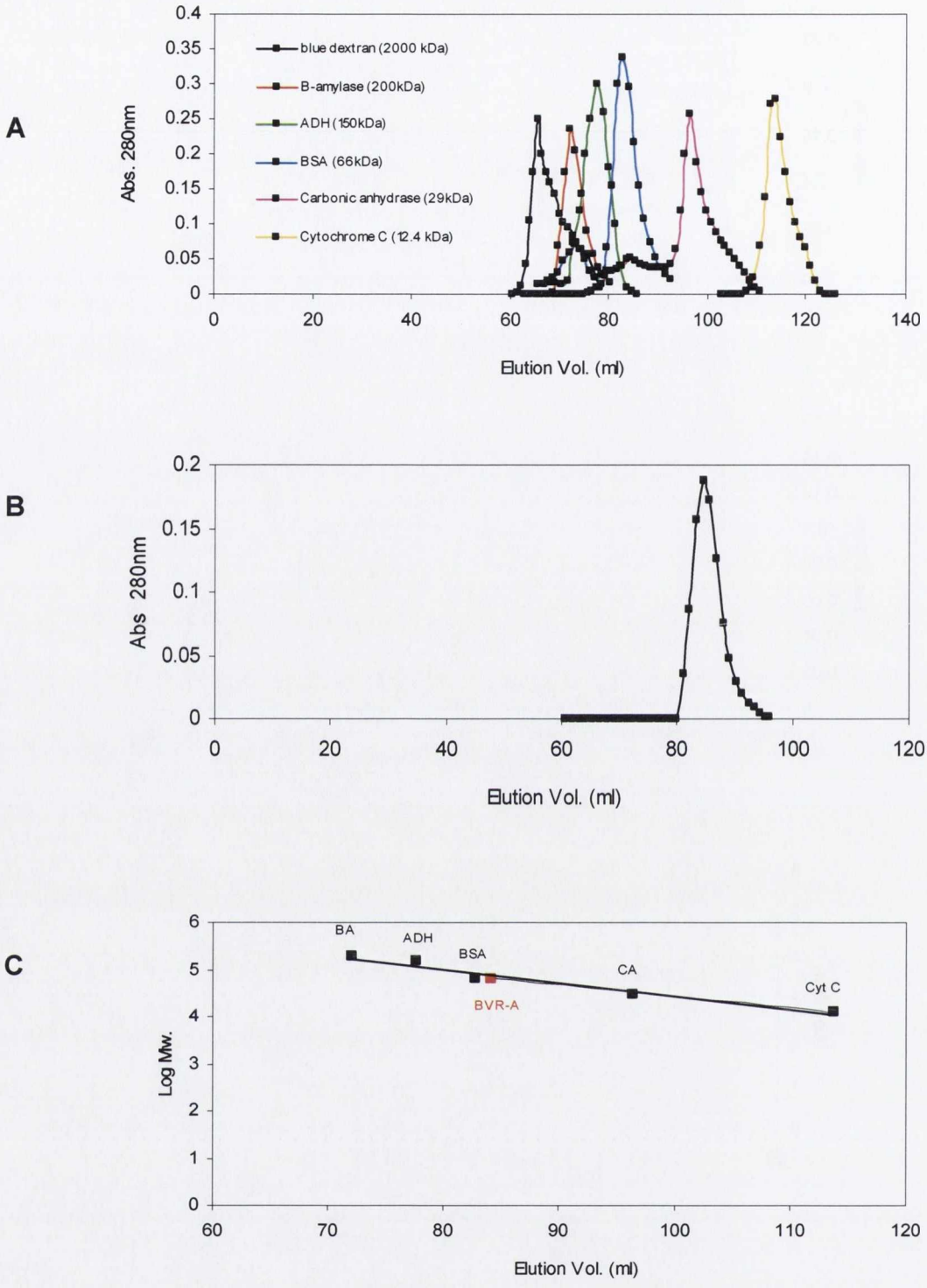

Figure 2 Size-exclusion chromatography of sBVR-A at pH 7.5 and 4°C

A. Calibration of the S-200 column using various proteins of known molecular weight.
B. Elution profile of recombinant sBVR-A from the S-200 column. sBVR-A eluted in 84ml.
C. Calibration curve for the S-200 column at pH5 and room temperature and determination of the native molecular weight of sBVR-A. Under these conditions sBVR-A was shown to have an Mr of 64kDa

A

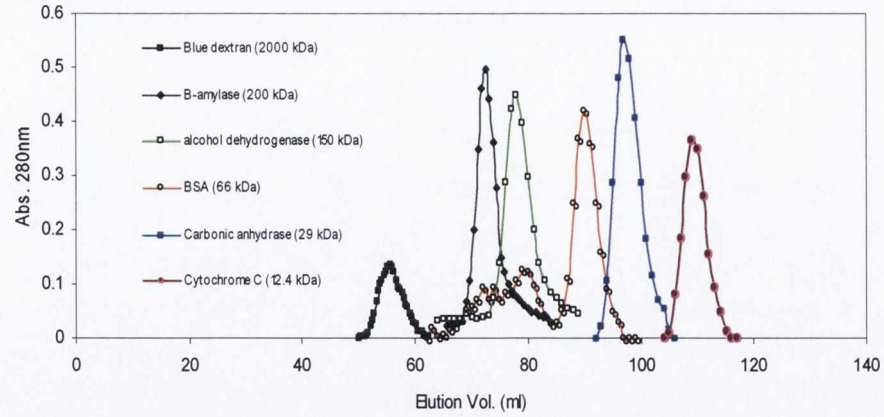

B

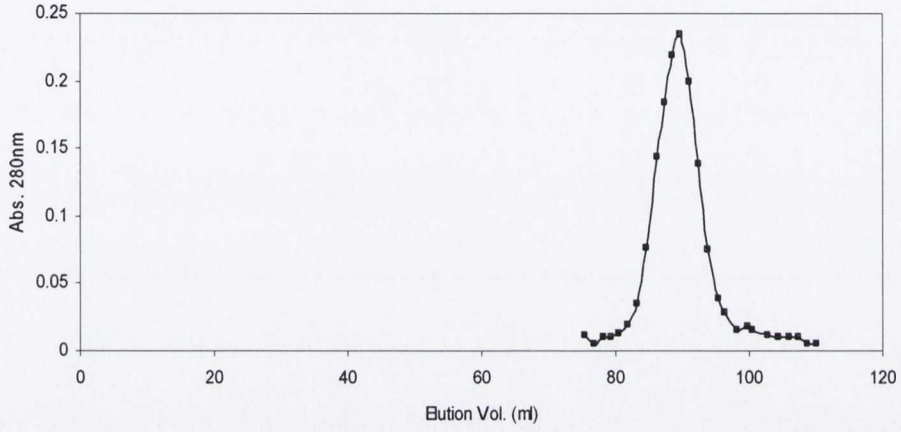

C

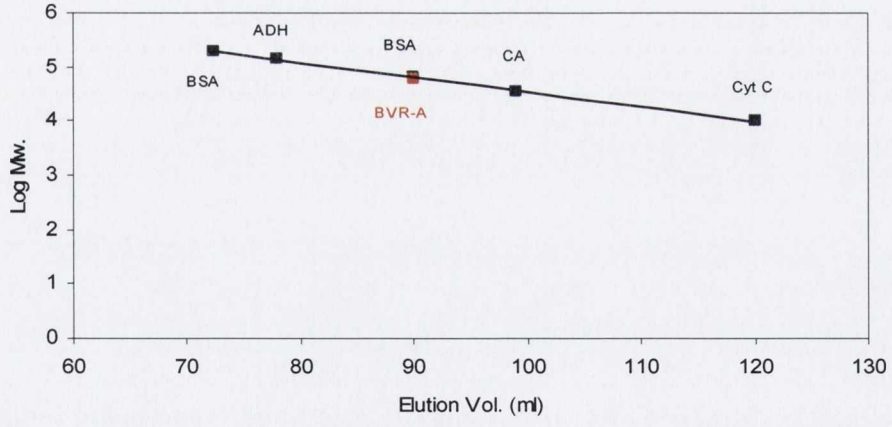

Figure 3 Size-exclusion chromatography of sBVR-A at pH 7.5 and room temperature (18-20°C)

A. Calibration of the S-200 column using various proteins of known molecular weight.
B. Elution profile of recombinant sBVR-A from the S-200 column. sBVR-A eluted in 90ml.
C. Calibration curve for the S-200 column at pH5 and room temperature and determination of the native molecular weight of sBVR-A. Under these conditions sBVR-A was shown to have an Mr of 66kDa

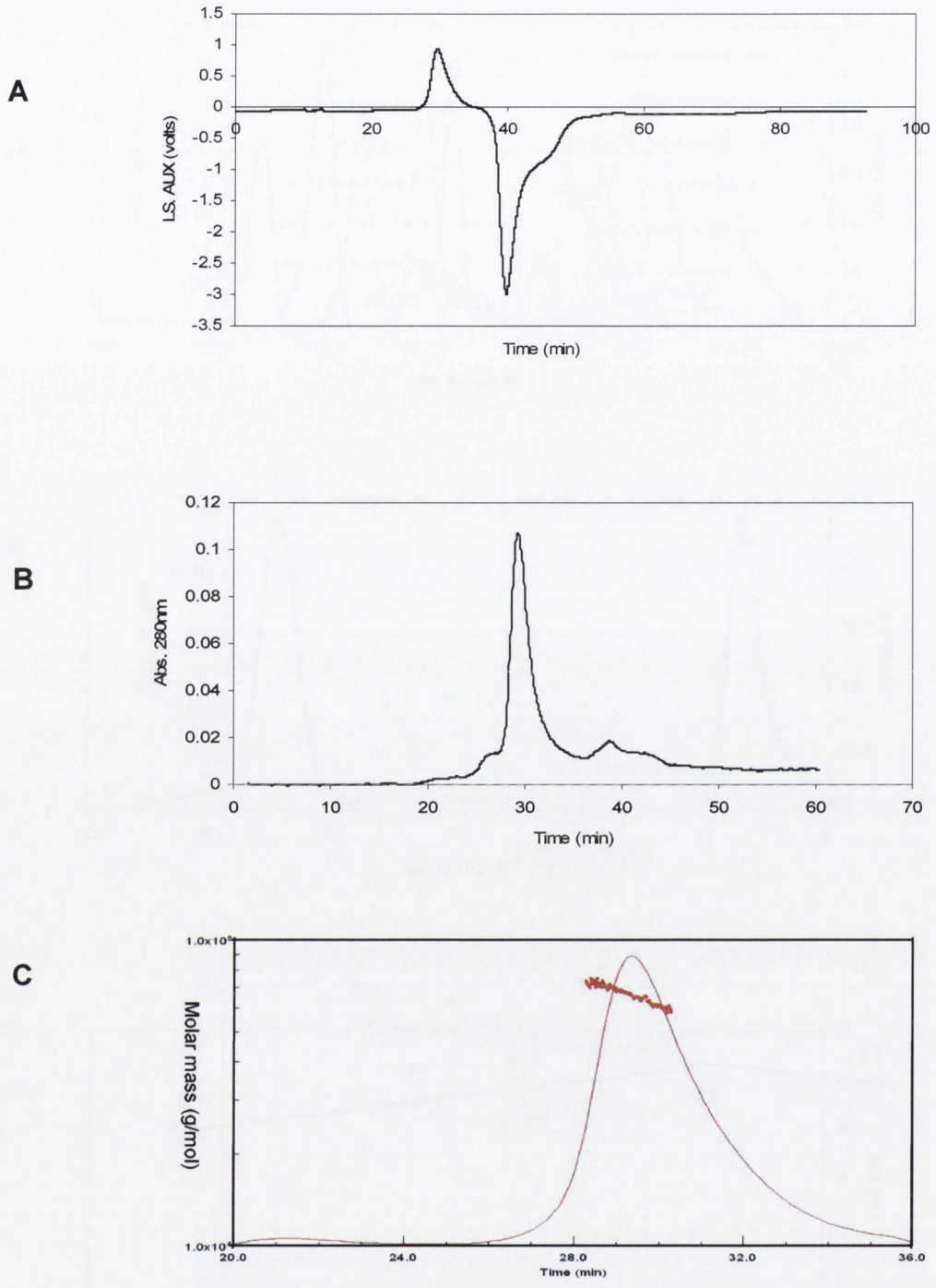

Figure 4. Light scattering analysis of sBVR-A at pH5 and room temperature (18-20°C)

A. Detection of sBVR-A by the light scattering detector following elution from the S-200 HR gel-filtration column. sBVR-A was detected following elution after 30min.
B. Detection of sBVR-A by the UV/Vis detector following elution from the S-200 HR gel-filtration column. sBVR-A was detected following elution after 30min.
C. Determination of the molar mass of sBVR-A at pH5 and room temperature. Mr determination was performed by Astra software which calculated an Mr of 66,210 g/mol for sBVR-A under these conditions.

A

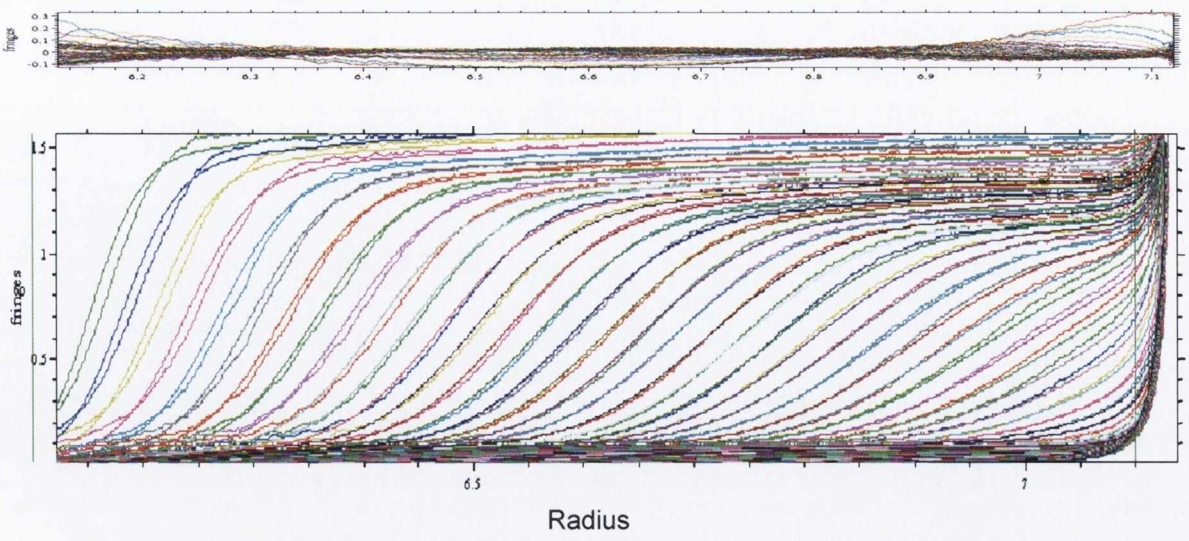

B

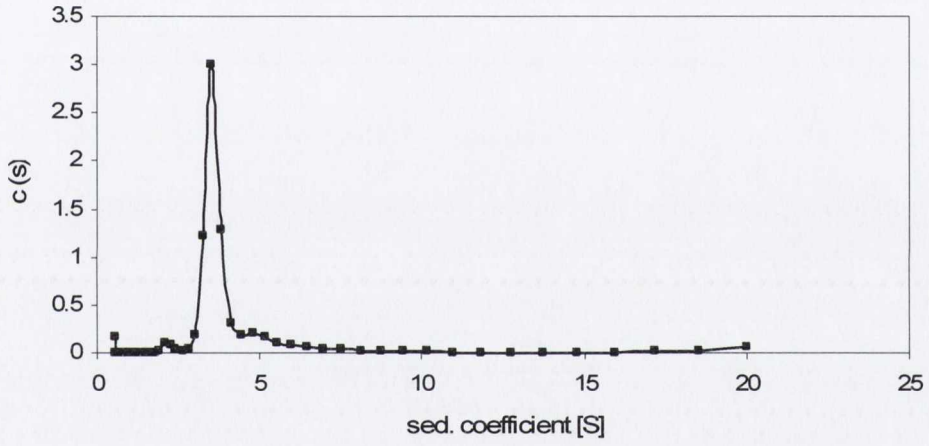

Figure 5 Sedimentation velocity analytical ultracentrifugation analysis of sBVR-A at pH5 and 21°C

A. Whole boundary analysis of sBVR-A. Changes in solute concentration were detected by Rayleigh interference. Experiments were performed as described in Section 2.2.24.1. Residuals are shown above the boundary analysis.
B. c (S) sedimentation co-efficient distribution analysis of sBVR-A. Whole boundary analysis was performed by Sedfit which produced a sedimentation co-efficient of 3.92 S and a molecular weight of 80.1kDa for sBVR-A

A

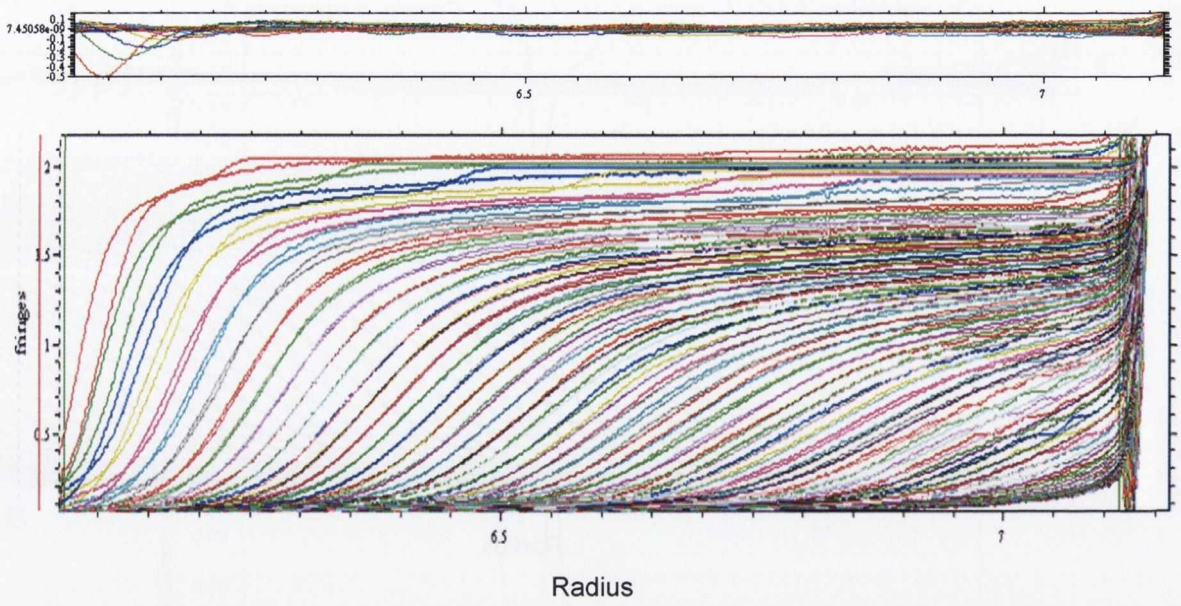

B

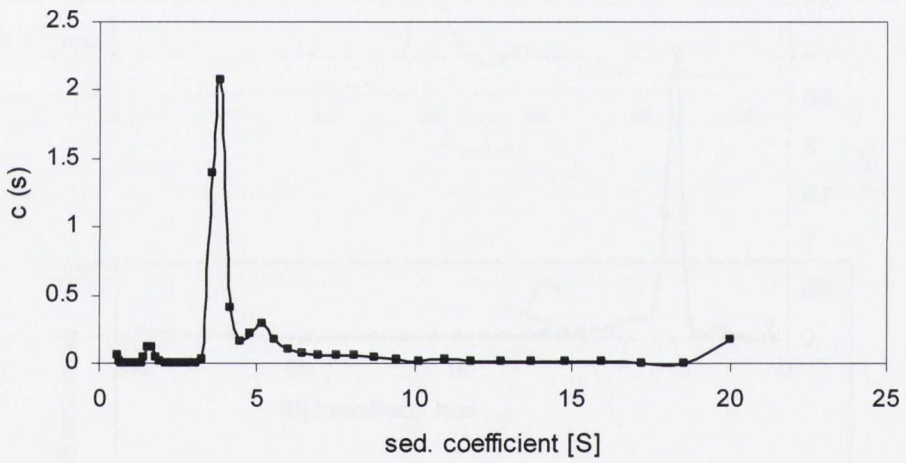

Figure 6 Sedimentation velocity analytical ultracentrifugation analysis of sBVR-A at pH7.5 and 11°C

A. Whole boundary analysis of sBVR-A. Changes in solute concentration were detected by Rayleigh interference. Experiments were performed as described in Section 2.2.24.1. Residuals are shown above the boundary analysis.

B. c (S) sedimentation co-efficient distribution analysis of sBVR-A. Whole boundary analysis was performed by Sedfit which produced a sedimentation co-efficient of 4.2S and a molecular weight of 80.4kDa for sBVR-A

A

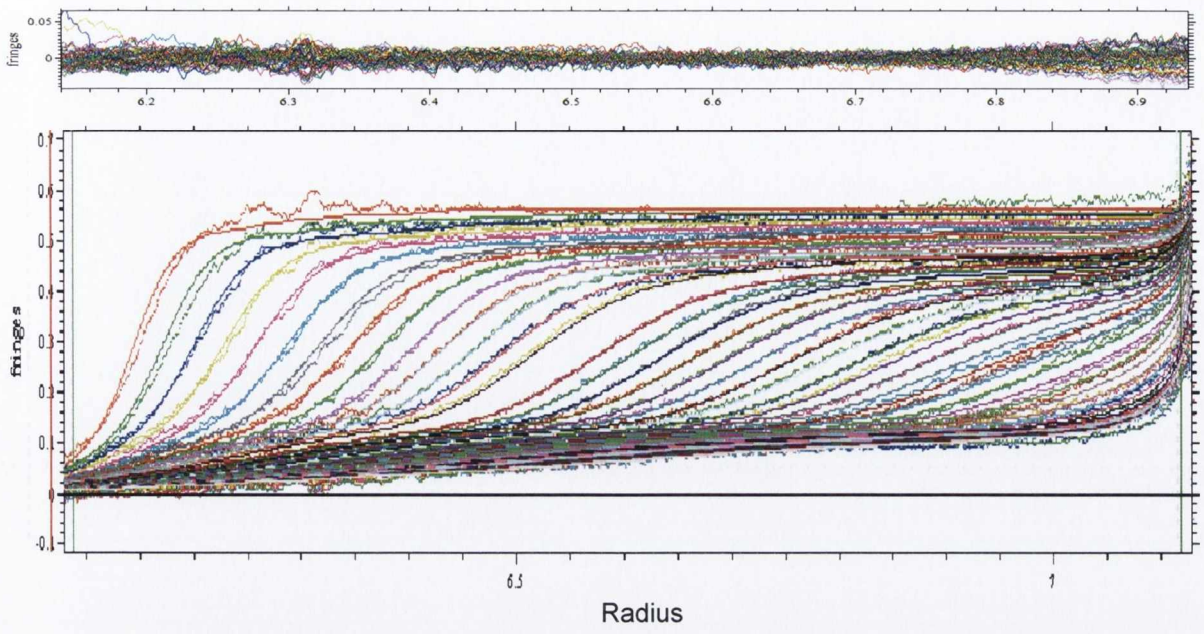

B

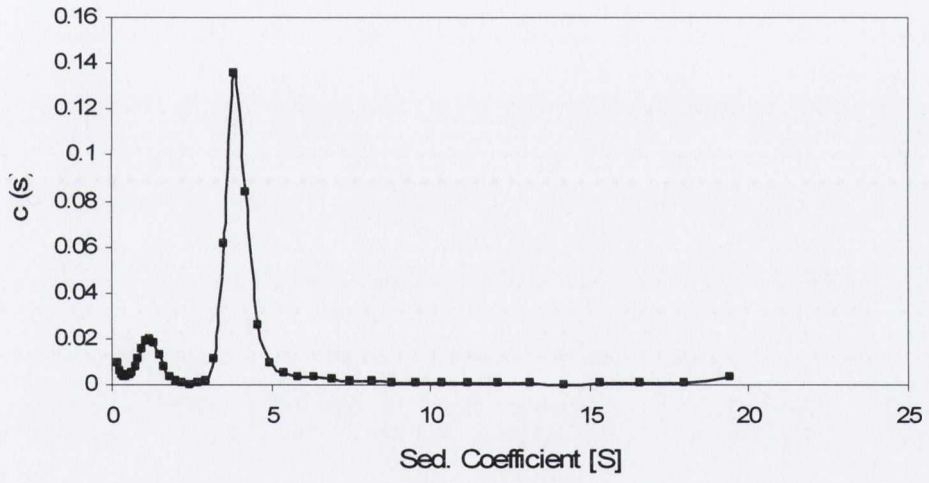

Figure 7 Sedimentation velocity analytical ultracentrifugation analysis of sBVR-A at pH7.5 and 21°C

A. Whole boundary analysis of sBVR-A. Changes in solute concentration were detected by Rayleigh interference. Experiments were performed as described in Section 2.2.24.1. Residuals are shown above the boundary analysis.

B. c (S) sedimentation co-efficient distribution analysis of sBVR-A. Whole boundary analysis was performed by Sedfit which produced a sedimentation co-efficient of 4.18S and a molecular weight of 80kDa for sBVR-A

REFERENCES

A

Abad-Zapatero, C., Griffith, JP., Sussman, JL., Rossmann, MG. (1987). Refined crystal structure of dogfish M4 apo-lactate dehydrogenase. J. Mol. Biol. **198**, 445-67.

B

Baier, K., Nicklisch, S., Grundner, C., Reinecke, J., Lockau, W. (2001) Expression of two nblA-homologous genes is required for phycobilisome degradation in nitrogen-starved Synechocystis sp. PCC6803.FEMS Microbiol Lett. **195**, 35-39.

Baranano, DE., Rao, M., Ferris, CD., Snyder, SH. (2002). Biliverdin reductase: a major physiologic cytoprotectant. PNAS, **99,** 16093-8.

Bassham, J., Benson, A., Calvin, M. (1950). The path of carbon in photosynthesis. J. Biol. Chem. **185**, 781-7.

Beale, SI. (1994) Biosynthesis of open-chain tetrapyrroles in plants, algae, and cyanobacteria. Ciba. Found Symp. **180**, 156-168.

Beale, SI. & Cornejo, J. (1991). Biosynthesis of phycobilins. Ferredoxin-mediated reduction of biliverdin catalyzed by extracts of Cyanidium caldarium. J. Biol. Chem. **266**, 22328-32.

Bellamacina, CR. (1996). The nicotinamide dinucleotide binding motif: a comparison of nucleotide binding proteins. FASEB J. **10**, 1257-69.

Benedikt, E., Gossauer, A., Köst, HP., Miki, W., Yamaguchi, K. (1988) Biliverdin IX delta and neobiliverdin IX delta, isolated from the ovaries of the marine snail, *Turbo cornutus*. Eur. J. Biochem. **175**, 643-648.

Berk, PD., Howe, RB., Bloomer, JR., Berlin, NI. (1969) Studies of bilirubin kinetics in normal adults. J. Clin. Invest. **48,** 2176-90.

Berman-Frank, I., Lundgren, P., Falkowski, P. (2003). Nitrogen fixation and photosynthetic oxygen evolution in cyanobacteria.Res Microbiol. **154,** 1571-64.

Blow, DM., Birktoft, JJ., Hartley, BS. (1969) Role of a buried acid group in the mechanism of action of chymotrypsin. Nature. **221**, 337-340.

Boucher, Y., Douady, CJ., Papke, RT., Walsh, DA., Boudreau, ME., Nesbo, CL., Case, RJ., Doolittle, WF. (2003) Lateral gene transfer and the origins of prokaryotic groups. Annu. Rev. Genet. **37**, 283-328.

Bradford, MM. (1976) A rapid and sensitive method for the quantitation of microgram quantities of protein utilizing the principle of protein-dye binding. Anal. Biochem. **72**, 248-254.

Braggins, PE., Trakshel, GM., Kutty, RK., Maines, MD. (1986) Characterization of two heme oxygenase isoforms in rat spleen: comparison with the hematin-induced and constitutive isoforms of the liver. Biochem. Biophys. Res. Commun. **141**, 528-533.

Brodersen, R. (1979) Bilirubin. Solubility and interaction with albumin and phospholipid. J. Biol. Chem. **254**, 2364-2369.

Browne, S. (2005) Ph.D Thesis, University of Dublin.

C

Caignan, GA., Deshmukh, R., Wilks, A., Zeng, Y., Huang, HW., Moënne-Loccoz, P., Bunce, RA., Eastman, MA., Rivera, M. (2002) Oxidation of heme to beta- and delta-biliverdin by Pseudomonas aeruginosa heme oxygenase as a consequence of an unusual seating of the heme. J. Am. Chem. Soc. **50**, 14879-14892.

Carbone, V., Endo, S., Sumii, R., Chung, RP., Matsunaga, T., Hara, A., El-Kabbani, O. (2008) Structures of dimeric dihydrodiol dehydrogenase apoenzyme and inhibitor complex: probing the subunit interface with site-directed mutagenesis. Proteins.**70**, 176-187.

Carugo, O. & Argos, P. (1997a) NADP-dependent enzymes. I: Conserved stereochemistry of cofactor binding. Proteins. **28**, 10-28.

Carugo, O., Argos, P. (1997b) NADP-dependent enzymes. II: Evolution of the mono- and dinucleotide binding domains. Proteins. **28**, 29-40.

Colleran, E., Carra, PO. (1970) Specificity of biliverdin reductase. Biochem J. **119**, 16P-17P.

Cornejo, J., Willows, RD., Beale, SI. (1998). Phytobilin biosynthesis: cloning and expression of a gene encoding soluble ferredoxin-dependent heme oxygenase from Synechocystis sp. PCC 6803.Plant J. **15**, 99-107.

D

Dambe, TR., Kühn, AM., Brossette, T., Giffhorn, F., Scheidig, AJ. (2006) Crystal structure of NADP(H)-dependent 1,5-anhydro-D-fructose reductase from Sinorhizobium morelense at 2.2 A resolution: construction of a NADH-accepting mutant and its application in rare sugar synthesis. Biochemistry.**45**, 10030-10042.

Deisenhofer, J., Epp, O., Miki, K., Huber, R., Michel, H. (1984). X-ray structure analysis of a membrane protein complex. Electron density map at 3 A resolution and a model of the chromophores of the photosynthetic reaction center from Rhodopseudomonas viridis. J. Mol. Biol. **180**, 385-98.

Douglas, AE. & Raven, JA. (2003) Genomes at the interface between bacteria and organelles. Philos. Trans. R. Soc. Lond. B. Biol Sci. **358**, 5-17.

Dunne, A. (2000). Ph.D Thesis, University of Dublin.

E

Eaton-Rye, JJ. (2004). The construction of gene knockouts in the cyanobacterium *Synechocystis* sp. PCC 6803. Methods. Mol. Biol. **274**, 309-24.

Elliot, G. (1996) Ph.D Thesis, University of Dublin.

Elmore, CL. & Porter, TD. (2002) Modification of the nucleotide cofactor-binding site of cytochrome P-450 reductase to enhance turnover with NADH in Vivo.
J. Biol.Chem. **277**, 48960-48964.

Ennis, O. (1996) Ph.D Thesis, University of Dublin.

Ennis, O., Maytum, R., Mantle, TJ. (1997). Cloning and overexpression of rat kidney biliverdin IX alpha reductase as a fusion protein with glutathione S-transferase: stereochemistry of NADH oxidation and evidence that the presence of the glutathione S-transferase domain does not effect BVR-A activity. Biochem J. **328,** 33-6.

F

Fisher, CL. & Pei, GK. (1997) Modification of a PCR-based site-directed mutagenesis method. Biotechniques. **23**, 570-571.

Florini, JR. & Vestling, CS. (1957) Graphical determination of the dissociation constants for two-substrate enzyme systems. Biochim. Biophys. Acta. **25**, 575-578.

Frankenberg, N., Mukougawa, K., Kohchi, T., Lagarias, JC. (2001) Functional genomic analysis of the HY2 family of ferredoxin-dependent bilin reductases from oxygenic photosynthetic organisms. Plant Cell. **13,** 965-978.

Franklin, E., Browne, S., Hayes, J., Boland, C., Dunne, A., Elliot, G., Mantle, TJ. (2007) Activation of biliverdin-IXalpha reductase by inorganic phosphate and related anions. Biochem. J. **405**, 61-67.

G

Gerk, PM. & Vore, M. (2002).Regulation of expression of the multidrug resistance-associated protein 2 (MRP2) and its role in drug disposition. J. Pharmacol. Exp. Ther. **302**, 407-15.

Gilchrist, ML. Jr, Ball, JA., Randall, DW., Britt, RD. (1995) Proximity of the manganese cluster of photosystem II to the redox-active tyrosine YZ. PNAS. **92**, 9545-9.

Granick, S., & Beale, SI. (1978) Hemes, chlorophylls, and related compounds: biosynthesis and metabolic regulation. Adv. Enzymol. Rela.t Areas Mol. Biol. **46**, 33-203.

Guillouard, I., Lagoutte, B., Moal, G., Bottin, H. (2000) Importance of the region including aspartates 57 and 60 of ferredoxin on the electron transfer complex with photosystem I in the cyanobacterium *Synechocystis* sp. PCC 6803. Biochem. Biophys. Res. Commun. **271,** 647-653.

H

Hagiwara, Y., Sugishima, M., Takahashi, Y., Fukuyama, K. (2006) Crystal structure of phycocyanobilin:ferredoxin oxidoreductase in complex with biliverdin IXalpha, a key enzyme in the biosynthesis of phycocyanobilin. PNAS **103**, 27-32.

Hayashi, S., Omata, Y., Sakamoto, H., Higashimoto, Y., Hara, T., Sagara, Y., Noguchi, M. (2004). Characterization of rat heme oxygenase-3 gene. Implication of processed pseudogenes derived from heme oxygenase-2 gene. Gene, **336**, 241-50.

Hayes, JD., Flanagan, JU., Jowsey, IR. Glutathione transferases. (2005). Annu. Rev, Pharmacol. Toxicol. **45**, 51-88.

Huang, CY., Ayliffe, MA., Timmis, JN. (2003). Direct measurement of the transfer rate of chloroplast DNA into the nucleus. Nature **422**, 72-6.

Hübschmann, T., Börner, T., Hartmann, E., Lamparter, T. (2001) Characterization of the Cph1 holo-phytochrome from Synechocystis sp. PCC 6803. Eur. J. Biochem. **268**, 2055-2063.

I

Inoue, H., Nojima, H., Okayama, H. (1990). High efficiency transformation of Escherichia coli with plasmids. Gene. **96**, 23-8.

J

Jansen, PL., Chowdhury, JR., Fischberg, EB., Arias, IM. (1997) Enzymatic conversion of bilirubin monoglucuronide to diglucuronide by rat liver plasma membranes.
J Biol Chem. **252,** 2710-2716.

Jorissen, HJ., Quest, B., Remberg, A., Coursin, T., Braslavsky, SE., Schaffner, K., de Marsac, NT., Gärtner, W. (2002) Two independent, light-sensing two-component systems in a filamentous cyanobacterium. Eur. J. Biochem. **269**, 2662-2671.

K

Kikuchi, A., Park, SY., Miyatake, H., Sun, D., Sato, M., Yoshida, T., Shiro, Y. (2001) Crystal structure of rat biliverdin reductase. Nat. Struct. Biol. **8**, 221-5.

Kohchi, T., Mukougawa, K., Frankenberg, N., Masuda, M., Yokota, A., Lagarias, JC. (2001) The Arabidopsis HY2 gene encodes phytochromobilin synthase, a ferredoxin-dependent biliverdin reductase. Plant Cell. **2**, 425-436.

Kravets, A., Hu, Z., Miralem, T., Torno, MD., Maines, MD. (2004) Biliverdin reductase, a novel regulator for induction of activating transcription factor-2 and heme oxygenase-1.
J. Biol. Chem. **279**, 19916-19923.

Kutty RK. & Maines MD. (1981). Purification and characterization of biliverdin reductase from rat liver. J. Biol. Chem. **256,** 3956-3962.

L

Laemmli, UK. (1970) Cleavage of structural proteins during the assembly of the head of bacteriophage T4. Nature, **227**, 680-685.

Laue, T., Shah, B., Ridgeway, T. and Pelletier, S. (1992). In S.E. Harding, A.J. Rowe, J.C. Horton (Ed.) *Analytical Ultracentrifugation in Biochemistry and Polymer Science*, (Cambridge: Royal Society of Chemistry).

Lawrence, BA., Polse, J., De Pina, A., Allen, MM., Kolodny, NH. (1996) 31P NMR identification of metabolites and pH determination in the cyanobacterium Synechocystis sp. PCC 6308. Current Microbiology. **34**, 280–283

Lightner, DA., McDonagh, AF. (2001) Structure and metabolism of natural and synthetic bilirubins. J. Perinatol. **1**:S13-16.

Lobley, A., Whitmore, L., Wallace, BA. (2002) DICHROWEB: an interactive website for the analysis of protein secondary structure from circular dichroism spectra. Bioinformatics. **18**, 211-212.

Lott, JS., Halbig, D., Baker, HM., Hardman, MJ., Sprenger, GA., Baker EN.(2000) Crystal structure of a truncated mutant of glucose-fructose oxidoreductase shows that an N-terminal arm controls tetramer formation. J. Mol. Biol. **304**, 575-584.

M

Maines, MD. & Trakshel, GM. (1993) Purification and characterization of human biliverdin reductase. Arch. Biochem. Biophys. **300**, 320-6.

Maines, MD., Polevoda, BV., Huang, TJ., McCoubrey, WK. Jr. (1996) Human biliverdin IXalpha reductase is a zinc-metalloprotein. Characterization of purified and Escherichia coli expressed enzymes. Eur. J. Biochem. **235**, 372-381.

Maisels, MJ. & McDonagh, AF. (2008) Phototherapy for neonatal jaundice. New England journal of Medicine. **358**, 920-928.

Markham, KA., Sikorski, RS., Kohen, A. (2003) Purification, analysis, and preservation of reduced nicotinamide adenine dinucleotide 2'-phosphate. Anal Biochem. **322**, 26-32.

Markwell, MA., Haas, SM., Bieber, LL., Tolbert, NE. (1978) A modification of the Lowry procedure to simplify protein determination in membrane and lipoprotein samples. Anal. Biochem. **87**, 206-10.

Martin, W. & Kowallik, KV. (1993) Annotated English translation of Mereschkowsky's 1905 paper 'Über Natur und Ursprung der Chromatophoren im Pflanzenreiche'. European Journal of Phycology. **34**, 287-295.

Martin, W., Rujan, T., Richly, E., Hansen, A., Cornelsen, S., Lins, T., Leister, D., Stoebe, B., Hasegawa, M., Penny, D. (2002) Evolutionary analysis of Arabidopsis, cyanobacterial, and chloroplast genomes reveals plastid phylogeny and thousands of cyanobacterial genes in the nucleus.PNAS.**99**,12246–12251.

Martin, W., Stoebe, B., Goremykin, V., Hapsmann, S., Hasegawa, M., Kowallik, KV. (1998) Gene transfer to the nucleus and the evolution of chloroplasts. Nature. **393,** 162-5.

McCoubrey, WK. Jr, Huang, TJ., Maines, MD. (1997) Isolation and characterization of a cDNA from the rat brain that encodes hemoprotein heme oxygenase-3. Eur. J. Biochem. **247**, 725-732.

McDonagh, AF. (1979) in The Porphyrins (Dolphin, D., ed.), vol. **6**, p. 257, Academic Press, New York.

Mohamed, HE., Vermaas, W. (2004) Slr1293 in *Synechocystis* sp. strain PCC 6803 Is the C-3',4' desaturase (CrtD) involved in myxoxanthophyll biosynthesis. J. Bacteriol. **186,** 5621-5638.

Montorzi, M., Dziedzic, TS., Falchuk, KH. (2002) Biliverdin during Xenopus laevis oogenesis and early embryogenesis. Biochemistry **31**, 10115-22.

N

Nogales, D., Lightner, DA. (1995) On the structure of bilirubin in solution. 13C[1H] heteronuclear Overhauser effect NMR analyses in aqueous buffer and organic solvents.
J. Biol. Chem. **270**, 73-77.

Noguchi, M., Yoshida, T., Kikuchi, G. (1979). Purification and properties of biliverdin reductases from pig spleen and rat liver. J. Biochem. **86**, 833-48.

O

O' Carra, P., & Colleran, E. (1971) Properties and kinetics of biliverdin reductase. Biochem. J. **125**, 110.

P

Palma, PN., Lagoutte, B., Krippahl, L., Moura, JJ., Guerlesquin, F. (2005) *Synechocystis* ferredoxin/ferredoxin-NADP(+)-reductase/NADP+ complex: Structural model obtained by NMR-restrained docking. FEBS Lett. **579,** 4585-4590.

Pereira, PJ., Macedo-Ribeiro, S., Párraga, A., Pérez-Luque, R., Cunningham, O., Darcy, K., Mantle, TJ., Coll, M. (2001) Structure of human biliverdin IXbeta reductase, an early fetal bilirubin IXbeta producing enzyme. Nat. Struct, Biol. **8**, 215-220.

Phelan, D., Winter, GM., Rogers, WJ., Lam, JC., Denison, MS. (1998) Activation of the Ah receptor signal transduction pathway by bilirubin and biliverdin. Arch. Biochem. Biophys. **357**, 1551-63.

Phillips, O. (1981). Ph.D Thesis, University of Dublin.

Phillips, O. & Mantle, TJ. (1981) Some kinetic and physical properties of biliverdin reductase. Biochem. Soc Trans. **9**, 275-8.

Piubelli, L,, Aliverti, A., Bellintani, F., Zanetti, G. (1995) Spinach ferredoxin i: overproduction in Escherichia coli and purification. Protein. Expr. Purif. **6**, 298-304.

R

Ravenm JA, & Allenm JF. (2003) Genomics and chloroplast evolution: what did cyanobacteria do for plants? Genome Biol. **4,** 1-5.

Rigney, E. & Mantle, TJ. (1988) The reaction mechanism of bovine kidney biliverdin reductase. Biochim. Biophys. Acta. **957**, 237-242.

Rigney, E., Mantle TJ., Dickinson, FM. (1989) The kinetics of ox kidney biliverdin reductase in the pre-steady state. Evidence that the dissociation of bilirubin is the rate-determining step. Biochem. J. **259**, 709-713.

Rigney, EM., Phillips, O., Mantle, TJ. (1988) Some physical and immunological propertiesof ox kidney biliverdin reductase. Biochem. J. **255**, 431-435.

Rudiger, W., Klose, W., Vuillaume, M., Barbier, M. (1969) On the biosynthesis of biliverdin-IX-gamma in *Pieris brassicae*. Experientia. **5,** 487-488.

S

Saito, S., Itano, HA. (1982) Verdohemochrome IX alpha: preparation and oxidoreductive cleavage to biliverdin IX alpha. PNAS. **79**, 1393-1397.

Sambrook, J. (2000) Molecular cloning, a laboratory reference Hardcover, Cold Spring Harbour Laboratory Press. ISBN # 0879695773.

Schagerl, M. & Müller B. (2006) Acclimation of chlorophyll a and carotenoid levels to different irradiances in four freshwater cyanobacteria. J. Plant. Physiol.**163**, 709-716

Schluchter, WM. & Glazer, AN. (1997) Characterization of cyanobacterial biliverdin reductase. Conversion of biliverdin to bilirubin is important for normal phycobiliprotein biosynthesis. J. Biol. Chem. **272**, 13562-13569.

Schuck, P. (2000) Size distribution analysis of macromolecules by sedimentation velocity ultracentrifugation and Lamm equation modeling. Biophysical Journal **78**, 1606-1619.

Schulz, JM., Watson, AL., Sanders, R., Ross, KL., Thoden, JB., Holden, HM., Fridovich-Keil, JL. (2004) Determinants of function and substrate specificity in human UDP-galactose 4'-epimerase. J. Biol. Chem. **279**, 32796-32803.

Sedlak, TW. & Snyder, SH. (2004). Bilirubin benefits: cellular protection by a biliverdin reductase antioxidant cycle. Pediatrics. **6**, 1776-82.

Shalloe, F., Elliott, G., Ennis, O., Mantle, TJ. (1996) Evidence that biliverdin-IX beta reductase and flavin reductase are identical. Biochem. J. **316**, 385-387.

Singleton, JW. & Laster, L. (1965) Biliverdin reductase of guinea pig liver. J. Biol, Chem. **240**, 4780-4789.

Sivaraja, M., Goodin, DB., Smith, M., Hoffman, BM. (1989) Identification by ENDOR of Trp191 as the free-radical site in cytochrome c peroxidase compound ES. Science, **245**, 738-740.

Sjöberg, BM. & Gräslund, A. (1977) The free radical in ribonucleotide reductase from Escherichia coli. Biochem. Soc. Trans. **5**, 747-748

Smith, LJ., Browne, S., Mulholland, AJ., Mantle, TJ. (2008) Computational and experimental studies on the catalytic mechanism of biliverdin-IXbeta reductase. Biochem J. **411**, 475-84.

Stafford, W.F., Sherwood, PJ. (2004) Analysis of heterologous interacting systems by sedimentation velocity: curve fitting algorithms for estimation of sedimentation coefficients, equilibrium and kinetic constants. Biophysical Chemistry **108,** 231-243.

Stocker, R., Ames, BN. (1987) Potential role of conjugated bilirubin and copper in the metabolism of lipid peroxides in bile. PNAS. **84**, 8130-8134.

Sugishima, M., Hagiwara, Y., Zhang, X., Yoshida, T., Migita, CT., Fukuyama, K. (2005) Crystal structure of dimeric heme oxygenase-2 from Synechocystis sp. PCC 6803 in complex with heme. Biochemistry **44**, 4257-4266.

Sugishima, M., Migita, CT., Zhang, X., Yoshida, T., Fukuyama, K. (2004) Crystal structure of heme oxygenase-1 from cyanobacterium Synechocystis sp. PCC 6803 in complex with heme. Eur. J. Biochem. **271,** 4517-25.

T

Tanaka, N., Kusakabe, Y., Ito, K., Yoshimoto, T., Nakamura, KT. (2002) Crystal structure of formaldehyde dehydrogenase from Pseudomonas putida: the structural origin of the tightly bound cofactor in nicotinoprotein dehydrogenases. J. Mol. Biol. **324,** 519-533.

Tenhunen, R., Marver, HS., Schmid, R. (1968) T he enzymatic conversion of heme to bilirubin by microsomal heme oxygenase. PNAS **61**, 748-55.

Tu, SL., Gunn, A., Toney, MD., Britt, RD., Lagarias, JC. (2004) Biliverdin reduction by cyanobacterial phycocyanobilin:ferredoxin oxidoreductase (PcyA) proceeds via linear tetrapyrrole radical intermediates. J. Am. Chem. Soc. **126**, 8682-8693.

Tu, SL., Sughrue, W., Britt, RD., Lagarias, JC. (2006) A conserved histidine-aspartate pair is required for exovinyl reduction of biliverdin by a cyanobacterial phycocyanobilin:ferredoxin oxidoreductase. J. Biol. Chem. **281**, 3127-36.

Tenhunen, R., Ross, ME., Marver, HS., Schmid, R. (1970) Reduced nicotinamide-adenine dinucleotide phosphate dependent biliverdin reductase: partial purification and characterization. Biochemistry. **9**, 298-303.

V

Van Ophem, PW., Van Beeumen, J., Duine, JA. (1993) Nicotinoprotein [NAD(P)-containing] alcohol/aldehyde oxidoreductases. Purification and characterization of a novel type from Amycolatopsis methanolica. Eur. J. Biochem. **212**, 819-826.

W

Whitby, FG., Phillips, JD., Hill, CP., McCoubrey, W., Maines, MD. (2002) Crystal structure of a biliverdin IXalpha reductase enzyme-cofactor complex. J. Mol. Biol. **319**, 1199-1210

Whitmore, L. & Wallace, BA. (2000) DICHROWEB, an online server for protein secondary structure analyses from circular dichroism spectroscopic data. Nucleic Acids Res. **32**, W668-673.

Wiegert, T., Sahm, H., Sprenger, GA. (1997) The substitution of a single amino acid residue (Ser-116 --> Asp) alters NADP-containing glucose-fructose oxidoreductase of Zymomonas mobilis into a glucose dehydrogenase with dual coenzyme specificity. J. Biol. Chem. **272**, 13126-13133.

Wu, JT., Wu, LH., Knight, JA. (1986) Stability of NADPH: effect of various factors on the kinetics of degradation. Clin. Chem. **32**, 314-9.

Y

Yamaguchi, T., Komoda, Y., Nakajima, H. (1994) Biliverdin-IX alpha reductase and biliverdin-IX betareductase from human liver. Purification and characterization. J. Biol. Chem. **269**, 24343-24348.

Yamaguchi, T. & Nakajima, H. (1995) Changes in the composition of bilirubin-IX isomers during human prenatal development. Eur. J. Biochem. **233**, 467-472.

Yamashita, K., McDaid, J., Ollinger, R., Tsui, TY., Berberat, PO., Usheva, A., Csizmadia, E., Smith, RN., Soares, MP., Bach, FH. (2004) Biliverdin, a natural product of heme catabolism, induces tolerance to cardiac allografts. FASEB J. **6**, 765-767.

Yoshihara, S., Shimada, T., Matsuoka, D., Zikihara, K., Kohchi, T., Tokutomi, S. (2006) Reconstitution of blue-green reversible photoconversion of a cyanobacterial photoreceptor, PixJ1, in phycocyanobilin-producing Escherichia coli. Biochemistry. **45**, 3775-3784.

Z

Zhang, X., Migita, CT., Sato, M., Sasahara, M., Yoshida, T. (2005) Protein expressed by the ho2 gene of the cyanobacterium *Synechocystis* sp. PCC 6803 is a true heme oxygenase. Properties of the heme and enzyme complex. FEBS J. **272**, 1012-1022.

Zehr, JP., Mellon, MT., Zani, S. (1998) New nitrogen-fixing microorganisms detected in oligotrophic oceans by amplification of Nitrogenase (nifH) genes. Appl. Environ. Microbiol. **64**, 444-450.